Dissecting the role of the partition factor ParF in TP228 plasmid segregation

Gina Elizabeth Gamble

Doctor of Philosophy

University of York

Biology

September 2016

Abstract

Antibiotic resistance is one of the most significant health concerns for the public. Bacterial antibiotic resistance can occur due to the presence of drug resistant plasmids; therefore understanding the mechanism of how these plasmids are passed from one generation to the next is of high importance. Low copy number plasmids utilise partition cassettes in order to ensure faithful segregation at cell division. This work dissects the multidrug resistance plasmid TP228, which contains the *parFGH* partition cassette. *parH* is a *cis*-acting like centromere site, ParG is a centromere DNA binding protein and ParF is a Walker-type ATPase that assembles into extended filaments upon ATP binding. Recent structural data has shown that ParF forms dimer-of-dimer units, which create the building blocks of the filaments. ParF also binds non-specifically to DNA *in vitro* and associates with the nucleoid *in vivo*. In the presence of the complete partition system, *parFGH*, ParF oscillates from one pole of the nucleoid to the other leading to correct positioning of the plasmids.

In this study, the role that ParF plays in driving the accurate segregation of the TP228 plasmid is dissected. A range of *in vitro* biochemical assays and *in vivo* microscopy experiments have been used to study ParF DNA binding, assembly into higher order structures and ParF localisation. A triple mutant, harbouring changes at the dimer-dimer interface of ParF was shown to be unable to undergo ATP-dependent assembly into higher order structures, confirming the importance of this interface in this process. Changes in residues in a proline-rich motif positioned at the monomer-monomer interface cause ParF to form stronger monomer-monomer interactions and to self-associate into high order structures in the absence of ATP. The results also established that a triad of amino acids positioned at this monomer-monomer interface are crucial in the interaction between ParF and the binding partner ParG. Finally, three informative mutants were found to be unable to bind DNA *in vitro* however *in vivo* microscopy revealed the mutants could still associate with the nucleoid. Conventional fluorescence and super resolution microscopy demonstrated that all these ParF mutants were unable to oscillate over the nucleoid and displayed a different pattern compared to wild type ParF. Overall the results demonstrated that both ATP and DNA regulate the dynamic ParF higher order structures and this underpins plasmid segregation. Based on these findings, a new model for TP228 plasmid segregation is proposed

Table of Contents

Abstract **2**

Table of Contents **3**

List of Tables **10**

List of Figures **12**

Acknowledgements **20**

Author's declaration **21**

Chapter 1: Introduction **22**

1.1 Plasmids **23**

1.2 Plasmid partition systems **25**

1.2.1 Type I partition systems 28

1.2.1.1 The Type Ia partition system of P1 plasmid 29

1.2.1.2 The Type Ia partition system of F plasmid 33

1.2.1.3 Type Ib partition systems 35

1.2.2 Type II partition systems 41

1.2.2.1 The type II partition system of R1 plasmid 41

1.2.3 Type III partition systems 45

1.2.3.1 The type III partition system of pBtoxis plasmid 45

1.2.4 Type IV partition systems 48

1.3 Bacterial chromosome segregation **49**

1.3.1 *Bacillus subtilis* chromosome segregation system 50

1.3.2 *Caulobacter crescentus* chromosome segregation system 51

1.4 Mechanisms of plasmid segregation **52**

1.4.1 A filament model of plasmid segregation for type I partition systems 52

1.4.2 A diffusion-ratchet mechanism for plasmid segregation for type I partition systems 55

1.4.3 Mechanism of chromosome segregation by type I partition systems 57

1.4.4 The insertional polymerisation 'pushing' model for type II plasmid systems ... 59

1.4.5 The treadmilling model for type III partition systems 61

1.5 The partition system of plasmid TP228 63

1.5.1 Centromere site *parH* 63

1.5.2 Centromere binding protein ParG 66

1.5.3 Walker-type ATPase ParF 69

1.5.3.1 ParF self-associates into higher order structures 75

1.5.3.2. ParF localises to the nucleoid and shows a dynamic oscillatory behaviour .. 78

1.6 ParF related proteins 79

1.6.1 The MinD cell division protein of *E. coli* 81

1.7 Project aims 85

Chapter 2: Materials and Methods 87

2.1 Bacterial strains and plasmids 88

2.1.1 Bacterial Strains 88

2.1.2 Plasmids 89

2.2 Media and antibiotics 97

2.2.1 Media 97

2.2.1.1 Luria-Bertani solid and liquid media 97

2.2.1.2 MacConkey agar 97

2.2.1.3 M9 Medium 98

2.2.2 Antibiotics 99

2.3 Recombinant DNA techniques 100

2.3.1 Plasmid DNA isolation – small scale 100

2.3.2 Polymerase chain reaction (PCR) 100

2.3.3 Restriction Enzyme Digest....106
2.3.4 Ethanol precipitation....106
2.3.5 Alkaline phosphate treatment of DNA....107
2.3.6 Agarose gel electrophoresis....107
2.3.7 Gel extraction of DNA fragments....108
2.3.8 DNA ligation....108
2.3.9 Preparation of competent cells....108
2.3.10 Transformation of competent cells....109
2.3.11 Screening of recombinant plasmids....109
2.3.12 DNA sequencing....109
2.4 Mutagenesis and cloning....110
2.4.1 Site directed mutagenesis by overlap extension PCR for *parF* mutagenesis ..110
2.4.2 Cloning *parF* mutant gene into other vectors....112
2.4.2.1 pET22b....112
2.4.2.2 pT18 and pT25....112
2.4.2.3 pBM40....112
2.4.2.4 pBM20 and pBM22....112
2.5 Expression and Purification....113
2.5.1 Overproduction of ParF and ParF mutant proteins....113
2.5.2 Overproduction of ParG....113
2.5.3 Purification of ParG, ParF and ParF mutant proteins....114
2.5.4 Buffer exchange of ParF and ParG proteins....115
2.5.5 Protein concentration determination....116
2.6 Sodium dodecyl sulfate-polyacrylamide gel electrophoresis (SDS-PAGE) 117
2.6.1 Preparation of gel....117
2.6.2 Sample preparation....119
2.6.3 Electrophoresis....119

2.6.4 Staining of SDS Gels 119

2.7 Plasmid partition assay 119

2.8 ATPase assay 122

2.8.1 Intrinsic ATPase activity 122

2.8.2 ParG stimulation of ATPase activity 122

2.9 Bacterial two-hybrid and β-galactosidase assay 122

2.9.1 Bacterial two-hybrid assay 123

2.9.2 β-galactosidase assay 123

2.10 Circular dichroism (CD) 125

2.11 Chemical cross-linking 125

2.12 Dynamic light scattering (DLS) 126

2.13 Electron microscopy (EM) 126

2.14 Electrophoretic mobility shift assay (EMSA) 127

2.14.1 Biotinylated DNA fragment 127

2.14.2 Preparation of samples and gel electrophoresis 127

2.14.3 DNA transfer 129

2.14.4 Detection of Biotinylated DNA 129

2.15 Fluorescence anisotropy 130

2.15.1 ATP binding 130

2.15.2 DNA binding 131

2.16 Microscopy 131

2.16.1 Confocal microscopy 131

2.16.3 3D-Structured Illumination Microscopy 132

2.16.4 Immunofluorescence microscopy 132

2.17 Sedimentation assay 133

2.18 Tethered particle motion (TPM) 134

2.19 Western blot 135

2.19.1 Preparation of samples and running of gel electrophoresis 135

2.19.2 Protein transfer onto Hybond ECL nitrocellulose membrane..... 136

2.19.3 Detection of proteins..... 136

Chapter 3: Disruption of the ParF dimer-dimer interface affects protein self-assembly, localisation and dynamics over the nucleoid..... 138

3.1 The dimer-dimer interface of ParF 139

3.2 Construction of *parF-S185W* and *parF-S186F* at interface 2 of the ParF dimer 145

3.3 *In vivo* analysis of the effect of the changes S185W and S186F on plasmid retention 152

3.4 ParF-K64A-V89Y-M96A..... 154

3.4.1 ParF and ParF-K64A-V89Y-M96A overproduction and purification..... 154

3.4.2 Biochemical properties of ParF-K64A-V89Y-M96A and the ability of the mutant to form higher order structures..... 158

3.4.2.1 ParF-K64A-V89Y-M96A is able to bind ATP similarly to wild type ParF . 158

3.4.2.2 ParF-K64A-V89Y-M96A is unable to assemble into higher order structures upon the ATP binding..... 159

3.4.2.3 ParF-K64A-V89Y-M96A is able to form a dimer similar to that of the wild type protein..... 167

3.4.3 ParF-K64A-V89Y-M96A is homogenously distributed over the nucleoid *in vivo* and is unable to oscillate..... 174

3.5 Conclusions..... 189

Chapter 4: The ParF monomer-monomer interface: interplay and synergy between the proline-rich motif and the ATP-binding pocket..... 191

4.1 The monomer-monomer interface of ParF..... 192

4.2 *In vivo* analysis of the effects of the mutations constructed in the proline-rich motif on plasmid retention 197

4.3 ParF-P107A, ParF-S108A and ParF-P109R..... 200

4.3.1 Cloning of mutant *parF* alleles into the expression vector pET22b 201

4.3.2 Biochemical properties of ParF-P107A, ParF-S108A and ParF-P109R and ability of the mutants to form higher order structures.....203

4.3.2.1 ParF-P107A, ParF-S108A ParF-P109R are folded correctly and the mutations have no effect on the secondary structure of ParF 203

4.3.2.2 All three mutants are able to bind ATP similarly to wild type ParF.....205

4.3.2.3 ParF-S108A and ParF-P109R ATPase activity are not stimulated by ParG.207

4.3.2.4 ParF-P107A, ParF-S108A and ParF-P109R form dimers, however their interaction with ParG is disrupted.....213

4.3.2.5 ParF-P107A, ParF-S108A and ParF-P109R have a higher tendency to self-associate into higher order structures.....219

4.3.2.6 ParF-S108A and ParF-P109R form filament structures in the absence of nucleotide.....231

4.3.3 ParF-S108A is homogenously distributed over the nucleoid *in vivo* and is unable to oscillate over the nucleoid.....233

4.3.4 ParF-P109R forms many different patterns *in vivo* and is unable to oscillate.241

4.4 ParF-P107A, ParF-S108A and ParF-P109R conclusions.....248

4.5 The ParF – ParG interface.....253

4.5.1 The ParF-L110A – ParG interaction is disrupted 256

4.5.2 ParF-ParG interface conclusions.....259

4.6 Conclusions of the monomer-monomer interface of ParF 261

Chapter 5: The role of ParF non-specific DNA binding and association with the nucleoid to mediate TP228 plasmid segregation 263

5.1 The role of ParF non-specific DNA binding in TP228 plasmid segregation....264

5.2 ParF is able to bind nsDNA *in vitro*.....266

5.3 *In vivo* analysis of the effects of the changes in residues potentially involved in DNA binding on plasmid retention.....274

5.4 ParF-R139A, ParF-R169A and ParF-K160E-R163E 277

5.4.1 ParF-R139A displays weaker ATP binding compared to the wild type ParF .280

5.4.2 ParF-R139A is a hyperactive ATPase.....282

5.4.3 ParF-R139A – ParF- R139A interaction and ParF-R139A – ParG interaction are stronger than the wild type ParF interactions....287

5.4.4 ParF-R139A has a higher tendency to self-associate into higher order structures and the ability of ParF-K160E-R163E to assemble into higher order structures is disrupted....293

5.4.5 ParF-R139A, ParF-R169A and ParF-K160E-R163E nsDNA binding is disrupted *in vitro* 304

5.4.6 ParF-R139A, ParF-R169A and ParF-K160E-R163E are homogenously distributed over the nucleoid *in vivo* and are unable to oscillate 308

5.5 ParF-R139A, ParF-R169A and ParF-K160E-R163E conclusions....323

5.6 The link between ParF nsDNA binding and assembly into higher order structures 327

5.7 Conclusion of the nsDNA binding properties of ParF....327

Chapter 6: Discussion and Future Work....330

6.1 Discussion....331

6.1.1 Disruption of the dimer-dimer interface prevents ParF from forming higher order structures....331

6.1.2 The ParF monomer-monomer interface is crucial for both the ParF-ParF interaction and the ParF-ParG interaction....333

6.1.3 ParF is able to bind nsDNA and associates with the nucleoid *in vivo* 335

6.2 Summary of all ParF mutant proteins 336

6.3 A model for TP228 plasmid segregation 349

6.4 Future work 353

Abbreviations 356

References 360

List of Tables

Table 1.1 - Comparisons of type Ia and type Ib partition systems 29

Table 1.2 - Summary of important residues for nucleotide binding and dimer cross contacts identified from the structure of ParF 72

Table 1.3 - Comparisons of ParA Walker-type ATPase proteins from different type I partition systems 80

Table 2.1 – List of bacterial strains 88

Table 2.2 – List of Plasmids 89

Table 2.3 – Composition of LB medium 97

Table 2.4 – Composition of MacConkey agar 98

Table 2.5 - Components of 10X M9 stock solution 99

Table 2.6 – Components of M9 medium 99

Table 2.7 – Antibiotics 99

Table 2.8 – PCR reaction 100

Table 2.9 – List of Primers 101

Table 2.10 – Thermocycler programme 105

Table 2.11 – Restriction digest reactions 106

Table 2.12 - The composition of buffers used in ParF purifications 115

Table 2.13 - The composition of buffers used in ParG purifications 115

Table 2.14 - Bradford assay protein standard reaction set up. 116

Table 2.15 – Composition of resolving gels used 118

Table 2.16 – Composition of the stacking gel 118

Table 2.17 – Composition of 5X M63 medium 124

Table 2.18 – Composition of buffer Z 125

Table 2.19 – Reaction set up for EMSA 128

Table 2.20 – Composition of 6% native gel 128

Table 2.21 – Composition of 5X TBE buffer 129

Table 4.1 - Summary of *in vitro* and *in vitro* characteristics of ParF-P107A, ParF-S108A and ParF-P109R in comparison to wild type ParF. If highlighted in red there is a significant difference observed between the ParF mutant and the wild type protein.....252

Table 5.1 – Summary of *in vitro* and *in vitro* characteristics of ParF-R139A, ParF-R169A and ParF-K160E-R163E in comparison to wild type ParF. If highlighted in red there is a significant difference observed between the ParF mutant and the wild type protein.....325

Table 6.1 - Summary of ParF mutant proteins *in vitro* phenotypes. If highlighted in red it indicates differences to that of ParF. Grey boxes indicate work not primarily done in this study. 338

Table 6.2 – Summary of ParF mutant proteins *in vivo* phenotype. If highlighted in red it indicates differences to that of ParF. Grey boxes indicate work not primarily done in this study. 340

Table 6.3 - Summary of ParF mutant proteins and the effects on the three main properties of ParF. 341

List of Figures

Figure 1.1 - Classification of partition systems.. 27

Figure 1.2 - Schematic representation of the partition cassettes of P1 plasmid.....31

Figure 1.3 - Structure of ParA and ParB from the P1 plasmid.....32

Figure 1.4 - Schematic representation of the partition cassette of F plasmid. 34

Figure 1.5 - Schematic representation of the partition cassette of pSM19035 plasmid. 37

Figure 1.6 - Schematic representation of the partition cassettes of pB171 plasmid. 40

Figure 1.7 - Schematic representation of the partition cassette of R1 plasmid.....43

Figure 1.8 – The structure of ParM from R1 plasmid and ParR from pB171 plasmid. .44

Figure 1.9 - Schematic representation of the partition cassette of pBtoxis plasmid. 47

Figure 1.10 - Structures of TubZ and TubR from the pBtoxis plasmid. 48

Figure 1.11 - A molecular model for a filament based pulling mechanism used by type I partition systems. 54

Figure 1.12 - A diffusion ratchet model of plasmid segregation by type I partition systems. 56

Figure 1.13 - The insertional polymerisation 'pushing' model of plasmid segregation by a type II partition system. 60

Figure 1.14 - A treadmilling model for plasmid segregation by a type III partition system. 62

Figure 1.15 - Schematic representation of the partition cassette of plasmid TP228. 65

Figure 1.16 - Structure of ParG dimer. 67

Figure 1.17 - Structure of ParF. 71

Figure 1.18 - Structural homology of ParF to other ParA superfamily proteins. 74

Figure 1.19 - ParF dimer-of-dimer unit. 77

Figure 1.20 - A model of the oscillatory behaviour of the MinCDE system of *E. coli*. 84

Figure 2.1 - Schematic representation of overlap extension mutagenesis. 111

Figure 2.2 - Schematic representation of a plasmid partition assay. 121

Figure 3.1 - Structure of monomeric ParF. 140

Figure 3.2 - The dimer-of-dimer unit formation by ParF..... 142

Figure 3.3 - Structure of ParF showing the position of residues changed at interface 1 and interface 2. 144

Figure 3.4 - Vector map of pFH450 and pFH547. 146

Figure 3.5 - Schematic representation of the *parFGH* region inserted into pFH547... 147

Figure 3.6 - Agarose gel showing PCR products from overlap extension mutagenesis of *parF-S185W* and *parF-S186F*…….. 149

Figure 3.7 - Example of an agarose gel showing the restriction digest of pFH547 vector and PCR 3 fragment for *parF-S185W* mutagenesis. 149

Figure 3.8 - Example of an agarose gel showing a restriction digest screen of pFH547 plasmids potentially habouring the desired mutation, *parF-S185W*.. 150

Figure 3.9 - ABI sequence traces showing the relevant section of wild type *parF* sequence between the two restriction sites *Cla*I and *Hpa*I and the sections for the mutations leading to the amino acid changes S185W and S186F. 151

Figure 3.10 - Plasmid retention percentage of ParF mutants at the interface of the ParF dimer. 153

Figure 3.11 - ParF and ParF-K64A-V89Y-M96A overproduction trial and solubility assay.. 155

Figure 3.12 -SDS-PAGE analysis showing the purification of wild type ParF.. 156

Figure 3.13 - SDS-PAGE analysis showing purification of ParF-K64A-V89Y-M96A.. 157

Figure 3.14 –ParF and ParF-K64A-V89Y-M96A ATP binding. 159

Figure 3.15 – DLS of ParF and ParF-K64A-V89A-M96A..... 162

Figure 3.16 – DLS of ParF and ParF-K64A-V89Y-M96A in the presence of ParG. .. 163

Figure 3.17 – EM observations of ParF in the presence of ATP. 165

Figure 3.18 – EM observations of ParF and ParF-K64A-V89Y-M96A in the presence and absence of ATP. 166

Figure 3.19 – Crosslinking of ParF and ParF-K64A-V89Y-M96A. S 169

Figure 3.20 - Agarose gel showing cloning of *parF-K64A-V89Y-M96A* into pT18 and pT25 vectors for bacterial two-hybrid assay. 171

Figure 3.21 – Bacterial two-hybrid and β-galactosidase assay of ParF and ParF-K64A-V89Y-M96A. 173

Figure 3.22 - Bacterial two-hybrid and β-galactosidase assay of ParF and ParF-K64A-V89Y-M96A. 174

Figure 3.23 – Plasmid set used in microscopy studies to investigate ParF and ParG localisation *in vivo* 176

Figure 3.24 - Agarose gels showing cloning of *parF-K64A-V89Y-M96A* allele into pBM20 and pBM40 for microscopy experiments. 177

Figure 3.25 - Western blot to show the level of ParF-Emerald comparatively to ParF. 12% SDS-gel showing purified ParF and cell extract of BW25113 *E. coli* cells that were transformed with pBM20 and pBM40 and grown as for confocal microscopy. 178

Figure 3.26 – ParF localisation within the cell when the full partition cassette *parFGH* is present. 181

Figure 3.27 – Z stack images of a single cell when the partition cassette *parFGH* is present.. 182

Figure 3.28 – Individual time images of ParF and ParG localisation over a twenty minute time lapse. 183

Figure 3.29 – Localisation of ParF-K64A-V89Y-M96A. 185

Figure 3.30 – Patterns of the localisation of ParF-K64A-V89Y-M96A and ParG. 186

Figure 3.31 – Z stack images of ParF-K64A-V89Y-M96A and ParG. 187

Figure 3.32 – Super resolution images of ParF and ParF-K64A-V89Y-M96A. 188

Figure 4.1– Structure of ParF showing the position of the proline-rich motif. 193

Figure 4.2 – Structure of ParF highlighting residues identified as potentially being involved in cross-contacts between ParF monomers. 195

Figure 4.3 - Structure of ParF highlighting residues identified by computational alanine scanning as potentially involved in disrupting the monomer-monomer interface of the protein. 196

Figure 4.4 - Plasmid retention percentage of ParF harbouring changes in the proline-rich motif of ParF.. 199

Figure 4.5 - Example of agarose gels showing the cloning of *parF-S108A* into pET22b(+).. 202

Figure 4.6 - Circular dichroism spectra of ParF-P107A, ParF-S108A and ParF-P109R. 204

Figure 4.7 – Fluorescence anisotropy of ParF-P107A, ParF-S108A and ParF-P109R binding ATP. 207

Figure 4.8 - Intrinsic ATPase activity of ParF and ParF-S108A. 209

Figure 4.9 – ParF and ParF-S108A ATPase activity in the presence of ParG. 210

Figure 4.10 – Intrinsic ATPase activity of ParF and ParF-P109R. 211

Figure 4.11 – ParF and ParF-P109R ATPase activity in the presence of ParG. 212

Figure 4.12 – Crosslinking results for ParF-S108A and ParF-P109R. 214

Figure 4.13 – Bacterial two-hybrid and β-galactosidase assay of ParF-P107A, ParF-S108A and ParF-P109R. 217

Figure 4.14 - Bacterial two-hybrid assay and β-galactosidase assay of ParF-P107A, ParF-S108A and ParF-P109R interactions with ParG. 218

Figure 4.15 – DLS of ParF-P107A, ParF-S108A and ParF-P109R in the absence and presence of nucleotide. 222

Figure 4.16 – DLS of ParF-P109R in the absence and presence of nucleotide.. 223

Figure 4.17 - DLS of ParF-P107A in the presence of ParG. 224

Figure 4.18 - DLS of ParF-S108A in the presence of ParG. 225

Figure 4.19 - DLS of ParF-P109R in the presence of ParG. 226

Figure 4.20 - Sedimentation assays of ParF-P107A, ParF-S108A and ParF-P109R in the absence and presence of nucleotide. 229

Figure 4.21 - Sedimentation assays of ParF-S108A and ParF-P109R in the presence of ParG. 230

Figure 4.22 – EM ultrastructures of ParF-S018A and ParF-P109R in the absence and presence of nucleotide. 232

Figure 4.23 – Localisation of ParF-S108A and ParG. 234

Figure 4.24 – Localisation patterns of ParF-S108A and ParG.....235

Figure 4.25 - Statistical analysis of ParG position when ParF-S108A is present. 235

Figure 4.26 - Statistical analysis of ParG foci number and position when ParF is present. 236

Figure 4.27 - Statistical analysis of ParG foci number and position when ParF-S108A is present. 237

Figure 4.28 – Z stack images of ParF-S108A and ParG.. 239

Figure 4.29 – Individual time images of ParF, ParF-S108A and ParG localisation over a twenty minute time lapse experiment. 240

Figure 4.30 – Localisation of ParF-P109R and ParG. 242

Figure 4.31- Multiple cells showing the different *in vivo* localisations patterns formed by ParF-P109R and ParG. 243

Figure 4.32 - Examples of ParF-P109R and ParG *in vivo* patterning. 244

Figure 4.33 – Number of ParF-P109R foci and the pattern formed by the distinct foci in numerous cells. 245

Figure 4.34 – Statistical analysis of the number of ParG foci and position in cells with a ParF and ParF-P109R background. 246

Figure 4.35 – Z stack images of ParF-P109R and ParG. 248

Figure 4.36 - ParF structure highlights residues potentially involved in the ParF-ParG interaction. 254

Figure 4.37 - Plasmid retention of plasmids harbouring mutations of residues potentially involved in ParF-ParG interactions. 255

Figure 4.38 – Bacterial two-hybrid and β-galactosidase assays of ParF-L110A-ParG, ParF-F112A-ParG and ParF-V149F-ParG. 257

Figure 4.39 – Comparison of the β-galactosidase assay results for ParF-S108A, ParF-P109R, ParF-L110A, ParF-F112A and ParF-V149F. 258

Figure 4.40 - ParF structure highlighting residues involved in the ParF-ParG interaction. 260

Figure 5.1 - Structure of ParF highlighting surface exposed basic residues identified as potentially involved in nsDNA binding. 265

Figure 5.2 – Fluorescence anisotropy analysis of ParF and non-specific DNA binding. 267

Figure 5.3 – EMSA results of ParF binding ns-DNA. 269

Figure 5.4 - Schematic representation of the TPM approach. 272

Figure 5.5 – TPM analysis of ParF binding nsDNA.. 273

Figure 5.6 – Structure of ParF highlighting the position of the residues changed in the double mutant. 275

Figure 5.7 - Retention percentage of plasmids harbouring *parF* alleles with mutations affecting residues potentially involved in DNA binding. 276

Figure 5.8 - Structure of ParF highlighting the positions of residues R139 and R169 that are close to the ATP binding pocket. 278

Figure 5.9 - Circular dichroism spectra of ParF-R139A and ParF-K160E-R163E. 279

Figure 5.10 – Fluorescence anisotropy of ParF-R139A and ParF-K160E-R163E ATP binding. 281

Figure 5.11 – Intrinsic ATPase activity of ParF-R139A.....283

Figure 5.12 – ATPase activity of ParF-R139 in the presence of ParG. 284

Figure 5.13 - Intrinsic ATPase activity of ParF-K160E-R163E. 285

Figure 5.14 - ATPase activity of ParF-K160E-R163E in the presence of ParG. 286

Figure 5.15 – Crosslinking results of ParF-R139A and ParF-K160E-R163E. 288

Figure 5.16 – Bacterial two-hybrid and β-galactosidase assay of ParF-R139A and ParF-K160E-R163E. 291

Figure 5.17 - Bacterial two-hybrid and β-galactosidase assay of ParF-R139A-ParG and ParF-K160E-R163E-ParG.....292

Figure 5.18 – DLS of ParF-R139A and ParF-K160E-R163E.....296

Figure 5.19 – DLS of ParF-R139A in the presence of ParG. 297

Figure 5.20 – DLS of ParF-K160E-R163E in the presence of ParG. 298

Figure 5.21 – Sedimentation assay of ParF-K160E-R163E.....301

Figure 5.22 - Sedimentation assay of ParF - R139A. 302

Figure 5.23 - Sedimentation assay of ParF-R139A, ParF-R169A and ParF-K160E-R163E in the presence of ParG. 303

Figure 5.24 – Fluorescence anisotropy analysis of ParF-R139A, ParF-R169A and ParF-K160E-R163E nsDNA binding. 305

Figure 5.25 – EMSA of ParF-R139A, ParF-R169A and ParF-K160E-R163E.....307

Figure 5.26 – Localisation of ParF-R139A and ParG. 310

Figure 5.27 – Localisation of ParF-R169A and ParG. 311

Figure 5.28 – Number and position of ParG foci in cells containing ParF-R139A and ParF-R169A. 312

Figure 5.29 – Localisation patterns of ParF-R139A and ParG. 313

Figure 5.30 - Statistical analysis of ParG signal position when ParF-R139A is present. 313

Figure 5.31 - Localisation patterns of ParF-R169A and ParG. 314

Figure 5.32 - Statistical analysis of ParG position when ParF-R169A is present.....315

Figure 5.33 – Z stack images of ParF-R139A with ParG and ParF-R169A with ParG. 316

Figure 5.34 – Localisation of ParF-K160E-R163E and ParG. 318

Figure 5.35 - Number and position of ParG foci in cells containing ParF-K160E-R163E. 319

Figure 5.36 – ParG foci positions in cells harbouring ParF-K160E-R163E. 319

Figure 5.37 – Localisation patterns of ParF-K160E-R163E and ParG. 320

Figure 5.38 - Statistical analysis of ParG position when ParF-K160E-R163E is present. 321

Figure 5.39 – Z stack images of ParF-K160E-R163E and ParG. 322

Figure 6.1 - ParF DNA binding model. 344

Figure 6.2 - A schematic representation of the behaviour displayed by ParF and ParF mutant proteins. 348

Figure 6.3 - A model for TP228 plasmid segregation. 352

Acknowledgements

I would like to thank my supervisor Dr Daniela Bariallà for giving me the opportunity to be part of her research group and work on a fantastic project and for all her guidance and support throughout. I would also like to thank my co-supervisor Dr Leo Caves and my TAP members Professor Maggie Smith and Professor Fred Antson.

I would like to acknowledge several people who have helped me throughout my project without whom the project would not have been possible. Dr Andrew Leach for his continued help and support within the Technology Facility of the University of York. Graeme Park and Meg Stark for their assistance with microscopy at the University of York. Dr. Marcus Posch for his support with super resolution microscopy carried out at the University of Dundee. Dr Ramus Dame and Ramon Van Der Valk for their help with TPM experiments carried out at the University of Leiden. Finally all the present and past members of the Daniela Barillà lab, especially Madhuri Barge and Irene Ng who have helped and advised me throughout my PhD. I would also like to thank all members of the L1 corridor.

Finally I would like to thank all my friends and family who have supported me throughout my PhD, especially my husband Liam and my parents Lynn and Graham.

This project was funded by the BBSRC at the University of York.

Author’s declaration

I declare that this thesis is a presentation of original work and I am the sole author. This work has not previously been presented for an award at this, or any other, University. All sources are acknowledged as References.

Chapter 1: Introduction

1.1 Plasmids

Plasmids are extrachromosomal DNA elements, which are able to replicate independently of the chromosome (Lederberg, 1952). These mobile genetic elements are found in all three domains of life, however they are predominantly found in bacteria (Del Solar *et al*., 1998). In most cases plasmids are circular, double stranded DNA molecules, which vary in size (one thousand base pairs to more than 100 kilobases) although examples of linear plasmids have also been described (Norman *et al*., 2009). Generally, plasmids are not essential for the organism's growth, however plasmids often possess genes that may benefit the organism's survival. Naturally occurring plasmids can be beneficial for the host organism in many ways, for example they may encode genes for antibiotic resistance, heavy metal resistance, utilisation of a specific nutrient or virulence factors (Johnson and Nolan, 2009). Plasmids are widely used in recombinant DNA technology and have significant biological relevance in areas including clinical studies, biotechnology, and environmental studies.

Plasmids are self-replicating DNA molecules that are present in defined copies per cell. Plasmid copy numbers range from a few per cell (low copy number) to hundreds per cell (high copy number). Plasmid replication can occur via three mechanisms: theta type, strand displacement and rolling circle (RC) (Del Solar *et al*., 1998). The theta type mechanism is the most widely studied and is similar to chromosome replication, also it should be noted that plasmids, like chromosomes, have origins of replication (*ori*) where replication is initiated. A common feature of the theta replication mechanism is that, in most cases, the initiation of replication is carried out by plasmid-encoded Rep proteins that are able to bind to direct repeats (iterons). Other features, that are found at the *ori* are an adjacent AT-rich region where assembly of the host initiation factors occurs and one or more DnaA boxes in which the host DnaA initiator protein can bind (Del Solar *et al*., 1998). Theta replication can be subdivided into four groups based on the mode of replication initiation. Class A theta replication plasmids include R1, P and F. Class B includes ColE1 and ColE1-like plasmids. These plasmids rely solely on host replication factors and do not encode Rep proteins. Class C and Class D combine elements from Class A and Class B replication. Class C include ColE2 and ColE3 plasmids, Class D includes pSM19035 plasmid from *Streptococcus pyogenes* and pIP501 from *Streptococcus agalactiae* (Lilly and Camps, 2015).

Escherichia coli incompatibility group Q (IncQ) plasmids utilize the strand–displacement mechanism of replication. This mechanism relies on three plasmid encoded proteins: RepA (helicase), RepB (primase) and RepC (initiator). Host factors are not involved with the mechanism of initiation of replication (Lilly and Camps, 2015). In this mechanism lagging strand synthesis is not coupled with the leading strand synthesis. The third mechanism, the rolling circle mechanism, is mostly employed by smaller plasmids such as pT181, pC221, pUB110 and pC194 from staphylococcal species. Replication by this method is unidirectional and involves the plasmid-encoded Rep protein generating a site-specific nick at the plasmid leading strand origin. The 3'-OH end is then elongated by a DNA polymerase (Khan, 1997).

As mentioned above, plasmids are found in defined numbers per cell. The copy number is maintained by plasmid-encoded control elements that regulate the initiation of the replication step (Del Solar *et al*., 1998). After replication, the plasmids must be faithfully segregated to each daughter cell. High copy number plasmids are thought to be stably maintained via random diffusion, where it is unlikely that a daughter cell will not contain at least one plasmid given the high number of plasmids present in the dividing cell. However, recent research has demonstrated that these high copy number plasmids may not be randomly distributed within the cell, but they are actually excluded from the nucleoid with some observed to cluster at the cell poles (Million-Weaver and Camps, 2014, Reyes-Lamothe *et al*., 2014). Therefore there is growing speculation for an active segregation mechanism, which could potentially involve chromosomal encoded proteins.

Plasmids employ mechanisms, other than random diffusion, to ensure they are faithfully segregated within the cell. There are three types of plasmid-encoded maintenance systems: (1) multimer resolution systems, (2) toxin-antitoxin systems (addiction systems) and (3) active segregation systems. Multimer resolution systems, which are encoded by both high and low copy number plasmids, act to remove plasmid dimers or multimers that have resulted from homologous recombination. If these multimers are not removed, this error would lead to plasmid instability (Guynet and de la Cruz, 2011). Toxin-antitoxin (TA) systems ensure plasmid maintenance by inhibiting growth of plasmid-free daughter cells; this can be seen as a backup maintenance mechanism. In most cases, the TA cassette encodes an antitoxin and a stable toxin protein. The antitoxin is either a labile protein or an untranslated antisense RNA species. The TA complex is transferred to the daughter cell, however the antitoxin is unstable. In a

plasmid free cell, the antitoxin cannot be replenished and therefore the toxin cannot be neutralised and thus will have deleterious effects on the cell (Hayes, 2003, Stieber *et al*., 2008). F plasmid employs a toxin-antitoxin system, encoding an antitoxin - CcdA and a toxin – CcdB which targets *E. coli* DNA gyrase. Another example employing this system is plasmid R1 of *E. coli* that contains the *hok-sok* TA system.

As low copy number plasmids are unable to rely on random diffusion it is essential they employ active mechanisms to ensure stable maintenance from one generation to the next. This is, in most cases, mediated by an active segregation system (partition system). Low copy number plasmids possess partition (*par*) loci that typically encode for two proteins that assemble on a *cis*-acting centromere site. One of the plasmid-encoded proteins, namely ParA, is typically an NTPase motor protein and the other protein is a centromere binding protein, namely ParB (Ebersbach and Gerdes, 2005, Hayes and Barillà, 2006). Partition systems on low copy number plasmids have been widely studied and have provided a greater understanding of DNA segregation in bacteria, as well as archaea.

1.2 Plasmid partition systems

All cells must be able to carry out accurate DNA segregation to ensure stable genome transmission (Moller-Jensen *et al*., 2000). In the last couple of decades our understanding of prokaryotic DNA segregation has vastly improved and it is now known that prokaryotes employ active DNA segregation mechanisms. Both bacterial plasmids and chromosomes have been shown to utilise partition (*par*) systems in order to faithfully segregate the genome in the cell (Moller-Jensen *et al*., 2000, Schumacher *et al*., 2012). Low copy number plasmids have been important model systems, which have allowed further understanding of partition systems in prokaryotes. Partition systems are composed of just three components: a *cis*-acting centromere-like site, and two Par proteins, a force generating NTPase motor protein and a centromere binding protein (CBP) (Schumacher, 2008). The *trans*-acting proteins are generally encoded in an operon that is auto-regulated by one or both proteins. Together the NTPase and CBP, form a nucleoprotein complex that binds to the *cis*-acting centromere site on the plasmid or chromosome forming a segrosome (Hayes and Barilla, 2006). The partition systems utilise bacterial cytoskeletal proteins including eukaryotic actin and tubulin homologues and also prokaryotic specific polymerising proteins (Machón *et al*., 2007). The partition systems are divided into four classes based on the type of NTPase encoded and the

genetic organization of the cassette (Figure 1.1). Type I are the most abundant and they are the only partition system specified by both plasmids and chromosome. This system is characterised by a Walker-type ATPase. Type I systems can be further sub-divided depending upon the presence (type Ia) or absence (type Ib) of an N-terminal helix-turn-helix (HTH) DNA binding domain in the ATPase (Table 1.1) (Ebersbach and Gerdes, 2005, Schumacher, 2008). Type II systems encode an actin-like GTPase/ATPase and type III systems encode a tubulin-like GTPase protein (Salje and Lowe, 2008, Schumacher *et al*., 2012). Recently a fourth type of partition system was discovered; however details of this system are still to be elucidated. This partition system has been identified on the *Staphylococcus aureus* plasmid pSK1 and appears to only encode one protein. It has been speculated that this single protein plays the role of both the NTPase and the CBP (Schumacher, 2008, Guynet and de la Cruz, 2011).

Although the four types of partition systems display many differences, a common feature of all these partition systems is the way in which the segrosome is formed. Firstly the CBP binds specifically to the centromere site on the plasmid and then additional CBPs are recruited to the complex via protein-protein and protein-DNA (non-specific and specific) interactions. The NTPase protein is then recruited to this complex to form the segrosome and this then drives plasmid partition. What distinguishes each type of partition system is the mechanism underpinning plasmid partitioning. The four types of partition systems are reviewed below, discussing key features and the mechanism involved in plasmid partitioning.

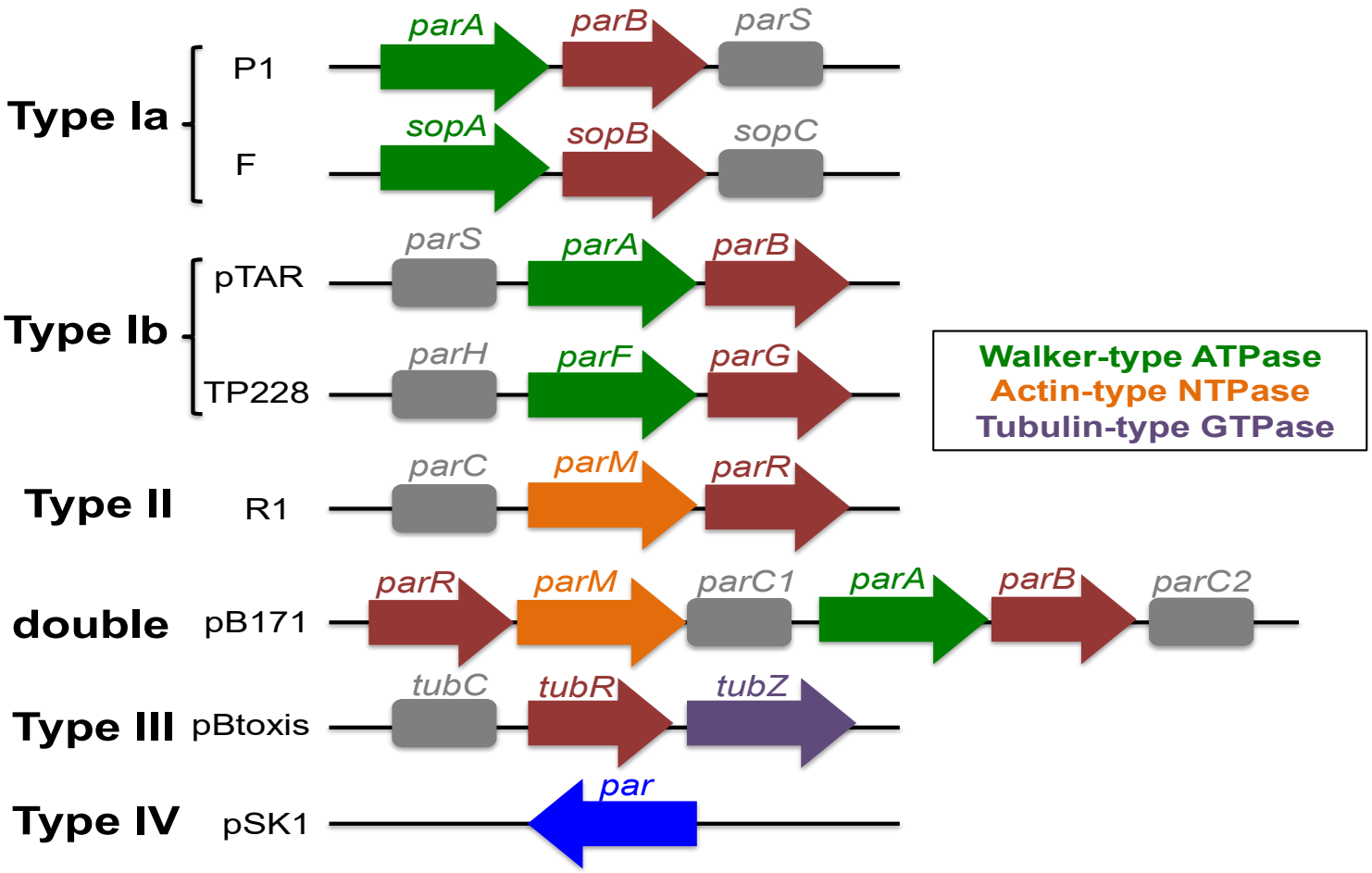

Figure 1.1 - Classification of partition systems. Schematic diagram of examples of the four types of partition systems highlighting the difference in genetic organisation and the type of NTPase**.** Genes that encode a Walker-type ATPase are shown as green arrows, actin-type NTPase as orange and tubulin-type GTPase as purple. Genes encoding the centromere binding proteins are shown as red arrows and the *cis*-acting centromere site is shown as a grey box. The activities of the protein encoded by the *par* gene on the pSK1 plasmid are still unknown and the gene is shown as a blue arrow.

1.2.1 Type I partition systems

Type I partition systems are the most abundant partition systems and are involved in both plasmid and chromosome segregation. The force generating motor protein specified by type I partition systems is an ATPase. These ATPase proteins are in fact members of a subgroup of the large P loop GTPase superfamily. The ATPase proteins have a deviant Walker-type (P loop) motif located at the N terminus, KGGXXGKT, known as the Walker A motif (Motallebi-Veshareh *et al*., 1990). The Walker A motif contains conserved lysine residues which are involved in the binding and hydrolysis of ATP, the second lysine is conserved in all the ATPase proteins from type I partition systems (Leipe *et al*., 2002, Lutkenhaus, 2012). These proteins also contain a Walker B motif, located on a strand close to the Walker A motif, which is involved in magnesium binding and catalysis. The Walker B motif is not as well conserved as the Walker A motif (Schumacher *et al*., 2012). The ATPase proteins from the type Ia and Ib partition systems share common features, such as binding ATP, binding DNA non-specifically and self-association. These proteins have a weak intrinsic ATPase activity, which is stimulated by the CBP and DNA. The ATPase proteins have also shown dynamic patterns over the nucleoid *in vivo* (Adachi *et al*., 2006, Baxter and Funnell, 2014, Ebersbach and Gerdes, 2004, Hatano and Niki, 2010, Marston and Errington, 1999). However, the mechanism by which the ATPase proteins promote plasmid partitioning is still not fully understood and is under much deliberation. A crucial question lies around the ability of these proteins to self-associate into higher order structures and what role this plays in the plasmid partitioning mechanism.

As mentioned above, type I partition systems are subdivided into two groups, Ia and Ib, based on the NTPase protein and the genetic organization. The main differences between Type Ia and Type Ib partition systems are detailed below in Table 1.1.

Table 1.1 Comparisons of type Ia and type Ib partition systems

Partition system	NTPase	CBP	Centromere	Model systems
Type Ia	Walker-type ATPase. Larger (321-420 amino acids) as contains HTH motif. Main transcriptional regulator	Shows some homology to other CBP proteins. Is a co-repressor of the operon.	Downstream of the operon	*parABS* of plasmid P1, *sopABC* of plasmid F, plasmid RK2 that encodes for KorB and IncC
Type Ib	Walker-type ATPase. Smaller (192-308 amino acids) as does not harbour the HTH motif	Sole transcriptional regulator of the operon. Diverse group of proteins with few homologues. Have a Ribbon-Helix-Helix (RHH) motif.	Upstream of the operon	*parFGH* of TP228, *parABS* of pB171

1.2.1.1 The Type Ia partition system of P1 plasmid

One of the most well studied Type Ia partition systems is that of P1, a prophage of bacteriophage P1 that exists as a low copy number plasmid in *E. coli*. The *par* system consists of the *trans*-acting proteins, ParA and ParB, and the *cis*-acting centromere site *parS* (Figure 1.2). The *parS* centromere site, which is downstream of the *parAB* genes, is ~ 80 bp and is described as having two arms that consist of four heptameric motifs and two hexameric motifs known as Box A and Box B, respectively (Funnell and Gagnier, 1993). These motifs are arranged asymmetrically and the two arms containing the motifs are separated by a 29 bp sequence that is recognised by the Integration Host Factor (IHF) protein. Dimeric ParB is able to recognize and bind these motifs of *parS.* Binding of IHF has been shown to increase the affinity of the binding of ParB by causing a bend in the *parS* site (Hayes and Austin, 1994). IHF binding is not essential for ParB binding; however in the absence of IHF partition is less efficient (Funnell, 1991). ParB, the CBP, is composed of three domains (Figure 1.3B): ParA binding

domain (residues 1 -141), a HTH domain (residues 147-270) and a C-terminal dimerisation domain (residues 275-333), which is connected to the HTH domain via a flexible linker (Schumacher, 2007). Mutational analysis has shown that both the HTH and dimerisation domain are essential for ParB binding *parS*. The nucleoprotein complex of ParB-*parS* is initially formed by one ParB dimer interacting with the recognition sequences on both sides of the sequence recognised by IHF. More ParB dimers are then recruited to the complex by protein-protein interactions (ParB-ParB) and protein-DNA interactions (Bouet *et al*., 2000, Rodionov *et al*., 1999).

ParA is the Walker-type ATPase that is composed of three domains: an elongated N-terminal region, a HTH motif and a large C-terminal domain (Figure 1.3A). ParA has two distinct roles: (1) transcriptional repressor of *parAB* and (2) association with the ParB-*parS* complex to form the segrosome which then drives plasmid segregation. These roles are dependent on the nucleotide bound state of ParA, where ParA-ADP is able to act as a transcriptional repressor and ParA-ATP promotes plasmid segregation (Bouet and Funnell, 1999, Davey and Funnell, 1994, Davis *et al*., 1996, Dunham *et al*., 2009). ParA has been shown to form a dimer both in the presence and absence of nucleotide, however nucleotide binding shifts the equilibrium towards the dimer (Davey and Funnell, 1997). ParA has been seen to form ATP dependent filaments *in vitro* (Dunham *et al*., 2009), however recently this has been disputed (Hatano and Niki, 2010, Vecchiarelli *et al*., 2010). ParA-ATP has also been shown to interact non-specifically with DNA; upon binding ATP, ParA-ATP undergoes a slow conformational change and this allows subsequent DNA binding (Vecchiarelli *et al*., 2010). ParA-ATP is seen to localise with the nucleoid *in vivo* and dynamically relocate (Hatano and Niki, 2010, Vecchiarelli *et al*., 2012). These findings have allowed a diffusion ratchet model to be proposed for P1 plasmid segregation: ParA binds ATP and undergoes a slow conformational change that allows binding to the nucleoid. Upon binding ParB tethered to the plasmid, ParA ATPase activity is stimulated and ParA-ATP becomes ParA-ADP. This causes ParA to be released from the nucleoid and a series of time delays due to ATP dependent transition allows ParA to diffuse before re-binding the nucleoid. This allows ParB bound to the plasmid to redistribute on the ParA gradient on the nucleoid (Hwang *et al*., 2013, Hu *et al*., 2015). This mechanism for plasmid segregation will be discussed later in more detail.

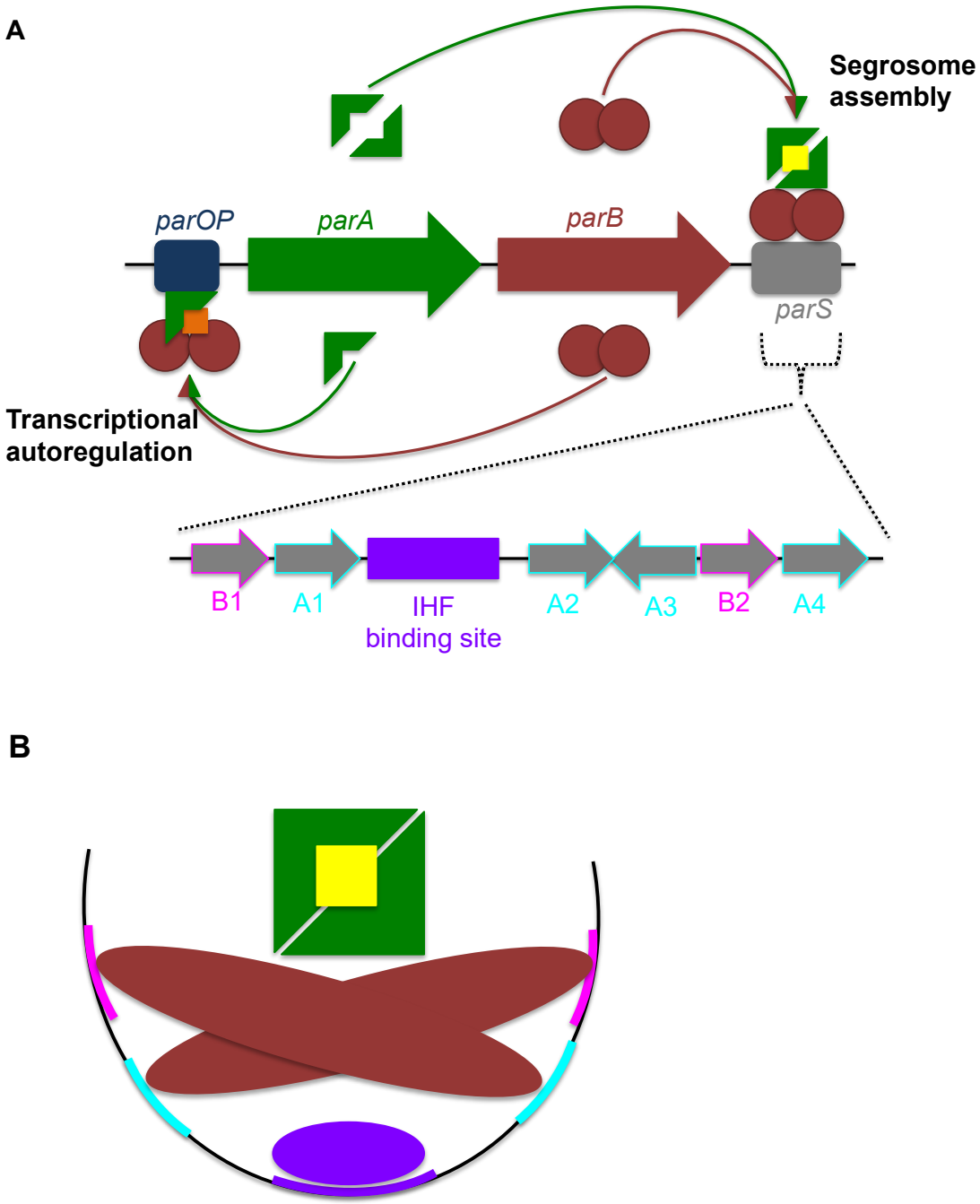

Figure 1.2 - Schematic representation of the partition cassettes of P1 plasmid. A) The P1 partition cassette encodes for two *trans*-acting proteins ParA, shown in green, and ParB, shown in red. The *cis*-acting centromere site, *parS*, is shown in grey. *parS* is expanded to show the heptameric (cyan) and hexameric (magenta) motifs as well as the position of the IHF binding site (purple). The operator/promoter region is shown in blue positioned upstream of *parA*. Dimeric ParB is shown binding to *parS* and recruiting ParA bound to ATP (yellow square). ParA bound to ADP (orange square) is able to bind *par*OP and act as a transcriptional repressor, with ParB acting as a co-repressor. B) Model of the P1 segrosome assembly. IHF shown as a purple oval binds its site and induces *parS* bending. This allows ParB to bind the repeat motifs and then ParA-ATP can be recruited to the segrosome. Adapted from (Hayes and Barillà, 2006).

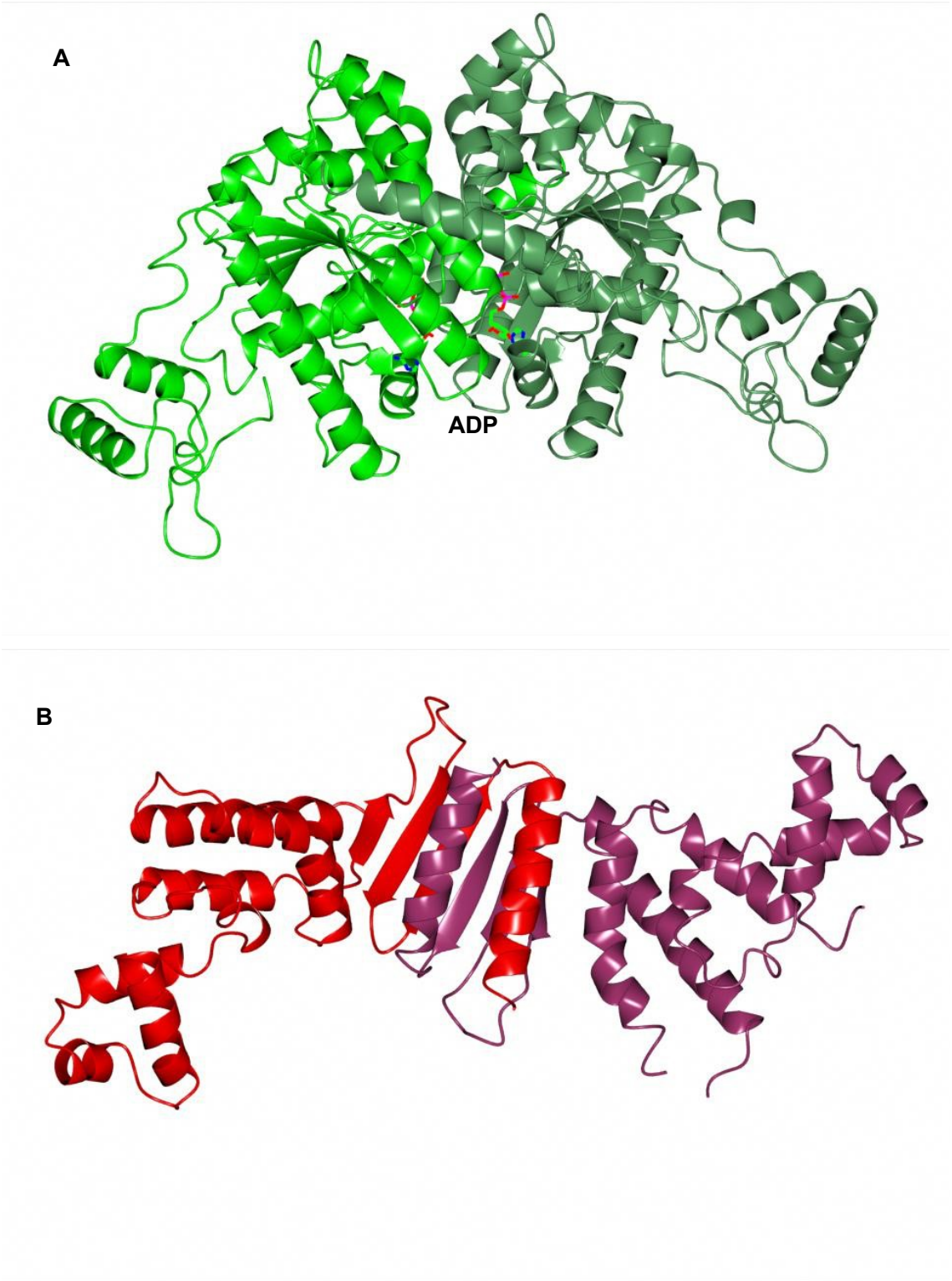

Figure 1.3 - Structure of ParA and ParB from the P1 plasmid. A) Ribbon diagram of ParA dimer bound to ADP. ADP is shown as sticks, with one monomer of ParA shown as light green and the other as dark green. B) Ribbon diagram of ParB dimer. One monomer is highlighted in red and the other in dark purple. The structural images were generated by using CCP4MG version 2.10.4 using the 3E76 and 1ZX4 PDB coordinates, respectively.

1.2.1.2 The Type Ia partition system of F plasmid

The *E. coli* F plasmid also employs a type Ia partition system in order to ensure faithful segregation from one generation to the next. The partition (*par*) system encodes SopA, the Walker-type ATPase, and SopB, the CBP. The centromere site, found downstream of the *sopAB* genes, is *sopC* (Figure 1.4). The centromere site on F plasmid, *sopC*, is not as complex as the centromere site found on plasmid P1. *sopC* is composed of 12 direct repeats of 43 bp, each of which contains a 16 bp inverted repeat. SopB, the CBP, binds *sopC* via these inverted repeats – specifically one SopB dimer is able to bind to one DNA repeat (Pillet *et al*., 2011, Schumacher *et al*., 2010). After one SopB dimer is bound additional SopB dimers are recruited to the complex via specific and non-specific DNA binding (Sanchez *et al*., 2015). This allows SopB to coat the DNA. SopB, like ParB, is composed of a SopA binding domain (residues 1-156), a HTH domain (residues 157-270) and a dimerisation domain (residues 271-323) each connected by a linker region. Unlike ParB, SopB was shown to have an additional dimerisation domain which is believed to be involved in DNA bridging and allows SopB to spread *in trans* on the DNA (Schumacher, 2012).

SopA, the Walker-type ATPase, contains a HTH motif that allows this protein to autoregulate the transcription of the *sopAB* genes. SopA shares many similarities with ParA, including ATP binding and non-specific DNA binding. It is proposed that binding ATP is necessary for binding to non-specific DNA but not for the specific binding to the promoter. Mutational analysis has shown that the C-terminal domain is important for the non-specific DNA binding (Castaing *et al*., 2008). *In vivo*, SopA showed an oscillatory pattern over the nucleoid (Ah-Seng *et al*., 2013, Hatano *et al*., 2007). As for ParA, it was originally proposed that SopA undergoes ATP dependent polymerisation and this was thought to be important for plasmid segregation (Bouet *et al*., 2006). SopB and non-specific DNA is able to stimulate SopA ATPase activity and thus cause depolymerisation, however SopB counteracts this by itself binding DNA non-specifically. This prevents SopA from non-specifically binding the DNA and thus allows polymerisation into higher order structures (Castaing *et al*., 2008). However, more recently this has been disputed and a diffusion ratchet model similar to that of P1 plasmid segregation has been proposed (Vecchiarelli *et al*., 2013, Vecchiarelli, 2014).

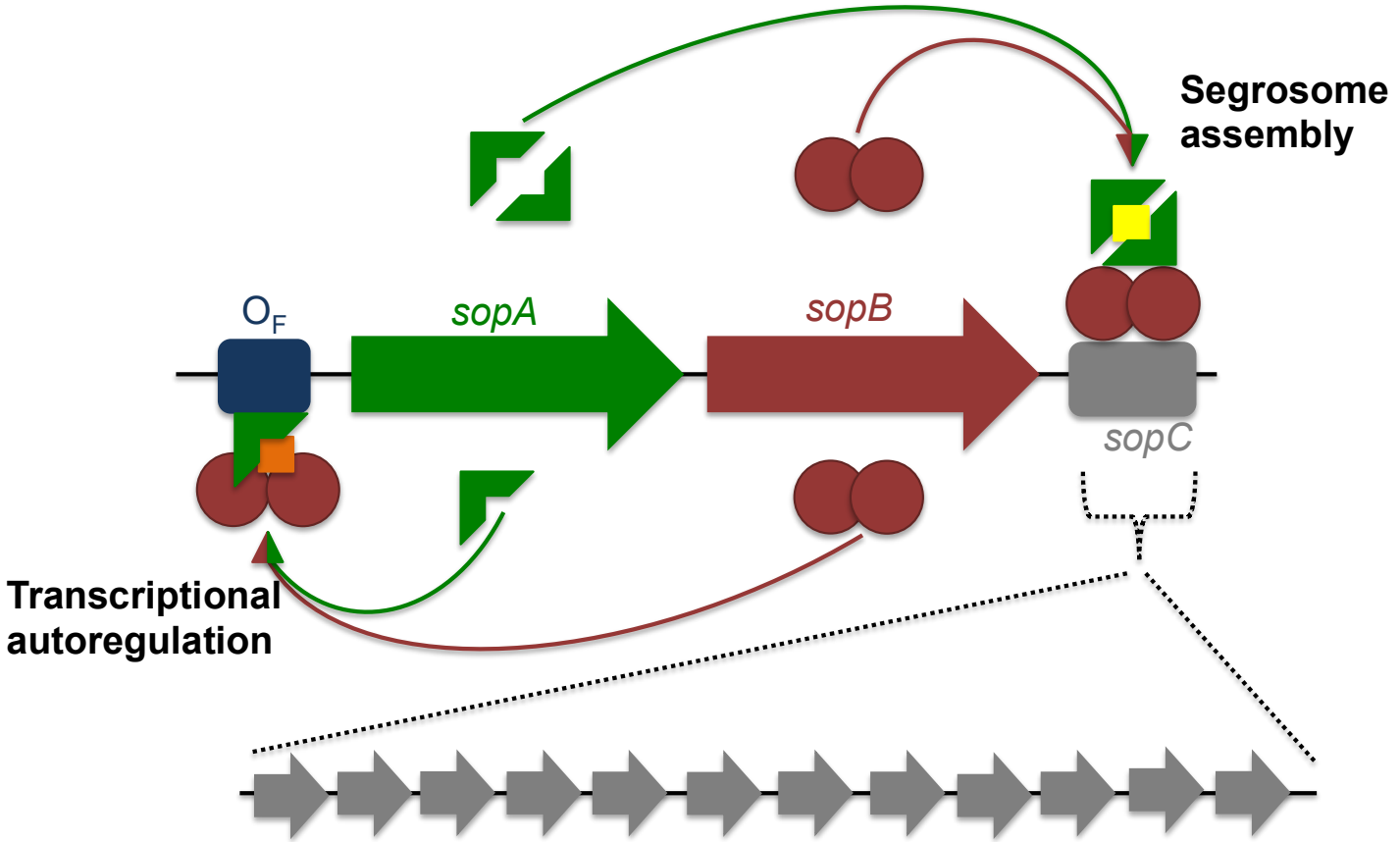

Figure 1.4 - Schematic representation of the partition cassette of F plasmid. The F plasmid partition cassette encodes for two *trans*-acting proteins SopA, shown in green, and SopB, shown in red. The *cis*-acting centromere site, *sopC*, is shown in grey. *sopC* is expanded to show the 12 direct repeats. The operator region, shown in blue, is positioned upstream of *sopA*. Dimeric SopB is shown binding to *sopC* and recruiting SopA bound to ATP (yellow square). SopA bound to ADP (orange square) is able to bind *parOP* and act as a transcriptional repressor, with SopB acting as a co-repressor.

1.2.1.3 Type Ib partition systems

Type Ib partition systems encode a Walker-type ATPase protein and a CBP. However the Walker-type ATPase protein is smaller than the type Ia counterpart and it is the CBP that acts as the transcriptional regulator protein. The centromere site is found upstream of the *trans*-encoded proteins. Type Ib partition systems are found on many plasmids including; the pSM19035 plasmid from *Streptococcus pyogenes*, pTAR plasmid from *Agrobacterium tumefaciens,* pB171 plasmid from *E. coli* and TP228 plasmid from *Salmonella enterica*. (Gerdes *et al*., 2000) The type Ib partition system of the TP228 plasmid is the most studied and the focus of this thesis and it will be discussed in detail later in this chapter.

pSM19035 is a low copy number plasmid from the Firmicutes multidrug resistant inC18 family. These plasmids are found in *Enterococcus* and *Streptococcus* species. The type Ib partition system harboured by this plasmid encodes for the *trans*-acting proteins δ_2 (ParA-like) and ω_2 (ParB-like) and six *cis*-acting *parS* sites (Figure 1.5). The *parS* sites are comprised of 9, 7 and 10 contiguous heptads sequences in direct or inverse orientation. The *parS* sites overlap with the promoter regions of the *δ, ω* and *copS* genes (Soberon *et al*., 2011). ω_2 acts a transcriptional repressor for *δ, ω* and *copS* genes by binding specifically to the promoter regions, as well as acting as a CBP for plasmid segregation as these promoter regions also act as the centromere sites (*parS*). The monomeric ω protein consists of a flexible N-terminal domain (residues 1-19) and a ribbon-helix-helix domain (20-71) that is required for DNA binding. However, ω is only functionally active when it is in the dimeric form (ω_2). The crystal structure of ω_2 in complex with DNA has been solved and shows that the protein makes specific base contacts in the DNA major groove using the β-sheets. Many ω_2 molecules are thought to bind to multiple repeats and this allows wrapping around the *parS* site, as a left-handed helix, without bending or distorting the DNA. It is believed binding non-specifically to DNA is not involved in this model and ω_2 therefore doesn't spread beyond the *parS* site (Murayama *et al*., 2001, Volante and Alonso, 2015).

As with other partition systems, the ATPase protein is recruited to the partition site via an interaction with ω_2 to form the segrosome. It has been shown that recruitment of the ATPase protein actually stabilises the ω_2–*parS* bound partition complex (Soberon *et al*., 2011). The Walker-type ATPase protein encoded by the pSM1905 partition systems is known as δ. The structure of the 284 residue monomeric protein has been solved and

shows that the protein is able to form a dimer in the presence or in the absence of ADP or ATP. Other ParA proteins have been shown to form dimers, however the majority require ATP for dimer formation. The structure revealed the δ_2 dimer is U-shaped with each arm representing one monomer, with the ATP binding site in the middle. As with other ParA proteins, δ_2 is able to bind non-specific DNA (Volante and Alonso, 2015). The surface charge of the dimer revealed the tips of the U-shaped arms were positively charged and therefore likely to interact with DNA. δ_2 was seen to localise with the nucleoid *in vivo*, and in the presence of ω_2 and *parS*, δ_2 appeared to form spiral-like structures that oscillated from one pole of the cell to the other (Pratto *et al*., 2008). δ_2 has been shown to polymerise into higher order structures when ATP was present; when ATP hydrolysis is stimulated by the partner protein ω_2, it results in depolymerisation. δ_2 forms nucleoprotein filaments on DNA, in the presence of ATP and ω_2. In the absence of DNA, but in the presence of ATP, δ_2 doesn't form filament structures but more globular-like structures containing 2-3 molecules of δ_2. As for P1 and F plasmid segregation, the model proposed for pSM19035 plasmid segregation does not involve a filament pushing-pulling system, but a diffusion - ratchet the details of which will be discussed later on in this chapter (Soberon *et al*., 2011, Volante and Alonso, 2015).

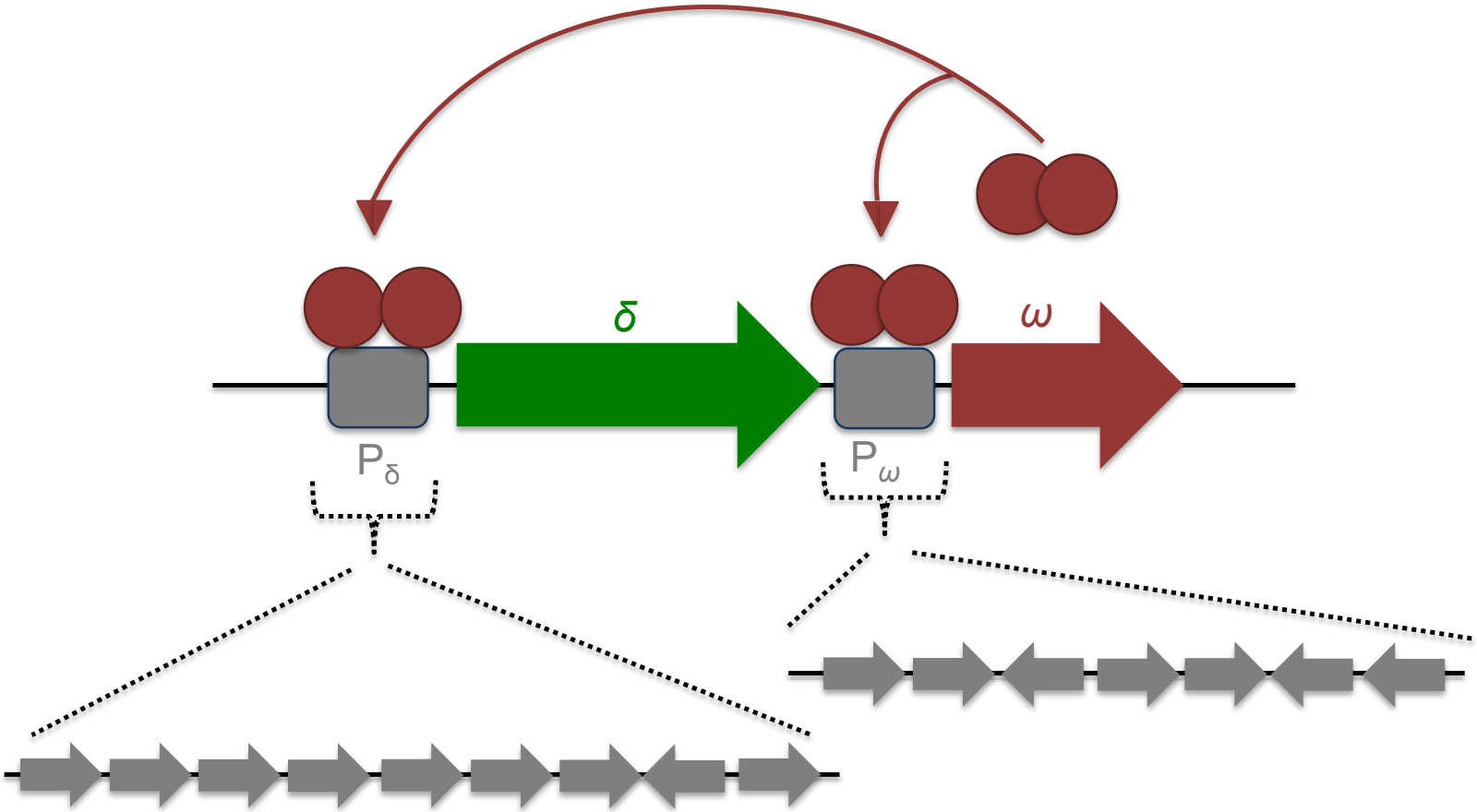

Figure 1.5 - Schematic representation of the partition cassette of pSM19035 plasmid. The pSM19035 plasmid encodes for two *trans*-acting proteins: the Walker-type ATPase, δ, shown in green and the CBP, ω, shown in red. The repeats of the *cis*-acting centromere sites overlap with the promoter sites and are shown in grey. Dimeric ω is able to bind to both *cis*-acting sites and act as a transcriptional repressor and a plasmid partition protein.

The *E. coli* virulence plasmid, pB171, is one of only few plasmids that encode two partition systems. The pB171 plasmid encodes a type Ib partition system (*par2*) and a type II partition system *(par1)*, both of which have been shown to be functional in plasmid segregation. The partition systems are both able to mediate plasmid segregation alone, however for optimal plasmid segregation both partition systems are required (Ebersbach and Gerdes, 2001). This system encodes a Walker-type ATPase, ParA, and a CBP, ParB. The partition loci contain two *cis*-acting centromere sites, *parC1* and *parC2* (Figure 1.6). *parC1* is the central *cis*-acting site found in-between *par1* and *par2,* both of which have been shown to utilise this central *parC1* site. *parC2* is found downstream of the *parAB* genes of the *par2* locus. Both the *cis*-acting sites contain a series of related 6 bp repeats organised into different clusters. *parC1* contains seventeen repeats organised into two clusters, one of thirteen and the other of four. *parC2* contains eighteen repeats organised into three clusters (Ebersbach and Gerdes, 2001). The CBP of *par2*, ParB, has been predicted to contain a ribbon-helix-helix domain and is able to bind, as a dimer, cooperatively to these direct repeats found in both of the *parC* sites (Ringgaard *et al*., 2007). ParB is therefore able to act as a segregation protein and a transcriptional repressor to auto-regulate the expression of *parAB*. Similar to other type Ib ParB proteins, ParB from pB171 is composed from a N-terminal domain that is believed to be involved in the ParA-ParB interaction and a C-terminal domain that contains the predicted RHH domain for DNA binding and is also involved in ParB dimerisation. It has also been proposed that ParB dimers are able to interact with other ParB dimers via the N-terminal domain, which enables multimer formation and larger nucleoprotein complexes to form (Ringgaard *et al*., 2007).

The Walker-type ATPase protein, ParA, of pB171 *par2* locus has been shown to form ATP dependent filaments and bundles *in vitro (Ebersbach et al., 2006)*. ParA has also been shown to bind non-specific DNA *in vitro*. *In vivo*, ParA has shown similar filament structures on the nucleoid and thus it has been proposed that the nucleoid functions as a scaffold for ParA filament assembly. ParA was also observed to form oscillating helical structures over the nucleoid in the presence of the ParB-*parC* complex and in the absence of ParB-*parC* no oscillation was seen. Oscillation was also shown to be dependent on ATP hydrolysis, suggesting this was the driving force behind the ParA oscillations. Mutational analysis suggested that the N-terminal of ParB was involved in stimulation of ParA ATPase activity and thus important in stimulating ParA depolymerisation and crucial to ParA oscillatory behaviour over the nucleoid

(Ebersbach and Gerdes, 2004, Ebersbach *et al*., 2006, Ringgaard *et al*., 2009). As with the other type I partition systems discussed, the mechanism underlying pB171 plasmid segregation is still under much deliberation. However, a model that involves the ParA polymerisation and depolymerisation cycle that drives plasmid positioning is still favoured for this system. A recent study supported this mechanism and disfavoured the diffusion ratchet mechanism (Ietswaart *et al*., 2014).

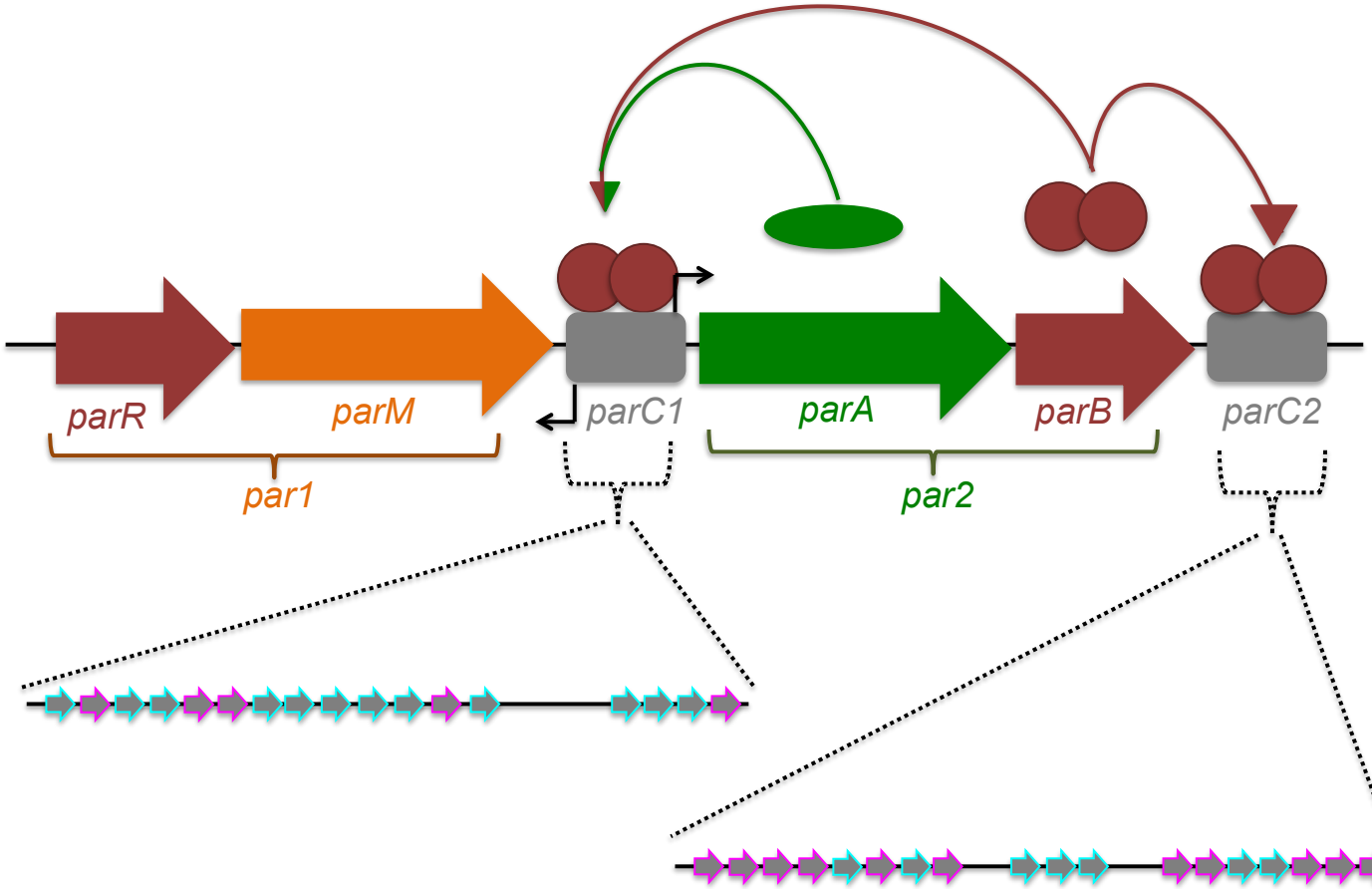

Figure 1.6 - Schematic representation of the partition cassettes of pB171 plasmid. The pB171 plasmid encodes for two partition systems. *par1*, highlighted in orange, is a type II partition system that encodes for the CBP ParR (shown in red) and the actin-like ATPase ParM (orange). *par2*, highlighted in green, is a type Ib partition system that encodes for the Walker-type ATPase ParA (green) and the CBP ParB (red). Two *cis*-acting centromere sites, *parC1* and *parC2* (grey), are positioned upstream and downstream of *par2* respectively. The *parC* sites are expanded to shown the clusters of direct repeats present; the repeats can be subdivided into two groups depending on the sequences, represented by magenta and cyan arrows. Dimeric ParB of *par2* is able to bind both *parC* sites.

1.2.2 Type II partition systems

The type II partition modules are the best understood systems with regards to the mechanism involved in the plasmid partitioning process. The type II partition systems typically encode an actin-like ATPase, known a ParM, and a CBP, known as ParR. The *cis*-acting centromere site, found upstream of *parMR*, is typically called *parC*. In type II partition systems, ParR typically contains a RHH domain similar to that of the CBP found in type Ib partition systems. ParR dimers are able to bind DNA and autoregulate the transcription of the *parMR* genes as well as acting as partition proteins. ParM, the motor protein, polymerises into filaments that push the plasmids apart to ensure faithful segregation. The R1 plasmid from *E. coli* is the best studied of these partition systems and has been the paradigm for understanding the partitioning process. Type II partition systems are also found on the pSK41 plasmid of *Staphylococcus aureus*, pLS20 and pLS32 plasmid of *Bacillus subtilis* and also one of the two partition systems on the pB171 plasmid of *E. coli* (Baxter and Funnell, 2014, Schumacher, 2012).

1.2.2.1 The type II partition system of R1 plasmid

The *parMRC* locus is the type II partition system found on the low copy number, multi-drug resistant plasmid R1 from *E. coli* (Figure 1.7). The *parC* site, which is positioned upstream of the *parMR* operon, contains ten 11 bp direct repeats that are organised into two sets of five. The two sets of five are separated by 39 bp that includes the promoter sequence for *parMR* (Dam and Gerdes, 1994). ParR is able to bind cooperatively to these ten direct repeats in order to form a large nucleoprotein complex, as well as binding to the promoter region as a transcriptional repressor of *parMR*. The structure of ParR from the R1 plasmid has not been solved, however the structure of two other ParR proteins from pB171 (Figure 1.8B) and pSK41 plasmids have been solved (Moller-Jensen *et al*., 2007, Schumacher *et al*., 2007). ParR binding to *parC* has been shown to cause distortion in the *parC* site: the DNA was seen to shorten which indicated that the *parC* site became wrapped around ParR. Structural data for pSK41 ParR and pB171 ParR supported these findings, confirming that six ParR dimers form a super helical structure in which the DNA is wrapped around the outside of the positively charged surface of the proteins. ParR dimers are able to bind cooperatively to the *parC* site via protein-protein interactions and protein-DNA interactions (Jensen *et al*., 1998, Schumacher *et al*., 2007). ParM, the motor protein, is able to bind to the ParR-*parC* complex via interactions with C-terminal region of ParR.

ParM is an actin-like ATPase protein that belongs to a superfamily of ATPase's that include actin, Hsp70, hexokinase and the bacterial protein MreB that is involved in maintaining bacterial cell shape. Therefore ParM is seen as a bacterial cytoskeletal protein that is homologous to eukaryotic actin proteins. ParM has been shown to polymerise into extended filaments in an ATP dependent manner, this polymerisation is bidirectional meaning the filaments are able to grow from both ends. ParM forms double helical protofilaments that are similar to eukaryotic actin filaments, although ParM filaments have a left-handed twist whereas actin is right handed. These ParM filaments are dynamically unstable and upon ATP hydrolysis the filaments are seen to depolymerise. However binding to the ParR-*parC* complex is able to stabilise these filaments, preventing depolymerisation and thus allow the filaments to grow. This then pushes the plasmids apart and is known as the insertional polymerisation mechanism for R1 plasmid segregation (Bharat *et al*., 2015, Moller-Jensen *et al*., 2002, Moller-Jensen *et al*., 2003, Salje and Lowe, 2008, Salje *et al*., 2010). The mechanism will be discussed in more detail later on in this chapter.

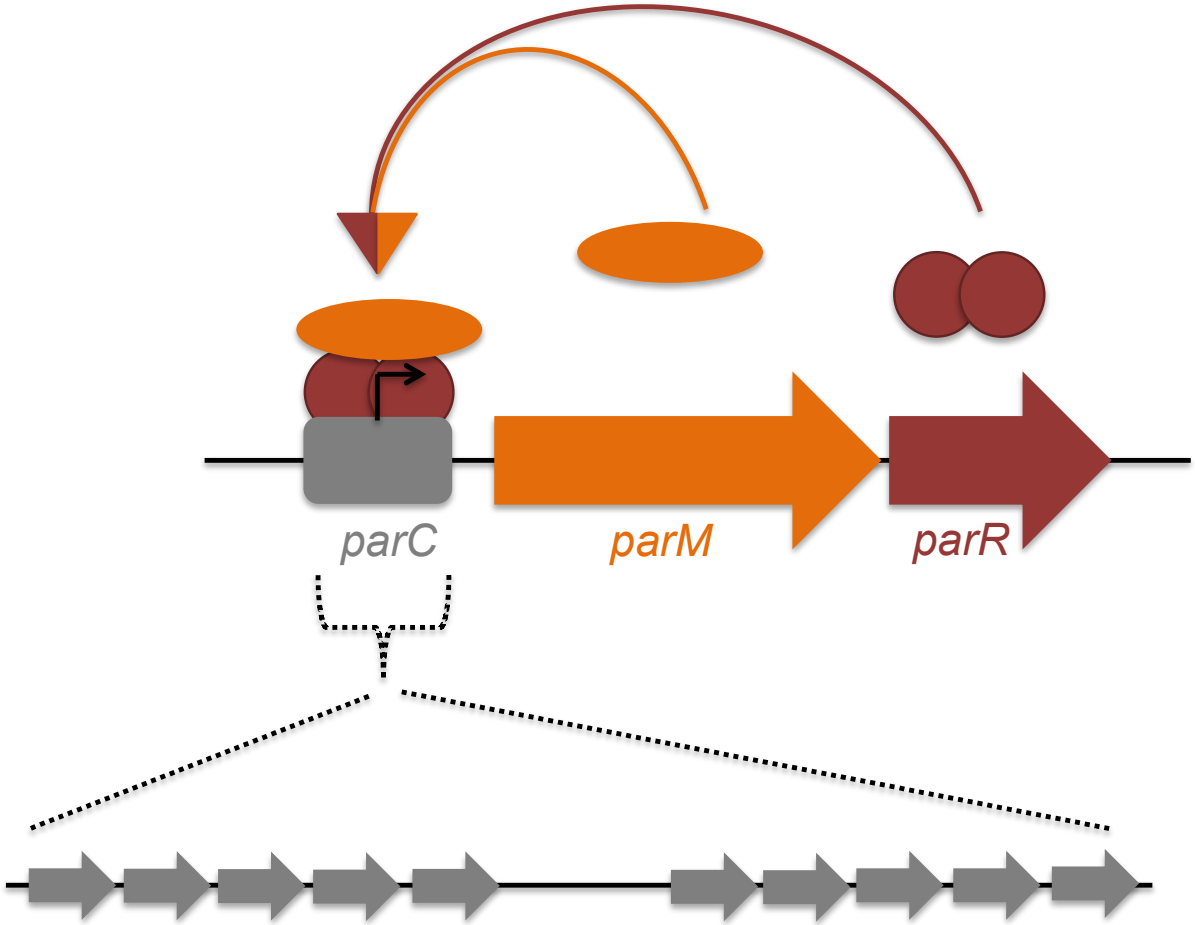

Figure 1.7 - Schematic representation of the partition cassette of R1 plasmid. The type II partition system of the R1 plasmid encodes for two *trans*-acting proteins: the actin-like ATPase, ParM (orange) and the CBP, ParR (red). The *cis*-acting centromere site, *parC* (grey), is found upstream of the *parMR* genes and is expanded to show the two groups of repeats that are separated by the promoter sequence. Dimeric ParR binds *parC* and acts as a transcriptional repressor and a partition protein; ParM interacts with the ParR-*parC* complex.

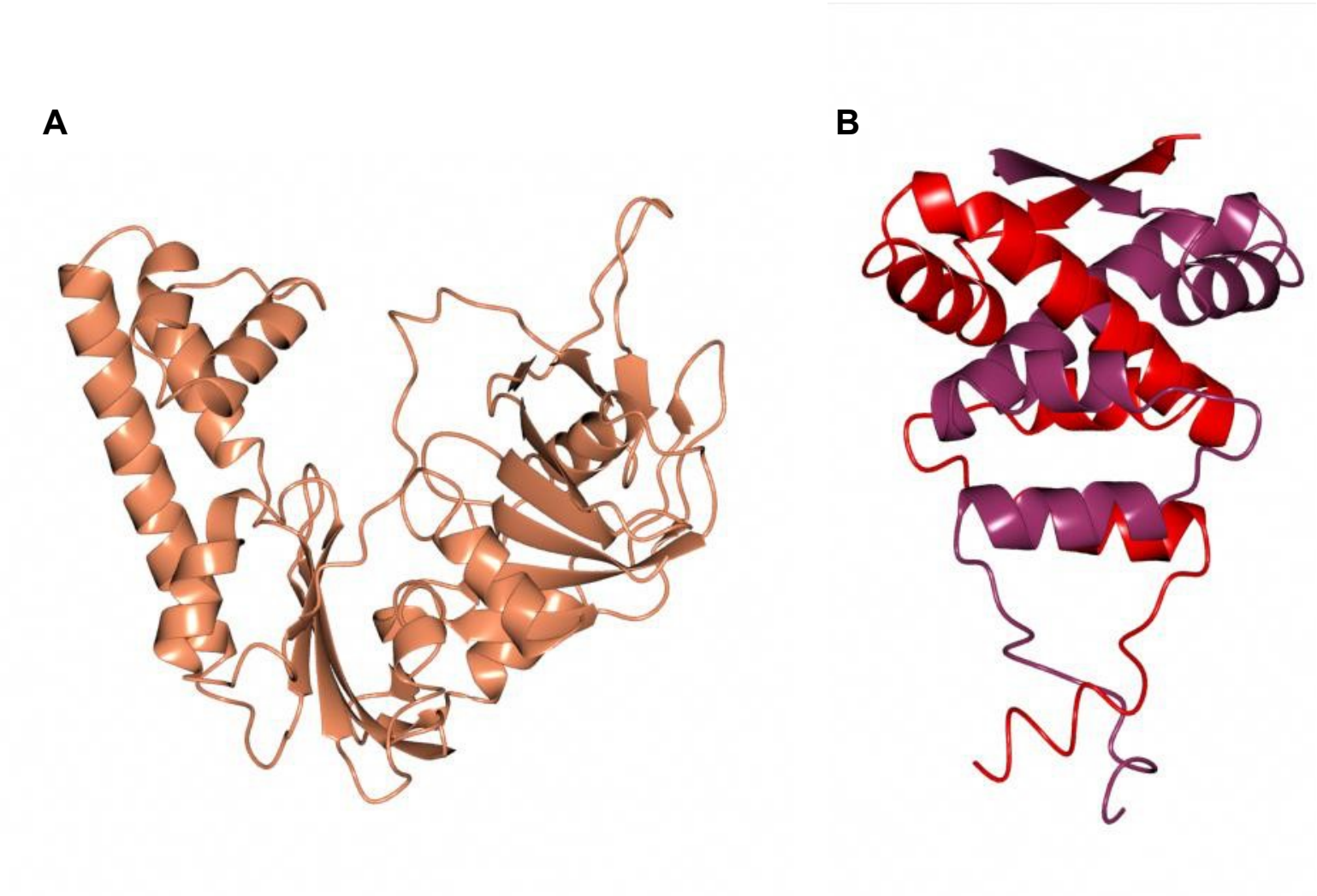

Figure 1.8 – The structure of ParM from R1 plasmid and ParR from pB171 plasmid. A) Ribbon diagram of ParM monomer in the Apo form. B) Ribbon diagram of ParR dimer. One monomer is highlighted in red and the other in dark purple. The structural images were generated by using CCP4MG version 2.10.4 using the 1MWK and 2JD3 PDB coordinates, respectively.

1.2.3 Type III partition systems

Type III partition systems have been identified on plasmids found in *Bacillus* species. These partition systems encode a tubulin-like GTPase protein, generally known as TubZ, and a CBP, generally know as TubR. The *cis*-acting centromere like site is known as *tubC*. In contrast to other partition systems, the gene encoding the CBP is found upstream of the gene encoding the motor protein. The *cis*-acting centromere site is found upstream of the genes. The first of these partition systems discovered was on the virulence plasmid pXO1 of *Bacillus anthracis*: RepX, now referred to as TubZ, showed homology to the GTPase tubulin-like protein FtsZ, which is necessary for cell division in bacteria (Tinsley and Khan, 2006). After this a similar system was identified on the endotoxin encoding plasmid pBtoxis of *Bacillus thuringiensis (Larsen et al., 2007).*

1.2.3.1 The type III partition system of pBtoxis plasmid

The pBtoxis plasmid from *B. thuringiensis* contains the type III partition system, *tubZRC* (Figure 1.9). The *cis*-acting centromere site, *tubC,* is composed of seven direct repeats arranged into two clusters, separated by 54 bp, the first cluster consisting of three and the second cluster consisting of four repeats. TubR has been shown to bind cooperatively to these direct repeats and acts as both a CBP and a transcriptional repressor of the *tubZR* genes (Aylett and Lowe, 2012, Larsen *et al*., 2007). The structure of TubR (Figure 1.10B) revealed that the protein contains a winged helix-turn-helix motif (Ni *et al*., 2010). Interestingly, the recognition helix of the HTH motif is not involved in DNA binding, because it is buried within the dimer interface of the protein. Mutational analysis revealed that a basic patch of residues in the wing and the helix next to the HTH motif are actually involved in DNA binding. This leads to a DNA binding model in which the wings of TubR could interact with minor grooves of the DNA and the exposed N-terminus of the HTH would insert into a single major groove (Ni *et al*., 2010).

TubZ, the tubulin-like GTPase, has been shown to polymerise into filament structures in a GTP dependent manner. The parallel double helical filament structures resemble that of tubulin and the filament structures formed by the bacterial cell division protein FtsZ. The polymerisation of TubZ into filaments is a dynamic process in which simultaneous plus end polymerisation and minus end depolymerisation occurs, this process is known as treadmilling. The TubZ filaments have been shown to be mostly composed of TubZ-

GDP and stabilised by a GTP cap. TubZ is able to bind to TubR-*tubC* complex via the C-terminal domain and GTP is not required for this binding. This C-terminal region is not required for TubZ polymerisation and therefore it is exposed in TubZ filaments and thus available for TubR binding. The proposed mechanism for plasmid segregation involves the TubR-*tubC* complex being moved along the filaments of TubZ to the poles of the cell (Chen and Erickson, 2008, Larsen *et al*., 2007, Ni *et al*., 2010). The treadmilling mechanism for plasmid segregation will be discussed in more detail later in this chapter.

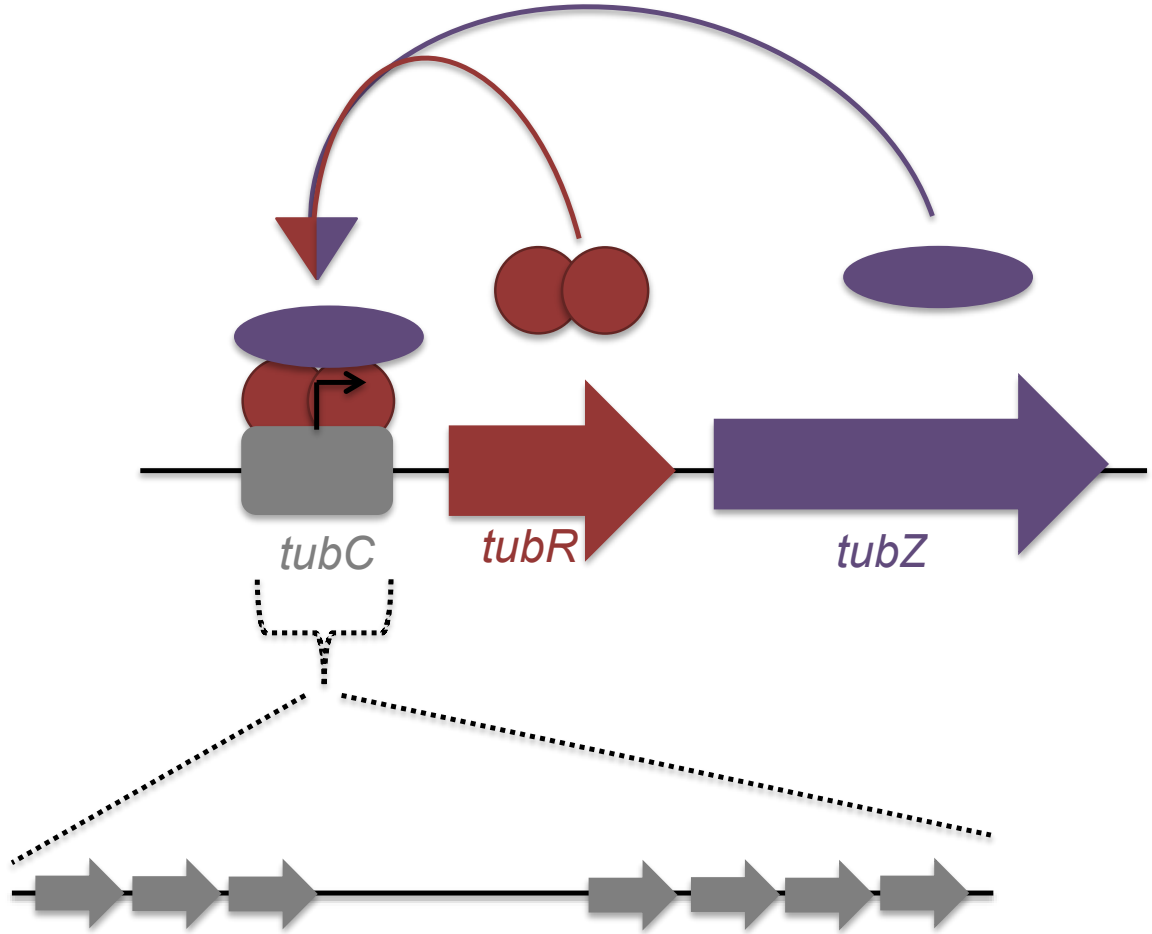

Figure 1.9 - Schematic representation of the partition cassette of pBtoxis plasmid. The type III partition system of the pBtoxis plasmid encodes for two *trans*-acting proteins: the CBP, TubR (red) and the tubulin-like GTPase, TubZ (purple). The *cis*-acting centromere site, *tubC* (grey), is found upstream of the *tubRZ* genes and is expanded to show the two groups of repeats that are separated by the promoter sequence. Dimeric TubR binds to *tubC* and acts as a transcriptional repressor and a partition protein; TubZ interacts with the TubR-*tubC* complex.

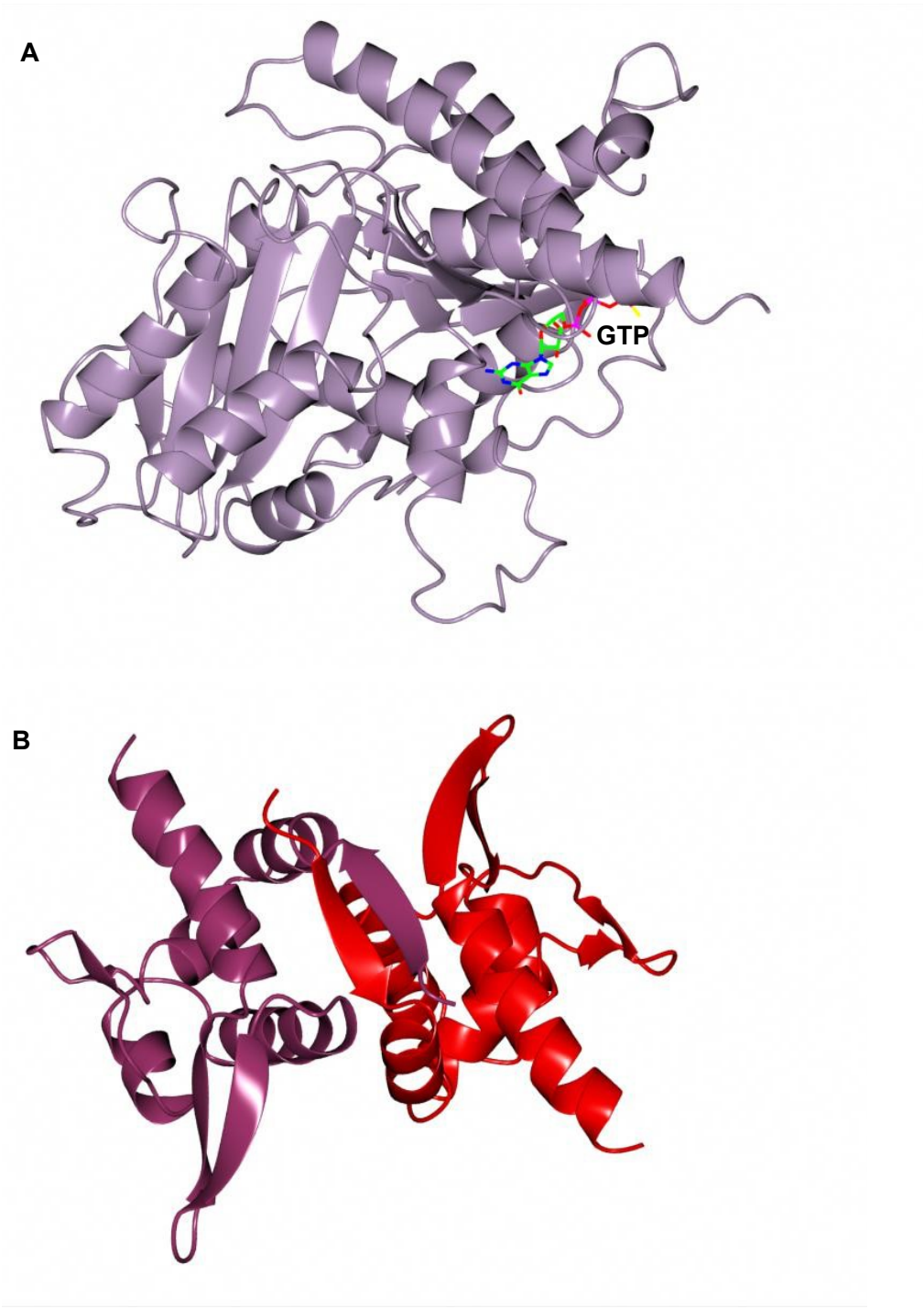

Figure 1.10 - Structures of TubZ and TubR from the pBtoxis plasmid. A) Ribbon diagram of TubZ bound to GTP. GTP is shown as sticks. B) Ribbon diagram of TubR dimer. One monomer is highlighted in red and the other in dark purple. The structural images were generated by using CCP4MG version 2.10.4 using the 3M89 and 3M8F PDB coordinates, respectively.

1.2.4 Type IV partition systems

An additional partition system has also been identified; this partition system that was identified on the *Staphylococcus aureus* plasmid pSK1 only utilises one partition

protein, named Par. This protein was unrelated to any other partitioning protein and therefore thought to represent a novel type of partitioning system, now referred to as type IV partitioning systems. Interestingly, Par homologues have been found on other plasmids from Gram-positive bacteria such as *Staphylococcus, Streptococcus, Lactococcus, Lactobacillus*, *Clostridium* and *Tetragenococcus.* Par from pSK1 plasmid, was predicted to contain a HTH motif and a central coiled-coiled domain. It has been proposed that this protein may play the role of both the CBP and the motor protein in this partition system. The HTH motif is thought to enable centromere binding and the coiled-coiled domain may allow dimerisation and act as a molecular switch. A 204 bp fragment was also identified upstream of the *par* operon, suggesting a possible centromere-like site (Simpson *et al*., 2003). However more research into this type of partitioning system is needed in order to confirm the role of the Par protein in plasmid segregation and to gain further understanding of this newly emerging partition system.

1.3 Bacterial chromosome segregation

The replicon model was the first proposed mechanism for bacterial chromosome segregation. This model postulated that the newly replicated bacterial chromosomes were attached to the cell membrane and cell growth was the driver of the segregation (Jacob *et al*., 1963). However it became evident that this model was unlikely, mainly due to the fact that the rate of chromosome segregation was much faster than cell growth. Evidence against the replicon model was also supported by *in vivo* fluorescence microscopy techniques (Gordon *et al*., 1997, Toro and Shapiro, 2010, Viollier *et al*., 2004). Other models for chromosome segregation were then proposed, however it was becoming evident that bacterial chromosomes employed an active mechanism with specific segregation proteins. It was then observed that many bacterial chromosomes contained homologous *par* loci, similar to those found on plasmids that encode partitioning proteins. Taken together with the observation that deletion of these partition genes often resulted in segregation defects it was believed that partition systems could drive the segregation of bacterial chromosomes (Gerdes *et al*., 2000).

Plasmid-like partition systems have been found on many bacterial chromosomes. The best studied systems are those harboured by *Bacillus subtilis, Caulobacter crescentus, Vibrio cholera, Streptomyces coelicolor, Pseudomonas aeruginosa* and *Pseudomonas putida*. Interestingly, no homologous partition system has been found in *E. coli*. To

date, all the partition systems found on bacterial chromosomes encode for a type Ib Walker-type ATPase and a CBP with a HTH motif.

1.3.1 *Bacillus subtilis* chromosome segregation system

The chromosome of *B. subtilis* contains a *parA* homologue, known as *soj*, and a *parB* homologue, *spo0J*. These proteins play many roles that are crucial for cellular processes in *B.subtilis*, these include: chromosome replication and segregation, chromosome origin localisation and separation, cell division, sporulation and developmental gene regulation. Spo0J was found to be crucial for both the initiation of sporulation and chromosome segregation (Ireton *et al*., 1994). On the other hand, the deletion of only *soj* does not cause significant chromosome segregation defects however, when the gene encoding the structural maintenance of chromosome protein (SMC) is also deleted chromosome segregation defects can be observed (Lee and Grossman, 2006). Soj is also believed to be involved in *B.subtilis* chromosome replication, Soj has been observed to act as a spatially regulated molecular switch that is able to activate or inhibit the DNA replication initiator protein, DnaA (Murray and Errington, 2008).

As well as the chromosomally encoded homologues of ParA and ParB, *B.subtilis* also possesses *parS* sites. Ten potential *parS*-like sequences were identified; these sites were located in the origin proximal region of the chromosomes. The *parS* sites consisted of 16 bp that contained an imperfect 8 bp inverted repeat. Eight of these were believed to be *parS* sites that Spo0J was able to bind (Lin and Grossman, 1998). Spo0J has been shown to bind DNA both specifically and non-specifically. Spo0J is able to bind site-specifically as a dimer to the *parS* sites and then is believed to undergo lateral spreading on the DNA flanking the *parS* sites (Murray *et al*., 2006). It has been proposed that Spo0J is able to bridge the DNA via adjacent and horizontal interactions between Spo0J dimers, this allows a large nucleoprotein complex to form over a large area of DNA (Chen *et al*., 2015, Graham *et al*., 2014). The structure of *B. subtilis* Spo0J has not been solved, however the structure of *Thermus thermophilus* and *Helicobacter pylori* Spo0J revealed the protein contains a flexible N-terminal region thought to be involved in interactions with the partner protein and also self-interactions, a HTH motif then enables DNA binding and a C-terminal dimerisation domain (Chen *et al*., 2015, Leonard *et al*., 2004).

Soj is a Walker-type ATPase that contains a P loop motif for ATP binding and hydrolysis. Soj has been shown to bind DNA in a specific manner, which allows Soj to

act as a transcriptional repressor for many genes involved in sporulation. Soj is monomeric when no nucleotide is present, however upon ATP binding is able to form a dimer. Upon ATP binding and dimerisation, Soj has been shown to bind DNA in a non-specific manner and a this has been shown to be mediated by an arginine patch found on the surface of the Soj dimer (Hester and Lutkenhaus, 2007). Upon this non-specific binding, Soj has been visualised forming nucleoprotein filaments (Leonard *et al*., 2005). Spo0J has been shown to stimulate Soj ATPase activity; two N-terminal lysine residues in Spo0J have been identified to be important in this stimulation (Leonard *et al*., 2005). Upon ATP hydrolysis Soj is no longer dimeric and therefore can no longer bind to DNA (Scholefield *et al*., 2011). *In vivo* Soj was seen to localise to the nucleoid and showed a dynamic oscillatory pattern when Spo0J was present (Marston and Errington, 1999, Quisel *et al*., 1999). Due to the parallels seen between the plasmid partitioning systems and the chromosome partitioning systems, it is believed the mechanism employed is similar and this will be discussed later in this chapter.

1.3.2 *Caulobacter crescentus* chromosome segregation system

Bacterial chromosome segregation has been well studied in *C. crescentus* and this is a good model system due to the fact that *C. crescentus* replicates its single chromosome only once per cell cycle. The partition proteins, ParA and ParB, have been shown to be essential for cell viability (Mohl and Gober, 1997). *C. crescentus* chromosome was found to have two *parS* sites, separated by 42 bp, positioned close to the origin of replication that contains an AT-rich sequence (Livny *et al*., 2007). ParB has been shown to bind specifically to these *parS* sites and it has been proposed that ParB, like other ParB proteins, is able to spread on DNA surrounding the *parS* in a non-specific manner to enable the formation of a large nucleoprotein complex (Lim *et al*., 2014, Toro *et al*., 2008). ParB is composed of three domains, a C-terminal dimerization domain, a central HTH domain for DNA binding and a N-terminal domain for interaction with the partner protein ParA. ParA, like many other type I ParA proteins previously discussed, is a Walker-type ATPase that binds ATP and forms a dimer. ATP hydrolysis is stimulated via interaction with the partner protein ParB. ParA has been observed to form filament structures and is able to bind DNA in a non-specific manner. This again has led to the proposal of either a model that involves polymerisation and depolymerisation driving chromosome segregation or a diffusion ratchet-like mechanism (Figge *et al*., 2003, Ptacin *et al*., 2010, Shelbelut *et al*., 2010, Toro *et al*.,

2008, Vecchiarelli *et al*., 2010). Additional proteins have also been identified that are thought to be involved in the mechanism which will be discussed later.

1.4 Mechanisms of plasmid segregation

As discussed above, partition systems typically consist of two proteins and a *cis*-acting centromere-like site. One of the proteins is a centromere binding protein (CBP) and is able to bind specifically to the *cis*-acting centromere-like site to form a nucleoprotein partition complex. The other protein is a NTPase motor protein that is recruited to the nucleoprotein partition complex to form a segrosome and uses the energy of nucleotide binding and hydrolysis to drive plasmid segregation. Even though partition systems utilise these three components, the molecular mechanism by which they segregate the plasmid are different. The mechanism employed by type II partition systems is the best understood and structural studies have allowed near atomic level understanding of the process involved. The type III partition system has been less extensively studied, mainly due to the fact it is the most recently discovered of the partition systems. However there is good evidence for the mechanism underpinning this type of plasmid segregation, which has not yet been disputed. On the other hand, the mechanism employed by type I partition systems is still under much deliberation. There are currently two main models of segregation that have been proposed that involve two very different mechanisms of segregation. The mechanism involved in plasmid segregation by type I partition systems is currently a hot topic of research.

1.4.1 A filament model of plasmid segregation for type I partition systems

In much of the early research into type I partition systems a ParA filament model was proposed. This model is based on the fact that several ParA proteins were seen to undergo ATP dependent polymerisation (Batt *et al*., 2009, Barilla *et al*., 2005, Bignell and Thomas, 2001, Bouet *et al*., 2006, Ringgaard *et al*., 2009). The model for plasmid segregation was thought to involve a polymerisation – depolymerisation cycle due to stimulation of the ParA ATPase activity by the partner protein. The ParA polymers, bound to the plasmid via the partner protein, were thought to either push or pull the plasmid upon this polymerisation and depolymerisation cycle and therefore moving the plasmids to either poles of the cell. This theory was further supported by many *in vivo*

studies in which ParA proteins were seen to dynamically relocate from one pole of the cell to the other (Ebersbach *et al*., 2006, Ringgaard *et al*., 2009, Hwang *et al*., 2013). These findings also lead to the observation that many of the ParA proteins were seen to localise on the nucleoid and it was then shown that these ParA proteins, when bound to ATP, were able to bind DNA in a non-specific manner (Castaing *et al*., 2008, Ringgaard *et al*., 2009, Vecchiarelli *et al*., 2010). The filament model of plasmid segregation was then modified to incorporate the nucleoid that acts as a scaffold for the polymerisation of ParA into filaments.

One example of filament model is that proposed for the pB171 plasmid. The type Ib partition system (*par2*) of pB171 encodes for the Walker –type ATPase - ParA, the CBP - ParB and two *cis*-acting centromeric sites, *parC1* and *parC2*. The model, shown in Figure 1.11, involves ParA moving the plasmid by a pulling mechanism. ParA is able to nucleate and polymerise into filaments, binding cooperatively and non-specifically to DNA and using the nucleoid as a scaffold. Upon capturing a ParB-bound plasmid, ParA then undergoes depolymerisation, which pulls the plasmid in the direction of the retracting polymer. The process is then repeated at the opposite pole. This continuous cycling of ParA polymerisation and depolymerisation allows the relocation of the plasmids to either pole and ensures faithful segregation. This model was supported by both experimental and mathematical modelling data (Ringgaard *et al*., 2009).

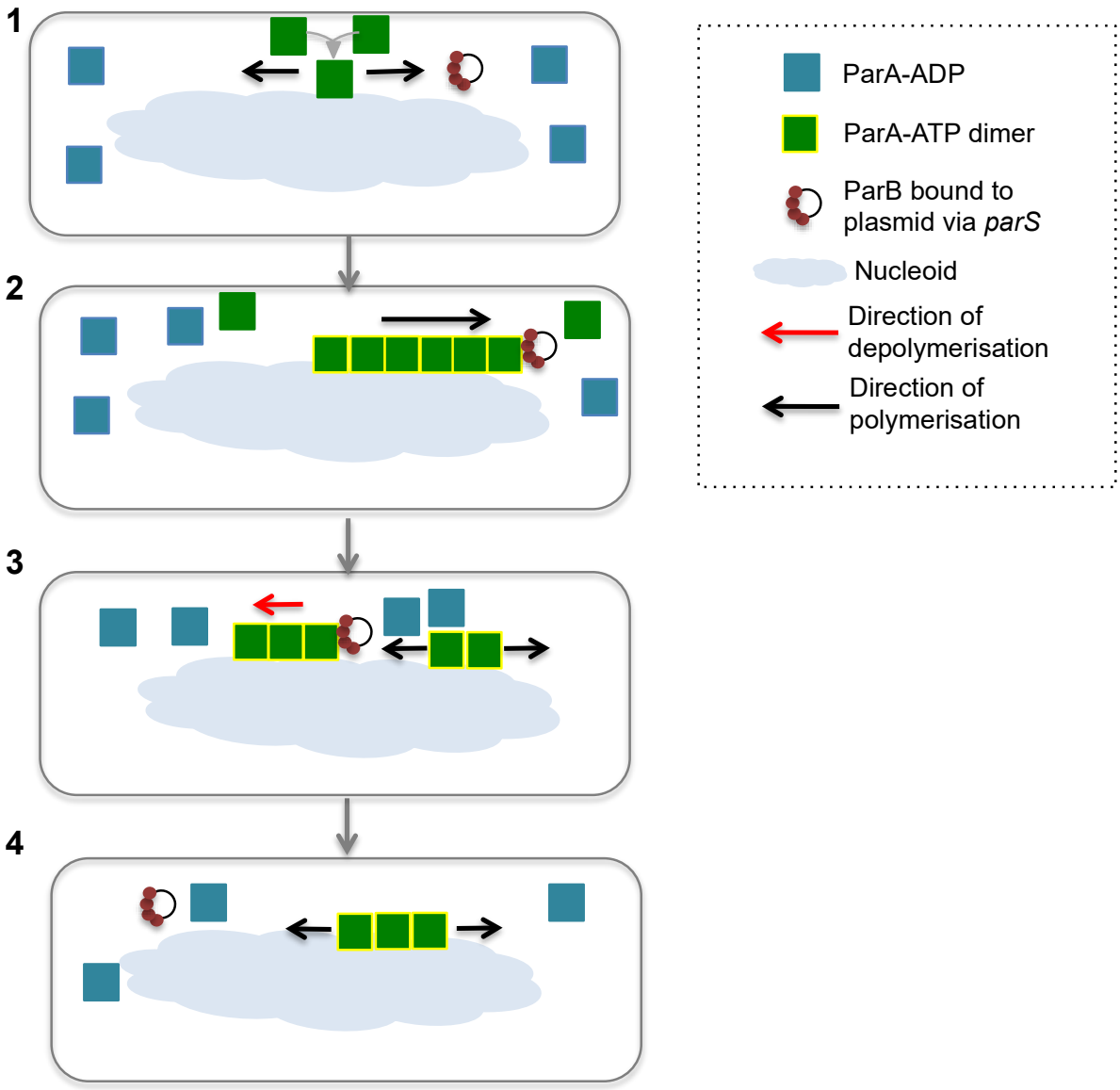

Figure 1.11 - A molecular model for a filament based pulling mechanism used by type I partition systems. Model proposed for the type Ib partition system of pB171. 1) ParA-ATP dimers bind to the nucleoid and are able to form filaments. 2) The growing ParA filament contacts a plasmid via an interaction with ParB, which then stimulates ParA ATPase activity. 3) The ParA filament then begins to depolymerise and pulls the bound plasmid in the direction of depolymerisation. 4) The plasmid is continually moved from one pole to the other as the depolymerisation in the previous step leaves a ParA-free zone in which recently released ParA, after exchange of ADP for ATP, can rebind and being polymerisation into filaments again. Adapted from (Ringgaard *et al.*, 2009)

1.4.2 A diffusion-ratchet mechanism for plasmid segregation for type I partition systems

Recently a new model that does not involve ParA polymerisation has been proposed. As with the filament-based model the process in which ParA-ATP binds the nucleoid is important, however ParA-ATP is proposed to associate with the nucleoid as a dimers or small oligomers not as a filament. The stimulation of ATP hydrolysis by the partner protein is again instrumental in allowing the dynamic relocation of ParA. This model predicts that ParB bound to *parS* creates and then follows a ParA gradient on the nucleoid surface. The model is known as a diffusion-ratchet mechanism as it proposes that the ParB-*parS* complex ratchets along the nucleoid following an oscillating wave of ParA. Initially the model was proposed for type Ia partition systems, namely the P1 and F plasmid (Hwang *et al*., 2013, Vecchiarelli, 2014). More recently, this model has been proposed for the type Ib partition system encoded by the pSM19035 plasmid (Volante and Alonso, 2015).

The diffusion ratchet model proposed for type I partition systems is outlined in figure 1.12. In this model ParA-ATP exists in two forms: one is able to bind the nucleoid (ParA-ATP*) as it has undergone a conformational change, the other is not yet able to bind. This time delay during the conformational change is a crucial step in this model. Firstly ParA-ATP* binds the nucleoid and ParB dimers bind the plasmid via the partition site. ParB, bound to the plasmid, then interacts with ParA-ATP* stimulating ParA ATPase activity and thus causes ParA to fall off the nucleoid. ParA-ADP now diffuses freely and this creates a ParA depletion zone on the nucleoid. ParA exchanges ADP for ATP and then undergoes a slow conformational change before rebinding the nucleoid in a different position. This continuous redistribution of ParA drives plasmid movement. After replication the plasmids follow high concentrations of ParA-ATP* in opposite directions and thus segregate bidirectionally (Vecchiarelli *et al*., 2012, Vecchiarelli, 2014).

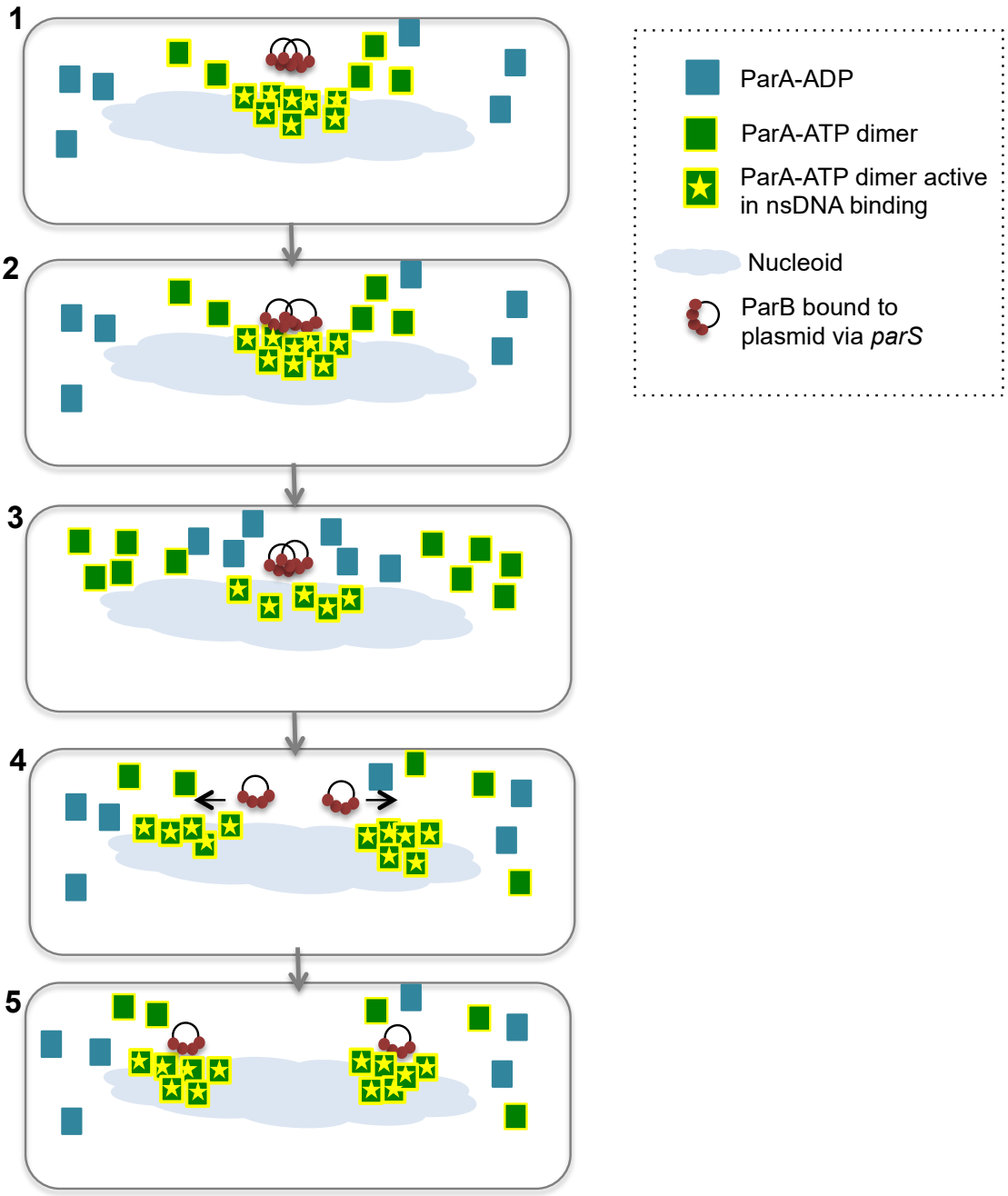

Figure 1.12 - A diffusion ratchet model of plasmid segregation by type I partition systems. Model proposed for the type I partition system of P1 plasmid and F plasmid. 1) ParA-ATP undergoes a slow conformational change which enables its binding to the nucleoid (ParA-ATP*). 2) ParB, bound to the plasmid via *parS*, interacts with ParA that allows the plasmid to be bridged to the nucleoid. 3) ParB stimulates ParA ATPase activity and ParA-ADP is then cleared from the nucleoid, ParA exchanges ADP for ATP and there is a slow conformational change before ParA-ATP is able to rebind the DNA and therefore ParA randomly diffuses. 4) ParA-ATP* then re-binds the nucleoid. This cycle allows a continuous redistribution of ParA-ATP* in which ParB bound to the plasmid constantly follows. 5) After the plasmid has undergone replication the two plasmids follow ParA gradients in opposite directions, the cycle then begins again. Adapted from (Vecchiarelli *et al*., 2012).

A similar model for pSM19035 plasmid segregation has recently been proposed. In this model the Walker-type ATPase, δ, binds ATP and this allows binding to the nucleoid. The CBP, ω, is able to bind to the plasmid, when dimeric, via the partition site. However this only forms a transient complex, which then becomes stabilized when dimeric δ interacts with ω. δ bound to the nucleoid then captures this complex of δ_2-ω_2-parS via protein-protein interactions between δ dimers. δ chases this complex and this leads to directional movement of the ω_2-*parS* complex towards a δ gradient. Again ω_2 stimulation of δ ATPase activity allows the diffusion of δ (Volante and Alonso, 2015).

1.4.3 Mechanism of chromosome segregation by type I partition systems

As with the type I plasmid segregation mechanism there has been much deliberation over the role and mechanism of partition proteins in chromosome segregation. The role of the partitioning proteins in chromosome segregation is often hard to determine as many other factors such as; SMC, DNA translocase and proteins involved in tethering chromosomes to the pole are thought to play a crucial role in the segregation process. However mechanisms have been proposed for chromosome segregation. These mechanisms are similar to those discussed above, a filament-based model and a diffusion-based model. This is due to the fact that many parallels have been observed between plasmid encoded and chromosome encoded ParA proteins. These similarities include the formation of higher order ParA structures in the presence of ATP and the ability of ParA to bind DNA non-specifically. Similar *in vivo* patterns have been seen for chromosome-encoded ParA proteins in which they are seen to dynamically relocate on the nucleoid (Reyes-Lamothe *et al*., 2011).

Filament-based models were originally proposed for chromosome segregation in two bacteria; *Vibrio cholerae* and *Caulobacter crescentus.* In these models the ParA proteins were thought to form filaments that extend from one pole to the ParB-*parS* complex. Upon disassembly of the filaments the chromosome is then pulled to the opposite pole of the cell (Fogel and Waldor, 2006, Ptacin *et al*., 2010, Shelbelut *et al*., 2010). However, as for plasmid segregation, there is much deliberation as to whether a filament-model is the most appropriate based on the available data. More recently a DNA-relay mechanism has been proposed for *Caulobacter crescentus* chromosome segregation. This model is similar to the diffusion-ratchet model proposed for the segregation of P1 and F plasmids. However the main difference between the diffusion-

ratchet model and the DNA-relay model is the importance of the elastic dynamics of the chromosome that play an essential role in the model. In the DNA-relay model ParA-ATP is able to bind non-specifically to nucleoid and ParB (bound to *parS*) then binds to ParA. ParA then acts as a tether and thus aids the movement of the ParB-*parS* complex from one region of DNA to another. Therefore the ParA-ParB complex is responsible for pulling the origin of replication region and thus the chromosome. The direction of movement is towards a ParA gradient and it is the elasticity of the chromosome that enables the ParB-*parS* complex to move in this direction. The continuous cycles of ParA binding DNA, ATP hydrolysis and ParA diffusion allow movement from one pole to the other (Lim *et al*., 2014, Wang *et al*., 2014a).

Many chromosome-encoded partitioning proteins have been shown to interact with other proteins such as DnaA initiator proteins and SMC (structural maintenance of chromosome) and this has been shown to be important in chromosome segregation. Polar anchoring proteins have also been shown to interact with partitioning proteins and they also play a crucial role in chromosome segregation. For example, in *C. crescentus,* the ParB-*parS* complex has been shown to interact with the polar anchor PopZ: this interaction allows PopZ to tether ParB-*parS*-*ori* sisters at the cell pole. Another protein TipN has been shown to be involved in tethering newly segregated ParB-*ori* at the new pole via interactions with ParA (Ptacin *et al*., 2010, Wang *et al*., 2013). In *B. subtilis* the CBP, Spo0J, is believed to recruit SMC to the origin region and this is believed to be involved in correct chromosome segregation (Wang *et al*., 2014b). The partitioning proteins, Soj and Spo0J, are also thought to interact with cell division proteins such as DivIB, FtsZ and MinD, which ensures the correct localisation of segregation proteins within the cell (Gruber and Errington, 2009, Sullivan *et al*., 2009).

The fact that chromosome encoded partitioning proteins interact with many other proteins and are potentially involved in other cellular processes other than chromosome segregation makes gaining an understanding of the protein roles much harder. However it is evident that parallels can be drawn between chromosome encoded and plasmid encoded partition systems. Therefore it is possible that advances in understanding the mechanism of type I partition systems can be gained from both chromosomes and plasmids. One interesting question is whether other factors are interacting with the plasmid encoded partitioning proteins and playing a role in the segregation mechanism.

1.4.4 The insertional polymerisation 'pushing' model for type II plasmid systems

The mechanism employed by type II partition systems is the best understood due to extensive studies on the *E. coli* R1 plasmid as well as pSK41 and pB171. ParM is a member of the bacterial actin-like proteins (ALPs), which are a large group of proteins believed to be bacterial cytoskeletal elements that are involved in many cellular processes (Derman *et al*., 2009, Shaevitz and Gitai, 2010). The insertional polymerisation mechanism involves ParM forming filaments, which push the plasmid apart (Figure 1.13). ParM has been shown to form double helical protofilaments, however these filaments display dynamic instability in the presence of ATP where both ends of the filament undergo rapid assembly and disassembly. However in the presence of ParR-*parC* complex the filaments become stabilized. Therefore the model proposed involves the ParR-*parC* capping the ends of the ParM filaments via ParM monomers interacting with the C-terminal domain of ParR. ParM is then able to grow via polymerisation at the capped end, the other extremity of the filament will carry on undergoing depolymerisation until another ParR-*parC* complex is found and the filament then becomes capped at both ends. This capping at both ends of the filament allows bidirectional pushing of the plasmid to opposite poles of the cell, upon which ATP hydrolysis will allow the release of the plasmid (Bharat *et al*., 2015, Garner *et al*., 2007, Gerdes *et al*., 2010, Salje *et al*., 2010, Salje and Lowe, 2008).

A similar model has also been proposed for another member of bacterial ALPs, Alp7A. The *alp7A* operon, found on the pLS20 plasmid from *B.subtilis*, consists of the *alp7R* gene and *alp7C* sequence as well as the *alp7A* gene. Alp7A is able to form dynamic filaments that play an important role in pLS20 plasmid segregation. Alp7A exhibits very similar characteristics to ParM, it has been shown to assemble into filaments which display dynamic instability and treadmilling properties (Derman *et al*., 2009). Alp7R is a DNA binding protein, which has been observed to bind to *alp7C*. Alp7R is involved in both stabilisation of Alp7A filaments and the regulation of expression of Alp7A (Derman *et al*., 2012). *In vivo* studies allowed a model to be proposed that is very similar to that of R1 plasmid segregation. The Alp7A filaments repeatedly assemble and dissemble until the filaments reach a plasmid, which stabilises the filaments and thus pushing the plasmids to the cell pole. The treadmilling property of Alp7A is proposed to keep the plasmids apart after they have been positioned at the poles of the cell (Derman *et al*., 2009, Derman *et al*., 2012).

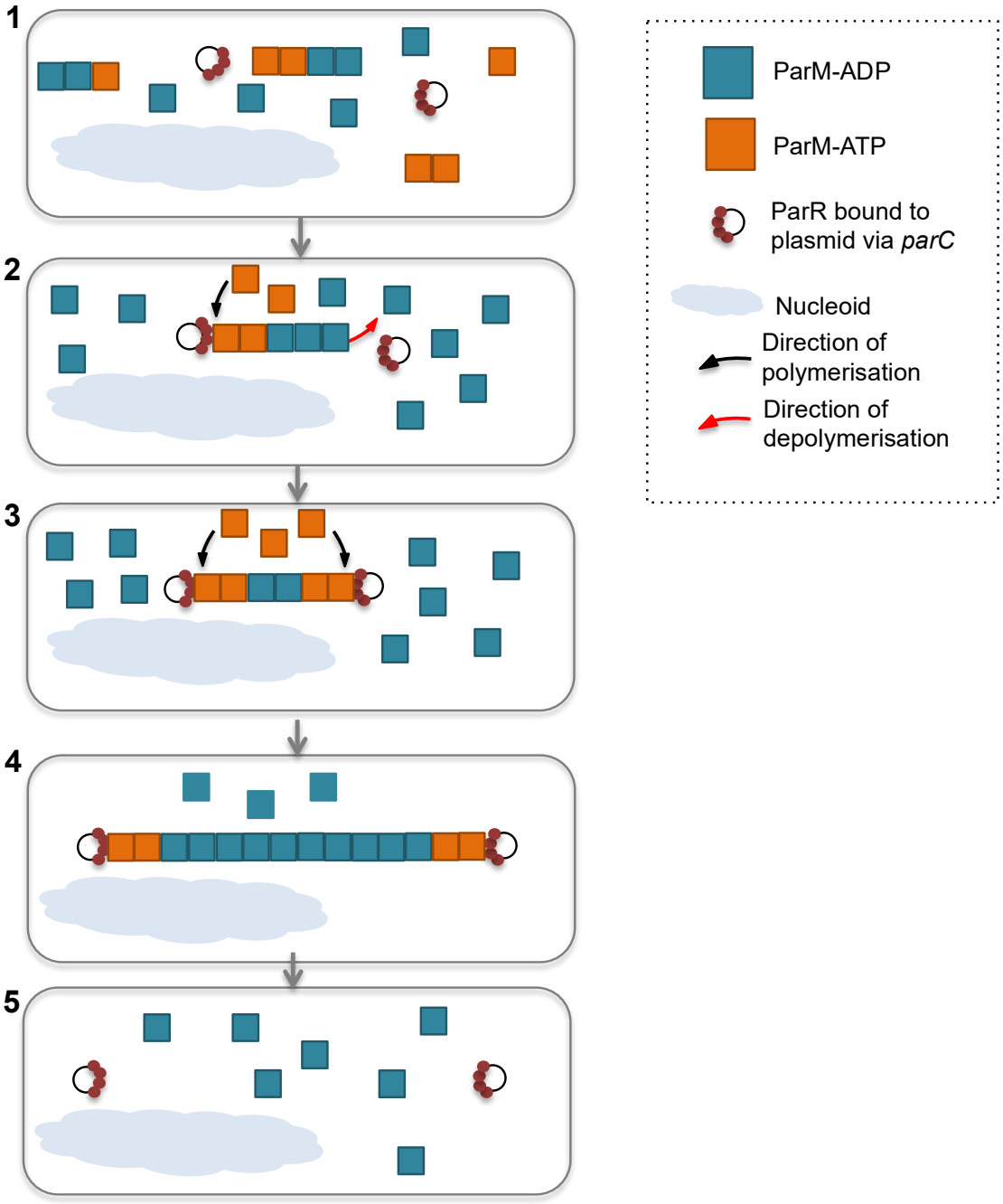

Figure 1.13 - The insertional polymerisation 'pushing' model of plasmid segregation by a type II partition system. Model based on the type II partition system of R1 plasmid. 1) A critical concentration of ParM allows polymerisation into filaments, these filaments are highly dynamic so are constantly undergoing polymerisation and depolymerisation until the reach a ParR-*parC* complex that caps and stabilises the filaments. 2) A ParM filament is capped at one end via an interaction with ParR, bound to a plasmid via *parC.* The ParM filament can continue to grow at the capped end and will continue to undergo polymerisation and depolymerisation at the other end in search of another plasmid bound by ParR. 3) The ParM filament is now capped at both end and this stabilises the filaments allowing growth. 4) The ParM filament elongates pushing the plasmids to opposite cell poles. 5) The plasmids are released at the pole and the ParM filament depolymerises. Adapted from (Salje *et al*., 2010).

1.4.5 The treadmilling model for type III partition systems

Type III partition cassettes encode a tubulin-like GTPase, another bacterial cytoskeletal element that is involved in driving plasmid segregation using a mechanism distinctly different from those of type I and type II partition systems. The best understood type III partition system is that encoded by the pBtoxis plasmid and it has led to the proposal for a treadmilling model (Figure 1.14). The tubulin-like GTPase, TubZ, has been shown to polymerise into parallel double helical filaments, which resemble that of tubulin, in the presence of GTP. The filaments, like those formed by ParM, are subject to dynamic instability and capping by GTP at one end allows polymerisation (Larsen *et al*., 2007). However, TubZ filaments differ from those of ParM as they show plus end polymerisation and minus end depolymerisation which is known as polymer treadmilling. The structure of TubZ revealed that it contains a flexible C-terminal tail and this is believed to interact with the partner protein TubR. Taken together this data allowed a model for plasmid segregation to be proposed. In the model the TubR-*tubC* complex interacts with TubZ filaments via the C-terminal tail. Upon addition of GTP TubZ undergoes polymerisation at the plus end and therefore growth of the filament, whereas GTP hydrolysis at the minus end causes depolymerisation. This treadmilling allows the plasmid, bound via TubR, to be moved along the TubZ filament towards the cell pole. It is believed that the TubZ filament curves around the cell pole. This might cause the plasmid to fall off the TubZ filament thus positioning it in the region of the cell pole ready for cell division (Aylett *et al*., 2010, Fink and Lowe, 2015, Ni *et al*., 2010).

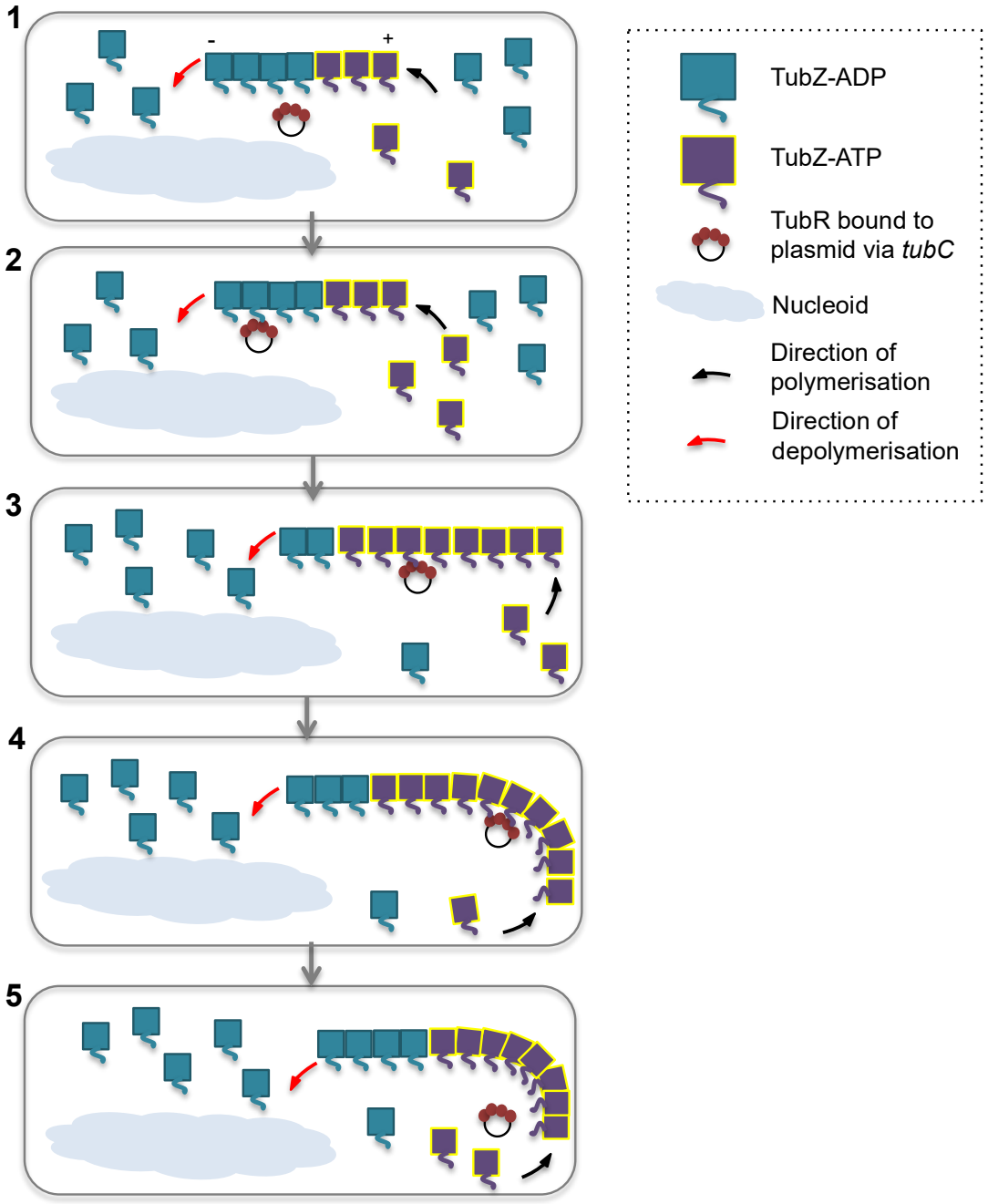

Figure 1.14 - A treadmilling model for plasmid segregation by a type III partition system. Model based on the type III partition system from pBtoxis. 1) TubZ is able to polymerise into filaments in a GTP dependent manner, these filaments are dynamic and polymerise at the + end and depolymerize at the – end. 2) The C-terminal tail of TubZ interacts with TubR, bound to the plasmid via *tubC*. 3) The TubZ filament continues to polymerise at the + end and depolymerize at the – end and TubR bound to the plasmid moves towards the + end. 4) The TubR bound plasmid continues to be passed along the TubZ filament until the cell pole is reached. 5) It has been proposed that when the TubZ filament bends around the cell pole it causes the release of the plasmid. Adapted from (Ni *et al*., 2010).

1.5 The partition system of plasmid TP228

This work aims to gain a further understanding of the partition system employed by the plasmid TP228, which ultimately will enable the molecular mechanism involved in segregation of the plasmid to be elucidated. Plasmid TP228 is a multidrug resistant plasmid originally isolated in *Salmonella newport* that has been shown to replicate at low copy numbers in *E. coli* (Hayes, 2000). Plasmid TP228, a member of the IncX1 incompatibility group, confers resistance to a wide range of antibiotics such as spectinomycin, kanamycin, neomycin, tetracycline streptomycin, sulfonamides and some metal ions (Jones *et al*., 1993). Plasmid TP228 has been shown to utilise a type Ib partition system that encodes two *trans*-acting proteins, ParF and ParG, and upstream of *parFG* a *cis*-acting centromere site *parH* (Figure 1.15). ParF is a Walker-type ATPase and ParG is the centromere binding protein that has been shown to bind specifically to the partition site *parH* to form a partition complex that is then able to recruit ParF (Barillà and Hayes, 2003, Hayes, 2000, Wu *et al*., 2011a). ParG has also been shown to bind to the operator site, upstream of *parFG*, and therefore ParG acts as the transcriptional repressor for *parF* and *parG* to autoregulate the expression of the two *trans*-acting proteins (Carmelo *et al*., 2005, Zampini *et al*., 2009). ParF, the Walker-Type ATPase, is the motor protein of the partition system and is responsible for driving the segregation of the plasmid, the exact mechanism of which is still not fully understood. However ParF has been shown to form higher order structures and this is thought to be important in the plasmid segregation mechanism (Barilla *et al*., 2005).

1.5.1 Centromere site *parH*

Positioned upstream of the *parFG* genes is an operator site, O_F, and a *cis*-acting centromere site *parH*. O_F is found immediately upstream of the 5' *parF* translational start codon. O_F consists of eight degenerate tetramer boxes of which five are arranged in inverted orientation and three in direct orientation. The variant repeats of 5'-ACTC-3' are separated by 4 bp AT-rich spacers. ParG has been shown to bind the O_F region, specifically each motif is bound by one ParG dimer and therefore it is proposed that the O_F region is coated by up to eight ParG dimers (Zampini *et al*., 2009). The binding of ParG to O_F allows it to act as a transcriptional repressor of the *parFG* genes (Carmelo *et al*., 2005).

Upstream of O_F, is a region of ~ 100 bp that is the *cis*-acting centromere site *parH*. The *parH* site consists of twelve degenerate 5'-ACTC-3' motifs that like O_F are separated by

AT-rich spacers. Eleven of the tetramer boxes are arranged in direct orientation whereas just one is arranged in an inverted orientation. All twelve of the repeats in the *parH* site have been shown to be essential for centromere function: sequential deletion of the tetramer boxes has been shown to progressively reduce the centromere function. The *parH* site lacks intrinsic bend, which is seen in other centromere sites, however the *parH* site does display highly elastic properties *in vivo*, which was demonstrated by rearrangement of boxes still showing centromere activity (Wu *et al*., 2011a). This indicated that *parH* could be flexed when in a complex with ParF and ParG if required, thus giving *parH* its elastic properties. ParG has been shown to bind specifically to the *parH* site, which then recruits ParF to form a nucleoprotein complex known as the segrosome (Wu *et al*., 2011a, Zampini *et al*., 2009). Segrosome assembly is the first step in plasmid segregation.

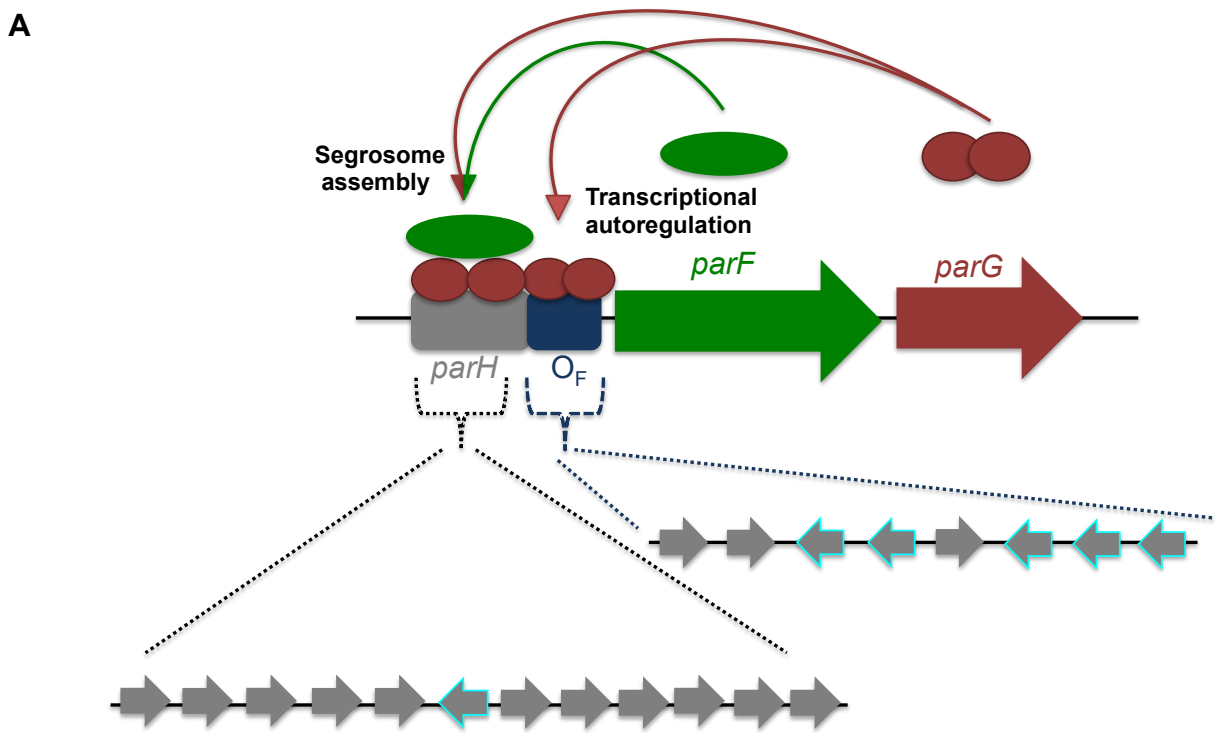

Figure 1.15 - Schematic representation of the partition cassette of plasmid TP228. A) The TP228 plasmid encodes for two *trans*-acting proteins, the Walker-type ATPase – ParF shown in green and the CBP – ParG shown in red. Upstream of *parFG* is the operator site, O_F shown in blue, and the *cis*-acting centromere site, *parH* shown in grey. The expanded view of the upstream regions indicates the twelve degenerate repeats of the *parH* site, one of which is in the inverted orientation (highlighted in cyan) and the eight degenerate repeats of O_F, five of which are in the inverted orientation. Dimeric ParG binds to the operator site to autoregulate the expression of *parFG*, as well as binding *parH* and then recruiting ParF to form a nucleoprotein complex (segrosome). B) DNA sequence of partition site *parH*. 12 degenerate repeats of 5'-ACTC-3' with AT rich spacers constitute the *parH* site of plasmid TP228. The repeats are boxed and denoted by arrows. The grey arrows indicate direct repeats and the cyan arrow represents the inverted repeat.

1.5.2 Centromere binding protein ParG

The partition system of TP228 encodes the CBP ParG, a 76 residue, 8.6 kDa protein that is a dimer in solution. The structure of ParG has been solved by NMR, which showed ParG consists of a flexible N-terminal tail (residues 1-32) and a C-terminal region (residues 33-76) that has a ribbon-helix-helix DNA binding motif (Figure 1.16). The C-terminal region is involved in ParG dimerization with hydrophobic contacts in this region responsible for holding the ParG dimer together. In addition to this the C-terminal domain is essential for ParG DNA binding, specifically the RHH motif within the C-terminal region (Golovanov *et al*., 2003).

The RHH domain is composed of residues 34-41 that form a β-sheet and residues 42-55 and 60-74 that form two α-helices. It is the RHH motif that enables ParG to bind DNA in a site-specific manner to the centromere site, *parH*, and the operator site O_F. ParG belongs to the Arc/MetJ superfamily, which comprises proteins that utilise a RHH motif for transcriptional repression. Proteins such as Arc and MetJ have been shown to bind DNA via the antiparallel β-sheets that are inserted into the major groove of the DNA (Golovanov *et al*., 2003, Schreiter and Drennan, 2007). ParG is likely to bind DNA in the same manner and key residues (R36, N38 and N40) located on one side of the β-strand have been shown to be important in making interactions with DNA (Golovanov *et al*., 2003). In addition to the RHH motif, the unstructured N-terminal tail of ParG is important in DNA binding. Other members of the Arc/MetJ superfamily have been shown to utilise the unstructured N-terminal domain in making additional specific DNA contacts (Knight and Sauer, 1989). The N-terminal tail of ParG was shown to be important in transcriptional repression of the *parFG* genes. Truncated versions of ParG that lacked 9, 19 or 30 N-terminal residues (Δ9, Δ19, Δ30) showed a gradual reduction in repression. Δ9 showed little effect on repression, whereas Δ19 and Δ30 displayed a much weaker repression therefore indicating the importance of the N-terminal tail in the transcriptional regulation activity of ParG (Carmelo *et al*., 2005, Zampini *et al*., 2009). The binding affinity of ParG for *parH* has also been shown to be altered by the N-terminal tail, demonstrating the importance of this region in *parH* binding. It has also been shown that removal of the N-terminal tail causes an increase in non-specific DNA binding by ParG (Wu *et al*., 2011a).

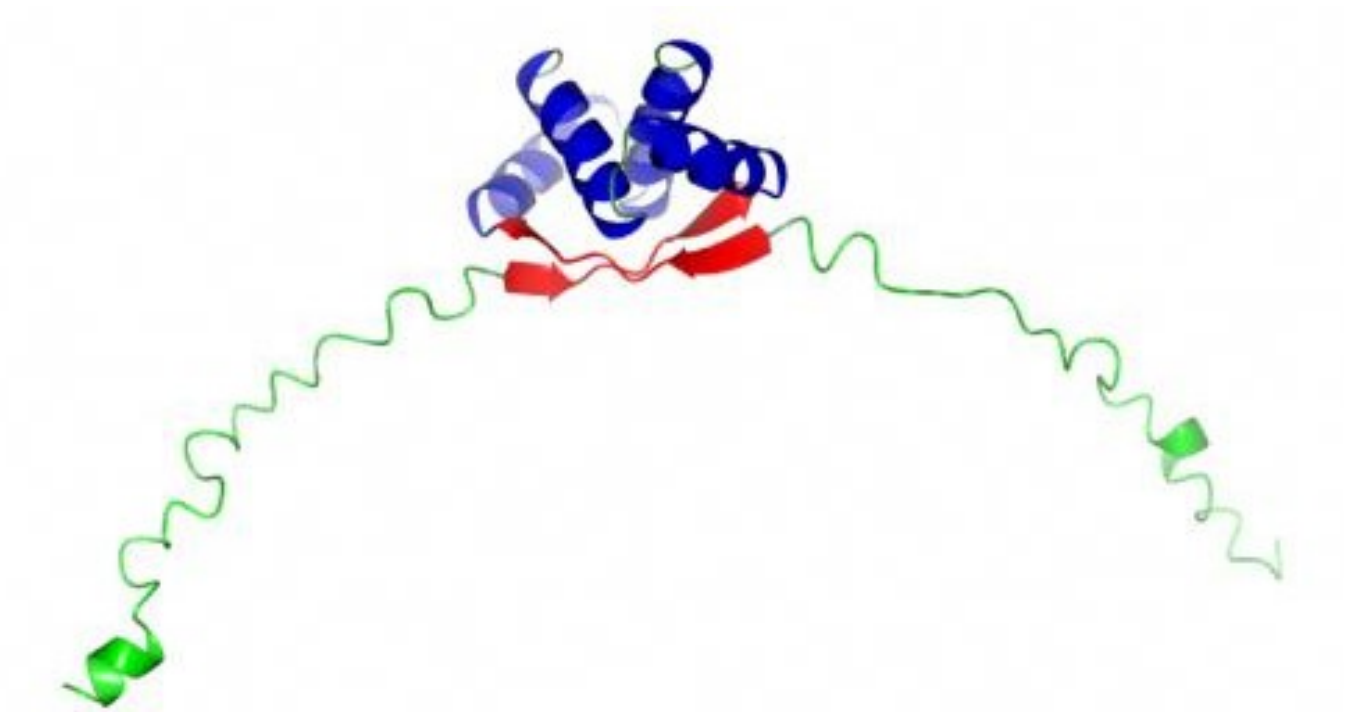

Figure 1.16 - Structure of ParG dimer. The unstructured N-terminal tails are shown in green, the β-sheets are shown in red and the α-helices are shown in blue. The dimer consists of two β-sheets and four α-helices.

As with other partition systems, the CBP is involved in recruiting the motor protein to the nucleoprotein complex to form the segrosome. ParG has been shown to interact with its partner protein, ParF (Barillà and Hayes, 2003). Both the C-terminal and N-terminal regions have been shown to contact ParF, and *in vivo* the ParF-ParG interaction has been shown to occur both in the absence and presence of the partition site, *parH* (Barillà and Hayes, 2003, Barilla *et al*., 2007). This interaction between ParF and ParG is important for three reasons: 1) it allows ParF to be recruited to the segrosome, 2) ParG stimulates the ATPase activity of ParF by ~ 30 fold *in vitro* and 3) ParG promotes the assembly of ParF into higher order structures (Barilla *et al*., 2005, Barilla *et al*., 2007). The role of the latter two functions in the mechanism of TP228 plasmid segregation is interesting due to the fact they have antagonistic effects on the assembly of ParF into higher order structures. Studies revealed that the N-terminal tail of ParG was crucial for both stimulation of ParF ATPase activity and assembly into higher order structures (Barilla *et al*., 2007, Barilla *et al*., 2005). The N-terminal truncated versions of ParG (Δ9, Δ19 and Δ30) showed a reduction in both stimulation of ATP hydrolysis by ParF and the enhancement of ParF assembly into higher order structures (Barilla *et al*., 2007).

The unstructured N-terminal tail of ParG contains an arginine finger-like motif. The N-terminal tail of ParG might be able to insert close to the ATP binding pocket of ParF and the arginine finger might be responsible for stimulating the ATPase activity by stabilising the transition state during ATP hydrolysis. Specifically, an arginine residue (R19) was identified to be essential for stimulation of ParF ATPase activity, as mutation of this residue was found to abolish stimulation of ATPase activity (Barilla *et al*., 2007). Recently, mutational analysis of the N-terminal tail of ParG has identified other residues that are important for stimulation of ParF ATPase activity (Madhuri Barge, unpublished data).

The ParG N-terminal tail has also been shown to be involved with the enhancement of ParF assembly into higher order structures. N-terminally truncated ParG proteins showed a reduction in the enhancement. An interesting observation was that particular residues when converted to different amino acids, abolished ATPase stimulation, but they did not affect the enhancement of ParF assembly into higher order structures thus suggesting a clear distinction between the two roles (Barilla *et al*., 2007). ParG has been shown to enhance ParF assembly into higher order structures both in the presence and absence of ATP, this was demonstrated by the fact that ParF mutants defective in ATP dependent assembly were still able to form higher order structures in the presence of

ParG (Dobruk-Serkowska *et al*., 2012). The exact mechanism by which ParG enhances the assembly of ParF into higher order structures is not fully understood, however it has been proposed that the N-terminal tail may bridge ParF monomers or may be able to cross-link adjacent ParF filaments. The ParG:ParF ratio has been demonstrated to be important in determining the role carried out by ParG. At low ParG:ParF ratios ParG is seen to stimulate ParF assembly into higher order structures, whereas at higher ratios it antagonises this assembly (Barilla *et al*., 2005, Barilla *et al*., 2007).

1.5.3 Walker-type ATPase ParF

The ParF Walker-type ATPase encoded by the TP228 partition system is a member of a subgroup of the large P-loop GTPase superfamily. A typical P-loop fold is characterised by an N-terminal Walker A motif, which consists of a flexible loop. The loop enables the correct positioning of the triphosphate moiety of bound nucleotides and the loop will often have a typical Walker A motif of GXXGXGK (Walker *et al*., 1982). ParF, and other ParA proteins, harbour a deviant Walker A motif of XKGGXXK. The ParA ATPase proteins show a conserved lysine residue at the second position in the sequence, which interacts with the terminal oxygen atom of the β-phosphate group of ATP across the interface (Leipe *et al*., 2002, Lutkenhaus and Sundaramoorthy, 2003). The deviant Walker A motif of ParF is composed of residues 9-16 and consists of the amino acid sequence PKGGSGKT. Also present in this class of proteins is a less well conserved Walker B motif and in ParF this is located at residues 73-83 with the sequence LADYDFAIVDG. The Walker B motif, positioned on a strand close to the Walker A motif, is important in magnesium binding and catalysis (Schumacher *et al*., 2012). The structure of ParF (206 residues, 22kDa protein) has been solved in the presence of ADP and a non-hydrolysable ATP analogue, phosphomethylphosphonic acid adenylate ester (AMPPCP) (Schumacher *et al*., 2012). The structure of ParF showed it consists of a single domain with a central seven-stranded twisted β-sheet, which are surrounded on each side by four α-helices. The structure revealed that ParF is monomeric when bound to ADP and dimeric when bound to AMPPCP (Figure 1.17). In the dimer structure the two nucleotide molecules appear to be sandwiched in between the monomers. The nucleotide binding pocket of ParF was identified as being composed of residues 9-16 (Walker A motif), residues 37-49 and residues 166-177 (important in providing contacts that specify the adenine nucleotide). In addition, other residues were identified as being important in nucleotide binding. The structure also indicated residues involved in the

cross contacts at the monomer-monomer interface (Schumacher *et al*., 2012). Some of the cross contacts identified were in addition to those between the nucleotide and the Walker A motif. Most notably was a proline-rich motif (residues 102-112) that was identified to make key contacts by inserting into a side pocket close to the nucleotide binding pocket in the adjacent monomer (Schumacher *et al*., 2012). The identified residues are summarised in Table 1.2.

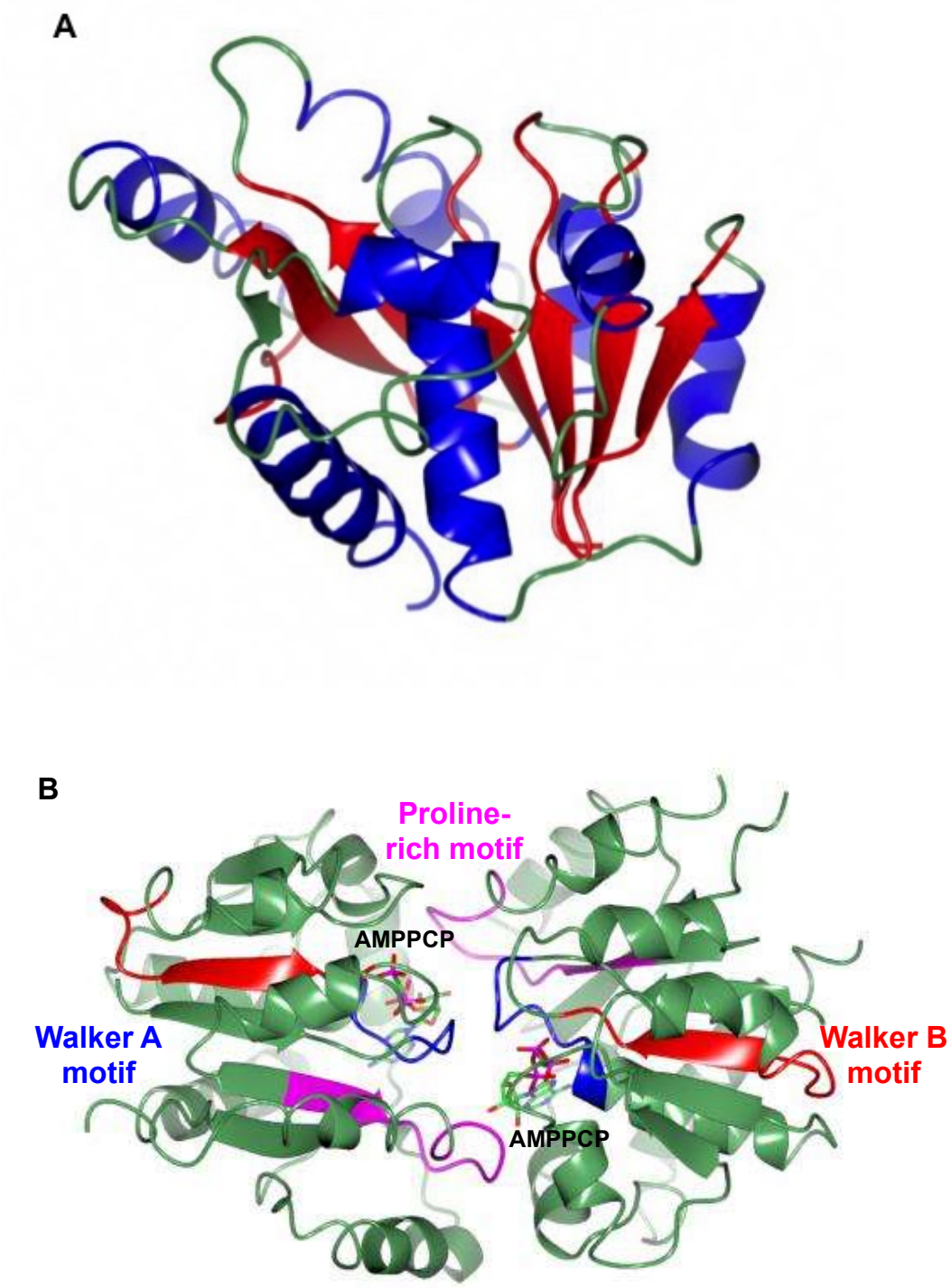

Figure 1.17 - Structure of ParF. A) Ribbon diagram of ParF monomer – the secondary structures are highlighted with the α-helices shown in blue, the β-sheets shown as red and the loops as green. B) Ribbon diagram of ParF dimer. ParF was shown to form a nucleotide sandwiched dimer in the presence of AMPPCP. AMPPCP is shown as sticks, the Walker A motif is highlighted in blue, the Walker B motif is highlighted in red and the proline-rich motif is highlighted in magenta. The structural images were generated by using CCP4MG version 2.10.4 using the 4E07 PDB coordinates.

Table 1.2 - Summary of important residues for nucleotide binding and dimer cross contacts identified from the structure of ParF

Residue	Importance
Lys10	Part of the Walker A motif and interacts with ϒ-phosphate of AMPPCP.
Asp37	Part of a triad of acidic residues that holds the hexacoordinated magnesium in position.
Asp39	Part of a triad of acidic residues that holds the hexacoordinated magnesium in position.
Asp82	Part of a triad of acidic residues that holds the hexacoordinated magnesium in position.
Arg139	Stacks over the adenine ring and makes a hydrogen bond with the ribose O4.
Thr167	Involved in specifying the adenine nucleotide by the carbonyl oxygen making a hydrogen bond to the N6 moiety of the adenine base.
Gln168	Involved in specifying the adenine nucleotide by interacting with the N3 moiety of the adenine base. Important in sealing the nucleotide sandwich dimer.
Arg169	Involved in specifying the adenine nucleotide by contacting the N1 group of the adenine base.
Thr17	Involved in stacking and hydrophobic interactions with the adenine base
Tyr172	Involved in stacking and hydrophobic interactions with the adenine base
Residues 102-112	Identified as the proline-rich motif and is seen to insert into a side pocket close to the nucleotide binding pocket and are important in maintaining the nucleotide sandwich dimer. Ser108 and Asp11 are involved in the stabilisation of the C3' *endo* conformation of the ParF dimer
Met146	Important in dimer cross contacts – stacks over the proline-rich motif and inserts into a hydrophobic pocket of the adjacent monomer
Val173	Forms the hydrophobic pocket that Met146 inserts into
Leu177	Forms the hydrophobic pocket that Met146 inserts into

The large P loop GTPase superfamily, which includes ParF, can be further divided into subgroups. The proteins in these subgroups are widely diverse and involved in many cellular processes such as DNA segregation, electron transport, and cell division. ParF, and ParF homologues, form one of these subgroups within the ParA superfamily and in fact were shown to be more closely related to the cell division protein MinD than to other plasmid and chromosome partitioning proteins such as ParA from P1 plasmid (Hayes, 2000). This was further confirmed when the structure of ParF was compared with that of other ParA proteins: it showed the strongest similarity to the *E. coli* MinD

structure as well as the *Thermus thermophilus* Soj structure (Figure 1.18) (Schumacher *et al*., 2012).

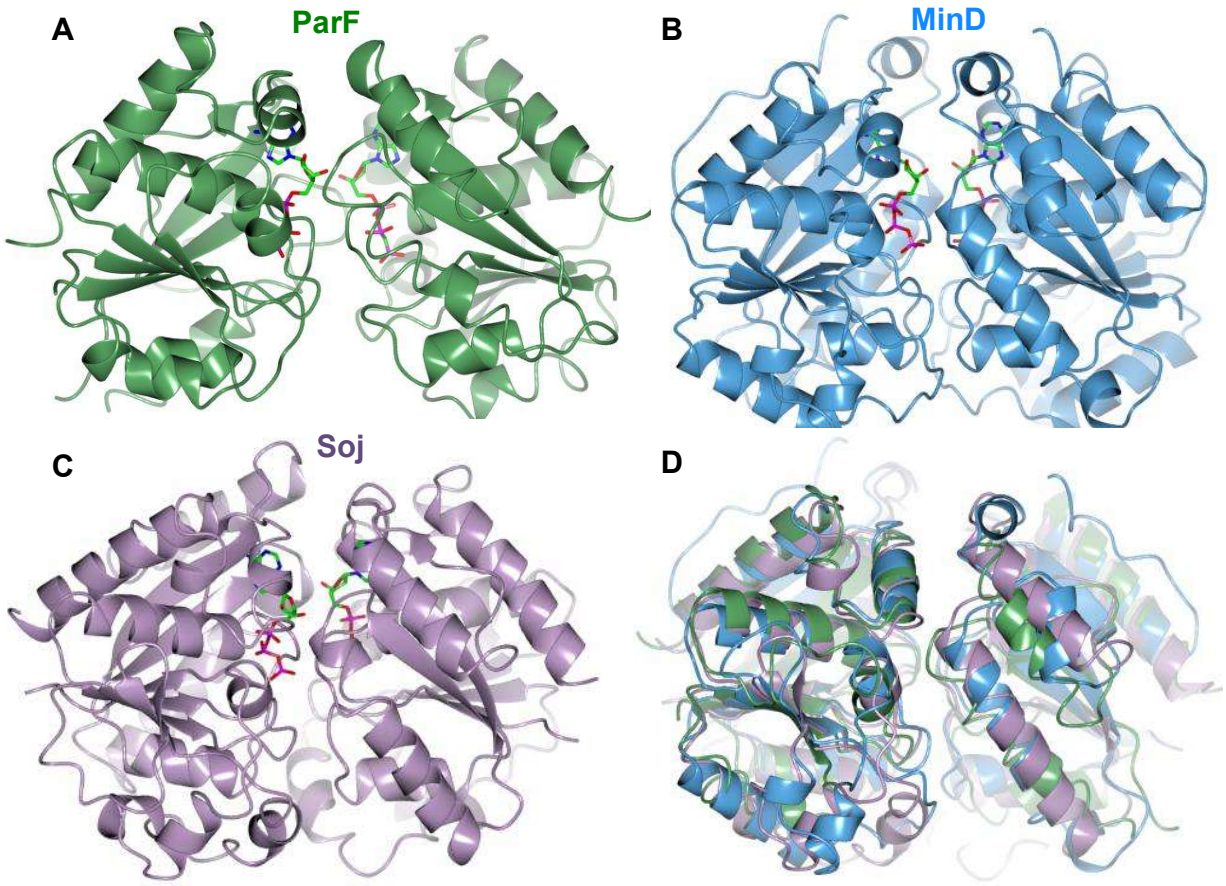

Figure 1.18 - Structural homology of ParF to other ParA superfamily proteins. A) A ribbon diagram of the ParF dimer, with AMPPCP molecules shown as sticks. B) A ribbon diagram of the *E. coli* MinD dimer, with ATP molecules shown as sticks. C) A ribbon diagram of the *T. thermophilus* Soj dimer, with ATP molecules shown as sticks. D) Superimposition of the three dimeric structures: ParF in green, MinD in blue and Soj in purple. The structural images were generated by using CCP4MG version 2.10.4 using the following PDB coordinates: A – 4E07. B- 3Q9L. C – 2BEJ.

1.5.3.1 ParF self-associates into higher order structures

ParF is able to bind ATP and has weak intrinsic ATPase activity, which is stimulated by its partner protein ParG (Barilla *et al*., 2007). It has been shown *in vivo* that upon binding ATP ParF assembles into extensive filaments and ATP hydrolysis then leads to filament disassembly. ADP antagonises the assembly of the filaments and therefore is thought to be an inhibitor of ParF filament assembly. It was proposed that the adenine-nucleotide cycling that drives ParF assembly and disassembly of filaments was important in the mechanism of TP228 plasmid segregation (Barilla *et al*., 2005, Schumacher *et al*., 2012). ParF was shown to have a tendency to self-associate into higher order structures even in the absence of nucleotide (Barillà and Hayes, 2003). The addition of ATP was seen to strongly enhance the formation of higher order structures *in vitro* and these structures were visualised by negative stain electron microscopy. The images revealed that in the presence of ATP, ParF could quickly form large filamentous structures of ~100 nm in length and after longer incubation extensive filament bundles were seen that ranged between 400-650 nm in length and 30 -70 nm in width. The filaments had a striking appearance in which they looked to have a compact end and a more irregular frayed end. ATP and ATP hydrolysis was clearly important in ParF dynamics; this was further supported by analysis of two ParF proteins that had mutations in the Walker A motif, ParF-G11V and ParF-K15Q. The mutant proteins, that had altered ATPase activity, failed to support plasmid partitioning and were shown to perturb ParF assembly into higher order structures. This not only confirmed the importance of ATP binding and hydrolysis in ParF assembly into higher order structures but also the link between ParF assembly into higher order structures and plasmid partitioning (Barilla *et al*., 2005). The link between ATP hydrolysis, assembly into higher order structures and plasmid segregation was further supported by analysis of hyperactive ATPase variants of ParF. ParF-P104A, ParF-R169A and ParF-G179A, are positioned close to the ATP binding pocket of ParF and were shown to be important in maintaining the architecture of the binding pocket. The mutant proteins showed a higher tendency to self-associate into higher order structures in the absence of nucleotide; the presence of nucleotides actually blocked the assembly of the mutant proteins into higher order structures. It has been suggested that this behaviour is due to a conformational change within ParF that primes it for self-association (Dobruk-Serkowska *et al*., 2012).

As discussed above, ParG plays an important role in the dynamics of the assembly and disassembly of the ParF filaments. The concentration of ParG determines whether ParG

promotes ParF assembly into higher order structures or antagonizes it. At low ParG:ParF ratios, ParG was seen to promote ParF assembly into higher order structures and EM images revealed the filament structures of ParF were thicker, longer and appeared more bundled in the presence of ParG. Two potential mechanisms by which ParG is thought to enhance ParF assembly into higher order structures are nucleation and bundling. Nucleation may occur by ParG N-terminal tails bridging adjacent ParF monomers. Bundling may result from the association of ParG dimers with ParF filaments and cross-linking adjacent filaments (Barilla *et al*., 2005). ParG has been shown to enhance ParF assembly into higher order structures in ParF variants that show disruption in ATP-dependent filament assembly. This was shown in both ParF variants that showed reduced ATPase activity compared to the wild type, and ParF variants that were hyperactive ATPase's (Barilla *et al*., 2005, Dobruk-Serkowska *et al*., 2012). These results indicate that the stimulatory effects of ATP and ParG on ParF assembly into higher order structures are independent but additive.

The structural data obtained for ParF provided further understanding of how ParF higher order filament structures form. Within the crystals, ParF-ATP was seen to form as extensive linear polymers in different experimental conditions. The ParF-ATP dimers were seen to interact with each other to form dimer-of-dimer units. It was proposed that these dimer-of-dimer units formed the building blocks of the ParF polymers (Figure 1.19). The dimer-of-dimer units are proposed to have interacting surfaces on all sides that are both geometrically and electrostatically complementary, and therefore allow long irregular polymers to form. Two interfaces that were identified on the surface of these ParF dimers (interface 1 and 2) were further investigated to try and gain a better understanding of these ParF higher order structures. A triple mutant, harbouring changes at interface 1, was constructed and found to disrupt plasmid segregation. The mutant was also unable to form higher order structures upon the addition of ATP (Schumacher *et al*., 2012).

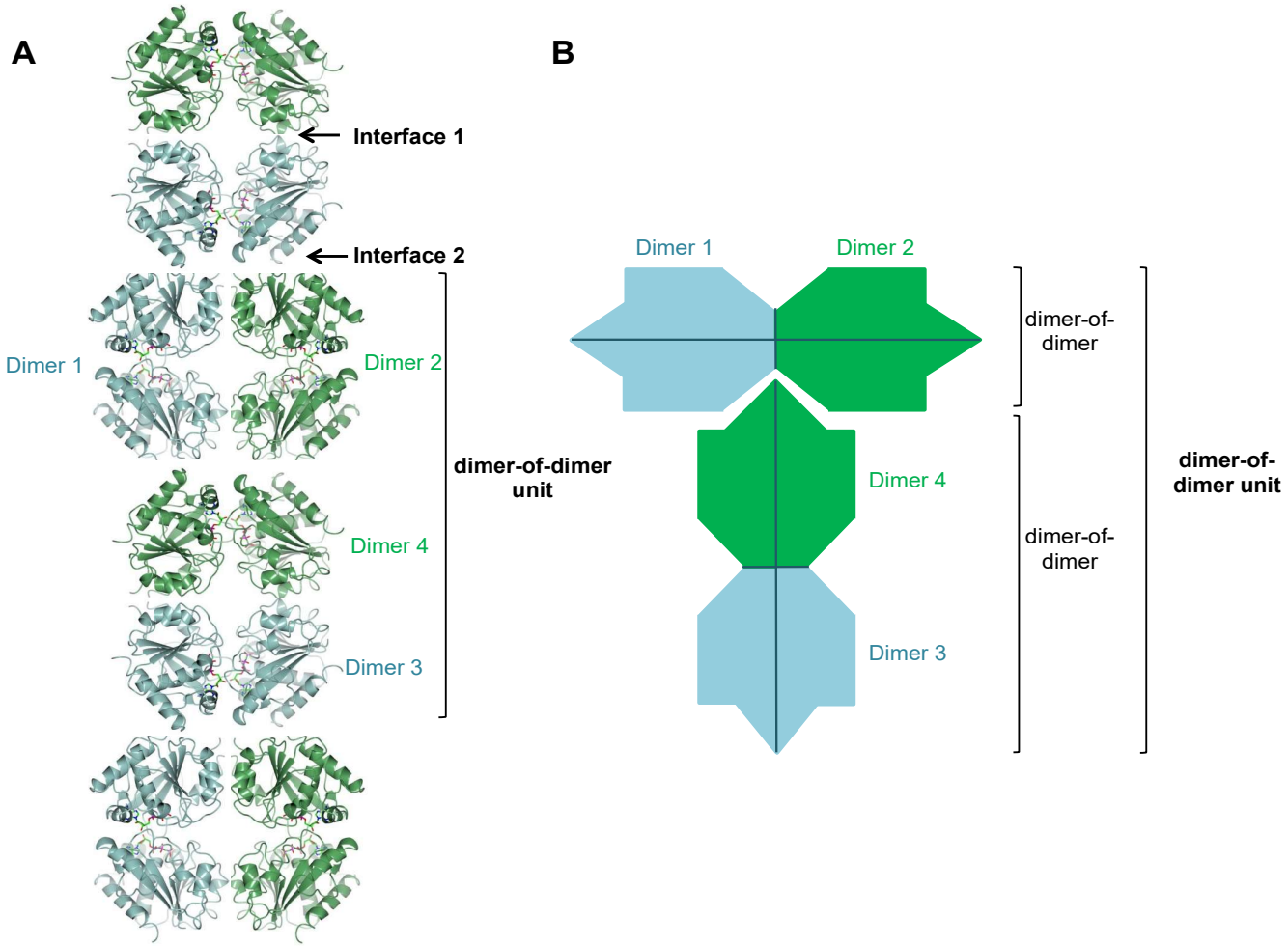

Figure 1.19 - ParF dimer-of-dimer unit. A) A ribbon diagram of ParF-AMPPCP dimers forming the units of the irregular ParF polymers. B) A schematic diagram of the ParF dimer-of-dimer unit. The structural images were generated by using CCP4MG version 2.10.4 using the 4E07 PDB coordinates.

Previously other ParA proteins of type I partition systems were thought to assemble into higher order structures and this was believed to drive plasmid segregation, however this has recently been under much deliberation. The recent models proposed by other type I partition systems, such as the type I partition systems of P1 plasmid and F plasmid, do not include a role for ParA assembly into higher order structures. However the evidence surrounding ParF assembly into higher order structures is clear and still believed to play a crucial role in plasmid segregation. ParF mutants that are unable to form these higher order structures fail to successfully segregate the plasmid, therefore indicating the importance of the assembly of higher order structures. The cycling of ParF assembly and disassembly of higher order filament structures is believed to drive TP228 plasmid segregation. However the link between ATP binding and hydrolysis, the role of ParG in stimulating ParF ATPase activity as well as ParF assembly into higher order structures is still not fully understood in terms of the mechanism behind TP228 plasmid segregation.

1.5.3.2. ParF localises to the nucleoid and shows a dynamic oscillatory behaviour

Many ParA proteins have been shown to display non-specific DNA binding properties *in vitro* and have been seen to localise on the nucleoid *in vivo* (Castaing *et al*., 2008, Hwang *et al*., 2013, Leonard *et al*., 2005, Pratto *et al*., 2008, Ptacin *et al*., 2010, Ringgaard *et al*., 2009). The ParA proteins have also shown dynamic behaviour *in vivo*, however the exact nature of this behaviour appears to be different for different systems. Some ParA proteins appear to move in helical or spiral like structures over the nucleoid to oscillate from one pole of the nucleoid to the other (Ebersbach *et al*., 2006, Ebersbach and Gerdes, 2004, Pratto *et al*., 2008, Ringgaard *et al*., 2009). Other ParA proteins have been seen to oscillate as clusters or distinct foci from one pole of the nucleoid to the other (Hatano *et al*., 2007, Hatano and Niki, 2010, Hwang *et al*., 2013). Even though there are some differences between ParA proteins, it is now evident that the dynamic redistribution of ParA proteins over the nucleoid is crucial to correct positioning and segregation of plasmids and chromosomes.

ParF also localises on the nucleoid *in vivo* and in the presence of ParG and *parH* has been shown to oscillate from one pole of the nucleoid to the other (Ringgaard et al., 2009, McLeod et al., 2016) In the absence of the entire partition system, ParF shows no oscillatory behaviour, thus indicating the importance of ParG in stimulating ParF

assembly and disassembly of higher order structures in the dynamic behaviour of ParF. It is therefore believed, that like other ParA proteins, ParF dynamic behaviour over the nucleoid is important in TP228 plasmid segregation. Structural data has allowed the identification of residues potentially involved in the non-specific DNA binding of ParF and this is investigated as part of this project.

1.6 ParF related proteins

As previously discussed, ParF forms a distinct subgroup within the ParA superfamily and evolutionarily ParF is more closely related to the MinD subgroup of cell division proteins than to other ParA proteins. However, database searches reveal that a number of plasmids encode ParF homologues that are of similar size and show homology throughout the protein to ParF. ParF shows the highest similarity to ParF homologues from plasmid pCL1 from *Chlorobium limicola*, pRA2 from *Pseudomonas alcaligenes* and pVS1 from *Pseudomonas aeruginosa*. However, pTAR from *Agrobacterium tumefaciens*, pVT745 from *Actinobacillus actinomycetemcomitans* and pB171 from *E. coli* also encode ParF homologues (Hayes, 2000, Machón *et al*., 2007). Interestingly, the ParF homologues of these plasmids are sometimes flanked with genes that encode diverse CBP that are unrelated to ParG or even ParB proteins (Fothergill *et al*., 2005).

Even though ParF forms a subgroup of the ParA superfamily, many similarities are seen between the ParF and other ParA Walker-type ATPase proteins involved in plasmid segregation. For example ParA from plasmid P1, SopA from plasmid F, δ from plasmid pSM19035 and ParA from plasmid pB171 share many common features with ParF. These are summarized in Table 1.3 however the partition systems that employ the ParA Walker –type ATPase proteins are discussed in detail earlier in this chapter. The parallels between the partition systems aids further understanding of the TP228 partition system as well as type I partition systems in general.

Table 1.3 - Comparisons of ParA Walker-type ATPase proteins from different type I partition systems

Walker-type ATPase protein	**1. ATPase activity**	**2. Dimeric protein**	**3. Assembles into higher order structures**	**4. Binds non-specific DNA**	**5. Dynamically relocates over the nucleoid**
ParA from plasmid P1	Weak intrinsic ATPase activity - stimulated by partner protein ParB	Yes - in the presence and absence of ATP	Does not form large filament structures but may associate to form small polymers	Yes – when bound to ATP	Yes
SopA from plasmid F	Weak intrinsic ATPase activity - stimulated by partner protein SopB	Yes - when bound to ATP	Does not form large filament structures but may associate to form small polymers	Yes – when bound to ATP	Yes
δ from plasmid pSM19035	Weak intrinsic ATPase activity - stimulated by partner protein ω	Yes - in the presence or absence of nucleotide	δ appears to form globular-like structures made up from 2 – 3 molecules of δ	Yes – when bound to ATP	Yes
ParA from plasmid pB171	Weak intrinsic ATPase activity - stimulated by partner protein ParB	Yes - when bound to ATP	Yes – in the presence of ATP ParA assembles into higher order structures	Yes – when bound to ATP	Yes
Soj from *B.subtilis* (Chromosome encoded)	Weak intrinsic ATPase activity - stimulated by partner protein Spo0J	Yes - when bound to ATP	Not seen to form filament structures	Yes – when bound to ATP	Yes
ParF from plasmid TP228	Weak intrinsic ATPase activity - stimulated by partner protein ParG	Yes - when bound to ATP	Yes - in the presence of ATP ParF assembles into higher order structures	Assumed to bind DNA in a non-specific manner	Yes

1.6.1 The MinD cell division protein of *E. coli*

ParA proteins have been shown to be similar in sequence, structure and activity to the cell division protein MinD from *E. coli* (Lutkenhaus, 2012). As previously discussed, ParF is more closely related to the MinD subgroup of proteins than to ParA partitioning proteins. ParF also shows strong structural homology to MinD (Schumacher *et al*., 2012). Many similarities between MinD and ParA proteins have been identified and it is believed that the proteins utilise a similar mechanism to carry out their cellular function.

The MinCDE system ensures cell division occurs at mid-cell by correctly positioning FtsZ, a tubulin-like GTPase that recruits all the other cell division proteins and actively constricts the membrane to enable cell division (Lutkenhaus, 2007, Osawa and Erickson, 2013). The MinCDE proteins prevent the formation of the Z-ring at poles due to the dynamic oscillatory behaviour displayed by MinD. The MinCDE system in *E. coli* consists of MinC, MinD – a Walker-type ATPase and MinE. MinC is the protein that is responsible for inhibiting cell division, however it has been shown to have a weak inhibition in the absence of MinD (de Boer *et al*., 1992). MinC is composed of two domains: the N-terminal domain is responsible for inhibiting FtsZ assembly into higher order structures and the C-terminal domain is involved in dimerisation as well as the interaction with MinD (Hu and Lutkenhaus, 2000). MinE is a topological specificity factor and is composed of two separable functional domains. The N-terminal domain is able to stimulate MinD ATPase activity and thus inactivates MinCD. The topological specificity comes from the C-terminal domain, which is responsible for MinE dimerisation and stabilises the interaction of MinE with the membrane (Hu and Lutkenhaus, 1999, Lutkenhaus, 2007). Therefore the system works by MinCD acting as a negative regulator of the formation of the Z ring, which is spatially coordinated by the MinE protein allowing the formation of the Z ring (produced from FtsZ) only at the mid-cell position.

MinD, the Walker-type ATPase protein, has been shown bind ATP and dimerise which is important for its function (Lutkenhaus and Sundaramoorthy, 2003). Structures for monomeric MinD have been solved for archaeal species (Cordell and Lowe, 2001, Hayashi *et al*., 2001, Sakai *et al*., 2001), and more recently the structure of C-terminal truncated MinD from *E. coli* was solved in the dimeric ATP-bound state (Wu *et al*., 2011b). The structure showed that Lys^{11} in the deviant Walker A motif is responsible for ATP binding and stabilises the dimer. MinD is at the centre of the MinCDE system

and is able to bind to both MinC and MinE as well as to the membrane. The C-terminal domain of MinD is responsible for membrane binding, where ten residues of the C-terminal domain form an amphipathic helix that inserts into the membrane bilayer (Lutkenhaus and Sundaramoorthy, 2003). The dimeric structure of MinD also revealed the orientation of the protein on the membrane. The C-terminal residues were shown to be in a fixed position towards the bottom of the MinD dimer, suggesting this face of MinD comes close to the membrane. As previously mentioned the structure of MinD and Soj are similar, the analogous face of the Soj dimer is the region involved in non-specific DNA binding (Hester and Lutkenhaus, 2007, Wu *et al*., 2011b). This is interesting as ParF shows structural homology with both MinD and Soj.

The binding sites for MinC and MinE are overlapping but they are exposed at the dimer interface of MinD. The C-terminal domain of MinC has been shown to be responsible for MinD binding, a highly conserved motif (RGSQ) is required for this interaction (Zhou and Lutkenhaus, 2005). The C-terminal domain of MinC is believed to bind near the top of the MinD dimer and in this orientation the N-terminal domain of MinC is free to contact FtsZ and inhibit the assembly of filaments. MinD is therefore able to bind to the membrane and then recruit MinC via this interaction. The binding site of MinE is believed to form upon MinD dimerisation, and the cleft within the dimer would allow the insertion of the MinE N-terminal domain. It was originally thought that a solvent exposed N-terminal domain of MinE would interact with MinD, however recent studies have shown that the binding domain is actually buried within the MinE dimer and therefore MinE must undergo a conformational change in order to allow binding to MinD (Ghasriani *et al*., 2010). MinE binding to MinD causes MinCD release from the membrane. This is due to the fact that MinE stimulates MinD ATPase activity, however only when MinD is membrane bound (Hu and Lutkenhaus, 2001).

As with other ParA proteins, there is much deliberation surrounding MinD assembly into filament structures and the role this plays in the dynamic oscillatory behaviour displayed by MinD. MinD has been shown to form filaments in the presence of ATP; incubation with phospholipid vesicles further promotes this filament formation. The addition of MinE both promotes filament formation by bundling the filaments but also causes the filaments to disassemble due to stimulation of MinD ATPase activity (Suefuji *et al*., 2002). MinD has been shown to bind cooperatively to lipid vesicles and therefore is believed to undergo surface dependent polymerisation and assemble into filaments (Lutkenhaus, 2007). More recently MinD was shown to form filaments,

however only in the presence of MinC. In this filament-forming model it was postulated that MinCD forms a copolymer with alternating MinC and MinD dimer and therefore the filaments do not resemble actin-like or tubulin-like filaments (Ghosal *et al*., 2014).

The oscillatory behaviour of the Min proteins is essential to ensure correct position of the Z ring (Figure 1.20). This oscillation is ATP driven and involves MinD binding ATP, associating with the membrane, MinD-ATPase activity being stimulated by MinE and thus MinD-ADP falling off the membrane and oscillating to the opposite pole of the cell. MinC follows this pole-pole oscillation and therefore inhibits Z ring formation at the poles of the cell (Hu and Lutkenhaus, 2001). As for ParA from plasmid P1, it has been proposed that an important step in MinD oscillation is the timer delay of the nucleoid exchange from ADP to ATP (Lutkenhaus, 2012). MinD was shown to move in a helical track as a protein filament *in vivo* and *in vitro* in the presence of ATP. The binding to phospholipid vesicles, and polymerisation of the protein into helical filaments was believed to reflect the dynamic action of MinD (Hu *et al*., 2002, Shih, 2003, Suefuji *et al*., 2002). More recently different models of the self-organising pattern formation of the Min proteins has been proposed including a diffusion ratchet mechanism (Loose *et al*., 2008). An alternative hypothesis is that mechanical stress by tethering MinD and MinE molecules to the membrane is responsible for the oscillation (Ivanov and Mizuuchi, 2010, Vecchiarelli *et al*., 2016).

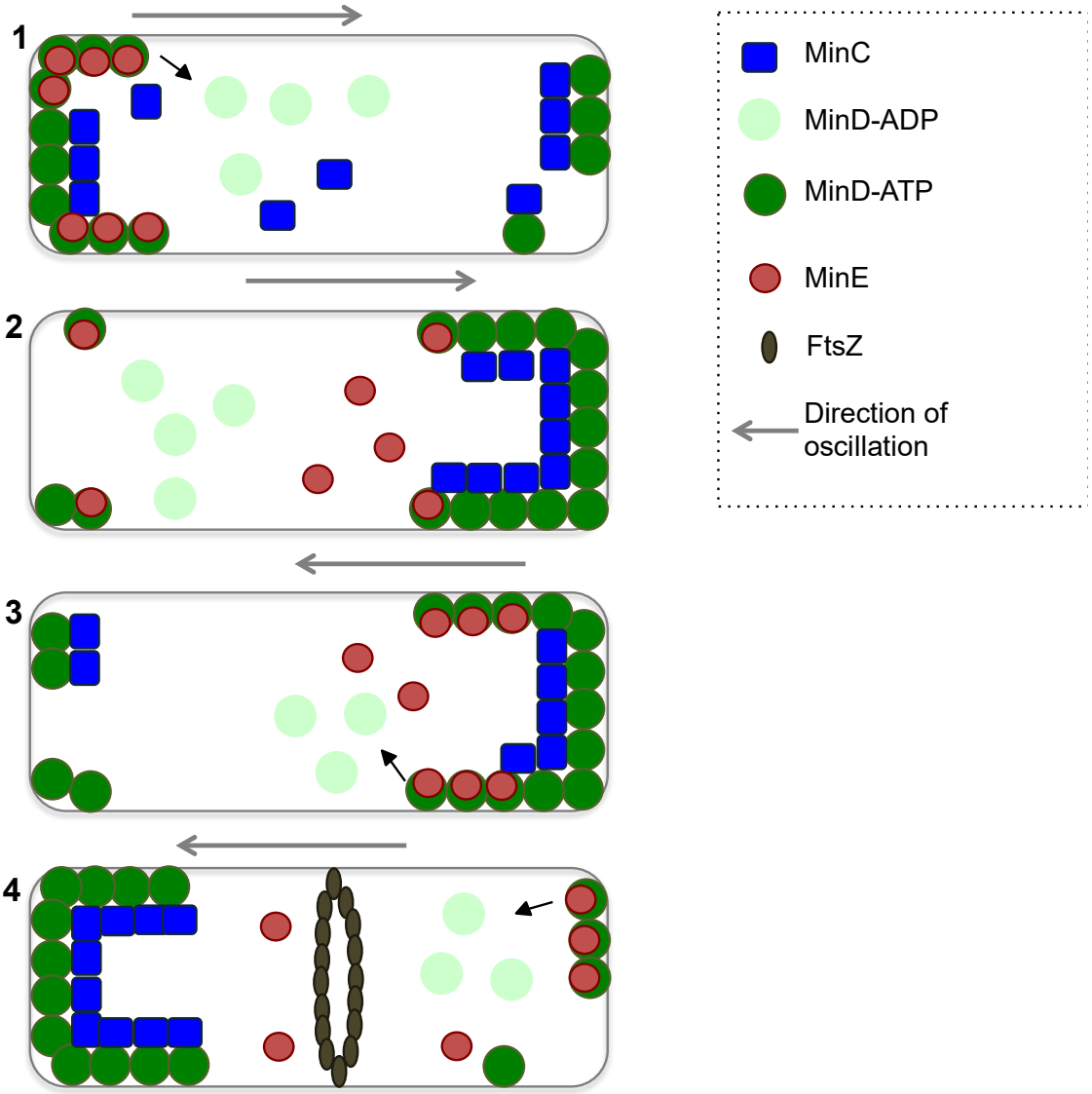

Figure 1.20 - A model of the oscillatory behaviour of the MinCDE system of *E. coli*. 1) MinD-ATP binds to the membrane and MinC is able to bind MinD. 2) MinE binds MinD, which stimulates MinD ATPase activity, and MinD-ADP falls off the membrane and oscillates to the other pole. 3) MinC and MinE follow MinD to the other pole, where MinC binds MinD and MinE begins to bind to MinD again stimulating ATP hydrolysis. 4) MinD-ADP oscillates to the other pole undergoes ADP-ATP exchange which allows rebinding at the new pole. MinC again follows. This oscillation prevents the formation of the Z ring at the poles therefore allowing the Z ring to form at mid cell for cell division. Adapted from (Lutkenhaus, 2007).

1.7 Project aims

Chromosome and plasmid segregation have been the subject of extensive studies, however there are still many areas that are not fully understood. Low copy number plasmids, many of which are multidrug resistant plasmids, have been important model systems that have provided further understanding of partition systems in prokaryotes. As antibiotic resistance is now becoming one of the most significant health concerns for the public, understanding how these drug resistant plasmids are passed from one generation to the next is critical and could provide potential drug targets to combat increasing antibiotic resistance. The aim of this project is to study the multidrug resistant, low copy number plasmid TP228 with an overall objective of gaining a better understanding of the molecular mechanism and dynamics employed by this plasmid to ensure accurate plasmid partitioning. Plasmid TP228 utilises a type Ib partition system that consists of the *parFGH* partition cassette, which harbours a partition site *parH* and encodes two *trans*-acting partition proteins ParF (a Walker-type ATPase) and ParG (a CBP). ParF is the motor protein that drives plasmid partitioning, the exact mechanism of which is still not fully understood. ParF has been shown to assemble into higher order structures, which are believed to be crucial for accurate plasmid partitioning. Other ParA Walker-type ATPase proteins have been shown to bind DNA in a non-specific manner and dynamically associate with the nucleoid, which is crucial for plasmid partitioning. ParF has also been shown to localise on the nucleoid, therefore understanding the role of ParF non-specific DNA binding properties and how this plays a role in plasmid partitioning is important. The main objectives for this study can broken down as follows:

1. Subunit association – how does ParF assemble and disassemble into higher order structures beginning with dimer formation and then dimer-dimer interactions
2. Analysing how ParF binds non-specific DNA and the way through which this function affects plasmid partition
3. Understanding the link between ParF assembly into higher order structures and the ability to bind to DNA non-specifically and to associate with the nucleoid *in vivo*.

Specifically these objectives will be achieved as detailed below:

- Analysing the monomer-monomer interface of ParF by constructing targeted mutations and analysing the resulting phenotype by a variety of different experimental techniques *in vitro* and *in vivo*
- Analysing the dimer-dimer interface of ParF by constructing targeted mutations at interfaces identified as being important in ParF assembly into higher order structures. The resulting phenotypes will be analysed using a variety of different experimental techniques *in vitro* and *in vivo*
- Confirming ParF is able to bind non-specific DNA *in vitro*
- Identifying residues potentially involved in ParF and non-specific DNA binding and constructing targeted mutations and analysing the resulting phenotype *in vitro*
- Investigating the cellular localisation of ParF and ParF mutants and also their dynamic behaviour *in vivo* using a range of microscopy techniques.

Chapter 2: Materials and Methods

2.1 Bacterial strains and plasmids

2.1.1 Bacterial Strains

All *Escherichia coli* strains used in this work are listed in Table 2.1. *E. coli* DH5α and BL21(DE3) were used for cloning and protein expression, respectively. Other strains were used in specific assays as indicated in Table 2.1. All strains were made chemically competent as described by the method in section 2.2.1.

Table 2.1 – List of bacterial strains

Strain	**Genotype**	**Application**
DH5α	F– Φ80*lac*ZΔM15 Δ(*lac*ZYA-*arg*F) U169 *rec*A1 *end*A1 *hsd*R17 (rK–, mK+) *pho*A *sup*E44 λ– *thi*-1 *gyr*A96 *rel*A1	Cloning
BL21 (DE3)	*fhu*A2 *[lon] omp*T *gal (λ DE3) [dcm]* Δ*hsd*S	Gene overexpression and protein production
BR825	*pol*A which has inactivated DNA polymerase gene for supporting only low copy number replication. When there is the mutation in polA, the mechanism for replication from the medium copy number origin MB1 is not supported and so the only option for replication is using the low copy origin. (Ludtke *et al*., 1989).	Plasmid partition assay
SP850	*rel*A1 *spo*T (*cya*-1400)::Km *thi*-1 e14-λ-	Bacterial two-hybrid assay
BW25113	[Δ(*ara*D-*ara*B)*567*Δ(*rha*D-*rha*B)*568* Δ*lacZ4787* (::rrnB-3) *hsd*R514 *rph*-1],	Microscopy

2.1.2 Plasmids

The plasmids used in this work are described in Table 2.2. Plasmids were either available from laboratory stocks or constructed during the course of this work.

Table 2.2 – List of Plasmids

Plasmid name	**Details**	**Antibiotic selection**
pFH450	A pBR322 derivative with P1 and ColE1 origins of replication without any partition elements Hayes (2000).	Chloramphenicol
pFH547	A pBR322 derivative with P1 and ColE1 origins of replication with the TP228 segregation cassette (~ 1.2 kb). pFH547 habours the wild type partition cassette *parFGH* (Hayes, 2000).	Chloramphenicol
pET22b(+)	An overexpression vector with the bacteriophage T7 promoter and $(His)_6$-tag at the C-terminal end (Novagen).	Ampicillin
pDB-ParG	The plasmid partition gene *parG* cloned into vector pET22b(+)(Barilla *et al*., 2005).	Ampicillin
pDB-ParF	The plasmid partition gene *parF* cloned into vector pET22b(+) (Barilla *et al*., 2005).	Ampicillin
pT25	A pACYC184 derivative with a T25 fragment corresponding to the amino acids 1–224 of the catalytic domain of adenylate cyclase, CyaA (Karimova *et al*., 1998).	Ampicillin
pT25-ParF	The plasmid partition gene *parF* cloned into pT25 (Barillà and Hayes, 2003).	Ampicillin

pT25-ParG	The plasmid partition gene *parG* cloned into pT25 (Barillà and Hayes, 2003).	Ampicillin
pT18	A derivative of pBluescript II KS having a T18 fragment corresponding to the amino acids 225–399 of the catalytic domain of adenylate cyclase, CyaA (Karimova *et al*., 1998).	Chloramphenicol
pT18-ParG	The plasmid partition gene *parG* cloned into pT18 (Barillà and Hayes, 2003).	Chloramphenicol
pBM20	A derivative of pFH547 in which the gene encoding the fluorescent protein mCherry is cloned in the frame with the partition gene *parG* (McLeod et al., 2016)	Chloramphenicol
pBM22	A derivative of pBM20 containing a $lacO_{120}$ (Lau *et al*., 2004) array (McLeod et al., 2016)	Chloramphenicol
pBAD-LacI-EBFP2	A plasmid harbouring a truncated version of *lacI* missing the last 12 codons and in frame with the gene encoding EBFP2 in pBAD-ebfp2 (Ai *et al*., 2007) (McLeod et al., 2016)	Spectinomycin
pBM40	A plasmid containing the *gfp* variant *gene emerald* cloned in the frame with *parF,* under the control of the arabinose-inducible promoter P_{BAD} in pBAD30 (McLeod et al., 2016)	Ampicillin
pGA-ParF-I102A	*parFI102A* allele cloned into pFH547 vector by using *Cla*I and *Stu*I restriction sites.	Chloramphenicol

pGA-ParF-I103A	*parFI103A* allele cloned into pFH547 vector by using *Cla*I and *Stu*I restriction sites.	Chloramphenicol
pGA-ParF-P104A	*parFP104A* allele cloned into pFH547 vector by using *Cla*I and *Stu*I restriction sites.	Chloramphenicol
pGA-ParF-V105A	*parFV105A* allele cloned into pFH547 vector by using *Cla*I and *Stu*I restriction sites.	Chloramphenicol
pGA-ParF-T106A	*parFT106A* allele cloned into pFH547 vector by using *Cla*I and *Stu*I restriction sites.	Chloramphenicol
pGA-ParF-P107A	*parFP107A* allele cloned into pFH547 vector by using *Cla*I and *Stu*I restriction sites.	Chloramphenicol
pGA-ParF-S108A	*parFS108A* allele cloned into pFH547 vector by using *Cla*I and *Stu*I restriction sites.	Chloramphenicol
pGA-ParF-P109R	*parFP109R* allele cloned into pFH547 vector by using *Cla*I and *Stu*I restriction sites.	Chloramphenicol
pGA-ParF-M146A	*parFM146A* allele cloned into pFH547 vector by using *Cla*I and *Stu*I restriction sites.	Chloramphenicol
pGA-ParF-V149F	*parFV149F* allele cloned into pFH547 vector by using *Cla*I and *Stu*I restriction sites.	Chloramphenicol

pGA-ParF-K151A	*parFK151A* allele cloned into pFH547 vector by using *Cla*I and *Stu*I restriction sites.	Chloramphenicol
pGA-ParF-K160A	*parFK160A* allele cloned into pFH547 vector by using *Cla*I and *Stu*I restriction sites.	Chloramphenicol
pGA-ParF-K160E-R163E	*parFK160E-R163E* allele cloned into pFH547 vector by using *Cla*I and *Stu*I restriction sites.	Chloramphenicol
pGA-ParF-S185W	*parFS185W* allele cloned into pFH547 vector by using *Cla*I and *Hpa*I restriction sites.	Chloramphenicol
pGA-ParF-S186F	*parFS186F* allele cloned into pFH547 vector by using *Cla*I and *Hpa*I restriction sites.	Chloramphenicol
pGA-ParF-K199A	*parFK199A* allele cloned into pFH547 vector by using *Cla*I and *Hpa*I restriction sites.	Chloramphenicol
pGA-ParF-R203A	*parFR203A* allele cloned into pFH547 vector by using *Cla*I and *Hpa*I restriction sites.	Chloramphenicol
pET-ParF-I102A	*parFI102A* allele cloned into pET-22b (+) vector by using *Nde*I and *Xho*I restriction sites.	Ampicillin
pET-ParF-P107A	*parFP107A* allele cloned into pET-22b (+) vector by using *Nde*I and *Xho*I restriction sites.	Ampicillin

pET-ParF-S108A	*parFS108A* allele cloned into pET-22b (+) vector by using *Nde*I and *Xho*I restriction sites.	Ampicillin
pET-ParF-P109R	*parFP109R* allele cloned into pET-22b (+) vector by using *Nde*I and *Xho*I restriction sites.	Ampicillin
pET-ParF-R139A	*parFR139A* allele cloned into pET-22b (+) vector by using *Nde*I and *Xho*I restriction sites.	Ampicillin
pET-ParF-K151A	*parFK151A* allele cloned into pET-22b (+) vector by using *Nde*I and *Xho*I restriction sites.	Ampicillin
pET-ParF-K160E-R163E	*parFK160E-R163E* allele cloned into pET-22b (+) vector by using *Nde*I and *Xho*I restriction sites.	Ampicillin
pET-ParF-S185W	*parFS185W* allele cloned into pET-22b (+) vector by using *Nde*I and *Xho*I restriction sites.	Ampicillin
pT18-ParF-K64A-V89Y-M96A	*parFK64A-V89Y-M96A* allele cloned into pT18 vector by using *Kpn*I and *Hind*III restriction sites.	Ampicillin
pT18-ParF-P107A	*parFP107A* allele cloned into pT18 vector by using *Kpn*I and *Hind*III restriction sites.	Ampicillin
pT18-ParF-S108A	*parFS108A* allele cloned into pT18 vector by using *Kpn*I and *Hind*III restriction sites.	Ampicillin
pT18-ParF-P109R	*parFP109R* allele cloned into pT18 vector	Ampicillin

	by using *Kpn*I and *Hind*III restriction sites.	
pT18-ParF-F112A	*parFF112A* allele cloned into pT18 vector by using *Kpn*I and *Hind*III restriction sites.	Ampicillin
pT18-ParF-R139A	*parFR139A* allele cloned into pT18 vector by using *Kpn*I and *Hind*III restriction sites.	Ampicillin
pT18-ParF-V149F	*parFV149F* allele cloned into pT18 vector by using *Kpn*I and *Hind*III restriction sites.	Ampicillin
pT18-ParF-K151A	*parFK151A* allele cloned into pT18 vector by using *Kpn*I and *Hind*III restriction sites.	Ampicillin
pT18-ParF-K160E-R163E	*parFK160E-R163E* allele cloned into pT18 vector by using *Kpn*I and *Hind*III restriction sites.	Ampicillin
pT25-ParF-K64A-V89Y-M96A	*parFK64A-V89Y-M96A* allele cloned into pT25 vector by using *Kpn*I and *Pst*I restriction sites.	Chloramphenicol
pT25-ParF-P107A	*parFP107A* allele cloned into pT25 vector by using *Kpn*I and *Pst*I restriction sites.	Chloramphenicol
pT25 ParF-S108A	*parFS108A* allele cloned into pT25 vector by using *Kpn*I and *Pst*I restriction sites.	Chloramphenicol
pT25-ParF-P109R	*parFP109R* allele cloned into pT25 vector by using *Kpn*I and *Pst*I restriction sites.	Chloramphenicol
pT25-ParF-L110A	*parFL110A* allele cloned into pT25 vector by using *Kpn*I and *Pst*I restriction sites.	Chloramphenicol
pT25-ParF-F112A	*parFF112A* allele cloned into pT25 vector	Chloramphenicol

	by using *Kpn*I and *Pst*I restriction sites.	
pT25-ParF-R139A	*parFR139A* allele cloned into pT25 vector by using *Kpn*I and *Pst*I restriction sites.	Chloramphenicol
pT25-ParF-K151A	*parFK151A* allele cloned into pT25 vector by using *Kpn*I and *Pst*I restriction sites.	Chloramphenicol
pT25-ParF-K160E-R163E	*parFK160E-R163E* allele cloned into pT25 vector by using *Kpn*I and *Pst*I restriction sites.	Chloramphenicol
pBM20-ParF-K64A-V89Y-M96A	*parFK64A-V89Y-M96A* allele cloned into pBM20 vector by using *Mfe*I and *Hpa*I restriction sites (McLeod et al., 2016)	Chloramphenicol
pBM20-ParF-S108A	*parFS108A* allele cloned into pBM20 vector by using *Mfe*I and *Hpa*I restriction sites.	Chloramphenicol
pBM20-ParF-P109R	*parFP109R* allele cloned into pBM20 vector by using *Mfe*I and *Hpa*I restriction sites.	Chloramphenicol
pBM20-ParF-R139A	*parFR139A* allele cloned into pBM20 vector by using *Mfe*I and *Hpa*I restriction sites.	Chloramphenicol
pBM20-ParF-K151A	*parFK151A* allele cloned into pBM20 vector by using *Mfe*I and *Hpa*I restriction sites.	Chloramphenicol
pBM20-ParF-K160E-R163E	*parFK160E-R163E* allele cloned into pBM20 vector by using *Mfe*I and *Hpa*I restriction sites.	Chloramphenicol

pBM20-ParF-R169A	*parFR169A* allele cloned into pBM20 vector by using *Mfe*I and *Hpa*I restriction sites.	Chloramphenicol
pBM22-ParF-S108A	*parFS108A* allele cloned into pBM22 vector by using *Mfe*I and *Hpa*I restriction sites.	Chloramphenicol
pBM22-ParF-K160E-R163E	*parFK160E-R163E* allele cloned into pBM22 vector by using *Mfe*I and *Hpa*I restriction sites.	Chloramphenicol
pBM40-ParF-K64A-V89Y-M96A	*parFK64A-V89Y-M96A* allele cloned into pBM40 vector by using *Spe*I and *Xba*I restriction sites (McLeod et al., 2016)	Ampicillin
pBM40-ParF-S108A	*parFS108A* allele cloned into pBM40 vector by using *Spe*I and *Xba*I restriction sites.	Ampicillin
pBM40-ParF-R139A	*parFR139A* allele cloned into pBM40 vector by using *Spe*I and *Xba*I restriction sites.	Ampicillin
pBM40-ParF-P109R	*parFP109R* allele cloned into pBM40 vector by using *Spe*I and *Xba*I restriction sites.	Ampicillin
pBM40-ParF-K151A	*parFK151A* allele cloned into pBM40 vector by using *Spe*I and *Xba*I restriction sites.	Ampicillin
pBM40-ParF-K160E-R163E	*parFK160E-R163E* allele cloned into pBM40 vector by using *Spe*I and *Xba*I restriction sites.	Ampicillin
pBM40-ParF-R169A	*parFR169A* allele cloned into pBM40 vector by using *Spe*I and *Xba*I restriction	Ampicillin

	sites.	
pBM40-Emerald	*emerald* gene cloned into pBM40 without *parF* using the restriction sites *Xba*I and *Spe*I	Ampicillin

2.2 Media and antibiotics

2.2.1 Media

2.2.1.1 Luria-Bertani solid and liquid media

Bacteria were grown in Luria-Bertani (LB) broth (Fisher Scientific) or on LB agar (Formedium). The composition of the medium is given in Table 2.3. LB broth and LB agar were prepared as per manufacturer's instructions by dissolving the specified amount of powder in the required volume of distilled water. LB broth and agar were sterilised by autoclaving at 121 °C for 20 minutes. The media were supplemented with the appropriate antibiotic when required.

Table 2.3 – Composition of LB medium

Component	**Concentration g/L**
Tryptone	10
Yeast extract	5
Sodium Chloride	10
Agar – for solid medium only	12

2.2.1.2 MacConkey agar

MacConkey agar (Oxoid) was used for bacterial two-hybrid assays. The composition of MacConkey agar is given in Table 2.4. The agar was prepared as per manufacturer's instructions by dissolving 40 g of the powder in 1 L of dH_20. To make the agar more

solid, 6 g of agar (technical no. 3) (Oxoid) were added. The medium was sterilised by autoclaving at 121 °C for 20 minutes.

Table 2.4 – Composition of MacConkey agar

Component	**Concentration g/L**
Peptone	20
Lactose	10
Bile salts	5
Sodium chloride	5
Neutral red	0.075
Agar	12
pH 7.4 ± 0.2	

2.2.1.3 M9 Medium

A 10X M9 stock solution was prepared as per Table 2.5. The components were dissolved in distilled water to a final volume of 1 L and autoclaved at 121°C for 20 minutes. M9 medium was then prepared as per Table 2.6. Other than 10X M9 stock solution the components of M9 medium were filter sterilised using a 0.2 μm filter.

Table 2.5 - Components of 10X M9 stock solution

Component	Quantity (g)
$Na_2HPO_4.7H2O$	64
KH_2PO_4	15
NaCl	2.5
NH_4Cl	5

Table 2.6 – Components of M9 medium

Components
1X M9 stock solution
2 mM $MgSO_4$
0.1 mM $CaCl_2$
0.2 % Glycerol

2.2.2 Antibiotics

Antibiotics used in this work are described in Table 2.7.

Table 2.7 – Antibiotics

Antibiotic	Stock concentration (mg/ml)	Final concentration used (μg/ml)
Chloramphenicol (Cm)	30 (dissolved in ethanol)	30 for cloning 10 for partition assays
Ampicillin (Amp)	100	100
Kanamycin (Kan)	50	10
Spectinomycin (Spec)	50	50

2.3 Recombinant DNA techniques

2.3.1 Plasmid DNA isolation – small scale

A bacterial colony was selected and inoculated in 5 ml of sterile LB broth containing the appropriate antibiotic using aseptic technique throughout. The culture was incubated overnight at 37 °C with shaking. Following incubation plasmid DNA isolation was carried out using Macherey-Nagel Nucleospin Plasmid miniprep kit as per the manufacturer's instructions. The 5 ml cultures were centrifuged at 11 000 x g for 1 minute to pellet the cells. To lyse the cells, the supernatant was discarded and the cell pellet was resuspended in 250 µl Buffer A1 before 250 µl of Buffer A2 was added and the mixture incubated for 5 minutes at room temperature. 300 µl of Buffer A3 was added and the mixture was inverted to mix. This was then centrifuged at 11 000 x g for 10 minutes and the supernatant removed and loaded onto the column to bind the DNA. This was then centrifuged at 11 000 x g for 1 minute and the flow through was discarded. Two wash steps were then carried out firstly with 600 µl of AW and then 500 µl of Buffer 4. After each the column was centrifuged at 11 000 x g for 1 minute. After the flow through was discarded the column was centrifuged one final time to remove any excess wash. The plasmid DNA was eluted in 50 µl of sterile Milli-Q water. Isolated plasmid DNA was stored at -20 °C. Details of all buffers are in the kits.

2.3.2 Polymerase chain reaction (PCR)

Amplification of DNA was carried out using PCR in an Eppendorf- Mastercycler Personal. PCR reactions were prepared on ice as per Table 2.8 with a final reaction volume of 60 µl. 5 mM stocks of each deoxynucleotide triphosphate (dNTPs) (Roche) were prepared by diluting 100 mM stocks with Milli-Q water. Specifically designed primers, listed in Table 2.9 were synthesised by Sigma Aldrich. The primers were resuspended in 1 ml of Milli-Q water to give the concentration as specified by the manufacturer for each individual primer. Primer stocks are then diluted to a final concentration of 5 pmol/µl. The PCR programme used is shown in Table 2.10, the annealing temperature was altered according to the primers being used and the extension time was dependent on the length of the PCR product.

Table 2.8 – PCR reaction

Component	Volume (µl)
Template DNA (1:10 dilution of plasmid DNA prepared as in 2.2.1)	3
Forward primer (5 pmol/ µl)	3
Reverse Primer (5 pmol/ µl)	3
dNTPs (dATP, dCTP, dGTP, dTTP) (5 mM)	2.4 of each
10x Pfu buffer	6
dH_2O	34.4
Pfu polymerase (Thermo Scientific)	1 (2 units)

Table 2.9 – List of Primers

Primer Name	**Sequence 5' – 3'**
ParF-S185W-Forw	AGCGTGTTTGAATGGAGTGATGGCGCT
ParF-S185W-Rev	AGCGCCATCACTCCATTCAAACACGCT
ParF-S186W-Forw	GTCTTTGAATCCTGGGATGGCGCTGCA
ParF-S186W-Rev	TGCAGCGCCATCCCAGGATTCAAACAC
ParF-S186F- Forw	GTGTTTGAATCCTTTGATGGCGCTGCA
ParF-S186F-Rev	TGCAGCGCCATCAAAGGATTCAAACAC
ParF-P104A-Forw	CTGGTAATTATCGCTGTCACCCCCAGC

ParF-P104A-Rev	GCTGGGGGTGACTGCGATAATTACCAG
ParF-P107A - Forw	ATCCCTGTCACCGCCAGCCCTCTGGAT
ParF-P107A-Rev	ATCCAGAGGGCTGGCGGTGACAGGGAT
ParF-I102A-Forw	AGCGACCTGGTAGCTATCCCTGTCACC
ParF-I102A - Rev	GGTGACAGGGATAGCTACCAGGTCGCT
ParF-I103A-Forw	GACCTGGTAATTGCCCCTGTCACCCCC
ParF-I103A - Rev	GGGGGTGACAGGGGCAATTACCAGGTC
ParF-V105A-Forw	GTAATTATCCCTGCCACCCCCAGCCCT
ParF-V105A-Rev	AGGGCTGGGGGTGGCAGGGATAATTAC
ParF-T106A-Forw	ATTATCCCTGTCGCCCCCAGCCCTCTG
ParF-T106A-Rev	CAGAGGGCTGGGGGCGACAGGGATAAT
ParF-S108A - Forw	CCTGTCACCCCCGCCCCTCTGGATTTC
ParF-S108A - Rev	GAAATCCAGAGGGGCGGGGGTGACAGG
OrF44upBT	AAATATTATTATGCTCTATGATTAACATAGA GCAAACATGGGA
OrF44upcomplement	TCCCATGTTTGCTCTATGTTAATCATAGAG CATAATAATATTT
ParF-K151A-Forw	TTGAATGTGCTTGCAGAAAGTATCAAA
ParF-K151A-Rev	TTTGATACTTTCTGCAAGCACATTCAA
ParF-K160A-Forw	GACACCGGTGTTGCAGCATTTCGTACA

ParF-K160A-Rev	TGTACGAAATGCTGCAACACCGGTGTC
ParF-K199A-Forw	GAAATCCTTACAGCAGAGATAGTTAGA
ParF-K199A-Rev	TCTAACTATCTCTGCTGTAAGGATTTC
ParF-R203A-Forw	AAAGAGATAGTTGCAATATTTGAGTAA
ParF-R203A-Rev	TTACTCAAATATTGCAACTATCTCTTT
ParF-K160A-Forw21	ACCGGTGGTGCAGCATTTCGT
ParF-R203A-Rev30	CTCAAATATTGCAACTATCTCTTTTGTAAG
ParF-EGFP-pBAD30-XbaI-F21	CCGGTCTCTAGAAAGAAGGAGATATACATA TGAAAGTGATCTCATTTCTG
ParF-M146A-Forw	GAAATGGCAACCGCGTTGAATGTGCTT
ParF-M146A-Rev	AAGCACATTCAACGCGGTTGCCATCTT
hypE700-Forw(btn)	TTGAACAATATACAACTCGCCCAC
hype700-Rev(DIG)	ACTCATGGGCGACCGCATTCACGC
hpaD700-Forw(btn)	ATGGGCAAGTTAGCGTTAGCAGCA
hpaD700-Rev(DIG)	AGTCGGCGTACTCCGGCAACATGG
ParF-P109R-Forw-New	GTCACCCCCAGCCGTCTGGATTTCTCC

ParF-P109R-Rev-New	GGAGAAATCCAGACGGCTGGGGGTGAC
ParF-K160E-R163E-Forw	ACCGGTGGTGAAGCATTTGAAACAGCTATT
ParF-K160E-R163E-Rev	AATAGCTGTTTCAAATGCTTCAACACCGGT
EGFP-Forw-XbaI	CCGGTCTCTAGAAAAGAAGGAGATATACAT ATGCCACCTACGGCA
ParF-V149F-Forw	ACCATGTTGAATTTTCTTAAAGAAAGT
ParF-V149F-Rev	ACTTTCTTTAAGAAAATTCAACATGGT
ParF-Forward	GAGGAAACCATATGAAAGTGATCTCATTT
ParF-Back	CACACACTCGAGCTCAAATATTCTAAC
ParF-ClaIupstream-F	ACCGGTGTTAAAGCATTTCGTACA
ParG2 - R	TTCTTTCTCGAGTTCGTTCTCTTTGAG
DNA20merHH Forward	AATTACTCAATTACTCAATT
DNA20merHH Reverse	AATTGAGTAATTGAGTAATT
206	GCAAATGATCAGGCCTCTTTCCCT
InvertRepPromoForBT	AACCTTTACTCATACAAAGAGTATG
InvertRepPromoRev	ACCTGAACCCCCTTTCGGATTCAGA
ParF-T18-Forw	TCTCTCGGTACCATGAAAGTGATCTCATTT

ParF-T18-Rev	TCTCTCAAGCTTTCCTCAAATATTCTAAC
ParF-T25-Forw	ATATATCTGCAGGGATGAAAGTGATCTCATTT
ParF - T25- Rev	TCTCTCGGTACCTTTACTCAAATATTCTAAC
ParF-EGFP-Forw	CGCACTGCAGTAATAAGAAGGAGATATACA TATGAAAGTGATCTCAAAG
ParF-EGFP-Rev	CCGCGTACTAGTCTCAAATATTCTAACTATCTC
pBAD-R	GTTTTATCAGACCGCTTCTGCG
ParF-EGFP-pBAD30-hind-R	CCGCGACAAGCTTTTACTTGTACAGCTCGTCCATGCC

Table 2.10 – Thermocycler programme

Step	Temperature (°C)	Time (Minutes)	Number of cycles
1. Initial Denaturation	93	3	1
2. Denaturation	92	1	30
3. Annealing	Dependent on primers used (range 40-70)	1	
4. Extension	72	30 seconds – 2 minutes dependent on product size	
6. Final Extension	72	6	1
7. Hold	10	Unlimited	

2.3.3 Restriction Enzyme Digest

Restriction enzyme digests were used as part of the cloning process throughout the project. All restriction enzymes were sourced from Promega, New England Biolabs and Thermo Scientific. All restriction enzymes were at a concentration of 10 units/µl. Primers were designed in order to incorporate specific restrictions sites on the DNA during a PCR that corresponded to restriction sites on the plasmid. Both the PCR DNA product and the plasmid could then be digested with the same restriction enzymes. Restriction enzyme digests were also used to check for positive clones. All purified plasmid DNA was at a concentration of 80 – 100 ng/µl. Digestion reactions were set up as per Table 2.11. Restriction digestion reactions were carried out at 37 °C for 2 hours.

Table 2.11 – Restriction digest reactions

Component	**Volume for cloning restriction digests (µl)**		**Volume for checking positive clones (µl)**
	PCR product	Purified plasmid DNA	
Purified DNA	40	30	16
Restriction Enzyme 1	1.5	3	1
Restriction Enzyme 2	1.5	3	1
10X Buffer – compatible for both enzymes as specified by manufacture	6	6	3
dH_2O	11	18	9
Total reaction volume	60		30

2.3.4 Ethanol precipitation

Ethanol precipitation was carried out to purify DNA from PCRs or restriction enzyme digests. The volume of DNA was made up to 60 µl if not so already. 20 µl of 3M sodium acetate (pH5.3) and 220 µl of 100% ice cold ethanol was added to the DNA and

then mixed thoroughly by inverting the tube several times. The mixture was then incubated at -20 °C for 2 hours. After incubation, the mixture was centrifuged at 4 °C for 30 minutes at 11,000 xg. The supernatant was carefully removed using a pipette avoiding disrupting the DNA pellet and 500 µl of 70% ice cold ethanol was added. The mixture was centrifuged again at 4 °C for 10 minutes at 11,000 xg. The supernatant was carefully removed with a pipette and any remaining ethanol was removed by leaving the tube open on a heating block (30 °C – 37 °C) for 10 minutes. The DNA was resuspended in 30 – 40 µl of Milli-Q water.

2.3.5 Alkaline phosphate treatment of DNA

Alkaline phosphatase was used to dephosphorylate restriction enzyme digested plasmid DNA in order to prevent re-ligation of the plasmid during the ligation reaction. Digested plasmid DNA was made up to a volume of 86 µl with Milli-Q water. To this 10 µl of 10X phosphatase buffer (NEB) and 2 µl (1 unit) of Alkaline Phosphatase enzyme was added. The reaction was incubated at 37 °C for 30 minutes and then another 2 µl of Alkaline phosphatase enzyme was added before a further 30 minute incubation at 37 °C. After incubation, 10 µl of 200 mM ethylene glycol tetraacetic acid (EGTA) was added to the reaction, which was then incubated at 75 °C for 10 minutes. A QIAGEN gel extraction kit was used to clean up the reaction. To a spin column provided in the kit, the reaction mixture and 300 µl of QG buffer was added and then centrifuged for 1 minute at 11,000 xg. The flow-through was discarded and the column washed twice with 750 µl of PE buffer (with 100% ethanol added). The flow-through was discarded and the empty column centrifuged for a further 2 minutes at 11,000 xg to remove any residual ethanol. The plasmid DNA was then eluted in 40 µl of Milli-Q water.

2.3.6 Agarose gel electrophoresis

All PCR products and DNA digestions were analysed using 1% w/v agarose gel electrophoresis. The gel was prepared by dissolving the required amount of agarose in 1X TAE buffer (40 mM Tris, 20 mM acetic acid, 1 mM EDTA) and adding 0.01% v/v SYBR Safe (fluorescent dye that intercalates with the DNA to allow visualisation under UV light). 6X loading dye (10 mM Tris.HCl, pH 7.6, 60% glycerol, 0.3% xylene cyanol, 0.3% bromophenol blue, 60 mM EDTA) was added to the DNA samples before loading on the gel (5 µl – 20 µl samples loaded). 1 µl of a 1 Kb DNA ladder (Thermo

scientific), with defined band sizes, was run on the gel to allow the size of the DNA fragments to be estimated. Agarose gels were electrophoresed at 110 V for 30 minutes or until DNA fragments were well separated. The DNA fragments were visualised using the BIORAD Gel doc EZ imager using Image lab 4.0.1 software to analyse the images. Flash gels (Lonza) were also used to analyse DNA. The Flash gel is a precast, prestained agarose gel and buffer in which samples can be loaded and bands visualised within 5 minutes.

2.3.7 Gel extraction of DNA fragments

DNA samples were ran on 1% w/v agarose gel and then gel extracted using a QIAGEN gel extraction kit following the manufacturer's instructions.

2.3.8 DNA ligation

After the DNA fragment (insert) and plasmid DNA (vector) were digested as per section 2.3.3 and the vector was dephosphorylated as per section 2.3.5, the ligation reaction was set up. The insert to vector ratio was 2:1 in the ligation reaction unless after visualisation on an agarose gel the ratio needed to be altered to ensure successful ligation. To the insert and vector, 3 µl of 10X T4 ligation buffer (Thermo scientific) and 1 µl (2.5 units) of T4 ligase (Thermo scientific) were added and the reaction was made up to 30 µl with Milli-Q water. The reactions were incubated at room temperature for 3 hours and then transformed into competent *E. coli* DH5α cells.

2.3.9 Preparation of competent cells

The desired strain of *E. coli* was streaked aseptically onto a sterile LB agar plate and incubated at 37 °C overnight. Following incubation, a single colony was picked from the plate and inoculated in 10 ml of LB broth. The culture was incubated at 37 °C overnight with shaking. 0.3 ml of the overnight culture was inoculated in 60 ml of sterile LB broth and grown at 37 °C with shaking until the required growth was reached. The bacterial growth was monitored by measuring the absorbance at 600 nm (A_{600}) using a spectrophotometer. The A_{600} was taken until the culture reached the optimal A_{600} of 0.4 - 0.6. The culture was then incubated on ice for 10 minutes and then centrifuged at 2,000 xg, 4 °C for 5 minutes to pellet the cells. The supernatant was discarded and the cell pellet was resuspended in 20 ml of chilled RF1 buffer (15% glycerol, 100 mM RbCl, 50 mM $MnCl_2$, 30 mM KCH_3CO_2, 10 mM $CaCl_2$, pH 5.8,

filter-sterilised and stored at 4ºC). The resuspended cells were then incubated on ice for 30 minutes before centrifuging again at 2,000 xg, 4 °C for 5 minutes to pellet the cells. The supernatant was removed and the cells resuspended in 4.8 ml of RF2 buffer (15% glycerol, 10 mM MOPS, 10 mM RbCl and 75 mM $CaCl_2$, pH 6.8, filter-sterilised and stored at 4ºC). The resuspended cells were then chilled on ice for 15 minutes before being divided into 400 µl aliquots, which were then snap-frozen with liquid nitrogen. The competent cells were stored at -80 °C until required.

2.3.10 Transformation of competent cells

The required competent cells were thawed on ice. Either 1 µl of purified plasmid DNA or the ligation mixture as described in 2.3.8 was added to 100 µl of competent cells. The cells were then incubated on ice for 40 minutes. The cells were heat-shocked at 42 °C for 90 seconds and then returned to the ice. 400 µl of sterile LB broth was added to the cells which were then incubated at 37 °C for 1 hour with shaking. Following incubation, 100 µl of the cells were plated onto LB agar containing the required antibiotic. The plates were incubated overnight at 37 °C.

2.3.11 Screening of recombinant plasmids

In order to check if the cloning of a DNA insert in a plasmid was successful, 10 individual transformants were screened. 10 individual colonies were inoculated each in 5 ml of LB broth and the required antibiotic and grown overnight at 37 °C with shaking. Plasmid DNA was then isolated as per 2.3.1 and a restriction enzyme digest was set up as per 2.3.3. The restriction digestion reaction was then run on a 1% w/v agarose gel. This allowed the identification of plasmids that contain the insert of the correct size. Those plasmids are then sent for sequencing to confirm the plasmid habours the desired mutation.

2.3.12 DNA sequencing

All sequencing reactions were carried out by GATC Biotech Limited, Constance, Germany. The primers used for sequencing are given in Table 2.9. The sequence data was analysed using Chromas software.

2.4 Mutagenesis and cloning

2.4.1 Site directed mutagenesis by overlap extension PCR for *parF* mutagenesis

During this work a number of *parF* mutants were generated in order to investigate the role played by certain amino acids in ParF function. Overlap extension mutagenesis was the method employed in order to create these mutations. This method involves four primers and three PCR steps (Figure 2.1). Two internal primers were designed to contain the *parF* gene sequence with the mutation. The external primers were dependent on the position of the mutation and the restriction site to be used. The forward external primers contained either the *parF* upstream sequence or *parH* upstream sequence. The reverse external primers contained either the *parF* downstream sequence or *parG* downstream sequence. The first part of the method involved two PCRs, PCR 1 uses an external forward primer and the internal reverse primer whereas PCR 2 uses the internal forward primer and an external reverse primer. The PCR was carried out as described in 2.3.2 and pFH547 was used as the template DNA. The products from these PCRs were purified using ethanol precipitation (2.3.4) and then run on an agarose gel to confirm the PCR had been successful. The products of PCR 1 and PCR 2 were then incubated together in a 1:1 ratio for a pre-cycle reaction to allow the overlapping sequences to anneal. The pre-cycle reaction contained 12.5 µl of PCR 1 product and 12.5 µl of PCR 2 product plus 2.4 µl of each dNTP, 5 µl of 10X Pfu buffer and was made up to 50 µl with Milli-Q water. After the initial denaturation step of 3 minutes at 93 °C, 1 µl of Pfu was added and the pre-cycle started. The pre-cycle was 10 cycles of incubation at 94 °C for 40 seconds and 72 °C for 40 seconds. On completion of the pre-cycle PCR 3 was carried out by adding 5 µl of the forward and reverse external primer (5 pmol/ µl) to the tube. The PCR 3 program was carried out as described in Table 2.10 except the initial denaturation step was not needed. The PCR product was run on an agarose gel, gel extracted and again purified by ethanol precipitation. The product of PCR 3 and the vector, pFH547, were then digested with the appropriate restriction enzymes as per 2.3.3 and ligation of the digested PCR product and vector could then be carried out as per 2.3.8. The mutation was confirmed by sequence analysis (GATC Biotech).

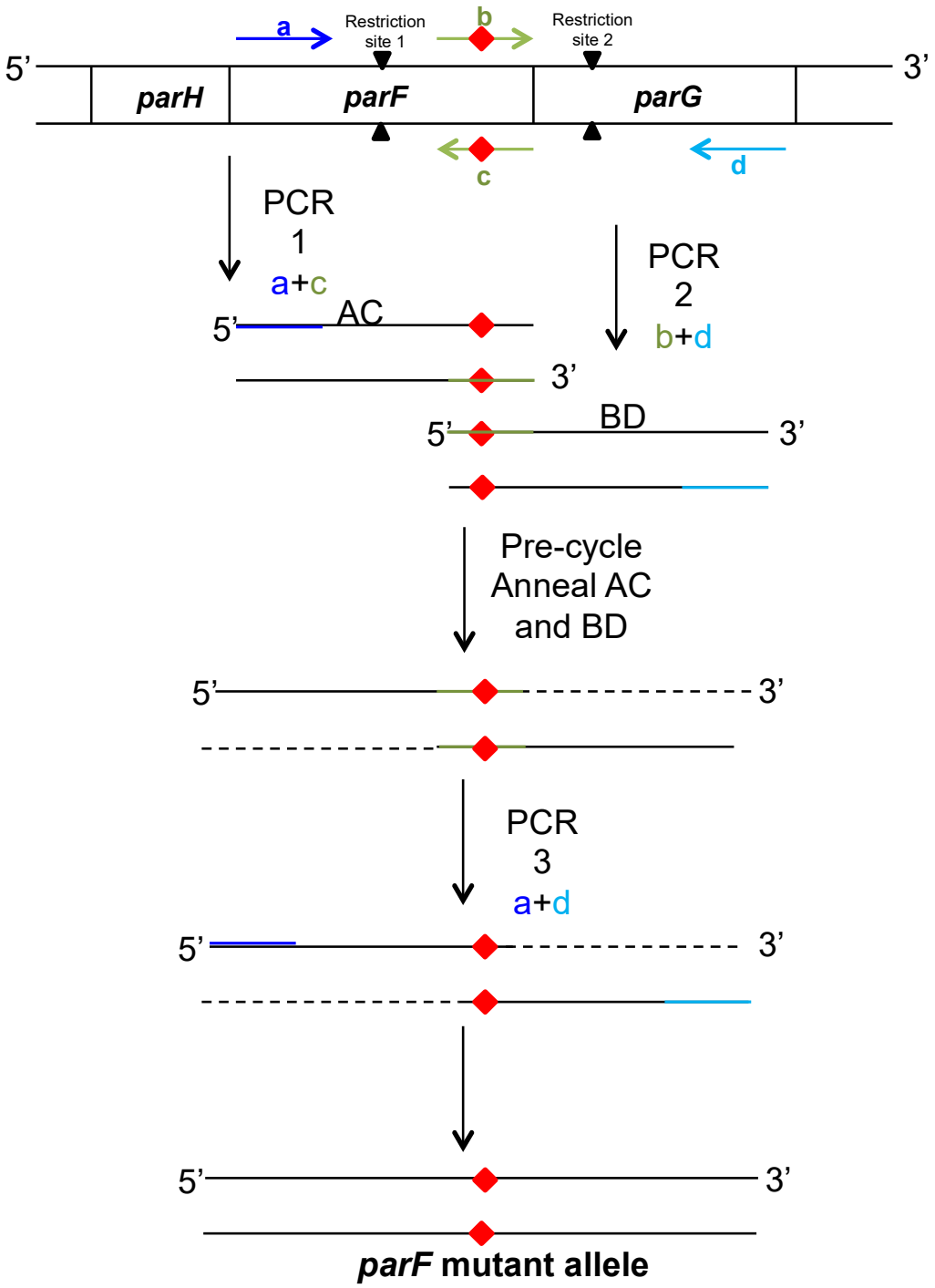

Figure 2.1 - Schematic representation of overlap extension mutagenesis. Three PCR reactions are carried out in order to generate *parF* mutant alleles. The primers used in are a – forward external primer (dark blue), b- forward internal primer with the desired mutation (green, red diamond indicates mutation), c – reverse internal primer with the desired mutation (green, red diamond indicates mutation), reverse external primer (light blue).

2.4.2 Cloning *parF* mutant gene into other vectors

2.4.2.1 pET22b

The forward primer, at the start of the *parF* gene, was designed to incorporate an *Nde*I restriction site and the reverse primer, at the end of the *parF* gene, was designed to incorporate an *Xho*I restriction site. PCR was then carried out with the pFH547 vector harbouring the desired mutation. The PCR was set up and ran as detailed in 2.3.2. The PCR products and pET22b vector were then digested with *Nde*I (NEB) and *Xho*I (Thermo Scientific) restriction enzymes as detailed in 2.3.3. The vector was dephosphorylated (2.3.5), run on an agarose gel to allow the digested vector to be extracted (2.3.7) and purified by ethanol precipitation (2.3.4). The digested PCR product was also purified using ethanol precipitation. The digested vector and PCR product were then ligated (2.3.8) and sent for sequencing to GATC Biotech to confirm the insertion of the desired mutation into the vector.

2.4.2.2 pT18 and pT25

As for pET22b, the forward and reverse primers were designed at the start and end of *parF* respectively and incorporated specific restriction sites. The forward primer for cloning into pT18 incorporated *Kpn*I site and the forward primer for cloning into pT25 incorporated *Pst*I. The reverse primer for cloning into pT18 incorporated *Hind*III and for cloning into pT25 incorporated *Kpn*I. Using these primers, the cloning was then carried out as for pET22b with pT18 and pT25 used as the vectors.

2.4.2.3 pBM40

The forward primer was designed at the start of *parF* and incorporated *Xba*I restriction site. The reverse primer was designed at the end of parF and incorporated SpeI restriction site. Again the cloning was carried out as for pET22b with pBM40 being used as the vector.

2.4.2.4 pBM20 and pBM22

Both pBM20 and pBM22 vectors contain the partition cassette *parFGH* with *mCherry* cloned in frame with *parG*. In order to clone a mutant *parF* allele into these vectors native restriction sites in the *parF* and *parG* genes were used to carry out restriction digests. The partition vector (pFH547) containing the mutant *parF* alleles and pBM20 or pBM22 were digested with *Mfe*I (New England Biolabs) and *Hpa*I (Thermo

Scientific) restriction enzymes as per 2.3.3. The restriction digests were then ran on an agarose gel and the digested pBM20 or pBM22 vector was gel extracted as per 2.3.7. The digested DNA fragment from pFH547 that contained the *parF* mutant allele was also gel extracted. After purification the DNA fragment and the vector were ligated as per 2.3.8 and then transformed into *E. coli* DH5α cells. Transformants were screened by restriction digests and those that contained the insert were sent to GATC Biotech for sequencing.

2.5 Expression and Purification

2.5.1 Overproduction of ParF and ParF mutant proteins

The pET22b vector, which contains a T7 promoter and the *parF* in frame with the codons for a hexa histine-tag was transformed into *E. coli* BL21(DE3) cells as per 2.3.10. After incubation overnight, 8-10 colonies were inoculated in 10 ml of LB broth with ampicillin and grown at 37 °C for ~1 hour with shaking. After incubation, the starter culture was then inoculated in 300 ml of pre-warmed LB broth containing ampicillin in a 2 L conical flask with baffled sides. The culture was then grown at 30°C with shaking until the OD_{600} = 0.8-0.9. The culture was then induced with isopropyl-beta-D-thiogalactopyranoside (IPTG) (Melford) at a final concentration of 1 mM and incubated for a further 3 hours at 30 °C. Cells were then harvested at 15,000 xg 4 °C for 15 minutes. The cell pellets were stored at -20 °C until needed for protein purification.

2.5.2 Overproduction of ParG

The pET22b vector, which contains a T7 promoter and *parG* in frame with the codons for a hexa histine-tag was transformed into *E. coli* BL21(DE3) cells as per 2.3.10. After incubation overnight, 8-10 colonies were inoculated in 10 ml of LB broth with ampicillin and grown at 37 °C for ~1 hour with shaking. After incubation, the starter culture was then inoculated in 300 ml of pre-warmed LB broth containing ampicillin in a 2 L conical flask with baffled sides. The culture was then grown at 37 °C with shaking until the OD_{600} = 0.8-0.9. The culture was then induced with isopropyl-beta-D-thiogalactopyranoside (IPTG) (Melford) at a final concentration of 1 mM and incubated for a further 2 hours at 37 °C. Cells were then harvested at 15,000 xg, 4 °C for 15 minutes. The cell pellets were stored at -20 °C until needed for protein purification.

2.5.3 Purification of ParG, ParF and ParF mutant proteins

The proteins were purified by Ni^{2+} affinity chromatography. The buffers, which differ for ParF and ParG, used for the purifications are given in Table 2.12 and Table 2.13 (Barillà and Hayes, 2003). The cell pellets were resuspended in 15 ml of the appropriate 1X binding buffer and to the resuspended cells 150 µl of lysozyme (10 mg/ml) (Sigma) and 1 EDTA free protease inhibitor tablet (Roche) were added. The cells were then incubated at 30°C for 15 minutes before another 150 µl of lysozyme (10 mg/ml) was added and a further incubation of 15 minutes at 30°C followed. The cells were sonicated 12 times for 30 seconds with 1 minute intervals on ice. The sonicated cells were then centrifuged at 11,000 xg at 4°C for 40 minutes and the supernatant was collected. The column was prepared with ~ 2.5 ml settled bed of His-binding resin (Novagen). The resin was charged with 1X 50 mM $NiSO_4$ and equilibrated with 1X binding buffer. The supernatant was loaded onto the column on a closed loading-elution circle for 1 hour 30 minutes at a peristaltic pump flow rate of 3. The column was then washed with 30 ml of 1X binding buffer and 50 ml of 1X wash buffer. The protein was then eluted with 12 ml of 1X elution buffer into 12 fractions of one ml each. To ParF fractions 1 µl of 2 mM Dithiothreitol (DTT) was added immediately. Protein fractions were then quantified by a Bradford assay using the Bio-Rad protein assay reagent as described in 2.5.5 The fractions of highest protein concentrations were then buffer exchanged into storage buffer with a 5 ml HiTrap desalting column as detailed in 2.5.4. The buffer exchanged fractions were then aliquoted into 100 µl and immediately snap-frozen using liquid nitrogen and stored at -80°C.

Table 2.12 - The composition of buffers used in ParF purifications

1X ParF Binding Buffer	1X ParF Wash Buffer	1X ParF Elution Buffer	ParF Storage Buffer
50 mM Tris, pH 7.5-8.0	50 mM Tris, pH8.0	50 mM Tris, pH 8.0	30 mM Tris, pH7.5-8.0
500 mM NaCl	1 M NaCl	150 mM NaCl	100 mM KCl
10 mM Imidazole	70 mM Imidazole	300 mM Imidazole	10 % Glycerol
10% Glycerol	10 % Glycerol	10 % Glycerol	2 mM DTT
All buffers were pH checked and filter sterilised before use.			

Table 2.13 - The composition of buffers used in ParG purifications

1X ParG Binding Buffer	1X ParG Wash Buffer	1X ParG Elution Buffer	ParG Storage Buffer
20 mM Tris, pH 7.5-8.0	20 mM Tris, pH8.0	20 mM Tris, pH 8.0	50 mM HEPES-KOH, pH 7.0
500 mM NaCl	1 M NaCl	500 mM NaCl	50 mM KCl
15 mM Imidazole	90 mM Imidazole	400 mM Imidazole	10 % Glycerol
10% Glycerol	10 % Glycerol	10 % Glycerol	2 mM DTT
All buffers were pH checked and filter sterilised before use.			

2.5.4 Buffer exchange of ParF and ParG proteins

Buffer exchange was carried out using a HiTrap desalting column (GE Healthcare). The column was first washed with 20 ml of Milli-Q water before being equilibrated with 20 ml of the appropriate storage buffer. 1.5 ml of protein fractions with high concentrations were then loaded onto the column and eluted in two 1 ml fractions in the storage buffer. Protein concentrations were again determined by a Bradford assay using the Bio-Rad

protein assay reagent as described in 2.5.5. Protein fractions were then analysed on SDS-PAGE as described in 2.6.

2.5.5 Protein concentration determination

Protein concentrations were determined by using a Bradford assay. Bovine serum albumin (BSA) was used as a protein standard. The protein standards were set up as detailed in Table 2.14. The reactions were incubated for 5 minutes and then the absorbance was measured at 595 nm. All samples were tested in triplicate. A graph of protein concentration versus absorbance (595 nm) was plotted to allow a standard curve to be obtained. Unknown protein concentrations could then be determined from the curve. 10 µl of the protein sample was added to 790 µl of Milli-Q water and 200 µl of Bradford reagent was added and the reaction incubated for 5 minutes before the absorbance at 595 nm was taken.

Table 2.14 - Bradford assay protein standard reaction set up.

BSA concentration (µg/ml)	Volume of BSA (0.2 mg/ml) (µl)	Volume of Milli-Q water (µl)	Volume of Bradford reagent (µl)
0	0	800	200
0.4	2	798	200
1	5	795	200
2	10	790	200
4	20	780	200
6	30	770	200

2.6 Sodium dodecyl sulfate-polyacrylamide gel electrophoresis (SDS-PAGE)

2.6.1 Preparation of gel

Gel plates were assembled as per the manufacturer's instructions in order to form the glass plate sandwich. A 12% resolving gel was used when running ParF samples and a 15% resolving gel was used when running ParG samples, the stacking gel was the same for both. The components of the gel are detailed in tables 2.15 and 2.16, the ammonium persulfate (APS) and tetramethylethylenediamine (TEMED) solutions were added last and just before pouring the gel. The resolving gel was poured between the glass plates leaving enough space for the stacking gel to be added on the top. To the top of the resolving gel 1 ml of 100 % isopropanol was added to ensure the gel was not exposed to air and the resolving gel was then left to solidify for ~ 30 minutes. The stacking gel was then prepared, again the APS and TEMED were added just before pouring. The isopropanol was removed from the top of the solidified resolving gel using filter paper and this was then washed with Milli-Q water and any excess water removed with the filter paper. The stacking gel was then added to the top of the resolving gel and the comb inserted before leaving the gel to solidify for ~30 minutes.

Table 2.15 – Composition of resolving gels used

Component	**Volume for 10 ml resolving gel solution for a 12 % gel (ml)**	**Volume for 10 ml resolving gel solution for a 15 % gel (ml)**
Deionised water	4.9	3.4
30% Acrylamide mix	6	7.5
1.5 M Tris (pH8.8)	3.8	3.8
10% Sodium dodecyl sulfate (SDS)	0.15	0.15
10% Ammonium persulfate (APS)	0.15	0.15
Tetramethylethylenediamine (TEMED)	0.006	0.006

Table 2.16 – Composition of the stacking gel

Component	**Volume for 5 ml stacking gel solution (ml)**
Deionised water	2.7
30% Acrylamide mix	0.67
1 M Tris (pH6.8)	0.5
10% Sodium dodecyl sulfate (SDS)	0.04
10% Ammonium persulfate (APS)	0.04
Tetramethylethylenediamine (TEMED)	0.004

2.6.2 Sample preparation

5 µl of 4X SDS loading buffer (100 mM Tris pH 6.8, 200 mM DTT, 4% SDS, 0.2% Bromophenol Blue and 20% Glycerol) were added to 15 µl of protein sample and the mixture was incubated at 95 °C for 5 minutes. Either 5 µl of PageRuler Prestained or Unstained Protein Ladder (Thermo Scientific) was loaded onto the gel to estimate the molecular weight of the protein samples.

2.6.3 Electrophoresis

Gels were run using the Mini-PROTEAN (Bio-Rad) system as per the manufacturer's instructions. After adding the gels to the tank it was filled with 1X SDS running buffer (Made from 5X SDS running buffer – 125 mM Tris, 1.25 M Glycine and 0.5% SDS). After removing the comb and rinsing the wells, the protein ladder and protein samples were loaded. Gels were run at 150 V for ~30 minutes until the samples could be seen to pass the stacking gel. Then the gel was run at 190 V for a further 30 minutes or until the dye front reached the bottom of the gel.

2.6.4 Staining of SDS Gels

SDS gels were stained with Coomassie Brilliant Blue dye (1.25 g of dye was added to 250 ml methanol, 50 ml acetic acid and 250 ml sterile water) for 1 hour with gentle shaking. Gels were then rinsed with water before adding destain solution (700 ml sterile water, 200 ml methanol and 100 ml of acetic acid) and gently shaking overnight or until the protein bands were clearly visible.

2.7 Plasmid partition assay

To analyse plasmid retention *in vivo* plasmid partition assays were carried out (Figure 2.2). Partition assays were used to assess whether a mutation had an effect on plasmid retention. This was done by transforming the plasmids harbouring the partition cassette with the mutation (pGA series of plasmids with specific mutations) into *E. coli* BR825. In parallel to this, the plasmid harbouring the wild type partition cassette (pFH547) and a plasmid with no partition cassette (pFH450) were also transformed into *E. coli* BR825 cells to allow comparisons to be made between the wild type partition cassette and the one containing the mutation. The transformations were plated onto LB medium plates with chloramphenicol (concentration) and grown overnight at 37°C. From these plates 10 colonies were picked and streaked onto fresh LB medium plates with

chloramphenicol (one plate was section into 5 to allow 5 streaks per plate) in order to obtain isolated colonies and again grown overnight at 37°C. One colony from each of the streaked sections was then picked and streaked on LB medium plates with no antibiotics. After overnight growth at 37 °C this step was repeated again. This streaking on non-antibiotic medium provides ~25 generations of non-selective growth. After incubation at 37°C overnight, 10 isolated colonies from each streaked section were stabbed onto LB medium and then LB medium plates with chloramphenicol. In total 100 isolated colonies were picked and stabbed onto both plates. After overnight growth at 37°C the number of colonies that had grown on the LB medium with chloramphenicol were counted and this allowed the percentage of plasmid retention to be calculated. Any inconsistencies when observing colony growth were accounted for and the maintaining of accurate statics was carried out throughout. Partition assays were performed in triplicate as a minimum.

When none of the colonies have any resistance at the end of the assay the rate of plasmid loss leading to that point is unknown as you go through the subcultures.

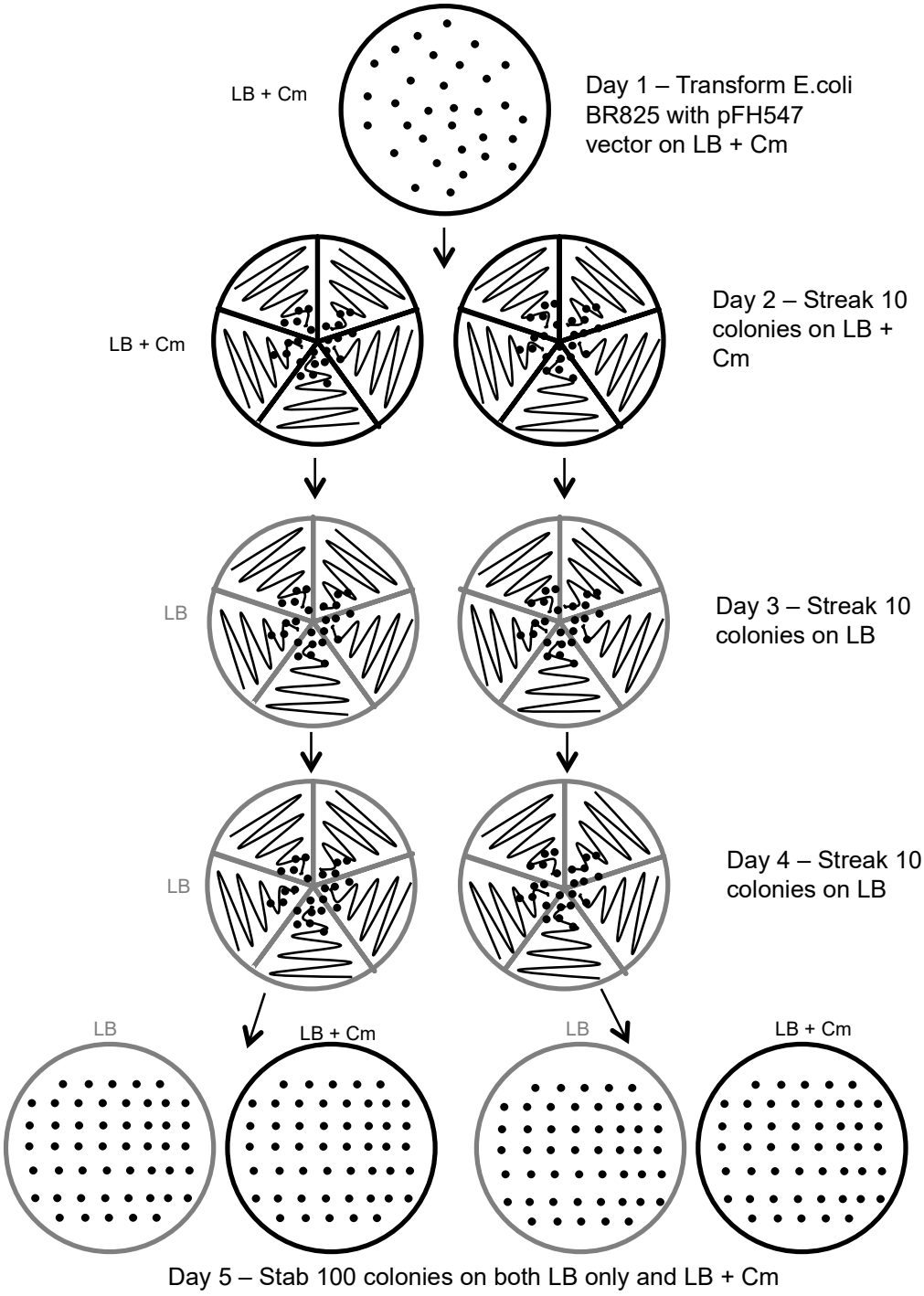

Figure 2.2 - Schematic representation of a plasmid partition assay. Transformation of the partition vector with no partition cassette, with the wild type partition cassette or a mutant partition cassette is carried out on day one. On day two 10 colonies are streaked onto LB medium with chloramphenicol. Day three and four the streaking is carried out on plates without chloramphenicol to allow ~25 generations of non-selective growth. On day five 100 colonies are stabbed onto one plate with chloramphenicol and one without.

2.8 ATPase assay

ATPase assays were used in order to quantify the level of ATP hydrolysis of ParF and ParF mutants in the presence and absence of ParG. ATPase assays were performed using thin layer chromatography (TLC) and [α^{35}S] ATP (Perkin Elmer, UK). A polyethyleneimine (PEI)-cellulose plate (Macherey-Nagel) was pre-run in Milli-Q water in a tank until the water level reached the top of the plate, the plate was then allowed to dry overnight.

2.8.1 Intrinsic ATPase activity

ParF or ParF mutant proteins were added at a final concentration of 0, 0.5, 1, 2, 4, and 8 µM. To this 4 µl of 4X ATPase buffer (120 mM Tris pH7.5, 400 mM KCl, 20 mM $MgCl_2$ and 8 mM DTT) and 1 µl of [α35S] ATP (25-100Ci/mmol) were added. To make the concentration of ATP to 250 µM, 0.4 µl of cold ATP (10 mM) was added to the reaction. The reaction was made up to 16 µl with Milli-Q water. The reactions were incubated at 30°C for 1 hour before 2.5 µl of each reaction was spotted onto the (PEI)-cellulose plate. The spots were air dried for ~ 15 minutes before the (PEI)-cellulose plate was subject to TLC using 0.5 M KH_2PO_4, pH 3.5 buffer in a TLC tank for 4 hours. The plate was then air dried and exposed to a BIOMAX MR Kodak film overnight and the ATP and ADP spots were quantified using a Phosphor Screen Scanner (Bio-rad Personal Molecular Imager) and normalized for the non-enzymatic hydrolysed ADP in the control lane.

2.8.2 ParG stimulation of ATPase activity

ParF or ParF mutant proteins were used at a final concentration of 0.5 µM and ParG was used at increasing concentrations of 0, 0.5, 1, 2 and 5 µM. 4 µl of 4X ATPase buffer was added to the reactions. 1 µl of a 1 in 10 dilution of [α35S] ATP (25-100Ci/mmol) was used to have a final concentration of ATP of 50 nM. The rest of the protocol was followed as described above in 2.81.

.

2.9 Bacterial two-hybrid and β-galactosidase assay

Bacterial two-hybrid assays were used in order to analyse both ParF/ParF mutants – ParG interaction and ParF or ParF mutants' self-interaction. β-galactosidase assays were then used to quantify these interactions.

2.9.1 Bacterial two-hybrid assay

E. coli SP850 cells were co-transformed with the two plasmids one with T18 fused to a protein of interest and the other with T25 fused to the other protein of interest. This was dependent on the interaction being analysed, if it was a ParF-ParG interaction *parG* was fused to the DNA encoding T18 and *parF/parF* mutant allele was fused to the DNA encoding T25. When protein self-interaction studies were carried out the same *parF/parF* mutant allele was fused to both the DNA encoding T18 and T25. As a negative control T18 and T25 were not fused to any protein and therefore no interaction would be seen. For the positive control T18 and T25 were fused to two fragment of the leucine zipper region of the yeast protein, GCN4, to produce T18-zip and T25-zip.The co-transformations were carried out as detailed in 2.3.10 with 1 µl of each plasmid being added to the 100 µl of competent *E. coli* SP850 cells. The transformations were plated on LB medium with both chloramphenicol (concentration) and ampicillin (concentration) to select for cells containing both plasmids. The plates were incubated at 30°C for ~36 hours. MacConkey agar plates were prepared fresh each time as detailed in 2.2.1.2. To 200 ml of prepared MacConkey agar chloramphenicol (concentration) and ampicillin (concentration) were added along with 10 ml of 20% (w/v) maltose (Sigma) (prepared by dissolving 2 g of maltose in 10 ml of Milli-Q water and filter sterilising). Plates were then poured and allow to completely dry for 1 hour. Colonies from the transformations were then streaked onto the MacConkey agar plates using a sterile loop and then the plates were incubated at 30°C for 16 hours or until red colonies can be seen.

2.9.2 β-galactosidase assay

Co-transformations were carried out as detailed in 2.3.10 with 1 µl of each plasmid (80 ng/ml) being added to the 100 µl of competent *E. coli* SP850 cells. The transformations were plated on LB medium with both chloramphenicol (concentration) and ampicillin (concentration) to select for cells containing both plasmids. The plates were incubated at 30°C for ~36 hours. Single colonies were then inoculated into 5 ml of LB broth with chloramphenicol (concentration), ampicillin (concentration) and 0.5 mM IPTG. The cultures were incubated overnight at 30°C with shaking. After incubation, cultures were incubated on ice for 20 minutes and then 1 ml of each culture was diluted with 4 ml of M63 medium (Table 2.17) supplemented with 1 ml 1 M $MgSO_4$ and 20% maltose. A_{600} for each culture was taken before 3x 500 µl aliquots were taken and centrifuged for 10

minutes at 11,000 xg to pellet the cells. The supernatant was removed carefully and cell pellets resuspended in 700 µl of buffer Z (Table 2.18). To this, 20 µl of $CHCl_3$ and 20 µl of 0.1% SDS were added and vortexed for 20 seconds to mix. The samples were then incubated at 28°C for 5 minutes before 200 µl of O-Nitrophenyl-β-D-Galactopyranoside (ONPG) (4 mg/ml) (Sigma) were added. The time taken to develop a yellow colour was recorded and at this point the reaction was stopped by adding 500 µl of 1 M Na_2CO_3. Samples were then centrifuged for 1 minute at 11,000 xg and then the supernatant was removed and the A_{420} and A_{550} was taken. Miller units could then be calculated by using the following equation:

$$\mathbf{MU=1000 \times A_{420} - (1.75 \times A_{550})/ T \times V \times A_{600}}$$

MU = Miller units
A = absorbance
T = time
V = volume

Table 2.17 – Composition of 5X M63 medium

Component	**Amount (g)**
$(NH_4)_2SO_4$	10
KH_2PO4	68
$FeSO_4.7H2O$	0.0025
Dissolved in 1 L of dH_2O and adjusted to pH 7	

Table 2.18 – Composition of buffer Z

Component	Final concentration (M)
$Na_2HPO_4.7H_2O$	0.06
$NaH_2PO_4.H_2O$	0.04
KCl	0.01
$MgSO_4$	0.001
Made to 1 L with dH_2O and adjusted to pH 7 To 20 ml of buffer Z 54 µl of (0.05 M) β-mercaptoethanol (Sigma) was added before use.	

2.10 Circular dichroism (CD)

CD was carried out to check ParF mutant proteins were correctly folded and that the amino acid change did not affect the secondary structure of the protein. ParF and mutant ParF proteins were buffer exchanged into CD buffer (30 mM Tris, pH 7.5, 50 mM KCl) with HiTrap desalting column as per 2.5.4 and diluted to a final concentration of 0.2 mg/ml. 200 µl of protein were added into a quartz cuvette with a path length of 0.1 mm. CD spectra were recorded at 25°C from 260 – 190 nm on a Jasco J810 CD spectrophotometer.

2.11 Chemical cross-linking

Chemical cross-linking was used to determine if ParF mutants were able to dimerise like the wild type ParF protein. The crosslinker used in these experiments was dimethyl pimelimidate (DMP). DMP is an imidoester, which is reactive towards primary amines at alkaline pH values to form an amidine bond. All crosslinking reactions were carried out in the following buffer, 50 mM HEPES-KOH (pH 8.5), 50 mM KCl and 5 mM MgCl2 therefore ParF proteins were buffer exchanged into this buffer using HiTrap desalting columns as described in 2.5.4. ParF and ParF mutant proteins were used at a final concentration of 12 µM in all reactions. DMP was added at increasing concentrations of 0, 0.1, 0.5, 1 and 10 mM. ParF forms dimers in the presence of ATP, therefore ATP was used at a final concentration of 1 mM in all reactions. The final reaction volume used was 15 µl. Reactions were incubated at 37°C for 2 hours and then

the reactions were stopped by adding 1 µl of 0.5 M Tris-HCL pH 6.8 and incubating at room temperature for 1 hour. The reactions were then analysed using SDS-PAGE as per 2.6.

2.12 Dynamic light scattering (DLS)

Dynamic light scattering was used to measure ParF and ParF mutant proteins' ability to form higher order structures. The Malvern Zetasizer Nano system was used for this as it allows the intensity of light scattering of a sample to be measured and from this the hydrodynamic radius (Z-average) can be inferred. Proteins were centrifuged for 30 minutes at 11,000 xg, 4°C and the supernatant was removed and quantified by Bradford assay as detailed in 2.5.5. All proteins were analysed at a final concentration of 50 ng/µl. All buffers used in DLS for sample dilutions were filtered sterilised with Anotop 10 syringe filter 0.02 µm (GE Healthcare). The samples were analysed in 50 µl quartz cuvettes. The samples were prepared by adding 46.25 µl of ParF (final concentration of 2.16 µM diluted with ParF storage buffer, Table 2.12) to the cuvette and placing it in the Zetasizer chamber at 30°C and initially taking 20 readings to establish a baseline. After this, 2.5 µl of 100 mM $MgCl_2$ (final concentration of 5 mM) and 1.25 µl of 20 mM nucleotide to give a final concentration of 500 µM (ADP, ATP or ATP- γ-s diluted in 20 mM Tris, pH 7.5) are added and mixed with a pipette. The cuvette was then placed back in the chamber and more readings were taken, the number of readings taken was dependent on whether the polymerisation was observed over a short or a long time period. If the effect of ParG on polymerisation were also being analysed, the cuvette would be removed and 2.16 µM ParG would be added and mixed using a pipette. Volumes of other components would have been adjusted accordingly in order to ensure final concentrations remain as detailed.

2.13 Electron microscopy (EM)

Ultrastructures of ParF and ParF mutant protein structures were analysed using negative-stain electron microscopy (EM). The protein samples were prepared as for DLS, concentrations and volumes were kept as detailed in 2.12. DLS assays were carried out in parallel with preparation of samples for EM to allow comparison on the EM images with the DLS results. The samples for EM were snap-frozen with liquid nitrogen at the point at which the analysis of polymers was to be taken. When ready samples were thawed and applied to carbon-coated copper grids (200 mesh size) that

had been glow discharged. After 30 s, the drops were blotted, the grids were stained with 1% uranyl acetate for 1 min and then blotted dry with filter paper. Grids were examined with a FEI Tecnai 12 BioTWIN G2 transmission electron microscope with a SIS CCD camera.

2.14 Electrophoretic mobility shift assay (EMSA)

2.14.1 Biotinylated DNA fragment

Electromobility shift assays (EMSA) were carried out in order to analyse ParF and ParF mutant proteins binding to DNA. ParF is able to bind DNA in a non-specific manner therefore the sequence of DNA used for the EMSA was irrelevant. EMSA were carried out with two different DNA fragments. One was the *parFG* promoter sequence, which was produced using PCR with the forward primer designed to have a biotin label at the 5' end. This DNA fragment was 123 bp in length. The PCR was carried out as in 2.3.2. The DNA concentration was determined using the Nanodrop (ThermoScientific). The other DNA fragment used was generated from annealing two primers, one of which had a biotin label at the 5' end. The forward and reverse primer, at a final concentration of 1μM, were mixed with 10 mM Potassium Phosphate buffer and a heat denaturation step was carried out at 93 °C for 5 minutes. The reaction was then left at room temperature for 1 hour allowing the primers to anneal. This produced a random sequence 43 bp DNA fragment.

2.14.2 Preparation of samples and gel electrophoresis

Increasing concentrations of ParF and ParF mutant proteins (0, 0.5, 1, 2, 4 and 8 μM) were added to 2 μl of 120 nM DNA (final concentration of 12 nM). The reaction set up is given in Table 2.19. The reactions were incubated at 30°C for 30 minutes. A 6% native gel was prepared (Table 2.20) and this was pre-run for 20 minutes at 100 V with 0.5X TBE buffer (Table 2.21). The 20 μl reactions were then loaded onto the gel along with 2 μl loading buffer in a separate lane in order to determine when the gel should be stopped.

Table 2.19 – Reaction set up for EMSA

Component	**Amount (µl)**
Protein	X
DNA (12 nM final concentration)	2
50 % glycerol	1
100 mM $MgCl_2$	1
100 mM ATP	0.4
10 X binding buffer (10 mM Tris pH 7.5, 50 mM KCl, 1 mM DTT, 5mM $MgCl_2$, 2.5% glycerol and 0.05% NP-40)	2
Milli-Q water	Make up to 20 µl

Table 2.20 – Composition of 6% native gel

Component	**Volume needed for 2 gels**
5X TBE	1.2 ml
30% Acrylamide	2.4 ml
10% APS	70 µl
TEMED	10 µl
Distilled water	8.4 ml

Table 2.21 – Composition of 5X TBE buffer

Component	Quantity
Tris	54 g
Boric acid	27.5 g
0.5 M EDTA, pH 8.0	20 ml
Distilled water	To make 1 L

2.14.3 DNA transfer

DNA from the native gel was transferred onto a positively charged nylon membrane (Roche). The nylon membrane and 4 pieces of 3MM Whatman paper were cut to the size of the gel and soaked, along with 2 sponges, for 10 minutes in 0.5X TBE. The transfer cassette (Bio-rad system) was then assembled first with the addition of one sponge and two pieces of Whatman 3MM paper followed by the gel and then the nylon membrane was placed on top of gel carefully, avoiding air bubbles. The remaining two pieces of Whatman 3MM paper and sponge were placed on the top of the membrane. The cassette was then placed in to the tank and the DNA transfer was carried out at 380 mA for 30 minutes in 0.5X TBE buffer. The cassette was then disassembled, the membrane was removed carefully and the positions of the lanes were marked. The membrane was wrapped in Saran wrap and the DNA was cross-linked to the membrane by placing DNA side down onto a UV transilluminator for 5 minutes.

2.14.4 Detection of Biotinylated DNA

The Detection of Biotinylated DNA was carried out using the LightShift™ Chemiluminescent EMSA kit (Pierce). The blocking buffer and 4X wash buffer were warmed to 50°C in order to ensure the component were completely dissolved. The membrane was then transferred into a clean tray and 20 ml of blocking buffer was added and incubated at room temperature with shaking for 15 minutes. The blocking buffer was then discarded and then another 10 ml of blocking buffer was added to the membrane with 1 µl streptavidin-horseradish peroxidase conjugate (Sigma-Aldrich) and again incubated at room temperature with shaking for 15 minutes. The membrane was then transferred to a clean tray and washed 4 times, each for 5 minutes with shaking in 20 ml of 1X wash buffer (prepared by doing a 1 in 4 dilution of 4X wash buffer in

Milli-Q water). After washing, the membrane was transferred to a clean tray and 30 ml of equilibration buffer was added and incubated for 5 minutes at room temperature. The substrate solution was prepared by adding 1 ml of luminol/enhancer solution to 1 ml stable peroxide solution and transferred to a clean tray. The membrane was carefully removed from the equilibration buffer with tweezers and allowed to drip dry before being placed DNA side down in the substrate solution. The membrane was incubated for 5 minutes at room temperature after which the membrane was removed and allowed to air dry on tissue paper. The membrane was then placed in a film cassette and covered with an acetate sheet before being exposed to an X-ray film. Initial exposure was for 1 minute and then this time would be adjusted dependent on the signal.

2.15 Fluorescence anisotropy

Fluorescence anisotropy was carried out on a Fluoromax-3 using FluorEssence 2.1 software. This technique was used to investigate DNA binding by ParF and ParF mutant protein as well as to check the ParF mutant proteins are able to bind ATP like the wild type ParF protein. In this technique the difference in polarized light can be measured as binding of a small molecule (DNA or ATP) causes a change in the rotational time of the protein. Upon binding the rate at which the protein tumbles is reduced and this can be measured to give binding constants and kinetics of binding. The fluorimeter was allowed to warm up for 30 minutes before use and the water bath was set to 25°C. Prior to use, the fluorimeter was calibrated with Milli-Q water as per the manufacturer's instructions.

2.15.1 ATP binding

ParF and ParF mutant proteins were centrifuged for 30 minutes at 11,000 xg, 4°C and the supernatant was removed and quantified using a Bradford assay as detailed in 2.5.5. Increasing concentrations of ParF and ParF mutant proteins (0, 0.25, 0.5, 1, 2, 4, 8, 10 and 12 µM) were prepared by diluting in sample buffer (20 mM Tris pH 7, 50 mM NaCl and 5 mM MgCl2). 1 µl (1 unit) of MANT-ATP (2'/3'-O-(N-Methyl-anthraniloyl)-adenosine-5'-triphosphate, Triethylammonium salt – a fluorescent ATP analog) was added to a total reaction volume of 150 µl. The reactions were then incubated at room temperature for 10 minutes before being added to a quartz microcuvette (Hellma). The excitation wavelength (λ_{ex}) was 356 nm and the emission wavelength (λ_{em}) was 442 nm. Ten measurements of fluorescence anisotropy were taken

for each reaction and then averaged. This value was then plotted against ParF or ParF mutant protein concentration. The assay was carried out in at least in triplicate.

2.15.2 DNA binding

Fluorescently labeled DNA fragments 20 bp and 40 bp in size were used to measure WT and mutant ParF protein binding to non-specific DNA. The DNA was prepared by annealing two primers, where the forward primer has a Cy3 label at the 5' end. The DNA fragments were prepared by adding 3 µl of the forward and reverse primer, at a final concentration of 1 µM, to 294 µl of 10 mM Potassium Phosphate buffer and carrying out a heat denaturation step at 93 °C for 5 minutes. The reaction was then left at room temperature for 1 hour allowing the primers to anneal. The concentration of the DNA was determined on the Nanodrop. The protein samples were prepared as for ATP binding reactions as detailed in 2.15.1. The DNA was kept at a constant concentration of 5 nM and the protein concentration was increased from 0.25 – 12 µM. To the reaction 3 µl of 100 mM nucleotide (ADP, ATP or ATP-γ-s) was added to give a final concentration of 2 mM. The sample buffer used is the same as for ATP binding and again the final reaction volume was 150 µl. The reactions were incubated for 10 minutes at room temperature before being added to the quartz microcuvette. The excitation wavelength (λ_{ex}) was 550 nm and the emission wavelength (λ_{em}) was 561 nm. Ten measurements of fluorescence anisotropy were taken for each reaction and then averaged. This value was then plotted against ParF or ParF mutant protein concentration. The assay was carried out in at least triplicate.

2.16 Microscopy

2.16.1 Confocal microscopy

Confocal microscopy was used to visualise ParG, ParF and ParF mutants *in vivo* in live cells. Transformations were carried using *E. coli* BW25113 and plated on LB medium with the appropriate antibiotics. Either pBM40 (pBAD-ParF), pBM20 or both plasmids were transformed as per 2.3.10. If ParF mutant proteins were to be visualised *in vivo* the appropriate plasmids were transformed that contain the *parF* mutant allele. From the transformation, 7-8 colonies were picked with a sterile loop and inoculated in 1 ml of M9 medium (Table 2.6) in the presence of the desired antibiotics. The cells were grown at 37°C for 1 hour with horizontal shaking. After the 1 hour incubation, 3 µl of 10% arabinose (final concentration on 0.03%) was added to induce other overproduction of

ParF-Emerald. The cells were then grown for a further 3 hours at 30°C with horizontal shaking. The cells were harvested at 8,000 xg for 1 minute and 950 µl of the supernatant was removed to leave 50 µl. The cells were then resuspended in the remaining 50 µl. Agarose (1.2% in M9 medium with glycerol and 4',6-diamidino-2-phenylindole (DAPI) at a final concentration of 2 µg/ml) pads were prepared on a microscopy slide with gene frames (ABgene). 0.4 µl of the cell suspension was placed on the agarose pad and covered with a glass coverslip. Confocal microscopy was performed using a Zeiss Invert LSM880. The 405 nm laser was used to visualise DAPI, the 488 nm laser was used to visualise GFP Emerald and the 561 nm laser for mCherry. Images were analysed using the Volocity software (Perkin Elmer).

2.16.3 3D-Structured Illumination Microscopy

Three Dimensional-Structured Illumination Microscopy (3D-SIM) was employed to study ParF localisation in greater detail as the images acquired display a higher level of resolution that would otherwise be beyond the diffraction limit. Super resolution microscopy employs patterned illumination to excite the sample and the resulting emission is the product of the structured illumination pattern superimposed on that of the sample. The cells are grown as for confocal microscopy (2.18.1) and the agarose pads are also prepared in the same way. Images were acquired at SULSA, University of Dundee with a 100x 1.4NA, oil immersion objective lens (Olympus, Center Valley, PA) and an electron-multiplying charge - coupled device (EMCCD) cameras (Photometrics, Tucson, AZ) on the Delta Vision OMX version 3 system (Applied Precision) equipped with 405-, 488-, and 593-nm solid-state lasers. Samples were illuminated by a coherent scrambled laser light source that had passed through a diffraction grating to generate the structured illumination by interference of light orders in the image plane to create a 3D sinusoidal pattern, with lateral stripes approximately 0.2 µm apart. Raw images were processed and reconstructed to reveal structures with greater resolution implemented on SoftWorx, ver. 6.0 (Applied Precision, Inc.). The channels were then aligned in x, y and rotationally. The images were analysed by 3D opacity using the Volocity software (Perkin Elmer).

2.16.4 Immunofluorescence microscopy

Immunofluorescence microscopy was used in addition to confocal microscopy to gain further understanding of ParF localisation *in vivo*. *E. coli* BR825 cells were transformed

with the vector pFH547, which contains the wild type partition cassette. An individual colony was picked from the transformants and used to inoculate 10 ml of LB broth supplemented with chloramphenicol (concentration) and grown overnight at 37°C with shaking. After incubation, 0.3 ml of the overnight culture was used to inoculate 10 ml of fresh LB broth containing chloramphenicol (concentration) and grown at 37°C until the A_{600} reached 0.6-0.7. 500 µl of the cells were then fixed by adding 100 µl of 16 % paraformaldehyde, 20 µl of 1 M NaH_2PO_4 and 5 µl of 0.25% glutaraldehyde and incubating at room temperature for 15 minutes. After incubation, the cells were centrifuged at 6,000 xg for 1 minute to pellet the cells. The cells were then washed three times by resuspending the cells in 1X PBS and centrifuging at 4,500 xg for 1 minute between each wash. After the final centrifugation, the cells were resuspended in 50 µl of GTE buffer (50 mM Glucose, 20 mM Tris pH 7.5 and 10 mM EDTA). The cells were then lysed by adding 5 µl of 1 µg/ml lysozyme solution. 20 µl of the cells were then immediately added to a poly-l-lysine coated cover slip and incubated at room temperature for 1 minute. The cover slip was then washed three times with 1X PBS and then air-dried completely. The cells were rehydrated with 20 µl of 1X PBS and incubated for 2 minutes at room temperature before 20 µl of 1X PBS with 4% (w/v) BSA (Sigma) was added and a further incubation of 20 minutes at room temperature was carried out. 10 µl of a 1:100 dilution (in 1X PBS, 4% BSA) of ParF serum was added to the slides and incubated at 37°C for 1 hour. The slides were then washed nine times with 1 X PBS and 10 µl of a 1:300 dilution (in 1X PBS, 4% BSA) of the secondary antibody was added – Alexa Fluoro 555 goat anti rabbit IgG (Life technologies) and incubated for 1 hour at room temperature in the dark. The slides were washed nine times with 1X PBS before the cover slips were air-dried. When the cover slips were dry they were placed onto microscope slides already treated with 20 µl of 2 µg/ml DAPI. The cover slips were then sealed and incubated over night at 30°C in the dark. Immunofluorescence microscopy was performed using a Zeiss Invert LSM880. The 405 nm laser was used to visualise DAPI and the 561 nm laser for Alexa Fluoro 555. Images were analysed using the Volocity software (Perkin Elmer).

2.17 Sedimentation assay

This assay was used to analyse ParF and ParF mutant proteins ability to form higher order structures in the presence and absence of nucleotides or ParG. Proteins were centrifuged for 30 minutes at 11,000 xg, 4°C and the supernatant was removed and

quantified using a Bradford assay as detailed in 2.5.5. ParF, ParF mutant proteins or ParG were used at a final concentration of 8 - 10 µM. A 60 µl reaction was set up with the protein, 5 mM $MgCl_2$, 2 mM nucleotide (ADP, ATP, ATP-γ-s) and made to the total reaction volume with ParF storage buffer. The reactions were then incubated for 10 minutes at 30°C. After the incubation, the reactions were centrifuged for 30 minutes at 11,000 xg, 4°C. 20 µl of the supernatant was collected and added to 10 µl 2X SDS loading buffer. The remaining supernatant was removed and the pellets were then dried by heating at 30°C for ~ 5 minutes or until no more supernatant was visible. The pellets were then resuspended in 15 µl of Milli-Q water and 10 µl of 2X SDS loading buffer were added. The supernatant and pellet samples were then denatured at 95°C for 5 minutes before subjecting them to a 12% SDS-PAGE (2.6). The bands were then quantified using Quantity One imaging software. The values were adjusted according to the fact that 100% of the pellet and only 33% of the supernatant was loaded on the gel.

2.18 Tethered particle motion (TPM)

Tethered particle motion (TPM) was carried out in order to gain greater understanding of the interaction between ParF and DNA, all experiments were carried out at the University of Leiden. As ParF binds DNA in a non-specific manner, a random sequence 700 bp DNA fragment was prepared using PCR as per 2.3.2. Primers were designed to amplify a 700 bp (59% GC content) region of *hypE*, a gene from *Salmonella enterica*. The forward primer was designed to incorporate biotin at the 5' end and the reverse primer was designed to incorporate digoxigenin (DIG) at the 3' end. The DNA fragment was purified using a GenElute Sigma-Aldrich kit as per the manufacturer's instructions. ParF was centrifuged at 11,000 xg, 4°C for 15 minutes and the supernatant was quantified using a Bradford assay as per 2.5.5. The protein was used at final concentrations ranging from 0.25 to 1 µM and any dilutions of the protein were made in ParF storage buffer (Table 2.12). Flow cells were prepared by heat-sealing two thin covers glasses using Parafilm as a spacer. The flow cells were incubated with 20 µg/ml antiDIG antibodies (Roche) for 10 minutes. Passivation of the surface was achieved by adding 0.4% (w/v) Blotting grade Blocker (BGB) (Bio-Rad) in buffer I (10 mM Tris (pH 7.5), 150 mM NaCl, 1 mM EDTA, 1 mM DTT, 3% glycerol, and 100 µg/mL acetylated BSA- Ambion) to the flow cell and incubating the sample for 10 minutes at the room temperature. The flow cell was then washed with 100 µl buffer I and 75 pM of the DNA labeled with biotin and DIG were added and incubated for 10 minutes. The

concentration of DNA added was increased (DNA used up to 6 nM) if the number of tethered beads was too low. After incubation, the flow cell was again washed with 100 µl of buffer I. Streptavidin-coated polystyrene beads (final concentration of 5 pM diluted in buffer I) with a diameter of 0.46 µm were added to the flow cell, and incubated for 10 minutes to allow binding to the biotin ends of the DNA. The flow cell was then washed with 100 µl of buffer I to remove any unbound beads. The flow cell was then washed with 100 µl of ParF storage buffer and incubated for 10 minutes before ParF was added at the desired concentration and the flow cell was sealed and incubated at room temperature for 10 minutes before the measurements were started. For a negative (DNA only) control another 100 µl of ParF storage buffer was added to the flow cell instead of ParF. TPM experiments were performed on a Nikon Diaphot 300 (on a TMC Vibracontrol clean top isolation table) using a 100x oil immersion objective (NA=1.25). Images were acquired using a Thorlabs CMOS camera (DCC1545M) at 25 Hz, with a camera exposure time of 20 ms. The x and y coordinates of individual beads were tracked in real time by custom-developed LabView software (National Instruments). Data was analysed manually to remove any beads that had double DNA tethers or that had fallen off the DNA during the experiment. The remaining beads were selected for further analysis and the root mean square displacement (RMS) was computed using the formula:

$$\sqrt{(x-\bar{x})^2+(y-\bar{y})^2}$$

The *x* and *y* values are the coordinates of the bead at each instant of time and are the mean values calculated from bead positions over 40 s time. Data analysis carried out with Origin 8.5 software.

2.19 Western blot

2.19.1 Preparation of samples and running of gel electrophoresis

Western blot was used to analyse the concentration of ParF, ParF-Emerald and ParG-mCherry expressed in cells analysed in confocal microscopy. Therefore the same competent cells, *E. coli* BW25113, were used. Transformations were carried out as per 2.3.10. After incubation, 8-10 colonies were inoculated in 30 ml of M9 minimal medium (with antibiotics) and grown at 37˚C for 1 hour with shaking. The cells were then induced with 3 µl of 10% arabinose (final concentration on 0.03%) and grown for a further 3 hours at 30°C with shaking. The cells were centrifuged at 2,000 xg, 4 °C for

10 minutes and the supernatant was removed. The cells were resuspended in 1 ml of binding buffer (20 mM Tris pH 7.5-8.0, 500 mM NaCl, 15 mM Imidazole, 10% Glycerol) and sonicated six times for 30 seconds each at a power of 70%. Cells were centrifuged at 11,000 xg, 4°C for 30 minutes. 60 µl of the supernatant was taken and 6 µl of 10X SDS loading buffer was added before the samples were heated to 95°C for 5 minutes. 60 µl were then loaded onto a 12% SDS-polyacrylamide gel and subjected to electrophoresis. 5 µl of a Prestained Page Ruler (Thermo Scientific) was loaded in order to estimate the size of the proteins. The gel was run for 60 minutes at 190 V.

2.19.2 Protein transfer onto Hybond ECL nitrocellulose membrane

Proteins from the gel were transferred onto a Hybond ECL nitrocellulose membrane (GE Healthcare). The membrane and 4 pieces of 3MM Whatman paper were cut to the size of the gel and soaked, along with 2 sponges, for 10 minutes in 1X Western transfer buffer (48 mM Tris pH 8.3, 39 mM Glycine, 0.037% SDS and 20% methanol). The transfer cassette (Bio-rad system) was then assembled first with the addition of one sponge and two pieces of Whatman 3MM paper followed by the gel and then the membrane was placed on top of gel carefully, avoiding air bubbles. The remaining two pieces of Whatman 3MM paper and sponge were placed on the top of the membrane. The cassette was then placed in to the tank and the DNA transfer was carried out at 30 mA overnight in western transfer buffer. The cassette was then disassembled and the membrane was removed carefully and the positions of the lanes were marked.

2.19.3 Detection of proteins

The membrane was rinsed with 1X Phosphate-buffered saline (PBS) (137 mM NaCl, 2.7 mM KCl, 10 mM Na_2HPO_4, 2 mM KH_2PO_4, pH 7.4) and the membrane was then blocked in 50 ml of blocking buffer which is 1X PBS with 0.1% Tween20 (Sigma) and 5% milk (Marvel original dried skimmed milk) with incubation at room temperature with shaking. After incubation, the membrane was rinsed briefly with 1X PBS-0.1% Tween 20. The affinity purified primary antibodies against ParF and ParG were used at 1:100 and 1:1000, respectively. Incubation of the primary antibodies was in 10 ml of blocking buffer for 4 hours at room temperature. The membrane was then washed twice with 1X PBS-0.1% Tween20, each for 10 minutes with shaking at room temperature. The secondary anti-rabbit antibody (Life technologies) was used at 1:30,000, again in 10 ml of blocking buffer. The membrane was incubated at room temperature with

shaking for 1 hour. The membrane was washed three times in 1X PBS-0.1% Tween20, each for 10 minutes with shaking at room temperature. Detection was carried out with the Pierce ECL Western blotting substrate (Thermo Fisher Scientific), 2 ml of luminol enhancer solution and 2 ml of peroxide solution was added to the membrane and incubated for 1 minute at room temperature. The membrane was removed placed in a film cassette and covered with an acetate sheet before being exposed to an X-ray film overnight.

Chapter 3: Disruption of the ParF dimer-dimer interface affects protein self-assembly, localisation and dynamics over the nucleoid

3.1 The dimer-dimer interface of ParF

The partition locus of plasmid TP228 consists of the *parFG* genes with an upstream centromere-like site, *parH*. ParF is the ATPase with the Walker-type ATP binding motif and ParG is the centromere binding protein (CBP) (Barilla *et al*., 2005). ParF has been shown to be monomeric when bound to ADP and dimeric when bound to ATP. Upon binding ATP and forming a dimer, ParF is seen to form higher order structures whereas binding of ADP antagonises this behaviour. The cycling between ADP and ATP bound states and the assembly and disassembly of these polymers of ParF is likely to be the driving force behind TP228 segregation, however the details of the mechanism are still to be elucidated. The structures of ParF bound to ADP and to AMPPCP (non-hydrolysable ATP analog) have been solved revealing the protein consists of a single domain with a central seven-stranded twisted β-sheet surrounded on each side by four α-helices (Figure 3.1) (Schumacher *et al*., 2012).

Figure 3.1 - Structure of monomeric ParF. Ribbon diagram of monomeric ParF indicating the secondary structural elements, helices are shown in blue, strands are shown in red and loops are green (Schumacher *et al*., 2012). The structural images were generated by using CCP4MG version 2.10.4 using the 4E07 PDB coordinates.

This structural data also provided further insight into the mechanism of how ParF forms higher order assemblies. The ParF-ATP dimers were seen to interact with each other to form dimer-of-dimer units. It was proposed that these dimer-of-dimer units formed the building blocks of the ParF polymers (Figure 3.2). The dimer-of-dimer units have possible interacting surfaces on all sides, which are both geometrically and electrostatically complementary, and therefore allow long irregular polymers to form. Two interfaces that were identified on the surface of the ParF dimers (interface 1 and 2) were further investigated to try and gain a better understanding of these ParF higher order structures. Residues were identified that make key interactions at ParF interfaces and were changed to a particular amino acid dependent upon the interaction that needed to be disrupted. A triple mutant harbouring changes at interface 1 was previously constructed (Schumacher *et al*., 2012) and found to disrupt plasmid segregation likely due to the inability of the mutant to form higher order structures upon ATP binding (Figure 3.3). A double mutant harbouring changes at interface 2 was also constructed however, the mutant protein presented purification challenges and therefore could not be further investigated (Schumacher *et al*., 2012).

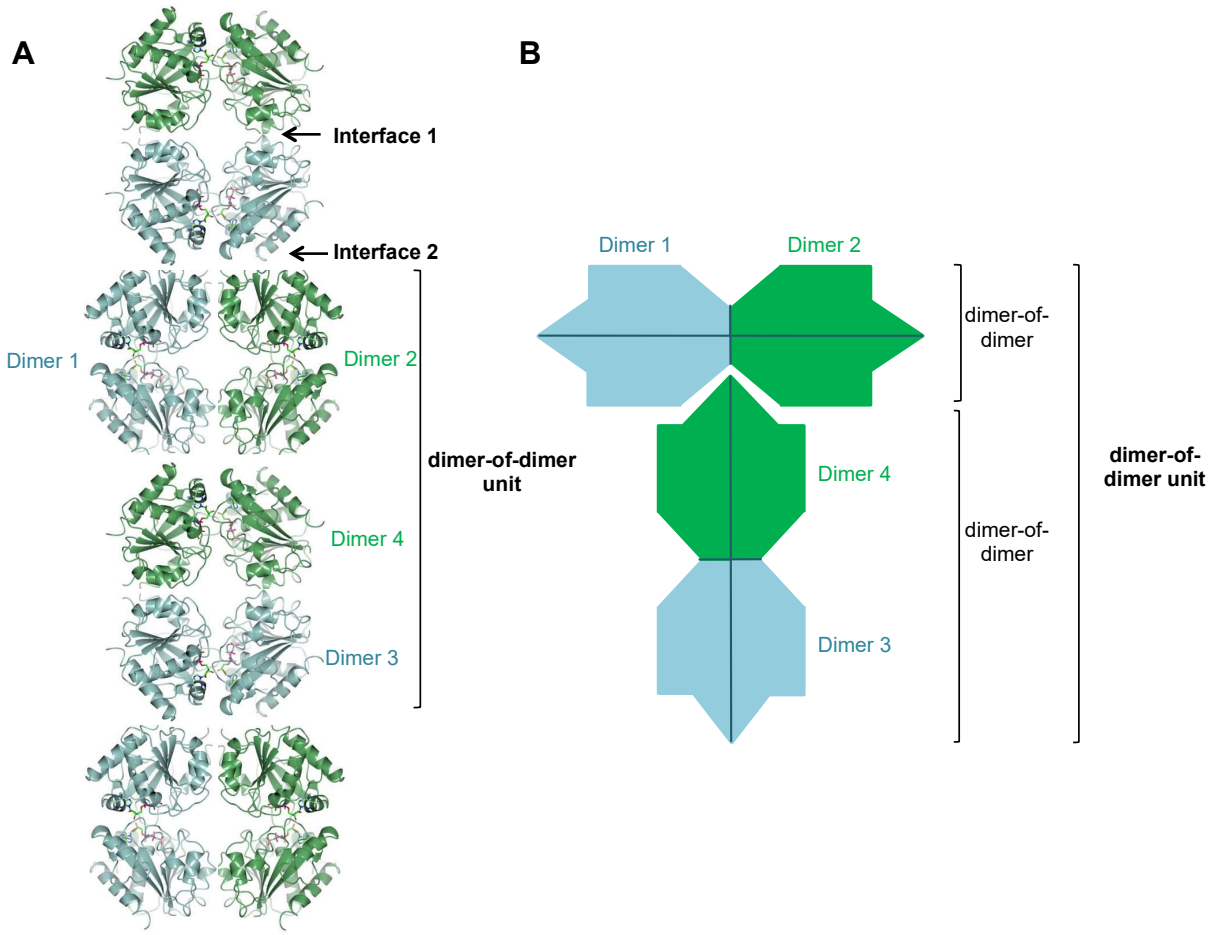

Figure 3.2 - The dimer-of-dimer unit formation by ParF. A) A ribbon diagram of ParF-AMPPCP dimers forming the units of the irregular ParF polymers. B) A schematic diagram of the ParF dimer-of-dimer unit. Adapted from (Schumacher *et al*., 2012). The structural images were generated by using CCP4MG version 2.10.4 using the 4E07 PDB coordinates.

The aim of this part of the study was to further investigate the effects of the changes in the triple mutant on the ability of ParF to form higher order structures and to construct a mutant at interface 2 that would be predicted to disrupt ParF dimer-of-dimer unit formation. The triple mutant, ParF-K64A-V89Y-M96A, has been shown to disrupt TP228 plasmid segregation *in vivo* through the use of plasmid partition assays (Hayes, 2000). Plasmids which contain the wild type partition cassette have a plasmid retention of ~70±10%, however a plasmid containing the partition cassette with *parF-K64A-V89Y-M96A* have a plasmid retention of 25±10%. *In vitro* analysis of the triple mutant showed that although the mutant was able to bind and hydrolyse ATP similarly to the wild type protein, the triple mutant was unable to form higher order structures upon addition of ATP. This suggested that disrupting interface 1 of the protein does affect ParF assembly of higher order structures and further work was carried out in order to support this view, the results of which are discussed in the following sections. S185W-G188W was the double mutant originally constructed to try and disrupt interface 2 (Schumacher *et al*., 2012). The mutant protein was refractory to purification, which suggested that disrupting this interface has a serious effect on ParF and therefore worth further investigation. Two single mutations were instead constructed at interface 2 in order to try and disrupt the interface without causing deleterious effects on the protein stability. S185 and S186 were selected for mutagenesis studies; S185 was a residue in the double mutant previously constructed and S186 was observed to protrude out at interface 2 of ParF and therefore was a plausible target for disrupting this interface (Figure 3.3). S185 and S186 were converted to tryptophan and phenylalanine, respectively, in order to try and disrupt the interface by replacing serine with large bulky amino acids.

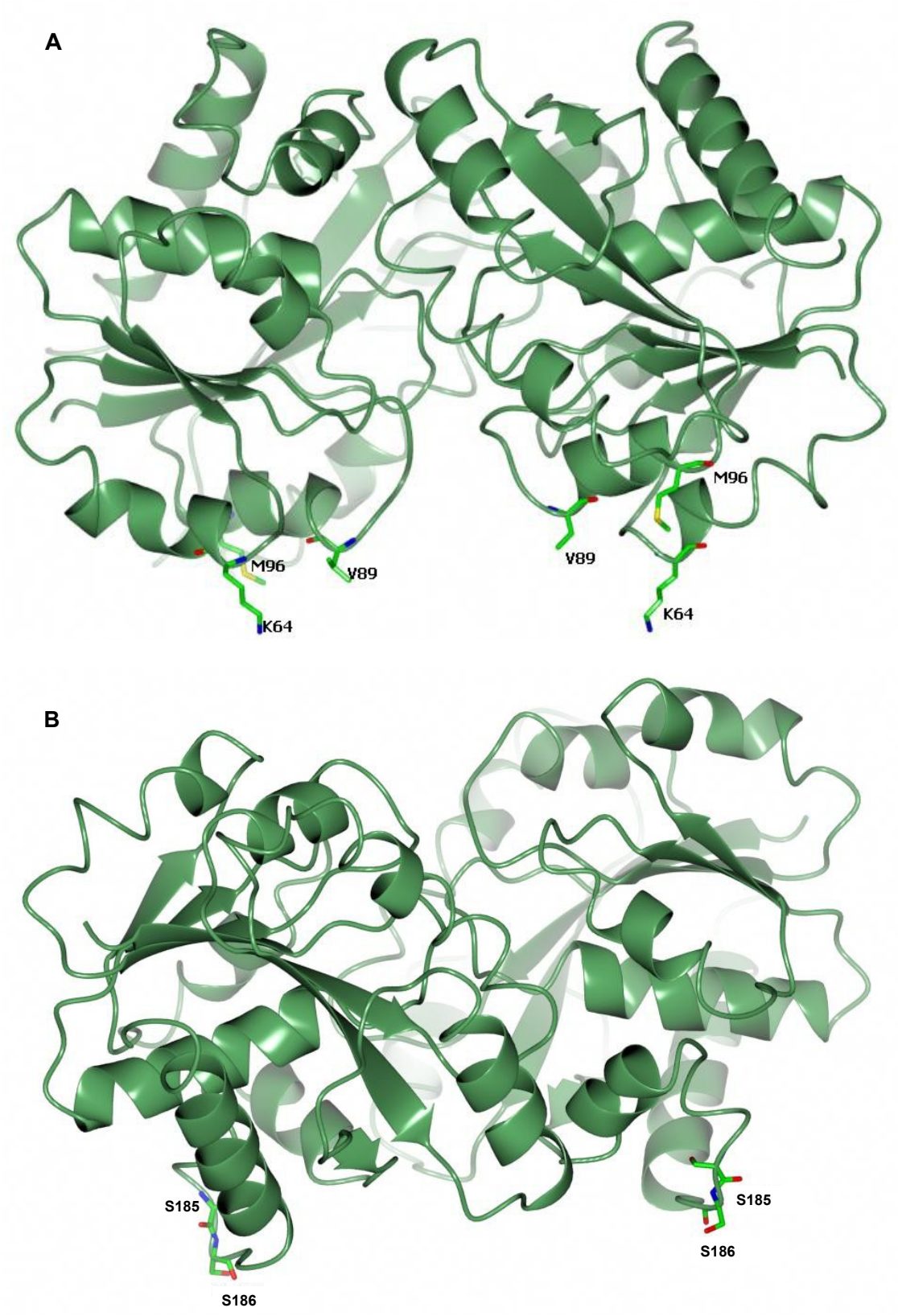

Figure 3.3 - Structure of ParF showing the position of residues changed at interface 1 and interface 2. A) The residues changed in the triple mutant – K64-V89-M96 at interface 1. B) The position of the two single residues changed at interface 2, S185 and S186. The structural images were generated by using CCP4MG version 2.10.4 using the 4E07 PDB coordinates

3.2 Construction of *parF-S185W* and *parF-S186F* at interface 2 of the ParF dimer

In this study two vectors were used, pFH450 and pFH547, which were derived from the stability probe vector pALA136. The pALA136 plasmid, a pBR322 derivative that has two origins of replication, P1 for low copy number and ColE1 for medium copy number, has been used to investigate plasmid segregation as the vector is highly unstable under conditions that support low copy number replication. If DNA partition genes are introduced then the plasmid become more stable (Macartney *et al*., 1997). pFH450 was generated by introducing multiple cloning sites into pALA136 and pFH547 was then produced by inserting the *parFGH* region from the TP228 plasmid into pFH450 using the restrictions sites *Sal*I and *Eco*RI (Hayes, 2000) (Figure 3.4). pFH547 contains the wild type *parFGH* partition cassette and is used throughout this study as a template for mutagenesis and for the analysis *of parF* mutations. pFH547 contains unique restriction sites within the *parF* and *parG* genes and these were used to swap the wild type regions with a fragment containing the desired mutation. Restriction sites were selected on the basis of the position of the mutation (Figure 3.5).

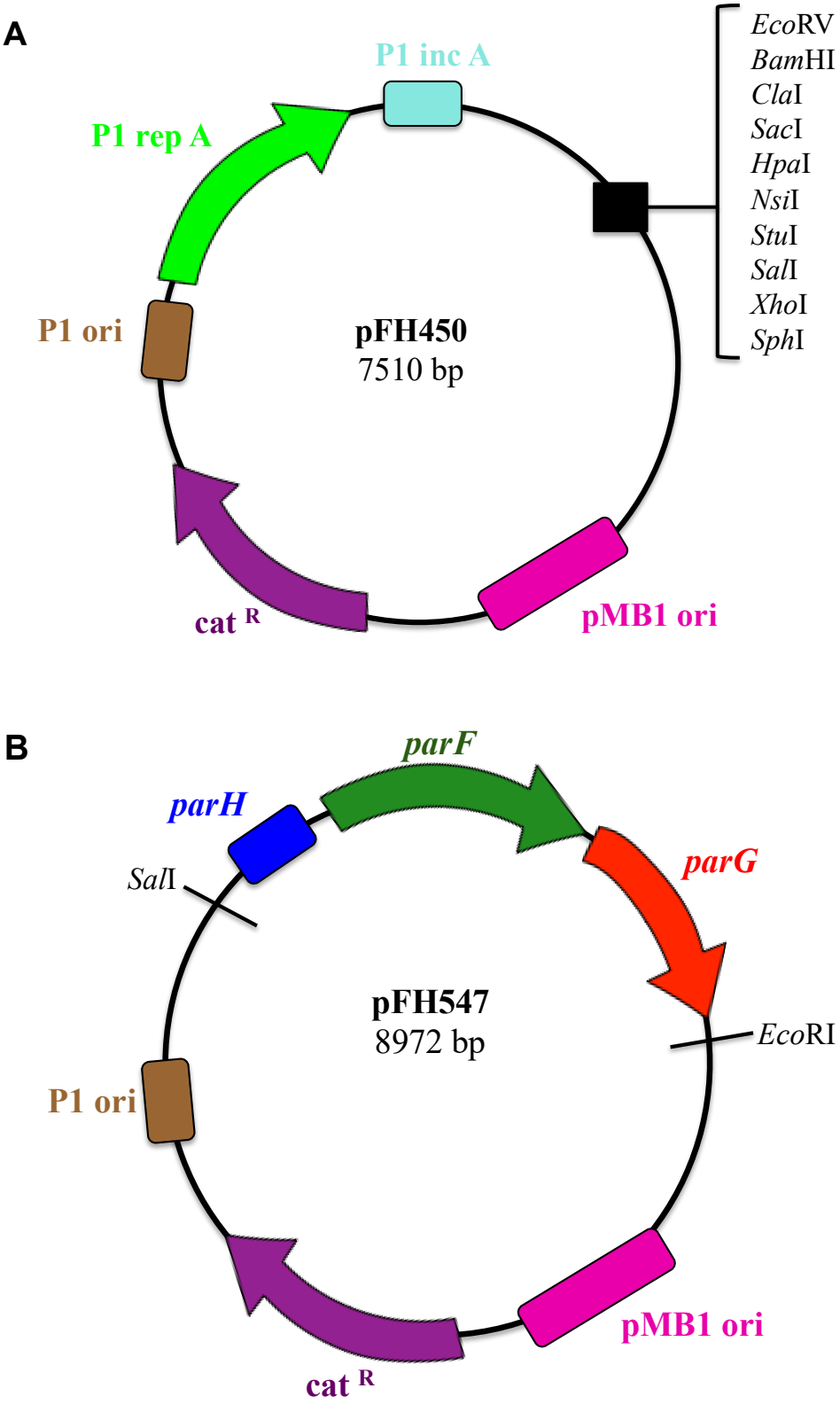

Figure 3.4 - Vector map of pFH450 and pFH547. A) pFH450 containing multiple cloning sites, chloramphenicol resistance gene and two origins of replication for low and medium copy number. B) pFH547 habouring the wild type *parFGH* partition cassette.

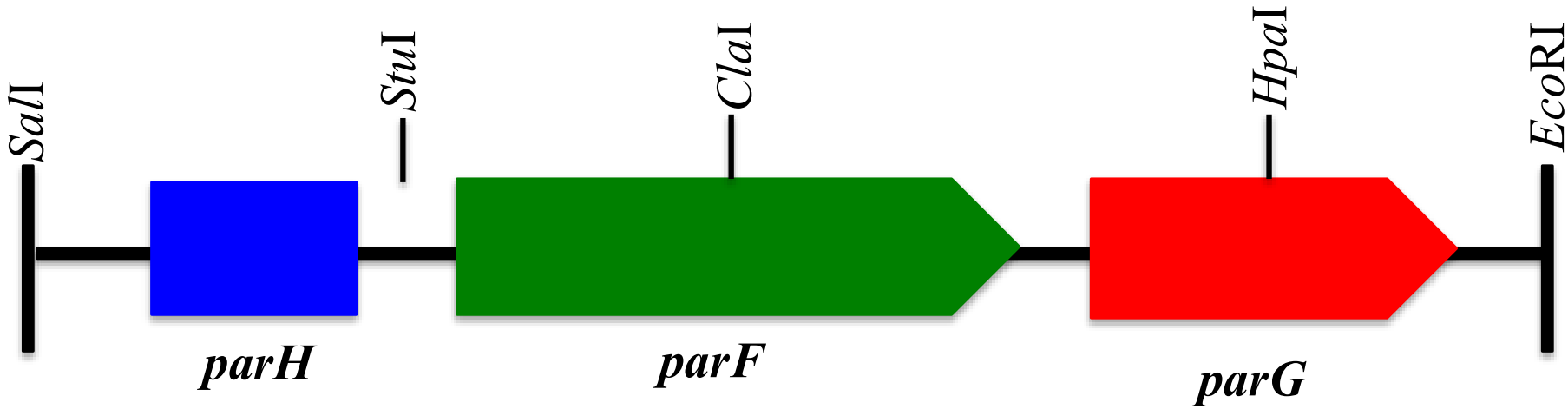

Figure 3.5 - Schematic representation of the *parFGH* region inserted into pFH547. The *parF, parG* and *parH* loci are shown with restriction sites used for construction of ParF mutants.

Overlap extension mutagenesis was carried out as detailed in section 2.4. Two single changes were constructed at interface 2, ParF-S185W and ParF-S186F, and the internal primers were designed accordingly. In both cases, the PCR 1 product amplified was of approximately 100 bp in size and PCR 2 was 360 bp. The two fragments of PCR 1 and PCR 2 were annealed, before PCR 3 was carried out as detailed in 2.4, to amplify a PCR product of 434 bp (Figure 3.6).

The PCR fragment from PCR 3 and the pFH547 vector were then digested with *Cla*I and *Hpa*I restriction enzymes as detailed in section 2.3.3 (Figure 3.7). The PCR fragment was subjected to ethanol precipitation (Section 2.3.4) and the vector subjected to alkaline phosphatase treatment (Section 2.3.5) before the ligation reaction was set up as detailed in section 2.3.8. *E. coli* DH5α cells were transformed with the ligation mixture and ten colonies were picked to screen for positive clones as detailed in 2.3.11 (Figure 3.8). Potential positive clones were sent for sequence analysis to GATC Biotech. The resulting sequencing data was then analysed to check the desired mutation was present and to confirm the remainder of the sequence contained no additional mutations. ABI sequence traces are shown in Figure 3.9, the wild type *parF* sequence is shown between the two restriction sites and the sequence of the two mutations constructed.

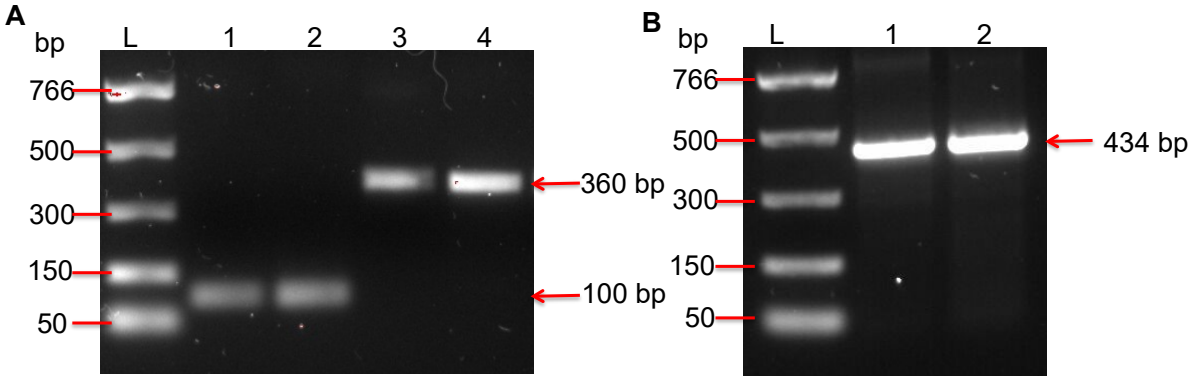

Figure 3.6 - Agarose gel showing PCR products from overlap extension mutagenesis of *parF-S185W* and *parF-S186F*. A) Agarose gel of the products of PCR 1 and PCR 2. Lanes: L – NEB PCR marker; 1, product of PCR 1 of *parF-S185W* mutagenesis; 2, product of PCR 1 of *parF-S186F* mutagenesis; 3, product of PCR 2 of *parF-S185W* mutagenesis; 4, product of PCR 2 of *parF-S186F* mutagenesis. B) Agarose gel of the products from PCR 3. Lanes: L – NEB PCR marker; 1, product of PCR 3 of *parF-S185W* mutagenesis; 2, product of PCR 3 of *parF-S186F* mutagenesis.

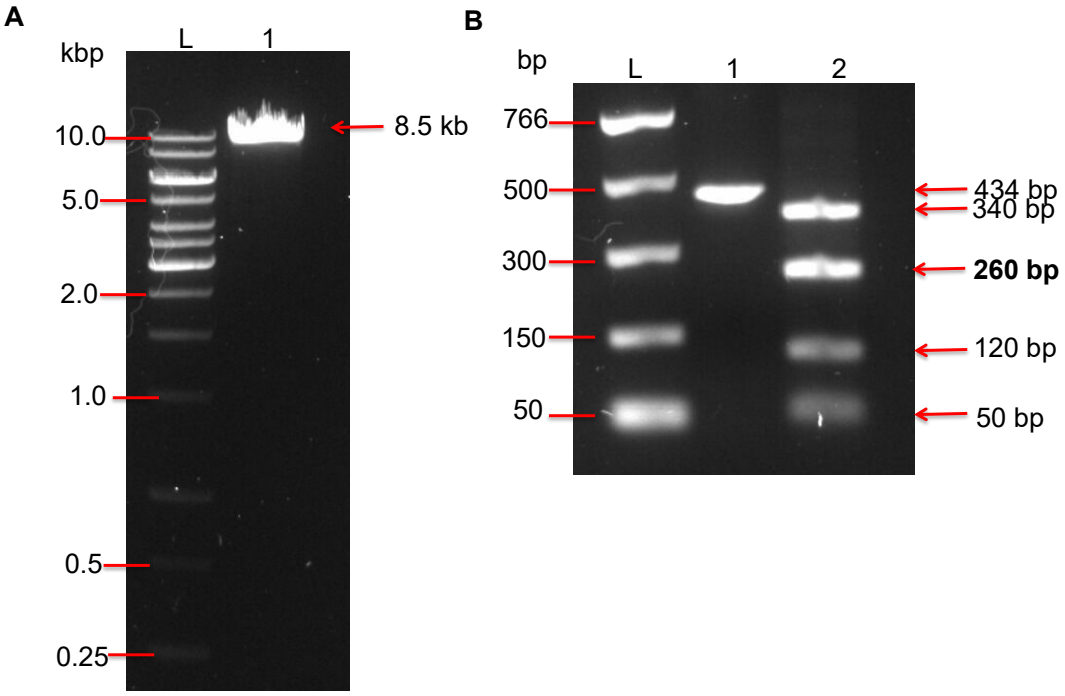

Figure 3.7 - Example of an agarose gel showing the restriction digest of pFH547 vector and PCR 3 fragment for *parF-S185W* mutagenesis. A) Digested pFH547 vector. Lanes: L, Gene Ruler 10 kbp ladder; 1 pFH547 digest. B) Digested PCR 3 fragment from annealed PCR 1 and PCR 2 products of *parF-S185W* mutagenesis. Lanes: L, Gene Ruler 10 kbp ladder; 1, Product of PCR 3 of parF-S185W mutagenesis after ethanol precipitation; 2, Digested products of PCR 3 which generates 4 fragments – the 260 bp fragment is the desired fragment that contains the mutation.

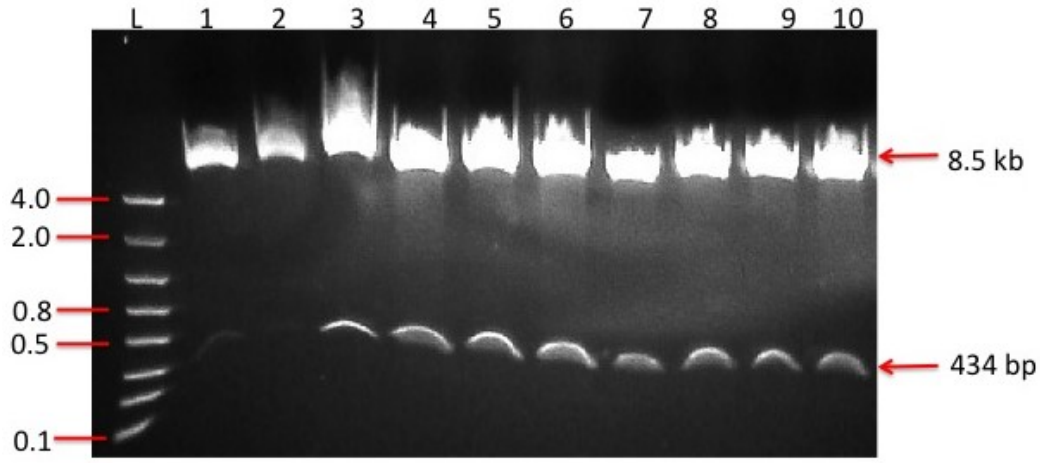

Figure 3.8 - Example of an agarose gel showing a restriction digest screen of pFH547 plasmids potentially habouring the desired mutation, *parF-S185W*. Lanes: L, FlashGel DNA marker (Lonza); 1 – digests of ten plasmids potentially harbouring the desired mutation.

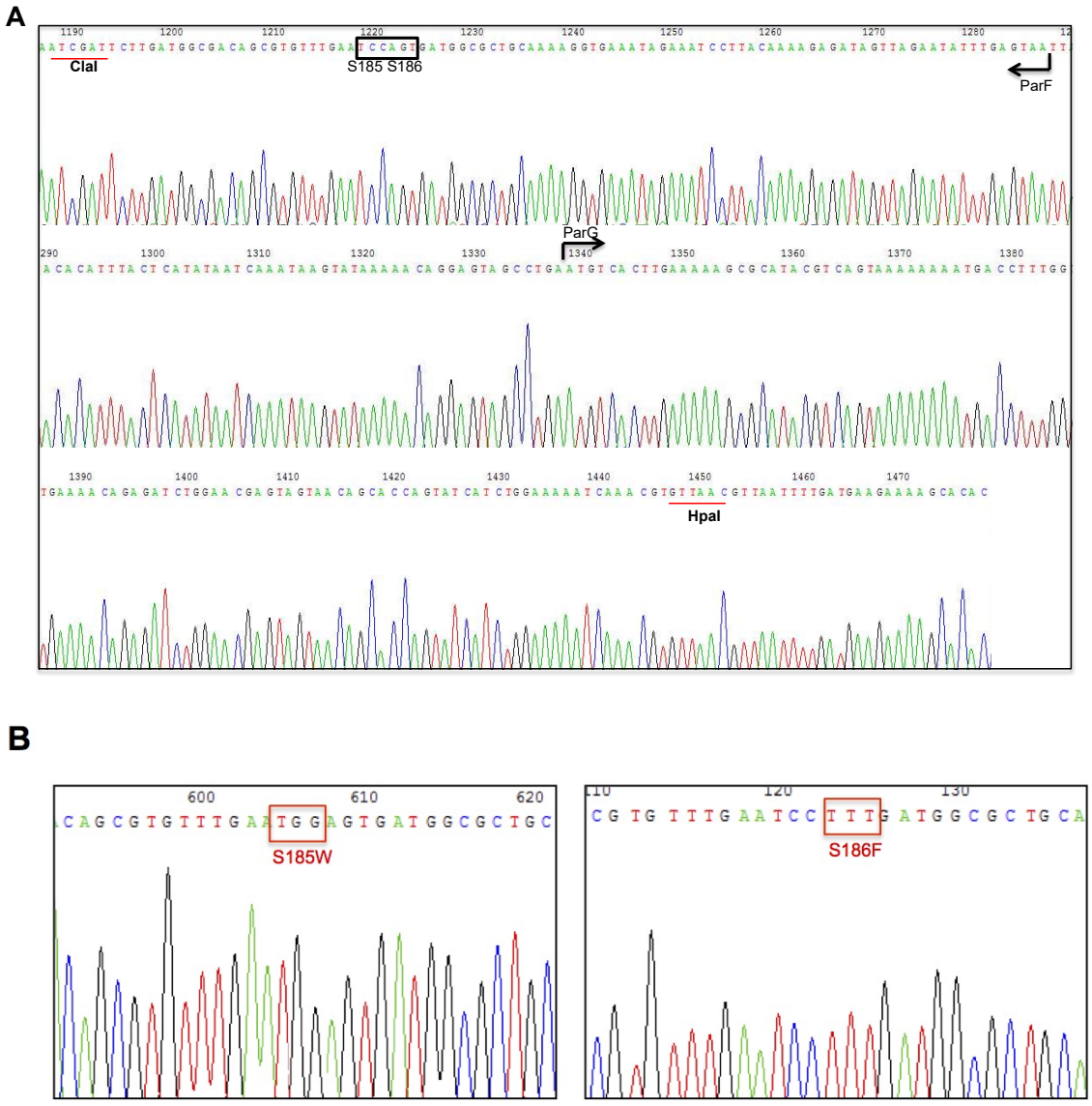

Figure 3.9 - ABI sequence traces showing the relevant section of wild type *parF* sequence between the two restriction sites *Cla*I and *Hpa*I and the sections for the mutations leading to the amino acid changes S185W and S186F. All sequencing data was obtained from GATC Biotech and the ABI sequence traces were analysed with Chromas software. A) ABI sequence trace of wild type *parF* and *parG* sequence between the two restriction sites *Cla*I and *Hpa*I indicated by a red line, black arrows shows the end of the *parF* sequence and the start of *parG* sequence. The codons for residues S185 and S186 and shown in a black box. B) Section of ABI sequence showing the two desired mutations resulting in S185W and S186F indicated by a red box.

3.3 *In vivo* analysis of the effect of the changes S185W and S186F on plasmid retention

Partition assays were employed to determine what effect the mutations have on plasmid retention (Section 2.7). The plasmids containing *parF-S185W* and *parF-S186F* were transformed into the *E. coli* BR825 (*polA*) strain that harbours a defective DNA polymerase I which therefore only supports replication from the P1 low copy number origin. After selection on LB medium with chloramphenicol, the cells were grown for approximately 25 generations on non-selective medium where only the plasmids containing an active partition cassette would be retained. The segregation activity of plasmids bearing the *parF* mutations was compared to that of the empty vector plasmid pFH450 and the plasmid pFH547, which contains the wild type *parFGH* partition cassette. The empty vector, pFH450, that doesn't contain a partition cassette is unstable in this *E. coli polA* strain and on average shows a plasmid retention of <5%. The vector with the wild type partition cassette, pFH547, has a plasmid retention of ~70%. Plasmid assays are carried out in at least triplicate to calculate the average plasmid retention of plasmids bearing *parF* mutants. As a general rule, if the retention is less than ~40% it is concluded that the mutation has a significant effect on plasmid retention and therefore further analysis is carried out. The results of the partition assay for ParF-S185W, ParF-S186F and also ParF-K64A-V89Y-M96A are shown in Figure 3.10. The partition assays showed that the plasmids containing either *parF-S185W* or *parF-S186F* did not show a significant reduction in plasmid retention and therefore no further analysis was carried out on ParF-S185W or ParF-S186F. The results of the partition assays for ParF-K64A-V89Y-M96A are consistent with those previously obtained (Schumacher *et al*., 2012).

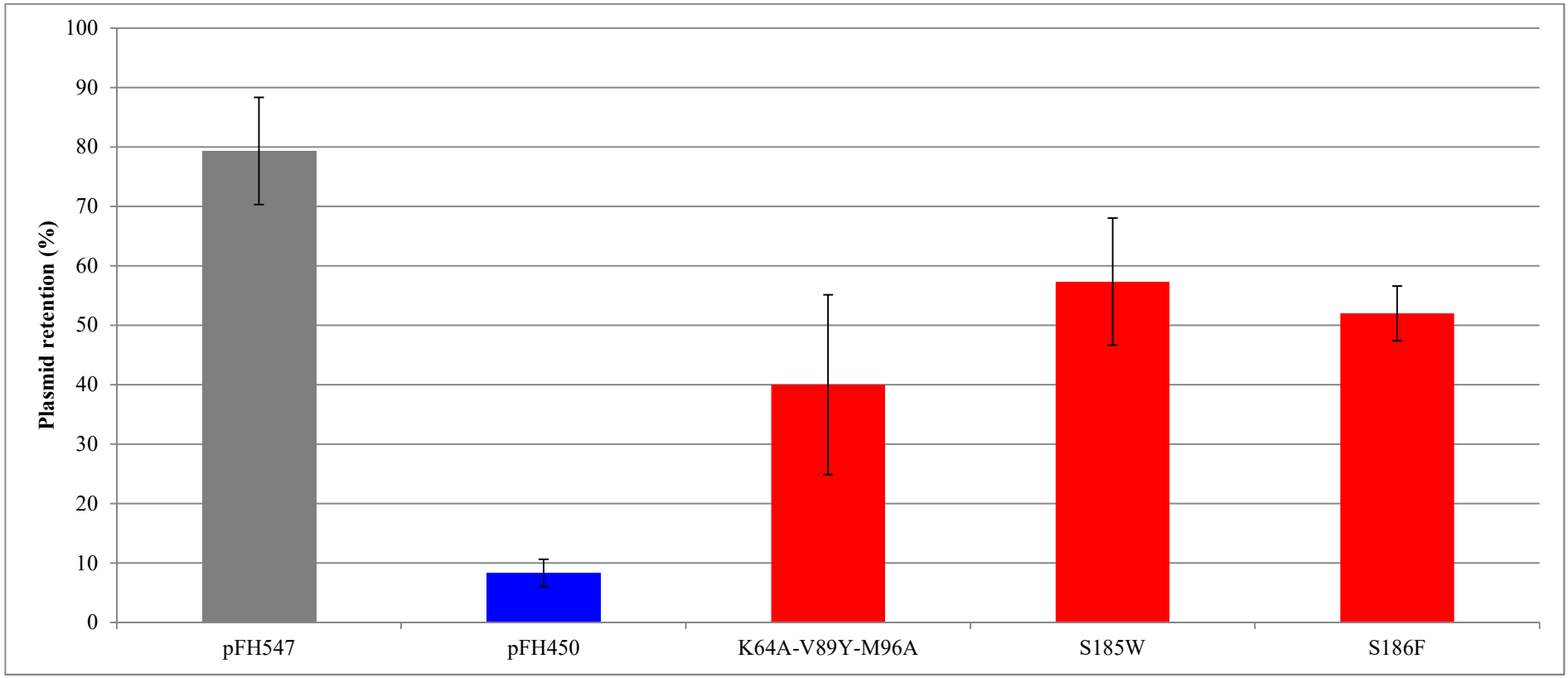

Figure 3.10 - Plasmid retention percentage of ParF mutants at the interface of the ParF dimer. pFH547 is the plasmid that contains the wild type *parFGH* partition cassette and pFH450 lacks a partition cassette. Plasmid retention shown is calculated from an average of at least three assays with the standard deviation.

3.4 ParF-K64A-V89Y-M96A

Partition assays, both in this study and as detailed in Schumacher *et al* (2012), have shown the retention of the plasmid bearing *parF-K64A-V89Y-M96A* is significantly lower than that of a plasmid containing the wild type *parFGH* partition cassette. ParF-K64A-V89Y-M96A has previously been purified and *in vitro* analysis has been carried out on the mutant (Schumacher *et al*., 2012). In this study, firstly the results that were reported by Schumacher *et al* (2012) were confirmed and subsequently additional *in vitro* and *in vivo* analysis was carried out to further characterise the mutant.

3.4.1 ParF and ParF-K64A-V89Y-M96A overproduction and purification

ParF and ParF-K64A-V89Y-M96A were overproduced using a pET expression system. The pET22b(+) expression vector was used, which contains a T7 promoter, *lac* operator and a C-terminal His-tag. The plasmids pDB-ParF and pET-ParF-K64A-V89Y-M96A were already constructed and available in the laboratory plasmid collection. For overproduction of the His-tagged ParF and ParF-K64A-V89Y-M96A, the appropriate pET vector was transformed into *E. coli* BL21(DE3) cells, which contain a chromosomal copy of the gene for T7 RNA polymerase under the control of the *lac* promoter. Upon addition of IPTG, production of T7 RNA polymerase allows expression of the gene cloned downstream of the T7 promoter, which in this case is *parF* or *parF-K64A-V89Y-M96A*. His-tagged proteins have been shown to have a similar plasmid retention *in vivo* as that of the native proteins, therefore it can be assumed that the His-tagged proteins are functional (Barillà and Hayes, 2003). The His-tagged proteins were purified using Ni^{2+} affinity chromatography (Section 2.5.3). Prior to purification, a pilot protein overproduction was carried out to confirm an appropriate induction time, (which in almost all cases was three hours) in order to produce the best level of ParF or ParF mutant overproduction. The solubility of the His-tagged protein was also assessed at this point (Figure 3.11). After this, purification was then carried out and the eluted ParF fractions were buffer exchanged and quantified by Bradford assay before analysing the purified proteins by SDS-PAGE (Figures 3.12 and 3.13). ParF and ParF mutants have a MW of 23.11 kDa including the His-tag.

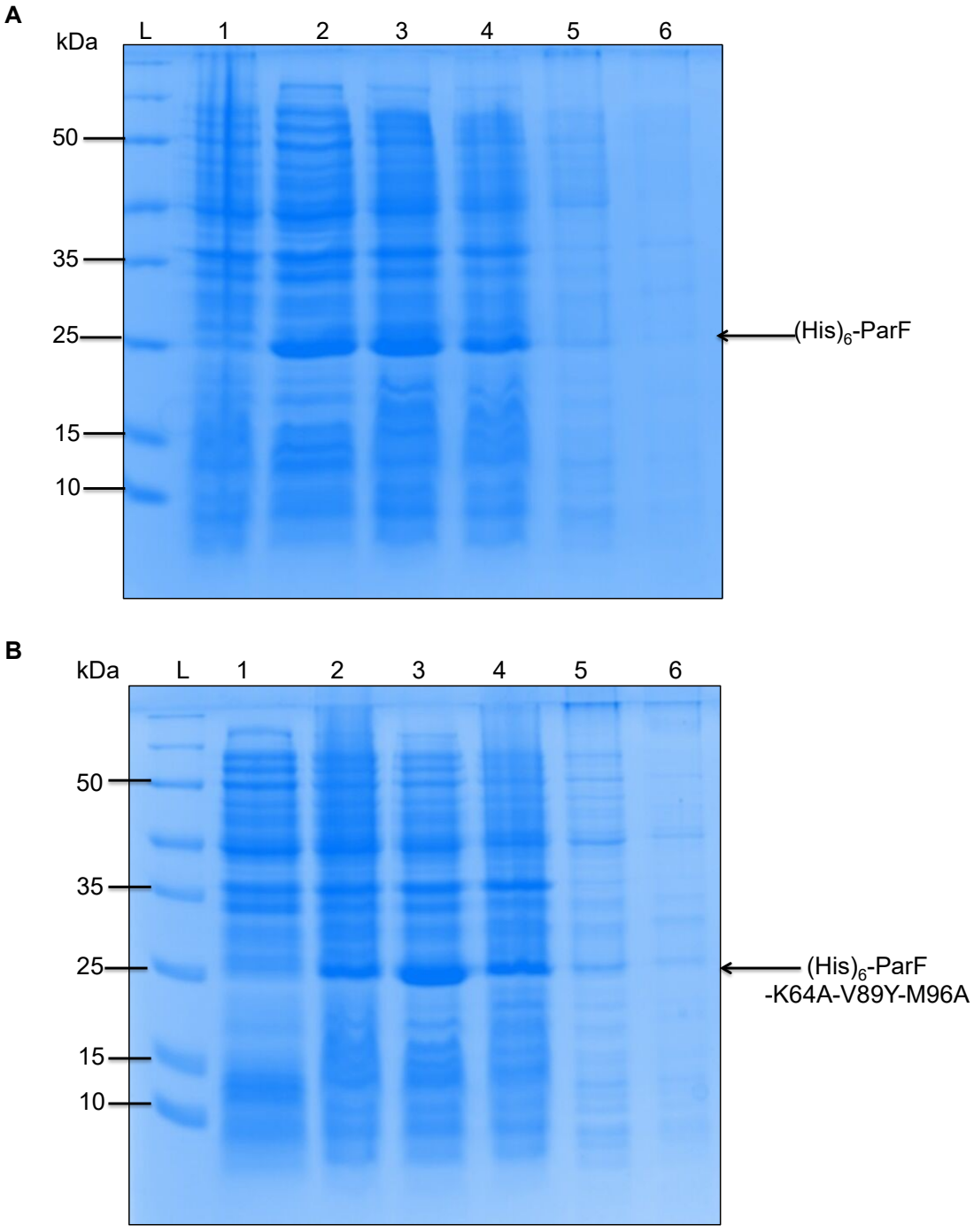

Figure 3.11 - ParF and ParF-K64A-V89Y-M96A overproduction trial and solubility assay. SDS-polyacrylamide gel showing various samples collected during the overproduction trial and solubility assay. Lanes: Ladder - PageRuler Prestained Protein Ladder, 1 - before induction, lane 2 – after 1 hour induction with IPTG, 3 – after 2 hours induction with IPTG, 4 – after 3 hours induction with IPTG, 5 – supernatant collected in solubility assay, 6 – pellet from solubility assay. A) Wild type ParF and B) ParF-K64A-V89Y-M96A.

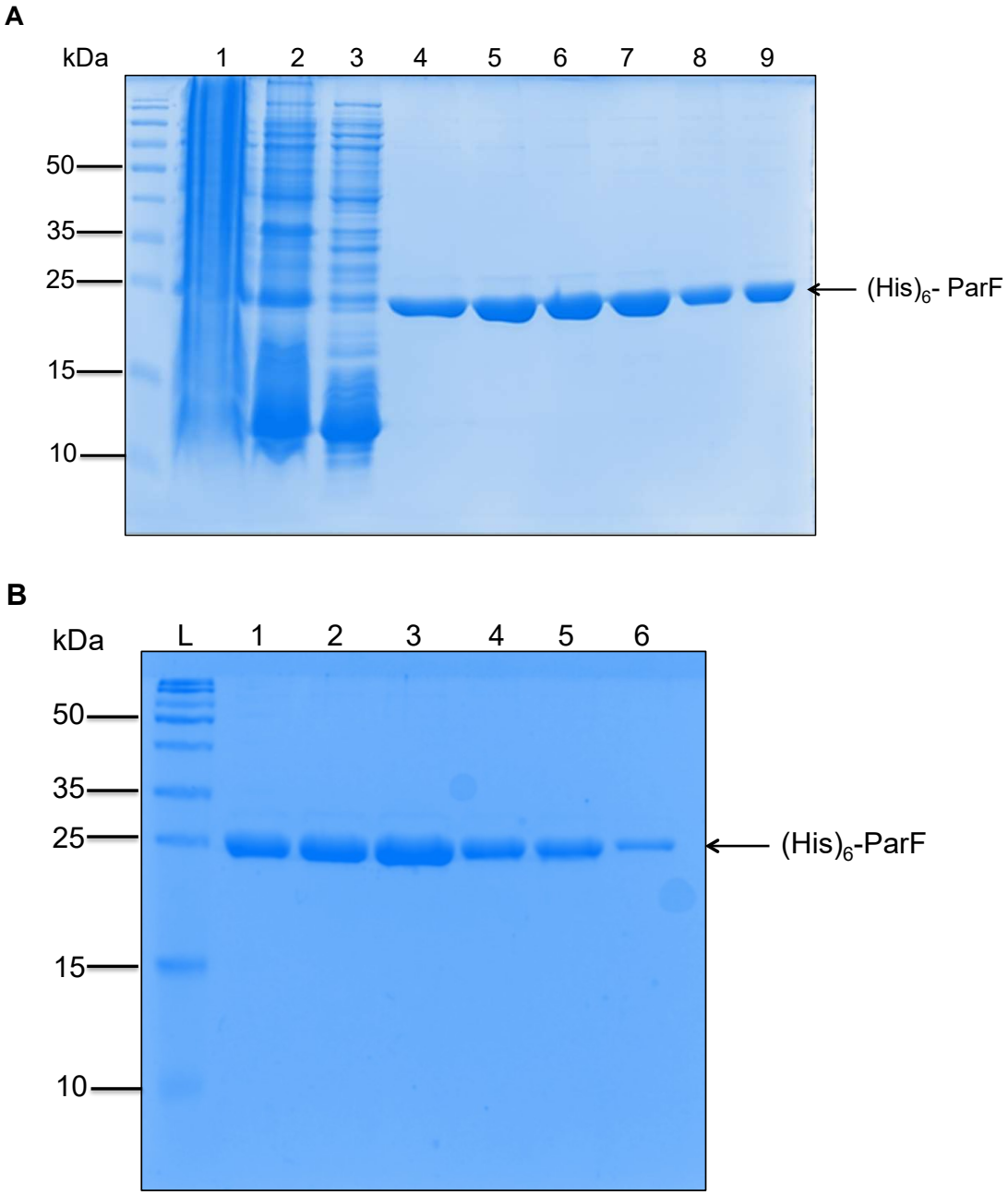

Figure 3.12 -SDS-PAGE analysis showing the purification of wild type ParF. His-tagged ParF is indicated by an arrow. A) Fractions collected during ParF purification. Lanes: Ladder – PageRuler Prestained Protein Ladder; 1, pellet fraction after centrifugation of sonicated cells; 2, supernatant of induced cell extract containing total soluble protein; 3, supernatant of induced cell extract after passing over the Ni^{2+} column; 4 – 9, selected elution fractions. B) ParF fractions after buffer exchange. Lanes: Ladder – PageRuler Prestained Protein Ladder; 1 – 6 buffer exchanged elution fractions of ParF protein.

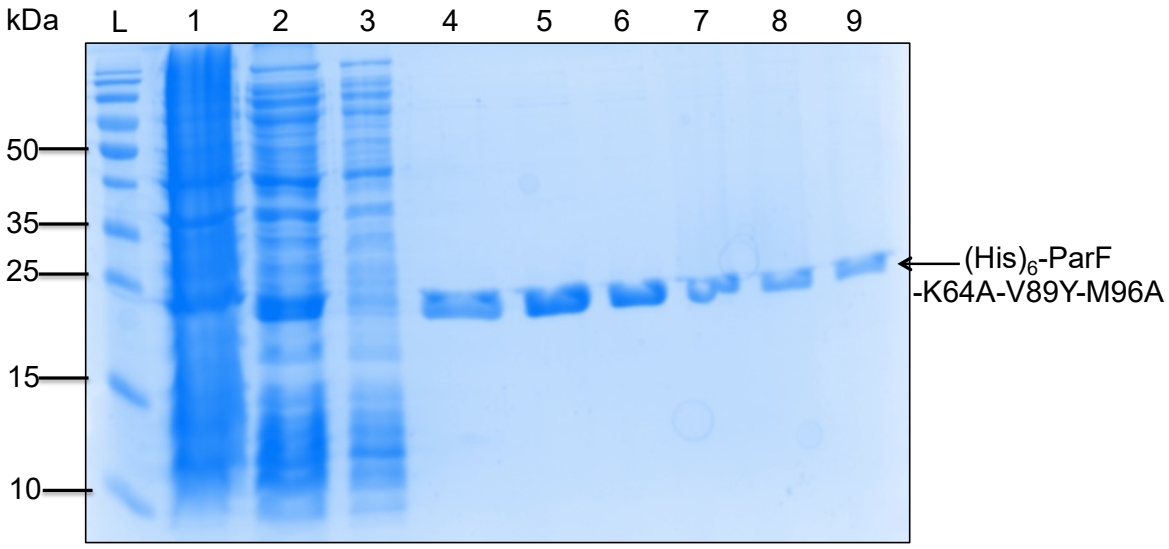

Figure 3.13 - SDS-PAGE analysis showing purification of ParF-K64A-V89Y-M96A. His-tagged ParF-K64A-V89Y-M96A is indicated by an arrow. A) Various fractions collected during ParF- K64A-V89Y-M96A purification. Lanes: Ladder – PageRuler Prestained Protein Ladder; 1, pellet fraction after centrifugation of sonicated cells; 2, supernatant of induced cell extract containing total soluble protein; 3, supernatant of induced cell extract after passing over the Ni^{2+} column; 4 – 9, selected buffer exchanged elution fractions.

3.4.2 Biochemical properties of ParF-K64A-V89Y-M96A and the ability of the mutant to form higher order structures

3.4.2.1 ParF-K64A-V89Y-M96A is able to bind ATP similarly to wild type ParF

Previous studies on ParF have shown that the protein is able to form polymers *in vitro* upon the addition of ATP (Barilla *et al*., 2005). Different techniques have been employed in order to analyse ParF polymer formation, two of which are Dynamic Light Scattering (DLS) and sedimentation assays. DLS measures the hydrodynamic radius of the protein in solution and allows ParF polymerisation to be analysed in real time. DLS allows particle abundance and size to be measured. Sedimentation assays are then performed to further support results observed with DLS. These techniques were therefore chosen to examine whether ParF-K64A-V89Y-M96A was able to form polymers *in vitro*. As previously shown, ParF forms polymers upon binding of ATP and thus fluorescence anisotropy experiments were carried out in order to check ParF-K64A-V89Y-M96A was able to bind ATP. A fluorescent ATP analog (MANT-ATP) was incubated with increasing concentrations of ParF and ParF-K64A-V89Y-M96A to analyse the protein's ability to bind ATP. ParF-K64A-V89Y-M96A was shown to bind MANT-ATP similarly to wild type ParF with K_d values of 0.44 μM and 0.43 μM, respectively (Figure 3.14). ParF is intrinsically a weak ATPase and the partner protein ParG stimulates this ATPase activity. Therefore it was also important to check ParF-K64A-V89Y-M96A ATPase activity, which was also shown to be similar to that of the wild type (Schumacher *et al*., 2012).

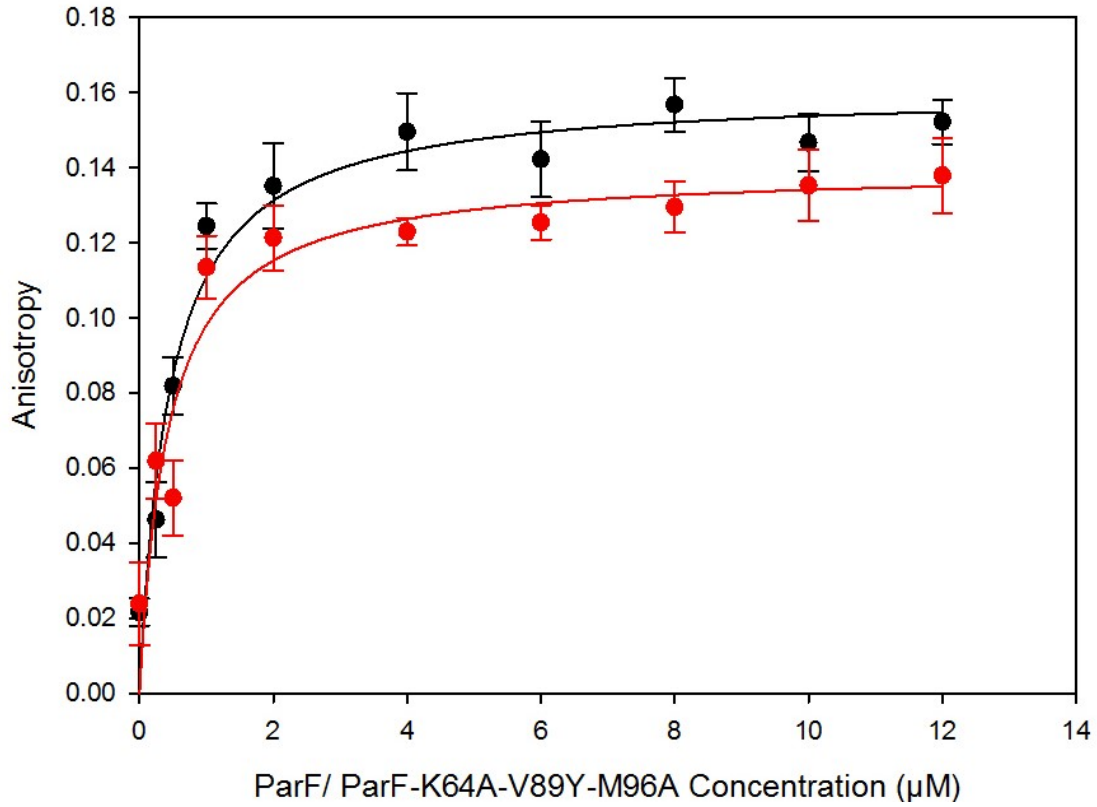

Figure 3.14 –ParF and ParF-K64A-V89Y-M96A ATP binding. ParF is shown in black, ParF-K64A-V89Y-M96A is shown in red. Ten anisotropy values are taken for each concentration and an average value is calculated and the standard deviation shown. Assays were carried out in triplicate.

3.4.2.2 ParF-K64A-V89Y-M96A is unable to assemble into higher order structures upon the ATP binding

After establishing the mutant protein showed ATP binding properties and ATPase activity similar to the wild type, the ability of the mutant to form higher order assemblies was analysed. In DLS experiments, ParF or ParF mutants (2.16 µM) are initially monitored, in the absence of nucleotides, at 30°C in order to establish a baseline. Generally, ParF proteins will remain stable for three minutes with an average intensity of ~150 kilocounts/second (kct/s) and an average particle size of ~ 25 nm and this allows a baseline measurement to be established. Upon addition of ATP or ATP-γ-S (500 µM) the intensity of light scattering will increase, almost immediately, to values ranging between 2000 – 10 000 kct/s. Measurements are then taken for a further six minutes or until the intensity plateaus. If ParF is monitored over a longer timer period, without nucleotide, a steady increase in intensity and particle size is seen, this is due to the fact that ParF has an intrinsic tendency to self-associate into polymers. When ADP is added, instead of ATP, no increase in intensity of light scattering is seen and even over a longer time period no increase in intensity is observed, thus indicating ADP

inhibits ParF polymer formation (Barilla *et al*., 2005). It has also been observed that ParG promotes ParF polymer formation, both in the presence and absence of ATP. It has been proposed that ParG is able to promote assembly of ParF higher order structures via two mechanisms, nucleation and bundling. In the absence of nucleotide it is thought that the N-terminal flexible tail of ParG bridges adjacent ParF monomers and thus aids the formation of ParF polymers (Barilla *et al*., 2007). In the presence of ATP, it is thought that ParG dimers associate with ParF polymers and thus crosslinks adjacent filaments (Barilla *et al*., 2005). In DLS experiments where ATP has already been added and the intensity has plateaued, the addition of ParG at the same final concentration of ParF results in a large increase in intensity with values up to ~ 25 000 kct/s. It should be noted that ParG alone does not show any increase in light scattering and therefore the increase in intensity seen when ParG is added is due to ParF forming higher order structures.

The ability of ParF-K64A-V89Y-M96A to form polymers was analysed firstly by carrying out a number of DLS experiments, in parallel with wild type ParF. Both ParF and ParF-K64A-V89Y-M96A were monitored over 60 minutes in the absence of nucleotide and upon addition of ADP, ATP and ATP–γ-S. When no nucleotide was present ParF shows a slow increase in intensity of light scattering due to the fact that ParF is seen to self-associate. ParF-K64A-V89Y-M96A shows a slight increase in intensity of light scattering but not to the same extent of the wild type protein (Figure 3.15A). When ADP is present both the mutant protein and the wild type protein show no increase in intensity of light scattering, which is consistent with the notion that ADP antagonises polymer formation (Figure 3.15B). Upon the addition of ATP, ParF shows a large increase in intensity of light scattering indicating the protein is forming higher order structures. In contrast, no increase in intensity of light scattering is seen for ParF-K64A-V89Y-M96A when ATP is added, indicating this mutant is unable to form higher order structures (Figure 3.15C). The same is observed upon the addition of ATP-γ-S (Figure 3.15D). Upon the addition of ParG, ParF-K64A-V89Y-M96A does show an increase in light scattering intensity therefore indicating that ParG is still able to promote the assembly of higher order structures of the mutant even though ATP is unable to do so. However the increase in light scattering intensity does not equal the level of the wild type even when the mutant is monitored over a longer time period (Figure 3.16). All these results were confirmed with sedimentation assays (data not shown).

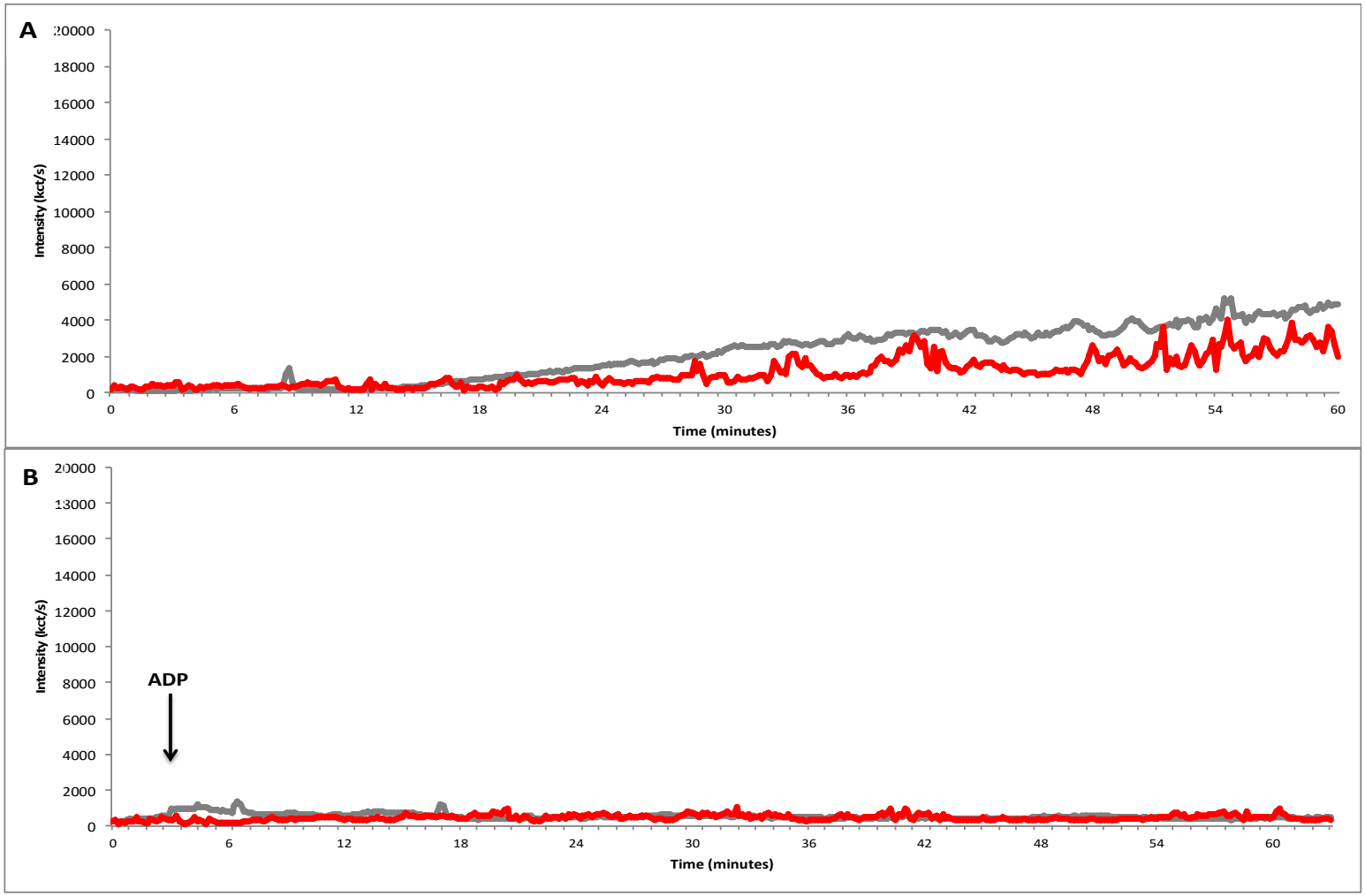
A
Intensity (kct/s)
20000
18000
16000
14000
12000
10000
8000
6000
4000
2000
0
0
6
12
18
24
30
36
42
48
54
60
Time (minutes)
B
Intensity (kct/s)
ADP
Time (minutes)

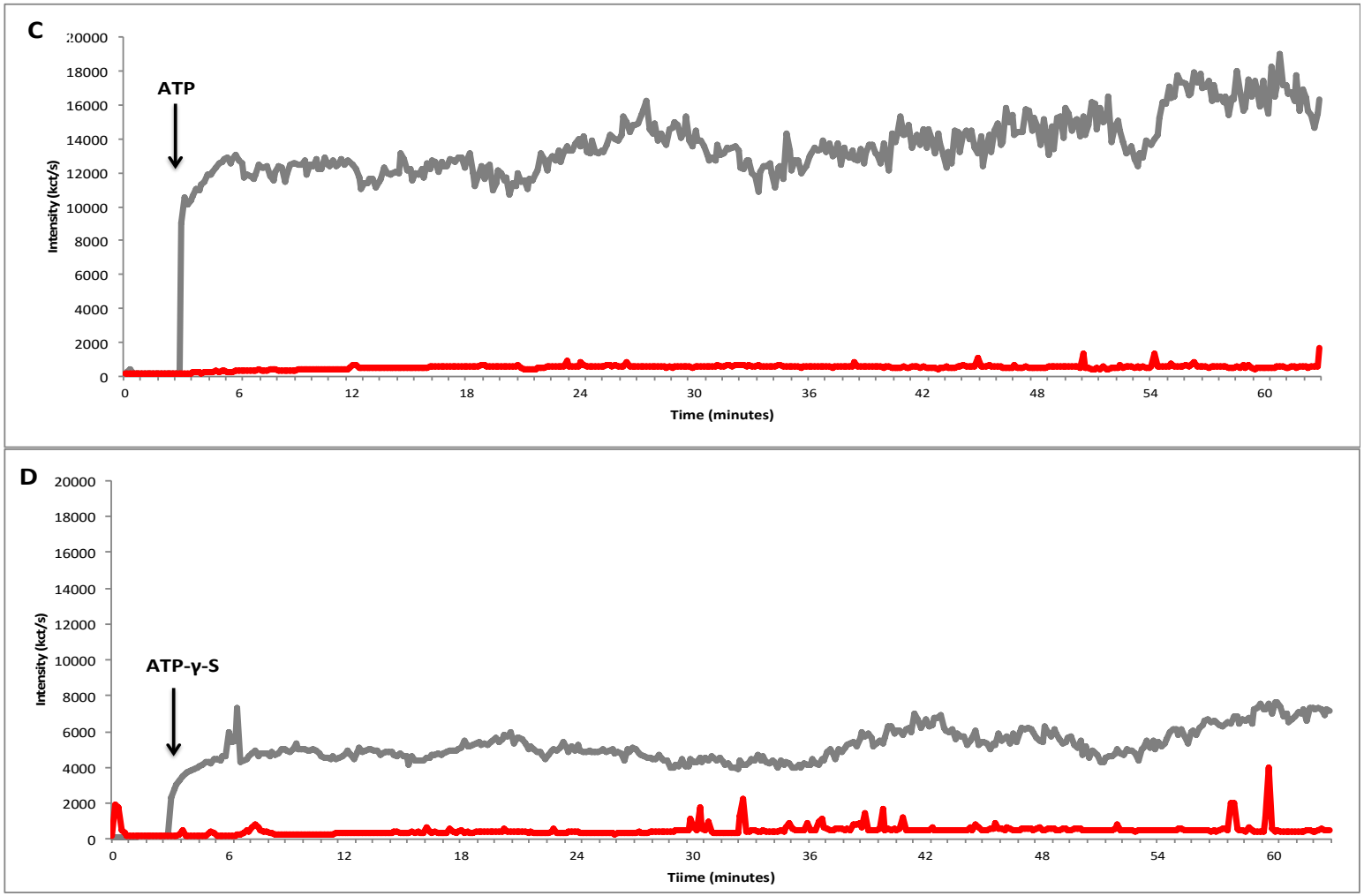

Figure 3.15 – DLS of ParF and ParF-K64A-V89A-M96A. DLS experiments were carried out and the increase in light scattering intensity (kct/s) was recorded for ParF and ParF-K64A-V89Y-M96A. ParF and ParF-K64A-V89Y-M96A were added at a final concentration of 2.16 µM and a baseline was obtained for three minutes and then nucleotide was added (500 µM) with $MgCl_2$ (5 mM). The point of addition is indicated by a black arrow. The light scattering intensity was then recorded for further 60 minutes. ParF is shown in grey and ParF-K64A-V89Y-M96A is shown in red. A) No nucleotide. B) ADP. C) ATP. D) ATP-γ-S. This is a representative experiment. Each experiment was repeated at least three times.

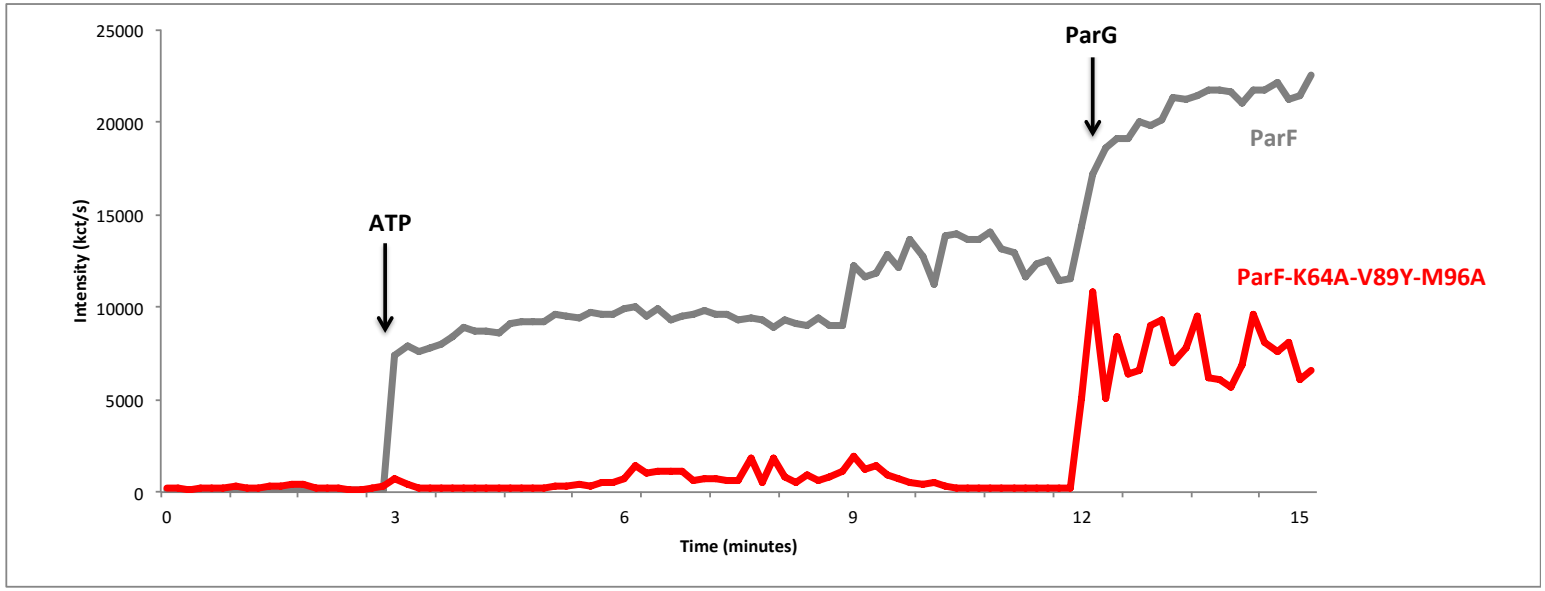

Figure 3.16 – DLS of ParF and ParF-K64A-V89Y-M96A in the presence of ParG. DLS experiments were carried out and the increase in light scattering intensity (kct/s) was recorded for ParF and ParF-K64A-V89Y-M96A. ParF and ParF-K64A-V89Y-M96A were added at a final concentration of 2.16 µM and a baseline was obtained for three minutes and then ATP was added (500 µM) with $MgCl_2$ (5 mM). The point of addition is indicated by a black arrow. The light scattering intensity was then recorded for a further nine minutes before ParG was added at a final concentration of 2.16 µM, as indicated by a black arrow, and the intensity recorded for further three minutes. ParF is shown in grey and ParF-K64A-V89Y-M96A is shown in red. This is a representative experiment. Each experiment was repeated at least three times.

Negative stain electron microscopy has been used to visualise the ultrastructures of ParF filaments (Barilla *et al*., 2005). Samples for electron microscopy were prepared in parallel with DLS experiments; protein and nucleotide concentrations were the same. This allowed results from the DLS experiments to be confirmed and also enabled comparisons between results seen for the DLS, as well as the appearance of the higher order structures to be visualised using electron microscopy. In the absence of ATP, ParF can be seen as small globular dots due to the tendency of ParF to self-associate. Upon addition of ATP ParF appears to form filament structures ranging from ~100 to ~500 nm in length (Figure 3.17). ParF-K64A-V89Y-M96A appears to form very small globular dots but upon the addition of ATP, unlike wild type ParF, larger filament structures cannot be seen. In fact, very little difference can be seen between the sample with no nucleotide and that containing ATP for ParF-K64A-V89Y-M96A and identifying any form of structure is very difficult (Figure 3.18). This supports the results seen in the DLS experiments; ParF-K64A-V89Y-M96A is unable to form higher order structures, as previously observed (Schumacher *et al*., 2012)

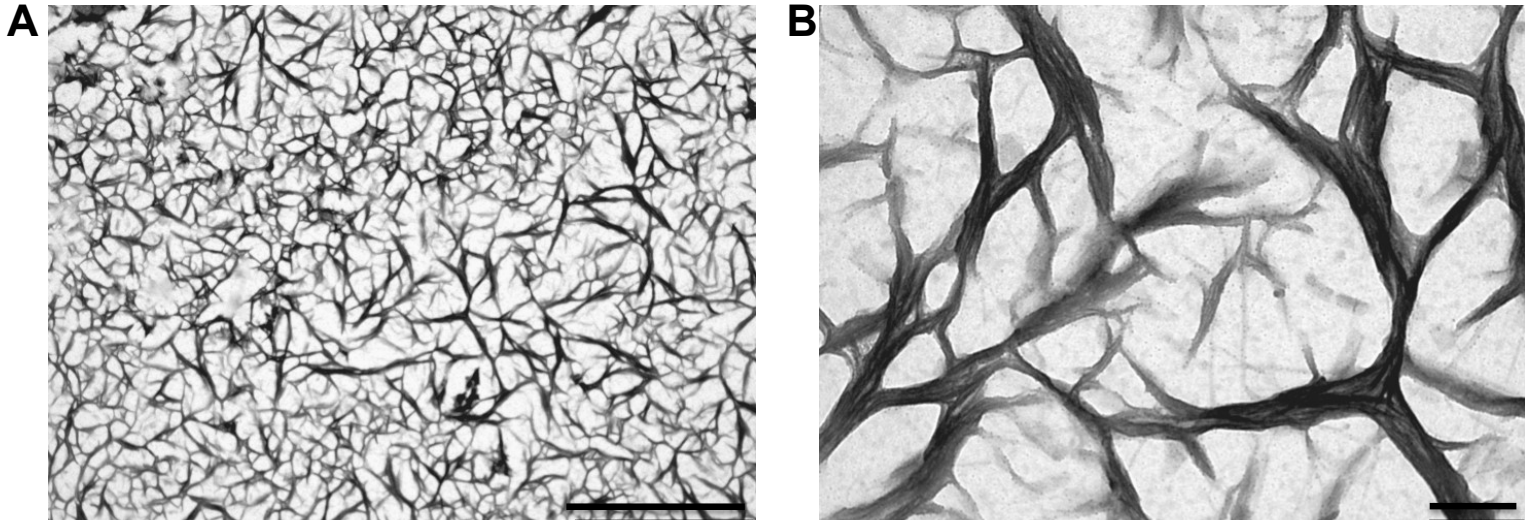

Figure 3.17 – EM observations of ParF in the presence of ATP. Ultrastructures of ParF observed by negative stain electron microscopy. ParF (2.16 μM) was visualised after the addition of ATP (2 mM). A) ParF structures shown at lower magnification. Scale bar = 2 μm. B) ParF structures shown at higher magnification. Scale bar = 200 nm.

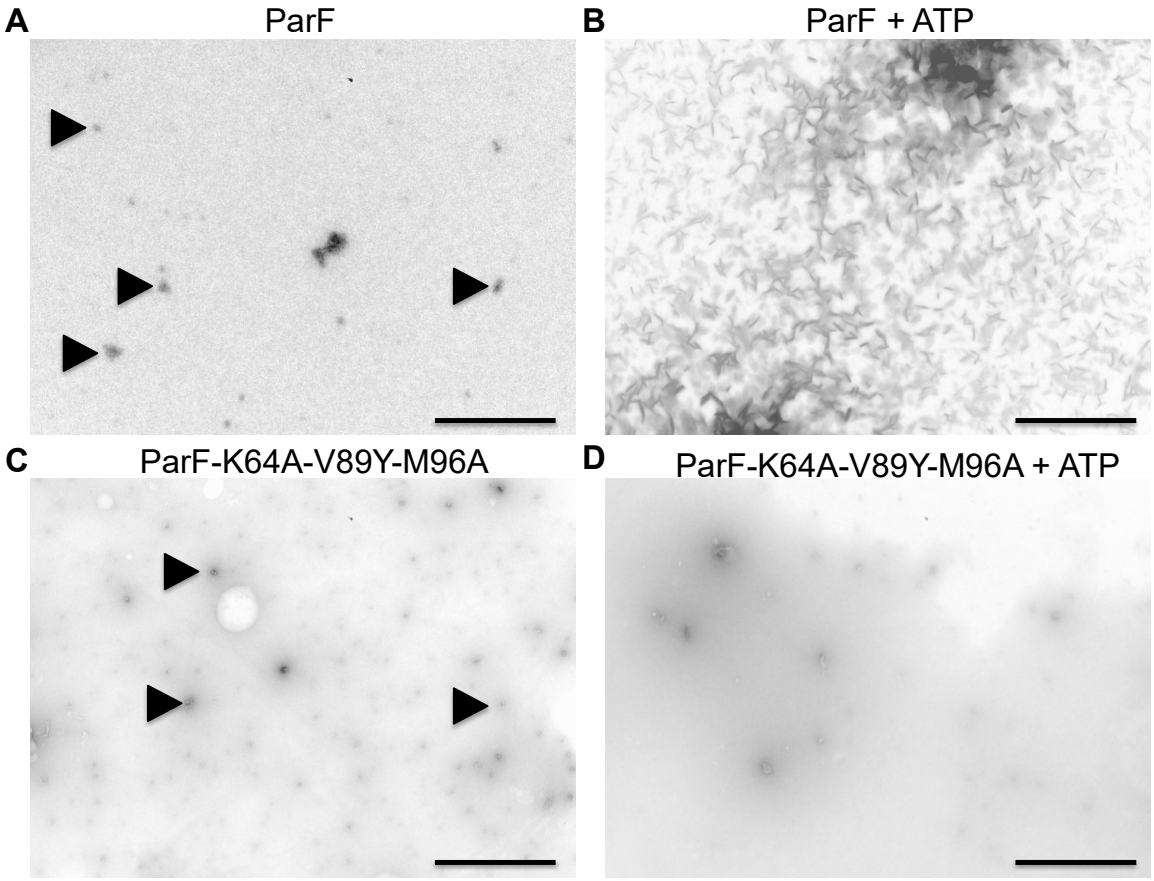

Figure 3.18 – EM observations of ParF and ParF-K64A-V89Y-M96A in the presence and absence of ATP. ParF or ParF-K64A-V89Y-M96A (2.16 μM) were visualised both in the absence and presence of ATP (2 mM). A) ParF. B) ParF + ATP. C) ParF-K64A-V89Y-M96A. D) ParF-K64A-V89Y-M96A + ATP. Small globular structures are indicated by black arrowheads. Scale bar = 1 μm.

3.4.2.3 ParF-K64A-V89Y-M96A is able to form a dimer similar to that of the wild type protein

It was proposed that ParF-K64A-V89Y-M96A might be unable to form higher order structures due to the fact that the interface at the dimer-of-dimer was disrupted. Therefore it was important to confirm the mutant was still able to form a dimer upon binding ATP. This would provide further support to the hypothesis that it is the disruption of the dimer-dimer interface that is preventing assembly of the mutant ParF into higher order structures. The ability of the mutants to form a dimer was firstly analysed by chemical cross-linking and then by using a bacterial two-hybrid system followed by quantification using a β-galactosidase assay.

Chemical cross-linking involves chemically joining two molecules by a covalent bond. Dimethyl pimelimidate (DMP) was used to chemically cross-link ParF dimers. DMP is an amine-reactive imidoester that reacts with primary amines to form amidine bonds. In the absence of DMP, ParF runs as a monomer (23 kDa) on a denaturing SDS-gel, however upon the addition of DMP ParF monomers are cross-linked, showing they interact to form a dimer, migrating on a SDS-gel at the position of a 46 kDa protein. ParF and ParF-K64A-V89Y-M96A (12 μM) were incubated with increasing concentrations of DMP (0 – 10 mM) for 2 hours at 37°C. ATP was added to the final reactions at a final concentration of 1 mM due to the fact that ParF is seen as dimer only in the presence of ATP. Figure 3.19 (B and D) show examples of SDS-gels in which ParF and ParF-K64A-V89Y-M96A were incubated with ADP, no presence of dimer was observed at any concentrations of DMP. ParF forms a dimer in the presence of 0.5 mM DMP and at the higher concentrations of DMP the intensity of the dimeric band increases. ParF-K64A-V89Y-M96A, like the wild type protein, forms a dimer at 0.5 mM DMP and again the band intensity of the dimer increase with increasing DMP concentrations (Figure 3.19).

A

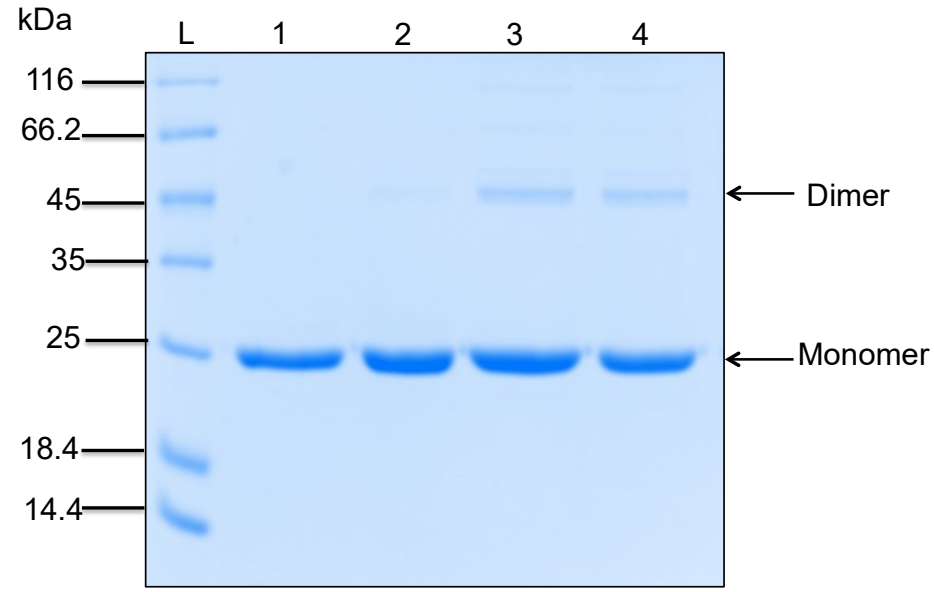
kDa
L
1
2
3
4
116
66.2
45
35
25
18.4
14.4
Dimer
Monomer

B

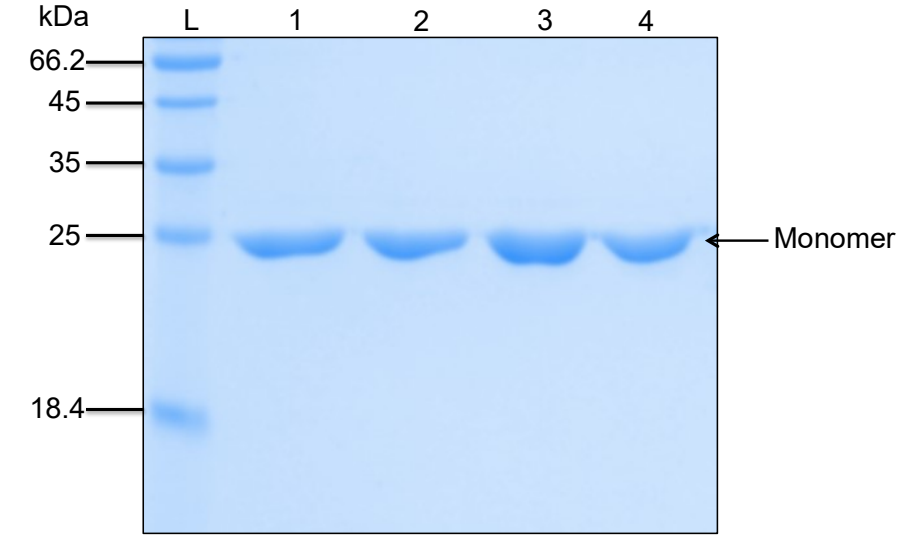
kDa
L
1
2
3
4
66.2
45
35
25
18.4
Monomer

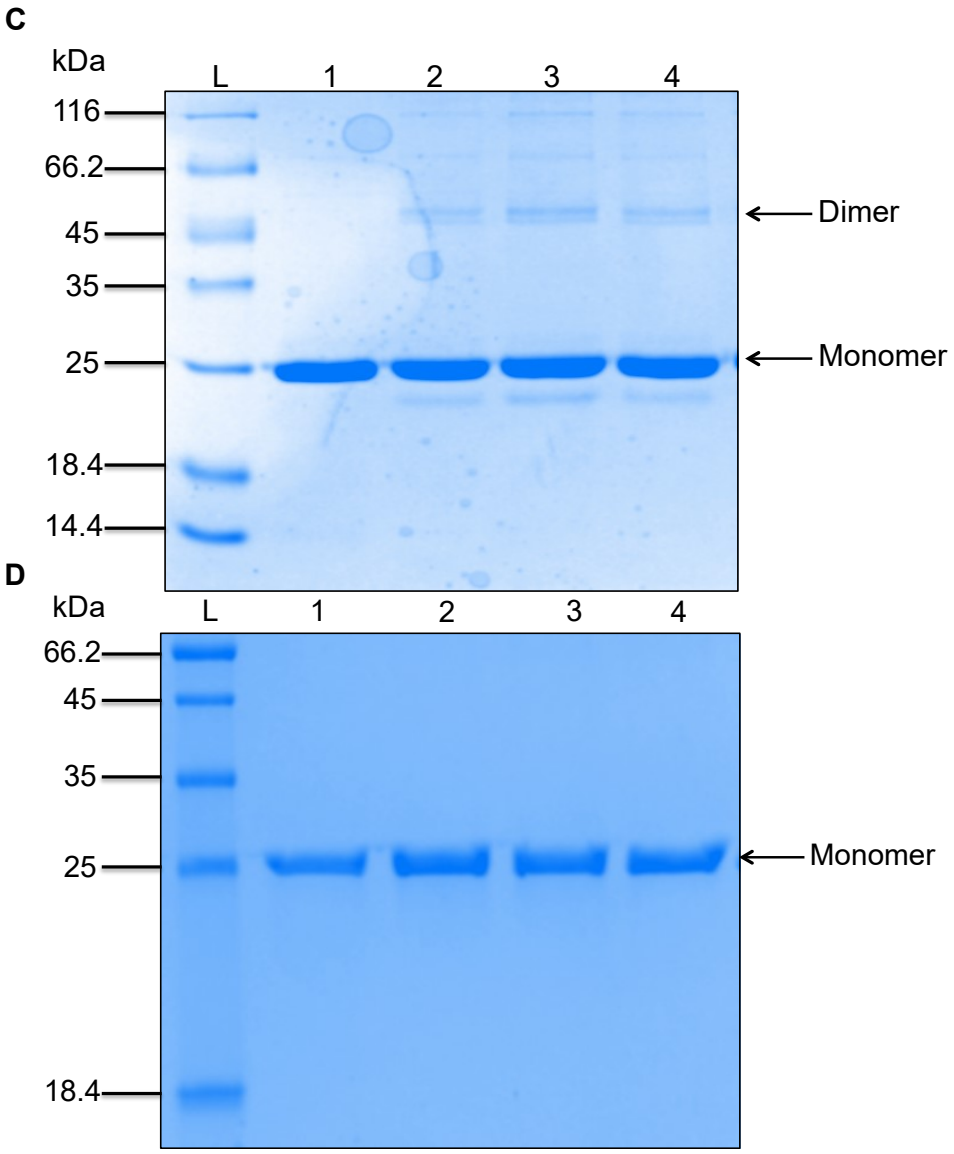

Figure 3.19 – Crosslinking of ParF and ParF-K64A-V89Y-M96A. SDS-polyacrylamide gels showing cross-linked products following two hours incubation with increasing concentrations of DMP. Lanes: L, Unstained Protein MW marker; 1, Protein only; 2, 0.5 mM DMP; 3, 1 mM DMP; 4, 10 mM DMP. A) ParF with ATP B) ParF with ADP C) ParF-K64A-V89Y-M96A with ATP D) ParF-K64A-V89Y-M96A with ADP

To further confirm that ParF-K64A-V89A-M96A is able to form a dimer a bacterial two-hybrid assay was employed and to quantify this interaction a β-galactosidase assay was carried out. These assays were also used to investigate whether ParF-K64A-V89Y-M96A was able to interact with ParG similarly to the wild type protein. As previously shown, ParG is able to stimulate ParF-K64A-V89Y-M96A assembly into higher order structures, which suggests that the mutant is able to interact with ParG. The bacterial two-hybrid system is used to study protein-protein interactions *in vivo* (Karimova *et al*., 1998). The system is based on complementation of two fragments of adenylate cyclase (CyaA), T18 and T25, from *Bordetella pertussis.* When T18 and T25 are fused to two proteins that interact, this enables the two fragments to re-associate and leads to the synthesis of cAMP. cAMP binds to the catabolite activator protein (CAP) and forms the cAMP/CAP complex that is able to trigger transcription of many genes, including those for maltose and lactose utilisation. In the bacterial two-hybrid assay maltose degradation is monitored and in the β-galactosidase assay the induction of the lactose operon in monitored. If ParF-ParF interaction was to be investigated, the *parF* gene (or a desired mutant) was fused to both T18 and T25 whereas if the ParF-ParG interaction was to be investigated the *parG* gene was fused to T18 and *parF* to T25. pT18ParF, pT25ParF and pT18 ParG were available in the laboratory plasmid collection. Cloning of *parF* mutant genes was carried out as described in 2.4.2 (Figure 3.20). All clones were checked by sequencing.

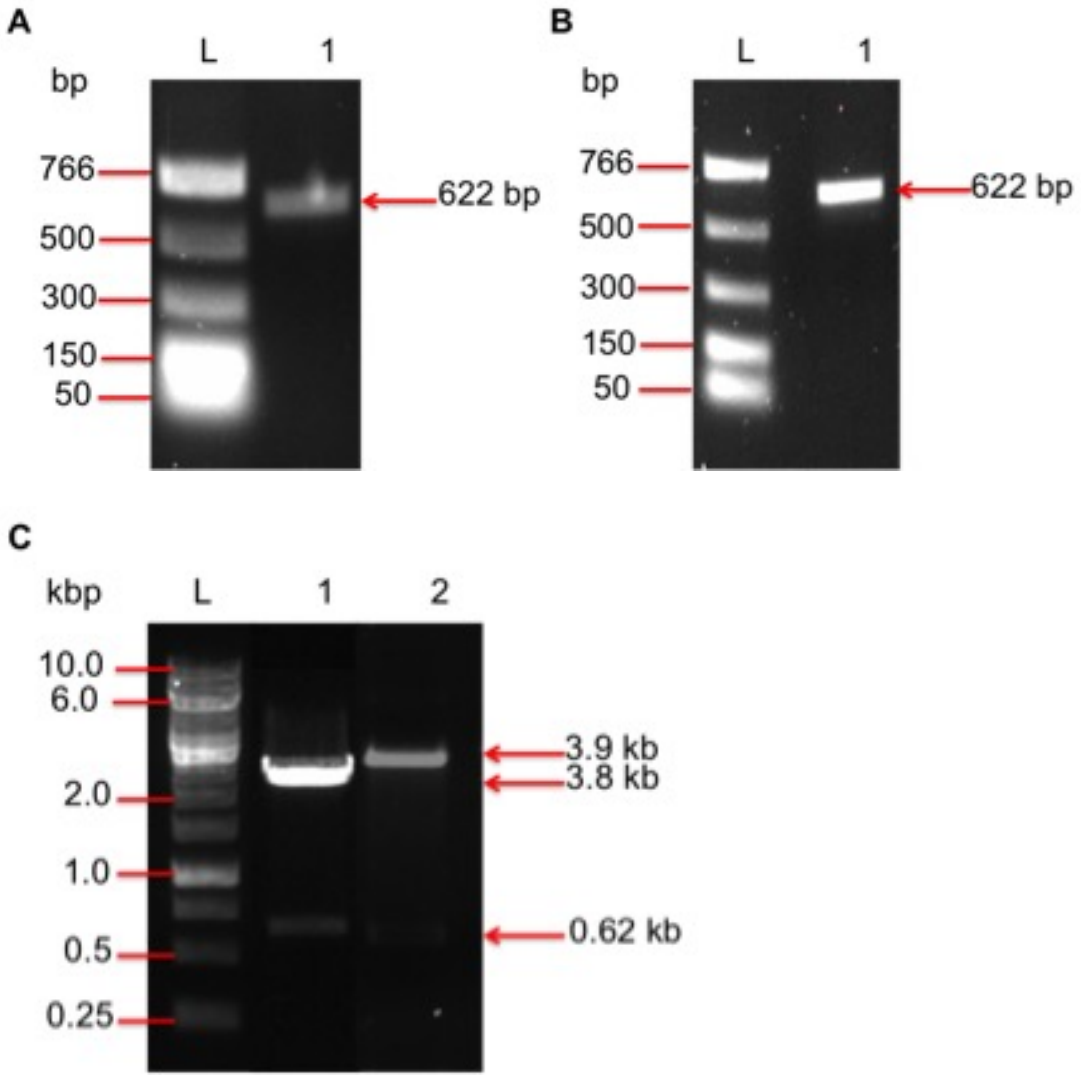

Figure 3.20 - Agarose gel showing cloning of *parF-K64A-V89Y-M96A* into pT18 and pT25 vectors for bacterial two-hybrid assay. A) Agarose gel of PCR products for pT18 cloning. L, NEB PCR marker; 1, PCR product. B) Agarose gel of PCR products for pT25 cloning. L, NEB PCR marker; 1, PCR product. C) Digested pT18 vector and pT25 vector. L, Gene Ruler 10 kbp ladder; 1, digested pT18; 2, digested pT25.

For the bacterial two-hybrid and β-galactosidase assays the desired plasmids pairs (pT18ParF+pT25ParF, pT18ParF-K64A-V89Y-M96A+pT25ParF-K64A-V89Y-M96A, pT18ParG+pT25ParF and pT18ParG+pT25ParF-K64A-V89Y-M96A) were co-transformed into SP850 *E. coli* competent cells as described in 2.3.10. As controls all plasmids were also co-transformed with the either pT18 and pT25, these plasmids contained only the T18 or T25 fragment without any gene fused to them. Therefore these controls should show no interactions (pT18+pT25, pT18ParF+pT25, pT18ParF-K64A-V89Y-M96A+pT25, pT18+pT25ParF, pT18+pT25ParF-K64A-V89Y-M96A, pT18ParG+pT25). For the bacterial two-hybrid assay the transformants were streaked onto MacConkey agar supplemented with 1% maltose and the ability of the cells to ferment sugar could be confirmed by the colour of the colonies. A dark red colour indicated that the two proteins fused to the T18 and T25 fragments were able to interact and therefore cAMP was synthesized. In the absence of interaction between the two proteins fused to the adenylate cyclase fragments, the colonies would be pale pink. In the β-galactosidase assay the controls, in which there was no interaction, would give a Miller units value of less than 100. On average the pT18ParF-pT25ParF pair would give a value of approximately 1500 Miller units and pT18ParG+pT25ParF would give a value of approximately 1000 Miller units. pT18ParF-K64A-V89Y-M96A + pT25ParF-K64A-V89Y-M96A showed a reduced interaction (average of 657.5 Miller units) compared to the wild type, however it was still evident that there was an interaction therefore confirming ParF-K64A-V89Y-M96A was able to form a dimer (Figure 3.21). pT18ParG + pT25ParF-K64A-V89Y-M96A showed a similar interaction to the wild type protein and ParG, this confirmed that ParF- K64A-V89Y-M96A is still able to interact with ParG (Figure 3.22).

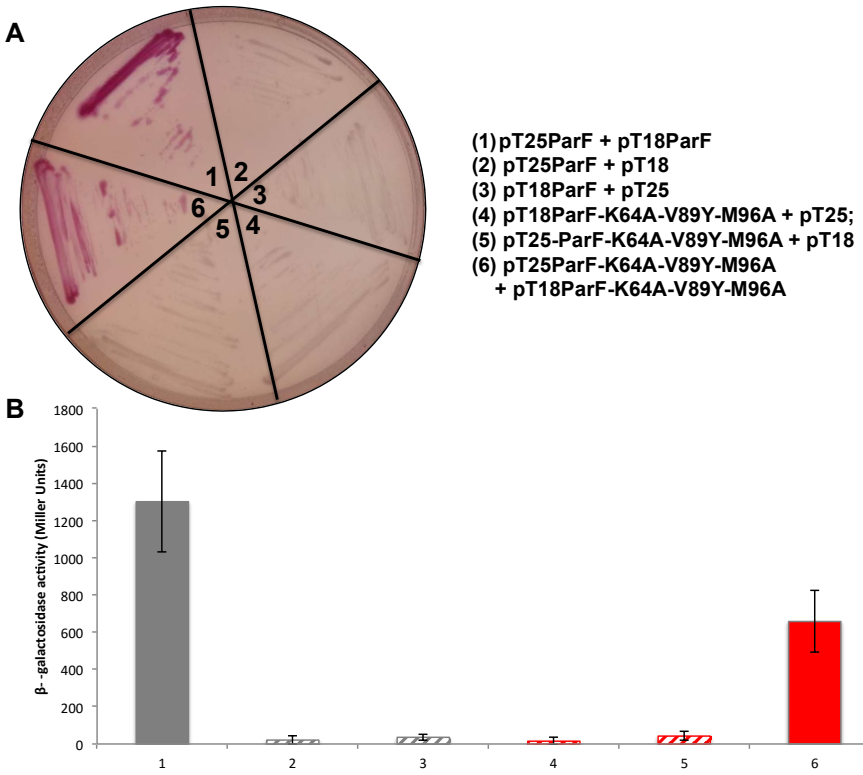

Figure 3.21 – Bacterial two-hybrid and β-galactosidase assay of ParF and ParF-K64A-V89Y-M96A. A) Bacterial two-hybrid assay. Plasmids carrying *parF* or *parF-K64A-V89Y-M96A* fused to T25 and T18 fragments were co-transformed into *E. coli* SP850 and streaked on MacConkey-maltose plates. B) β-galactosidase assay. ParF-ParF interaction is shown in grey and ParF-K64A-V89Y-M96A- ParF-K64A-V89Y-M96A interaction is shown in red. The assay was carried out in triplicate and error bars represent the standard error of mean.

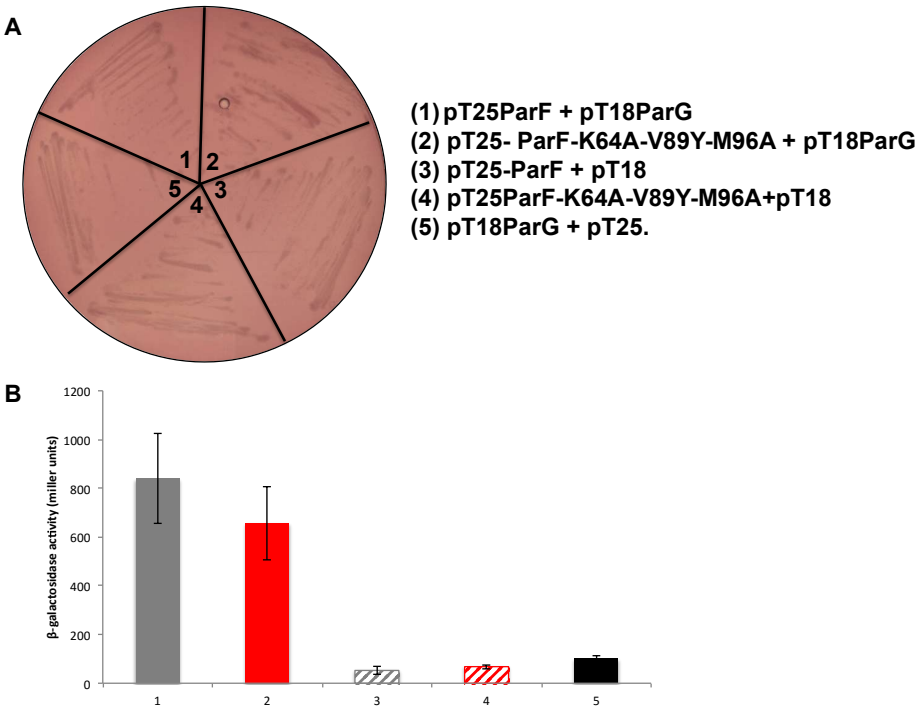

Figure 3.22 - Bacterial two-hybrid and β-galactosidase assay of ParF and ParF-K64A-V89Y-M96A. A) Bacterial two-hybrid assay. Plasmids carrying *parF* or *parF-K64A-V89Y-M96A* fused to T25 and *parG* fused to T18 were co-transformed into *E. coli* SP850 and streaked on MacConkey-maltose plates. B) β-galactosidase assay. ParF-ParG interaction is shown in grey and ParF-K64A-V89Y-M96A- ParG interaction is shown in red. The assay was carried out in triplicate and the error bars represent the standard error of mean.

3.4.3 ParF-K64A-V89Y-M96A is homogenously distributed over the nucleoid *in vivo* and is unable to oscillate

Many members of the ParA superfamily have been shown to form higher order structures and display dynamic characteristics *in vivo*. Some ParA proteins have been shown to oscillate over the nucleoid and this oscillatory behaviour appears similar to that of MinD. ParF is homologous to MinD and the two proteins share strong structural similarities. Interestingly, ParF has been shown to be more closely related to MinD than other well characterised ParA proteins, such as ParA from the P1 plasmid (Barilla *et al*., 2005). MinD is an *E. coli* protein involved in correct positioning and spatial regulation of the FtsZ ring. MinD, an ATPase, is able to associate with the membrane and activate MinC, an inhibitor of FtsZ assembly. MinE stimulates MinD ATPase activity, which causes MinD to disassociate from the membrane. This allows MinD to rapidly oscillate between cell poles (Lutkenhaus, 2007).

ParA from plasmid pB171 has been shown to dynamically relocate over the nucleoid and also displays an oscillatory pattern (Ringgaard *et al*., 2009). In addition to this, ParA from the P1 plasmid has been observed to form a dynamic pattern on the nucleoid

(Vecchiarelli *et al*., 2010). Therefore it was proposed that ParF may show similar characteristics *in vivo*.

It has recently been observed that ParF does show similar oscillatory behaviour and is able to form a dynamic pattern on the nucleoid (McLeod et al., 2016). Therefore, confocal microscopy was used to gain further understanding of how ParF forms dynamic assemblies and to investigate the effect of the triple residue changes on ParF *in vivo.* Cells were also imaged by three-dimensional structured illumination microscopy (3D-SIM) using an OMX microscope, which allowed higher resolution images to be acquired. Characterising how ParF and ParF mutants localise and oscillate *in vivo* allows more in depth knowledge to be gained and is key to understanding how the TP228 plasmid is segregated in the cell.

In order to visualise the proteins *in vivo* a fluorescent tagging system was employed. Two plasmid vectors that were used for microscopy experiments were available in the laboratory plasmid collection (provided by Brett McLeod). One plasmid encoded ParF fused to the monomeric Green Fluorescent Protein (GFP) Emerald variant and the other encoded ParG fused to the fluorescent protein mCherry. The first plasmid (pBM40) harbours *parF* cloned under the control of the arabinose inducible promoter P_{BAD} and fused with the Emerald gene. The other plasmid, known here after as pBM20, contains *parHFG-mCherry* partition cassette that encodes a ParG-mCherry fusion protein (Figure 3.23). Partition assays were used to ensure pBM20 showed a similar plasmid retention to that of the partition plasmid pFH547. Results showed the retention of pBM20 was similar and therefore the partition cassette was functional. Both ParF and ParG proteins have also been shown to be functional when fused to the fluorescent proteins(McLeod et al., 2016). The mutant *parF* alleles were cloned into both plasmids as detailed in 2.4.2 to allow the effects of the mutations to be studied *in vivo* (Figure 3.24). All clones were checked by sequencing.

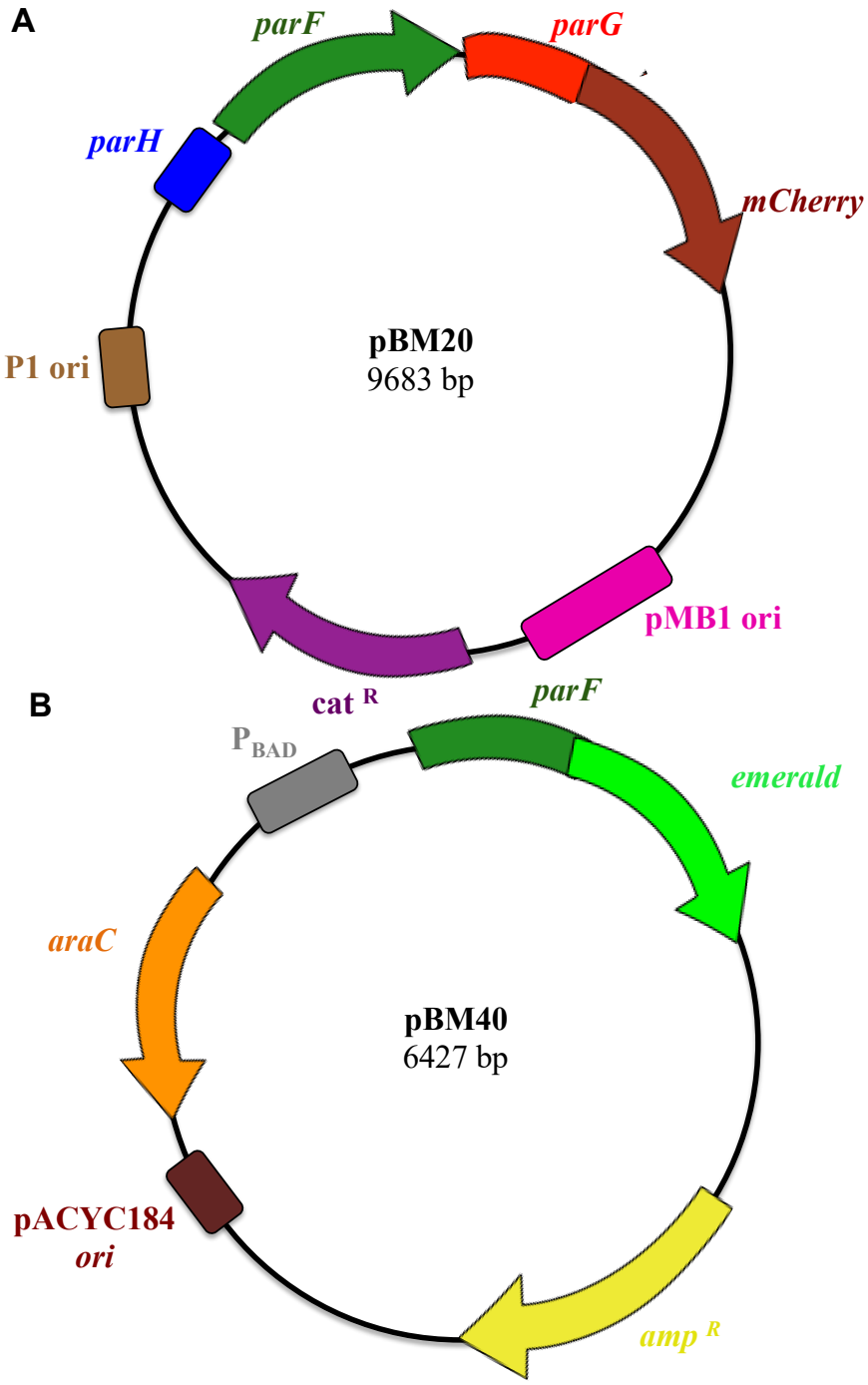

Figure 3.23 – Plasmid set used in microscopy studies to investigate ParF and ParG localisation *in vivo*. A) pBM20 contains the wild type partition cassette *parFGH* encoding ParG fused to mCherry. B) pBM40 contains *parF* fused to Emerald under the control of the P_{BAD} inducible promoter.

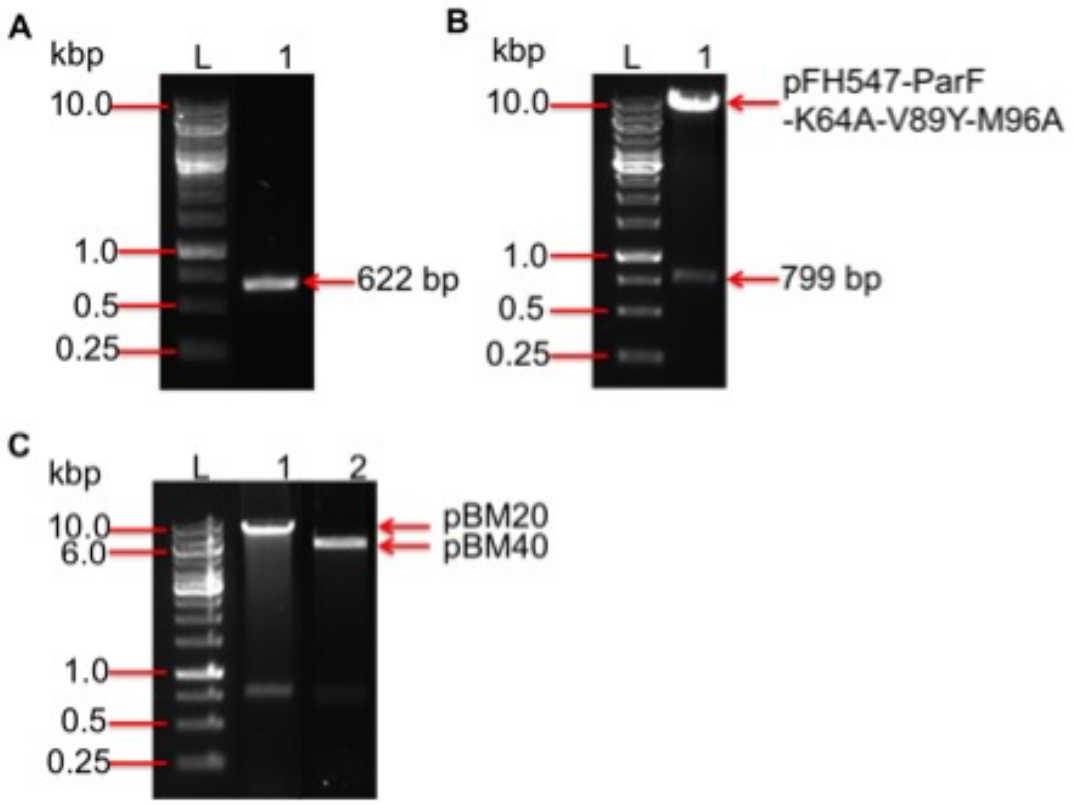

Figure 3.24 - Agarose gels showing cloning of *parF-K64A-V89Y-M96A* allele into pBM20 and pBM40 for microscopy experiments. A) Agarose gel showing PCR product of the *parF-K64A-V89Y-M96A* allele amplified with primers to incorporate *Xba*I and *Spe*I restriction sites. L, Gene Ruler 10 kbp ladder; 1, PCR product. B) Agarose gel showing pFH547-ParF-K64A-V89Y-M96A digested with *Mfe*I and *Hpa*I to give the desired fragment of 799 bp that contains the triple mutation. L, Gene Ruler 10 kbp ladder; 1, digested pFH547-ParF-K64A-V89Y-M96A. C) Agarose gel showing digested pBM20 and pBM40. L, Gene Ruler 10 kbp ladder; 1, pBM20 digested with *Mfe*I and *Hpa*I; 2, pBM40 digested with *Xba*I and *Spe*I.

In order to study the localisation of ParF/ParF mutants and ParG, the appropriate pBM20 and pBM40 plasmids were co-transformed into BW25113 *E. coli* cells and grown for four hours in the presence of antibiotics. In these experiments, the aim was to investigate the localisation of the proteins rather than plasmid retention or loss. The cells were grown in the presence of L-arabinose for three hours in order to induce expression of *parF-emerald*. In order to ensure the level of overproduced ParF-Emerald is within a reasonable range and that the protein is full-length, a Western blot was carried out. This experiment showed that the fusion protein is not degraded and allowed the ratio of ParF:ParF-Emerald to be determined as 1:1.5 (Figure 3.25). The nucleoid is visualised using DAPI, a fluorescent stain that is able to pass through an intact cell membrane and bind DNA.

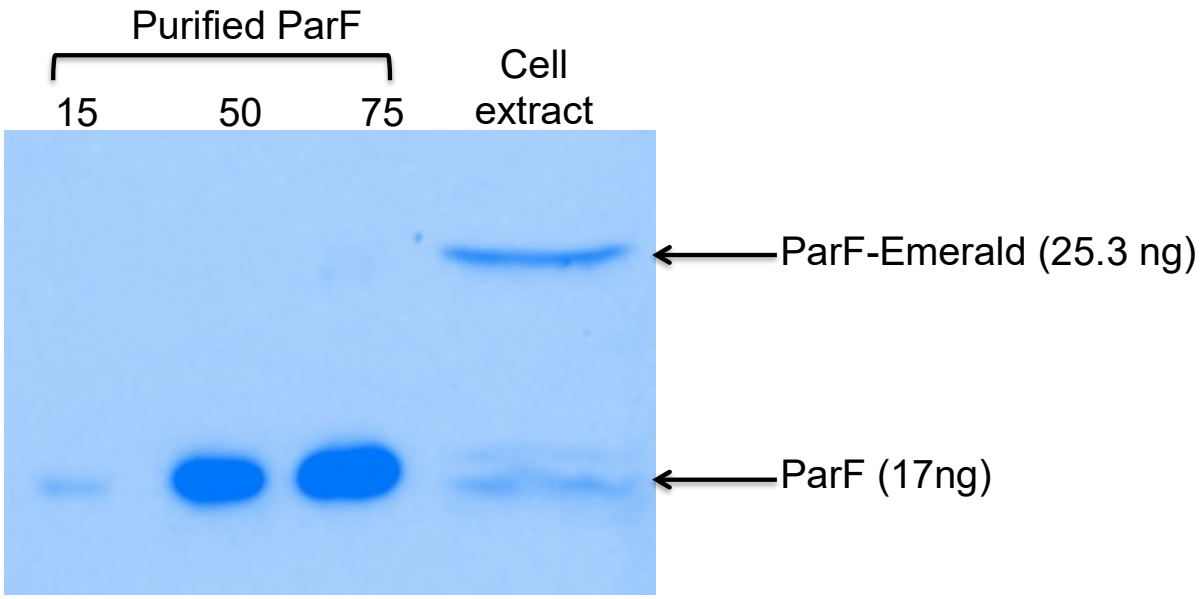

Figure 3.25 - Western blot to show the level of ParF-Emerald comparatively to ParF. 12% SDS-gel showing purified ParF and cell extract of BW25113 *E. coli* cells that were transformed with pBM20 and pBM40 and grown as for confocal microscopy.

Fluorescence microscopy revealed the ParF-Emerald signal is asymmetrically distributed over the nucleoid, whereas the ParG-mCherry red signal appears more evenly dispersed. The ParF-Emerald signal has a compact 'head' at one pole of the nucleoid and then a more dispersed 'tail' and the pattern could be described as comet-like. Even though the ParG-mCherry signal appears dispersed throughout the nucleoid, often distinct, higher density ParG foci can be identified within the dispersed signal. When a single focus is observed, it is normally positioned at midcell, whereas if two foci are seen they are positioned at one-quarter and three-quarters of the cell length (Figure 3.26, this study; (McLeod et al., 2016).

To determine whether the ParF-Emerald and ParG-mCherry signals were distributed throughout the nucleoid volume or just present on the surface of the chromosome, z-stacks of the cells were taken. Incremental images were taken through the z-plane of the cell every 0.19 μm. The ParF-Emerald and ParG-mCherry signals were observed through the nucleoid in all cells imaged (n=100) (Figure 3.27). The signals were more intense in the z stack images taken in the center of the cell, indicating that both ParF and ParG are found within the nucleoid during the plasmid segregation process. Time-lapse experiments allowed the dynamics of the proteins to be observed *in vivo* and cells were observed over twenty minutes with images taken every minute. Time-lapse experiments revealed that ParF-Emerald oscillated from one pole of the nucleoid to the other, and over twenty minutes the signal would be seen on average to oscillate 4-5 times, confirming the pattern previously observed (McLeod et al., 2016). ParG-mCherry was also seen to oscillate, interestingly ParG-mCherry signal lagged slightly behind the ParF-Emerald signal (Figure 3.28). When only pBM40 was transformed into the cells meaning there was only ParF-Emerald present in the cell and no TP228 partition cassette, ParF-Emerald was homogenously spread throughout the nucleoid. No asymmetric localisation or oscillation over the nucleoid was observed. This result indicated that both ParG and *parH* are required for ParF to be asymmetrically distributed and oscillate from one pole to pole over the nucleoid. 100 cells were observed over a twenty minute time-lapse and this pattern of concurrent oscillation of ParF and ParG was detected in 82% of the cells.

When cells were imaged by 3-dimensional structured illumination microscopy (3D-SIM) using an OMX microscope, higher resolution images were acquired. These images allowed much more detailed structures of ParF-Emerald to be visualised as well as a more defined ParG-mCherry signal. Firstly, the images confirmed the pattern seen using

confocal fluorescence microscopy: ParF-Emerald was asymmetrically distributed over the nucleoid and ParG-mCherry was more evenly distributed over the nucleoid with distinct foci being identified. As previously observed by McLeod *et al*., the higher resolution images revealed that ParF protrudes into the nucleoid volume forming a lattice of ParF bundles. This result is consistent with the pattern seen from z-stack images acquired using confocal microscopy. ParF is associated with the nucleoid and the ParF signal appears to fill 'gaps' in the nucleoid, however it should be noted that some of the Emerald signal could be seen above the nucleoid indicating ParF is not entirely associated with the nucleoid. The ParG-mCherry signal also appeared to be spread through the nucleoid and appears to be captured by the ParF lattice that extends throughout the nucleoid (Figure 3.32).

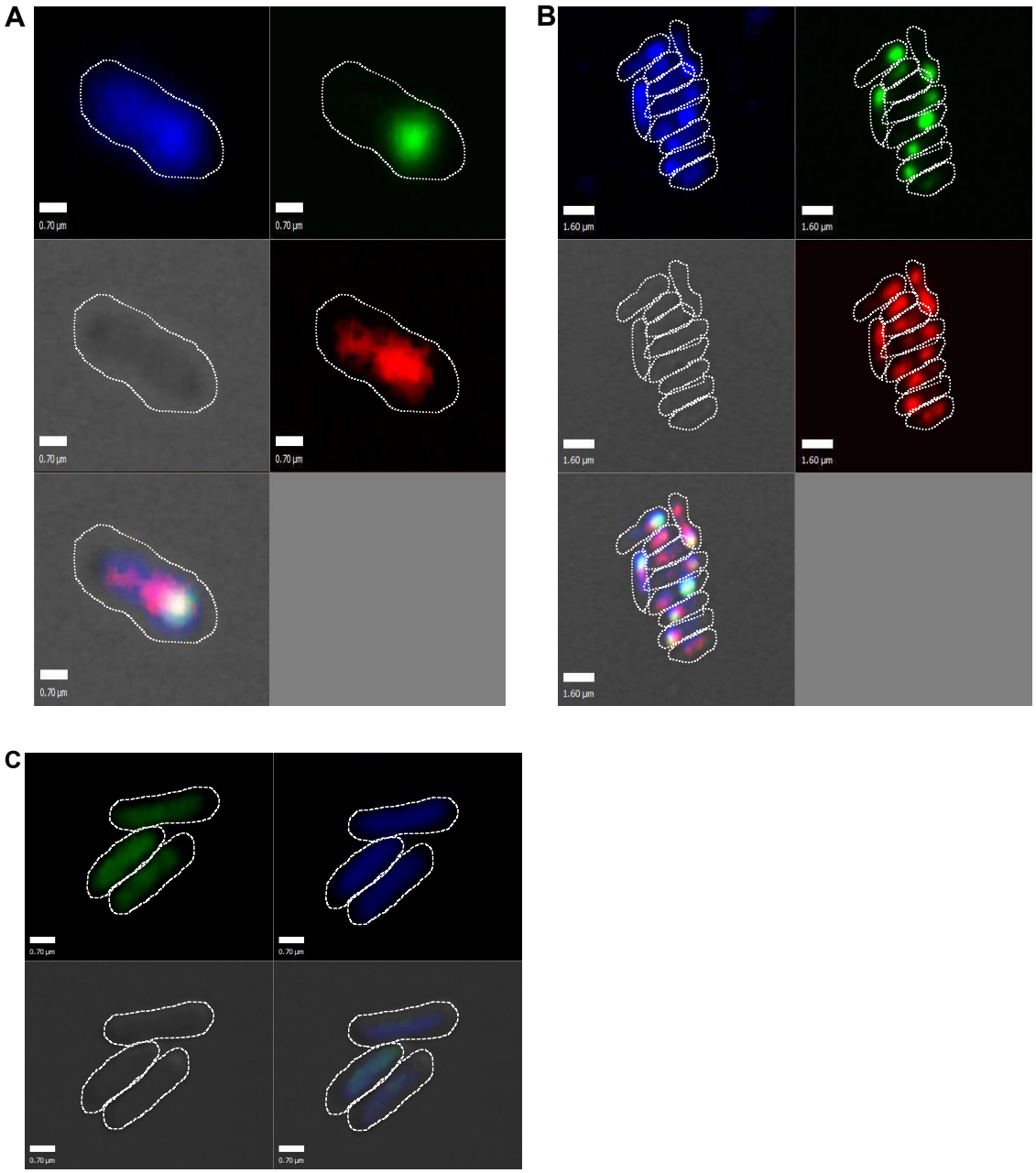

Figure 3.26 – ParF localisation within the cell when the full partition cassette *parFGH* is present. Images of *E. coli* cells acquired using the confocal microscope A) BW25113 *E. coli* cell habouring a plasmid carrying the partition cassette *parFG-mCherry-parH* (pBM20) and a plasmid expressing *parF-emerald* from the P_{BAD} promotor (pBM40). Top left - individual channel for DAPI, top right – individual channel for ParF-Emerald, middle left – bright field image, middle right – individual channel for ParG-mCherry, bottom left – merged image. Scale bar = 0.7 µm. B) Multiple BW25113 *E. coli* cells habouring a plasmid carrying the partition cassette *parFG-mCherry-parH* (pBM20) and a plasmid expressing *parF-emerald* from the P_{BAD} promoter (pBM40). Top left - individual channel for DAPI, top right – individual channel for ParF-Emerald, middle left – bright field image, middle right – individual channel for ParG-mCherry, bottom left – merged image. Scale bar = 1.60 µm. C) Multiple BW25113 *E. coli* cells expressing *parF-emerald* only (pBM40). Top left - individual channel for ParF-Emerald, top right – individual channel for DAPI, bottom left – bright field image, bottom right –merged image. Scale bar = 0.70 µm.

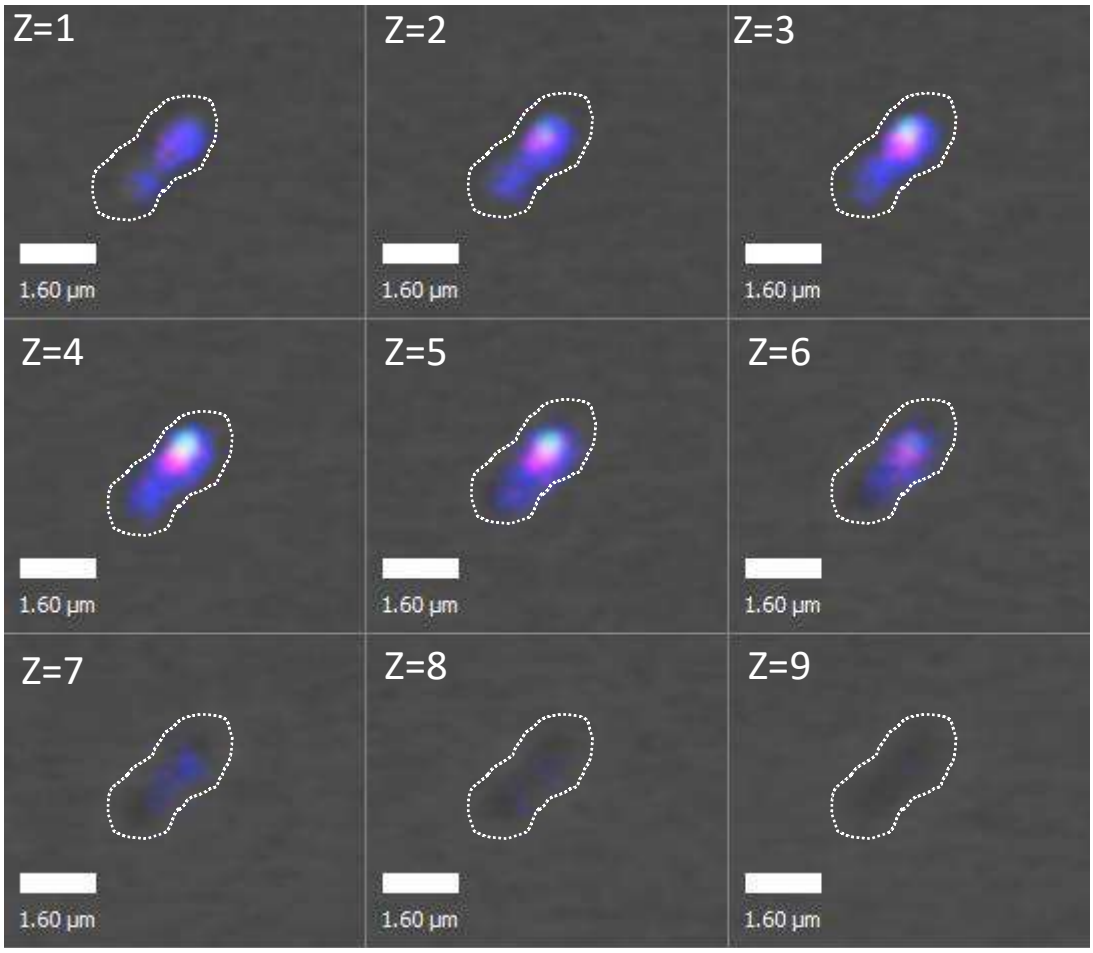

Figure 3.27 – Z stack images of a single cell when the partition cassette *parFGH* is present. Images of *E. coli* cells acquired with the confocal microscope. Nine z-stacks were taken at intervals of 190 nm. The merged images shown are cells harbouring the plasmid carrying the *parFG-mCherry-parH* cassette and the plasmid expressing *parF-emerald* from the P_{BAD} promoter. The nucleoid is stained with DAPI. Scale bar = 1.60 µm.

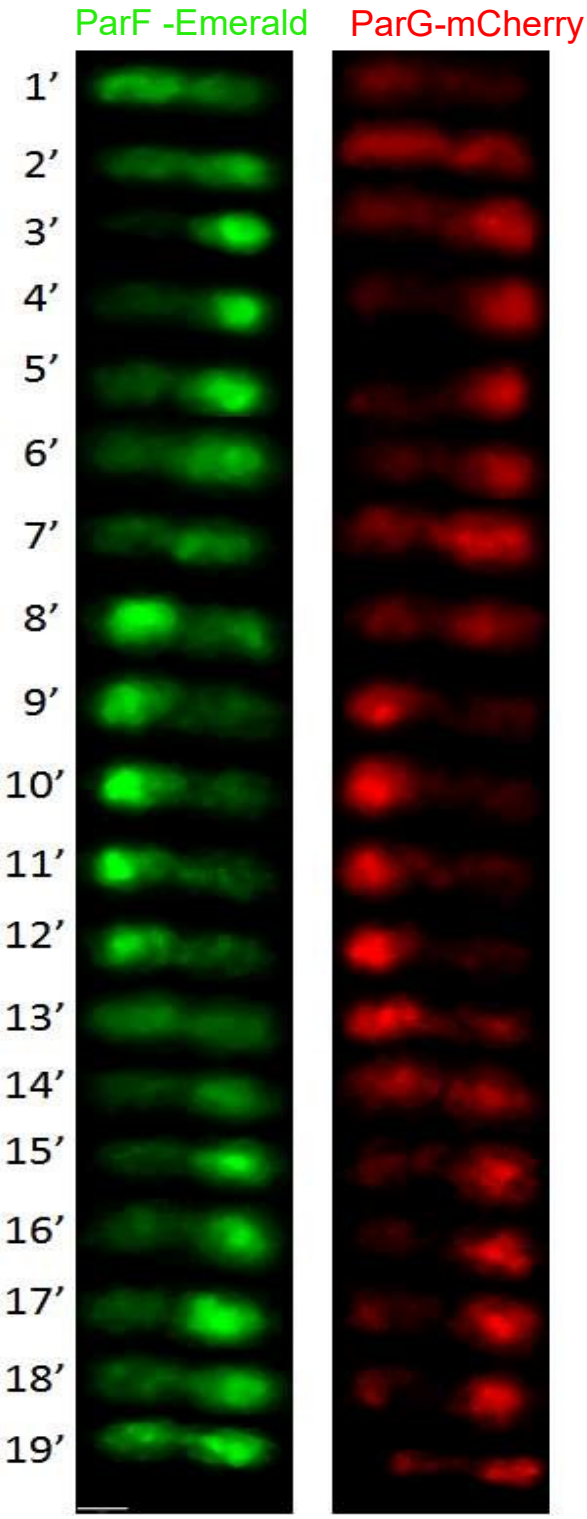

Figure 3.28 – Individual time images of ParF and ParG localisation over a twenty minute time lapse. A representative example of a twenty minute time-lapse experiment showing a cell habouring the plasmid carrying the *parFG-mCherry-parH* cassette and the plasmid expressing *parF-emerald* from the P_{BAD} promoter. ParF-Emerald is shown in the left column and ParG-mCherry shown in the right column. Scale bar = 0.7 μm.

The effect of the triple mutation on ParF localisation and dynamics was investigated by acquiring confocal and super resolution microscopy images; z-stacks and time-lapse experiments were also performed. Cells habouring the plasmids that contained the partition cassettes with the *parF-K64A-V89Y-M96A* allele (pBM20-ParF-K64A-V89Y-M96A) and the plasmid encoding ParF-K64A-V89Y-M96A-Emerald (pBM40-ParF-K64A-V89Y-M96A) were grown and imaged exactly as the wild type cells. ParF-K64A-V89Y-M96A-Emerald is not asymmetrically distributed over the nucleoid like the wild type protein, but in fact spread homogenously over the nucleoid. ParG is also homogenously spread over the nucleoid (Figure 3.29). The interaction between ParF-K64A-V89Y-M96A and ParG is not disrupted, therefore it is likely that ParF-K64A-V89Y-M96A recruits ParG bound to the plasmid to the nucleoid and this is reflected in the same patterning observed for both proteins (Figure 3.30). Z-stacks revealed, that like the wild type protein, ParF-K64A-V89Y-M96A-Emerald is spread throughout the nucleoid volume (Figure 3.31). The images acquired using super resolution microscopy confirmed these findings (Figure 3.32). In addition, when a twenty minute time-lapse experiment was carried out, no oscillation was seen for either ParF-K64A-V89Y-M96A-Emerald or ParG-mCherry. Both the green and red signals remained distributed throughout the nucleoid for the entire twenty minutes (data not shown). ParF oscillation and asymmetric patterning is likely due to the cycling of binding ATP, forming higher order structures followed by stimulation of ATPase activity by ParG, which would cause disassembly and remodeling of the ParF bundles. ParF does not oscillate in the absence of *parH*, ParG or both. Moreover, when a ParG mutant that is unable to stimulate ParF ATPase activity replaces the wild type ParG, ParF cannot oscillate(McLeod et al., 2016). ParF-K64A-V89Y-M96A is known to bind and hydrolyse ATP similarly to the wild type ParF (Madhuri Barge, unpublished data) and the mutants' interaction with ParG is largely unaffected. Therefore, the mutant is homogenously spread throughout the nucleoid and is unable to oscillate possibly as a consequence of the inability to form higher order structures because of the disruption at interface 1 of the dimer-of-dimer.

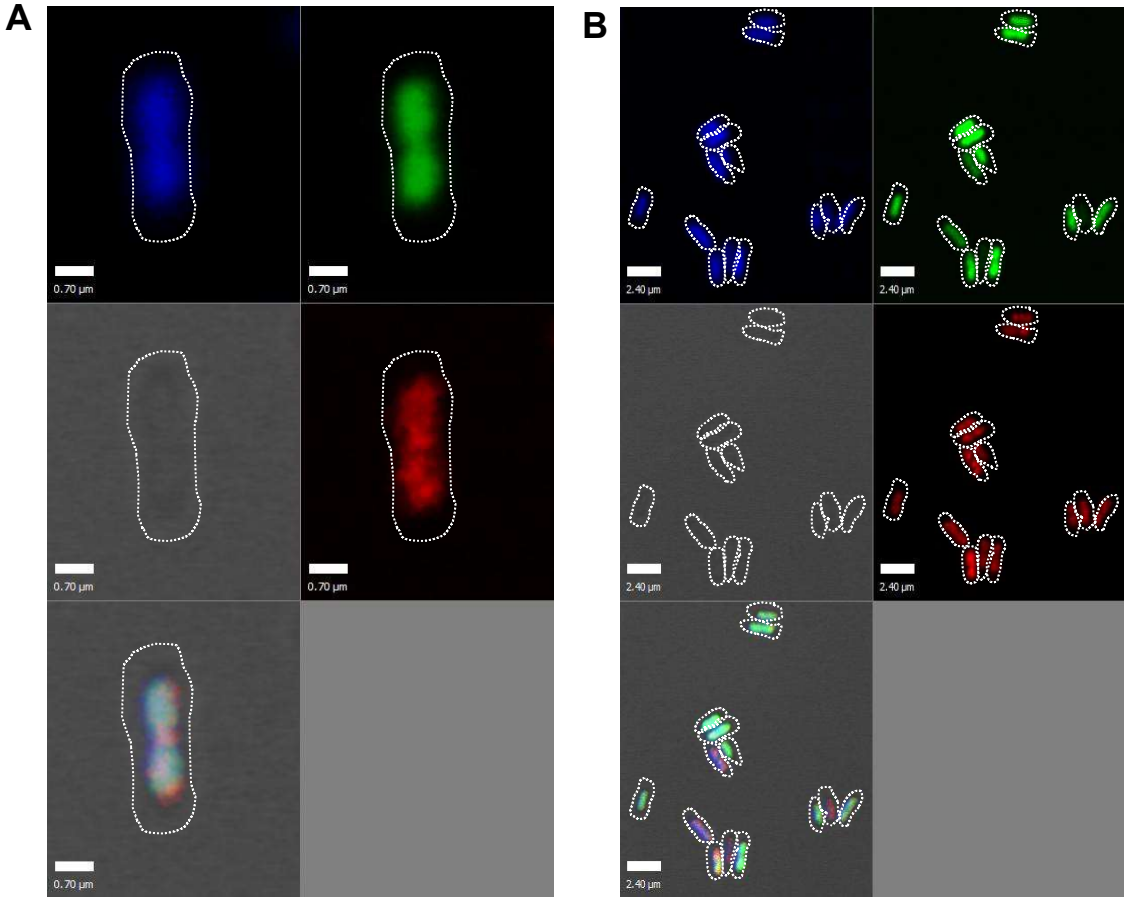

Figure 3.29 – Localisation of ParF-K64A-V89Y-M96A. Images of *E. coli* cells acquired with the confocal microscope. A) BW25113 *E. coli* cell habouring a plasmid carrying the partition cassette *parF-K64A-V89Y-M96A-parG-mCherry-parH* (pBM20-ParF-K64A-V89Y-M96A) and a plasmid expressing *parFK64A-V89Y-M96A-emerald* from the P_{BAD} promoter (pBM40-ParF-K64A-V89Y-M96A). Top left - individual channel for DAPI, top right – individual channel for ParF-K64A-V89Y-M96A-Emerald, middle left – bright field image, middle right – individual channel for ParG-mCherry, bottom left – merged image. Scale bar = 0.7 µm. B) Multiple BW25113 *E. coli* cells habouring a plasmid carrying the partition cassette *parF-K64A-V89Y-M96A-parG-mCherry-parH* (pBM20ParF--K64A-V89Y-M96A) and a plasmid expressing *parF-K64A-V89Y-M96A-emerald* from the P_{BAD} promotor (pBM40-ParF-K64A-V89Y-M96A). Top left - individual channel for DAPI, top right – individual channel for ParF-eGFP, middle left – bright field image, middle right – individual channel for ParG-mCherry, bottom left – merged image. Scale bar = 2.40 µm.

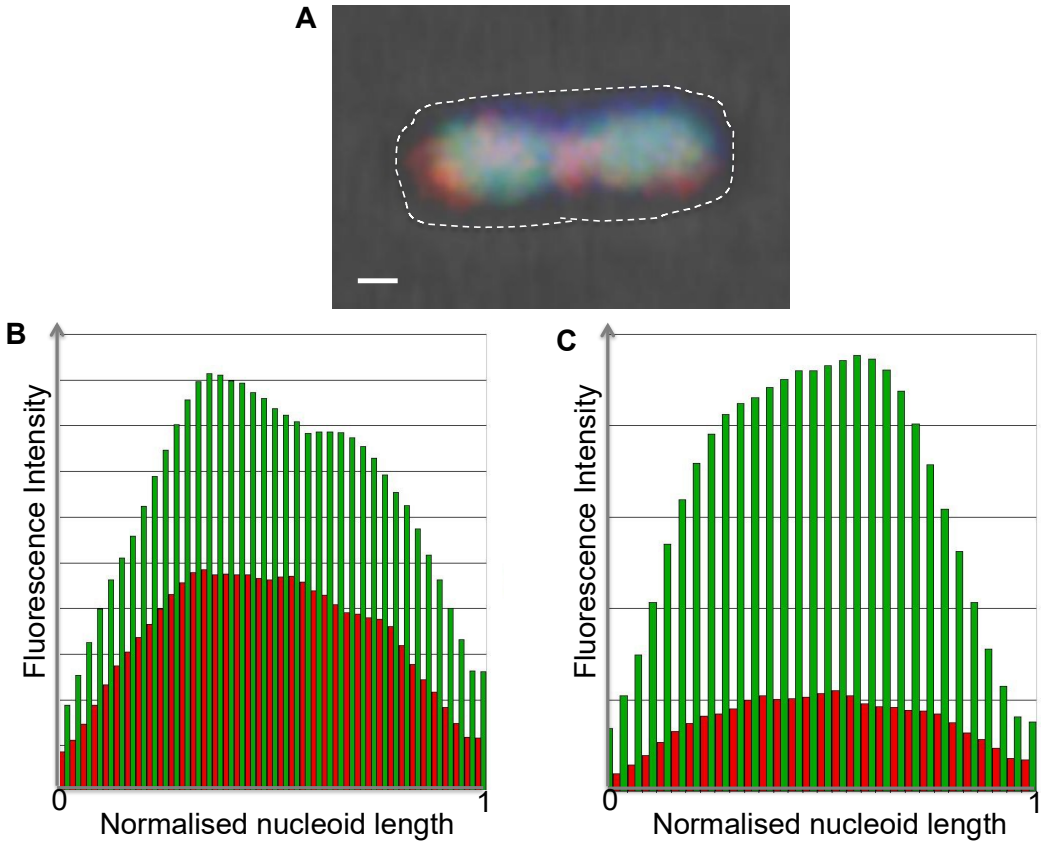

Figure 3.30 – Patterns of the localisation of ParF-K64A-V89Y-M96A and ParG. Images of *E. coli* cells acquired with the confocal microscope. BW25113 *E. coli* cell harbouring a plasmid carrying the partition cassette *parF-K64A-V89Y-M96AparG-mCherry-parH* (pBM20-ParF-K64A-V89Y-M96A) and a plasmid expressing *parF-K64A-V89Y-M96A-emerald* from the P_{BAD} promoter (pBM40-ParF-K64A-V89Y-M96A). This analysis is done by measuring signal of ParF-K64A-V89Y-M96A and ParG throughout the nucleoid rather than the perimeter of the cell as this can cause discrepancies due to the difficulty in identifying the perimeter of the cell. A) A merged image. Scale bar = 0.3 μm. B) Fluorescence intensity plot of the cell shown in (A) showing the spread of ParG-mCherry (red) signal and the spread of the ParF- K64A-V89Y-M96A -eGFP (green) signal. C) Fluorescence intensity plot of another cell (image not shown) demonstrating the overlap of both the ParG-mCherry (red) signal and the ParF- K64A-V89Y-M96A-Emerald (green) signal.

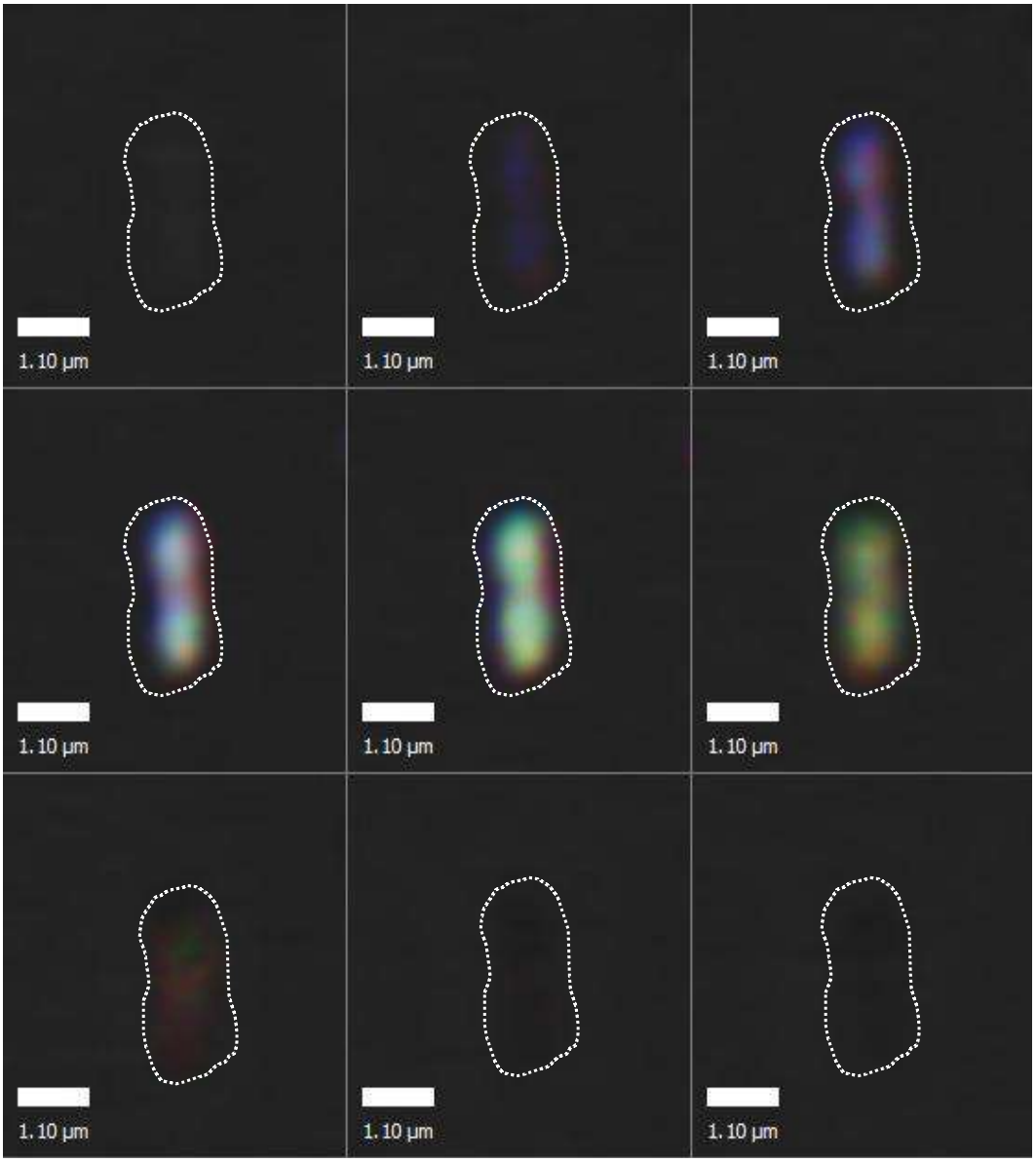

Figure 3.31 – Z stack images of ParF-K64A-V89Y-M96A and ParG. Images of *E. coli* cells acquired with the confocal microscope. Nine z-stacks were taken at intervals of 190 nm. The merged images shown are cells harbouring the plasmid carrying the *parF-K64A-V89Y-M96A-parG-mCherry-parH* cassette and a plasmid expressing *parF-K64A-V89Y-M96A-emerald* from the P_{BAD} promoter. The nucleoid is stained with DAPI. Scale bar = 1.60 µm.

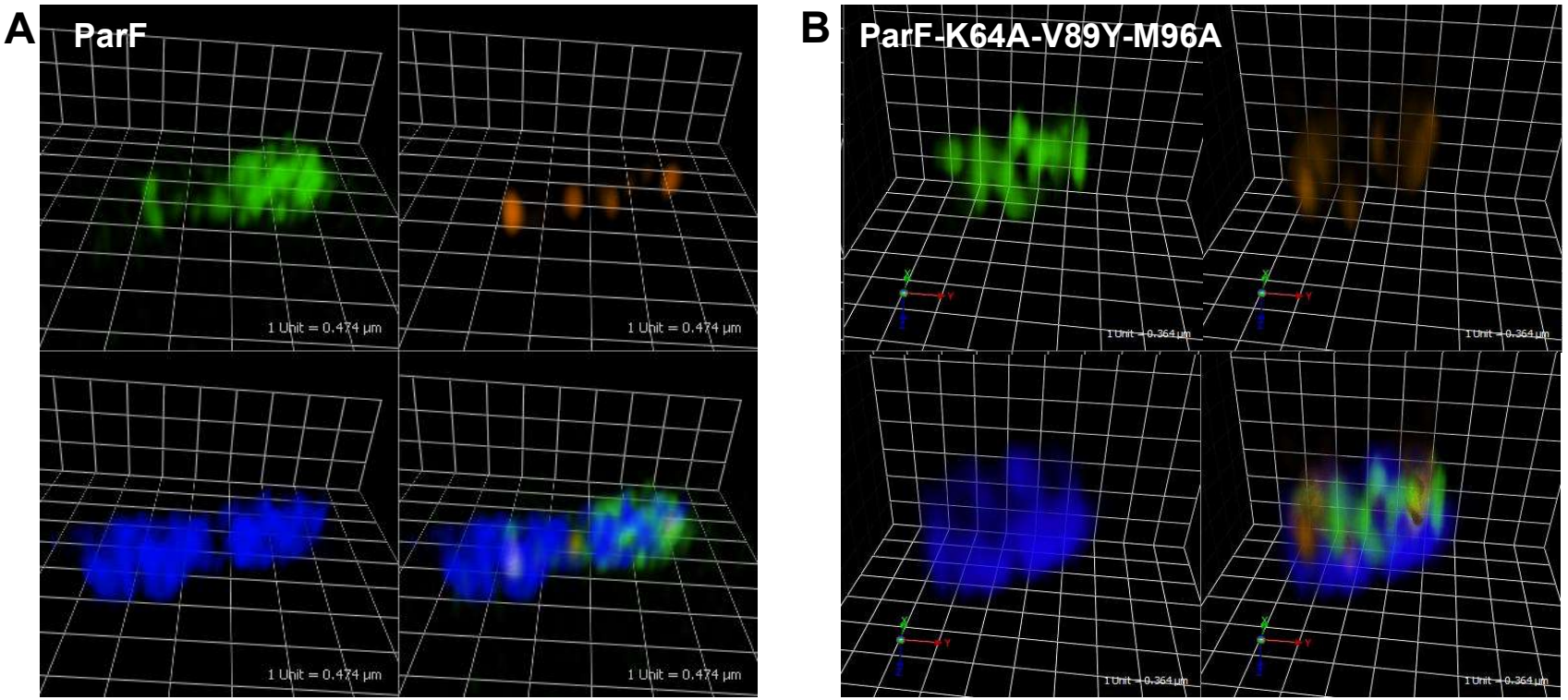

Figure 3.32 – Super resolution images of ParF and ParF-K64A-V89Y-M96A. Three dimensional rendering of 3D-SIM images of *E. coli* cells acquired with the OMX microscope. The channels are shown as: top left – ParF-Emerald; top right – ParG-mCherry; bottom left – nucleoid stained with DAPI; bottom right – merged image. A) Cell harbouring the plasmid carrying the *parFG-mCherry-parH* cassette and a plasmid expressing *parF-emerald* from the P_{BAD} promoter. Scale bar, 1 unit = 0.474 µm. B) Cell harbouring the plasmid carrying the *parF-K64A-V89Y-M96A-parG-mCherry-parH* cassette and a plasmid expressing *parF-K64A-V89Y-M96A-emerald* from the P_{BAD} promoter. Scale bar, 1 unit = 0.364 µm.

3.5 Conclusions

The mechanism underpinning TP228 plasmid segregation is still unclear. There is still much deliberation as to whether ParA proteins, from the Walker-type ATPase group of partition proteins, are able to assemble into higher order structures and the role of these assemblies in plasmid segregation. When bound to ATP, ParF is able to form higher order structures. Structural data revealed that ParF-ATP dimers interacted with each other to form dimer-of-dimer units. It was proposed that these dimer-of-dimer units formed the building blocks of ParF polymers. It was suggested that by disrupting two interfaces on the surface of these ParF dimers (interface 1 and 2) that ParF polymer formation would be abolished. Results obtained here support previous findings on ParF. Upon the addition of ATP, ParF was shown to form higher order structures using DLS and sedimentation assays. The addition of ADP had an antagonistic effect on the formation of these higher order structures. Electron microscopy was used to visualise the formation of these assemblies and again this showed that the formation of these structures was observed only in the presence of ATP. ParF has a tendency to self-associate in the absence of nucleotide, which was shown both in the DLS experiment and by the small globular structures seen in the EM images. Confocal microscopy, along with higher resolution images acquired from super resolution microscopy, demonstrated that ParF is asymmetrically distributed over the nucleoid and is able to oscillate from one pole to pole over the nucleoid, when the full partition cassette *parFGH* is present. ParF appeared to protrude into the nucleoid and form a lattice. The fact that ParF localises to the nucleoid suggests ParF can bind DNA in a non-specific manner; this topic is investigated in this study later (Chapter 5).

Schumacher *et al* (2012) constructed a double mutant, harbouring changes at interface 2, which was impossible to purify and therefore could not be further investigated. In this study two single changes were constructed at interface 2, S185W and S186F. Partition assays showed that the plasmids containing either *parF-S185W* or *parF-S186F* did not show a significant reduction in plasmid retention. This suggests that a single mutation at this interface is not sufficient to disrupt plasmid segregation. This interface was not further investigated in this study, however in the future it would be informative to construct a different double mutant at this interface to try and disrupt plasmid segregation without affecting the proteins solubility.

Schumacher *et al* (2012) also constructed a triple mutant, harbouring changes at interface 1 and proposed these mutations disrupted plasmid segregation, as the mutant ParF was unable to assemble into higher order structures upon the addition of ATP. Results obtained here supported previous findings by Schumacher *et al* (2012), ParF-K64A-V89Y-M96A is unable to form higher order structures upon the addition of ATP. Even though this mutant is able to bind and hydrolyse ATP, DLS experiments showed no increase in light scattering intensity upon the addition of ATP. These results were supported by images obtained from EM, no higher order structures could be seen when ATP was added and little difference between no nucleotide and ATP samples could be identified. Bacterial two-hybrid assays and chemical cross-linking demonstrated this mutant could still form a dimer (although to a lesser extent compared to wild type protein), which clarified this was not the reason ParF-K64A-V89Y-M96A could not form these higher order structures. All these results support the theory that disruption of this interface can prevent ParF from forming higher order structures. Furthermore, it supports the model of ParF forming dimer-of-dimer units that form the building blocks of the higher order structures.

ParF-K64A-V89Y-M96A *in vivo* localisation and dynamics were investigated by conventional and super resolution microscopy. Unlike the wild type protein, ParF-K64A-V89Y-M96A does not form an asymmetric pattern over the nucleoid but in fact is homogenously spread through the nucleoid. ParF-K64A-V89Y-M96A does however still appear to protrude into the nucleoid. Time-lapse experiments revealed that the mutant is unable to oscillate from pole to pole over the nucleoid. Wild type ParG also shows no oscillation. The cycling between assembly and disassembly of higher order structures is likely to drive the oscillation; therefore the inability of ParF-K64A-V89Y-M96A to assemble into any detectable higher order structures might explain why no oscillation is observed. The *in vivo* studies further support the importance of ParF to form these higher order structures, as cells harbouring the ParF triple mutant display low plasmid stability (Schumacher *et al*., 2012). The lack of formation of higher order structures and resulting ablation of ParF-K64A-V89Y-M96A relocation over the nucleoid is likely to be the cause of the partition deficient phenotype, indicating that ParF assembly into organized assemblies on the nucleoid template plays an important role in plasmid partitioning.

Chapter 4: The ParF monomer-monomer interface: interplay and synergy between the proline-rich motif and the ATP-binding pocket

4.1 The monomer-monomer interface of ParF

The structure of ParF of the TP228 plasmid partition locus has recently been solved to 2.90 Å resolution (Schumacher *et al*., 2012). The structure revealed that ParF is monomeric when bound to ADP and dimeric when bound to AMPPCP. The structural data also provided further insight into the mechanism of how ParF forms higher order structures, as linear polymers of ParF were seen to form within the crystals. The ParF-ATP dimers were seen to interact to form dimer-of-dimer units. These dimer-of-dimer units are proposed to form the building blocks of the ParF polymers. This is supported by results observed for the ParF triple mutant, ParF-K64A-V89Y-M96A, harbouring changes at the dimer interface (Schumacher *et al*., 2012), that was found to disrupt plasmid segregation, likely due to the inability of the mutant to form higher order structures upon the addition of ATP (Chapter 3). It is evident that ParF must be bound to ATP and dimeric in order to assemble into these higher order structures, therefore preventing dimer formation is likely to disrupt this process. Disrupting the monomer-monomer interface of ParF would hopefully disrupt ParF dimer formation and offer an insight into the interfaces and specific residues involved in assembly of ParF into higher order structures. Ultimately, the aim would be to gain further understanding of the role of ParF higher order structures in TP228 plasmid segregation.

In the dimer structure the nucleotide appears to be sandwiched in between the monomers. The nucleotide binding pocket of ParF was identified as being composed of residues 9-16 (Walker A motif), residues 37-49 and residues 166-177. In addition, other residues were identified that were important in forming cross-contacts at the monomer-monomer interface of ParF. Some of the cross-contacts identified were in addition to those between the nucleotide and the Walker A motif. Schumacher *et al* (2012) identified a proline-rich motif in ParF (Figure 4.1). In each ParF monomer, this motif is seen to insert into the adjacent monomer close to the ATP binding pocket and allows cross-contacts to form between subunits within the dimer. The proline-rich motif consists of eleven residues that are highly conserved in ten ParF homologues, therefore indicating the importance of these residues (Schumacher *et al*., 2012).

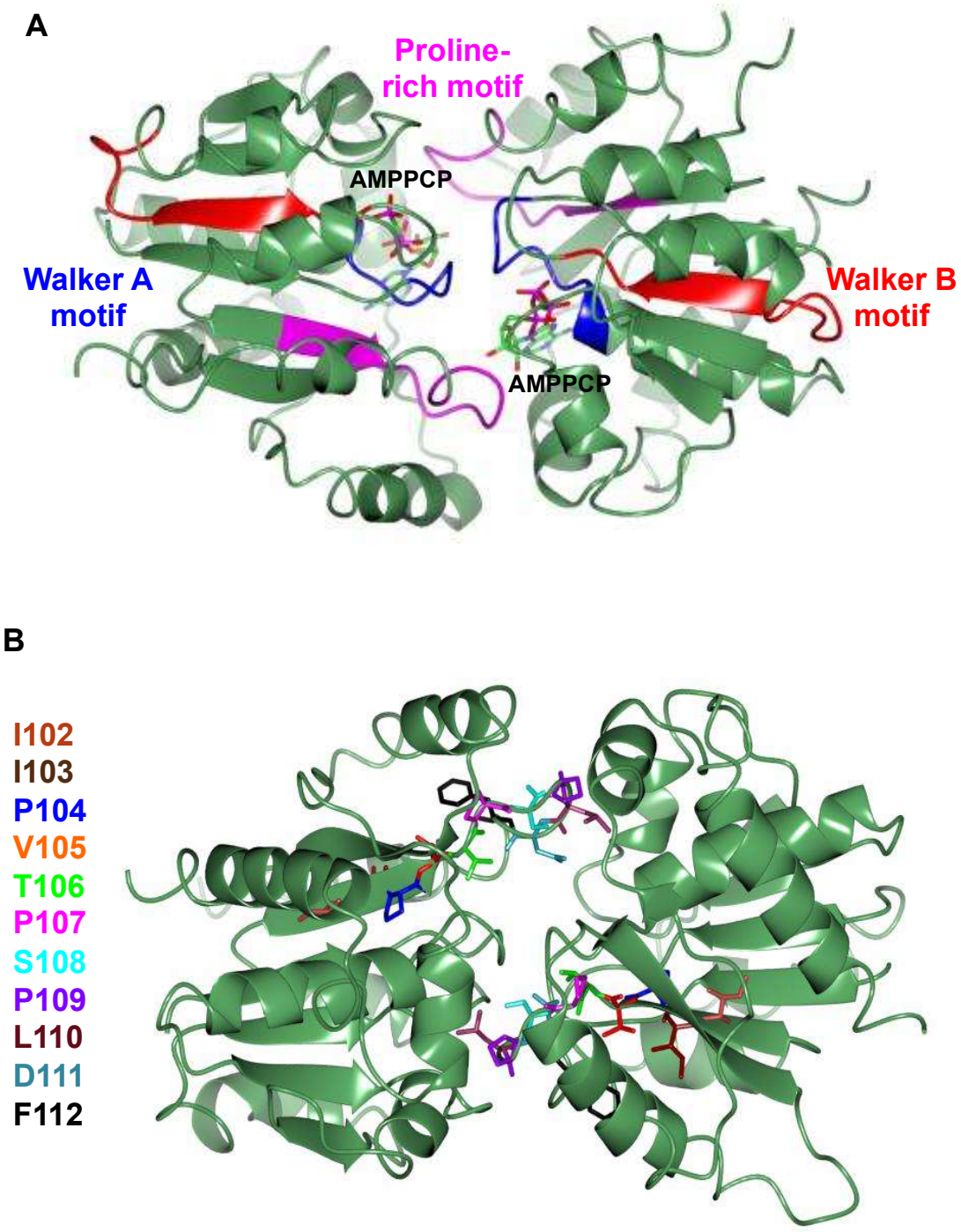

Figure 4.1– Structure of ParF showing the position of the proline-rich motif. A) Ribbon diagram of ParF dimer. ParF forms a nucleotide sandwich dimer in the presence of AMPPCP. AMPPCP is shown as sticks, the Walker A motif is highlighted in blue, the Walker B motif is highlighted in red and the proline-rich motif is highlighted in magenta. B) Ribbon diagram of ParF dimer. The residues that are part of the proline-rich motif are shown as sticks. Each residue is individually coloured as per the key on the left of the structure. The structural images were generated by using CCP4MG version 2.10.4 using the 4E07 PDB coordinates.

In addition to the proline-rich motif, additional key residues were identified that make cross-contacts within the monomer-monomer interface and with the proline-rich motif. The structural data revealed the side chain of P109 and Met146 insert into a hydrophobic cleft between Val173 and Leu177 of the adjacent subunit (Figure 4.2). Computational alanine scanning was also carried out in order to obtain further indication as to which residues may be important at the ParF monomer-monomer interface. Computational alanine scanning uses a simple free energy function to calculate the effects of alanine mutations on the binding free energy of a protein-protein complex. This allows energetically important residues, “hot spots”, to be identified and indicates which amino acids are critical at an interface (Kortemme and Baker, 2002). Gln41, Ser43, Leu110, Met143, Met146, Val173 and Leu177 were identified as being important residues at the monomer-monomer interface of ParF (Figure 4.3). Interestingly Met146, Val173 and Leu177 were identified by both structural predictions and computational analysis and therefore are likely to play a role in the dimer formation of ParF.

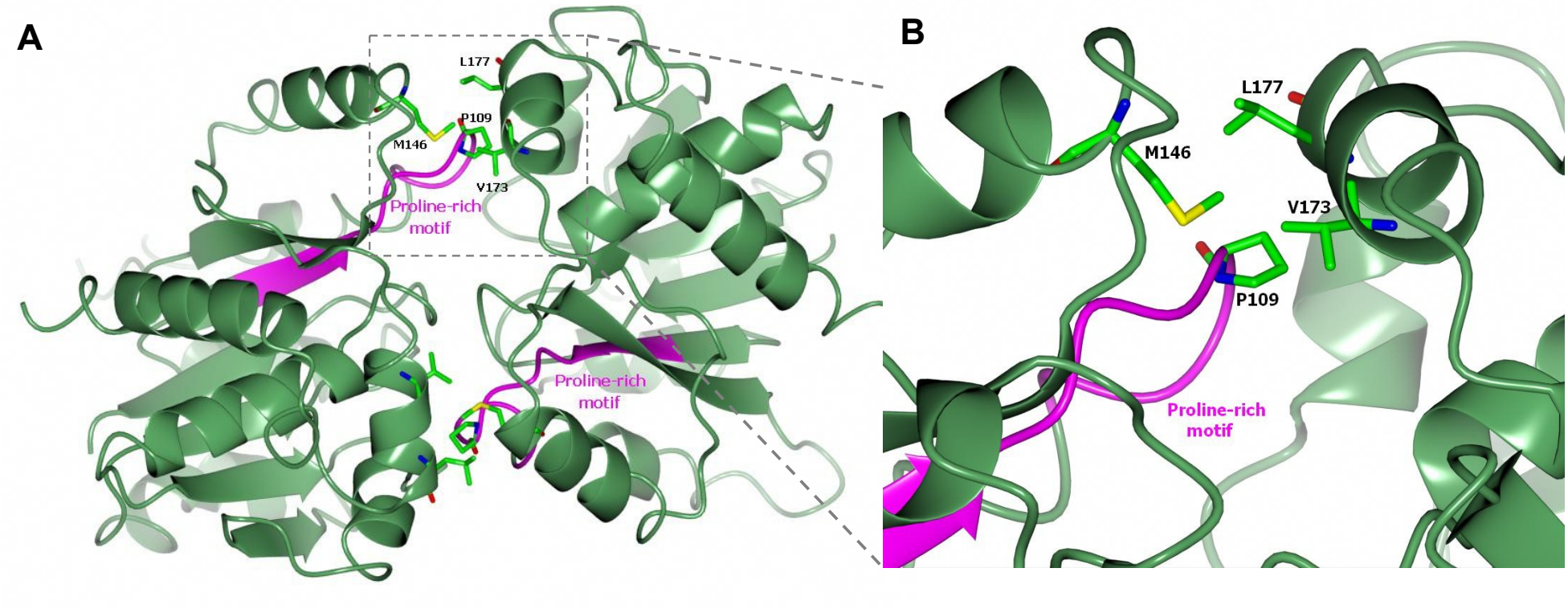

Figure 4.2 – Structure of ParF highlighting residues identified as potentially being involved in cross-contacts between ParF monomers. A) Ribbon diagram of ParF dimer. The proline-rich motif is highlighted in magenta with additional residues identified as potentially being involved in the monomer-monomer interaction shown as sticks. B) Zoomed image of the ribbon diagram of ParF dimer. M146 and P109 can be seen to insert into the hydrophobic pocket created by V173 and L177 on the adjacent monomer. The structural images were generated by using CCP4MG version 2.10.4 using the 4E07 PDB coordinates.

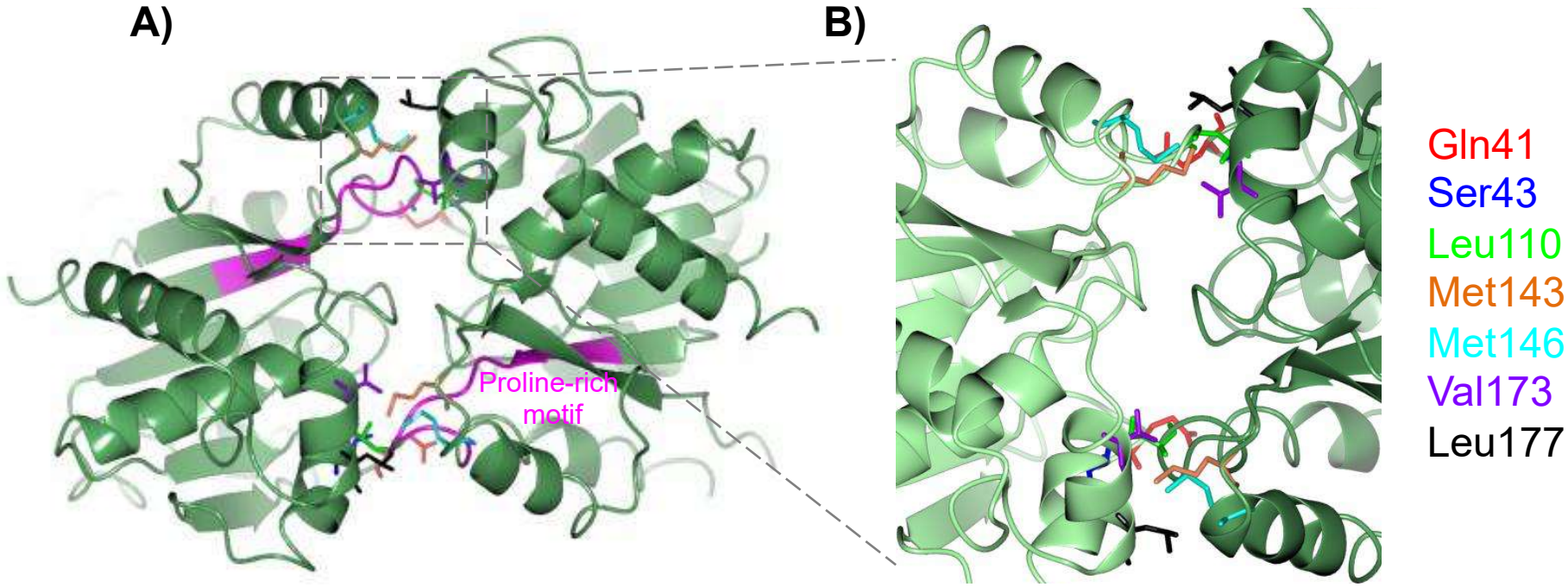

Figure 4.3 - Structure of ParF highlighting residues identified by computational alanine scanning as potentially involved in disrupting the monomer-monomer interface of the protein. A) Ribbon diagram of ParF dimer. The proline-rich motif is highlighted in magenta with additional residues identified as potentially being involved in the monomer-monomer interaction shown as sticks. Each residue is individually coloured as per the key on the right of the figure. B) Zoomed image of the ribbon diagram of ParF dimer. One monomer is shown in light green and the other in dark green. The structural images were generated by using CCP4MG version 2.10.4 using the 4E07 PDB coordinates.

The aim of this part of the study was to try and disrupt the monomer-monomer interface of ParF resulting in the obstruction of dimer formation and thus assembly into higher order structures. The roles of individual residues in the proline-rich motif were investigated. This was initially achieved using alanine scanning mutagenesis. Alanine is often chosen for mutagenesis studies, due to the fact that it is a small, uncharged amino acid and normally does not create any conformational change in the protein or electrostatic or steric effects. The role of each of the residues in the proline-rich motif was analysed in terms of the effect on the monomer-monomer interface of ParF. In particular, the initial investigation focused specifically on the three proline residues found in the proline rich motif, P104, P107 and P109. It is postulated that the proline residues may act as a molecular switch for ParF assembly into higher order structures. Proline is able to undergo *cis-trans* isomerisation and this is believed to play a role in molecular switches in proteins involved in cellular growth and regulation. Proline residues have been found to play both structural and dynamic roles in protein folding, fibre formation and protein-protein interactions (Deber *et al*., 2010). Therefore, taken with this and the fact that the proline residues in the proline-rich motif are well conserved in ParF homologues, it is reasonable to believe the proline residues may play a crucial role in ParF assembly into higher order structures.

4.2 *In vivo* analysis of the effects of the mutations constructed in the proline-rich motif on plasmid retention

Overlap extension mutagenesis was employed to mutate individual residues within the proline-rich motif to alanine. The experimental setup was the same as described in Chapter 3 for the construction of ParF-S185W. The partition vector, pFH547, was the template for the mutagenesis and restriction sites within the *parF* and *parG* genes were used in order to swap the wild type region with the fragment containing the desired mutations in the region encoding the proline-rich motif. The mutagenesis was carried out as detailed in 2.4. The proline-rich motif is composed of eleven residues, four of these residues had already been mutated to alanine and characterised in terms of the effect the change has on plasmid retention. ParF-P109A, L110A, D111A and F112A were constructed by the Hayes laboratory (unpublished data), therefore the first seven residues of the proline-rich motif were mutated to alanine in this study.

Partition assays were employed to determine what effects the mutations have on plasmid retention (Section 2.7). The constructed plasmids containing *parF* mutations in the proline-rich motif were transformed into the *E. coli* strain BR825 (*polA*) and the partition assays were carried out as described in Chapter 2. The results of the assays for the proline-rich motif mutagenesis are shown in Figure 4.4. The plasmid harbouring the *parF-P109A* mutation showed a plasmid retention of ~60 %, which is close to the wild type partition cassette and therefore this mutation had very little effect on plasmid retention (data not shown). On the other hand plasmids harbouring *parF-L110A, parF-D111A* or *parF-F112A* showed a significant reduction in plasmid retention (<10%), close to that of the plasmid that doesn't contain a partition cassette (Caccamo and Hayes, unpublished data).

The next step in this part of the study was to further investigate the role P109 played in the cross-contacts between ParF monomers. P109 was highlighted by the structural data as being involved in these cross-contacts. Schumacher *et al* (2012) observed that P109 from one monomer inserted into a hydrophobic pocket of the other monomer formed by residues Val173, Ile176 and Leu177. Although P109 is part of the proline-rich motif and had already been mutated to alanine and shown to have little effect on plasmid retention (Caccamo and Hayes, unpublished data) it was proposed that it may be possible to disrupt the cross-contacts by mutating P109 to either a larger or a charged amino acid. Therefore P109 was changed to arginine and characterised in terms of the effect the mutation had on plasmid retention.

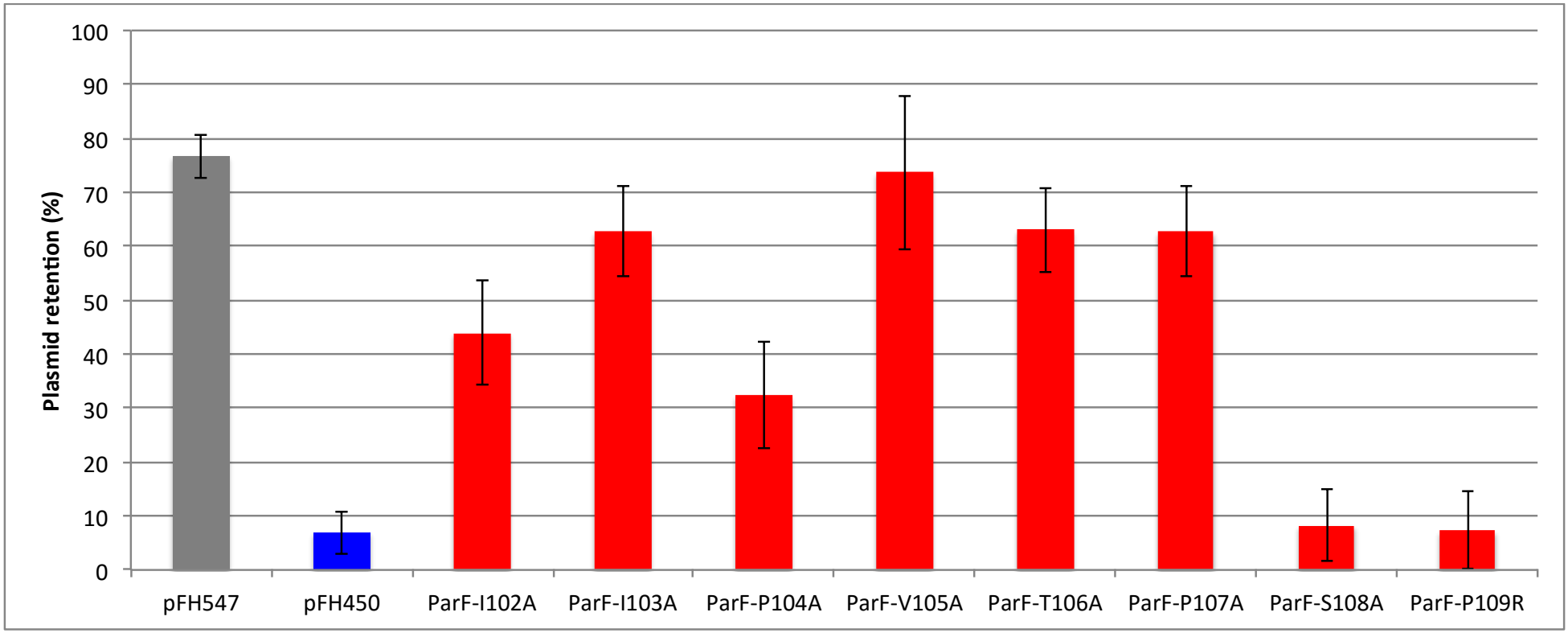

Figure 4.4 - Plasmid retention percentage of ParF harbouring changes in the proline-rich motif of ParF. pFH547 plasmid contains the wild type *parFGH* partition cassette and pFH450 lacks a partition cassette. Plasmid retention shown is calculated from an average of at least 3 assays with the standard deviation. Error bars represent the standard error of the mean. Partition assays of the first eight residues in the proline-rich motif.

The results of the partition assays identified I102A, P104A, S108A and P109R as showing informative phenotypes. However, ParF-P104A has already been characterised in Dobruk-Serkowska *et al*. (2012) and therefore no further work was carried out on this mutant in this study. ParF-P104A was expected to exert short-range impact on the ATP binding pocket conformation due to its proximity to the pocket. The results showed that ParF-P104A attenuated ATP binding and converted ParF to a hyperactive ATPase. ParF-P104A was also shown to form higher order structures even in the absence of nucleotide, indicating that the mutant self-associates more readily than the wild-type ParF. In contrast to wild type ParF, ParF-P104A assembly into higher order structures was inhibited by the addition of nucleotide. The results suggested that the P104A residue change may alter the conformation of the ATP binding pocket and cause a conformational change that locks ParF in a configuration that causes the increase in self-association (Dobruk-Serkowska *et al*., 2012).

The plasmid bearing *parF-I102A* showed a slight reduction in plasmid retention and therefore attempts were made to purify ParF-I102A in order to carry out *in vitro* analysis. However, after several attempts, it was not possible to purify ParF-I102A as it was insoluble and therefore no further work on ParF-I102A was carried out. The plasmid bearing *parF-S108A* and the plasmid bearing *parF-P109R* showed a significant reduction in plasmid retention close to that of the empty vector. Therefore further analysis on ParF-S108A and ParF-P109R was carried out in this study. Even though the plasmid bearing *parF-P107A* only showed a slight reduction in plasmid retention, further analysis was carried out on ParF-P107A. This was motivated by the originally proposed hypothesis on the role of the proline residues in ParF assembly into higher order structures and the results observed for ParF-P104A reported in Dobruk-Serkowska *et al.* (2012).

4.3 ParF-P107A, ParF-S108A and ParF-P109R

In order to analyse the effects of changes in the proline-rich motif on the monomer-monomer interface of ParF, ParF-P107A, ParF-S108A and ParF-P109R were studied using a range of *in vitro* and *in vivo* experimental approaches. Throughout the *in vitro* analysis it became evident that ParF-S108A and ParF-P109R showed more pronounced phenotypes than ParF-P107A, which is reasonable due to the difference observed in the partition assays. Therefore analysis became much more focused on ParF-S108A and

ParF-P109R throughout this part of the study, and ParF-P107A was only analysed by certain techniques.

4.3.1 Cloning of mutant *parF* alleles into the expression vector pET22b

ParF-P107A, ParF-S108A and ParF-P109R were overproduced using a pET expression system. The *parF* mutant alleles were cloned into the pET22b(+) expression vector, which contains a T7 promoter, *lac* operator and a C-terminal His-tag. The expression vector containing wild type *parF*, pDB-ParF, was already part of the laboratory stocks and used as a template for cloning of mutant *parF* alleles. Cloning involved the amplification of *parF-P107A*, *parF-S108A* and *parF-P109R* (from pFH547 vector containing the desired mutations) to incorporate restriction sites that enabled the wild type region to be swapped with the fragment containing the desired mutation in pET22b(+). Cloning was carried out as detailed in section 2.4.2 and an example of the cloning of *parF-S108A* into pET22b(+) is shown in Figure 4.5. All potential clones were sent for sequencing analysis (GATC) to ensure the desired mutation was present in the recombinant plasmid.

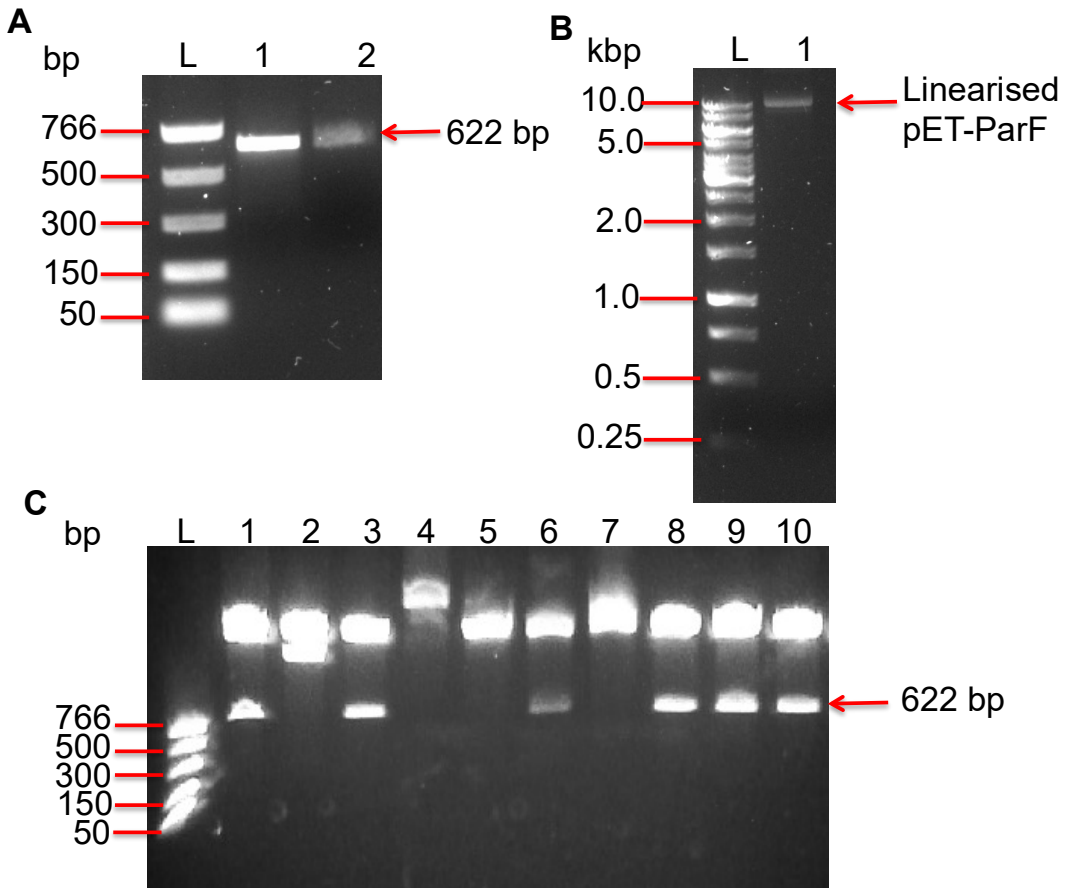

Figure 4.5 - Example of agarose gels showing the cloning of *parF-S108A* into pET22b(+). A) Agarose gel showing the PCR product of amplification of *parF-S108A* allele from pFH547. Lanes: L – NEB PCR marker; 1, *parF-S108A* PCR product; 2, PCR product after digestion with *Nde*I and *Xho*I restriction enzymes. B) Digested pET22b(+) – ParF vector. Lanes: L, Gene Ruler 10 kbp ladder; 2, pET22b(+)-ParF digest. C) Example of flash gel (Lonza) showing a restriction digest screen of pET22b(+) plasmids potentially harbouring the desired mutation, *parF-S108A*. Lanes: L,NEB PCR marker; 1 – 10 digests of ten plasmids potentially harbouring the desired mutation.

The overproduction and purification of the His-tagged ParF-P107A, ParF-S108A and ParF-P109R was carried out as detailed in section 2.5. Solubility assays were initially carried out to ensure the ParF mutant proteins were soluble prior to purification using Ni^{2+} affinity chromatography. An example of a solubility assay and purification of a ParF mutant protein is described in Chapter 3 and therefore no example is shown for ParF-P107A, ParF-S108A or ParF-P109R.

4.3.2 Biochemical properties of ParF-P107A, ParF-S108A and ParF-P109R and ability of the mutants to form higher order structures

4.3.2.1 ParF-P107A, ParF-S108A ParF-P109R are folded correctly and the mutations have no effect on the secondary structure of ParF

Prior to carrying out detailed *in vitro* analysis on ParF-P107A, ParF-S108A and ParF-P109R to investigate the effects of the changes on the monomer-monomer interface, circular dichroism (CD) was carried out in order to ensure the mutations had no effect on the structure of ParF. CD was carried out as detailed in section 2.10 and the results are shown in Figure 4.6. The CD spectra of ParF- P107A and ParF-S108A were very similar to that of wild type ParF, indicating the proteins were correctly folded and the mutations had little or no effect on ParF secondary structure. ParF-P109R also showed a similar spectrum to ParF, the slight difference observed between the spectra is due to the fact that the concentration of ParF-P109R was slightly lower (0.05 mg/ml) than that of the wild type ParF (0.2 mg/ml), therefore the ParF-P109R spectrum was adjusted by a factor of 4 to take this into account. Therefore this assay would need to be repeated with ParF and ParF-P109R at the same final concentration to conclude that ParF-P109R does have a similar structure to wild type ParF.

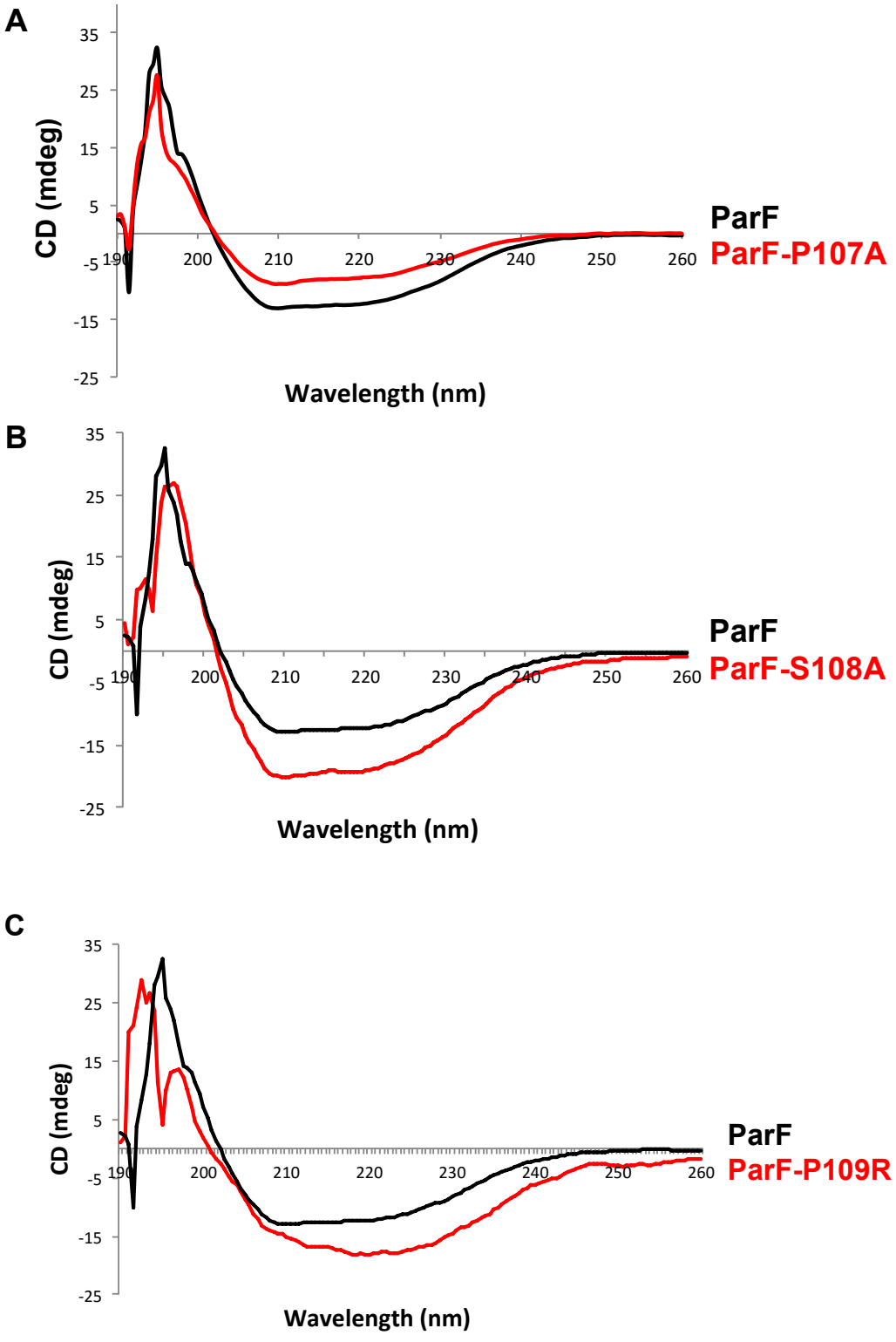

Figure 4.6 - Circular dichroism spectra of ParF-P107A, ParF-S108A and ParF-P109R. A) ParF-P107A. ParF spectrum is shown in black and the mutant in red. B) ParF-S108A. ParF spectrum is shown in black and the mutant in red. C) ParF-P109R. ParF spectrum is shown in black and the mutant in red.

4.3.2.2 All three mutants are able to bind ATP similarly to wild type ParF

Fluorescence anisotropy experiments were carried out in order to check whether ParF-P107A, ParF-S108A and ParF-P109R were able to bind ATP. A fluorescent ATP analog (MANT-ATP) was incubated with increasing concentrations of ParF and ParF-P107A/S108A/P109R to analyse the proteins ability to bind ATP. ParF-P107A, ParF-S108A and ParF-P109R were observed to bind MANT-ATP similarly to wild type ParF. ParF-P109R bound MANT-ATP similarly to wild type ParF, with almost identical K_d values. ParF has an observed K_d value of 0.44 μM and ParF-P109R has a K_d value of 0.37 μM. It should be noted that for ParF-P109R the binding curve does not fit exactly to all concentrations points. This is due to the fact that obtaining high concentrations of ParF-P109R is problematic as the protein isn't as soluble as the wild type protein. This means different protein aliquots were used in one experiment, which can lead to slight variations of results. However it should be noted that this experiment was repeated at least in triplicate and the K_d value was very similar for all. The K_d values for ParF-P107A and ParF-S108A indicate the mutants have a slightly lower affinity for ATP compared to that of the wild type protein. ParF-P107A and ParF-S108A had K_d values of 1.9 μM and 2.3 μM, respectively (Figure 4.7).

A

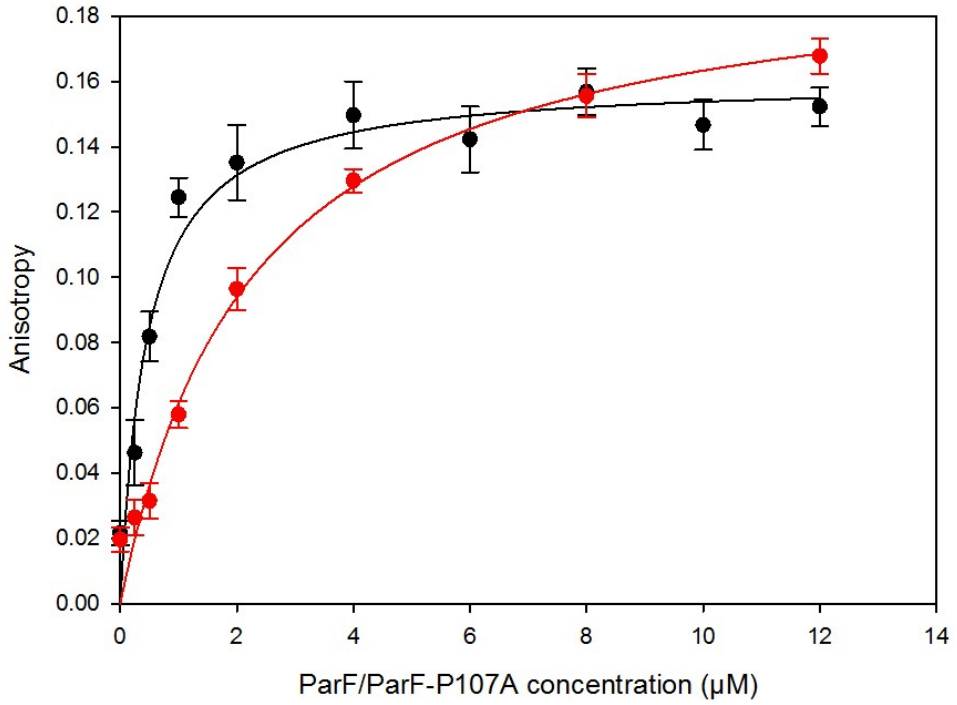
Anisotropy
0.18
0.16
0.14
0.12
0.10
0.08
0.06
0.04
0.02
0.00
0
2
4
6
8
10
12
14
ParF/ParF-P107A concentration (μM)

B

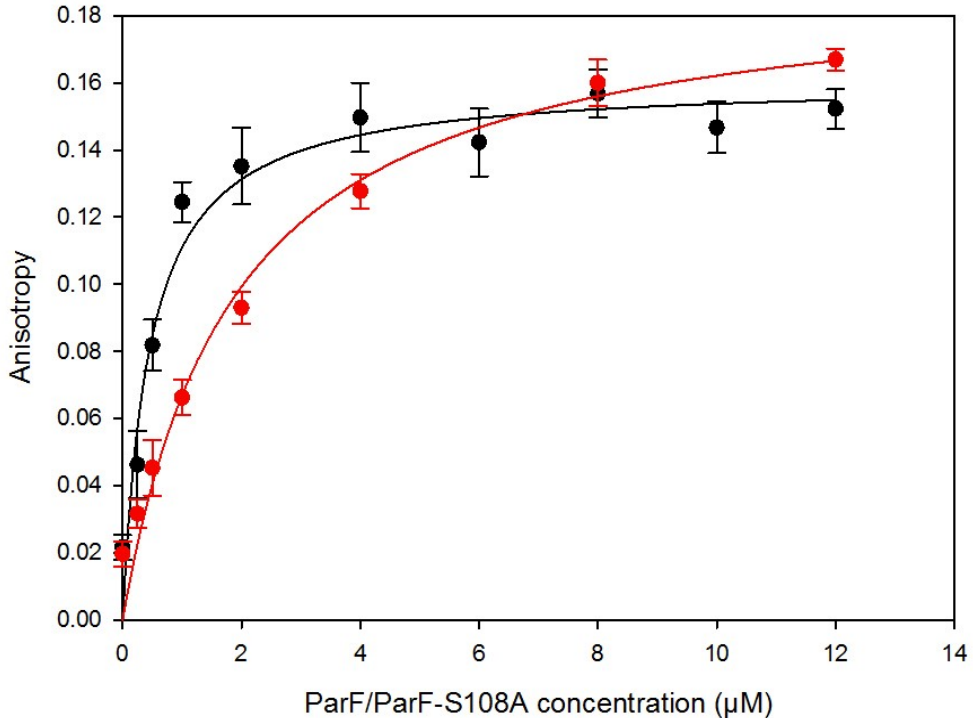
Anisotropy
0.18
0.16
0.14
0.12
0.10
0.08
0.06
0.04
0.02
0.00
0
2
4
6
8
10
12
14
ParF/ParF-S108A concentration (μM)

C

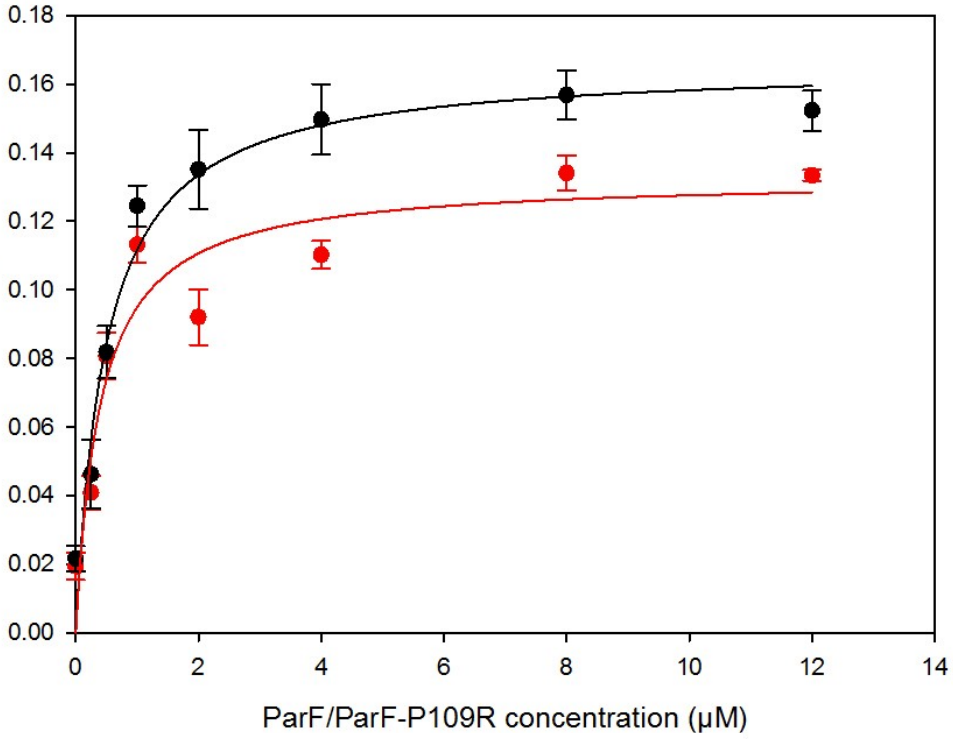

Figure 4.7 – Fluorescence anisotropy of ParF-P107A, ParF-S108A and ParF-P109R binding ATP. ParF is shown in black, ParF mutants are shown in red. Ten anisotropy values are taken for each concentration and an average value is calculated from this. Assays are carried out in triplicate. Error bars represent the standard error of the mean. A) ParF-P107A. B) ParF-S108A. C) ParF-P109R

4.3.2.3 ParF-S108A and ParF-P109R ATPase activity are not stimulated by ParG

ParF is an intrinsically weak ATPase and the partner protein ParG stimulates this activity. As ParF-S108A and ParF-P109R were shown to bind ATP similarly to wild type ParF, the next step involved checking ParF-S108A and ParF-P109R ATP hydrolysis. The ATPase activity of ParF and ParF mutants was analysed using thin layer chromatography (TLC) as described in section 2.8. In this assay, ParF/ParF mutant is incubated with radioactive ATP and ATP and its hydrolysis product, ADP, is separated using TLC. The ATP and ADP spots can be visualised on autoradiography films and quantified using a phosphorimager instrument. In the ATPase assays ParF/ParF mutant ATPase activity is tested both in the presence and absence of ParG. When ParG is added to wild type ParF, the increase in ATP hydrolysis results in a larger amount of ADP due to the stimulation of ParF ATPase activity by the N-terminal tail of ParG. The results demonstrated that ParF-S108A shows an intrinsic ATPase activity similar to that of the wild type protein ParF (Figure 4.8). However, stimulation of ParF-S108A

ATPase activity by ParG was lower than that observed for wild type ParF (Figure 4.9). At high ParG concentrations, ParF-S108A ATPase activity was not stimulated beyond 50 % of the maximum stimulation. The level of stimulation of ParF-S108A ATPase activity when 1 μM ParG was added appears higher than expected based on the level of stimulation when higher concentrations of ParG are added. This is likely due to experimental error within different ATPase assays. As the intrinsic ATPase activity of ParF-S108A is similar to wild type ParF, the reduced stimulation by ParG suggests ParF-S108A may not be able to interact with ParG to the same extent as ParF interacts with ParG.

ParF-P109R also showed a weak intrinsic ATPase activity similarly to the wild type protein ParF and again ParG was unable to stimulate the ATPase activity of ParF-P109R to the same extent as seen for ParF (Figure 4.10 and 4.11). Even in the presence of the highest concentration of ParG, the ATPase activity of ParF-P109R was not stimulated beyond 40% of the stimulation produced by ParG on ParF ATPase activity. As ParG is unable to stimulate the ATPase activity of both ParF-S108A and ParF-P109R it is likely that both mutants display a disruption in the interaction with ParG. Therefore analysing the interaction between the mutant proteins and ParG was investigated using a bacterial two-hybrid assay to try and support this hypothesis.

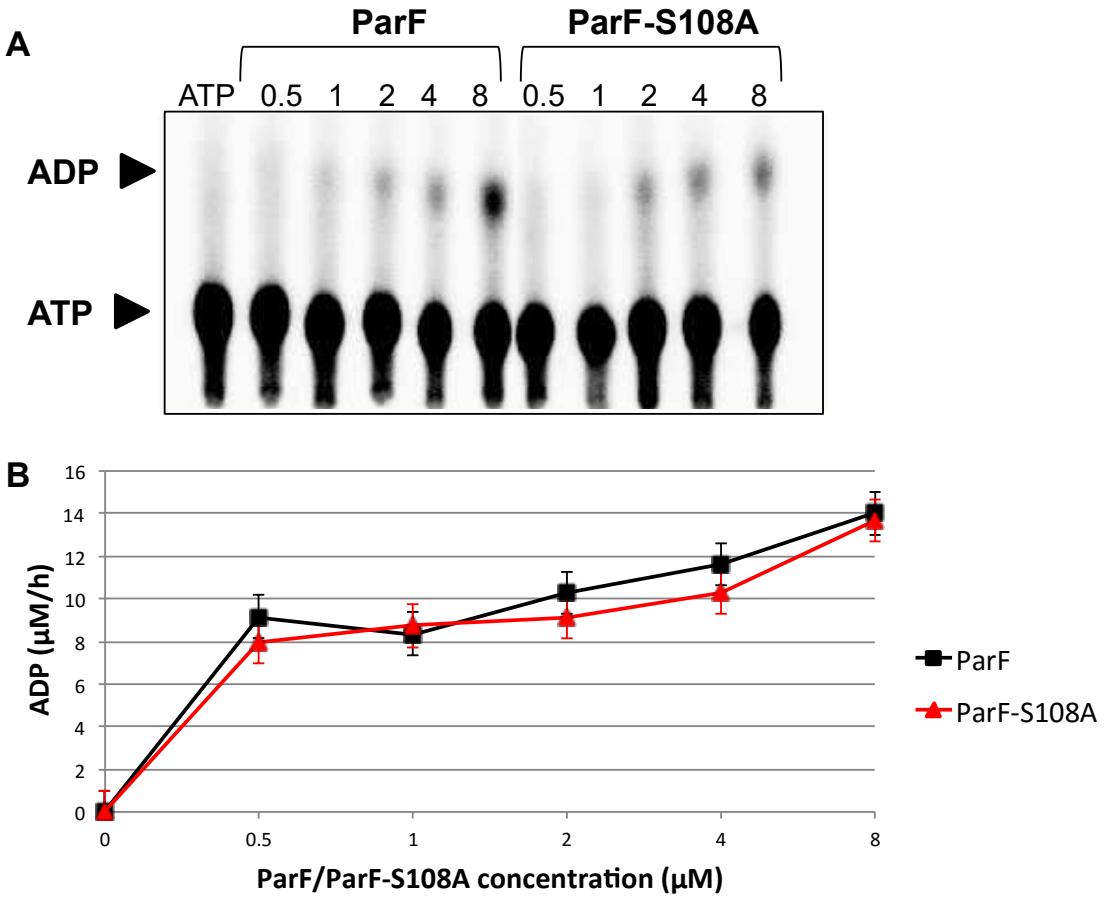

Figure 4.8 - Intrinsic ATPase activity of ParF and ParF-S108A. A) An example autoradiographic image showing the results of a representative ATPase assay in which radioactive ATP ([α^{35S}] ATP) was incubated with ParF and ParF-S108A. ATP and ADP (indicated by black arrow heads) were separated by TLC. Experiments were performed in triplicate. B) ATP hydrolysis plotted as a function of ParF/ParF-S108A concentration. The graph represents the average of three experiments and therefore the differences in intensities as shown in A don't quite match the quantitation shown in the graph. ParF is shown in black and ParF-S108A is shown in red. Error bars represent the standard error of the mean.

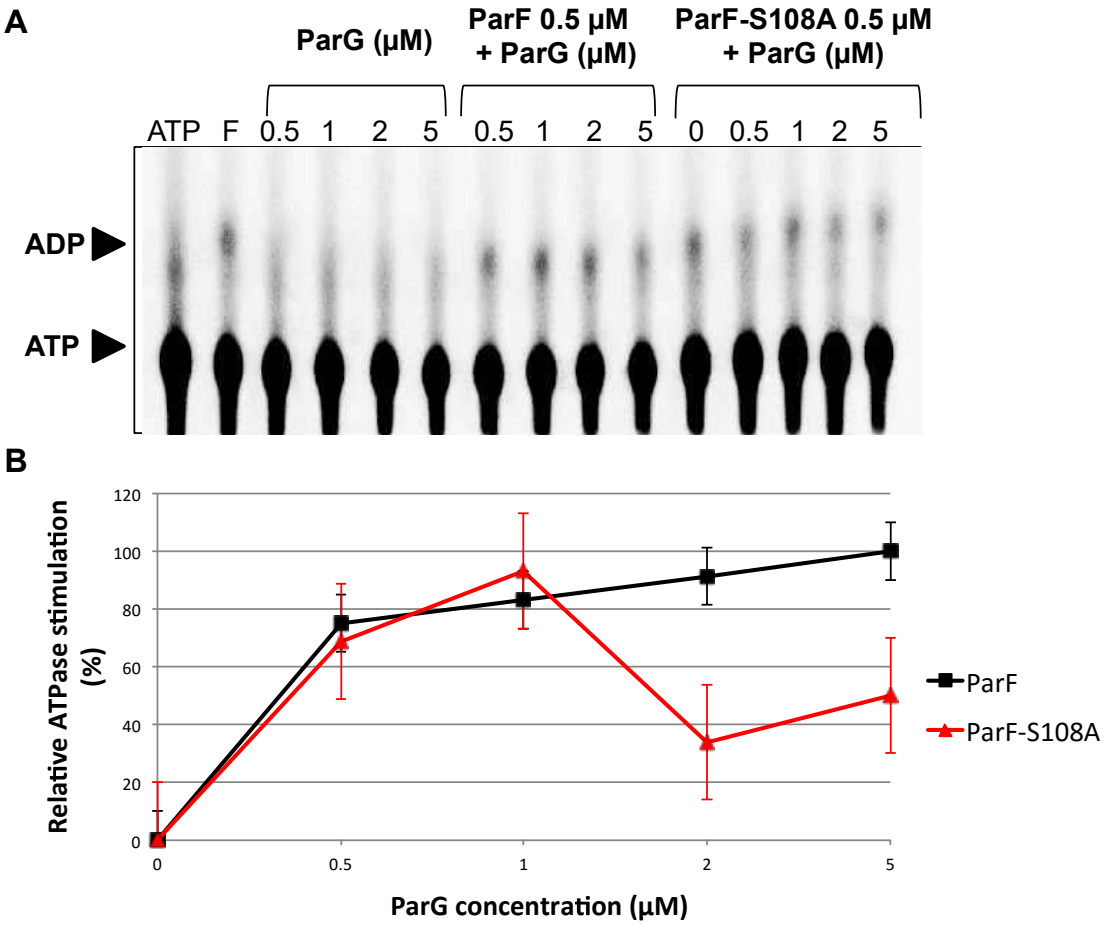

Figure 4.9 – ParF and ParF-S108A ATPase activity in the presence of ParG. A) Autoradiographic image showing the results of a representative ATPase assay in which radioactive ATP ([α^{35S}] ATP) and ParG were incubated with ParF and ParF-S108A. ParG was tested without ParF to check for the presence of potentially contaminating ATPase activities. ATP and ADP (indicated by black arrow heads) were separated by TLC. Experiments were performed in triplicate. B) Relative ATPase stimulation (%) plotted as a function of increasing ParG concentration. ParF is shown in black and ParF-S108A is shown in red. Error bars represent the standard error of the mean.

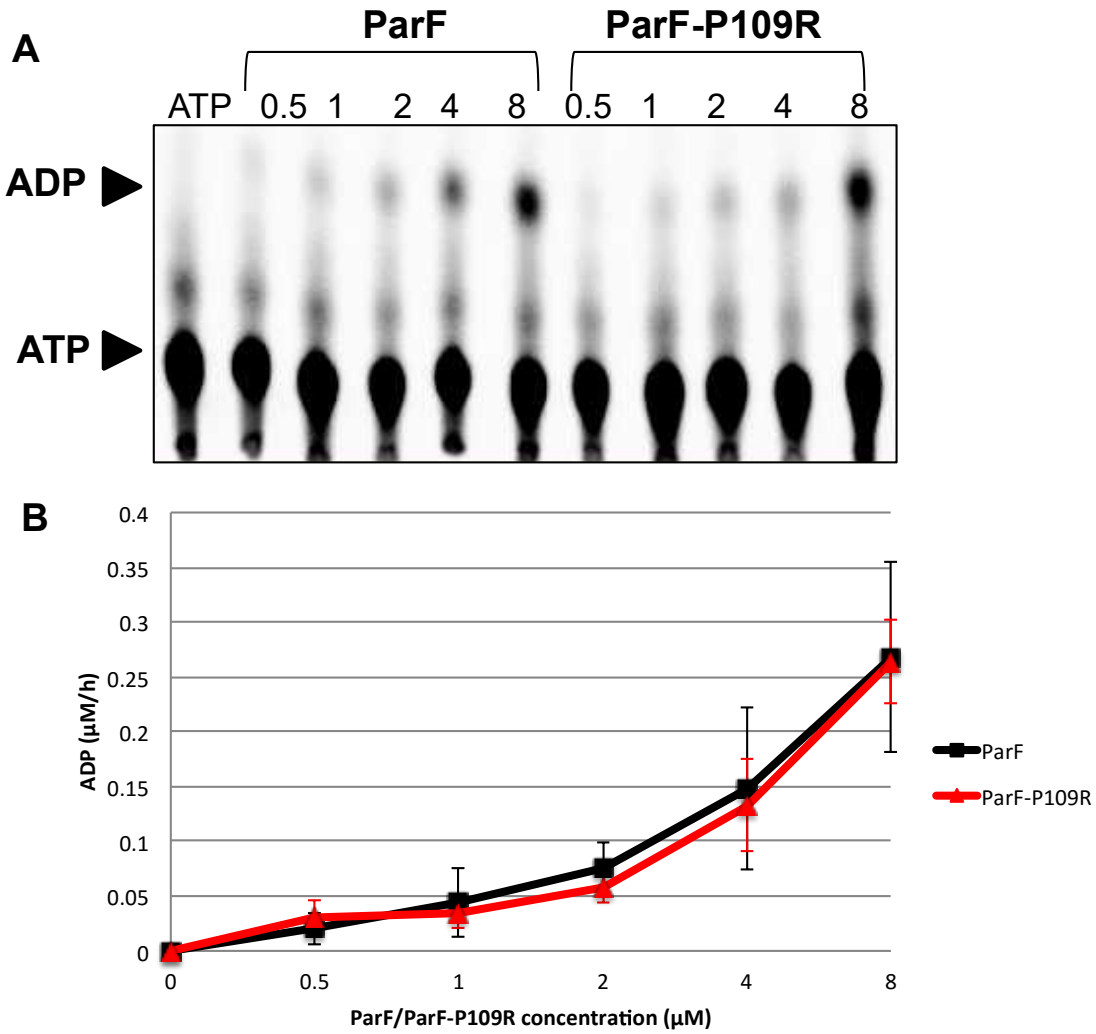

Figure 4.10 – Intrinsic ATPase activity of ParF and ParF-P109R. A) Representative autoradiographic image showing the results of an ATPase assay in which radioactive ATP ([α^{35S}] ATP) was incubated with ParF and ParF-P109R. ATP and ADP (indicated by black arrow heads) were separated by TLC. Experiments were performed in triplicate. B) ATP hydrolysis plotted as a function of ParF/ParF-P109R concentration. The graph represent the average of three experiments and is not directly representing the image shown in A. ParF is shown in black and ParF-P109R is shown in red. Error bars represent the standard error of the mean.

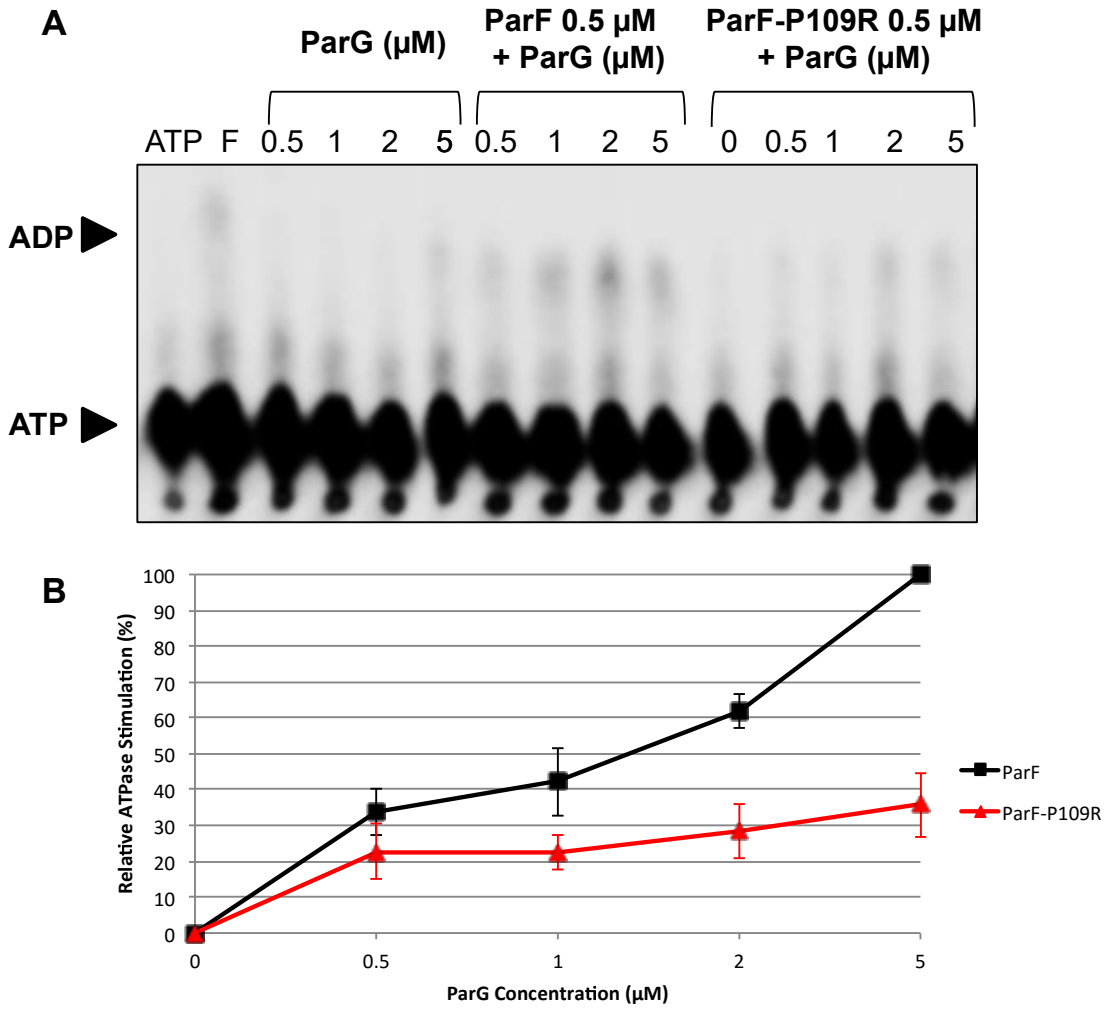

Figure 4.11 – ParF and ParF-P109R ATPase activity in the presence of ParG. A) Representative autoradiographic image showing the results of an ATPase assay in which radioactive ATP ([α^{35S}] ATP) and increasing concentrations of ParG were incubated with ParF and ParF-P109R. ParG was tested without ParF to check for the presence of potential contaminating ATPase activities. ATP and ADP (indicated by black arrow heads) were separated by TLC. Experiments were performed in triplicate. B) Relative ATPase stimulation (%) plotted as a function of increasing ParG concentration. The graph represent the average of three experiments and is not directly representing the image shown in A. ParF is shown in black and ParF-P109R is shown in red. Error bars represent the standard error of the mean.

4.3.2.4 ParF-P107A, ParF-S108A and ParF-P109R form dimers, however their interaction with ParG is disrupted

The original hypothesis was that disrupting residues in the proline-rich motif, which is positioned at the monomer-monomer interface, would affect dimer formation by ParF. The ability of the mutants to form a dimer was firstly analysed by chemical cross-linking and then by using a bacterial two-hybrid system followed by quantification using a β-galactosidase assay. The bacterial two-hybrid and β-galactosidase assays were also employed to analyse the interaction of the mutants with ParG, as the ATPase assay suggested that the interaction between both ParF-S108A and ParF-P109R with ParG might be disrupted.

Chemical cross-linking with dimethyl pimelimidate (DMP) was carried out as detailed in section 2.11. In the absence of DMP ParF runs as a monomer (23 kDa) on a denaturing SDS-gel, however upon the addition of DMP ParF monomers are cross-linked, showing they interact to form a dimer, running on a SDS-gel at 46 kDa. ParF, ParF-S108A and ParF-P109R (12 μM) were incubated with increasing concentrations of DMP (0 – 10 mM) for 2 hours at 37°C. ATP was added to the final reactions at a final concentration of 1 mM, as ParF dimerises only upon binding ATP. Upon addition of ADP and not ATP no dimerisation can be observed (data not shown). At 0.5 mM DMP ParF is able to be visualised as a dimer and at the higher concentrations of DMP the intensity of the dimeric band increases. Bands at higher molecular weights can also be seen at the higher concentrations of DMP, these bands are due to larger ParF complexes also being cross-linked. ParF-S108A and ParF-P109R, like the wild type protein, both formed a dimer at 0.5 mM DMP and again the band intensity of the dimer and higher molecular weight species increase with increasing DMP concentrations (Figure 4.12).

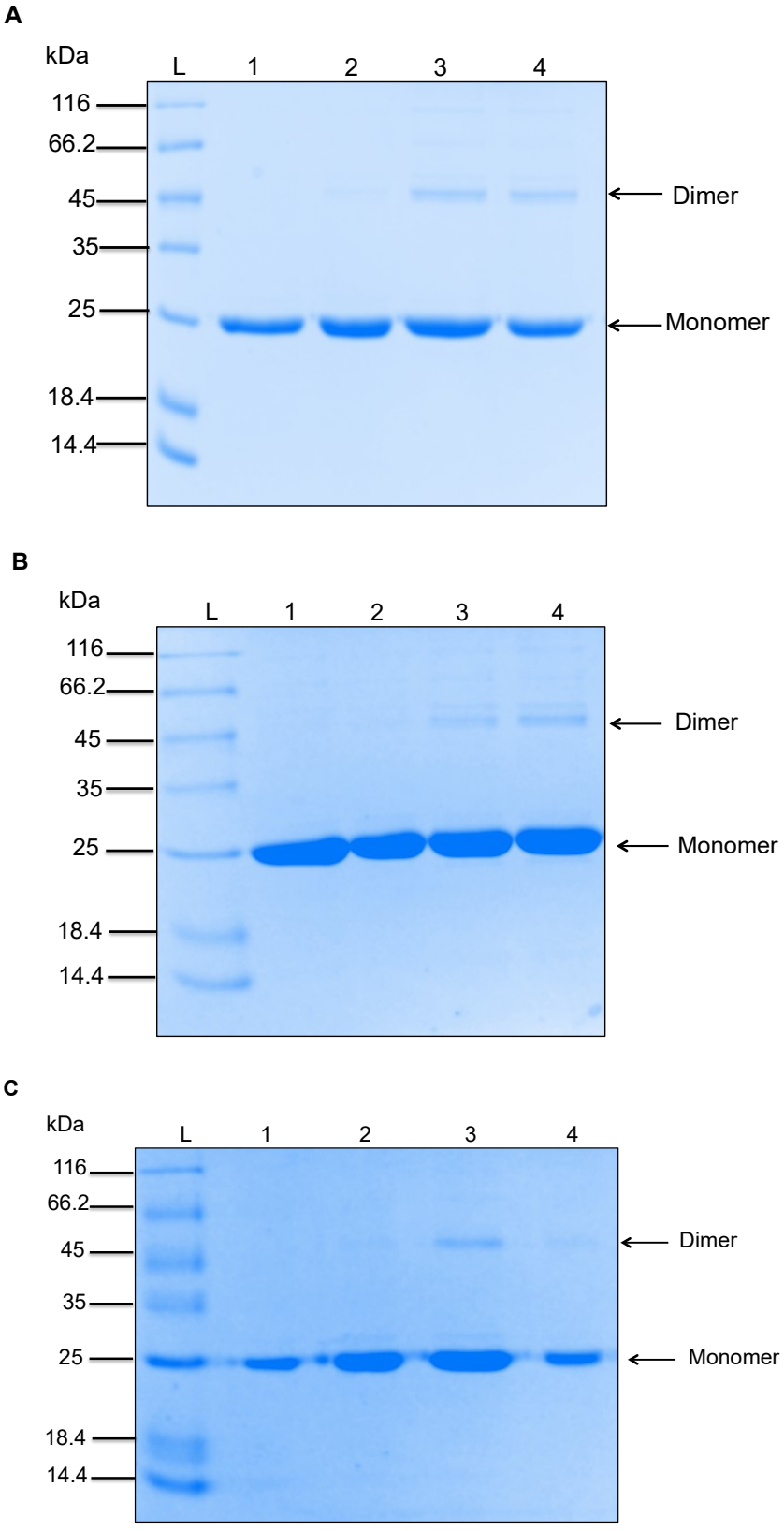

Figure 4.12 – Crosslinking results for ParF-S108A and ParF-P109R. SDS-polyacrylamide gels showing cross-linked products following two hours incubation with increasing concentrations of DMP. Lanes: L, Unstained Protein MW marker; 1, Protein only; 2, 0.5 mM DMP; 3, 1 mM DMP; 4, 10 mM DMP. A) ParF B) ParF-S108A C) ParF-P109R.

To examine whether ParF-P107A can form a dimer and to further confirm that ParF-S108A and ParF-P109R are able to dimerise, a bacterial two-hybrid assay was employed and to quantify this interaction a β-galactosidase assay was carried out. These assays were also used to investigate if the mutant proteins were able to interact with ParG similarly to the wild type protein. The bacterial two-hybrid system used to study protein-protein interactions *in vivo* (Karimova *et al*., 1998) was carried out as detailed in section 2.9. Cloning of *parF-P107A*, *parF-S108A* and *parF-P109R* were carried out as described in 2.4.2. Examples of cloning for bacterial two-hybrid assays for other *parF* mutants are detailed in Chapter 3. Examples of negative controls carried out in β-galactosidase assays are also shown in Chapter 3.

For the bacterial two-hybrid and β-galactosidase assays the desired plasmid pairs were co-transformed into SP850 *E. coli* competent cells as described in 2.3.10. pT18ParF-P107A+pT25ParF- P107A showed a slightly reduced interaction (average of ~1000 Miller units) compared to the wild type, however it was still evident that there was an interaction and therefore confirmed that ParF-P107A was able to form a dimer (Figure 4.13). The results for ParF-S108A and ParF-P109R confirmed those observed for the cross-linking; both mutant proteins are able to form a dimer (Figure 4.13). Interestingly the bacterial two-hybrid appeared to show a slightly darker red colour for pT18ParF-S108A+pT25ParF-S108A and for pT18ParF-P109R+pT25ParF-P109R compared to pT18ParF+pT25ParF, suggesting the interaction of ParF-S108A-ParF-S108A and ParF-P109R –ParF-P109R may be slightly stronger than ParF-ParF. This was confirmed in the β-galactosidase assay as pT18ParF-S108A+pT25ParF-S108A showed on average 100 Miller units more than pT18ParF+pT25ParF. ParF-P109R self-association showed on average an increase of 200 Miller units compared to ParF. Surprisingly, these results not only disprove the original hypothesis that changing the amino acids within the proline-rich motif would disrupt the dimer formation, but actually indicates the opposite effect. ParF-S108A and ParF-P109R appear to form a dimer with a self-interaction stronger than that of ParF-ParF.

The ParF-P107A-ParG, ParF-S108A-ParG and ParF-P109R-ParG interactions were then investigated. ParF-P107A showed a slightly stronger interaction with ParG compared to the wild type protein and ParG, confirming that ParF-P107A is still able to interact with ParG. On average ParF-P107A-ParG interaction is ~ 300 Miller units higher than ParF-ParG. However the error bar is large for ParF-P107A-ParG due to one result in the repeats of the β-galactosidase assay. If this result is excluded and only two

repeats are taken into account, the interaction of ParF-P107A with ParG is almost identical to that of wild type ParF. Therefore it can be concluded that the interaction of ParF-P107A with ParG is similar to ParF-ParG and not significantly higher. On the other hand, both ParF-S108A and ParF-P109R showed significantly weaker interactions with ParG compared to ParF (Figure 4.14). This was supported in both the bacterial two-hybrid assay and relative quantitation through the β-galactosidase assay. The interaction of ParG with ParF-S108A produced on average ~ 240 Miller units compared to ~ 840 for the interaction with ParF. This indicates the ParF-S108A-ParG interaction is ~ 70% weaker than ParF-ParG. The interaction of ParF-P109R with ParG showed on average ~ 532 compared to ~ 840 Miller units for the wild type proteins interaction. This indicates the interaction of ParF-P109R with ParG is ~ 40% weaker than ParF-ParG. These results help rationalise the results from the ATPase assay: if the ParF-S018A-ParF-ParG interaction and ParF-P109R-ParG interaction are disrupted, ParG is unable to stimulate the ATPase activity as efficiently.

The results described so far indicate that converting S108 to alanine and P109 to arginine does have an effect on the ParF monomer-monomer interface. However, the outcome is not the one originally envisaged, as the monomer-monomer interaction is augmented rather than abolished.

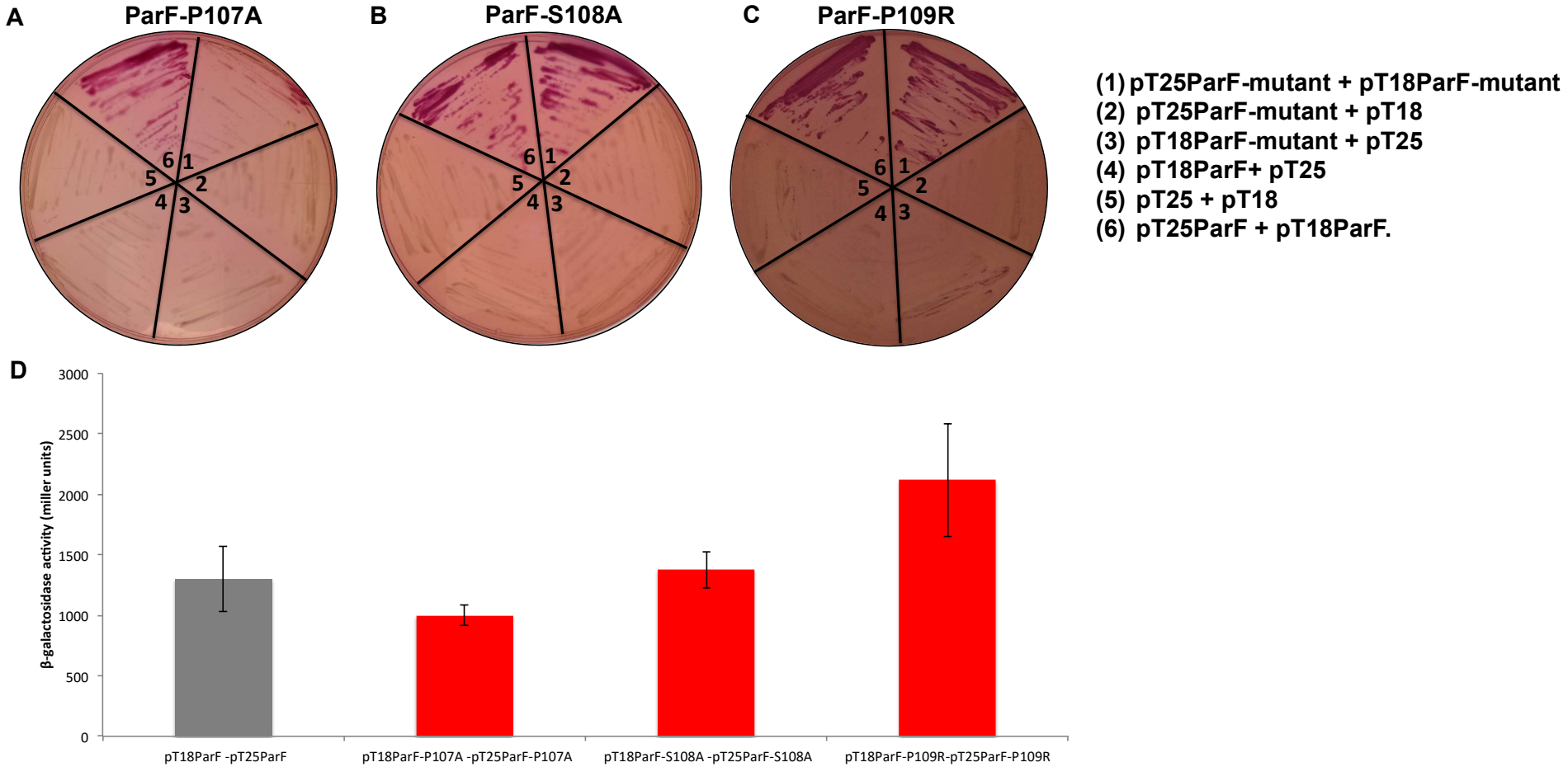

Figure 4.13 – Bacterial two-hybrid and β-galactosidase assay of ParF-P107A, ParF-S108A and ParF-P109R. A) Bacterial two-hybrid assay for ParF-P107A. Plasmids carrying *parF* or *parF-p107A* fused to T25 and T18 fragments were co-transformed into *E. coli* SP850 and streaked on MacConkey-maltose plates.. B) Bacterial two-hybrid assay for ParF-S108A. Plasmids carrying *parF* or *parF-S108A* fused to T25 and T18 fragments were co-transformed into *E. coli* SP850 and streaked on MacConkey-maltose plates. C) Bacterial two-hybrid assay for ParF-P109R. Plasmids carrying *parF* or *parF-P109R* fused to T25 and T18 fragments were co-transformed into *E. coli* SP850 and streaked on MacConkey-maltose plates. D) β-galactosidase assay. ParF-ParF interaction is shown in grey, ParF-P107A-ParF-P107A, ParF-S108A-ParF-S108A and ParF-P109R-ParF-P109R interactions are shown in red. The assay was carried out in triplicate. Error bars represent the standard error of the mean.

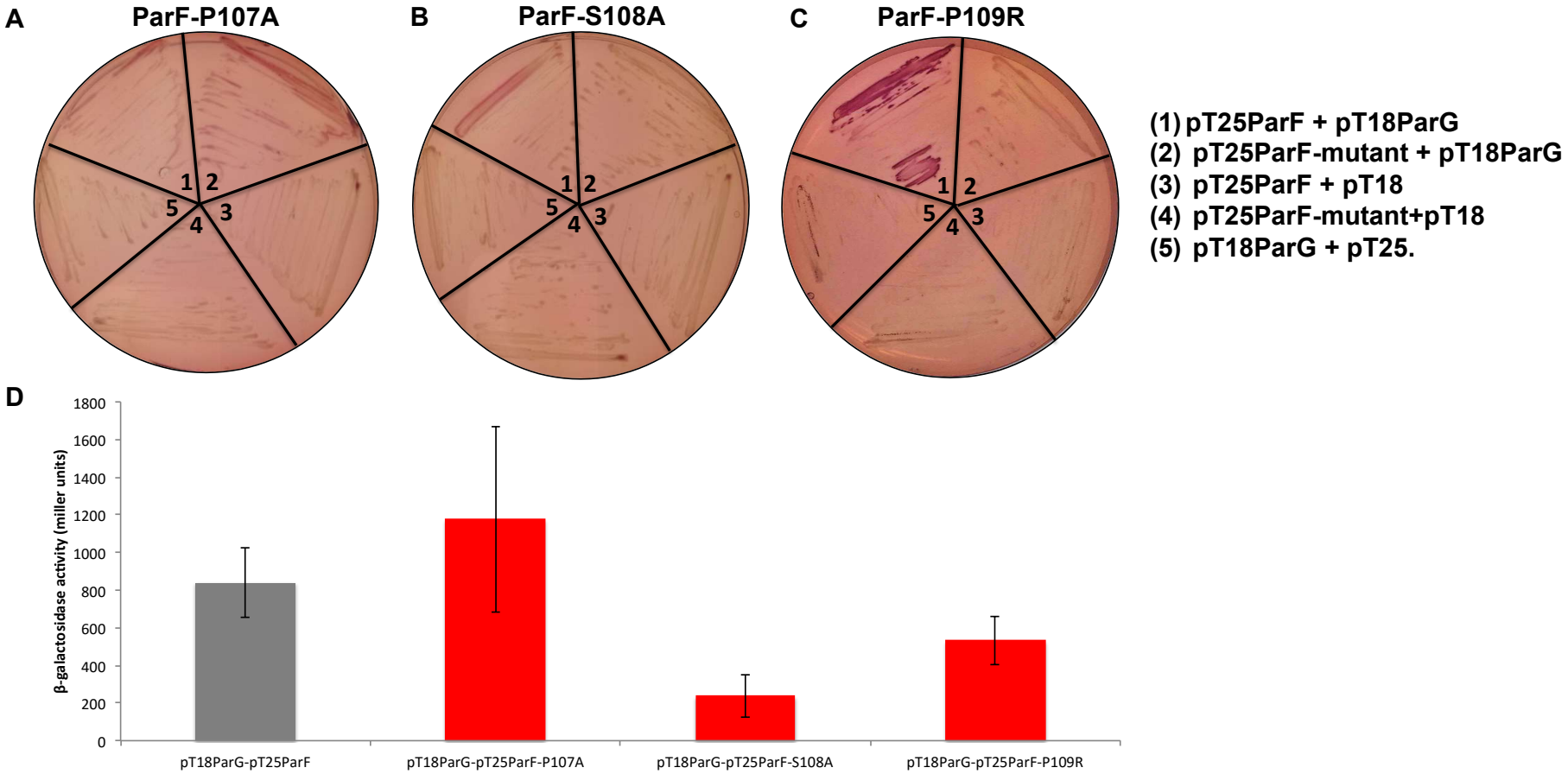

Figure 4.14 - Bacterial two-hybrid assay and β-galactosidase assay of ParF-P107A, ParF-S108A and ParF-P109R interactions with ParG. A) Bacterial two-hybrid assay for ParF-P107A-ParG interaction. Plasmids carrying *parF* or *parF-P107A* fused to T25 and *parG* fused to T18 were co-transformed into *E. coli* SP850 and streaked on MacConkey-maltose plates. B) Bacterial two-hybrid assay for ParF-S108A-ParG interaction. Plasmids carrying *parF* or *parF-S108A* fused to T25 and *parG* fused to T18 were co-transformed into *E. coli* SP850 and streaked on MacConkey-maltose plates. C) Bacterial two-hybrid assay for ParF-P109R-ParG interaction. Plasmids carrying *parF* or *parF-P109R* fused to T25 and *parG* fused to T18 were co-transformed into *E. coli* SP850 and streaked on MacConkey-maltose plates. D) β-galactosidase assay. ParF-ParG interaction is shown in grey, ParF-P107A- ParG, ParF-S108A-ParG and ParF-P109R-ParG interactions are shown in red. The assay was carried out in triplicate. Error bars represent the standard error of the mean.

4.3.2.5 ParF-P107A, ParF-S108A and ParF-P109R have a higher tendency to self-associate into higher order structures

Originally it was proposed that changing amino acids within the proline-rich motif would disrupt the ParF dimer formation and thus prevent the assembly of ParF into higher order structures. During the course of the investigations, it became apparent that the monomer-monomer interface of these mutant proteins does differ from wild type ParF, however the interaction between the monomers is actually stronger rather than weaker, which means a dimer is still formed. It was therefore important to establish the effect that this behaviour has on ParF assembly into higher order structures. The ability of ParF-P107A, ParF-S108A and ParF-P109R to form higher order structures *in vitro* was first investigated using DLS as detailed in section 2.12 and then with sedimentation assays (section 2.17) to cross-check and validate the DLS results. As previously shown (Barilla *et al*., 2005) and discussed in Chapter 3, ParF is able to assemble into higher order structures in the presence of ATP and this property is antagonised by ADP. ParF was also shown to have an intrinsic tendency to self-associate into higher order structures in the absence of nucleotide. In addition, it has also been observed that ParG promotes ParF polymer formation, both in the presence and absence of ATP. Therefore in this study, the assembly of ParF-P107A, ParF-S108A and ParF-P109R into higher order structures was observed in the absence of nucleotide and in the presence of ADP, ATP, ATP-γ-S and ParG. All DLS experiments were carried out in parallel with ParF, the proteins were monitored over 60 minutes and changes in intensity of light scattering were observed (Figure 4.15).

The results observed for ParF-P107A and ParF-S108A were very similar, with ParF-S108A showing a slightly more distinctive behaviour. In the absence of nucleotide ParF-P107A and ParF-S108A showed an increase in light scattering intensity over time, therefore demonstrating the proteins were self-associating. Compared to the wild type ParF, ParF-P107A and especially ParF-S108A showed a higher tendency to self-associate, as evidenced by the higher increase in intensity of light scattering (Figure 4.15A). Unlike wild type ParF, the addition of ATP did not augment the assembly of ParF-P107A and ParF-S108A into higher order structures, but in contrast appeared to inhibit the formation of the higher order structures. In fact, upon addition of any nucleotide, ADP, ATP or ATP-γ-s, the mutants' ability to self-associate was decreased (Figure 4.15).

ParF-P109R showed an even more distinctive phenotype than ParF-P107A and ParF-S108A but this also suggests that ParF-P109R had a stronger tendency to self-associate. In the absence of nucleotide ParF-P109R showed an increase in intensity of light scattering over time and, compared to the wild type ParF, the increases was significantly higher (Figure 4.15A). In some instances, the intensity of light scattering would start ~ 8000 – 10000 kct/s and increase to a maximum of ~35000 – 40000. This level of intensity is extremely high and even in the presence of ATP for 60 minutes ParF rarely generates this level of scattering. Interestingly, the addition of nucleotides had little or no effect on the intensity of light scattering and over time it showed a steady increase (Figure 4.15). Therefore ParF-P109R appears to self-associate independently of the presence of ATP. Figure 4.16 shows DLS experiments in which ParF-P109R was incubated without nucleotide and with ADP, ATP and ATP-γ-s on the same graph to demonstrate the limited effect of nucleotides on the propensity of ParF-P109R to self-associate.

The ability of ParG to promote ParF-P107A, ParF-S108A and ParF-P109R assembly into higher order structures was also investigated. ParG was observed to promote ParF-P107A assembly into higher order structures to some extent both in the presence and absence of ATP, although in the absence of nucleotide this was more prominent (Figure 4.17). In the absence of nucleotide ParG promoted the assembly of ParF-P107A into higher order structures to a similar extent as the wild type ParF, if any difference can be observed the initial increase in light scattering is more gradual for ParF-P107A. When ATP was added first and then ParG only a slight increase in intensity of light scattering could be seen, that was significantly lower than ParF. Therefore ParG is not able to override the effects of nucleotides on ParF-P107A assembly into higher order structures but in the absence of nucleotide ParG is able to stimulate the assembly of higher order structures. ParF-S108A and ParF-P109R, like ParF-P107A, show a very slight increase in intensity of light scattering when ATP and then ParG are added indicating ParG is unable to promote ParF-S108A and ParF-P109R assembly into higher order structures (Figure 4.18 and 4.19). This is likely to reflect previous findings that both ParF-S108A and ParF-P109R show a much weaker interaction with ParG than ParF-ParG and also ParF-P107A-ParG.

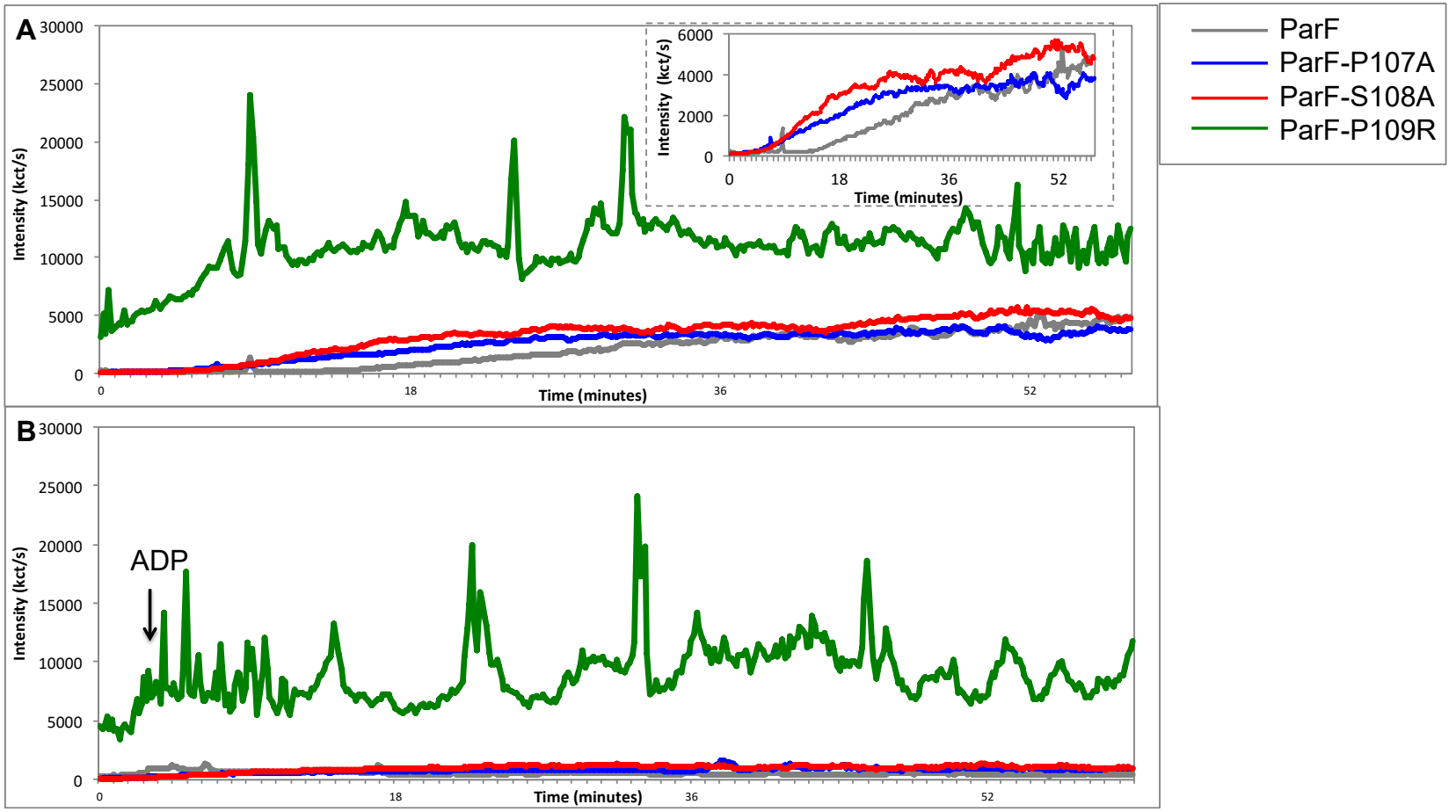
A
B
Intensity (kct/s)
Time (minutes)
ADP
ParF
ParF-P107A
ParF-S108A
ParF-P109R

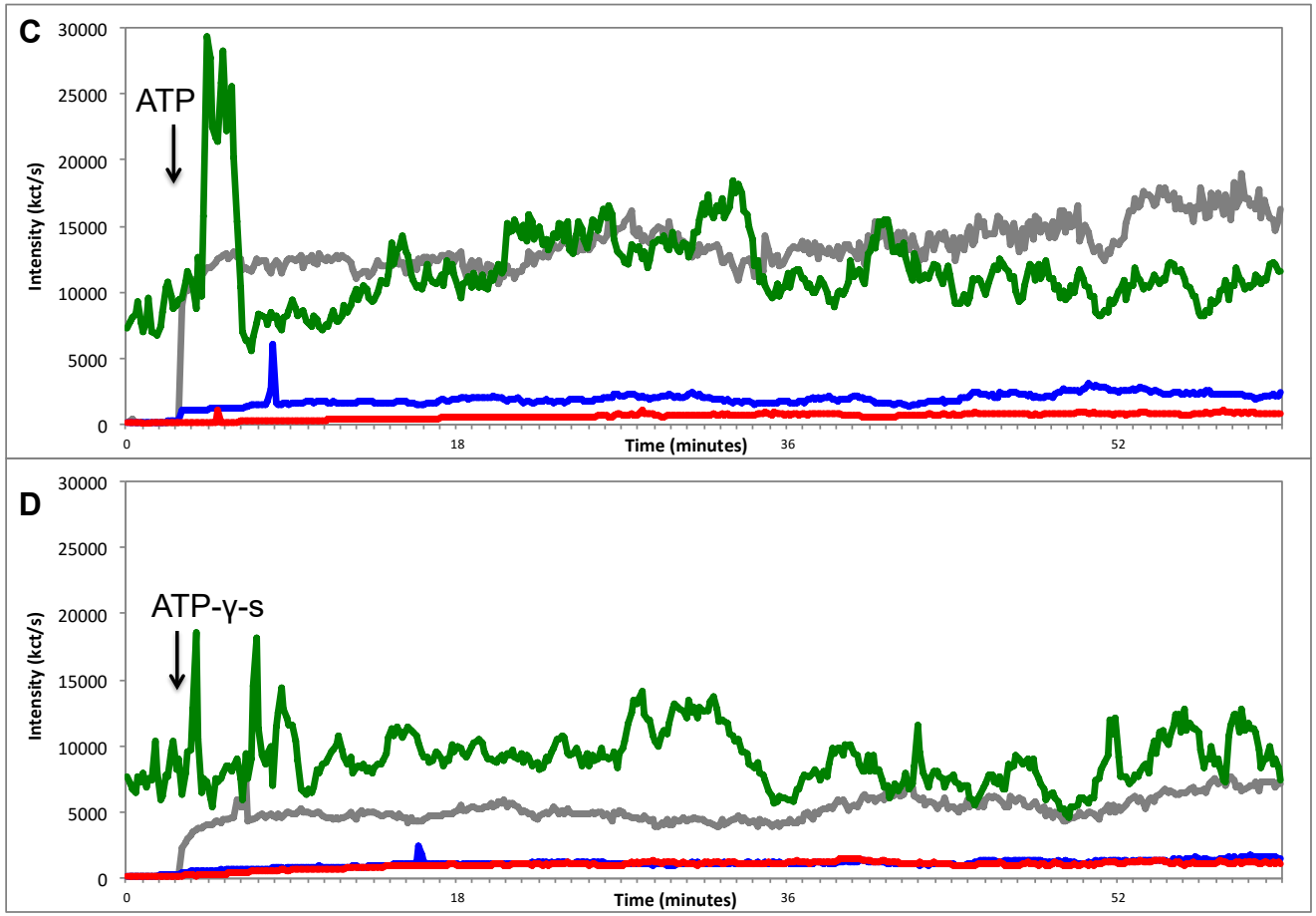

Figure 4.15 – DLS of ParF-P107A, ParF-S108A and ParF-P109R in the absence and presence of nucleotide. DLS experiments were carried out and the increase in light scattering intensity (kct/s) was recorded for ParF, ParF-P107A, ParF-S108A and ParF-P109R. ParF, ParF-P107A, ParF-S108A and ParF-P109R were added at a final concentration of 2.16 μM and a baseline was obtained for three minutes and then nucleotide was added (500 μM) with $MgCl_2$ (5 mM); the point of addition is indicated by a black arrow. The light scattering intensity was then recorded for further 60 minutes. ParF is shown in grey, ParF-P107A in blue, ParF-S108A is shown in red and ParF-P109R in green. A) No nucleotide – inset graph shows the results on a smaller scale to demonstrate the differences more clearly. B) ADP. C) ATP. D) ATP-γ-S. This is a representative experiment. Each experiment was repeated at least in triplicate.

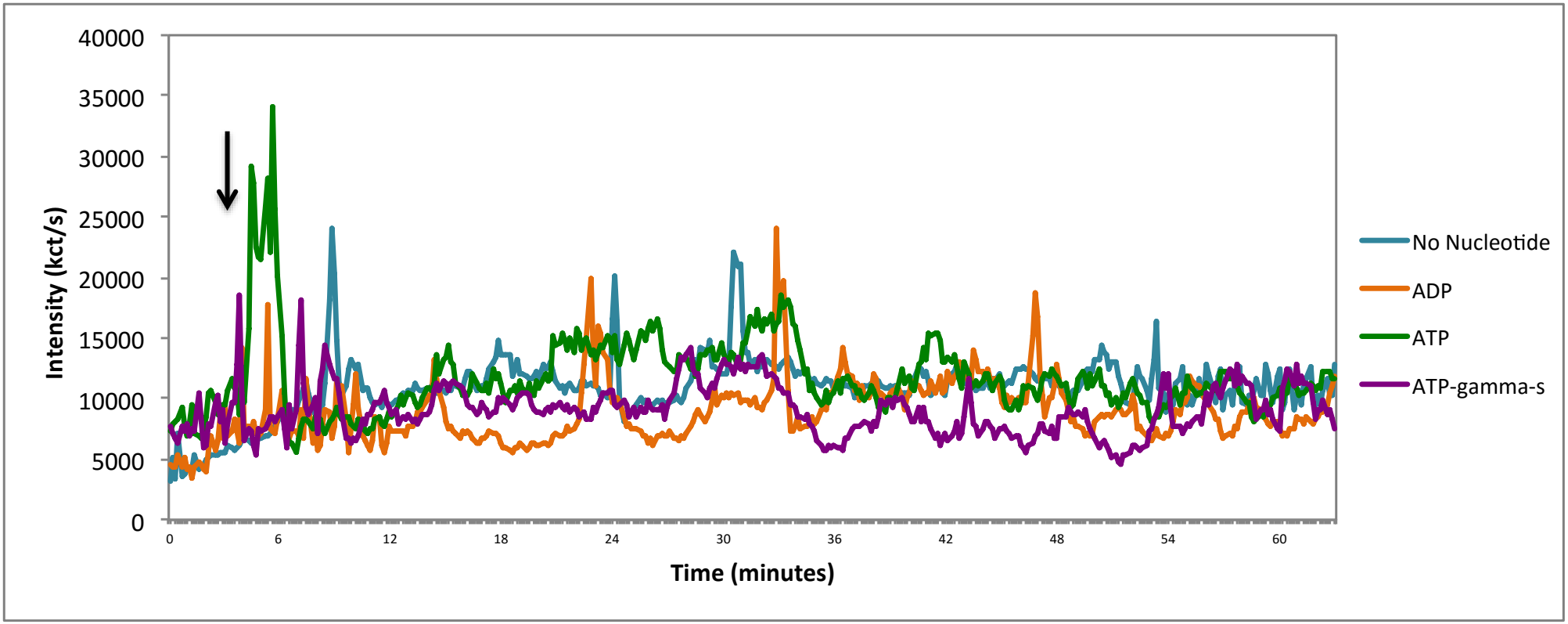

Figure 4.16 – DLS of ParF-P109R in the absence and presence of nucleotide.. DLS experiments were carried out and the increase in light scattering intensity (kct/s) was recorded for ParF and ParF-P109R. ParF and ParF-P109R were added at a final concentration of 2.16 μM and a baseline was obtained for three minutes and nucleotide was added (500 μM) with $MgCl_2$ (5 mM). The point of addition is indicated by a black arrow.

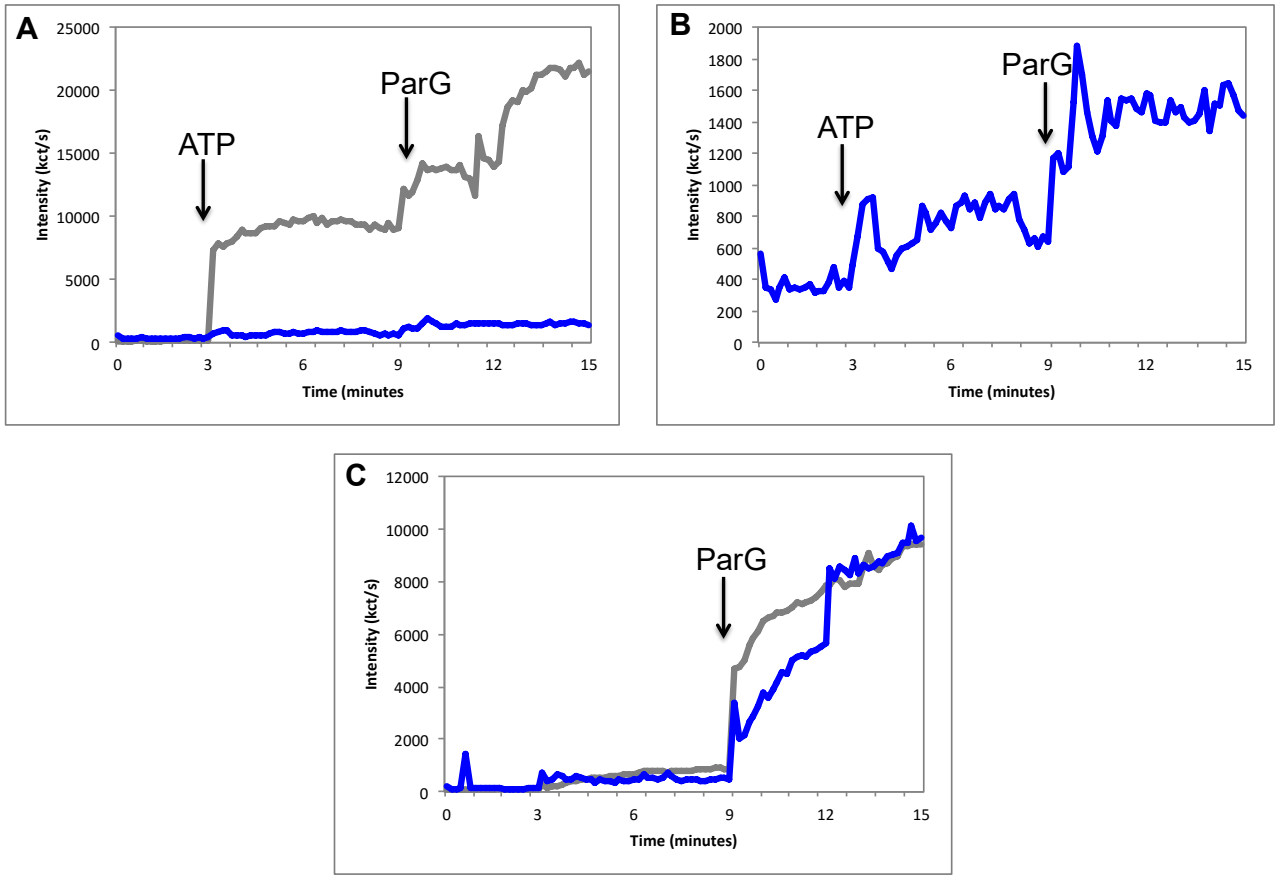

Figure 4.17 - DLS of ParF-P107A in the presence of ParG. DLS experiments were carried out and the increase in light scattering intensity (kct/s) was recorded for ParF and ParF-P107A. ParF and ParF-P107A were added at a final concentration of 2.16 µM and a baseline was obtained for three minutes and then if ATP was added (500 µM) with $MgCl_2$ (5 mM), it is indicated by a black arrow. The light scattering intensity was then recorded for a further six minutes before ParG was added at a final concentration of 2.16 µM, indicated by a black arrow, and the intensity recorded for a further 6 minutes. ParF is shown in grey and ParF-P107A is shown in blue. A) The effect of both ATP and ParG on the assembly of ParF-P107A into higher order structures. B) The effect of both ATP and ParG on the assembly of ParF-P107A into higher order structures, only ParF-P107A (blue) is shown on a smaller scale to indicate more clearly any changes in intensity of light scattering. C) The effect of only ParG on the assembly of ParF-P107A into higher order structures. This is a representative experiment. Each experiment was repeated at least in triplicate.

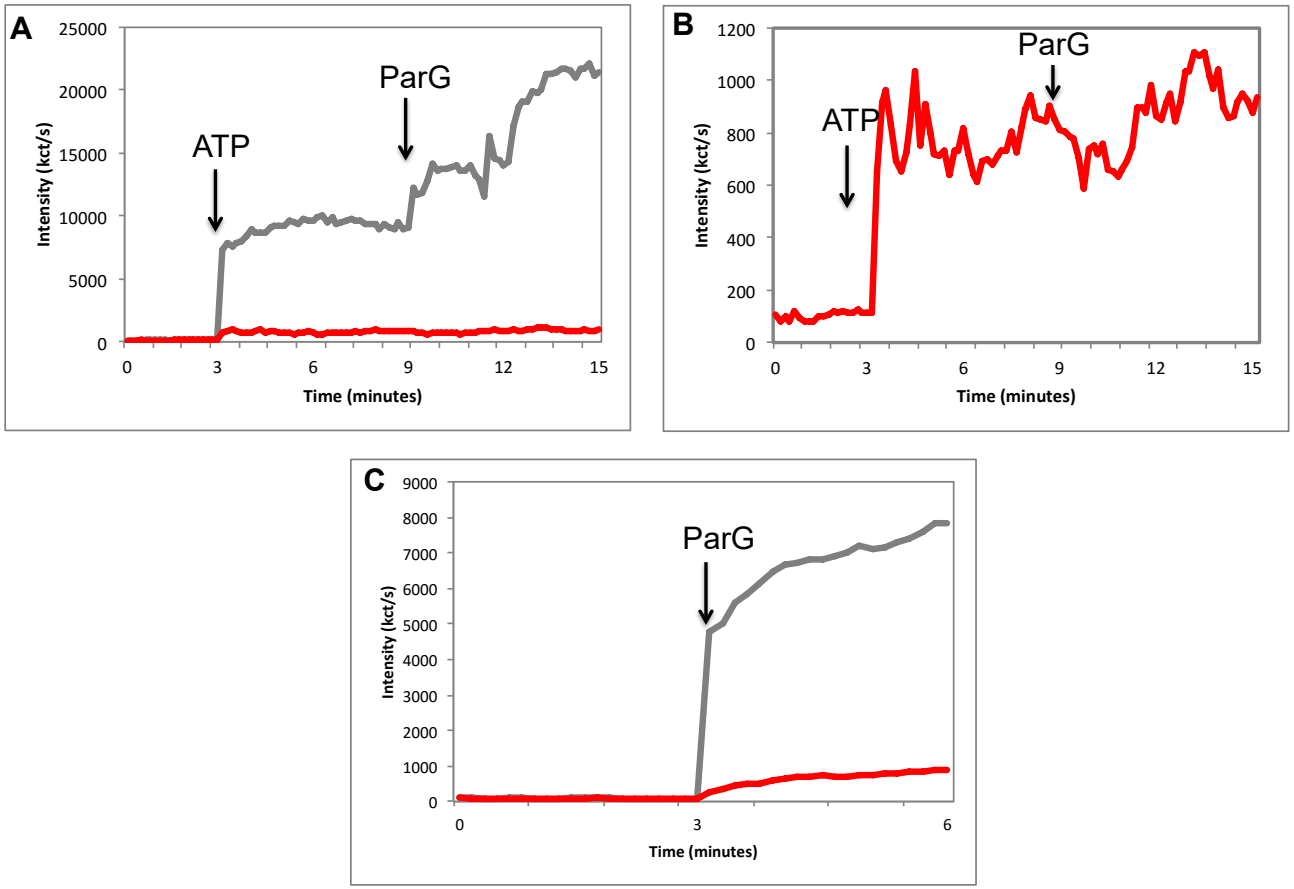

Figure 4.18 - DLS of ParF-S108A in the presence of ParG. DLS experiment was carried out and the increase in light scattering intensity (kct/s) was recorded for ParF and ParF-S108A. ParF and ParF-S108A were added at a final concentration of 2.16 µM and a baseline was obtained for three minutes and then if ATP was added (500 µM) with $MgCl_2$ (5 mM), it is indicated by a black arrow. The light scattering intensity was then recorded for a further six minutes before ParG was added at a final concentration of 2.16 µM, indicated by a black arrow, and the intensity recorded for a further six minutes. ParF is shown in grey and ParF-S108A is shown in red. A) The effect of both ATP and ParG on the assembly of ParF-S108A into higher order structures. B) The effect of both ATP and ParG on the assembly of ParF-S108A into higher order structures, only ParF-S108A (red) is shown on a smaller scale to indicate more clearly any changes in intensity of light scattering. C) The effect of ParG only on the assembly of ParF-S108A into higher order structure. This is a representative experiment. Each experiment was repeated at least in triplicate.

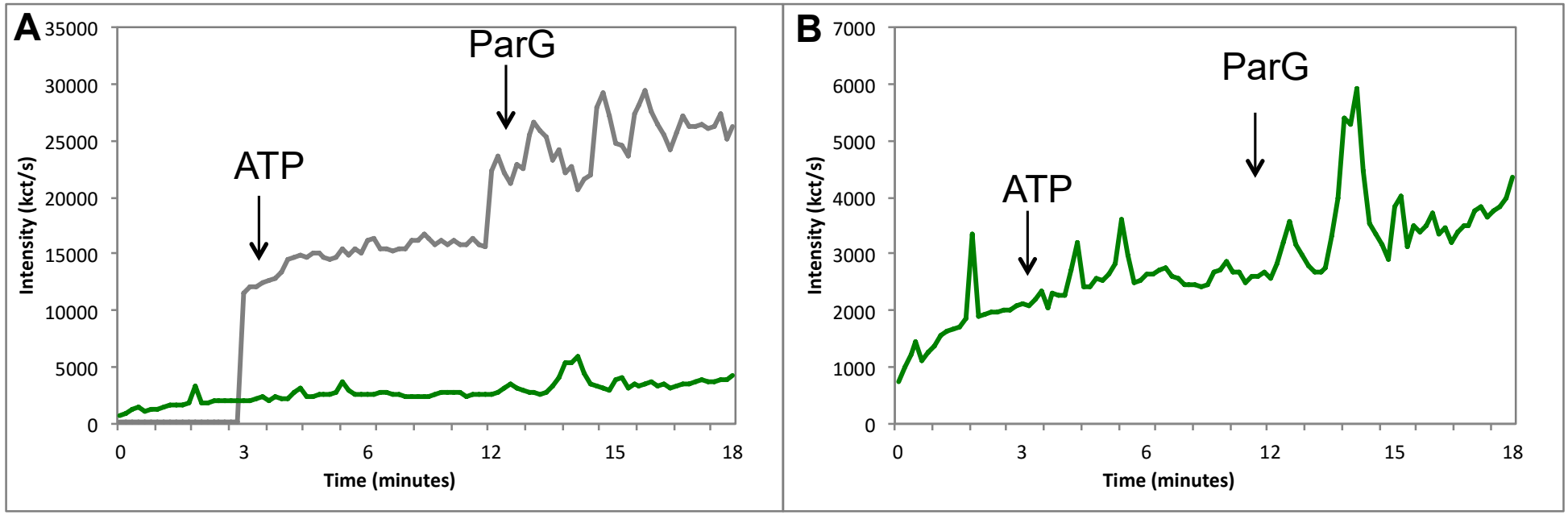

Figure 4.19 - DLS of ParF-P109R in the presence of ParG. DLS experiments were carried out and the increase in light scattering intensity (kct/s) was recorded for ParF and ParF-P109R. ParF and ParF-P109R were added at a final concentration of 2.16 μM and a baseline was obtained for three minutes and ATP was added (500 μM) with $MgCl_2$ (5 mM). The point of addition is indicated by a black arrow. The light scattering intensity was then recorded for a further six minutes before ParG was added at a final concentration of 2.16 μM, as indicated by a black arrow, and the intensity recorded for a further six minutes. ParF is shown in grey and ParF-P109R is shown in green. A) The effect of both ATP and ParG on the assembly of ParF-P109R into higher order structures. B) The effect of both ATP and ParG on the assembly of ParF-P109R into higher order structures, only ParF-P109R (green) is shown on a smaller scale to indicate more clearly any changes in intensity of light scattering. Experiments were carried out at least in triplicate and shown above is a representative experiment.

In order to confirm findings from DLS and also to allow a more quantitative approach to be taken, sedimentation assays were carried out. In the sedimentation assays ParF, ParF-P107A, ParF-S108A and ParF-P109R (10 μM) were incubated in the absence or presence of nucleotides (2 mM) and $MgCl_2$ (5 mM). The reactions were incubated at 30˚C for 10 minutes and centrifuged at 4˚C, 11,000 xg for 30 minutes in order to separate the pellet and the supernatant. Protein levels in the supernatant and pellet were analysed by SDS-PAGE and stained using His-tag gel stain or Coomassie blue. Sedimentation assays also demonstrated that ParF-P107A, ParF-S108A and ParF-P109R have a greater tendency to self-associate as shown by the increased proportion of the mutant proteins detected in the pellet compared to that of the wild type. Upon addition of any nucleotide, the amount of ParF-P107A and ParF-S108A detected in the pellet is reduced indicating the addition of nucleotides solubilises the proteins and thus antagonises the ability to form higher order structures (Figure 4.20). This is especially evident for ParF-S108A, as in the absence of nucleotides the amount of protein found in the pellet fraction is almost double that of ParF (53% for ParF-S108A compared to 28% for ParF). When ADP, ATP or ATP-γ-S nucleotide was added, the amount in of ParF-S108A in the pellet is reduced drastically and over 90% of the protein is found in the supernatant fraction (Figure 4.20A) clearly indicating the addition of nucleotide solubilises the protein. For ParF-P109R almost all (~80%) of the protein is detected in the pellet in the absence of nucleotide. Upon addition of any nucleotide the amount of ParF-P109R detected in the pellet is reduced slightly, however a significant amount of ParF-P109R still remains in the pellet (Figure 4.20B). These results support those observed in the DLS experiments.

Sedimentation assays were also carried out with the addition of ParG, only for ParF-S108A and ParF-P109R in order to support the findings from DLS experiments and to confirm the disruption of the ParF-S108A-ParG interaction and ParF-P109R-ParG interaction (Figure 4.21). In this sedimentation assay ParG was added to ParF or ParF-S108A/P109R in the presence and absence of ATP. In the absence of ATP, ParG slightly promotes ParF assembly into higher order structures. However in the presence of ATP, ParG causes almost all of ParF to be detected in the pellet thus indicating the ParG significantly increases the assembly of ParF into higher order structures (Figure 4.21). However, both in the presence and absence of ATP, ParG only caused a slight increase in the amount of ParF-S108A detected in the pellet and had little effect on the amount of ParF-P109R detected in the pellet. The amount of ParG detected in the pellet

fraction is also calculated in these experiments, as a control ParG only and ParG + ATP were analysed (gel not shown) and < 5% of ParG was detected in the pellet. The amount of ParG found in the pellet is shown to significantly increase when ParF is also in the sample, therefore confirming the interaction between ParF and ParG, which enables ParG to promote the assembly of ParF into higher order structures. The amount of ParG detected in the pellet when ParF-S108A or ParF-P109R is present is significantly lower (Figure 4.21), providing further evidence that the interaction between ParF-S108A and ParF-P109R with ParG is disrupted and that ParG is unable to stimulate the assembly of ParF-S108A or ParF-P109R into higher order structures as for the wild type ParF.

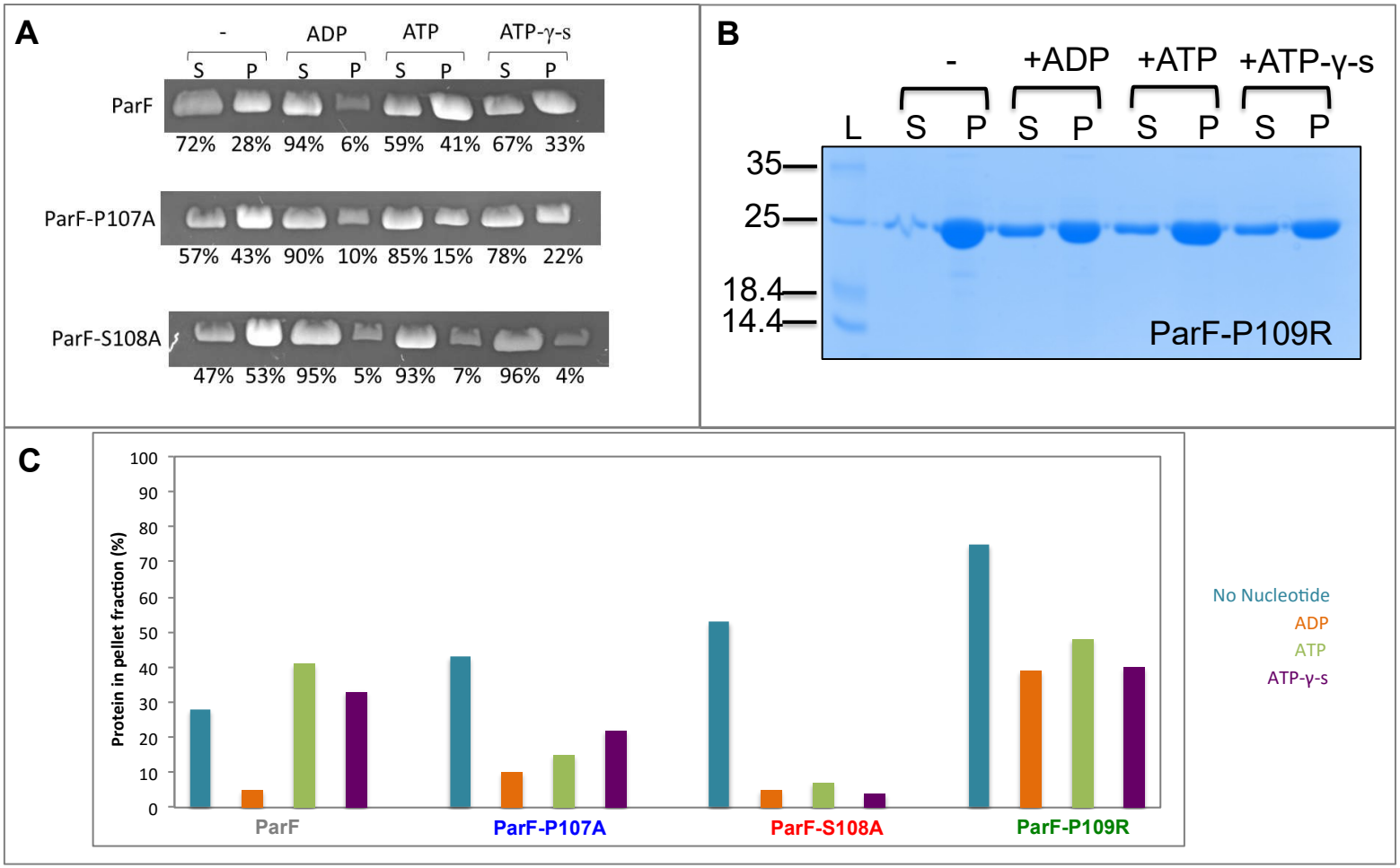

Figure 4.20 - Sedimentation assays of ParF-P107A, ParF-S108A and ParF-P109R in the absence and presence of nucleotide. ParF, ParF-P107A, ParF-S108A and ParF-P109R (10 µM) were incubated with and without nucleotide and separated on a 15 % SDS gel. 100% of pellet (P) and 33% of supernatant (S) fractions were resolved on gels. A) Representative gel of sedimentation assay of ParF, ParF-P107A and ParF-S108. Assays were repeated in triplicate. The percentage of the proteins found in the pellet and supernatant shown under each respective band. B) Representative gel of sedimentation assay of ParF-P109R. Assays were repeated in triplicate. C) Graph showing the percentage of the proteins found in the pellet.

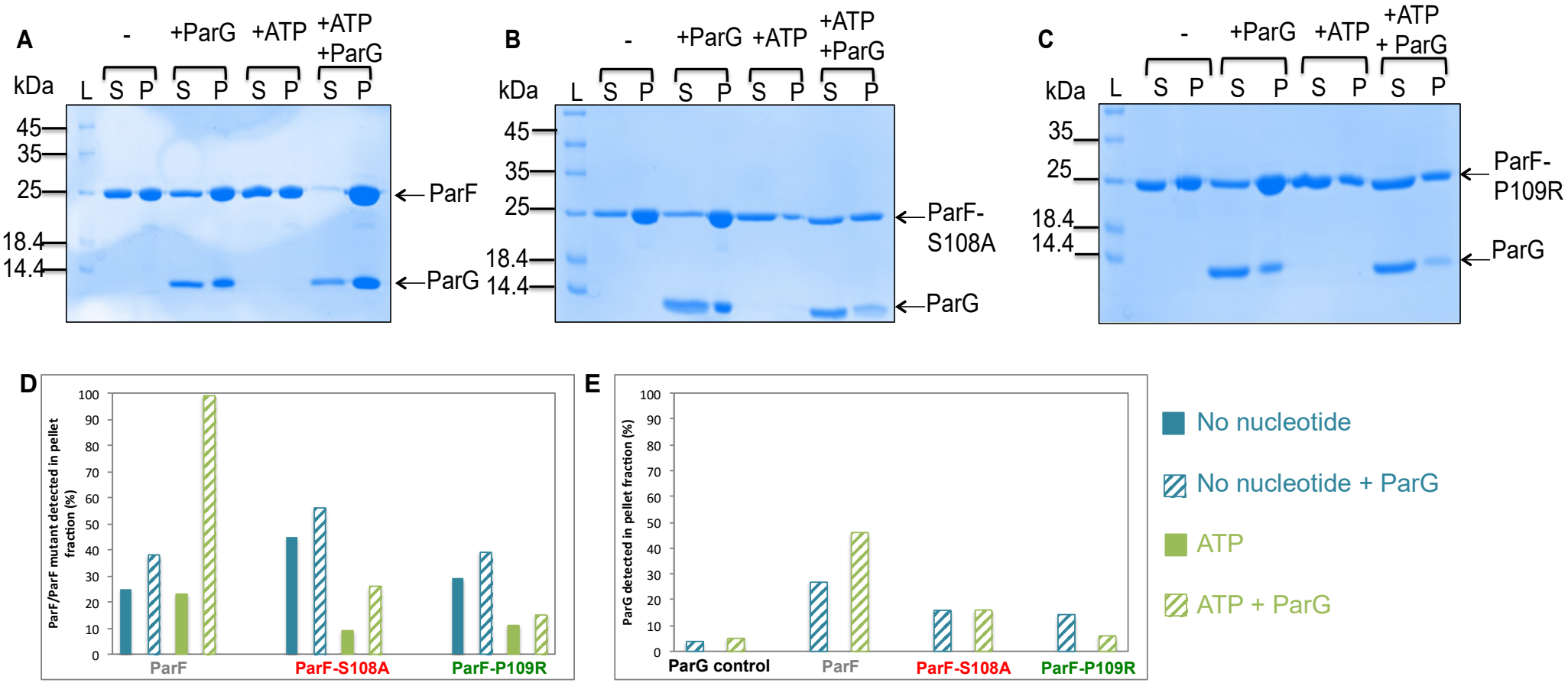

Figure 4.21 - Sedimentation assays of ParF-S108A and ParF-P109R in the presence of ParG. ParF, ParF-S108A and ParF-P109R (10 µM) were incubated with and without ATP and ParG and separated on a 15 % SDS gel. 100% of pellet (P) and 33% of supernatant (S) fractions were resolved on gels. Assays were repeated in triplicate. A) Representative gel of sedimentation assay of ParF with ParG. B) Representative gel of sedimentation assay of ParF-S108A with ParG. C) Representative gel of sedimentation assay of ParF-P109R with ParG. D) Graph to show the percentage of the ParF, ParF-S108A and ParF-P109R found in the pellet when incubated with ATP and ParG. E) Graph showing the percentage of ParG found in the pellet from the same sedimentation assay. A ParG only control is shown on this graph.

4.3.2.6 ParF-S108A and ParF-P109R form filament structures in the absence of nucleotide

Negative stain electron microscopy has been used to visualise the ultrastructures of ParF filaments (Barilla *et al*., 2005). Samples for electron microscopy were prepared in parallel with DLS experiments; protein and nucleotide concentrations were the same. This allowed results from the DLS experiments to be confirmed and also comparisons between results seen for the DLS and the appearance of the higher order structures observed using electron microscopy. In the absence of ATP ParF can be seen as small globular dots due to the tendency of ParF to self-associate. Upon addition of ATP ParF appears to form filament structures ranging in length from ~100 to 500 nm (Figure 4.22 A and 4.22B). In the absence of ATP both ParF-S108A and ParF-P109R appeared to form large filament structures, often bigger than those observed for ParF in the presence of ATP. The filament structures of the ParF-S108A and ParF-P109R were thick extensive filaments that appeared to form bundles (Figure 4.22C an 4.22E). However in the case of ParF-S018A in the presence of ATP, these extensive filament structures were not observed, instead small needle-like structures were detected (Figure 4.22D). These results support the observations of the DLS and sedimentation assay: ParF-S108A has a higher tendency to self-associates into higher order structures in the absence of nucleotide. However upon addition of ATP (or any nucleotide) this behaviour is inhibited and the protein becomes more soluble. On the other hand, in the presence of ATP, ParF-P109R still appeared to form filament structures (Figure 4.22F). This again supported the results observed in the DLS and sedimentation assays. The differences between the filament structures of ParF compared to those of ParF-S108A and ParF-P109R, in the presence and absence of ATP, are clear and it is becoming evident that disrupting the monomer-monomer interface of ParF impacts on the ability of the protein to assemble into higher order structures.

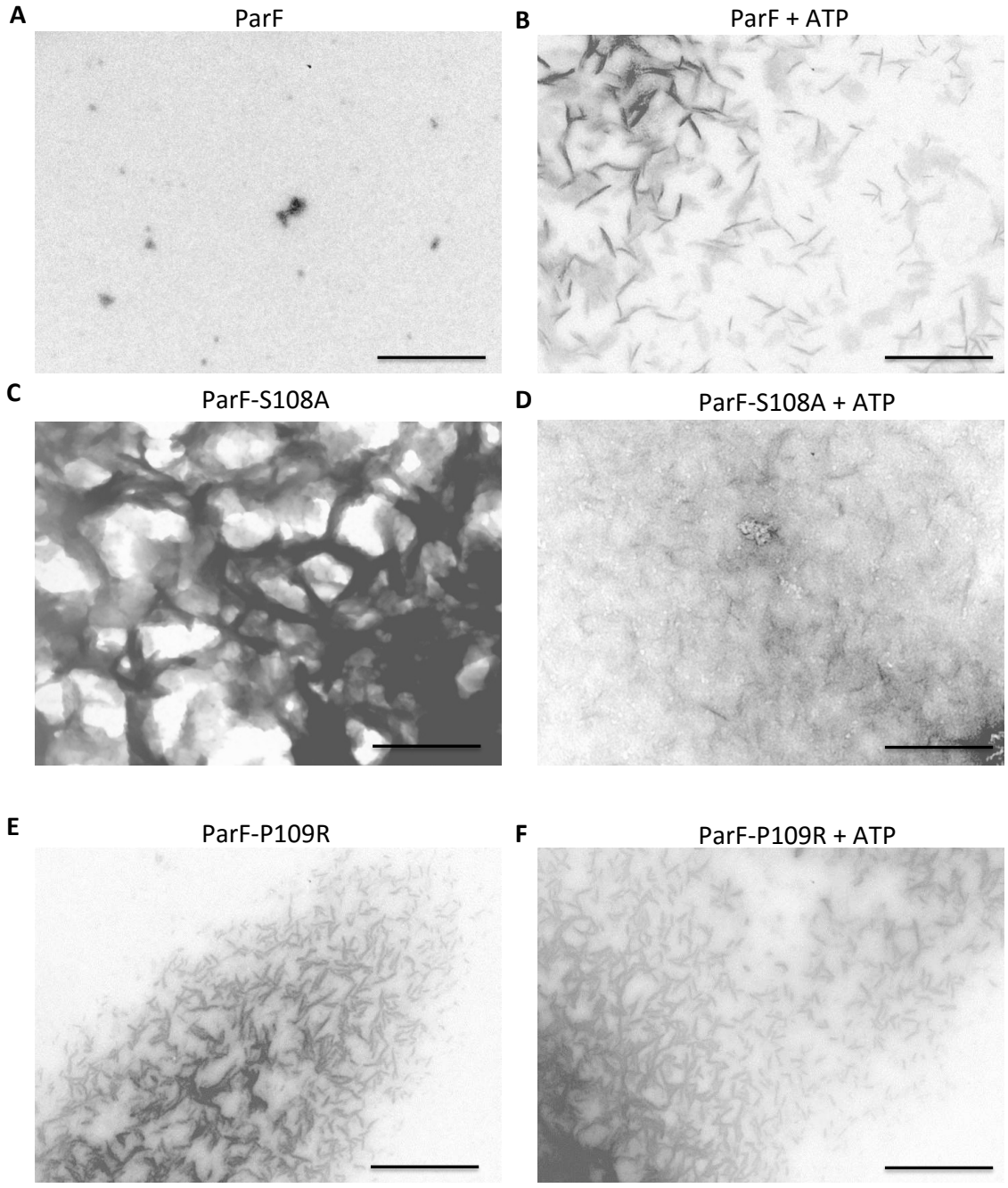

Figure 4.22 – EM ultrastructures of ParF-S018A and ParF-P109R in the absence and presence of nucleotide. Ultrastructures of ParF, ParF-S108A and ParF-P109R observed by negative stain electron microscopy. Aliquots of ParF, ParF-S108A or ParF-P109R (2.16 μM) are visualised. A) ParF structures. Scale bare = 500 nm. B) ParF structures in the presence of ATP. Scale bar 500 nm. C) ParF-S108A structures. Scale bar = 500 nm. D) ParF-S108A structures in the presence of ATP. Scale bar = 500 nm. E) ParF-P109R structures. Scale bar = 500 nm. D) ParF-P109R structures in the presence of ATP. Scale bar = 500 nm.

4.3.3 ParF-S108A is homogenously distributed over the nucleoid *in vivo* and is unable to oscillate over the nucleoid

As previously discussed many other members of the ParA superfamily have been shown to display dynamic behaviour over the nucleoid. It has been observed that ParF shows an oscillatory behaviour and is able to form a dynamic pattern on the nucleoid (McLeod et al., 2016) and Chapter 3 of this work). Mutant *parF* alleles can be cloned into two plasmids, pBM20 and pBM40, in order to investigate the *in vivo* localisation. Details of the plasmids used for microscopy and cloning mutant *parF* alleles have been described in Chapter 3. In order to visualise ParF, ParF-S108A and ParG, the appropriate pBM20 and pBM40 plasmids were co-transformed into BW25113 *E. coli* cells and grown for four hours in the presence of antibiotics. The cells are grown in the presence or L-arabinose for three hours in order to induce expression of *parF-emerald*. The nucleoid was visualised during the microscopy using DAPI.

The effect of the S108A change on ParF localisation and dynamics were investigated by acquiring confocal microscopy images, z-stacks and time-lapse videos. Cells harbouring the plasmids containing the partition cassettes with the *parF-S108A* allele (pBM20-ParF-S108A) and the plasmid expressing ParF-S108A-Emerald (pBM40-ParF-S108A) were grown and imaged exactly as the wild type (detailed in Chapter 3). ParF-S108A-Emerald is not asymmetrically distributed over the nucleoid like the wild type protein, but in fact it is spread homogenously over the nucleoid (Figure 4.23). ParG forms, in most cases, a single focus which is often positioned at midcell or the extreme pole of the cell (Figure 4.24 and 4.25). This single focus appeared more compact than foci observed in cells containing the wild type cassette. ParF-S108A is not seen to localise with ParG, which is predicted to be due to the weaker interaction observed *in vitro* for ParF-S108A-ParG. In the presence of the wild type partition casette and ParF-Emerald, ParG is observed to form 1-4 foci per cell. Often these foci are distinct, but not compact and appear slightly diffuse. The majority of the cells contain one or two ParG foci. If the cell contains one focus, it is generally positioned at midcell, whereas if two foci are present they are often positioned at one quarter and three quarter positions (Figure 4.26). This positioning of two foci is likely to be just before segregation, therefore the plasmids will be accurately inherited from one generation to the next. It was observed that 89% of the cells containing ParF-S108A-Emerald had a single ParG focus. This percentage is significantly higher than that observed in cells containing wild

type ParF, as only 40% of these cells contain a single ParG focus (Figure 4.26 and 4.27).

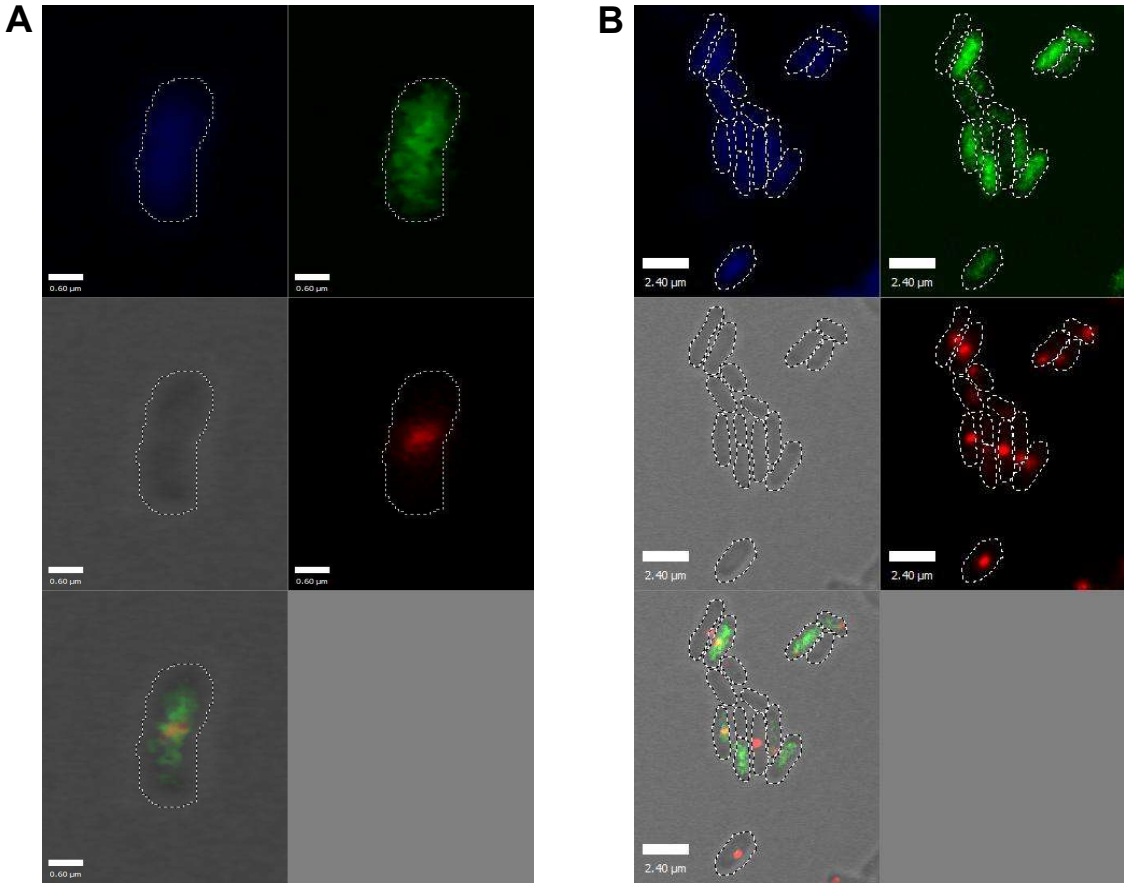

Figure 4.23 – Localisation of ParF-S108A and ParG. Images of *E. coli* cells acquired with the confocal microscope A) BW25113 *E. coli* cell harbouring a plasmid carrying the partition cassette *parF-S108AparG-mCherry-parH* (pBM20-ParF-S108A) and a plasmid expressing *parF-S108A-emerald* from the P_{BAD} promoter (pBM40-ParF-S108A). Top left - individual channel for DAPI, top right – individual channel for ParF-S108A-Emerald, middle left – bright field image, middle right – individual channel for ParG-mCherry, bottom left – merged image. Scale bar = 0.6 µm. B) Multiple BW25113 *E. coli* cells harbouring a plasmid carrying the partition cassette *parF-S108A-parG-mCherry-parH* (pBM20ParF—S108A) and a plasmid expressing *parF-S108A -emerald* from the P_{BAD} promoter (pBM40-ParF-S108A). Top left - individual channel for DAPI, top right – individual channel for ParF-S108A-Emerald, middle left – bright field image, middle right – individual channel for ParG-mCherry, bottom left – merged image. Scale bar = 2.40 µm.

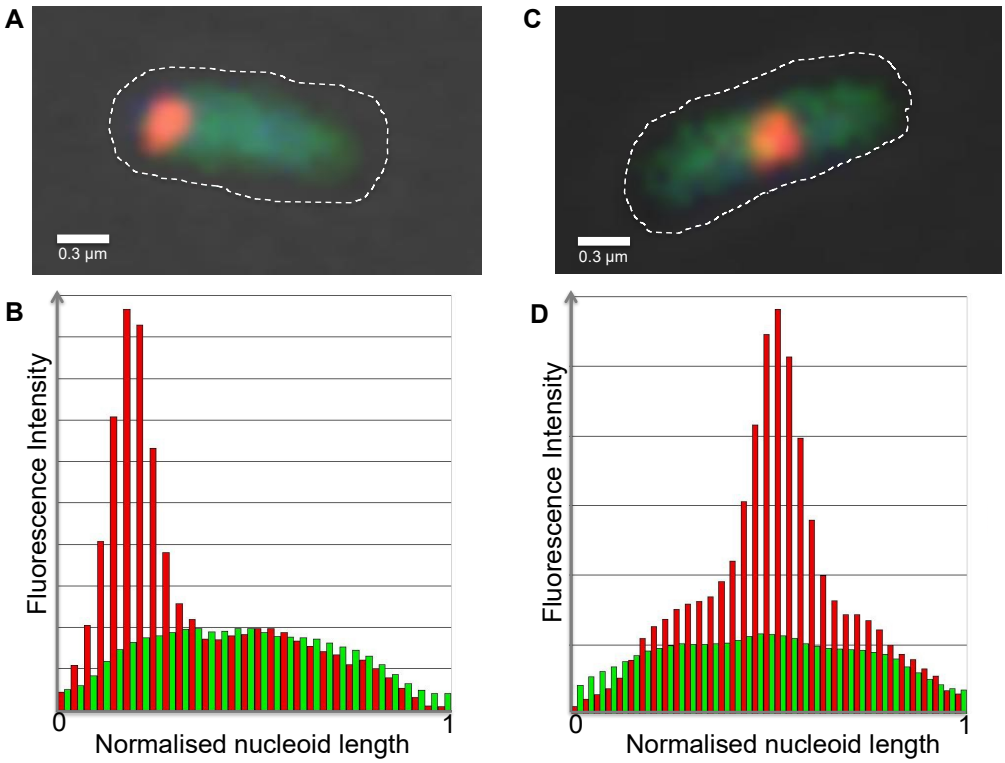

Figure 4.24 – Localisation patterns of ParF-S108A and ParG. Images of *E. coli* cells acquired with the confocal microscope. BW25113 *E. coli* cell harbouring a plasmid carrying the partition cassette *parF-S108AparG-mCherry-parH* (pBM20-ParF-S108A) and a plasmid expressing *parF-S108A-emerald* from the P_{BAD} promoter (pBM40-ParF-S108A). A) A merged image with ParG focus positioned at the pole. Scale bar = 0.3 µm. B) Fluorescence intensity plot of the cell shown in (A) indicating the position of ParG-mCherry (red) signal and the spread of the ParF-S108A-Emerald (green) signal. C) A merged image with ParG focus positioned at midcell. Scale bar = 0.3 µm. D) Fluorescence intensity plot of the cell shown in (C) showing the position of ParG-mCherry (red) signal and the spread of the ParF-S108A-Emerald (green) signal.

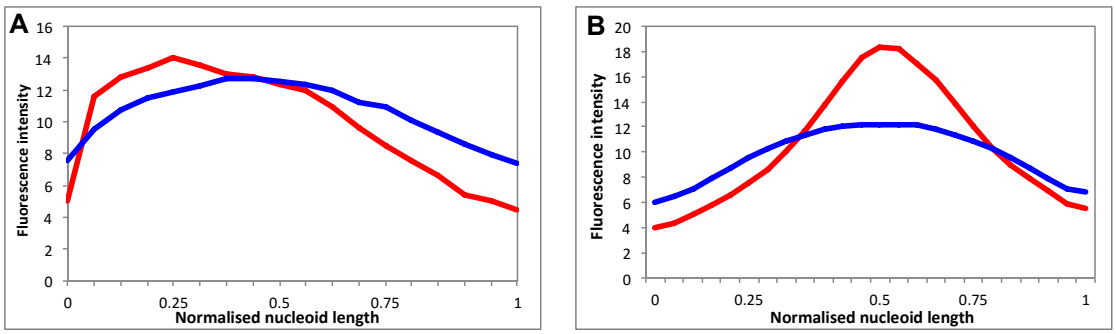

Figure 4.25 - Statistical analysis of ParG position when ParF-S108A is present. Quantitative analysis of ParG-mCherry localisation in *E. coli* cells harbouring a plasmid carrying the partition cassette *parF-S108A-parG-mCherry-parH* (pBM20-ParF-S108A) and a plasmid expressing *parF-S108A-emerald* from the P_{BAD} promoter (pBM40-ParF-S108A). A) Average position of ParG-mCherry focus when localised at the pole (n = 75 cells). ParG-mCherry signal is shown in red and the nucleoid-DAPI in blue. B) Average position of ParG-mCherry focus when positioned at midcell (n = 102 cells). ParG-mCherry signal is shown in red and nucleoid-DAPI in blue.

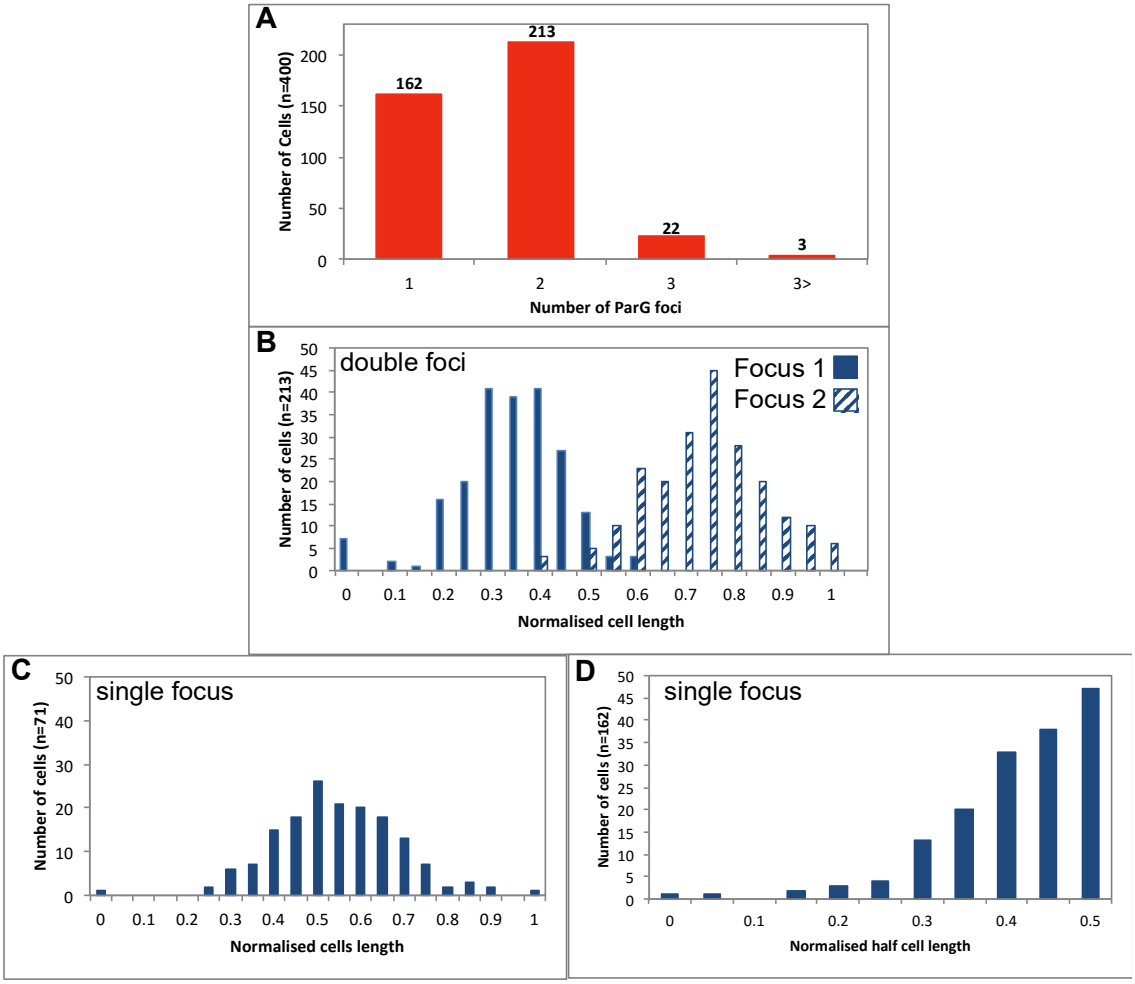

Figure 4.26 - Statistical analysis of ParG foci number and position when ParF is present. Quantitative analysis of ParG-mCherry localisation in *E. coli* cell harbouring a plasmid carrying the partition cassette *parF-parG-mCherry-parH* (pBM20-ParF) and a plasmid expressing *parF-emerald* from the P_{BAD} promoter (pBM40-ParF). A) Number of ParG-mCherry foci per cell (n = 400 cells). B) Position of double foci displayed as a function of the normalised cell length. C) Position of a single focus displayed as a function of the normalised cell length. D) Position of a single focus displayed as a function of the normalised half cell length.

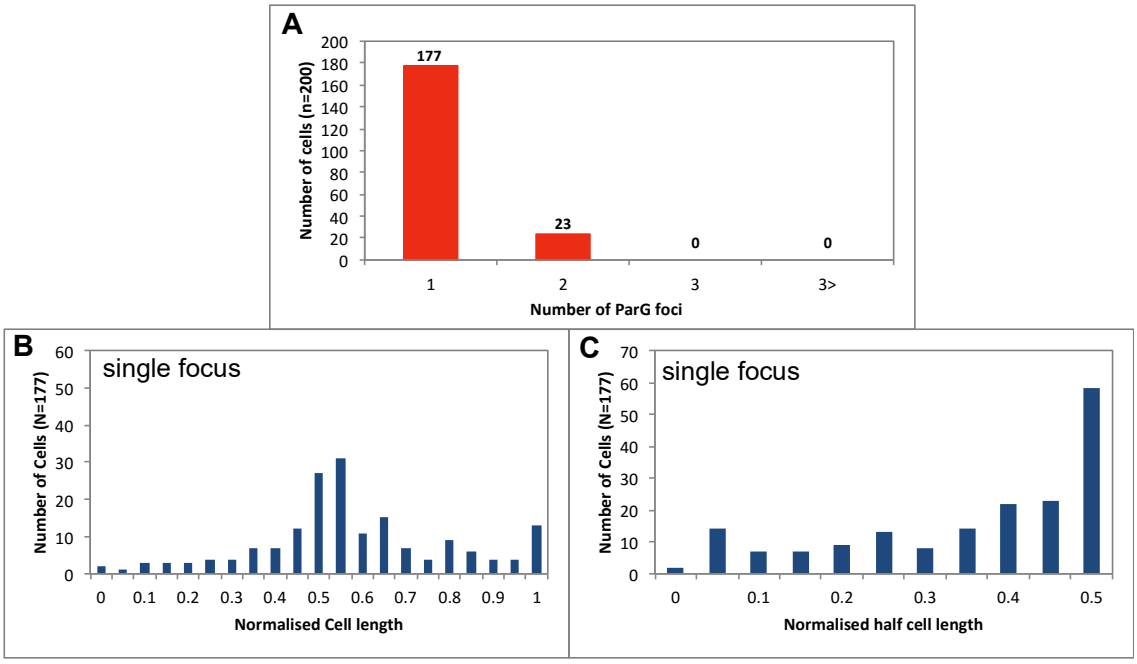

Figure 4.27 - Statistical analysis of ParG foci number and position when ParF-S108A is present. Quantitative analysis of ParG-mCherry localisation in *E. coli* cells harbouring a plasmid carrying the partition cassette *parF-S108A-parG-mCherry-parH* (pBM20-ParF-S108A) and a plasmid expressing *parF-S108A-emerald* from the P_{BAD} promoter (pBM40-ParF-S108A). A) Number of ParG-mCherry foci per cell (n = 200 cells). B) Position of a single focus displayed as a function of the normalised cell length. C) Position of a single focus displayed as a function of the normalised half cell length.

Z-stacks revealed, that like the wild type protein, ParF-S108A is spread throughout the nucleoid volume (Figure 4.28). In addition, when a twenty minute time-lapse experiment was carried out no oscillation was seen for either ParF-S108A-Emerald or ParG (Figure 4.29). The green signal remained spread throughout the nucleoid and the compact red signal remained in the same position for the entire twenty minutes. ParF oscillation and asymmetric patterning is likely due to the cycling of binding ATP, forming higher order filament structures followed by stimulation of ATPase activity by ParG. McLeod *et al*. has shown that ParF does not oscillate in the absence of *parH*, ParG or both. Also when a ParG mutant that is unable to stimulate ParF ATPase activity replaces the wild type ParG, wild type ParF cannot oscillate. ParF-S108A has been shown to be deficient in ATP-dependent stimulation of assembly into higher order structures and the mutants' interaction with ParG is disrupted. Therefore, it is likely that ParF-S108A is homogenously spread throughout the nucleoid and is unable to oscillate due to the fact that the mutant is unable to undergo cycling of assembly and disassembly of higher order polymeric structures because of (1) the disruption at the monomer-monomer interface that causes a conformational change in the protein and (2) ParF-S108A ATPase activity is unable to be stimulated by ParG.

When ParF-S108A is present, in most of the cells ParG forms a compact focus at midcell. It has been observed that ParG foci co-localise with the plasmid carrying the *parFGH* cassette (McLeod et al., 2016)and therefore it can be postulated that the same may occur in cells containing plasmids harbouring *parF* mutants. This would suggest that when S108 is mutated to alanine, in most cases, the plasmid becomes stuck at midcell and ParF-S108A is not able to oscillate to position the plasmid correctly. The fact that the ParG focus is mostly present at midcell or at the pole suggests that the plasmid-ParG complex is excluded from the nucleoid. This is likely because ParF-S108A does not interact with ParG and thus does not recruit the plasmid to the nucleoid region. The focus at midcell is likely to be between separated nucleoids. This would explain the disruption in plasmid segregation.

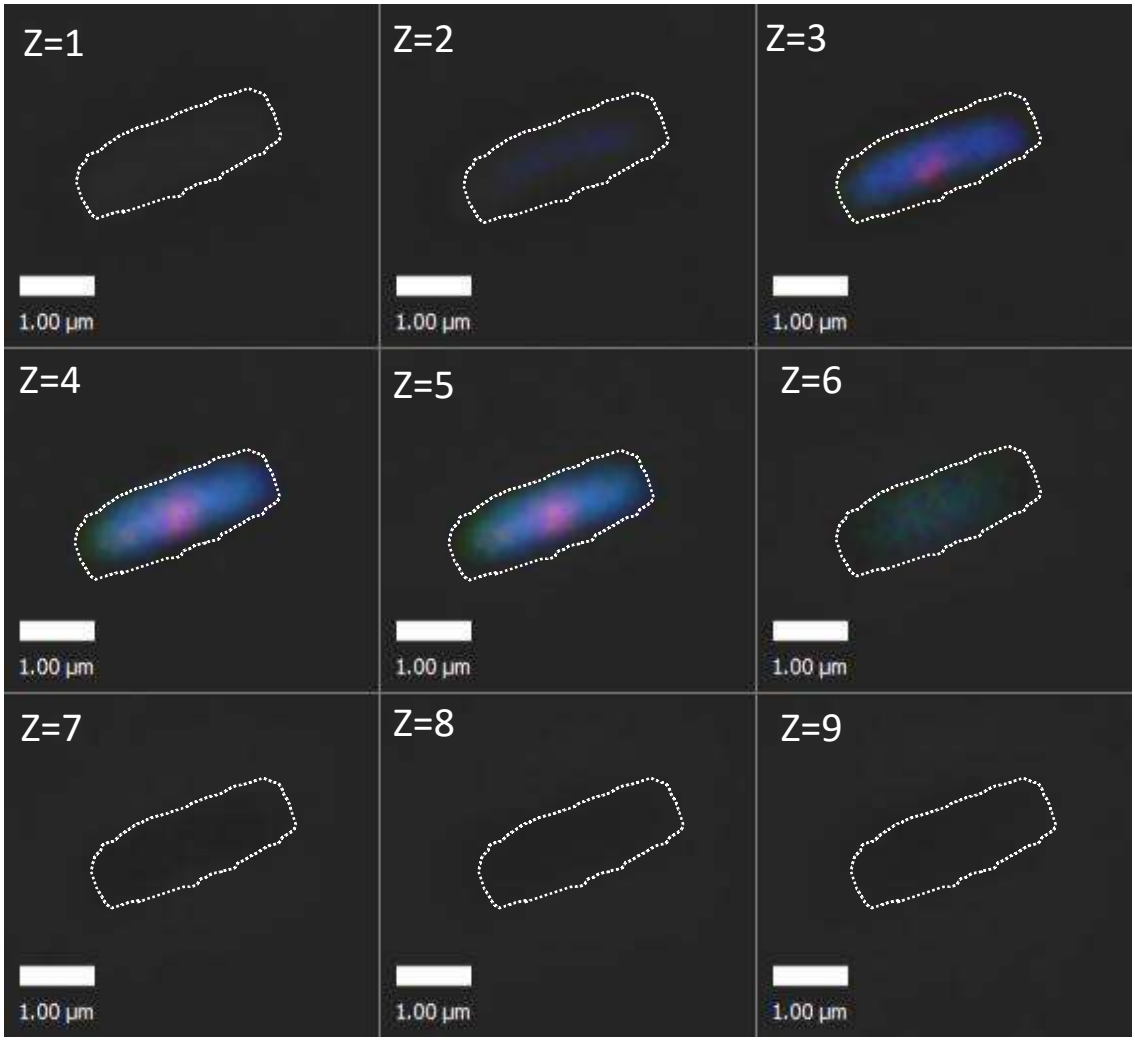

Figure 4.28 – Z stack images of ParF-S108A and ParG. Images of *E. coli* cells acquired with the confocal microscope. Nine z-stacks are taken at intervals of 190 nm. The merged images shown are cells harbouring the plasmid carrying the *parF-S108A-parG-mCherry-parH* cassette and a plasmid expressing *parF-S108A-emerald* from the P_{BAD} promoter. The nucleoid is stained with DAPI. Scale bar = 1.00 µm.

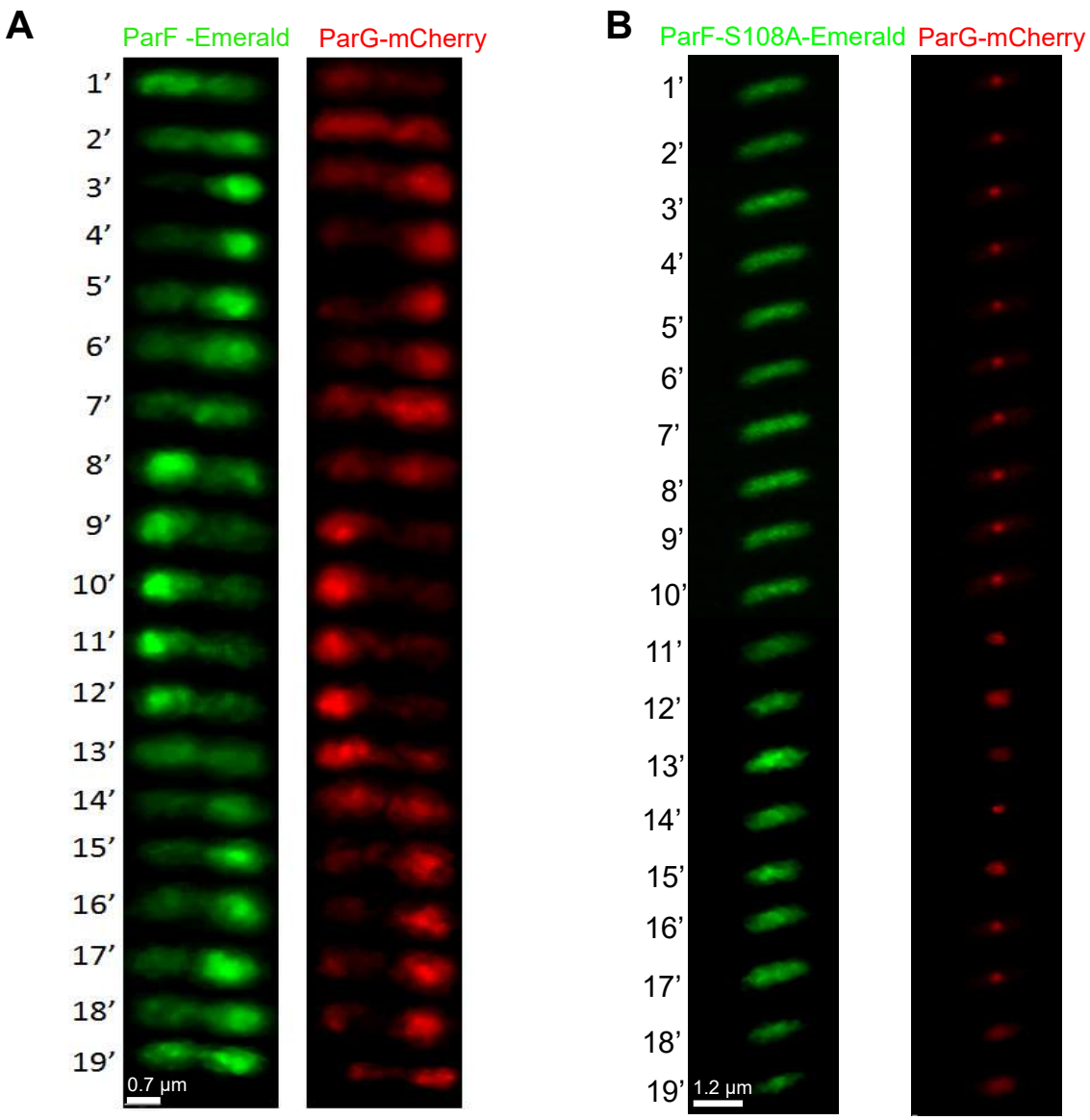

Figure 4.29 – Individual time images of ParF, ParF-S108A and ParG localisation over a twenty minute time lapse experiment. A) A representative twenty minute time-lapse experiment of a cell harbouring the plasmid carrying the *parFG-mCherry-parH* cassette and a plasmid expressing *parF-emerald* from the P_{BAD} promoter. ParF-Emerald is shown in the left column and ParG-mCherry shown in the right column. Scale bar = 0.7 µm. B) A representative twenty minute time-lapse experiment of a cell harbouring the plasmid carrying the *parF-S108AparG-mCherry-parH* cassette and a plasmid expressing *parF-S108A-emerald* from the P_{BAD} promoter. ParF-S108A-Emerald is shown in the left column and ParG-mCherry shown in the right column. Scale bar = 1.2 µm.

4.3.4 ParF-P109R forms many different patterns *in vivo* and is unable to oscillate

ParF-P109R was visualised *in vivo* exactly as discussed above for ParF-S108A. ParF-P109R did not form an asymmetric pattern on the nucleoid as seen for the wild type ParF. Interestingly, not a single defined pattern could be observed, but in fact many heterogeneous patterns of ParF-P109R were detected (Figure 4.30 and 4.31). In some cells ParF-P109R-Emerald was observed to spread throughout the nucleoid and in others distinct foci were clearly visible. Many of the cells had a compact single ParG focus mostly positioned at midcell, although cells with two compact foci were seen. Interestingly though, in some cells ParG was spread over the nucleoid and no foci were visible (Figure 4.32 and 4.33). In the presence of the wild type partition casette and ParF-Emerald, ParG forms foci that are discrete, but appear diffused slightly. The majority of the cells contain one or two ParG foci. When the cell contains one focus it is generally positioned at midcell, whereas if two foci are present, they are often positioned at one quarter and three quarter positions. While the percentage of cells containing one ParG focus when ParF-P109R is present is higher than that in the wild type background, the position of a single ParG focus and two ParG foci are similar to those observed in the wild type context (Figure 4.34). Surprisingly, in some cases ParF-P109R and ParG foci also appeared to overlap which is interesting as all the biochemical work has demonstrated that ParF-P109R has a weaker interaction with ParG. In 42 % of the cells analysed the number of ParF-P109R and ParG foci are the same. 50% of the cells that contain one ParF-P109R and one ParG focus show an overlay of the green and red signal, whereas 80 % of cells that contain two ParF-P109R and ParG foci show overlay of the signals. Analysis of the distribution of ParF-P109R and ParG revealed that there isn't a single pattern that occurs significantly more often than another.

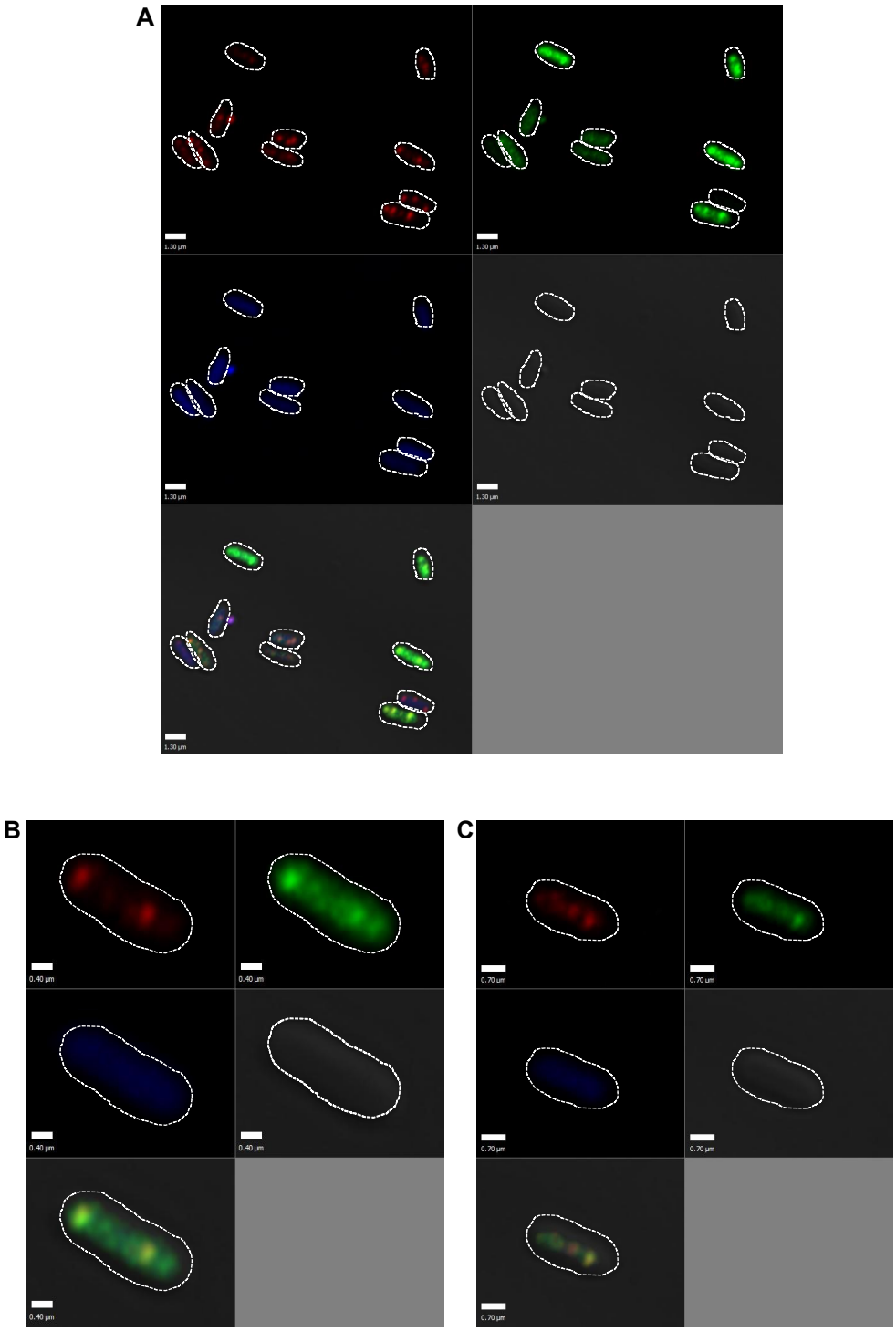

Figure 4.30 – Localisation of ParF-P109R and ParG. Images of *E. coli* cells acquired with the confocal microscope A) Multiple BW25113 *E. coli* cells harbouring a plasmid carrying the partition cassette *parF-P109R-parG-mCherry-parH* (pBM20-ParF-P109R) and a plasmid expressing *parF-P109R-emerald* from the P_{BAD} promoter (pBM40-ParF-P109R). Top left - individual channel for ParG-mCherry, top right – individual channel for ParF-P109R-Emerald, middle left – individual channel for DAPI, middle right – bright field image, bottom left – merged image. Scale bar = 1.3 µm. B) BW25113 *E. coli* cell harbouring plasmid carrying the partition cassette *parF-P109R-parG-mCherry-parH* (pBM20-ParF-P109R) and a plasmid expressing *parF-P109R-emerald* from the P_{BAD} promoter (pBM40-ParF-P109R). Top left - individual channel for ParG-mCherry, top right – individual channel for ParF-P109R-Emerald, middle left – individual channel for DAPI, middle right – bright field image, bottom left – merged image. Scale bar = 0.4 µm. C) Same as (B) Scale bar = 0.7 µm.

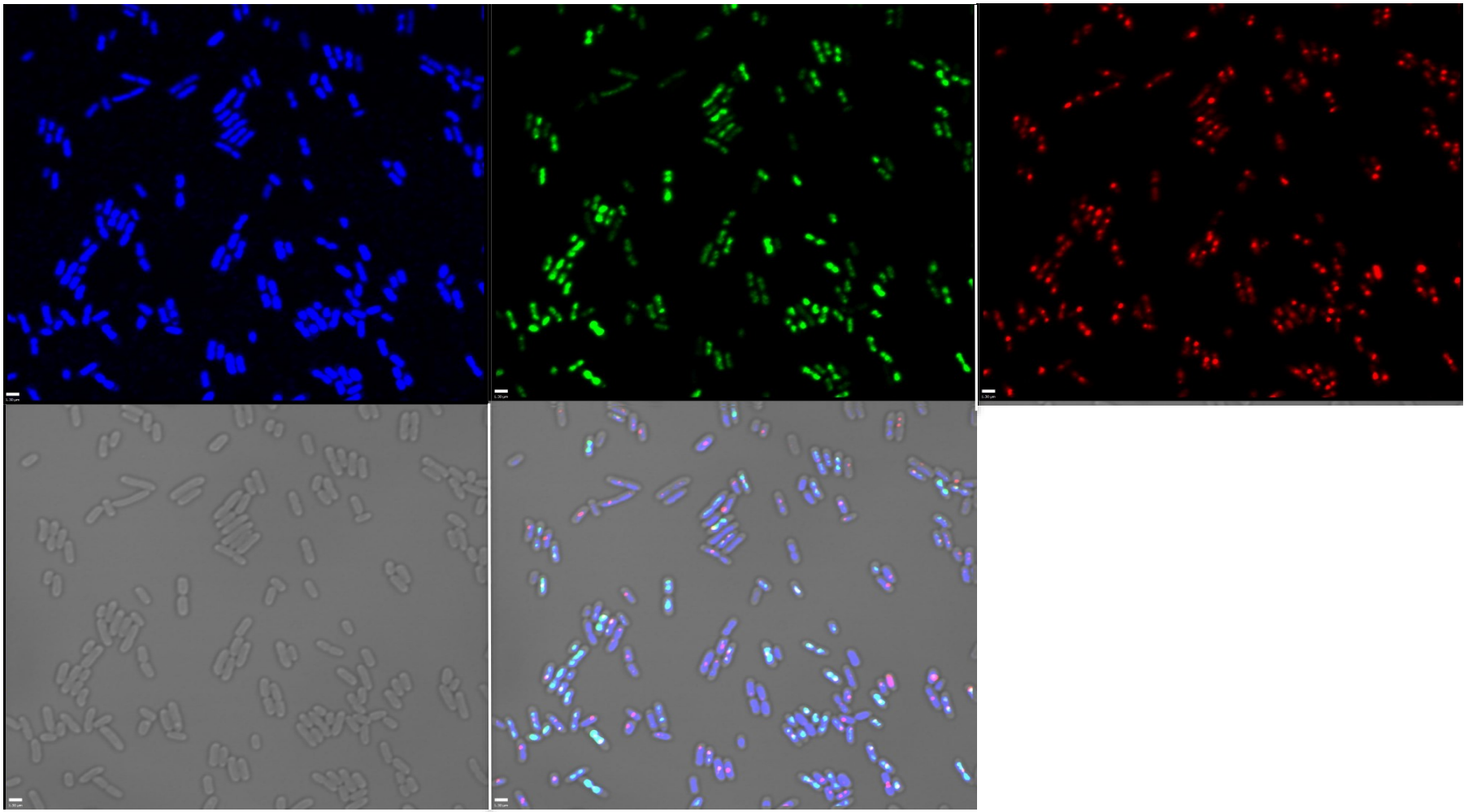

Figure 4.31- Multiple cells showing the different *in vivo* localisations patterns formed by ParF-P109R and ParG. Images of *E. coli* cells acquired with the confocal microscope. Multiple BW25113 *E. coli* cells harbouring a plasmid carrying the partition cassette *parF-P109R-parG-mCherry-parH* (pBM20-ParF-P109R) and a plasmid expressing *parF-P109R-emerald* from the P_{BAD} promoter (pBM40-ParF-P109R). Top left – individual channel for DAPI, top middle – individual channel for ParF-P109R-Emerald, top right – individual channel for ParG-mCherry, bottom left – bright field image, bottom middle – merged image. Scale bar = 1.3 µm. Examples of specific patterns are shown in Figure 4.32.

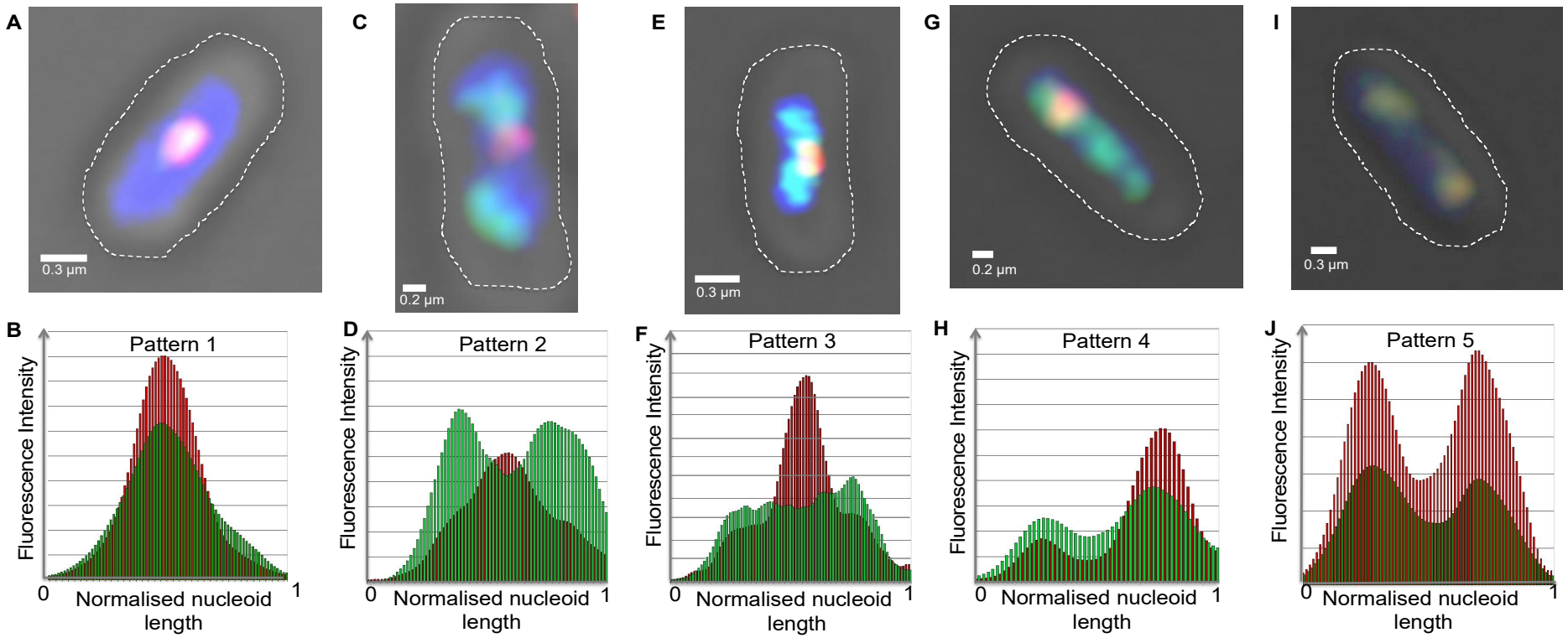

Figure 4.32 - Examples of ParF-P109R and ParG *in vivo* patterning. Images of *E. coli* cells acquired with the confocal microscope. BW25113 *E. coli* cells harbouring a plasmid carrying the partition cassette *parF-P109R-parG-mCherry-parH* (pBM20-ParF-P109R) and a plasmid expressing *parF-P109R-emerald* from the P_{BAD} promoter (pBM40-ParF-P109R). A) Merged-channel image of a cell with ParF-P109R and ParG focus positioned at midcell. Scale bar = 0.3 µm. B) Fluorescence intensity plot of the cell shown in (A) showing the position of ParG-mCherry (red) signal and the ParF-P109R-Emerald (green) signal. C) Merged-channel image of a cell with ParG focus positioned at midcell and two ParF-P109R foci positioned either side. Scale bar = 0.2 µm. D) Fluorescence intensity plot of the cell shown in (C) showing the position of ParG-mCherry (red) signal and of the ParF-P109R-Emerald (green) signal. E) Merged-channel image of a cell with ParG focus positioned at midcell and ParF-P109R spread. Scale bar = 0.3 µm. F) Fluorescence intensity plot of the cell shown in (E) showing the position of ParG-mCherry (red) signal and of the spread of the ParF-P109R-Emerald (green) signal. G) Merged image of a cell with ParG focus positioned at three quarter position and two ParF-P109R foci positioned at one quarter and three quarter positions. Scale bar = 0.2 µm. H) Fluorescence intensity plot of the cell shown in (G) showing the position of ParG-mCherry (red) signal and of the ParF-P109R-Emerald (green) signal. I) Merged-channel image of a cell with two ParF-P109R and two ParG foci positioned at one quarter and three quarter position. Scale bar = 0.3 µm. J) Fluorescence intensity plot of the cell shown in (I) showing the position of ParG-mCherry (red) signal and of the ParF-P109R-Emerald (green) signal.

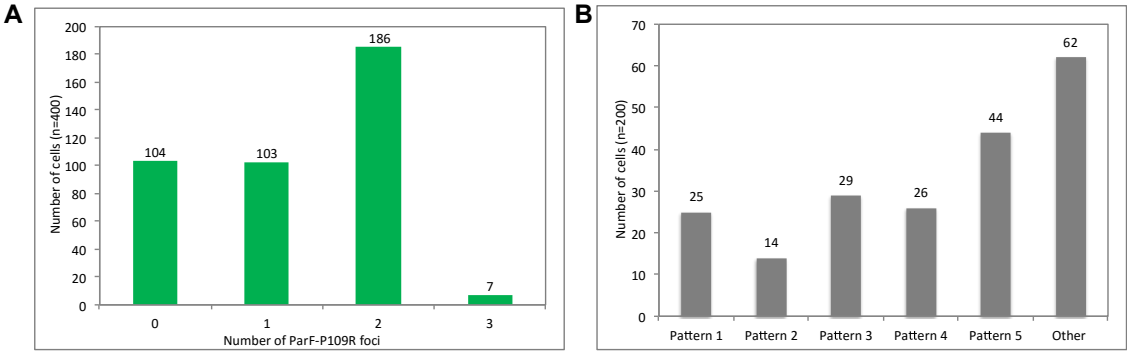

Figure 4.33 – Number of ParF-P109R foci and the pattern formed by the distinct foci in numerous cells. Quantitative analysis of ParG-mCherry and ParF-P109R-Emerald localisation from *E. coli* cell harbouring a plasmid carrying the partition cassette *parF-P109R-parG-mCherry-parH* (pBM20-ParF-P109R) and a plasmid expressing *parF-P109R-emerald* from the P_{BAD} promoter (pBM40-ParF-P109R). A) Number of ParF-P109R-Emerald foci per cell (n = 400 cells). B) Number of cells in which ParF-P109R and ParG form distinct patterns. The patterns are shown in Figure 4.32 (n = 200).

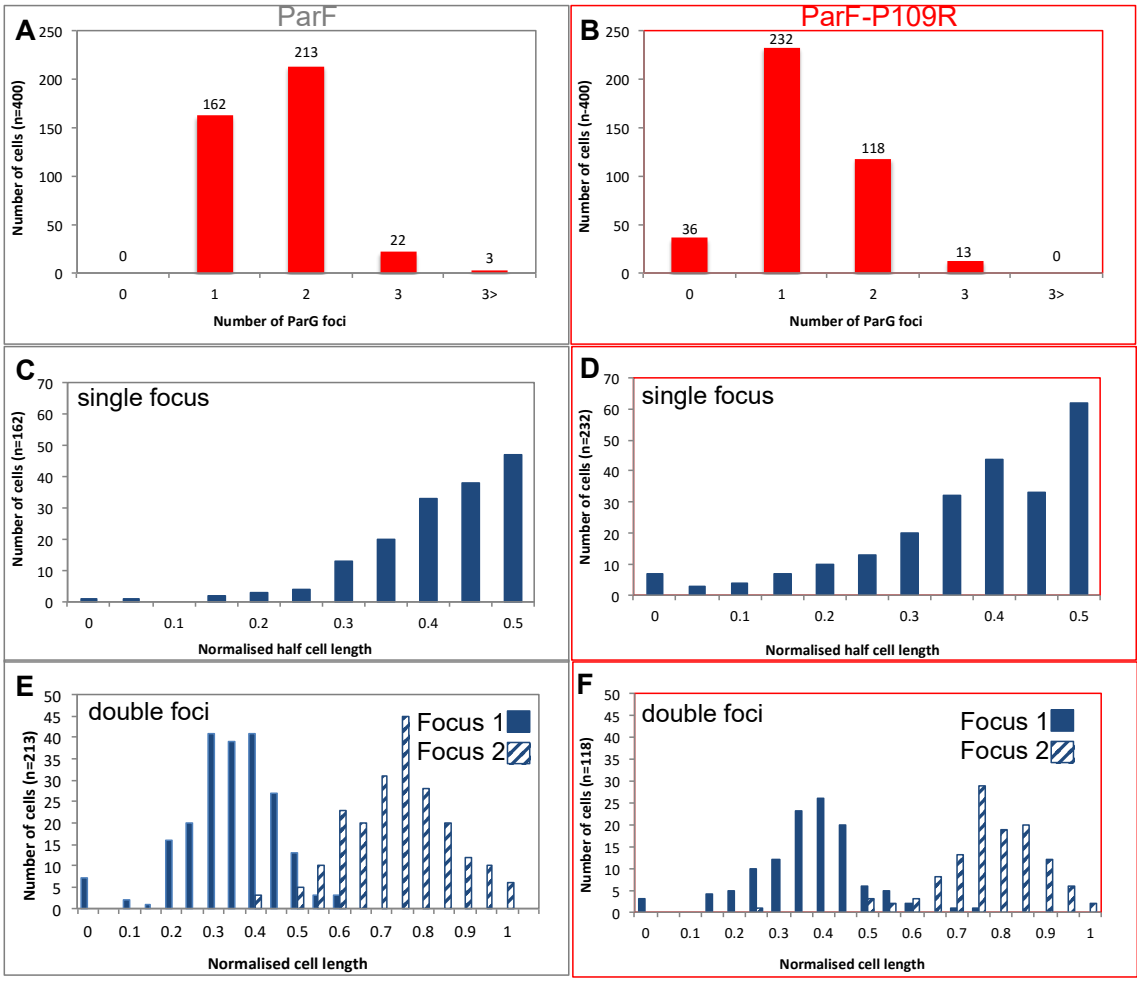

Figure 4.34 – Statistical analysis of the number of ParG foci and position in cells with a ParF and ParF-P109R background. Quantitative analysis of ParG-mCherry localisation in *E. coli* cell harbouring a plasmid carrying the partition cassette *parF-parG-mCherry-parH* (pBM20-ParF) and a plasmid expressing *parF- emerald* from the P_{BAD} promoter (pBM40-ParF) or a plasmid carrying the partition cassette *parF-P109R-parG-mCherry-parH* (pBM20-ParF-P109R) and a plasmid expressing *parF-P109R-emerald* from the P_{BAD} promoter (pBM40-ParF-P109R). A) Number of ParG-mCherry foci per cell (n = 400 cells) with wild type ParF. B) Number of ParG-mCherry foci per cell (n=400 cells) with ParF-P109R. C) Position of a single ParG-mCherry focus with wild type ParF present in the cell, displayed as a function of the normalised cell half length. D) Position of a single ParG-mCherry focus with ParF-P109R present in the cell, displayed as a function of the normalised cell half length. E) Position of two ParG-mCherry foci with wild type ParF present in the cell, displayed as a function of the normalised cell length. F) Position of two ParG-mCherry foci with ParF-P109R present in the cell, displayed as a function of the normalised cell length.

Z-stacks revealed that like the wild type protein ParF-P109R permeates the nucleoid volume in three dimensions (Figure 4.35). When a twenty minute time-lapse experiment was carried out, no oscillation was observed for either ParF-P109R-Emerald or ParG. The pattern of the green and the red signal remained identical throughout the twenty minutes and did not relocate (data not shown). ParF-P109R has been shown to be deficient in ATP-dependent assembly into higher order structures and the interaction with ParG is disrupted. Therefore, it is likely that ParF-P109R is unable to oscillate due to the fact that the mutant is unable to undergo cycling of assembly and disassembly of higher order structures because of (1) the disruption at the monomer-monomer interface that causes a conformational change in the protein and (2) ParF-P109R ATPase activity is not stimulated by ParG. The distribution of the ParF-P109R-Emerald signal is harder to rationalise due to the different patterns observed. *In vitro* the protein has a higher tendency to self-associate into higher order structures; therefore it is reasonable to propose that the same happens *in vivo*. Thus the fact that ParF-P109R is forming foci is likely to be due to the proteins forming higher order structures, within the spatial constraints of the nucleoid, that become localised and appear as foci. Super resolution microscopy may be able to support this hypothesis, as it would enable higher resolution images to be acquired. The fact that, in some cases, ParF-P109R foci and ParG foci overlap is unlikely to be due to an interaction between ParF-P109R and ParG, as *in vitro* data strongly suggest this interaction is significantly disrupted. In cells in which this pattern occurs, the ParF-P109R-Emerald signal can be observed as, but not restricted to, compact foci. Therefore it may just be that the red and green signals happen to co-localise and it is not a direct result of an interaction between ParF-P109R and ParG. It is challenging to speculate why, in the presence of ParF-P109R, ParG forms foci positioned in a similar way to when wild type ParF is present yet plasmid segregation is disrupted. As previously discussed in this chapter, it has been observed that ParG foci co-localise with the plasmid harbouring the *parFGH* partition cassette (McLeod et al., 2016). It should be possible to establish if the same colocalisation is observed when a partition cassette contains a *parF* mutant allele. This may offer an insight into the ParG foci position, when ParF-P109R is present in the cell, as it would allow the position of the plasmid to be established.

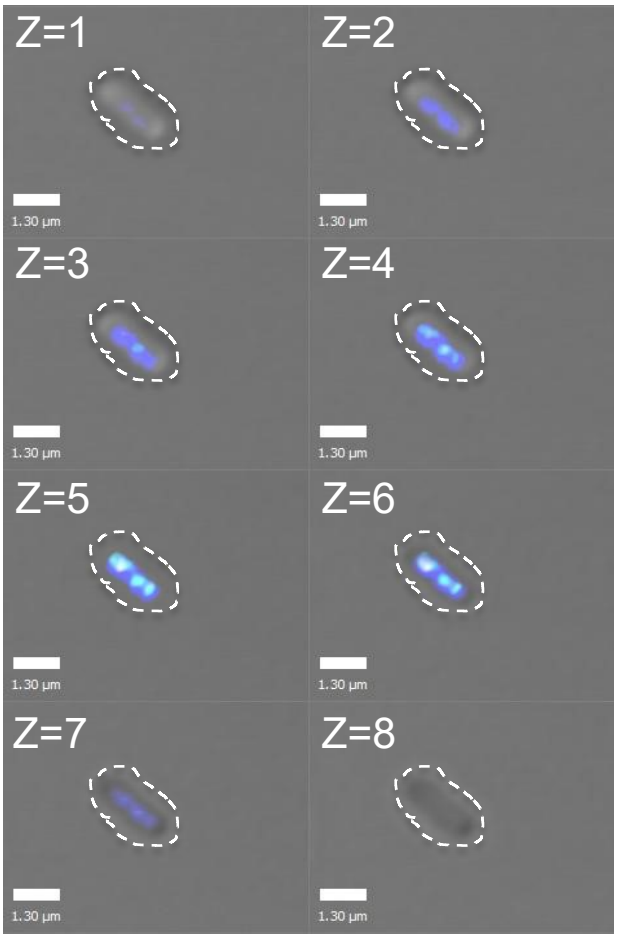

Figure 4.35 – Z stack images of ParF-P109R and ParG. Images of *E. coli* cells acquired with the confocal microscope. Eight z-stacks are taken at intervals of 190 nm. The merged images shown are cells harbouring the plasmid carrying the *parF-P109R-parG-mCherry-parH* cassette and a plasmid expressing *parF-P109R-emerald* from the P_{BAD} promoter. The nucleoid is stained with DAPI. Scale bar = 1.30 µm.

4.4 ParF-P107A, ParF-S108A and ParF-P109R conclusions

The aim of this part of the project was to disrupt the monomer-monomer interface of ParF, which would hopefully disrupt ParF dimer formation and offer an insight into the interfaces and specific residues involved in assembly of ParF into higher order structures. A proline-rich motif was identified by Schumacher *et al* (2012) and thought to be important in the cross-contacts of the monomers of ParF. It was postulated that the proline residues in this motif might act as a molecular switch for ParF assembly into higher order structures. The eleven residues of the proline-rich motif were individually mutated to alanine and characterised in terms of the effect the change had on plasmid retention. I102A, P104A and S108A were shown to have a significant effect on plasmid retention and P107A had a smaller effect (Figure 4.4). ParF-I102A could not be purified

as it was insoluble and ParF-P104A had already been characterised by Dobruk-Serkowska *et al* (2012). A number of residues were also identified by Schumacher *et al* (2012) that were thought to be important in the cross-contacts between the monomers of ParF, P109 being one of these residues. P109 was seen to insert into a hydrophobic pocket of the adjacent monomer formed by V173 and L177. As the converting P109 to alanine had little effect on plasmid retention, P109 was changed to arginine to try and disrupt this interaction. P109R had a significant effect on plasmid retention and therefore this study focused on ParF-P109R alongside ParF-P107A and ParF-S108A. Surprisingly, and in contrast to the original expectations, the changes in these amino acids did not prevent dimer formation, but in fact resulted in the opposite effect. Throughout this work it became evident that ParF-S108A and ParF-P109R had very distinctive phenotypes, although ParF-P107A did demonstrate some of the same *in vitro* characteristics as ParF-S108A and ParF-P109R. Table 4.1 summarises the similarities and difference observed for ParF-P107A, ParF-S108A and ParF-P109R. Bacterial two-hybrid assays demonstrated that ParF-S108A and ParF-P109R formed dimers and also that the self-interaction between these monomers were stronger than ParF monomer-monomer association (Figure 4.13). ParF-S108A showed a higher tendency to self-associate into higher order structures in the absence of nucleotide. The addition of nucleotides antagonised this feature (Figure 4.15). This is an interesting observation that was also shown for ParF-P104A (Dobruk-Serkowska *et al*., 2012). ParF-P109R also exhibited a higher tendency to self-associate into higher order structures but this was both in the absence and presence of nucleotides. Another significant observation was that both ParF-P109R and ParF-S108A displayed weaker interactions with ParG compared to that of ParF and ParG. These findings clearly demonstrate many similarities between ParF-S108A and ParF-P109R. It is likely that, due to the close proximity of the proline rich motif to the ATP binding pocket, the mutations may alter the conformation of the binding pocket and cause a conformational change that locks ParF in a configuration that favours self-association. It is possible the conversion of P109 to arginine has a more severe effect on the conformational change compared to the change of S108 to alanine due to the differences in the properties of the amino acids. Alanine is a reasonably small amino acid whereas arginine is not only a large amino acid but also positively charged and polar.

When ParF-S108A and ParF-P109R were visualised *in vivo* some differences could be observed. Fluorescence microscopy revealed ParF-S108A was homogenously spread

throughout the nucleoid and did not show any dynamic oscillatory behaviour. On the other hand, ParF-P109R formed many different patterns over the nucleoid, none of which resembled the pattern formed by wild type ParF, but not just restricted to a homogenous pattern like ParF-S108A. As for ParF-S108A, ParF-P109R did not show any dynamic oscillatory behaviour. The number and position of ParG foci were also different in cells with ParF-S108A and ParF-P109R. Even though the *in vivo* localisation does differ between ParF-S108A and ParF-P109R, the combination of assembling into higher order structures and the disruption of the interaction with ParG is likely to cause the partition deficient phenotype in both instances. The differences in the assembly into higher order structures are likely to be responsible for the differences in the patterning. *In vivo*, the presence of the nucleotides would inhibit the assembly of ParF-S108A into higher order structures and therefore the protein would appear homogenously spread over the nucleoid. This pattern is similar to that observed for ParF-K64A-V89Y-M96A, a ParF mutant harbouring changes at the dimer-dimer interface that is unable to assemble into higher order structures (Chapter 3). ParF-P109R on the other hand, in the presence of nucleotides *in vivo* will still assemble into higher order structures and therefore foci form in areas of high concentrations of ParF-P109R higher order structures. Wild type ParF forms patches due to the assembly into higher order structures, but in an ATP dependent manner. Therefore the difference in patterning of ParF and ParF-P109R and the lack of oscillation of ParF-P109R is due to the fact that that the dynamic assembly and disassembly of the ParF-P109R higher order structures is disrupted, due to the conformational change and the lack of stimulation of ATPase activity by ParG.

To conclude, the combination of assembling into higher order structures and the disruption of the interaction with ParG are likely to cause the partition deficient phenotype observed for both ParF-S108A and ParF-P109R. The fact that ParF-S108A and ParF-P109R do not interact with ParG prevent the recruitment of ParG bound plasmid to the nucleoid and leads to disruption of segregation of the plasmid, often due to the plasmid being excluded from the nucleoid at midcell or the pole of the nucleoid. ParF-S108A and ParF-P109R are clearly unable to assemble into the standard lattice observed for ParF in the cell, where ATP is present, but just bind diffusely to the nucleoid. More detailed investigations on the nature of the ParF-S108A and ParF-P109R structures on the nucleoid would need to be carried out in order to determine exactly how the lattice formed differs from that of the wild type protein. In conclusion,

these results indicate that the assembly of higher order structures plays an important role in plasmid partitioning, along side the interaction with ParG.

Table 4.1 - Summary of *in vitro* and *in vivo* characteristics of ParF-P107A, ParF-S108A and ParF-P109R in comparison to wild type ParF. If highlighted in red there is a significant difference observed between the ParF mutant and the wild type protein.

	ParF	ParF-P107A	ParF-S108A	ParF-P109R
Plasmid Retention	~70 %	~ 60 %	~ 8%	~ 7%
Binds ATP	Yes. K_d = 0.44 µM	Yes. K_d = 1.90 µM	Yes. K_d = 2.30 µM	Yes. K_d = 0.37 µM
Forms a dimer	Yes. MU = 1300	Yes. MU = 998	Yes. MU = 1377	Yes. MU = 2116
Interacts with ParG	Yes. MU= 839	Yes. MU = 1177	Yes. MU = 238	Yes. MU = 532
Intrinsic ATPase activity	Weak	-	Weak	Weak
ParG stimulates ATPase activity	Yes	-	No	No
Self –associates in the absence of nucleotide	Yes	Yes – higher tendency	Yes- higher tendency	Yes – significantly higher tendency
ATP dependent assembly into higher order structures	Yes	No – addition of nucleotide solubilises the protein	No– addition of nucleotide solubilises the protein	No – addition of nucleotide has no effect and the protein continues to self-associate
ParG promote assembly into higher order structures	Yes	Yes	No	No
ParF/ParF mutant cell localisation pattern	Asymmetrically distributed	-	Homogenously distributed	Different patterns
ParG cell localisation pattern	Distinct ParG foci can be identified within a dispersed signal		Compact focus mostly at midcell	Different patterns
Number of ParG foci	1-4	-	1	0-4
Protrudes into the nucleoid	Yes	-	Yes	Yes
Oscillates	Yes	-	No	No

4.5 The ParF – ParG interface

ParG interacts with ParF and both the C- and N-terminal regions of ParG have been shown to be important in the contacts with ParF (Barillà and Hayes, 2003, Barilla *et al*., 2007). This interaction between ParF and ParG is important for three reasons: 1) allows ParF to be recruited to the segrosome, 2) ParG stimulates the ATPase activity of ParF and 3) ParG promotes the assembly of ParF into higher order structures (Barilla *et al*., 2005, Barilla *et al*., 2007). The unstructured N-terminal tail of ParG contains an arginine finger-like motif, which is likely to be inserted into the ATP binding pocket of ParF to stimulate ATPase activity. The co-structure of ParF-ParG is yet to be solved, however some recent work has made progress towards solving this (Schumacher, M. – unpublished data). The preliminary structural data of ParF-ParG has revealed a potential interface, in which a patch of residues were identified (Figure 4.36). Four of these residues are position in the proline-rich motif. Two of these residues, S108 and P109, have already been shown in this work to have a weaker interaction with ParG than wild type ParF. L110 and F112 are the other two residues in this stretch that were thought to be potentially involved in the ParF – ParG interactions. Both these residues have been mutated to alanine and plasmids harbouring these changes have shown a significant reduction in plasmid retention (Caccamo and Hayes - unpublished data). V149 was the other residue identified, this was mutated to phenylalanine in order to try and disrupt the ParF-ParG interaction and characterised in terms of plasmid retention, which was significantly affected. Therefore bacterial two-hybrid assays have been employed to investigate whether the remaining residues, L110, F112 and V149 are also impaired in ParG interactions.

V149 was converted to phenylalanine and characterised in terms of the effect the change had on plasmid retention. The plasmid harbouring the *parF-V149F* mutation showed a plasmid retention of ~26% which is significantly lower than the plasmid harbouring the wild type partition cassette. The results of the partition assay for V149F, as well as the previously discussed residues S108A and P109R, are shown in Figure 4.37 As previously discussed the plasmids harbouring *parF-L110A* and *parF-F112A* showed a significant reduction in plasmid retention (<10%), close to that of the plasmid that doesn't contain a partition cassette (Caccamo and Hayes - unpublished data).

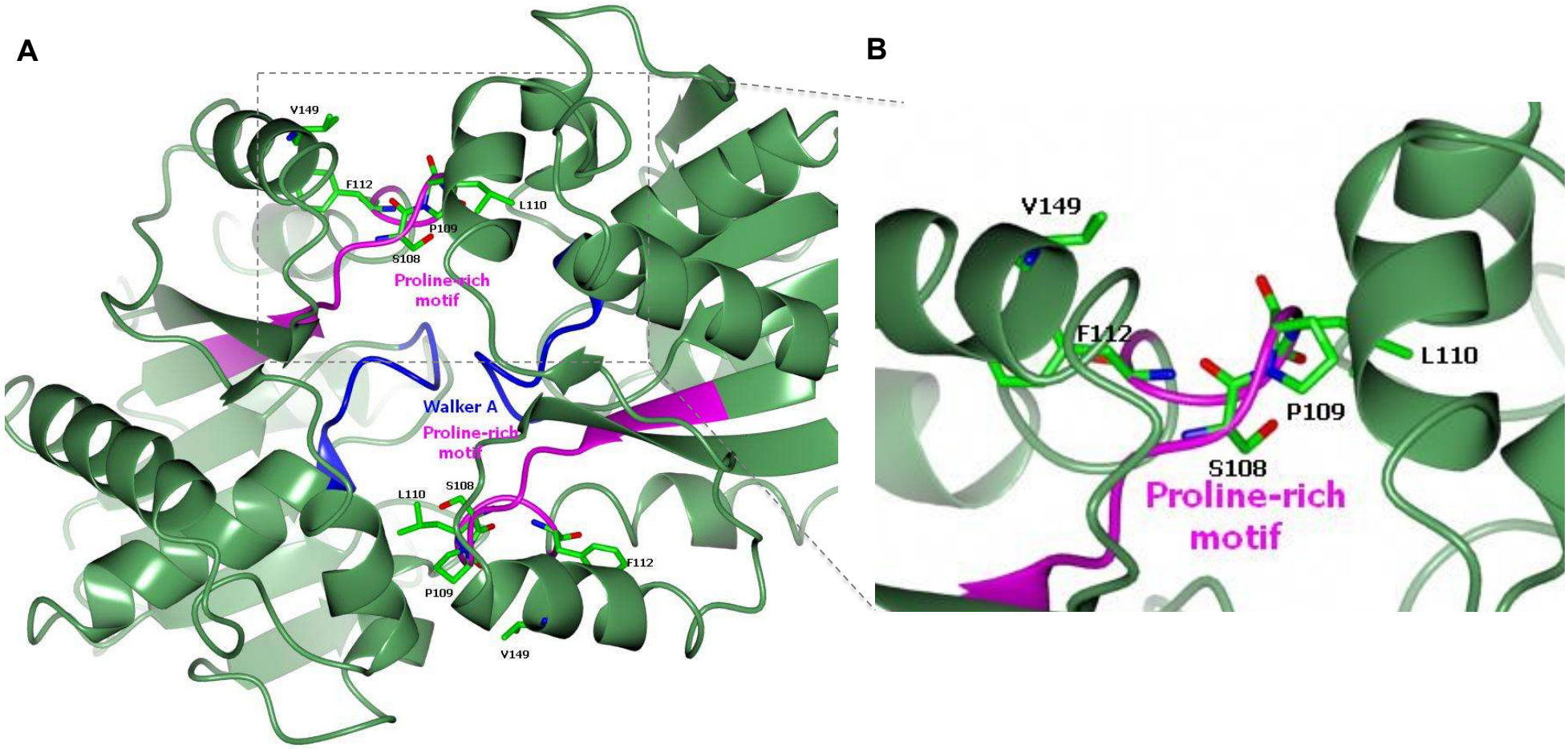

Figure 4.36 - ParF structure highlights residues potentially involved in the ParF-ParG interaction. A) Ribbon diagram of ParF dimer. The Walker A motif is highlighted in blue and the proline-rich motif is highlighted in magenta. Residues identified as potentially being involved in the ParF-ParG interaction shown as sticks. B) Zoomed image of the ribbon diagram of ParF dimer. The structural images were generated by using CCP4MG version 2.10.4 using the 4E07 PDB coordinates.

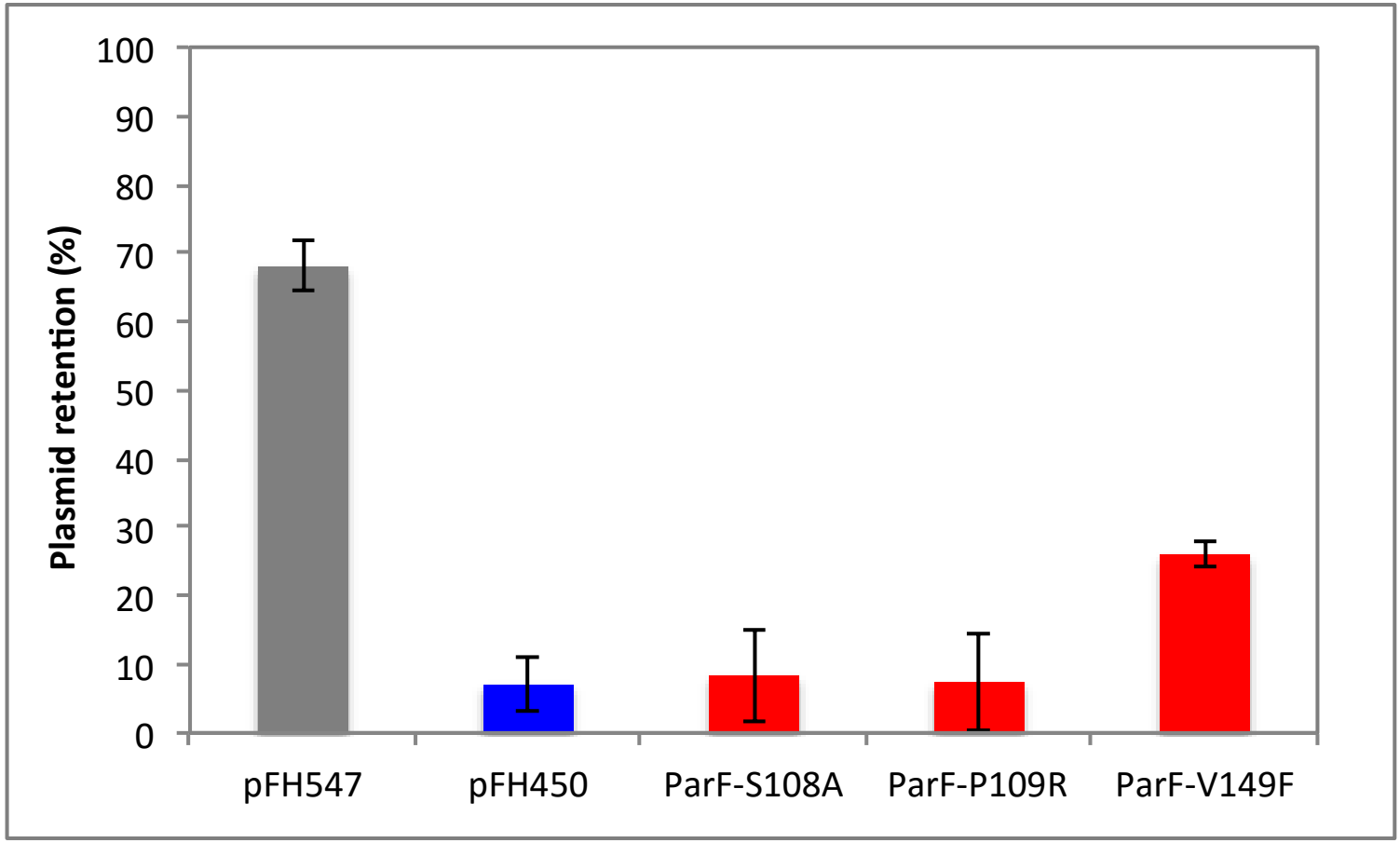

Figure 4.37 - Plasmid retention of plasmids harbouring mutations of residues potentially involved in ParF-ParG interactions. pFH547 plasmid contains the wild type *parFGH* partition cassette and pFH450 lack a partition cassette. Plasmid retention shown is calculated from an average of at least three assays with the standard deviation

4.5.1 The ParF-L110A – ParG interaction is disrupted

Bacterial two-hybrid assays were carried out as detailed in section 2.9 to investigate ParF-ParG interactions. β-galactosidase assays were then used to quantify these interactions. For the bacterial two-hybrid and β-galactosidase assays *parF-L110A, parF-F112A* and *parF-V149F* alleles were cloned into the pT25 plasmids as previously described. The desired plasmid pairs were co-transformed into SP850 *E. coli* competent cells as described in 2.3.10. The results showed that ParF-L110A has a weaker interaction with ParG, whereas ParF-F112A and ParF-V149F only show a slightly reduced interaction. ParF-L110A clearly exhibited a significantly weaker interaction with ParG compared to ParF-ParG (Figure 4.38). This is supported by both the bacterial two-hybrid assay plates and the β-galactosidase quantitation. pT18ParG+pT25ParF-L110A showed on average ~ 100 Miller units compared to ~ 1000 Miller units for pT18ParG+pT25ParF (Figure 4.38). This indicates the interaction of ParF-L110A with ParG is ~ 90% weaker than that of wild type ParF with ParG. In reality, the Miller units indicate little or no interaction between the two proteins as ~100 units are normally obtained for controls where the proteins that do not interact. The results for the interaction of ParF-F112A and ParF-V149F with ParG are less obvious. The colonies from the bacterial two-hybrid assays of both ParF-F112A-ParG and ParF-V149F-ParG appear a darkish red colour and it is hard to determine if there is a difference in the colour of the colonies compared to ParF-ParG. The β-galactosidase quantitations show that the interaction of ParG with ParF-F112A generates on average ~ 1500 Miller units. However, in this instance the average value of the experiments repeated in triplicate for the interaction of ParF and ParG was ~ 2500 units. Although this value is higher than the average value previously obtained, comparatively it does suggest that the interaction of ParF-F112A with ParG is ~ 40% weaker than that of ParF with ParG. In the β-galactosidase assays the interaction of ParF-V149F with ParG showed on average ~ 640 miller units compared to ~1300 for wild type proteins. This would suggest the ParF-F112A-ParG interaction is approximately half as strong as the association of ParF with ParG. Therefore for both ParF-F112A and ParF-V149F the bacterial two-hybrid solid plate colour does not clearly demonstrate a weaker interaction with ParG, however the β-galactosidase quantitations do show difference in the interaction compared to that of ParF-ParG. The results of all the β-galactosidase are shown in Figure 4.39, including those previously obtained for ParF-S108A-ParG and ParF-P109R-ParG. An average of each of the individual experiments average is plotted for ParF-ParG.

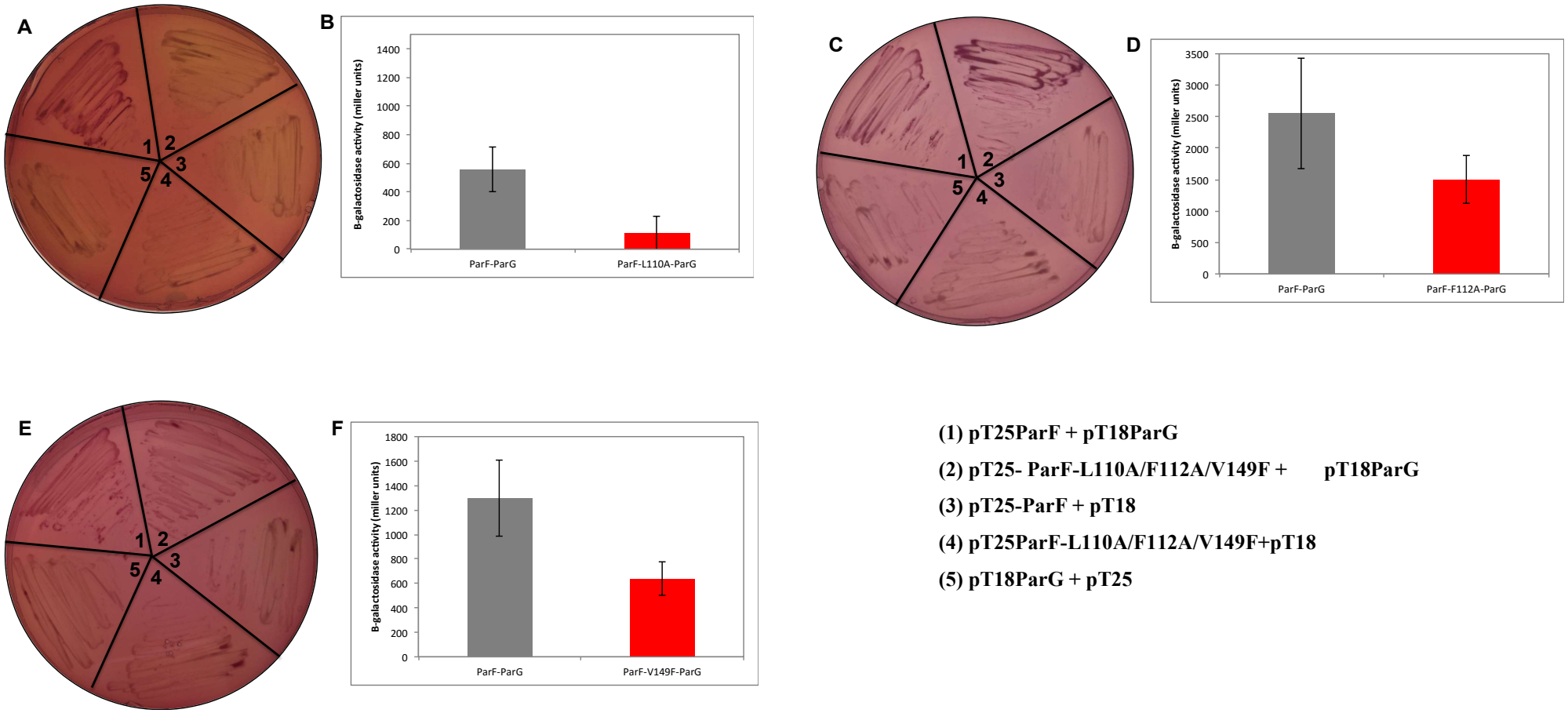

Figure 4.38 – Bacterial two-hybrid and β-galactosidase assays of ParF-L110A-ParG, ParF-F112A-ParG and ParF-V149F-ParG. Bacterial two-hybrid assays of the interaction of ParF-L110A, ParF-F112A and ParF with ParG. Plasmids carrying *parF* or *parF* mutant alleles were fused to T25 and *parG* fused to T18 and the plasmids co-transformed into *E. coli* SP850. Colonies were streaked on MacConkey-maltose plates. In the β-galactosidase assay ParF-ParG interaction is shown in grey and ParF-L110A/F112A/V149F-ParG interaction is shown in red. The assays were carried out in triplicate. A) Bacterial two-hybrid of ParF-L110A –ParG. B) β-galactosidase assay to quantify ParF-L110A –ParG interaction. C) Bacterial two-hybrid of ParF-F112A –ParG. D) β-galactosidase assay to quantify ParF-F112A –ParG interaction. E) Bacterial two-hybrid of ParF-V149F –ParG. F) β-galactosidase assay to quantify ParF-V149F –ParG interaction. Error bars represent the standard error of the mean.

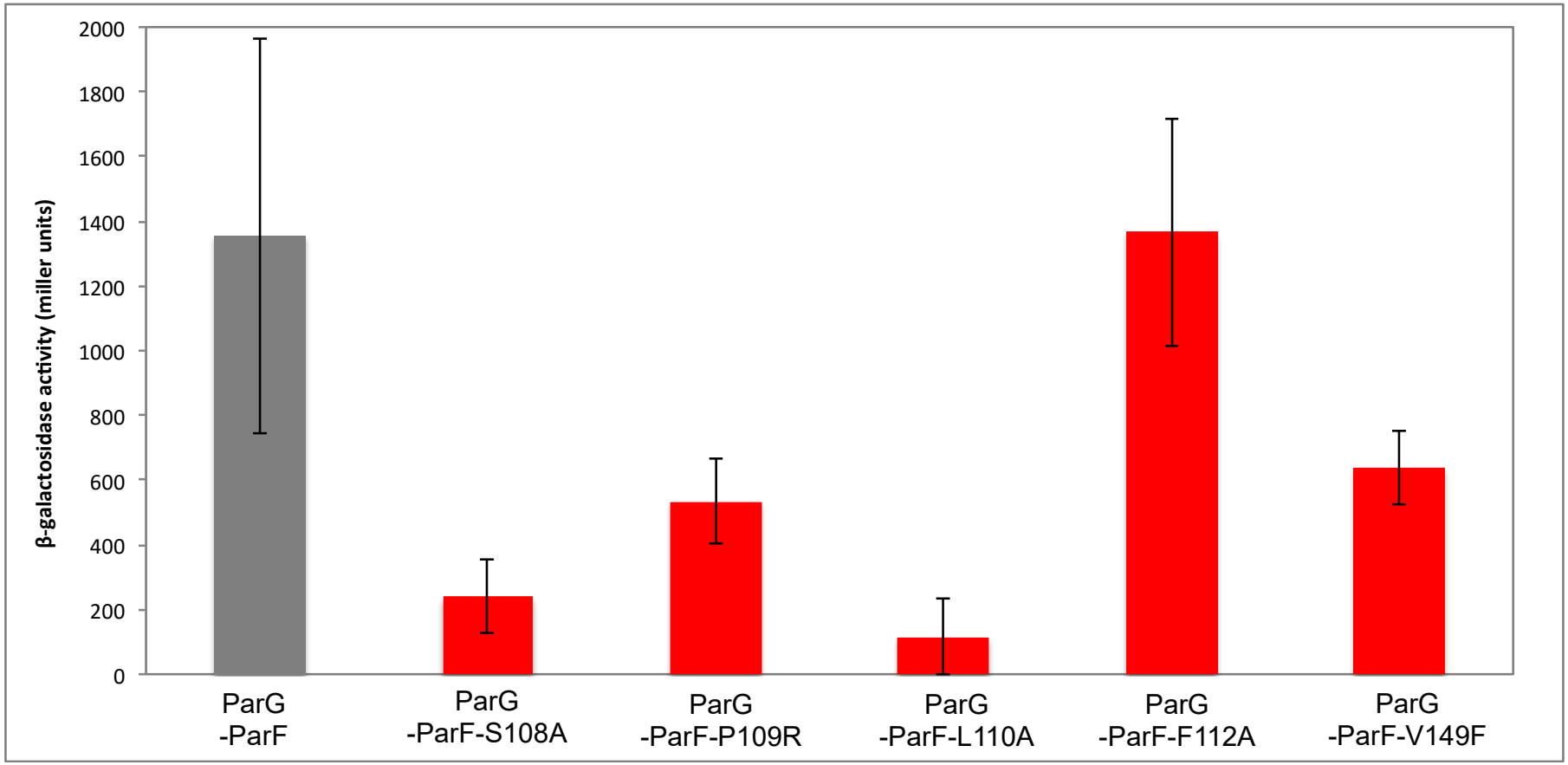

Figure 4.39 – Comparison of the β-galactosidase assay results for ParF-S108A, ParF-P109R, ParF-L110A, ParF-F112A and ParF-V149F. Results of the β-galactosidase quantitations for all ParF proteins with changes of residues potentially involved in the interaction with ParG. ParF-ParG shown in grey is an average of the averages from each individual experiment and therefore the error bar is large. All ParF mutants are shown in red. Error bars represent the standard error of the mean.

4.5.2 ParF-ParG interface conclusions

A patch of residues were identified at the monomer-monomer interface of ParF believed to be involved in the interaction with ParG. Four of these residues were positioned in the proline-rich motif and the other residue was positioned at the top on the monomer-monomer interface in the ParF dimer. The unstructured N-terminal tail of ParG is likely to insert into the ATP binding pocket of ParF in order to stimulate ParF ATPase activity via the arginine finger motif. The proline-rich motif is positioned in close proximity to the ATP binding pocket of ParF and therefore it is reasonable to propose that residues positioned at the interface of the ParF monomer make key interactions with the ParG N-terminal tail. The results of the bacterial two-hybrid and β-galactosidase assays demonstrated that ParF-S108A, ParF-P109R and ParF-L110A show significantly weaker interactions with ParG compared to the wild type ParF protein. The interaction of ParF-F112A and ParF-V149F with ParG is slightly weaker than the ParF-ParG interaction. These results suggest that S108, P109 and L110 are likely to make key interactions with ParG, whereas F112 and V149 may make interactions but these residues do not appear to be essential. It is possible to suggest that S108, P109 and L110 are required for direct interactions with ParG whereas F112 and V149 may be required indirectly. In the structure of ParF, S108, P109 and L110 appear to protrude more obviously into the monomer-monomer interface of ParF monomers compared to F112 and V149 (Figure 4.40).

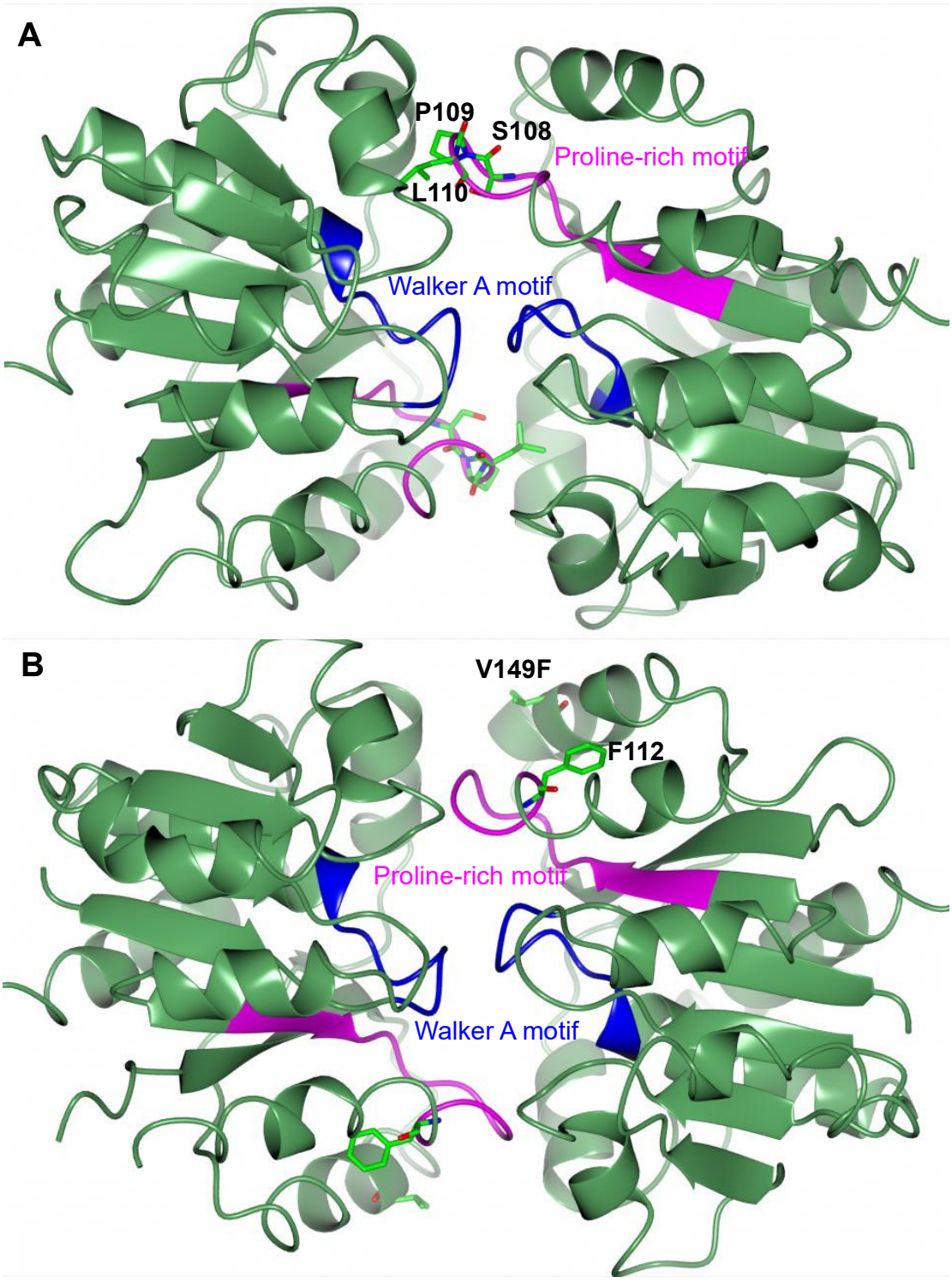

Figure 4.40 - ParF structure highlighting residues involved in the ParF-ParG interaction. A) Ribbon diagram of ParF dimer. The Walker A motif is highlighted in blue and the proline-rich motif is highlighted in magenta. S108, P109 and L110 (shown as sticks) are seen to protrude into the ParF monomer-monomer interface. B) Ribbon diagram of ParF dimer. The Walker A motif is highlighted in blue and the proline-rich motif is highlighted in magenta. F112 and V149 (shown as sticks) don not protrude into the ParF monomer-monomer interface to the same extent as S108, P109 and L110. The structural images were generated by using CCP4MG version 2.10.4 using the 4E07 PDB coordinates.

4.6 Conclusions of the monomer-monomer interface of ParF

The structure of ParF has revealed that when bound to ADP the protein is monomeric and when bound to ATP is dimeric. Residues were identified that are important in forming cross-contacts at the monomer-monomer interface, these included a proline-rich motif that is inserted into the adjacent ParF monomer close to the ATP binding pocket. The crystal structure also gave an insight into how ParF can form higher order structures. ParF-ATP dimers were seen to interact with each other to form dimer-of-dimer units and it was proposed that these dimer-of-dimer units formed the building blocks of the ParF polymers. Therefore it was reasonable to propose that blocking dimer formation would prevent ParF from forming higher order structures and this would hopefully enable a greater understanding of how ParF is able to drive TP228 plasmid segregation. The aim of this part of the project was to disrupt the monomer-monomer interface of ParF with the intention of blocking ParF dimer formation. The approach taken to try and achieve this was investigating the role of individual residues in a well conserved proline-rich motif by employing mutagenesis.

The proline motif consists of 11 residues, 6 of which caused a significant reduction in plasmid retention, when converted to alanine, indicating residues within this motif are clearly important for ParF function. One residue, P109, when converted to alanine had little effect on plasmid retention, but when converted to the bulkier arginine residue did show a significant reduction in plasmid retention. In this work, S108A and P109R were characterised in terms of the effect on the ParF monomer-monomer interface. ParF-S108A and ParF-P109R showed many similarities *in vitro*, however the results were surprising, as both were still able to form dimers. In fact, rather than disrupting dimer formation, both ParF-S108A and ParF-P109R showed a stronger self-interaction than ParF-ParF. Moreover this then appeared to have an impact on the assembly of the proteins into higher order structures. Both ParF-S108A and ParF-P109R had a higher tendency to self-associate into higher order structures in the absence of nucleotide compared to wild type ParF, especially ParF-P109R. In the case of ParF-S108A, the addition of nucleotide inhibited this propensity and the protein became solubilised. On the other hand, the addition of nucleotide to ParF-P109R had almost no effect and the protein continued to self-associate into higher order structures. It should be noted this was not ATP-dependent assembly into higher order structures. Clearly the monomer-monomer interface was disrupted, but due to the close proximity of the proline rich-

motif to the ATP binding pocket, these amino acid substitutions may alter the conformation of the binding pocket and cause a conformational change that locks ParF in a configuration that favours self-association. The results suggest that to prevent ParF dimer formation it may be necessary to construct a double or a triple mutant.

In addition to the disruption of the monomer-monomer interface of ParF, the results indicate that S108 and P109 are important in the interaction of ParF with ParG. Both ParF-S108A and ParF-P109R showed a significantly weaker interaction with ParG and ParG was unable to stimulate either the ATPase activity or the assembly into higher order structures of the proteins. These findings are also interesting as recently there has been some progress made in solving the co-structure of ParF-ParG, and preliminary observations have identified a patch of residues that may form a potential ParF-ParG interface (Schumacher, M. – unpublished data). Four of the residues are part of the proline-rich motif, two of which are S108 and P109. The other two residues, L110 and F112 and an additional residue positioned at the top of the monomer-monomer interface were the remaining residues identified. ParF-L110A was also found to display a significantly weaker interaction with ParG, demonstrating that the triad of S108, P109 and L110 are clearly involved in the ParF-ParG interaction. These findings are starting to build a clearer picture of how the N-terminal tail of ParG inserts into the monomer-monomer interface of ParF to enable ParG to stimulate ATPase activity.

The monomer-monomer interface of ParF is important in both the ParF-ParF interaction and also the ParF-ParG interaction. Disrupting this interface has a knock on effect on the ATP-dependent assembly of ParF into higher order structures, due to a conformational change in the ParF dimer. It is likely that to disrupt the monomer-monomer interface in such a way that the ParF dimer would be unable to form multiple residues would need to be changed.

Chapter 5: The role of ParF non-specific DNA binding and association with the nucleoid to mediate TP228 plasmid segregation

5.1 The role of ParF non-specific DNA binding in TP228 plasmid segregation

Many ParA proteins have been shown to display non-specific DNA (nsDNA) binding properties *in vitro* and have been seen to localise on the nucleoid *in vivo.* ParA from P1 plasmid, SopA from F plasmid, δ from pSM19035 plasmid, ParA from pB171 plasmid and Soj from *B. subtilis* have all been shown to bind nsDNA (Leonard *et al*., 2005, Castaing *et al*., 2008, Pratto *et al*., 2008, Ringgaard *et al*., 2009, Ptacin *et al*., 2010, Hwang *et al*., 2013). It is becoming apparent that the non-specific DNA binding properties of these ParA proteins are important in the plasmid segregation mechanism and all recently proposed models for plasmid segregation involve ParA proteins associating with the nucleoid. The nsDNA binding of the ParA proteins has been shown to be ATP-dependent. In the case of ParA from the P1 plasmid, the binding of ATP allows ParA to undergo a slow conformational change that enables ParA to bind nsDNA (Vecchiarelli *et al*., 2010). Residues within the C-terminal region are thought to be crucial for the nsDNA binding of the ParA proteins, mutations of residues within this region have been shown to abolish nsDNA binding and allowed specific residues involved in nsDNA binding to be identified (Castaing *et al*., 2008, Pratto *et al*., 2008, Hester and Lutkenhaus, 2007). Surface exposed basic residues have been identified both by mutational and structural analysis of the ParA proteins. Some of the residues are well conserved within the ParA proteins.

ParF has been shown to localise with the nucleoid *in vivo* (Ringgaard *et al*., 2009) and has been observed to bind nsDNA in an ATP-dependent manner *in vitro* (McLeod et al., 2016). The structure of ParF revealed surface exposed residues that could be involved in nsDNA binding (Figure 5.1). These residues are positioned on the surface of the dimer and would also be located on the surface of a ParF polymer, therefore being optimally positioned to associate with the nucleoid. The aim of this part of the study was to firstly confirm that ParF was able to bind nsDNA *in vitro* and to try and gain further understanding of the binding properties. This was achieved by employing biochemical ensemble techniques as well as a single molecule approach. Secondly, the study focused on identifying a potential interface of ParF that is involved in nsDNA binding. The roles of individual surface exposed basic residues, identified from the structure of ParF, were investigated in terms of the effect they have on nsDNA binding and plasmid segregation. The overall aim was to gain a greater understanding of nsDNA binding of ParF, specifically the role of the nucleoid in TP228 plasmid segregation.

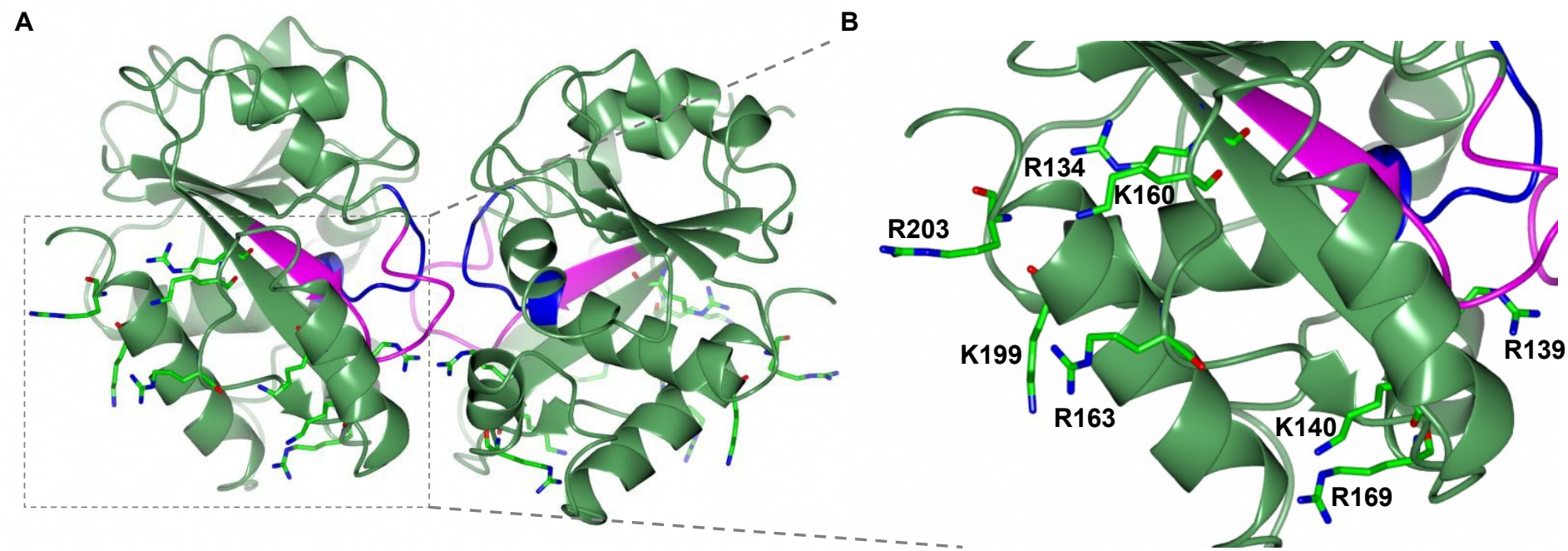

Figure 5.1 - Structure of ParF highlighting surface exposed basic residues identified as potentially involved in nsDNA binding. A) Ribbon diagram of ParF dimer. The proline-rich motif is shown in magenta and the Walker A motif is shown in blue. Residues identified as potentially involved in nsDNA binding are shown as sticks. B) Zoomed image of the ribbon diagram of ParF dimer. The structural images were generated by using CCP4MG version 2.10.4 using the 4E07 PDB coordinates.

5.2 ParF is able to bind nsDNA *in vitro*

It was previously observed that ParF is able to form a dynamic pattern on the nucleoid and that ParF could bind DNA *in vitro* (McLeod et al., 2016). Initially, fluorescence anisotropy and electrophoretic mobility-shift assays (EMSA) were employed in order to verify whether purified ParF binds DNA *in vitro*. It was previously observed that, like other ParA proteins, ParF binds to non-specific DNA in an ATP-dependent manner (McLeod et al., 2016). Therefore both assays in this study were carried out with numerous double stranded DNA fragments that differed in both size and sequence. The effect of the addition of nucleotides was also investigated and assays were carried out either in the absence of nucleotide or in the presence of ADP, ATP or ATP-γ-s. The results confirmed that as expected, ParF bound to nsDNA in an ATP-dependent manner. ParF bound to different DNA fragments of random sequence demonstrating the binding is non-specific. This was further supported by analysing the ability of ParF to bind DNA in the presence of increasing salt concentrations, McLeod *et al*. observed that higher ionic strength inhibited ParF DNA binding and this is consistent with non-specific DNA binding.

The overproduction and purification of the His-tagged ParF by Ni^{2+} affinity chromatography was carried out as detailed in section 2.5. Firstly, fluorescence anisotropy experiments were performed in order to analyse ParF DNA binding. 20 and 40 bp Cy3 (5') fluorescently labeled DNA fragments with random sequences were used in the fluorescence anisotropy experiments. The chosen fluorescent DNA fragment was incubated with increasing concentrations of ParF, either in the absence of nucleotide or in the presence of ADP, ATP or ATP-γ-s (2 mM). The change in anisotropy was then measured and plotted against ParF concentration. ParF was observed to bind the nsDNA in the presence of ATP and ATP-γ-s, but not in the presence of ADP or in the absence of nucleotide (Figure 5.2). No significant difference in the binding was observed between the 20 bp (data not shown) or the 40 bp DNA fragment, therefore subsequent fluorescence anisotropy experiments were carried out using only the 40 bp DNA fragment. The K_d value was ~ 300 nM for ParF DNA binding in the presence of ATP and ATP-γ-s.

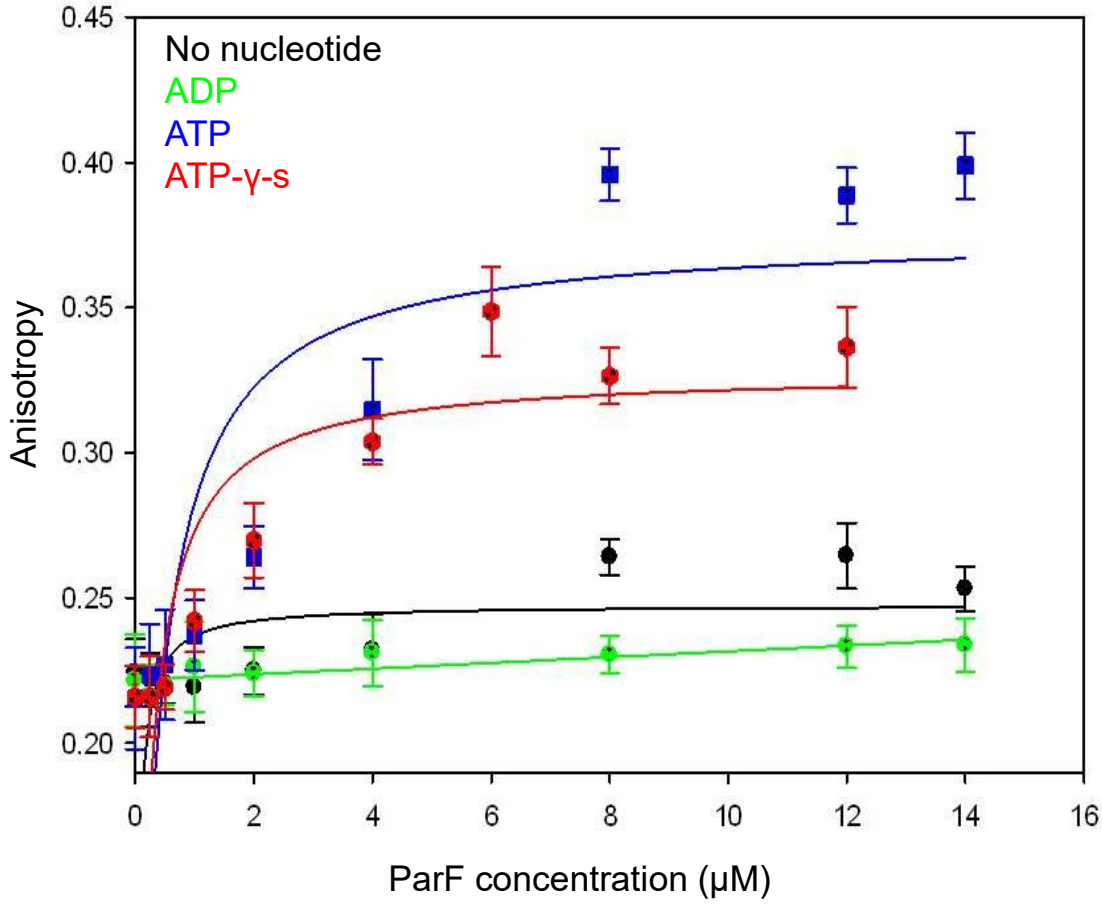

Figure 5.2 – Fluorescence anisotropy analysis of ParF and non-specific DNA binding. Fluorescence anisotropy studies in which increasing concentrations of ParF are incubated with a fluorescent 40 bp DNA fragment harbouring a random sequence. The analysis of DNA binding was carried out in the presence of different nucleotides. No nucleotide is shown in black, ADP is shown in green, ATP is shown in blue and ATP-γ-s is shown in red. K_d = 0.329 μM with ATP and the K_d = 0.2 μM with ATP-γ-s. Ten anisotropy values were recorded for each concentration and the average value was calculated. Assays were repeated in triplicate. Error bars represent the standard error of the mean.

EMSAs were performed in order to confirm the results observed for fluorescence anisotropy. EMSAs were carried out using two different DNA fragments, one was a 123 bp biotinylated DNA fragment that contained the *parFG* promoter sequence, and the other was a 43 bp biotinylated DNA fragment of random sequence. Increasing ParF concentrations were incubated with a biotinylated DNA fragment either in the absence of nucleotide or in the presence of ADP, ATP or ATP-γ-s (2 mM). EMSA is a technique often employed to analyse the ability of a protein to bind a specific DNA sequence. In general, when a protein binds to the DNA fragment, a band-shift can be observed in the gel. A control lane of DNA alone will contain a single band. Upon addition of the protein to the DNA fragment, a second band will be observed that corresponds to the

protein bound to the DNA. This nucleoprotein complex is larger than DNA fragment only and therefore is retarded in the gel and thus a band-shift is observed. Upon increasing concentrations of the protein, the amount of unbound DNA typically decreases and the intensity of the band representing the nucleoprotein complex will increase. EMSAs can also be employed to analyse the interaction between a protein and nsDNA. The band-shift can often appear different in this case. It can be clearly observed that when ParF was incubated with the biotinylated DNA fragment without nucleotide or in the presence of ADP no band-shift occurred. The lanes in which the ParF-DNA fragment reactions were loaded show bands that migrate to the same position as the DNA fragment only, indicating the protein is not binding to the DNA. On the other hand, when ATP and ATP-γ-s are present in the reaction a band-shift can be observed (Figure 5.3). At high ParF concentrations (2 – 8 μM) the bands are more retarded in the gel and this indicates ParF is binding the DNA fragment, causing a larger nucleoprotein complex to form which runs differently on the gel. The same results are observed both when ParF is incubated with the 43 bp DNA fragment (data not shown) or the 123 bp DNA fragment, confirming that ParF binds DNA in a non-specific manner. The results are consistent with those observed for fluorescence anisotropy experiments, where ParF binds nsDNA in an ATP-dependent manner.

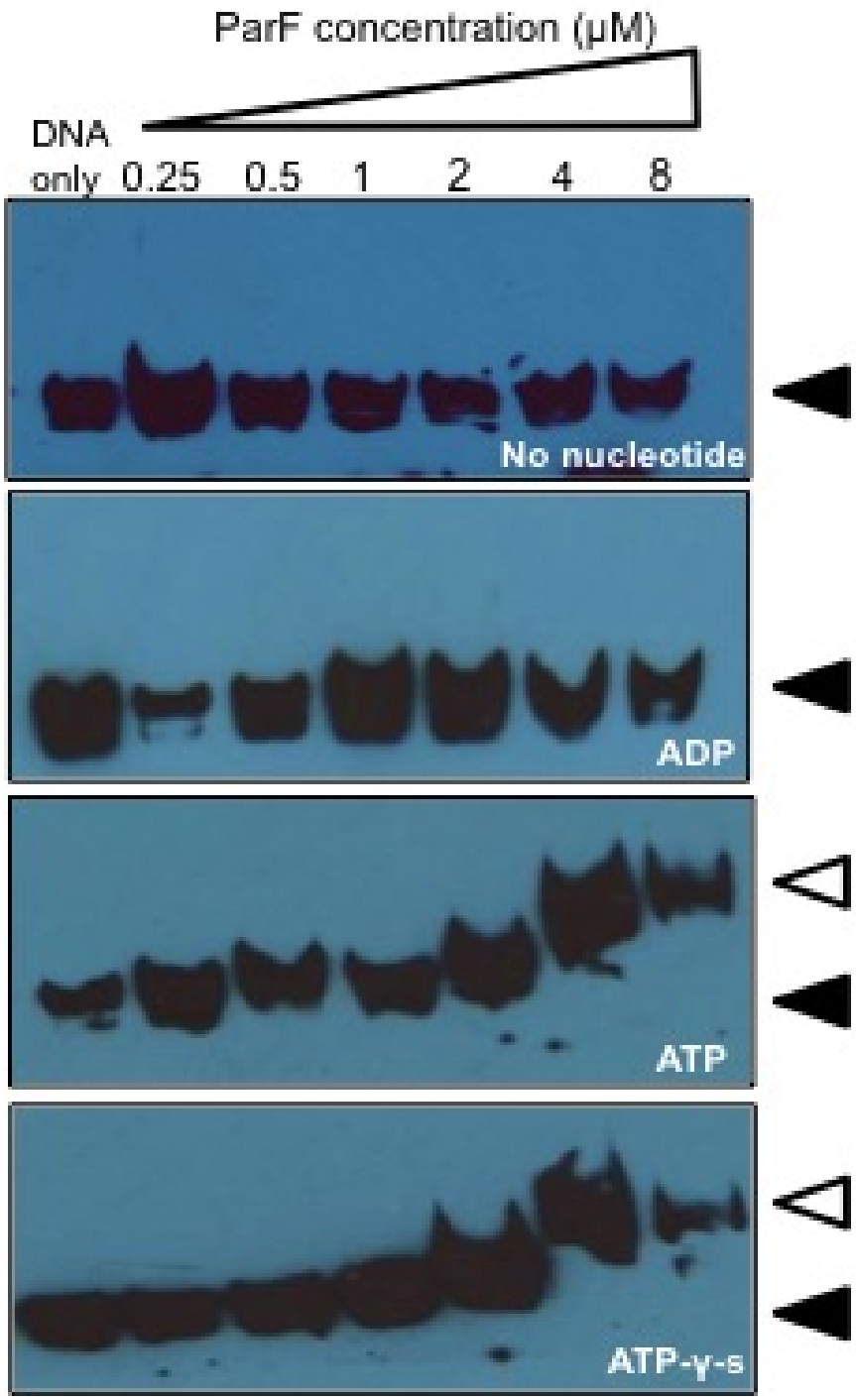

Figure 5.3 – EMSA results of ParF binding ns-DNA. Representative EMSA of reactions in which ParF was incubated with nsDNA. Increasing concentrations of ParF were incubated with a 123 bp biotinylated DNA fragment harbouring the *parFG* operator sequence in the absence of nucleotide or the presence of ADP, ATP or ATP-γ-s. Unbound DNA is indicated by a black arrowhead, a shifted nucleoprotein complex is indicated by a white arrow head. Assays were repeated at least in triplicate.

In order to try and gain further understanding of ParF nsDNA binding properties, a single molecule approach, Tethered Particle Motion (TPM), was employed. In a TPM experiment, increasing concentrations of ParF were incubated with a random sequence 700 bp DNA fragment either in the absence of nucleotide or in the presence of ADP or ATP. One end of the DNA fragment is attached to a small bead and the other is attached to a surface. The x and y coordinates of individual beads can be tracked in real time and the root mean square displacement (RMS) is calculated. If ParF binds to the DNA the motion of the bead would change and thus so would the RMS value. In general, if a protein binds and polymerises on the DNA, the RMS value will increase due to stiffening of the DNA. If a protein binds DNA and causes bends and loops in the DNA the RMS value will decrease due to the compaction of the DNA (Figure 5.4). The addition of ParF to the DNA in the absence of nucleotide or ADP showed little change in the RMS value, demonstrating no binding. These results are consistent with the previous DNA binding studies (Figures 5.2 and 5.3). Upon addition of ATP, the RMS value decreased thus indicating that ParF caused the DNA to become compacted. However, analysing the data was problematic due to the fact that at the higher concentrations of ParF many of the beads became completely stuck to the surface. This was likely due to the dense compaction of the DNA upon ParF binding. Therefore a manual analysis was carried out in which, after any extreme outliers were removed, a histogram for the RMS values of every bead was plotted giving an average RMS value. Then for each ParF concentration the RMS values were plotted for all the beads and this created peaks at different RMS values. The area under these peaks was then calculated. The percentage of the peaks was calculated for small and large RMS values and this was plotted on a graph (Figure 5.5). Clearly when ADP is present even at higher concentrations of ParF the majority of the beads had a large RMS value, similar to that of the DNA only control, indicating no ParF binding to the DNA fragment. When ATP was present at higher concentrations of ParF more beads had a small RMS value indicating ParF was binding the DNA fragment.

These results not only confirm that ParF binds nsDNA in an ATP-dependent manner, but also provides further insight into the mechanism by which ParF binds the DNA. The results suggest that ParF doesn't form a one-dimensional filament structure on the DNA, as this would have resulted in an increase of RMS value upon the addition of ParF. Instead the results suggest that multiple ParF-ATP dimers may bind the DNA and the interaction of many ParF dimers forming larger higher order structures may cause

the bending and looping of the DNA. This provides further evidence for the *in vivo* observations by McLeod *et al*. and this work (Chapter 3), in which higher resolution images revealed that ParF appears to protrude into the nucleoid forming a lattice of ParF bundles.

Additional techniques were also employed in order to try and further characterise the interaction of ParF with DNA such as DNase I footprinting and Surface Plasmon Resonance (SPR). However an interaction was not detected with these approaches, which suggests a transient and dynamic nature of the association of ParF with DNA.

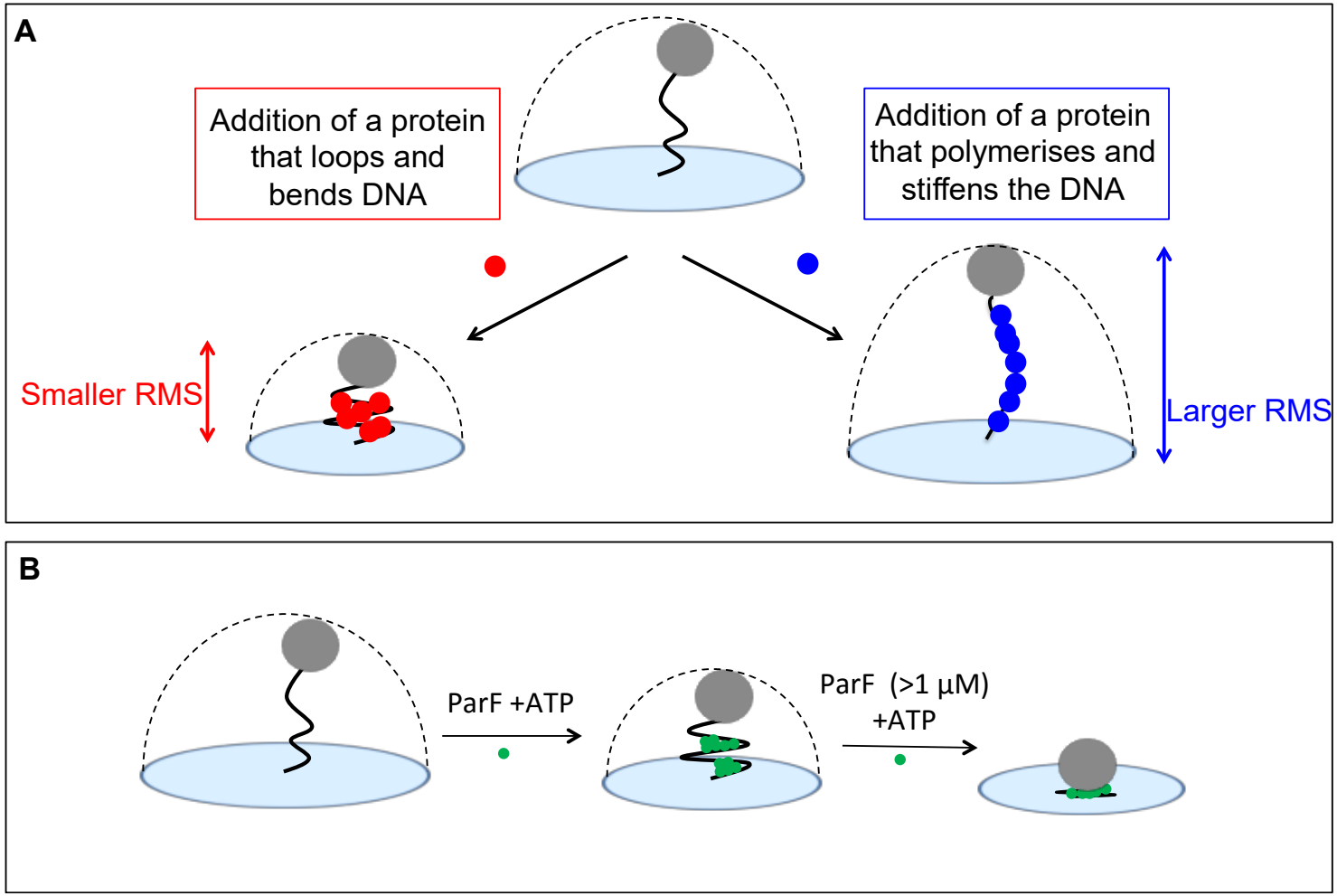

Figure 5.4 - Schematic representation of the TPM approach. A) Schematic diagram of possible outcomes of a TPM experiment. The addition of a protein that compacts the DNA by looping and bending would cause a decrease in RMS value, whereas the addition of a protein that polymerises on the DNA would cause an increase in RMS. B) Schematic diagram of the results of a TPM experiment, in which ParF was added to DNA in the presence of ATP. At lower concentrations of ParF the DNA becomes compacted and the RMS value decreases. At high ParF concentrations the bead becomes completely stuck to the surface.

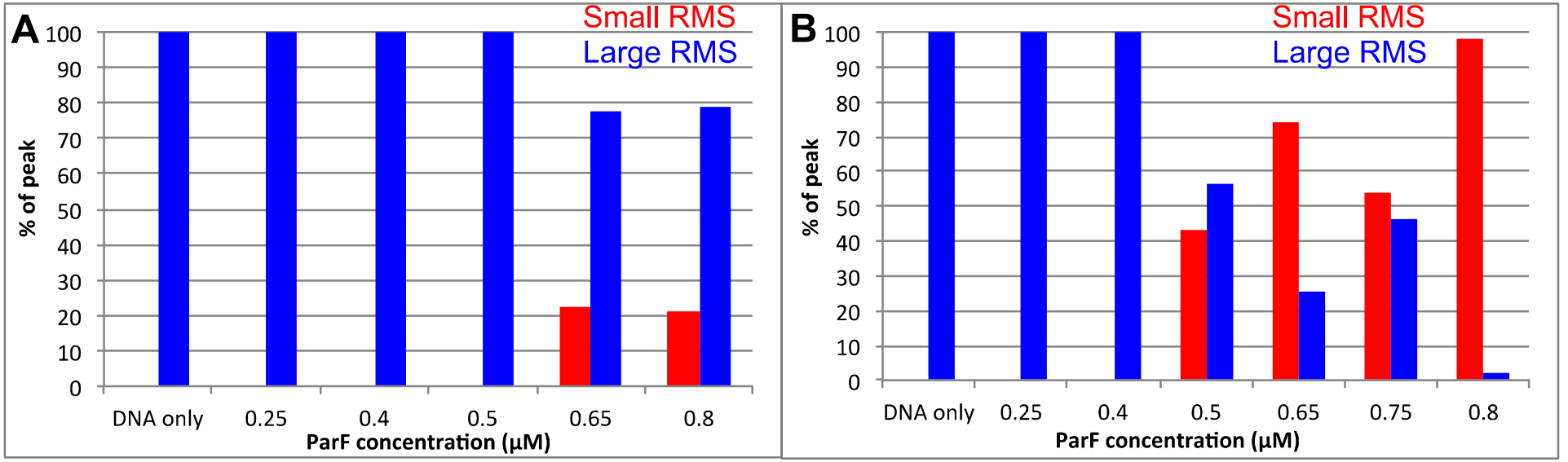

Figure 5.5 – TPM analysis of ParF binding nsDNA. TPM experiment in which increasing concentrations of ParF were incubated with a 700 bp DNA fragment harbouring a random sequence. The percentage of the peaks of small and large RMS values is plotted, large RMS value is shown in blue and small RMS value is shown in red. A) In the presence of ADP. B) In the presence of ATP.

5.3 *In vivo* analysis of the effects of the changes in residues potentially involved in DNA binding on plasmid retention

Overlap extension mutagenesis was employed to change individual residues potentially involved in DNA binding to alanine. The experimental setup was the same as described in Chapter 3 for the construction of ParF-S185W. The partition vector, pFH547, was the template for the mutagenesis and restriction sites within the *parF* and *parG* genes were used in order to swap the wild type region with the fragment containing the desired mutations. The mutagenesis was carried out as detailed in 2.4. Eight surface exposed basic residues were identified as potentially involved in ParF nsDNA binding. Initially, all eight residues (R134, R139, K140, K160, R163, R169, K199 and R203) were mutated to alanine and characterised in terms of the effect the mutation had on plasmid stability.

Partition assays were employed to determine what effects the mutations have on plasmid retention (Section 2.7). The segregation activity of plasmids bearing the *parF* mutations were compared to empty vector plasmid pFH450 and the plasmid pFH547 which contains the wild type *parFGH* partition cassette. The results of the partition assay are shown in Figure 5.7. The plasmid harbouring the *parF-R139A* and *parF-R169A* mutations showed a significant reduction in plasmid retention (<10%), close to that of the plasmid that doesn't contain a partition cassette. ParF-R169A has been characterised in Dobruk-Serkowska, A. *et al*. (2012). R169 was identified as being important in shaping the ATP binding site of ParF and it was observed that converting R169 to alanine causes ParF to become a hyperactive ATPase. In addition, ParF-R169A was shown to self-associate more readily than the wild type ParF and also ParF-R169A displayed a stronger interaction with ParG. However, the effect of the mutation on ParF DNA binding was not investigated and this was carried out in this work. Further detailed analysis on ParF-R139A was carried out in this study alongside additional characterisation of ParF-R169A.

In addition to the nine single mutations constructed, a double mutant was also constructed. It was postulated that to completely abolish the ability of ParF to bind DNA multiple residues would need to be mutated. Single amino acid changes are likely to have a smaller effect on ParF DNA binding as the other basic exposed residues can compensate. Of the eight originally identified surface exposed basic residues partition assays identified R139A and R169A as being informative mutations as they caused a

significant decrease in plasmid retention. The six remaining residues had little or no effect on plasmid retention when mutated to alanine. Two of these residues, K160 and R163, were selected for further mutagenesis studies based on their limited effect on protein fold (Figure 5.6). The residues were changed to glutamic acid in order to maintain the hydrophilic surface of the protein but to disrupt DNA binding by changing the positively charged residues to a negative charge. Due to time constraints multiple residues were not changed to alanine initially and then changed to glutamic acid. The plasmid harbouring the *parF-K160E-R163E* mutation showed a significant reduction in plasmid retention of ~10%, which again is close to that of the plasmid that doesn't contain a partition cassette. Therefore further analysis of ParF-K160E-R163E was also carried out in this study.

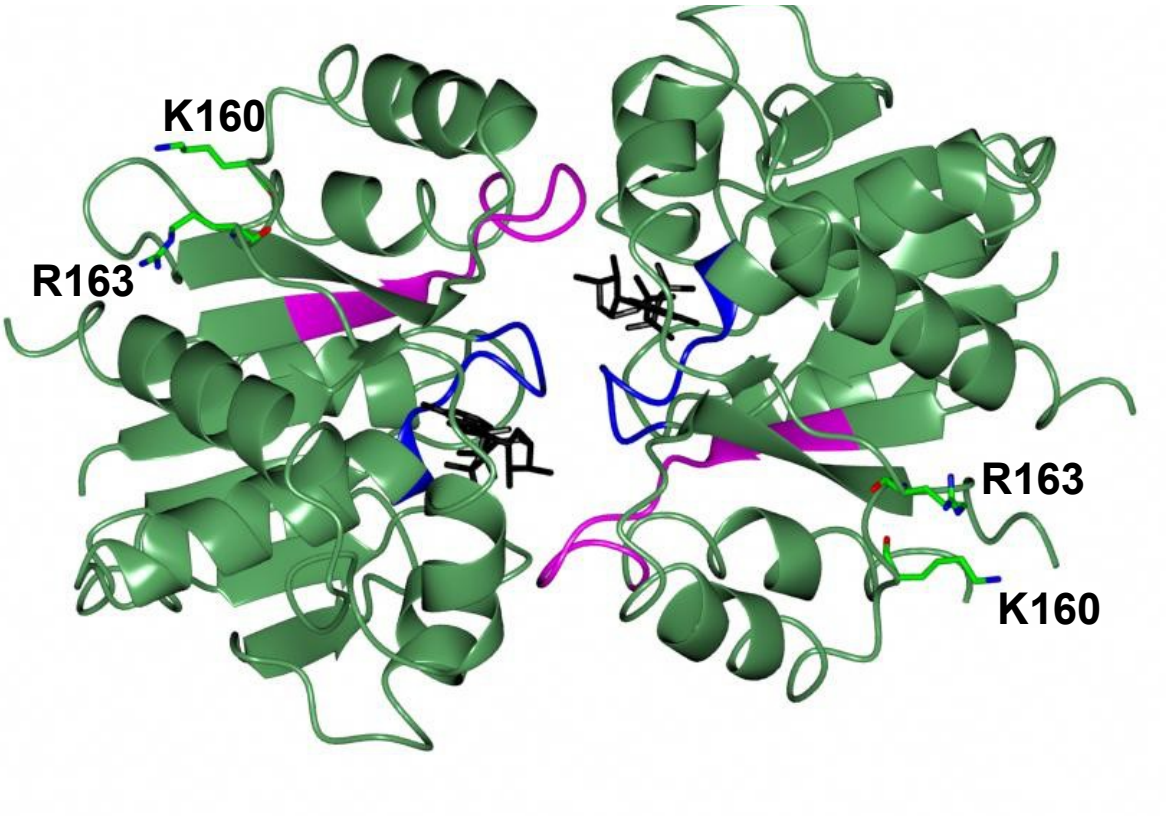

Figure 5.6 – Structure of ParF highlighting the position of the residues changed in the double mutant. Ribbon diagram of ParF dimer. The proline-rich motif is shown in magenta, the Walker A motif is shown in blue and AMPPCP is shown as sticks in black. K160 and R163 are shown as sticks. The structural images were generated by using CCP4MG version 2.10.4 using the 4E07 PDB coordinates.

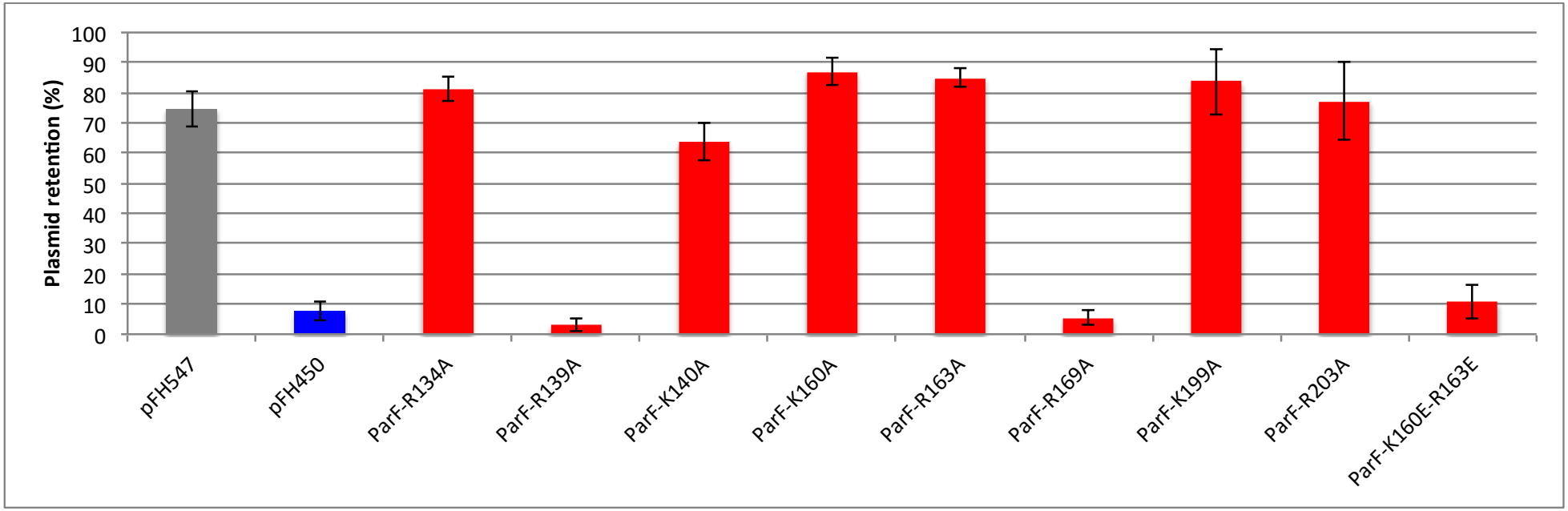

Figure 5.7 - Retention percentage of plasmids harbouring *parF* alleles with mutations affecting residues potentially involved in DNA binding. pFH547 plasmid contains the wild type *parFGH* partition cassette and pFH450 lack a partition cassette. Plasmid retention shown is calculated from an average of at least three assays. The error bars represent the standard error of the mean. Partition assays of the eight surface exposed residues identified and the double mutant also constructed

5.4 ParF-R139A, ParF-R169A and ParF-K160E-R163E

To analyse the effects of ParF-R139A, ParF-R169A and ParF-K160E-R163E on the DNA binding of ParF, a range of *in vitro* and *in vivo* experiments were carried out. These initially involved analysing whether these changes had any effect on ATP binding and hydrolysis, assembly into higher order structures and interaction with ParG in order to ensure a complete picture was gained. As previously discussed ParF-R169A has been characterised in Dobruk-Serkowska, A. *et al*. (2012) and shown to be a hyperactive ATPase that has a higher tendency to self-associate into higher order structures in the absence of nucleotide. ParF-R169A was also shown to have a stronger interaction with ParG compared to wild type ParF. During the course of this study it became evident that ParF-R139A shared many of the same characteristics as ParF-R169A, which is reasonable considering both these residues, as well as being surface exposed basic residues, are both involved in either shaping the ATP binding pocket or making contact with ATP (Figure 5.8). The features of ParF-R139A, ParF-R169A ParF-K160E-R163E are discussed in detail in the following sections.

ParF-R139A, ParF-R169A and ParF-K160E-R163E were overproduced using a pET expression system. The *parF mutant* allele was cloned into the pET22b(+) expression vector as detailed in Chapter 4 for other mutants. The overproduction and purification of His-tagged ParF-R139A, ParF-R169A and ParF-K160E-R163E was carried out as detailed in section 2.5. Solubility assays were initially performed to ensure the proteins were soluble and then the purification using Ni^{2+} affinity chromatography was carried out. Before any *in vitro* characterisation, CD was employed (section 2.10) to ensure the mutations had no effect on the protein fold. The results demonstrated ParF-R139A, ParF-R169A and ParF-K160E-R163E were correctly folded and the conversion of the residues had little or no effect on ParF secondary structure. The CD spectra of ParF-R139A and ParF-K160E-R163E are shown in Figure 5.9 and the CD spectrum for ParF-R169A is detailed in Dobruk-Serkowska, A. *et al*. (2012).

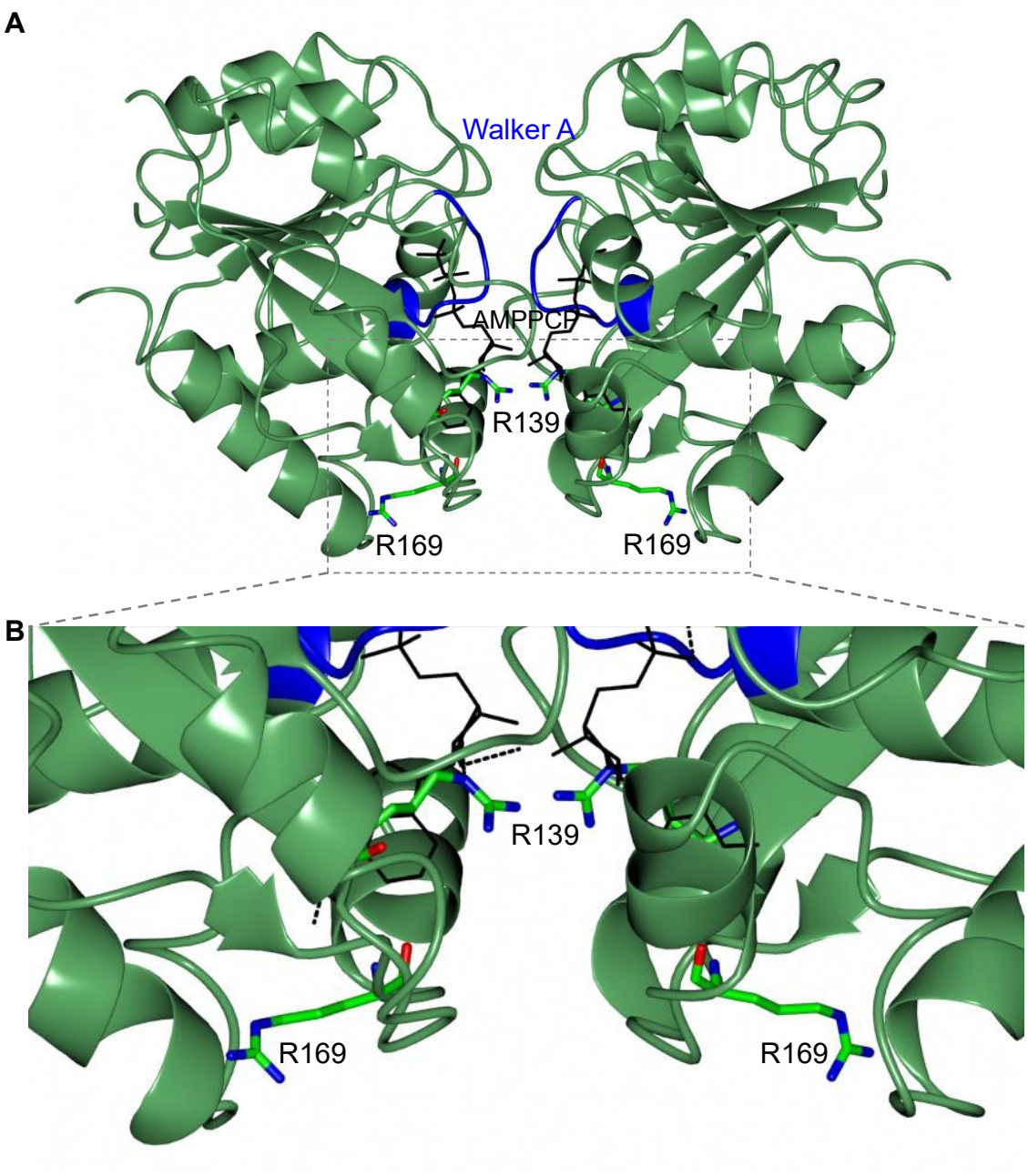

Figure 5.8 - Structure of ParF highlighting the positions of residues R139 and R169 that are close to the ATP binding pocket. A) Ribbon diagram of ParF dimer. The Walker A motif is shown in blue and AMPPCP is shown as sticks in black. R139 and R169 are shown as sticks. B) Zoomed image of the ribbon diagram of ParF dimer, AMPPCP is shown in black with hydrogen bonds from R139 to AMPPCP shown as a dashed black line. The structural images were generated by using CCP4MG version 2.10.4 using the 4E07 PDB coordinates.

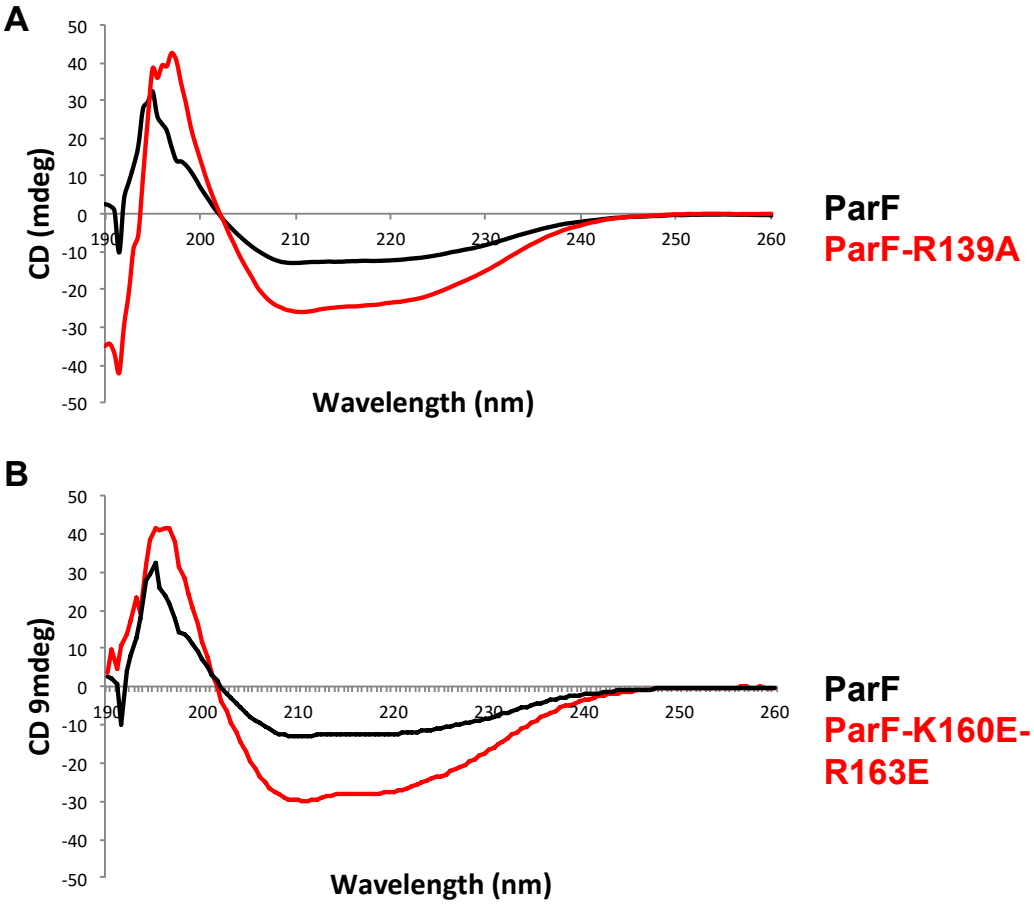

Figure 5.9 - Circular dichroism spectra of ParF-R139A and ParF-K160E-R163E. A) ParF-R139A. ParF spectrum is shown in black and the mutant in red. B) ParF-K160E-R163E. ParF spectrum is shown in black and the mutant in red.

5.4.1 ParF-R139A displays weaker ATP binding compared to the wild type ParF

Fluorescence anisotropy experiments were carried out in order to analyse whether ParF-R139A and ParF-K160E-R163E were able to bind ATP. A fluorescent ATP analog (MANT-ATP) was incubated with increasing concentrations of ParF and ParF-R139A/ ParF-K160E-R163E and the change in anisotropy value was measured. ParF-K160E-R163E was observed to bind ATP similarly to that of ParF as the results obtained for ParF-K160E-R163E fitted into a binding curve almost identical to that of ParF. The K_d value obtained for ParF-K160E-R163E was 0.7 μM, which is very similar to the ParF K_d value of 0.44 μM (Figure 5.10B). On the other hand, ParF-R139A was observed to bind MANT-ATP but the binding differed from that of the wild type ParF. At low concentrations ParF initially showed a sharp increase in anisotropy and then at higher concentrations the increase became more gradual before reaching a plateau. ParF-R139A showed more of a gradual increase in anisotropy and saturation was not completely reached: the final anisotropy value reached ~ 65% of that achieved by the wild type ParF protein. These findings are reflected in the difference in the K_d values, ParF has an observed K_d value of 0.44 μM, whereas ParF-R139A has a K_d value of 2.11 μM (Figure 5.10A). The structural data of ParF revealed that R139 makes the only hydrogen bond from ParF to the ribose group of AMPPCP and therefore it is expected that ATP binding is likely to be affected by the conversion of the arginine to alanine. The results for ParF-R139A are very similar to those observed in Dobruk-Serkowska, A. *et al*. (2012) for ParF-R169A ATP binding. ParF-R169A also showed weaker binding to ATP, the change in anisotropy only reached ~50% of the wild type ParF, with a K_d value > 1 μM.

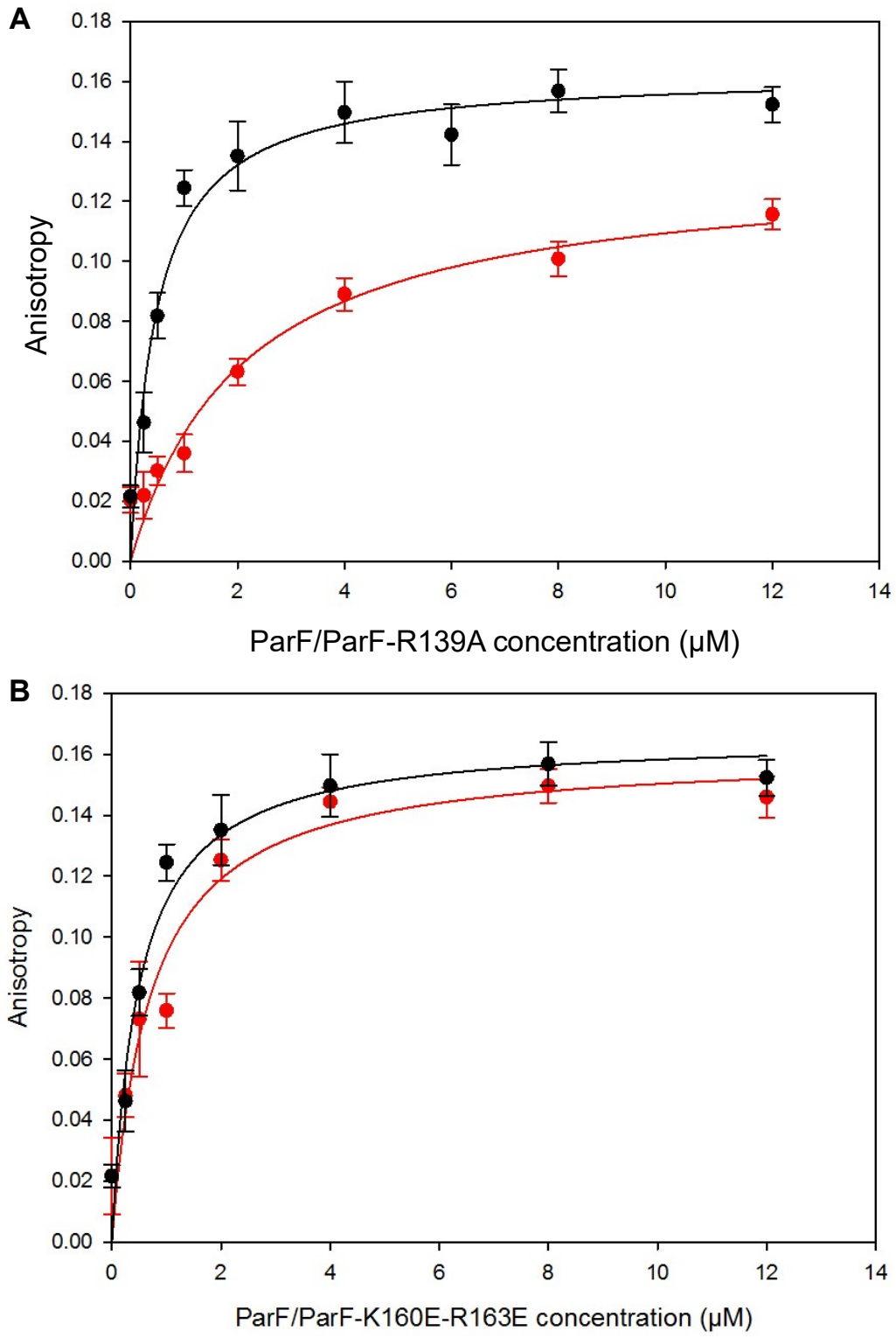

Figure 5.10 – Fluorescence anisotropy of ParF-R139A and ParF-K160E-R163E ATP binding. Fluorescence anisotropy studies of ATP binding by ParF, ParF-R139A and ParF-K160E-R163E. Increasing concentrations of ParF/ParF-R139A/ ParF-K160E-R163E are incubated with MANT-ATP and the change in anisotropy was measured. ParF is shown in black and mutant proteins shown in red. Ten anisotropy values are taken for each concentration and an average value is calculated. Assays are carried out in triplicate. Error bars represent the standard error of the mean. A) ParF-R139A. B) ParF-K160E-R163E.

5.4.2 ParF-R139A is a hyperactive ATPase

ParF is intrinsically a weak ATPase and the partner protein, ParG, stimulates this activity via an arginine finger-like motif in the N-terminal tail. As ParF-R139A ATP binding was attenuated similarly to the behaviour of ParF-R169A, it is reasonable to propose that ParF-R139A, like ParF-R169A, may be a hyperactive ATPase. The ATPase activity of ParF-R139A was analysed, as well as the ATPase activity of ParF-K160E-R163E, using thin layer chromatography (TLC) as described in section 2.8. In this assay, ParF, ParF-R139A and ParF-K160E-R163E were incubated with radioactive ATP and ATP and ADP were then separated using TLC. The ATP and ADP spots can be visualised on autoradiography films and quantified using a Phosphor imager. ParF, ParF-R139A and ParF-K160E-R163E ATPase activity was tested both in the presence and absence of ParG. The results demonstrated that ParF-K160E-R163E has a weak intrinsic ATPase activity similar to that of wild type ParF (Figure 5.13). ParG was able to stimulate the ATPase activity of ParF-K160E-R163E similarly to the enhancement observed for the wild type protein (Figures 5.14). Thus ParF-K160E-R163E is able to bind and hydrolyse ATP similarly to the wild type protein and therefore a different function must be responsible for the disruption in plasmid partition. This however was not the case for ParF-R139A and as expected ParF-R139A is a hyperactive ATPase. At the highest concentration of ParF-R139A the rate of ATP hydrolysis is almost three times higher than that of the wild type ParF (Figure 5.11). ParG was unable to stimulate the ATPase activity of ParF-R139A beyond the level reached by the ParF mutant alone (Figure 5.12). This may be due to an altered interaction with the N-terminal tail of ParG or due to the fact that as ParF-R139A is a hyperactive ATPase the level of ATP hydrolysis is already at a high level and therefore no further stimulation can be achieved. The interaction of ParF-R139A was then investigated using a bacterial-two hybrid assay to help rationalise the results observed here. It should be again noted that, in Dobruk-Serkowska, A. *et al.* (2012), ParF-R169A was observed to be a hyperactive ATPase and ParG was unable to stimulate the ATPase activity. The conversion of R169 to alanine was believed to (1) disrupt the shaping of the ATP binding site of ParF and (2) prevent the correct alignment of the arginine finger motif of the N-terminal tail of ParG.

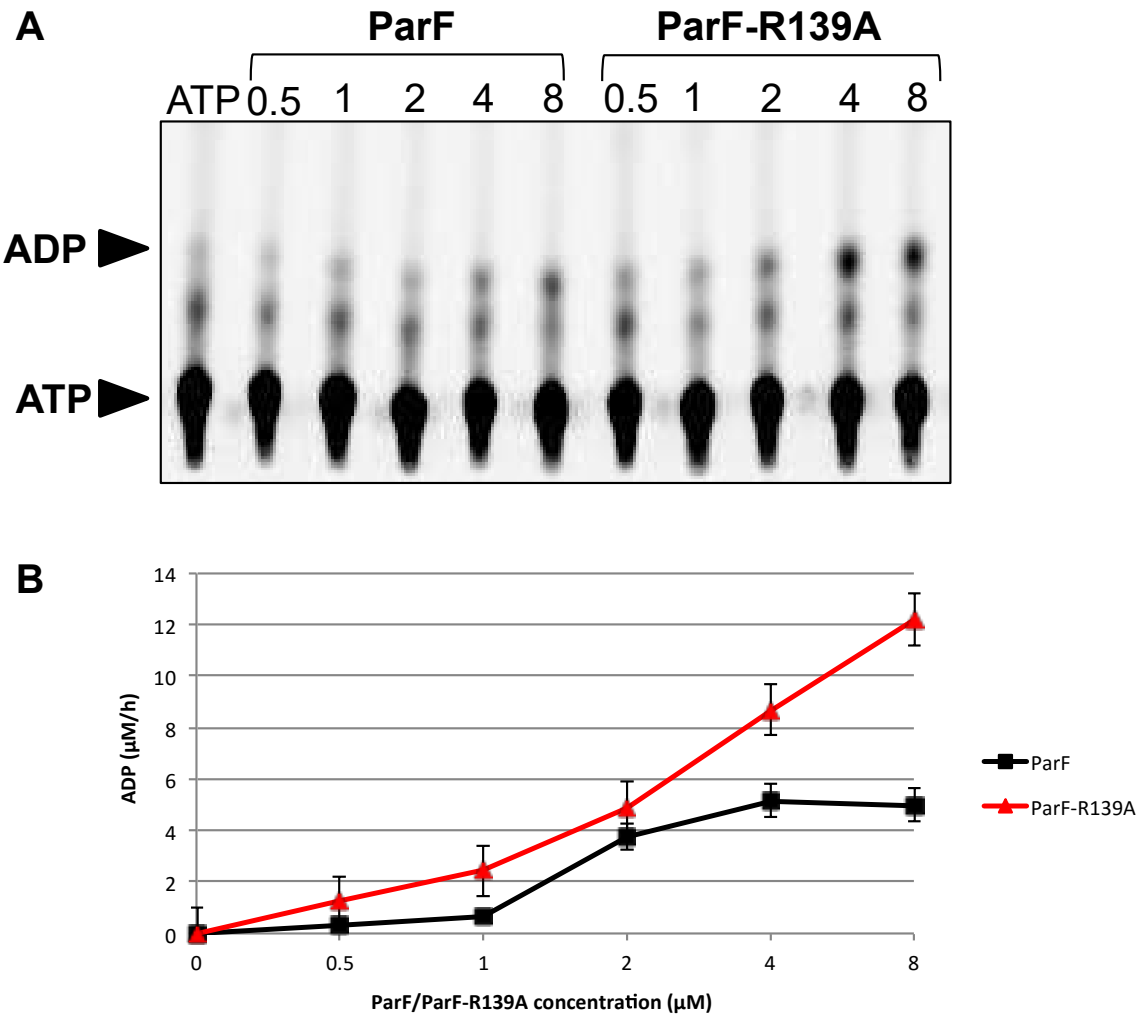

Figure 5.11 – Intrinsic ATPase activity of ParF-R139A. A) Autoradiographic image of a representative experiment showing the results of an ATPase assay in which radioactive ATP ([α^{35S}] ATP was incubated with ParF and ParF-R139A. ATP and ADP (indicated by black arrow heads) were separated by TLC. B) ATP hydrolysis plotted as a function of ParF/ParF-R139A concentration. ParF is shown in black and ParF-R139A is shown in red. Experiments were performed in triplicate and error bars represent the standard error of mean.

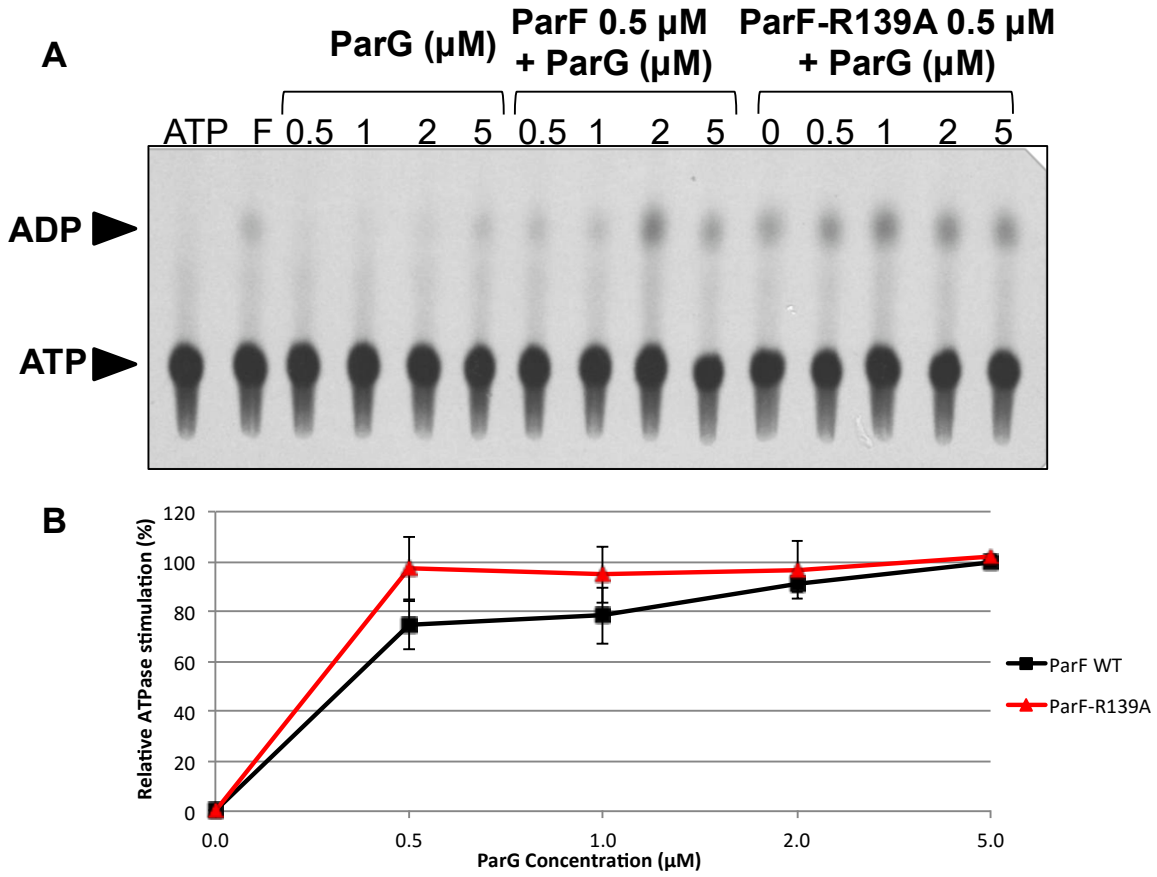

Figure 5.12 – ATPase activity of ParF-R139 in the presence of ParG. A) Autoradiographic image showing the results of a representative ATPase assay in which radioactive ATP ([α^{35S}] ATP) and ParG were incubated with ParF and ParF-R139A. ParG was tested without ParF to check for the presence of potentially contaminating ATPase activities. ATP and ADP (indicated by black arrow heads) were separated by TLC. B) Relative ATPase stimulation (%) plotted as a function of increasing ParG concentration. ParF is shown in black and ParF-R139A is shown in red. Experiments were performed in triplicate and error bars represent the standard error of mean.

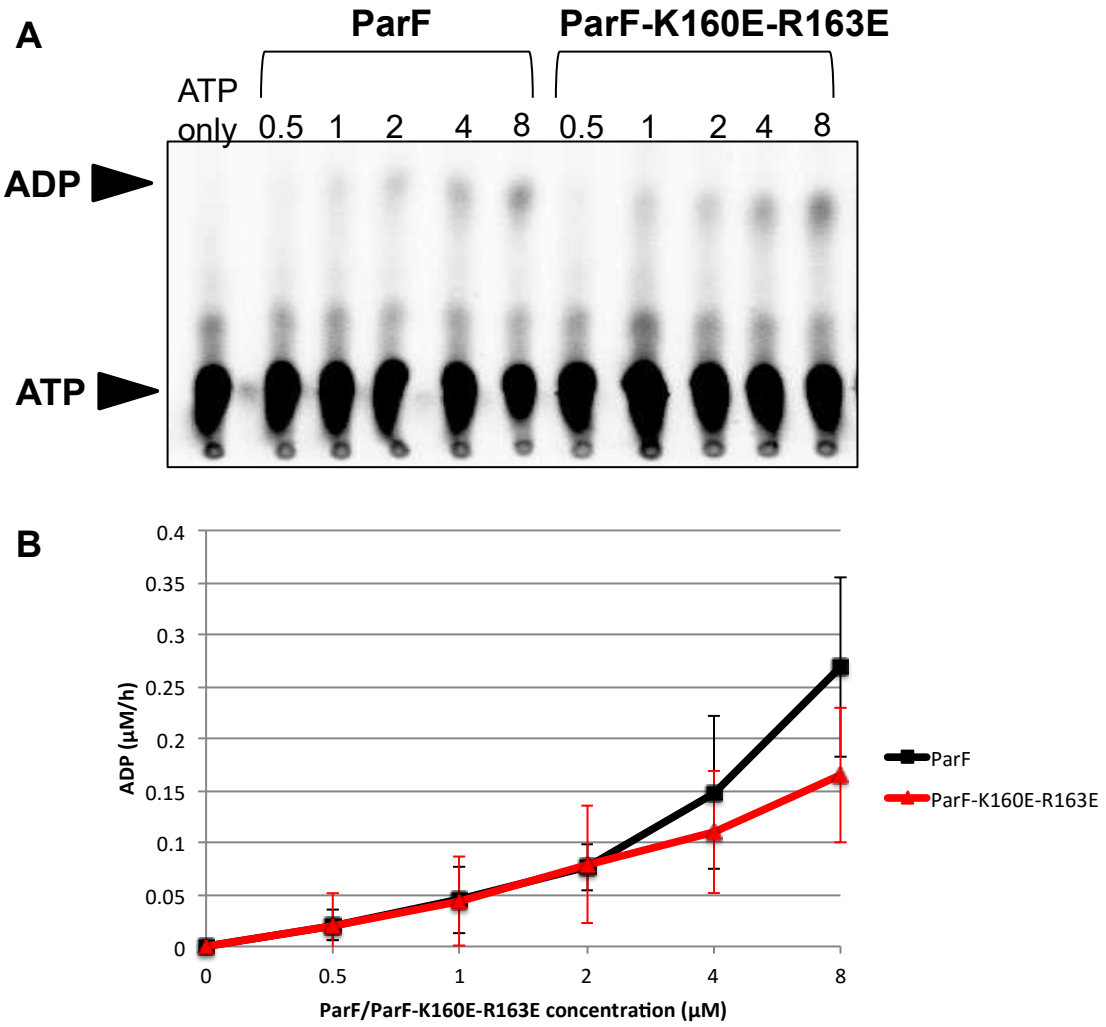

Figure 5.13 - Intrinsic ATPase activity of ParF-K160E-R163E. A) An example autoradiographic image showing the results of a representative ATPase assay in which radioactive ATP ([α^{35S}] ATP) was incubated with ParF and ParF-K160E-R163E. ATP and ADP (indicated by black arrow heads) were separated by TLC. Experiments were performed in triplicate and error bars represent the standard error of mean. B) ATP hydrolysis plotted as a function of ParF/ParF-K160E-R163E concentration. The graph represent the average of three experiments and is not directly representing the image shown in A. ParF is shown in black and ParF-K160E-R163E is shown in red.

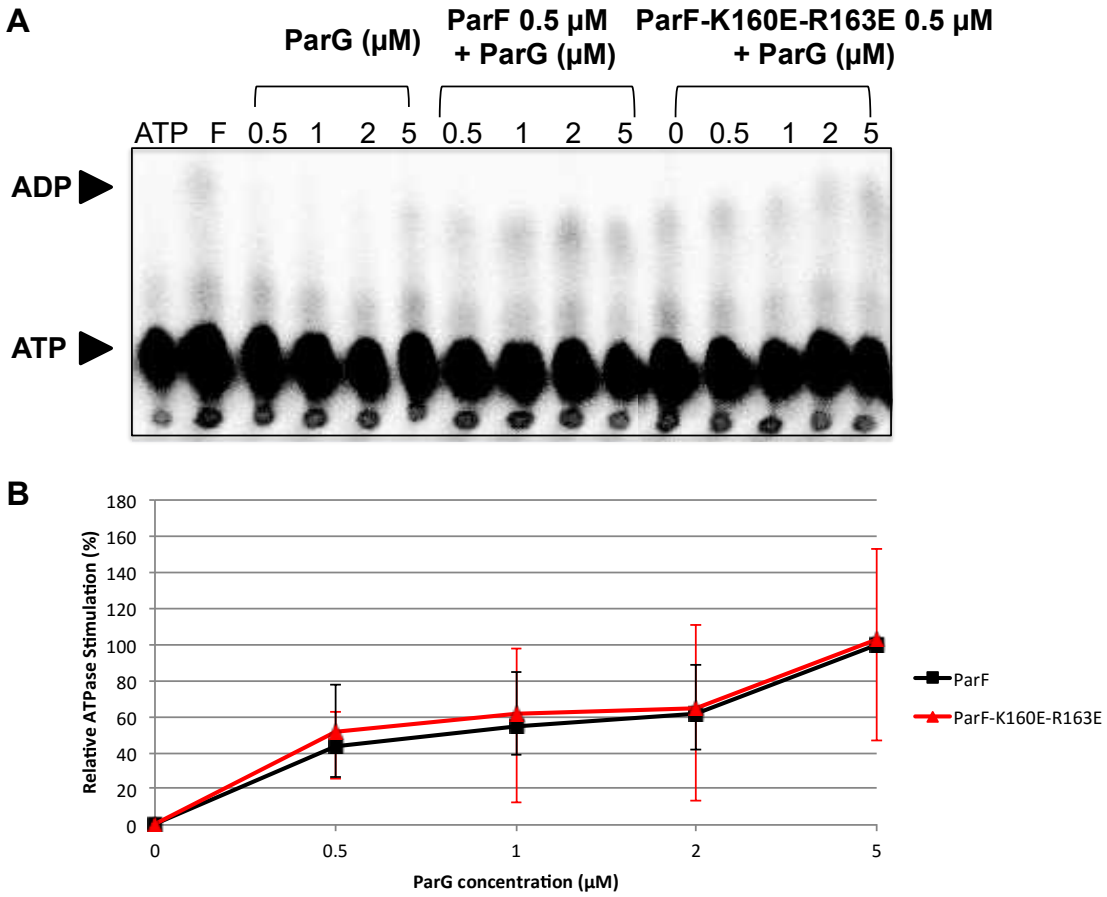

Figure 5.14 - ATPase activity of ParF-K160E-R163E in the presence of ParG. A) An example autoradiographic image showing the results of a representative ATPase assay in which radioactive ATP ([α^{35S}] ATP) and ParG was incubated with ParF and ParF-K160E-R163E. ParG was tested without ParF to check for the presence of potential contaminating ATPase activities. ATP and ADP (indicated by black arrow heads) were separated by TLC. Experiments were performed in triplicate and error bars represent the standard error of mean. B) Relative ATPase stimulation (%) plotted as a function of increasing ParG concentration. The graph represent the average of three experiments and is not directly representing the image shown in A. ParF is shown in black and ParF-K160E-R163E is shown in red.

5.4.3 ParF-R139A – ParF- R139A interaction and ParF-R139A – ParG interaction are stronger than the wild type ParF interactions

The ability of ParF-R139A and ParF-K160E-R163E to form a dimer was firstly analysed by chemical cross-linking and then by using the bacterial two-hybrid system followed by quantification using a β-galactosidase assay. The bacterial two-hybrid and β-galactosidase assays were also employed to analyse the interaction of the mutant proteins with ParG.

Chemical cross-linking with dimethyl pimelimidate (DMP) was carried out as detailed in section 2.11. ParF forms a dimer in the presence of 0.5 mM DMP and at higher concentrations the intensity of the dimeric band increases. Dimerisation is only observed in the presence of ATP and in addition of ADP no dimerisation is observed (data not shown). Bands at higher molecular weights can also be seen at the higher concentrations of DMP, these bands represent larger ParF complexes that are also being cross-linked. Both ParF-R139A and ParF-K160E-R163E, like the wild type protein, form dimers at 0.5 mM DMP and again the intensity of the dimer band and higher molecular weight species increase with increasing DMP concentrations (Figure 5.15).

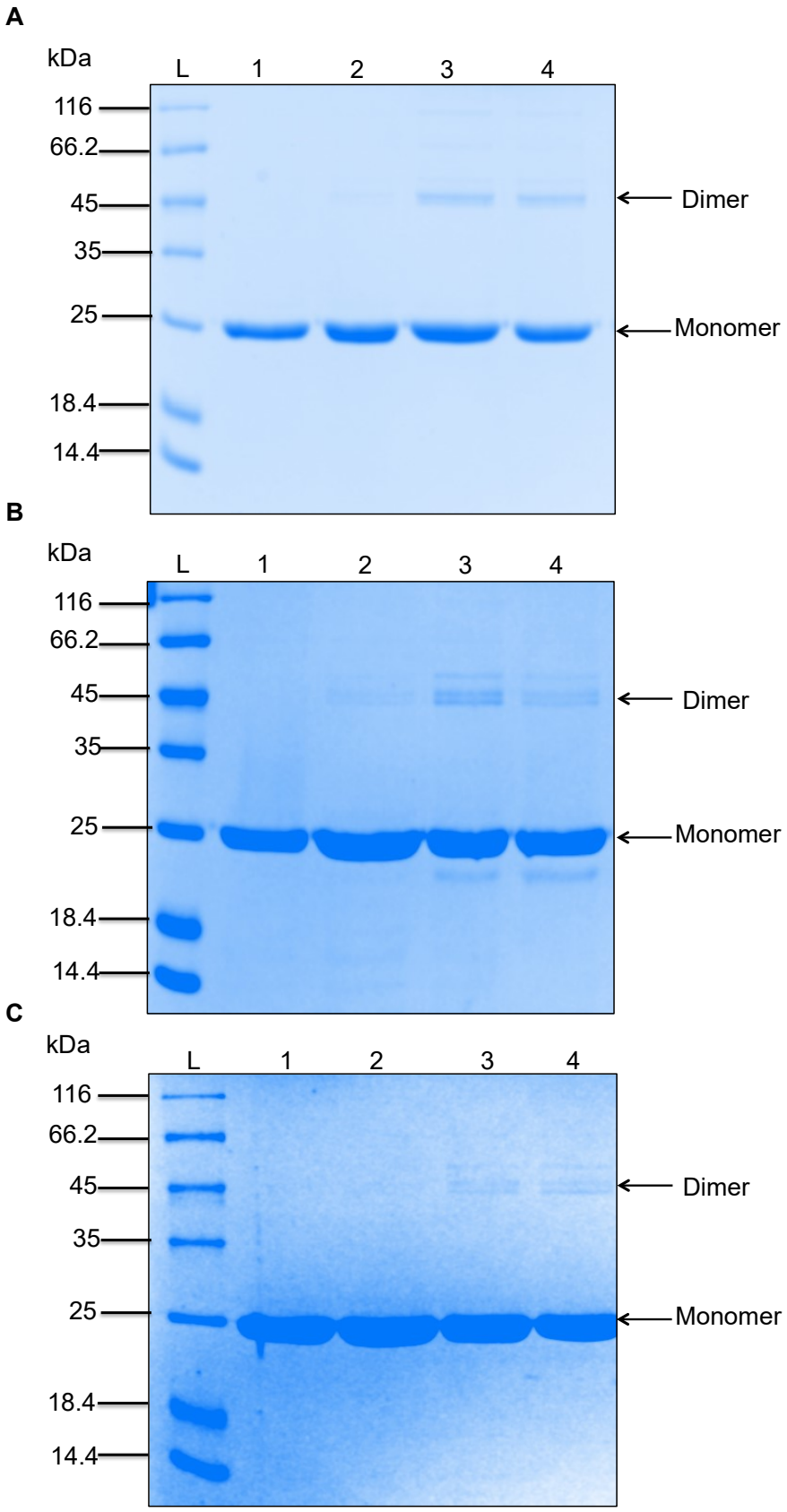

Figure 5.15 – Crosslinking results of ParF-R139A and ParF-K160E-R163E. SDS-polyacrylamide gels showing cross-linked products following two hours incubation with increasing concentrations of DMP. Lanes: L, Unstained Protein MW marker; 1, Protein only; 2, 0.5 mM DMP; 3, 1 mM DMP; 4, 10 mM DMP. A) ParF B) ParF-R139A.C) ParF-K160E-R163E

To further confirm that ParF-R139A and ParF-K160E-R163E were able to form a dimer, a bacterial two-hybrid assay was employed and to quantify this interaction a β-galactosidase assay was carried out. These assays were also used to investigate if ParF-R139A and ParF-K160E-R163E were able to interact with ParG similarly to the wild type protein. The bacterial two-hybrid system used to study protein-protein interactions *in vivo* (Karimova *et al*., 1998) was carried out as detailed in section 2.9. Cloning of *parF-R139A* and *parF-K160E-R163E* was carried out as described in 2.4.2. Examples of cloning for bacterial two-hybrid assays for other *parF* mutants are detailed in Chapter 3.

The results of both assays confirmed those observed for the cross-linking indicating that ParF-R139A and ParF-K160E-R163E are able to form dimers (Figure 5.16). The results obtained for ParF-K160E-R163E were almost identical to that of ParF and very little difference could be observed in both the bacterial two-hybrid results and the quantification of the β-galactosidase assay. As for ParF-R139A, the bacterial two-hybrid appeared to show a slightly darker red colour compared to that observed for ParF, suggesting the interaction of ParF-R139A with itself might be slightly stronger than the ParF-ParF interaction. This was confirmed in the β-galactosidase assay as the ParF-R139A-ParF- R139A interaction showed on average 100 Miller units more than ParF-ParF. It was reported in Dobruk-Serkowska, A. *et al.* (2012) that the self-association of ParF-R169A was detectably stronger than that of ParF-ParF, with ParF-R169A-ParF-R169A producing ~ 300 - 500 Miller units more than ParF-ParF. The self-association of ParF-R139A does not appear to be as strong as that for ParF-R169A, however it clearly demonstrates a stronger self-association than the wild type protein.

The interaction of ParF-R139A and ParF-K160E-R163E with ParG was then investigated. Again, the results obtained for ParF-K160E-R163E were almost identical to that of ParF and very little difference could be observed in both the bacterial two-hybrid results and the quantification of the β-galactosidase assay. ParF-R139A showed a slightly stronger interaction with ParG compared to the wild type protein, confirming that ParF- R139A was still able to interact with ParG. On average the ParF-P139A-ParG interaction produced ~ 300 Miller units more than ParF-ParG (Figure 5.17). Again these results are similar to those observed for ParF-R169A, in Dobruk-Serkowska, A. *et al.* (2012), that also showed a detectably stronger interaction with ParG. It is becoming

evident that disruption of the ATP binding pocket of ParF alters the self-association of the protein, as well as the interaction with ParG. As discussed in Chapter 4, residues that are positioned at the monomer-monomer interface and in proximity to the ATP binding pocket are important in the interactions of ParF with itself and ParG and now residue R139 has been shown to belong to this subset of amino acids. On the other hand, ParF-K160E-R163E is positioned away from the ATP binding pocket of ParF and these changes have not affected the ATP binding and hydrolysis or the monomer-monomer and ParG interactions.

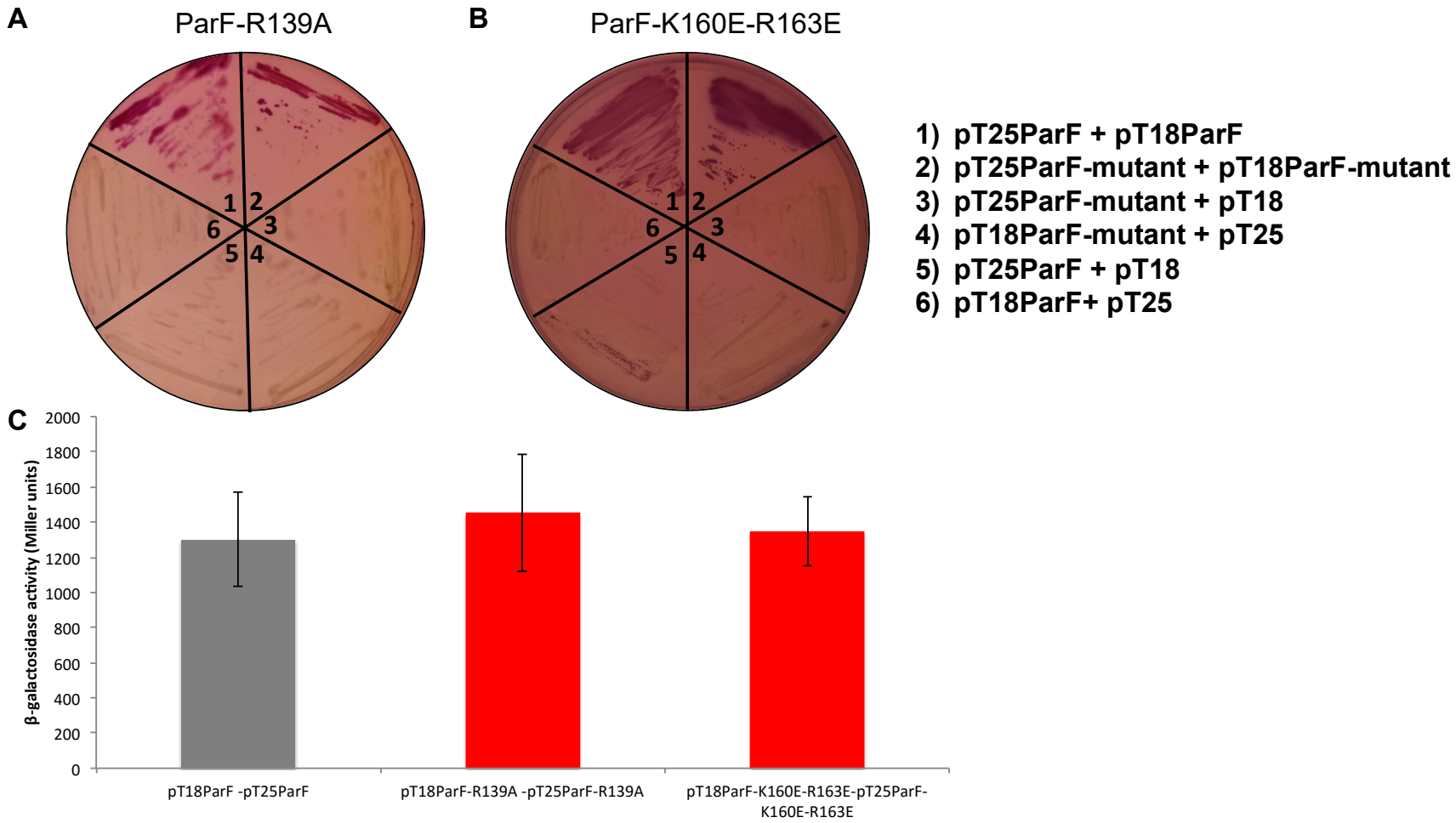

Figure 5.16 – Bacterial two-hybrid and β-galactosidase assay of ParF-R139A and ParF-K160E-R163E. A) Bacterial two-hybrid assay for ParF-R139A and ParF-K160E-R163E. Plasmids carrying *parF* or *parF-R139A* or *parF-K160E-R163E* are fused to T25 and T18 fragments were co-transformed into *E. coli* SP850 and streaked on MacConkey-maltose plates. A) ParF-R139A bacterial two-hybrid assay. B) ParF-K160E-R163E bacterial two-hybrid assay. C) β-galactosidase assay. The level of ParF-ParF interaction is shown in grey and mutant protein interactions in red. The assay was carried out in triplicate and error bars represent the standard error of mean.

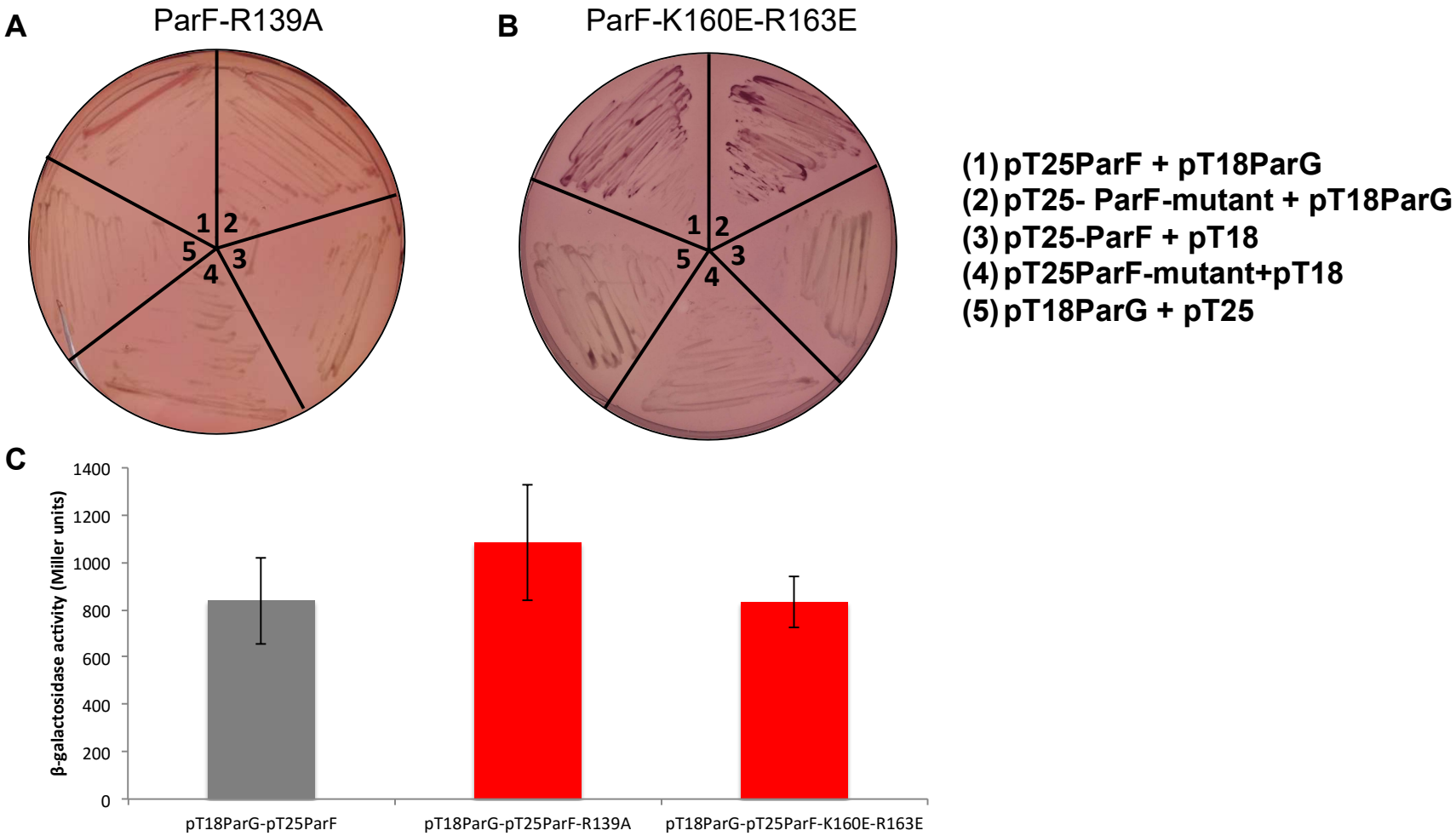

Figure 5.17 - Bacterial two-hybrid and β-galactosidase assay of ParF-R139A-ParG and ParF-K160E-R163E-ParG. A) Bacterial two-hybrid assay for ParF-R139A-ParG interaction and ParF-K160E-R163E-ParG interaction. Plasmids carrying *parF, parF-R139A or parF-K160E-R163E* are fused to T25 and *parG* fused to T18 were co-transformed into *E. coli* SP850 and streaked on MacConkey-maltose plates. A) ParF-R139A bacterial two-hybrid assay. B) ParF-K160E-R163E bacterial two-hybrid assay. C) β-galactosidase assay. The quantitation of ParF-ParG interaction is shown in grey and the mutant proteins interaction is shown in red. The assay was carried out in triplicate and error bars represent the standard error of mean.

5.4.4 ParF-R139A has a higher tendency to self-associate into higher order structures and the ability of ParF-K160E-R163E to assemble into higher order structures is disrupted

As previously shown in this work (Chapter 4), ParF mutants that have shown a stronger self-association than ParF have a higher tendency to self-associate into higher order structures. This was thought to be due to the fact that the residues that were changed were located close to the ATP binding pocket and caused a conformational change that favoured the self-association of the ParF mutants. In addition, ParF-R169A was also observed to have a higher tendency to self-associate into higher order structures in the absence of nucleotide (Dobruk-Serkowska *et al*., 2012). It was therefore reasonable to speculate that the same characteristic might be displayed by ParF-R139A. On the other hand, all previous *in vitro* characterisation of ParF-K160E-R163E demonstrated that the mutant protein displayed properties almost identical to those of the wild type protein and the reason for the disruption in plasmid segregation was still elusive. The ability of ParF-R139A and ParF-K160E-R163E to form higher order structures *in vitro* was investigated using dynamic light scattering (DLS) as detailed in section 2.12 and then with sedimentation assays (section 2.17) to further support the DLS results. As previously shown (Barilla *et al*., 2005) and discussed Chapter 3, ParF is able to assemble into higher order structures in the presence of ATP and this is antagonised by ADP. In addition, it has also been observed that ParG promotes ParF polymer formation, both in the presence and absence of ATP. The assembly of ParF-R139A and ParF-K160E-R163E into higher order structures was observed in the absence of nucleotide and in the presence of ADP, ATP, ATP-γ-S and ParG. All DLS experiments were carried out in parallel with ParF, the proteins were monitored over 60 minutes and changes in intensity of light scattering were observed (Figure 5.18).

In the absence of nucleotide ParF-R139A showed an increase in intensity of light scattering over time and compared to the wild type ParF the increase was higher. This suggests ParF-R139A has a higher tendency to self-associate as compared to wild type ParF. The addition of nucleotides appeared to inhibit this self-association: this observation held true also for ATP, demonstrating that ParF-R139A does not show ATP-dependent self-association into higher order structures (Figure 5.18). Upon the addition of ParG to ParF-R139A the intensity of light scattering did increase slightly, indicating that ParG could promote ParF-R139A assembly into bundles. However, this increase was relatively small compared to that observed when ParG is added to ParF

(Figure 5.19). The fact that ParF-R139A was observed to have a stronger interaction with ParG supports these findings and demonstrates that the addition of ParG, in this instance, is able to override the inhibitory effect of nucleotide on ParF-R139A self-association into higher order structures.

The results presented for ParF-K160E-R163E are notably different from those of ParF-R139A, and in fact from those of any other mutant proteins studied. In the absence of nucleotide, ParF-K160E-R163E showed no increase in intensity of light scattering indicating that the mutant was unable to self-associate into higher order structures. Upon the addition of ATP or ATP-γ-s, ParF-K160E-R163E did assemble into higher order structures as demonstrated by an increase in intensity of light scattering (Figure 5.18). However, unlike the wild type protein, this increase was not immediate upon addition of ATP or ATP-γ-s, instead a more gradual increase was observed. Although an obvious increase in intensity of light scattering is observed, the maximum intensity reached by ParF-K160E-R163E is lower compared to wild type ParF. This may be a result of the more gradual increase observed and it is reasonable to suggest that if ParF K160E-R163E was observed over a longer time period the same level of intensity might be reached. As for ParF-R139A, ParG was able to promote ParF-K160E-R163E assembly into higher order structures (Figure 5.20).

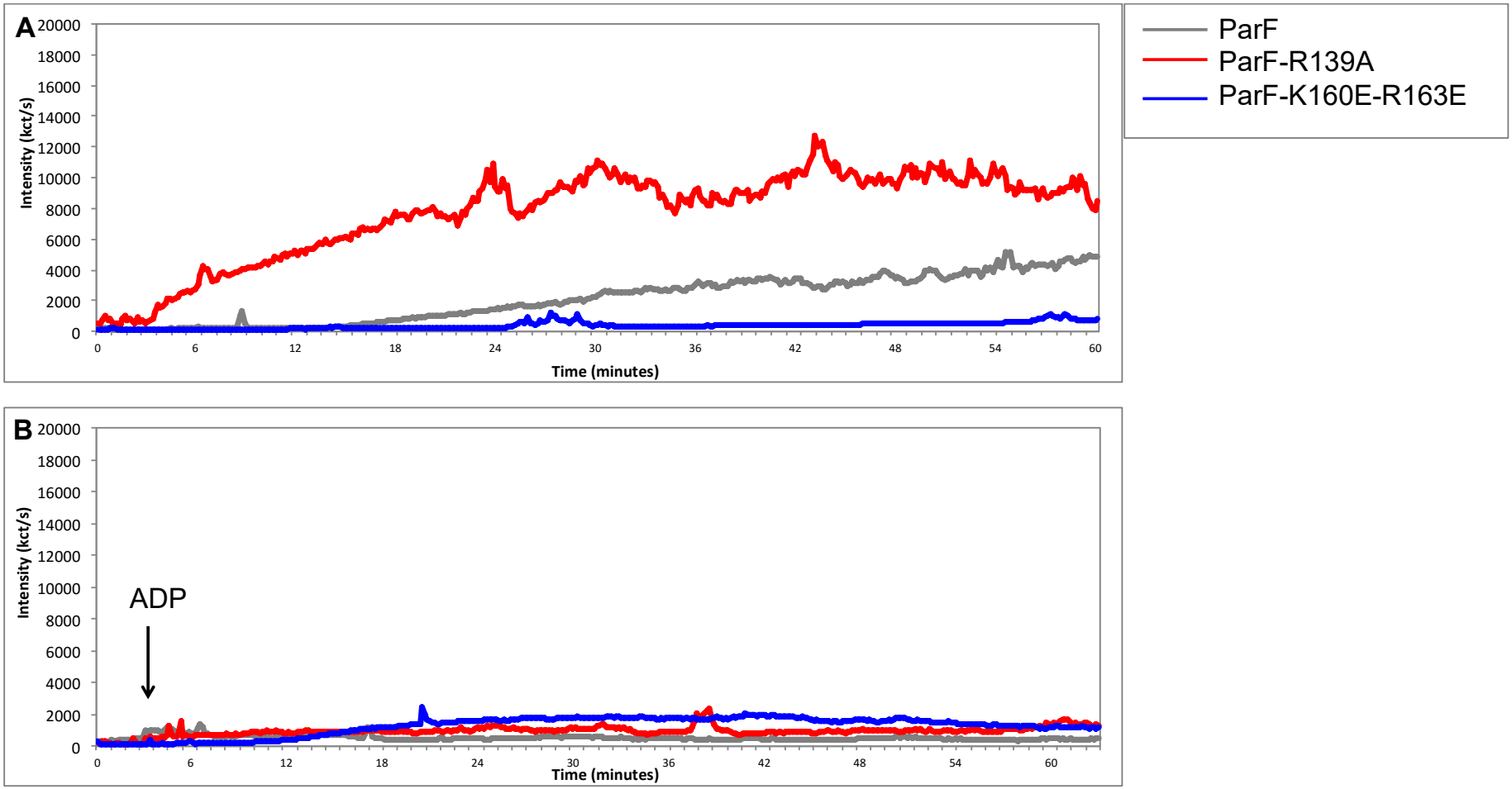
A
B
Intensity (kct/s)
Time (minutes)
ADP
ParF
ParF-R139A
ParF-K160E-R163E

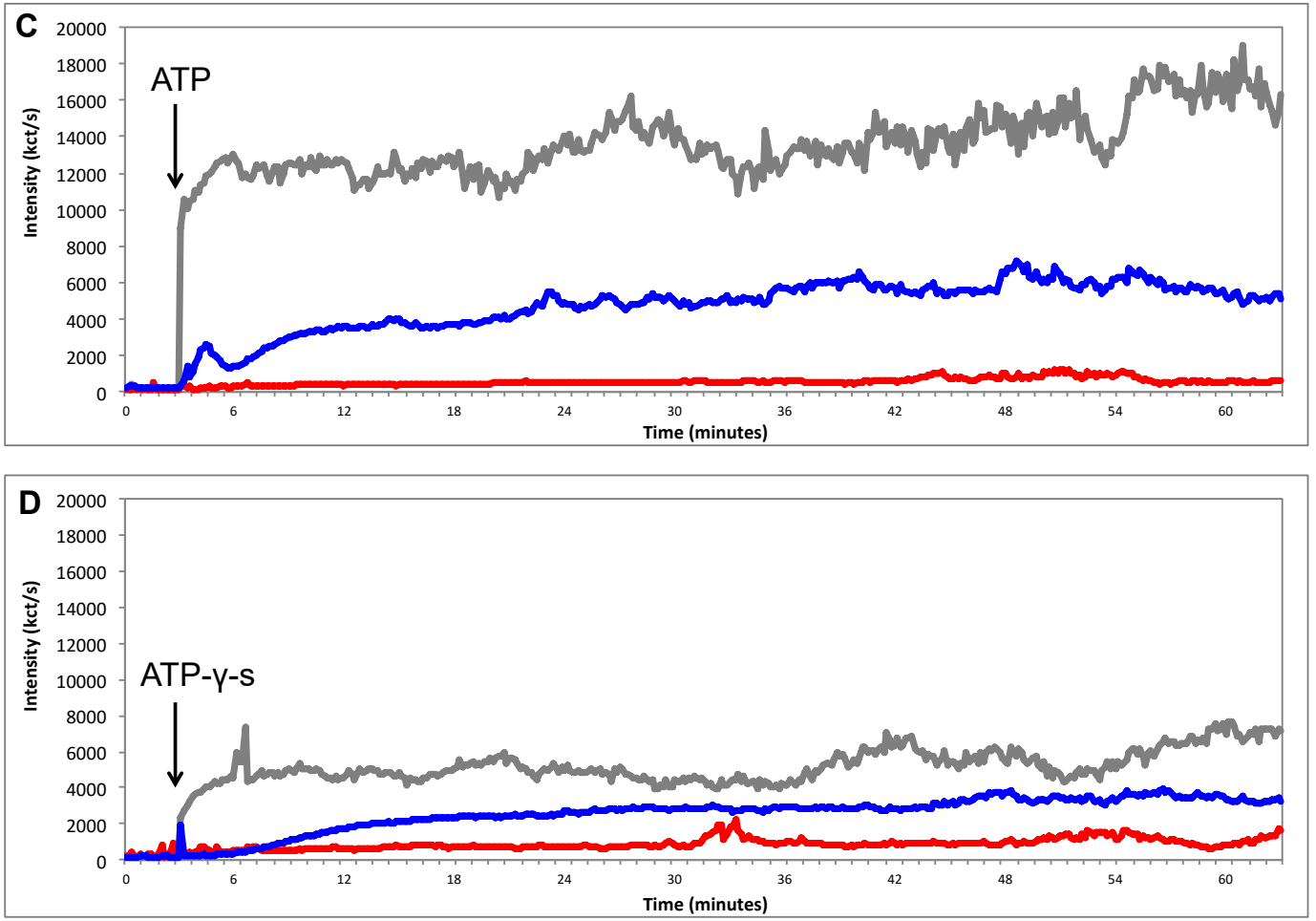

Figure 5.18 – DLS of ParF-R139A and ParF-K160E-R163E. DLS experiments were carried out and the increase in light scattering intensity (kct/s) was recorded for ParF, ParF-R139A and ParF-K160E-R163E. Proteins were present at a final concentration of 2.16 µM and a baseline was obtained for three minutes and then nucleotide was added (500 µM) with $MgCl_2$ (5 mM). The point of addition is indicated by a black arrow. The light scattering intensity was then recorded for further 60 minutes. ParF is shown in grey, ParF-R139A in red and ParF-K160E-R163E in blue. A) No nucleotide B) ADP C) ATP D) ATP-γ-S. This is a representative experiment. Experiments were carried out in triplicate.

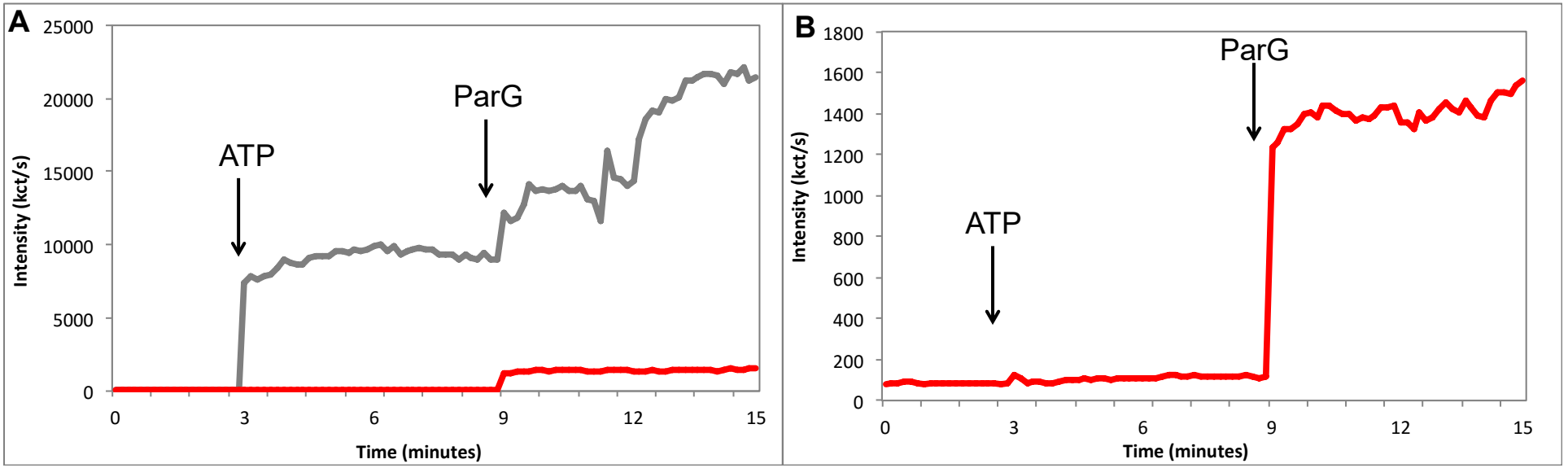

Figure 5.19 – DLS of ParF-R139A in the presence of ParG. DLS experiments were carried out and the increase in light scattering intensity (kct/s) was recorded for ParF and ParF-R139A. ParF and ParF-R139A were present at a final concentration of 2.16 µM and a baseline was obtained for three minutes. ATP was added (500 µM) with $MgCl_2$ (5 mM) at the point indicated by a black arrow. The light scattering intensity was then recorded for a further six minutes before ParG was added at a final concentration of 2.16 µM, as indicated by a black arrow, and the intensity recorded for a further six minutes. ParF is shown in grey and ParF-R139A is shown in red. A) The effect of both ATP and ParG on the assembly of ParF-R139A into higher order structures. B) The effect of both ATP and ParG on the assembly of ParF-R139A into higher order structures, only ParF-R139A (red) is shown on a smaller scale to indicate more clearly any changes in intensity of light scattering. This is a representative experiment. Experiments carried out in triplicate.

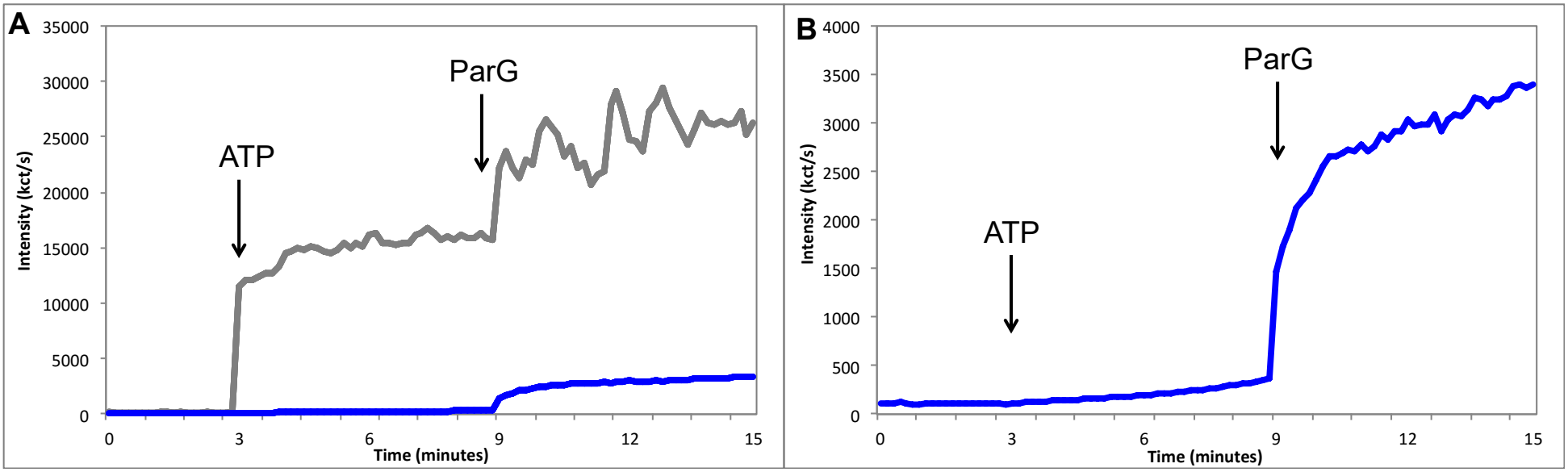

Figure 5.20 – DLS of ParF-K160E-R163E in the presence of ParG. DLS experiments were carried out and the increase in light scattering intensity (kct/s) was recorded for ParF and ParF-K160E-R163E. ParF and ParF-K160E-R163E were added at a final concentration of 2.16 µM and a baseline was monitored for three minutes. ATP was added (500 µM) with $MgCl_2$ (5 mM) at the point indicated by a black arrow. The light scattering intensity was then recorded for a further 6 minutes before ParG was added at a final concentration of 2.16 µM, indicated by a black arrow, and the intensity recorded for further six minutes. ParF is shown in grey and ParF-K160E-R163E is shown in blue. A) The effect of both ATP and ParG on the assembly of ParF and ParF-K160E-R163E into higher order structures. B) The effect of both ATP and ParG on the assembly of ParF-K160E-R163E into higher order structures, shown on a smaller scale to indicate more clearly any changes in intensity of light scattering. This is a representative experiment. Each experiment was repeated at least in triplicate.

Sedimentation assays were carried out in order to gather more quantitative results as well as to compare ParF-R139A assembly into higher order structures with ParF-R169A. The results did further support those observed in the DLS experiments. The results for ParF-K160-R163E did demonstrate that this mutant is unable to self-associate into higher order structures in the absence of nucleotide as only a very small amount of the protein was detected in the pellet fraction. In the presence of nucleotide the amount of ParF-K160-R163E detected in the pellet was still very small (Figure 5.21). In the DLS experiments upon the addition of ATP or ATP-γ-s, ParF-K160-R163E was observed to assemble into higher order structures gradually however this is not detected in the sedimentation assays. This is likely due to the fact that in the sedimentation assays the proteins are only incubated for ten minutes and clearly ParF-K160-R163E demonstrates a much slower response to ATP or ATP-γ-s. The results observed when ParG was added also supported the findings from the DLS experiments. In the absence of nucleotide but in the presence of ParG the amount of ParF-K160E-R163E detected in the pellet increases slightly. In the presence of both ATP and ParG, a significant increase in the amount of ParF-K160E-R163E detected in the pellet was observed clearly demonstrating that ParG is able to promote ParF- K160E-R163E assembly into higher order structures. It should also be noted that the amount of ParG detected in the pellet was almost identical for ParF and ParF-K160E-R163E demonstrating the interaction of the mutant proteins with ParG is similar to that of ParF-ParG (Figure 5.23).

The results for ParF-R139A demonstrated that an increased proportion of ParF-R139A was detected in the pellet fraction compared to that observed for ParF indicating that ParF-R139A has a higher tendency to self-associate into higher order structures in the absence of nucleotide. Upon the addition of nucleotide the amount of ParF-R139A detected in the pellet decreased, however there was still a noticeable amount. This feature is different from that observed in the DLS experiments, where upon addition of nucleotide the self-assembly of ParF-R139A appeared to be inhibited. However, when comparing the intensity of the bands for ParF and ParF-R139A with ATP/ATP-γ-s there is noticeably less ParF-R139A in the pellet fraction compared to the amount observed for ParF (Figure 5.22). The variation in the results observed for DLS and sedimentation assays is likely to be due to the accuracy of quantification of the bands in the sedimentation assays due to the intensity levels. However, the results upon the addition of ParG are much more apparent. In the absence of nucleotide but in the presence of

ParG the amount of ParF-R139A and ParF-R169A detected in the pellet increases slightly. In the presence of both ATP and ParG, the amount of ParF-R139A detected in the pellet more than doubles clearly demonstrating that ParG is able to promote ParF-R139A assembly into higher order structures. The results observed here for ParF-R169A confirm those shown in Dobruk-Serkowska, A. *et al.* (2012). The amount of ParG detected in the pellet increases when either ParF-R139A or ParF-R169A are present, this firstly confirms that ParF-R139A and ParF-R169A are able to interact with ParG and also that ParG is able to promote the assembly into higher order structures (Figure 5.23).

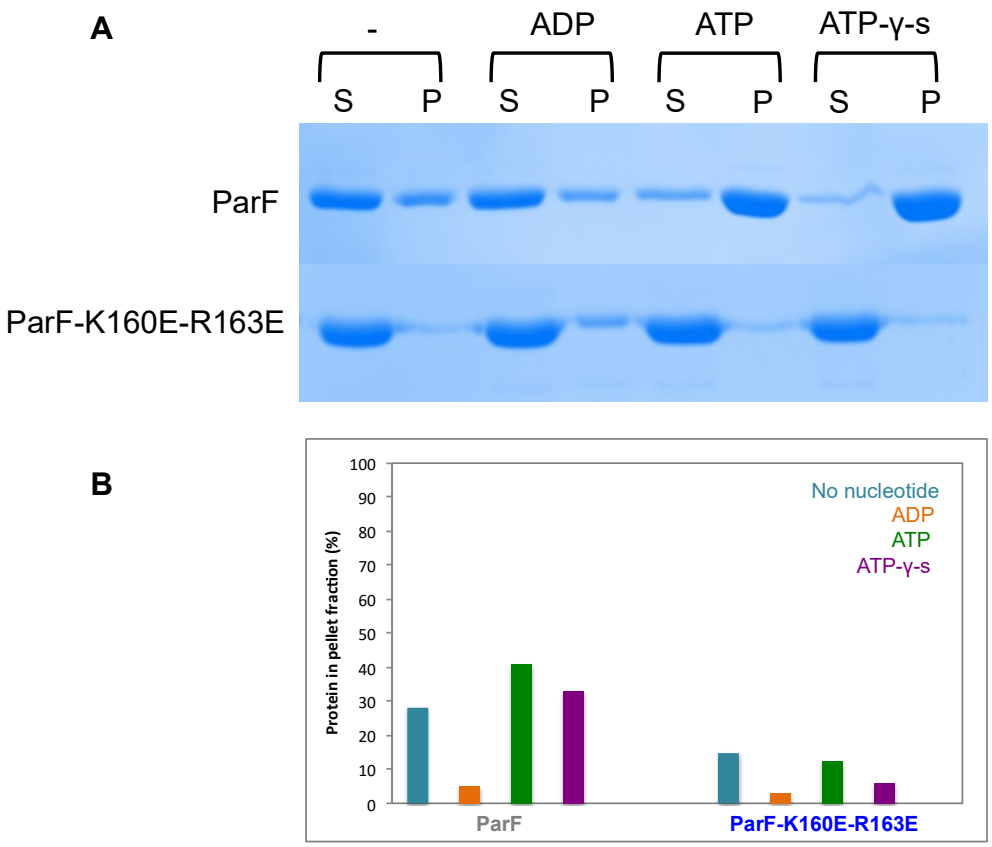

Figure 5.21 – Sedimentation assay of ParF-K160E-R163E. ParF and ParF-K160E-R163E (10 μM) were incubated with and without nucleotide and separated on a 15 % SDS gel. 100% of pellet (P) fraction and 33% of supernatant (S) fractions were resolved on gels. A) Representative gel of sedimentation assay of ParF and ParF-K160E-R163E. Assays are repeated in triplicate. B) Graph showing the percentages of ParF and ParF-K160E-R163E recovered in the pellet.

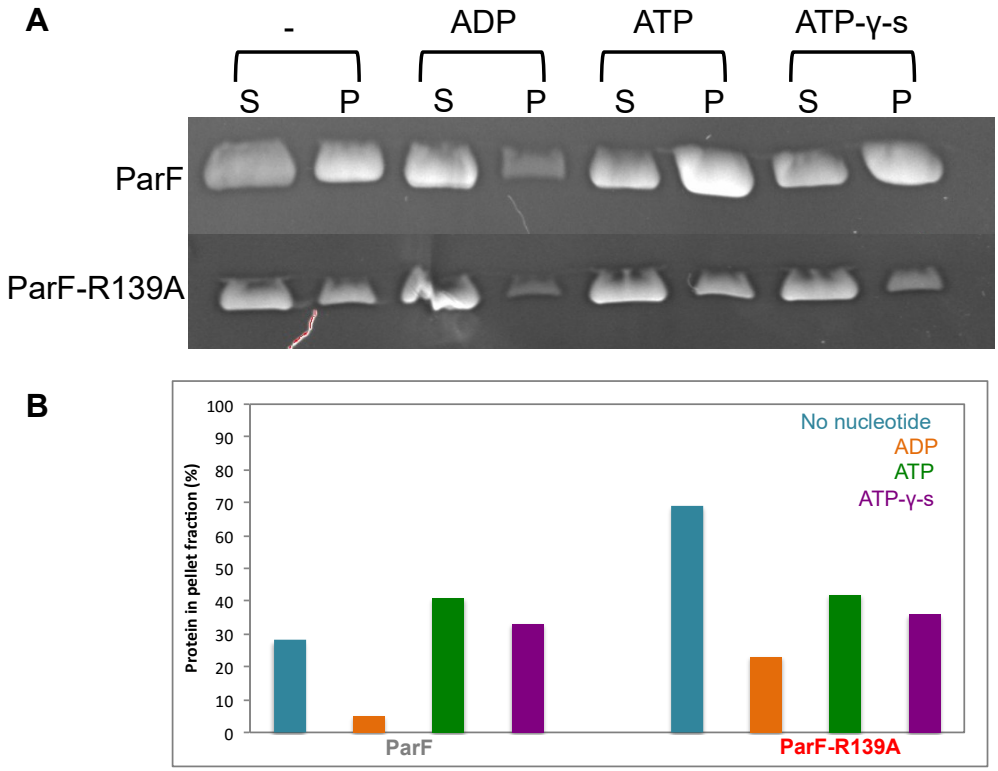

Figure 5.22 - Sedimentation assay of ParF - R139A. ParF and ParF-R139A (10 µM) were incubated with and without nucleotide and separated on a 15 % SDS gel. 100% of pellet (P) fraction and 33% of supernatant (S) fractions were resolved on gels. A) Representative gel of sedimentation assay of ParF-R139A. Assays were repeated in triplicate. B) Graph showing the percentages of ParF-R139A recovered in the pellet.

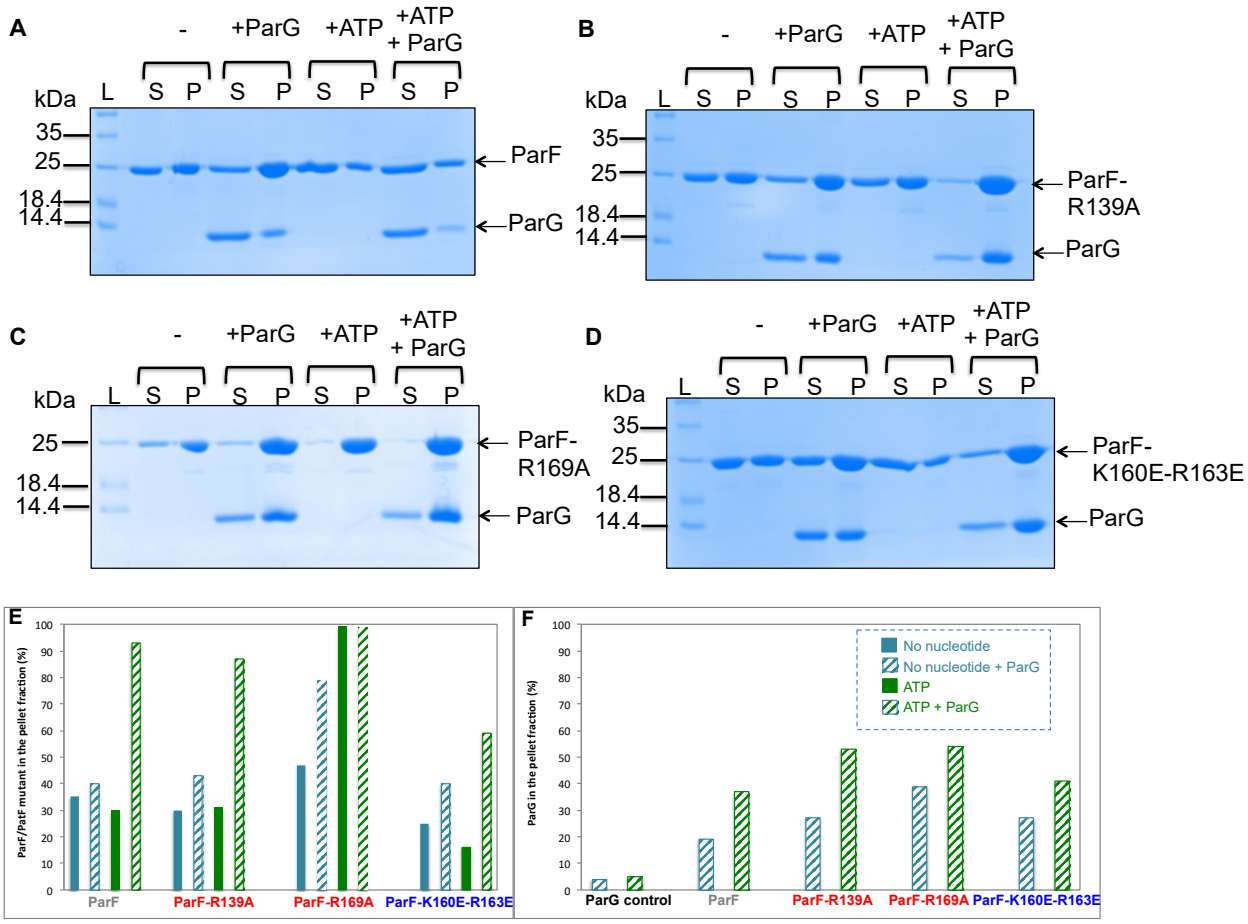

Figure 5.23 - Sedimentation assay of ParF-R139A, ParF-R169A and ParF-K160E-R163E in the presence of ParG. ParF, ParF-R139A, ParF-R169A and ParF-K160E-R163E (10 µM) were incubated with and without ATP and ParG and separated on a 15 % SDS gel. 100% of pellet (P) fraction and 33% of supernatant (S) fractions were resolved on gels. Assays were repeated in triplicate. A) Representative gel of sedimentation assay of ParF with ParG. B) Representative gel of sedimentation assay of ParF-R139A with ParG. C) Representative gel of sedimentation assay of ParF-R169A with ParG. D) Representative gel of sedimentation assay of ParF-K160E-R163E with ParG. E) Graph showing the percentage of ParF, ParF-R139A, ParF-R169A and ParF-K160E-R163E found in the pellet. F) Graph showing the percentage of ParG recovered in the pellet from the same sedimentation assay. A ParG only control is shown on this graph.

5.4.5 ParF-R139A, ParF-R169A and ParF-K160E-R163E nsDNA binding is disrupted *in vitro*

The ability of ParF-R139A, ParF-R169A and ParF-K160E-R163E to bind DNA *in vitro* was analysed by fluorescence anisotropy and EMSA. Firstly, fluorescence anisotropy experiments were carried out as per section 2.15. The experimental setup was identical to that described previously for wild type ParF, experiments were performed in parallel with ParF to enable fair comparisons of binding. ParF was observed to bind the nsDNA in the presence of ATP and ATP-γ-s with a K_d of ~ 300 nM, but not in the presence of ADP or in the absence of nucleotide. ParF-R139A, ParF-R169A and ParF-K160E-R163E were observed not to bind DNA, either in the absence or presence of nucleotide. No significant change in anisotropy could be seen under any of the conditions, any increase was small and when compared to wild type ParF clearly demonstrated there was no DNA binding (Figure 5.24).

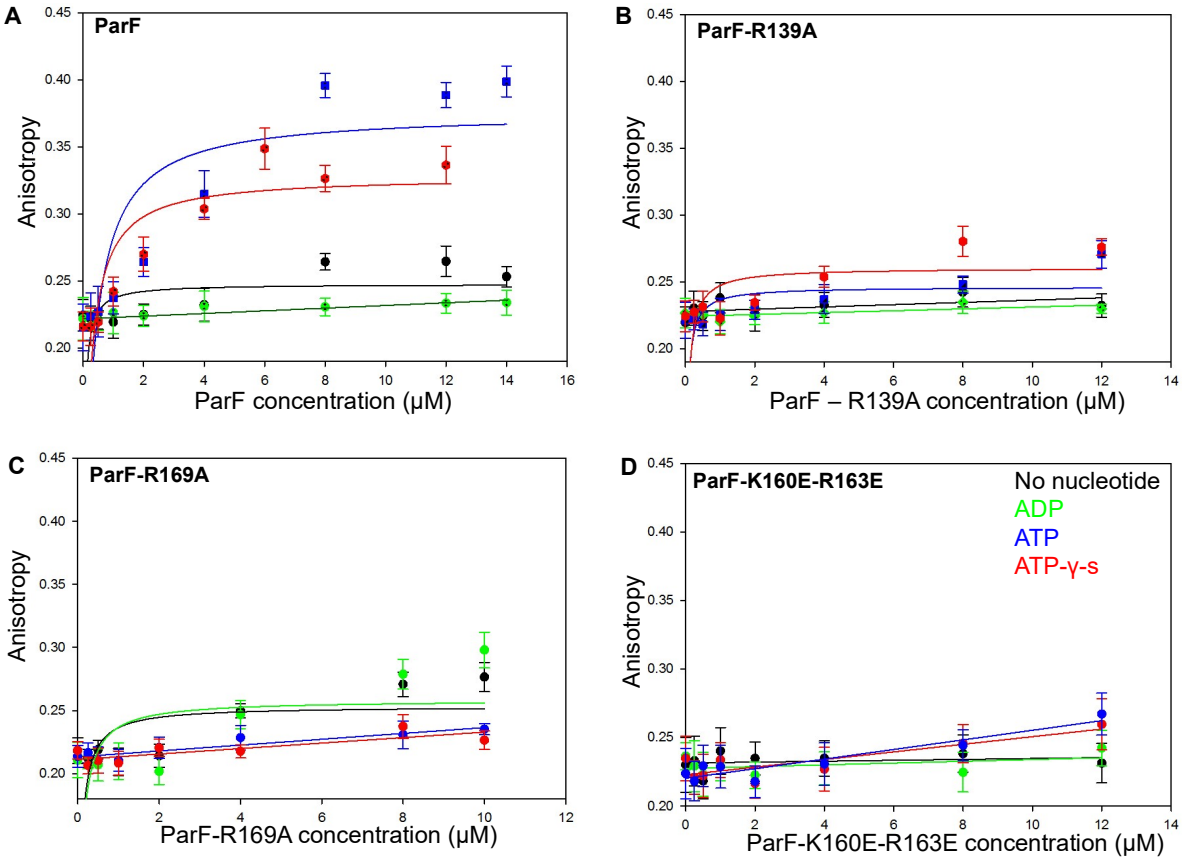

Figure 5.24 – Fluorescence anisotropy analysis of ParF-R139A, ParF-R169A and ParF-K160E-R163E nsDNA binding. Fluorescence anisotropy studies in which increasing concentrations of ParF or ParF mutants were incubated with a fluorescent 40 bp DNA fragment harbouring a random sequence. The analysis of DNA binding was carried out in the presence of different nucleotides. No nucleotide is shown in black, ADP is shown in green, ATP is shown in blue and ATP-γ-s is shown in red. Ten anisotropy values are taken for each concentration and the average value is calculated. Error bars represent the standard error of the mean. These are representative experiments. Assays were repeated in triplicate. A) ParF B) ParF-R139A C) ParF-R169A. D) ParF-K160E-R163E.

EMSAs were performed in order to confirm the results observed for fluorescence anisotropy (Figure 5.25). As previously discussed, when ParF was incubated with the biotinylated DNA fragment without nucleotide or in the presence of ADP, no band-shift occurred. When ATP and ATP-γ-s were present in the reaction a band-shift was observed, indicating ParF binds nsDNA in an ATP-dependent manner. No obvious band-shift was observed for ParF-R139A or ParF-K160E-R163E, confirming that both were unable to bind nsDNA *in vitro*. The results are similar for ParF-R169A, however a small band-shift was observed at the highest ParF-R169A concentration when ATP was present, suggesting nsDNA binding but with a lower affinity than wild type ParF. However, overall the results indicate that ParF-R139A, ParF-R169A and ParF-K160E-R163E are unable to bind to DNA *in vitro* in the same fashion as wild type ParF.

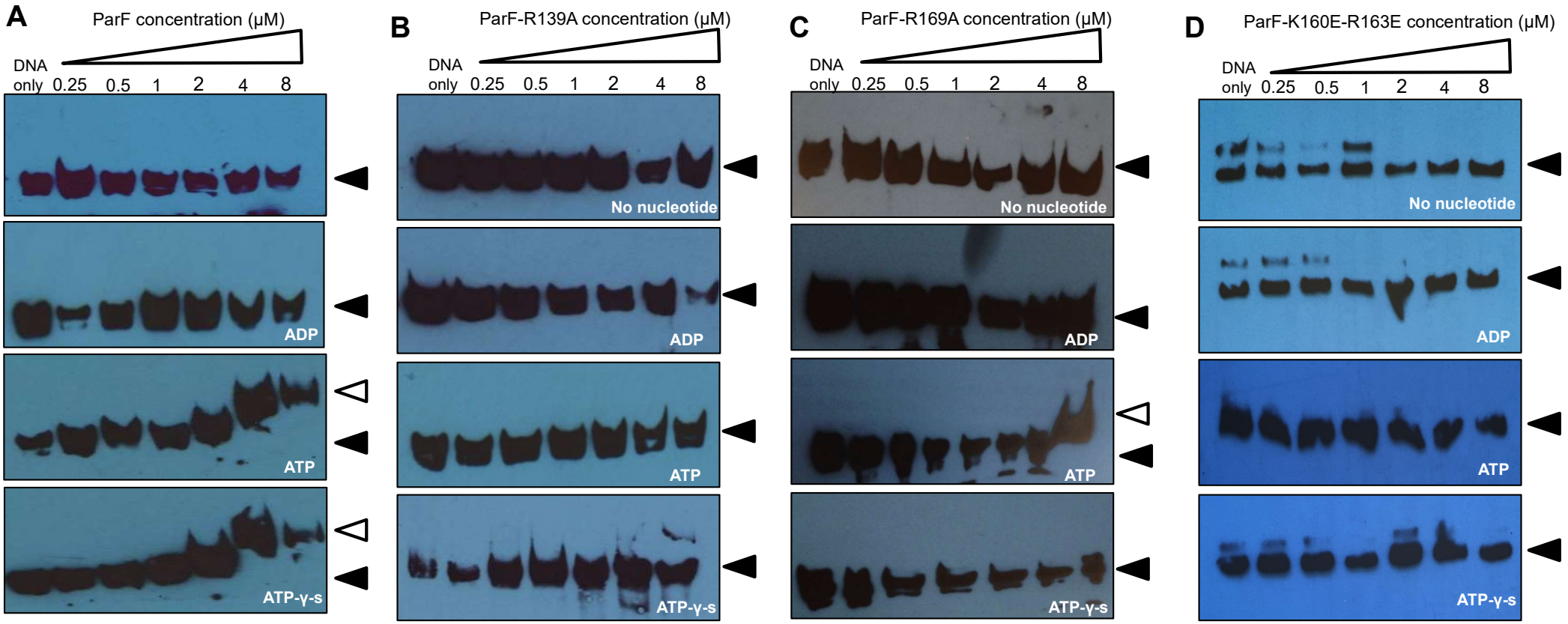

Figure 5.25 – EMSA of ParF-R139A, ParF-R169A and ParF-K160E-R163E. Representative EMSAs performed with ParF and ParF mutants. Increasing concentrations of ParF/ParF mutants were incubated with a 123 bp biotinylated DNA fragment harbouring the *parFG* operator sequence in the absence of nucleotide or the presence of ADP, ATP or ATP-γ-s. Unbound DNA is indicated by a black arrowhead, a shifted nucleoprotein complex is indicated by a white arrowhead. Assays are repeated in at least triplicate. A) ParF B) ParF-R139A C) ParF-R169A D) ParF-K160E-R163E.

5.4.6 ParF-R139A, ParF-R169A and ParF-K160E-R163E are homogenously distributed over the nucleoid *in vivo* and are unable to oscillate

ParF shows an oscillatory behaviour and is able to form a dynamic pattern on the nucleoid (McLeod et al., 2016) and Chapter 3 of this work. Mutant *parF* alleles have been cloned into two plasmids, pBM20 and pBM40, in order to investigate the *in vivo* localisation. Details of the plasmids used for microscopy and cloning mutant *parF* alleles are described in Chapter 3. In order to visualise ParF, ParF-R139A, ParF-R169A, ParF-K160E-R163E and ParG the appropriate pBM20 and pBM40 plasmids are co-transformed into BW25113 *E. coli* cells and grown for four hours in the presence of antibiotics. The cells are grown in the presence of L-arabinose for three hours in order to induce expression of *parF-emerald*. The nucleoid was visualised using DAPI.

The effect of the R139A, R169A and K160E-R163E on ParF localisation and dynamics were investigated by acquiring confocal microscopy images, Z-stacks and time-lapse videos. Cells harbouring plasmids that contained the partition cassettes with the *parF-R139A* allele, *parF-R169A* and *parF-K160E-R163E* (pBM20-ParF-R139A, pBM20-ParF-R169A and pBM20-ParF-K160E-R163E) and the plasmid expressing ParF-R139A-Emerald, ParF-R169A-Emerald or ParF-K160E-R163E-Emerald (pBM40-ParF-R139A, pBM40-ParF-R169A or pBM40- ParF-K160E-R163E) were grown and imaged exactly as the wild type (as detailed in Chapter 3). The results acquired for ParF-R139A and ParF-R169A appeared very similar whereas the results observed for ParF-K160E-R163E showed some distinctive differences.

Even though the DNA binding properties of ParF-R139A and ParF-R169A were observed to be disrupted *in vitro*, observations *in vivo* revealed that both mutants still appeared to associate with the nucleoid. However the patterning differed, ParF-R139A-Emerald and ParF-R169A-Emerald were not asymmetrically distributed over the nucleoid like the wild type protein, but in fact spread homogenously over the nucleoid (Figure 5.26 and 5.27). In most cases, ParF-R139A-Emerald and ParF-R169A-Emerald also appeared to form small foci that localised with ParG foci. The majority of cells containing either ParF-R139A-Emerald or ParF-R169A-Emerald exhibited a single ParG focus, 89% and 95% of cells, respectivelty (Figure 5.28). This percentage is significantly higher than in cells containing the wild type ParF protein of which only 40% contain a single ParG focus. Both ParF-R139A and ParF-R169A show stronger interactions with ParG and therefore it is reasonable to suggest that the ParF mutants are

interacting with and accumulating on the ParG-plasmid complex. In a twenty minute time-lapse experiment, no oscillation was observed for ParF-R139A-Emerald, ParF-R169A-Emerald or ParG. The green signal remained spread throughout the nucleoid and the compact red signal persisted in the same position for the entire twenty minutes (data not shown). Although in the presence of both mutants ParG forms mostly a single focus, the position of this focus slightly differs between the two mutant backgrounds (Figure 5.28). In cells containing ParF-R139A, the ParG focus is more randomly positioned over the nucleiod although the focus does appear to be localise at midcell and the pole more often than any other position (Figure 5.29 an 5.30). This pattern is similar to that observed by McLeod, B. *et al* for a plasmid harbouring a *parF* deletion but also to those resulting from alleles encoding ParF with changes in residues in the Walker A motif, G11V and K15Q. ParF-G11V and ParF-K15Q, like ParF-R139A, display disrupted ATP binding and altered ATPase activity (Barilla *et al*., 2005). The presence of the single ParG-plasmid focus suggests that post-replication plasmid separation has not occurred and the ParF mutants are unable to position the plasmid correctly due to the disruption in both the ATPase activity and the assembly into higher order structures. On the other hand, the position of the ParG focus in cells containing ParF-R169A is much more defined, the ParG focus in most cases is positioned at midcell (Figure 5.31 and 5.32). This patterning is similar to the pattern observed for ParF-S108A (Chapter 4 of this work), in which ParG also formed a single ParG focus mostly positioned at midcell with ParF-S108A-Emerald spread throught the nucleiod. Both ParF-R169A and ParF-S108A display a stronger self-interaction and have a high tendency to self-associate in the absence of nucleotide.

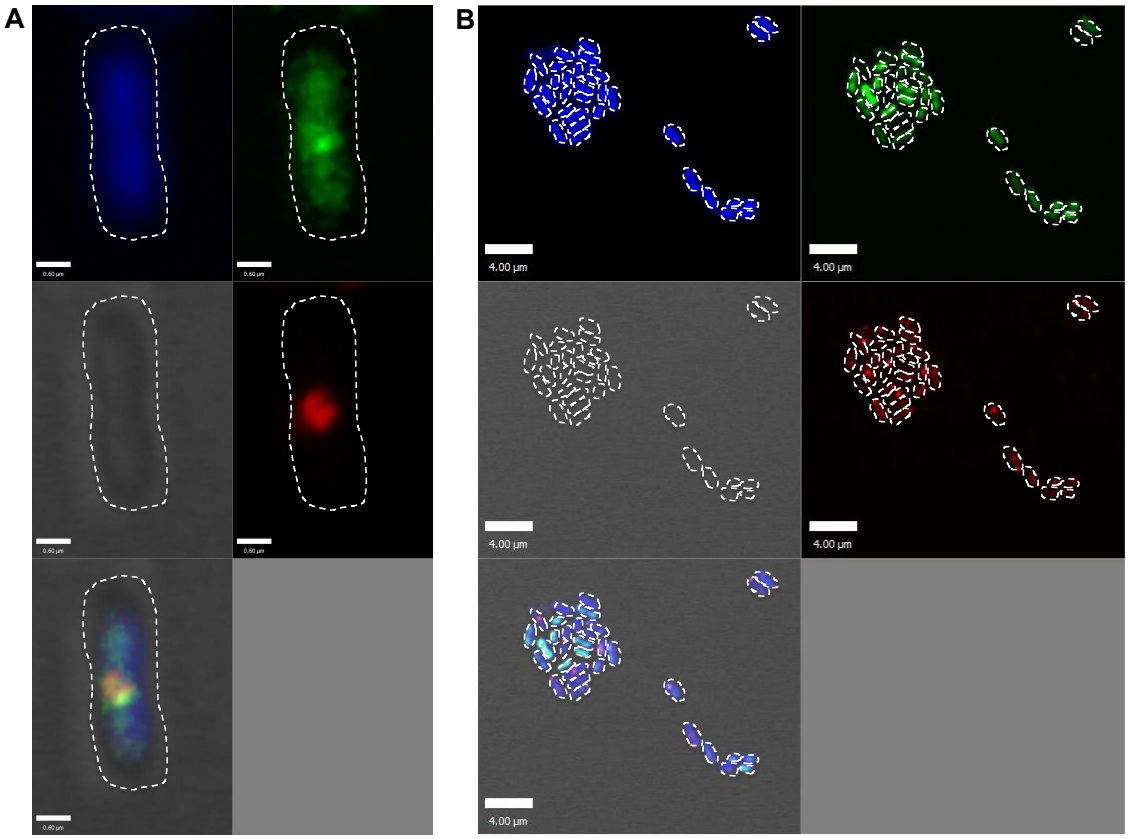

Figure 5.26 – Localisation of ParF-R139A and ParG. Images of *E. coli* cells acquired with the confocal microscope. A) BW25113 *E. coli* cell harbouring a plasmid carrying the partition cassette *parF-R139A-parG-mCherry-parH* (pBM20-ParF-R139A) and a plasmid expressing *parF-R139A-emerald* from the P_{BAD} promoter (pBM40-ParF-R139A). Top left - individual channel for DAPI, top right – individual channel for ParF-R139A-Emerald, middle left – bright field image, middle right – individual channel for ParG-mCherry, bottom left – merged image. Scale bar = 0.6 µm. B) Multiple BW25113 *E. coli* cells harbouring a plasmid carrying the partition cassette *parF-R139A-parG-mCherry-parH* (pBM20ParF—R139A) and a plasmid expressing *parF-R139A -emerald* from the P_{BAD} promoter (pBM40-ParF-R139A). Top left - individual channel for DAPI, top right – individual channel for ParF-R139A-Emerald, middle left – bright field image, middle right – individual channel for ParG-mCherry, bottom left – merged image. Scale bar = 4.00 µm.

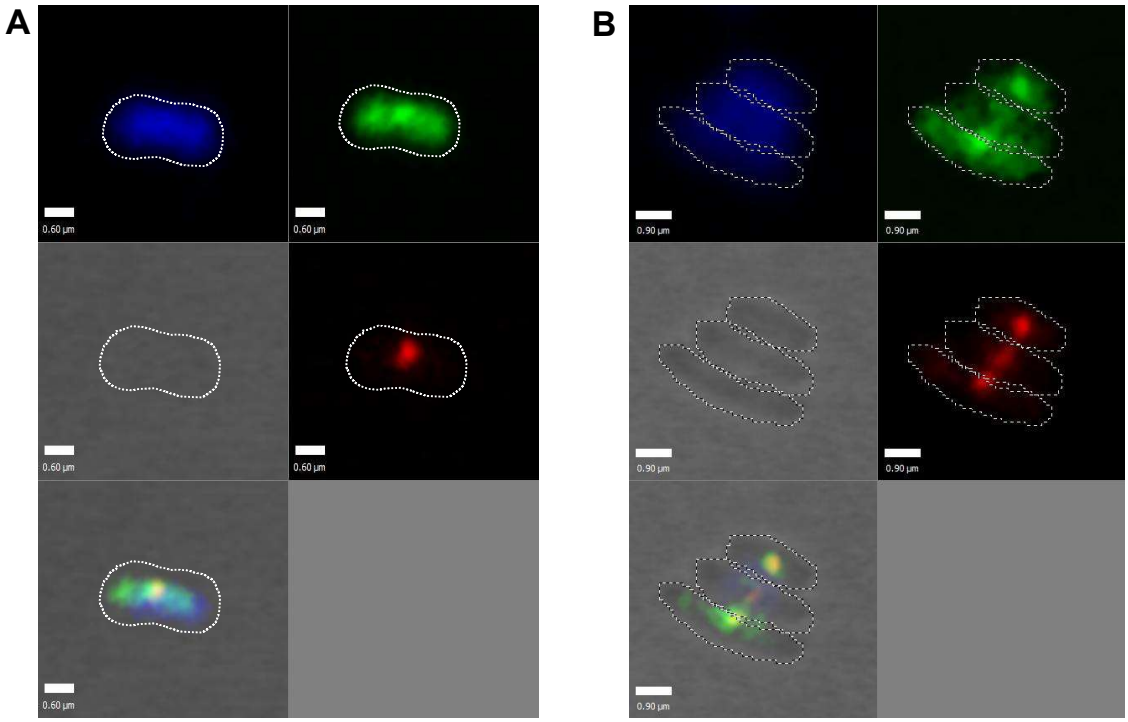

Figure 5.27 – Localisation of ParF-R169A and ParG. Images of *E. coli* cells acquired with the confocal microscope A) BW25113 *E. coli* cell harbouring a plasmid carrying the partition cassette *parF-R169A-parG-mCherry-parH* (pBM20-ParF-R169A) and a plasmid expressing *parF-R169A-emerald* from the P_{BAD} promoter (pBM40-ParF-R169A). Top left - individual channel for DAPI, top right – individual channel for ParF-R169A-Emerald, middle left – bright field image, middle right – individual channel for ParG-mCherry, bottom left – merged image. Scale bar = 0.6 µm. B) Multiple BW25113 *E. coli* cells harbouring a plasmid carrying the partition cassette *parF-R169A-parG-mCherry-parH* (pBM20ParF—R169A) and a plasmid expressing *parF-R169A -emerald* from the P_{BAD} promoter (pBM40-ParF-R169A). Top left - individual channel for DAPI, top right – individual channel for ParF-R169A-Emerald, middle left – bright field image, middle right – individual channel for ParG-mCherry, bottom left – merged image. Scale bar = 0.9 µm.

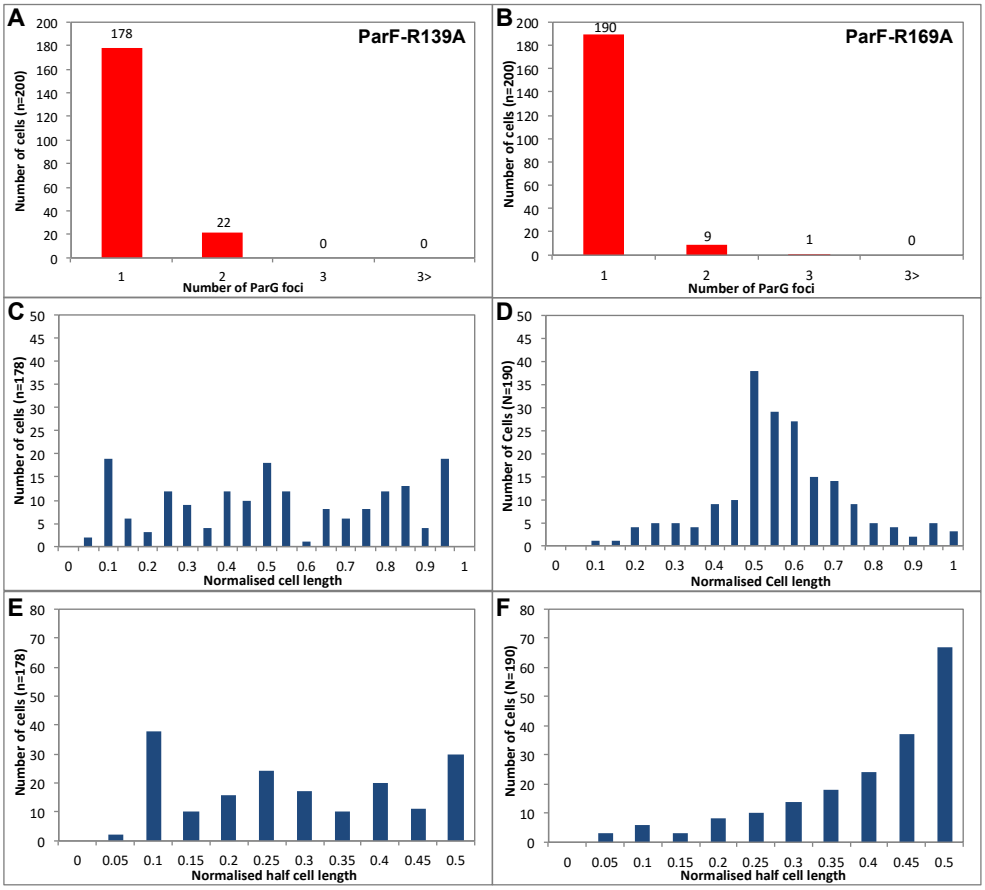

Figure 5.28 – Number and position of ParG foci in cells containing ParF-R139A and ParF-R169A. Quantitative analysis of ParG-mCherry localisation in *E. coli* cells harbouring a plasmid carrying the partition cassette *parF-R139A/R169A-parG-mCherry-parH* (pBM20-ParF-R139A/R169A) and a plasmid expressing *parF- R139A/R169A-emerald* from the P_{BAD} promoter (pBM40-ParF-R139A/R169A). A) Number of ParG-mCherry foci per cell (n = 200 cells) for ParF-R139A. B) Number of ParG-mCherry foci per cell (n = 200 cells) for ParF-R169A. C) Position of a single focus displayed as a function of the normalised cell length for ParF-R139A. D) Position of a single focus displayed as a function of the normalised cell length for ParF-R169A. E) Position of a single focus displayed as a function of the normalised half cell length for ParF-R139A. F) Position of a single focus displayed as a function of the normalised half cell length for ParF-R169A.

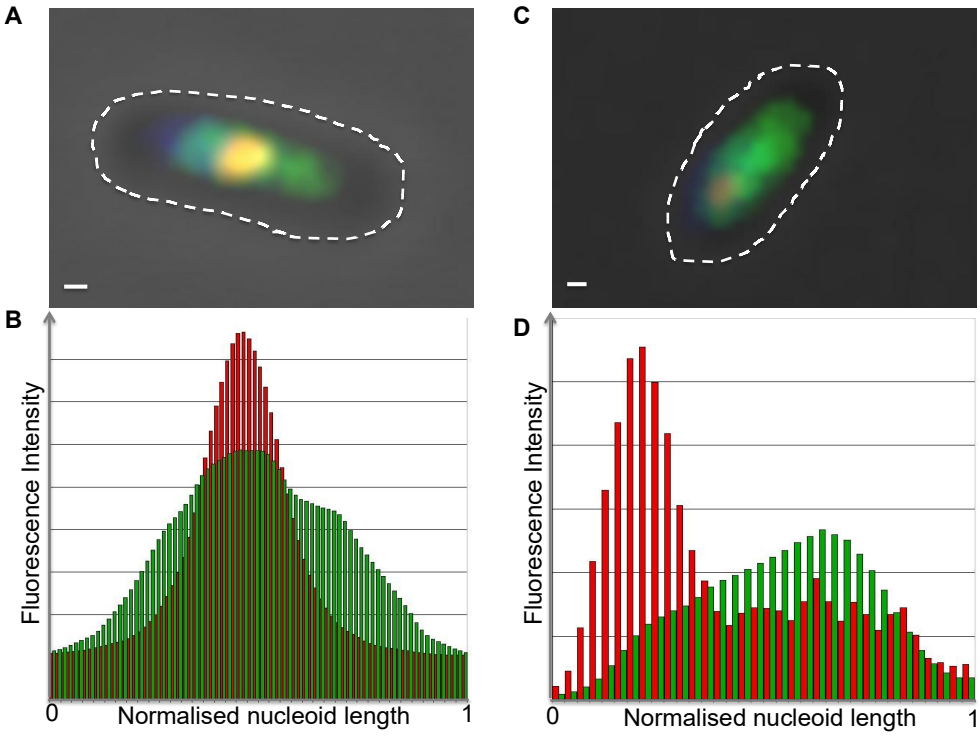

Figure 5.29 – Localisation patterns of ParF-R139A and ParG. Representative images of *E. coli* cells acquired with the confocal microscope. BW25113 *E. coli* cell harbouring a plasmid carrying the partition cassette *parF-R139A-parG-mCherry-parH* (pBM20-ParF-R139A) and a plasmid expressing *parF-R139A-emerald* from the P_{BAD} promoter (pBM40-ParF-R139A). A) A merged image with ParG focus positioned at midcell. Scale bar = 0.2 µm. B) Fluorescence intensity plot of the cell shown in (A) showing the position of ParG-mCherry (red) signal and the spread of the ParF-R139A-Emerald (green) signal. C) A merged image with ParG focus positioned at the pole. Scale bar = 0.2 µm. D) Fluorescence intensity plot of the cell shown in (C) showing the position of ParG-mCherry (red) signal and the spread of the ParF-R139A-Emerald (green) signal.

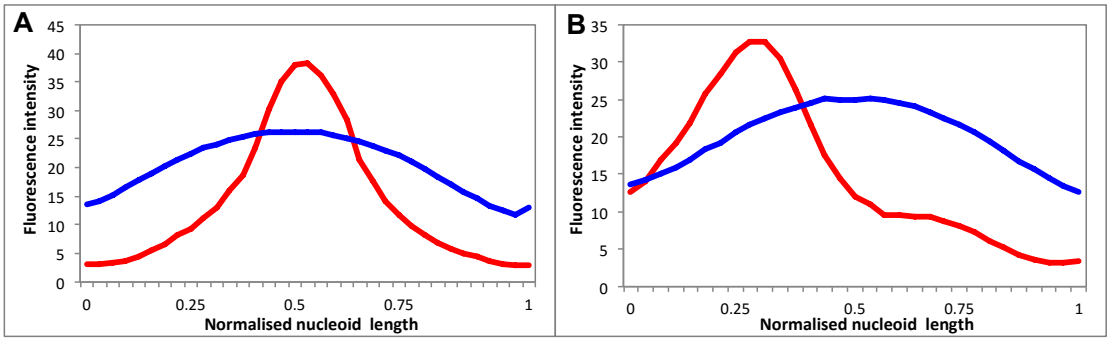

Figure 5.30 - Statistical analysis of ParG signal position when ParF-R139A is present. Quantitative analysis of ParG-mCherry localisation in *E. coli* cells harbouring a plasmid carrying the partition cassette *parF-R139A-parG-mCherry-parH* (pBM20-ParF-R139A) and a plasmid expressing *parF-R139A-emerald* from the P_{BAD} promoter (pBM40-ParF-R139A). A) Average position of ParG-mCherry focus when positioned at midcell (n = 88 cells). ParG-mCherry signal is shown in red and DAPI-stained nucleoid in blue. B) Average position of ParG-mCherry focus when positioned at the pole (n = 55 cells). ParG-mCherry signal is shown in red and DAPI-stained nucleoid in blue.

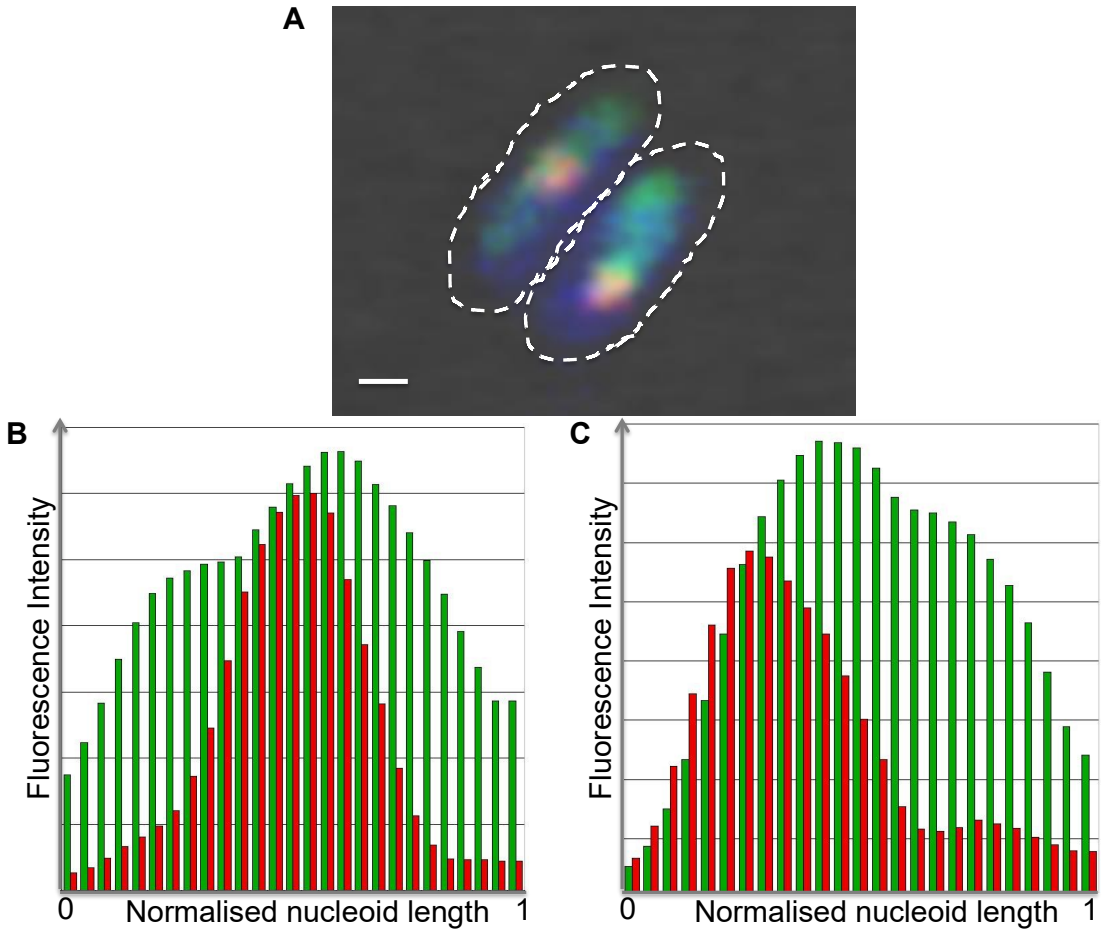

Figure 5.31 - Localisation patterns of ParF-R169A and ParG. Images of *E. coli* cells acquired with the confocal microscope. BW25113 *E. coli* cell harbouring a plasmid carrying the partition cassette *parF-R169AparG-mCherry-parH* (pBM20-ParF-R169A) and a plasmid expressing *parF-R169A-emerald* from the P_{BAD} promoter (pBM40-ParF-R169A). A) A merged image showing two cells, one of which shows the ParG focus positioned at midcell and the other at the pole. Scale bar = 0.4 μm. B) Fluorescence intensity plot of the left cell shown in (A) showing the position of ParG-mCherry (red) signal at midcell and the spread of the ParF-R169A-Emerald (green) signal. C) Fluorescence intensity plot of the right cell shown in (A) showing the position of ParG-mCherry (red) signal at the pole and the spread of the ParF-R169A-Emerald (green) signal.

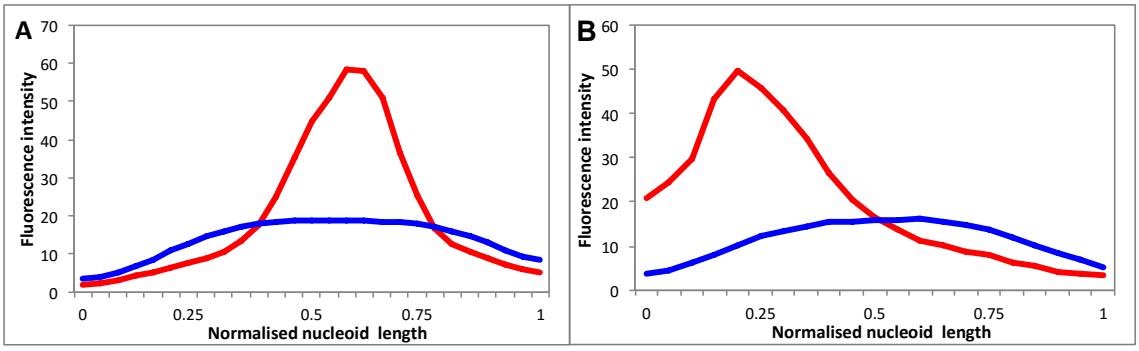

Figure 5.32 - Statistical analysis of ParG position when ParF-R169A is present. Quantitative analysis of ParG-mCherry localisation in *E. coli* cells harbouring a plasmid carrying the partition cassette *parF-R169A-parG-mCherry-parH* (pBM20-ParF-R169A) and a plasmid expressing *parF-R169A-emerald* from the P_{BAD} promoter (pBM40-ParF-R169A). A) Average position of ParG-mCherry focus when positioned at midcell (n = 147 cells). ParG-mCherry signal is shown in red and DAPI-stained nucleoid in blue. B) Average position of ParG-mCherry focus when positioned at the pole (n = 80 cells). ParG-mCherry signal is shown in red and DAPI-stained nucleoid in blue.

Z-stacks acquisition revealed, that like the wild type protein, ParF-R139A and ParF-R169A are spread throughout the nucleoid volume (Figure 5.33). Although *in vitro* both ParF-R139A and ParF-R169A display disrupted nsDNA binding, both mutants still associate with the nucleoid *in vivo*. It is reasonable to suggest that a single amino acid change is not sufficient to disrupt nsDNA binding *in vivo* and the mutants are able to retain some residual nsDNA, as other basic residues are able to compensate.

Overall, in both the ParF-R139A and ParF-R169A backgrounds, plasmid segregation is disrupted as the mutant proteins are unable to position the plasmid correctly. ParF oscillation and asymmetric patterning is likely due to the cycling of binding ATP, forming higher order filament structures followed by stimulation of ATPase activity by ParG. It is likely that the mutants are homogenously spread throughout the nucleoid and unable to oscillate due to the mutants' inability to undergo cycling of assembly and disassembly of higher order filament structures because of the disruption of ATP binding and hydrolysis. The impairment in DNA binding displayed by ParF-R139A and ParF-R169A might be a consequence of these mutant proteins' defective interaction with ATP rather than a direct effect on the association with the nucleoid. It is likely that the changes of these residues affect the structure of ParF on the nucleoid and as a consequence no splitting or positioning of the plasmids occurs. The changes in the ParF structure might be due to the weakened interaction with DNA.

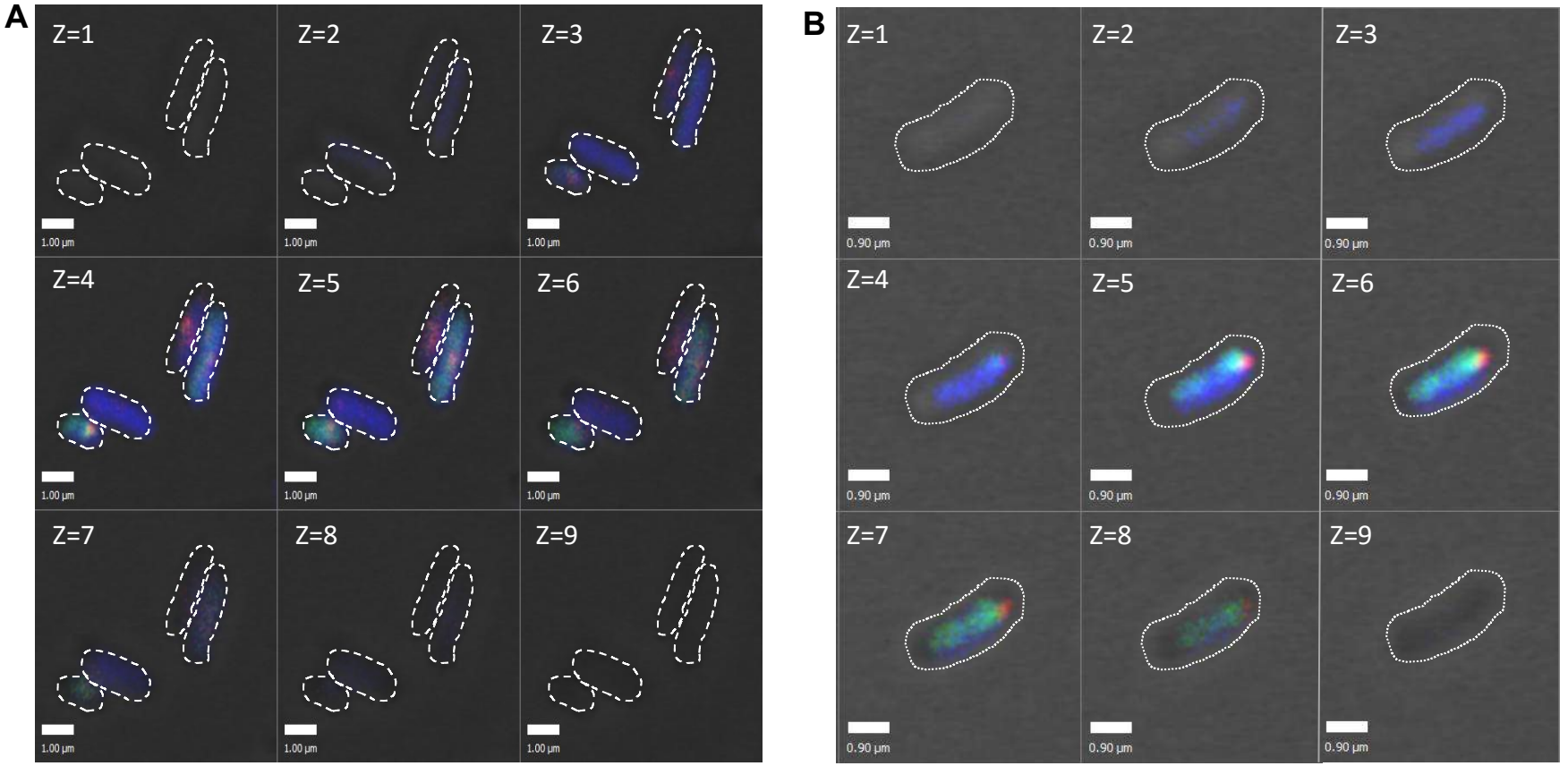

Figure 5.33 – Z stack images of ParF-R139A with ParG and ParF-R169A with ParG. Images of *E. coli* cells acquired with the confocal microscope. Nine Z-stacks were taken at intervals of 190 nm. A) Merged image of cells harbouring the plasmid carrying the *parF-R139A-parG-mCherry-parH* cassette and a plasmid expressing *parF-R139A-emerald* from the P_{BAD} promoter. The nucleoid is stained with DAPI. Scale bar = 1.00 µm. B) Merged image of a cell harbouring the plasmid carrying the *parF-R169A-parG-mCherry-parH* cassette and a plasmid expressing *parF-R169A-emerald* from the P_{BAD} promoter. The nucleoid is stained with DAPI. Scale bar = 0.90 µm.

The localisation and patterning of ParF-K160E-R163E was different from that observed for ParF-R139A and ParF-R169A and in fact displayed some similarities to ParF-K64A-V89Y-M96A (Chapter 3). ParF-K160E-R163E-Emerald is not asymmetrically distributed over the nucleoid but spread homogenously over the nucleoid (Figure 5.34). The localisation of the ParG-mCherry signal was very similar to that observed when wild type ParF is present in the cells (Figure 5.35 and 5.37). The ParG-mCherry signal appears present throughout the nucleoid, but often, distinct ParG foci can also be identified within the dispersed signal. These foci are not as compact as those observed in cells containing other ParF mutants discussed in this work. The number and position of ParG-plasmid foci were very similar to those observed in the wild type background. When ParF-K160E-R163E was present, 40% of the cells contained a single ParG focus mostly positioned at midcell. 42% of the cells contained two ParG foci, which were positioned at one-quarter and three-quarter of the cell length (Figure 5.36). However, in a twenty minute time-lapse experiment no oscillation was seen for ParF-K160E-R163E-Emerald or ParG. The green signal remained spread throughout the nucleoid and the red signal remained in the same position for the entire twenty minutes (data not shown).

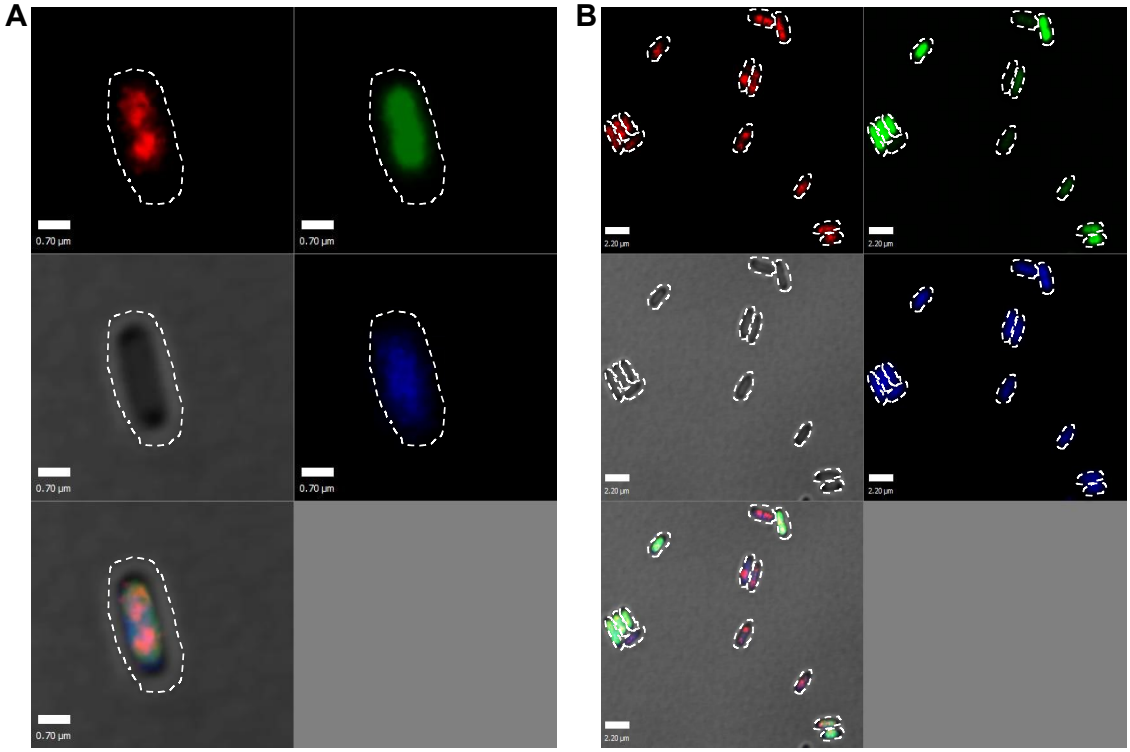

Figure 5.34 – Localisation of ParF-K160E-R163E and ParG. Images of *E. coli* cells acquired with the confocal microscope A) BW25113 *E. coli* cell harbouring a plasmid carrying the partition cassette *parF-K160E-R163E-parG-mCherry-parH* (pBM20-ParF- K160E-R163E) and a plasmid expressing *parF- K160E-R163E-emerald* from the P_{BAD} promoter (pBM40-ParF-K160E-R163E). Top left - individual channel for DAPI, top right – individual channel for ParF-K160E-R163E-Emerald, middle left – bright field image, middle right – individual channel for ParG-mCherry, bottom left – merged image. Scale bar = 0.7 µm. B) Multiple BW25113 *E. coli* cells harbouring a plasmid carrying the partition cassette *parF- K160E-R163E -parG-mCherry-parH* (pBM20ParF— K160E-R163E) and a plasmid expressing *parF- K160E-R163E-emerald* from the P_{BAD} promoter (pBM40-ParF- K160E-R163E). Top left - individual channel for DAPI, top right – individual channel for ParF-K160E-R163E-Emerald, middle left – bright field image, middle right – individual channel for ParG-mCherry, bottom left – merged image. Scale bar = 2.2 µm.

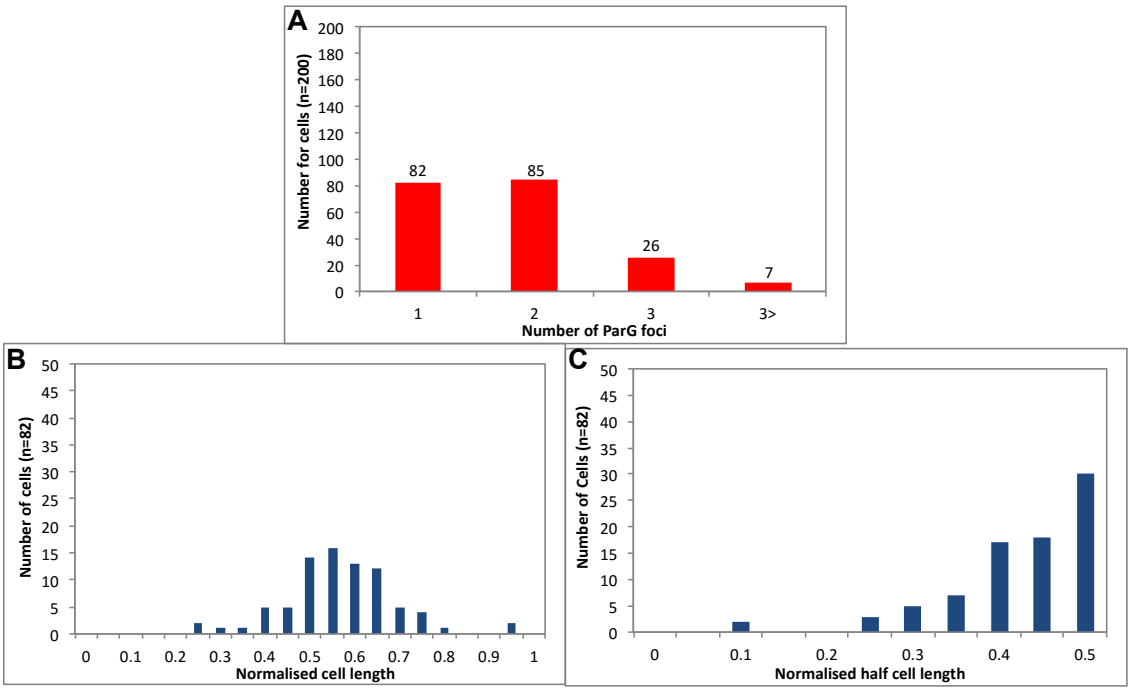

Figure 5.35 - Number and position of ParG foci in cells containing ParF-K160E-R163E. Quantitative analysis of ParG-mCherry localisation in *E. coli* cell harbouring a plasmid carrying the partition cassette *parF-K160E-R163E-parG-mCherry-parH* (pBM20-ParF- K160E-R163E) and a plasmid expressing *parF-K160E-R163E-emerald* from the P_{BAD} promoter (pBM40-ParF-K160E-R163E). A) Number of ParG-mCherry foci per cell (n = 200 cells) for ParF-K160E-R163E. B) Position of a single focus displayed as a function of the normalised cell length for ParF- K160E-R163E. C) Position of a single focus displayed as a function of the normalised half cell length for ParF- K160E-R163E.

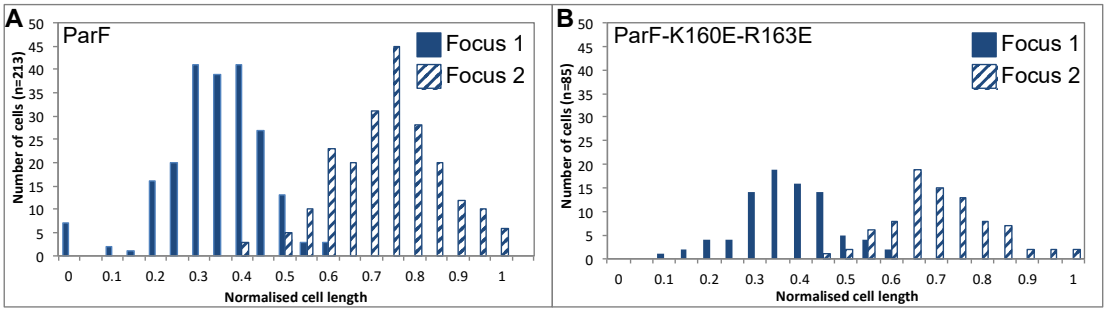

Figure 5.36 – ParG foci positions in cells harbouring ParF-K160E-R163E. Quantitative analysis of ParG-mCherry localisation in *E. coli* cell harbouring a plasmid carrying the partition cassette *parF- K160E-R163E-parG-mCherry-parH* (pBM20-ParF- K160E-R163E) and a plasmid expressing *parF- K160E-R163E -emerald* from the P_{BAD} promoter (pBM40-ParF-K160E-R163E). A) Position of double foci displayed as a function of the normalised cell length in cells with ParF. B) Position of double foci displayed as a function of the normalised cell length in cells with ParF-K160E-R163E.

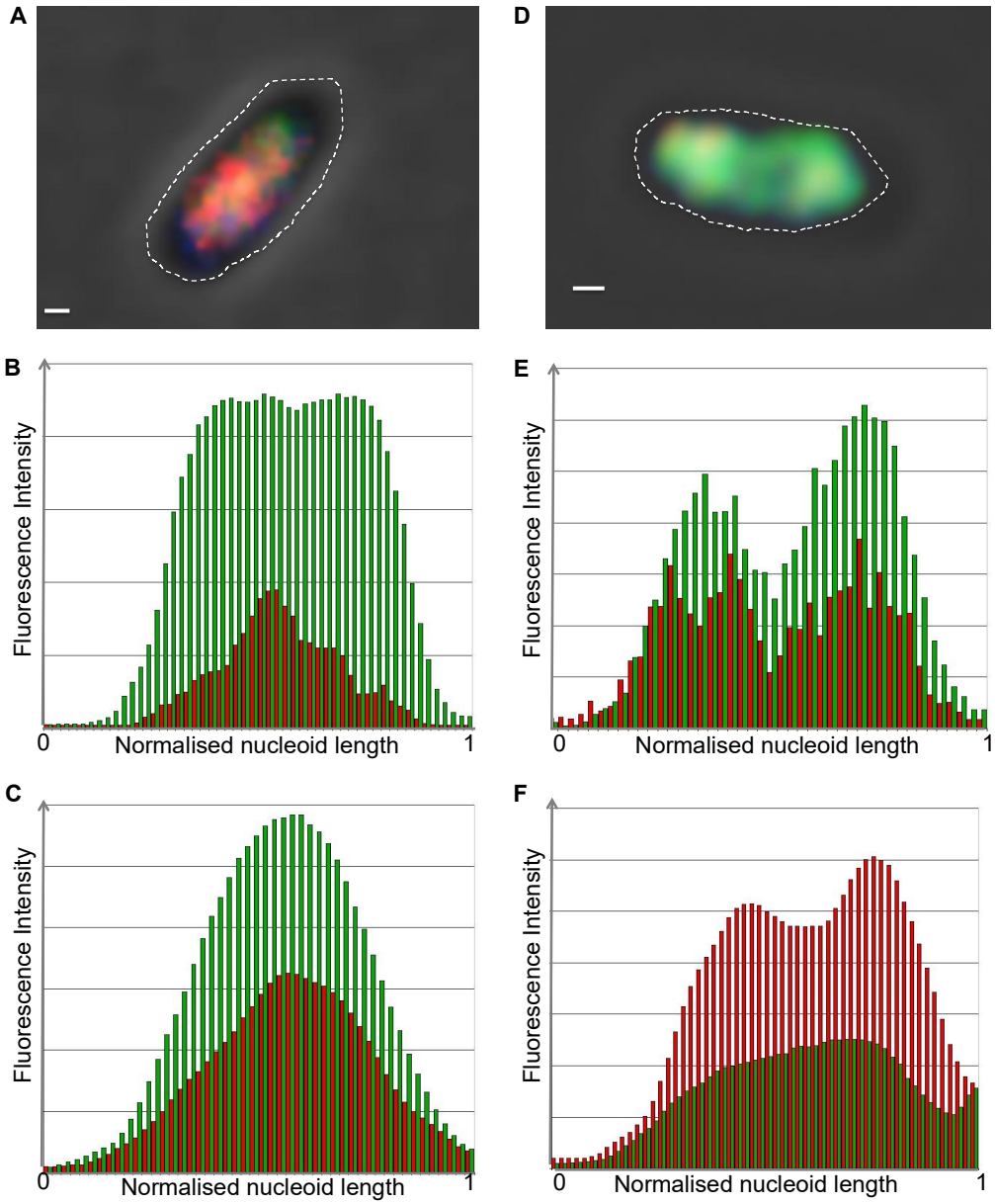

Figure 5.37 – Localisation patterns of ParF-K160E-R163E and ParG. Images of *E. coli* cells acquired with the confocal microscope. BW25113 *E. coli* cell harbouring a plasmid carrying the partition cassette *parF-K160E-R163E-parG-mCherry-parH* (pBM20-ParF-K160E-R163E) and a plasmid expressing *parF-K160E-R163E-emerald* from the P_{BAD} promoter (pBM40-ParF-K160E-R163E). A) A merged image with ParG focus positioned at midcell. Scale bar = 0.2 µm. B) Fluorescence intensity plot of the cell shown in (A) showing the position of ParG-mCherry (red) signal and the spread of the ParF-K160E-R163E-Emerald (green) signal. C) Fluorescence intensity plot of another cell (not shown) with ParG-mCherry (red) signal at midcell and ParF-K160E-R163E-Emerald (green) signal is a similar position. D) A merged image of a cell with two ParG foci positioned at one quarter and three quarter positions. Scale bar = 0.3 µm. E) Fluorescence intensity plot of the cell shown in (D) showing the position of ParG-mCherry (red) signal and the ParF-K160E-R163E-Emerald (green) signal overlapping. F) Fluorescence intensity plot of another cell (not shown) with ParG-mCherry (red) signal at one and three quarter position and with diffused ParF-K160E-R163E-Emerald (green) signal.

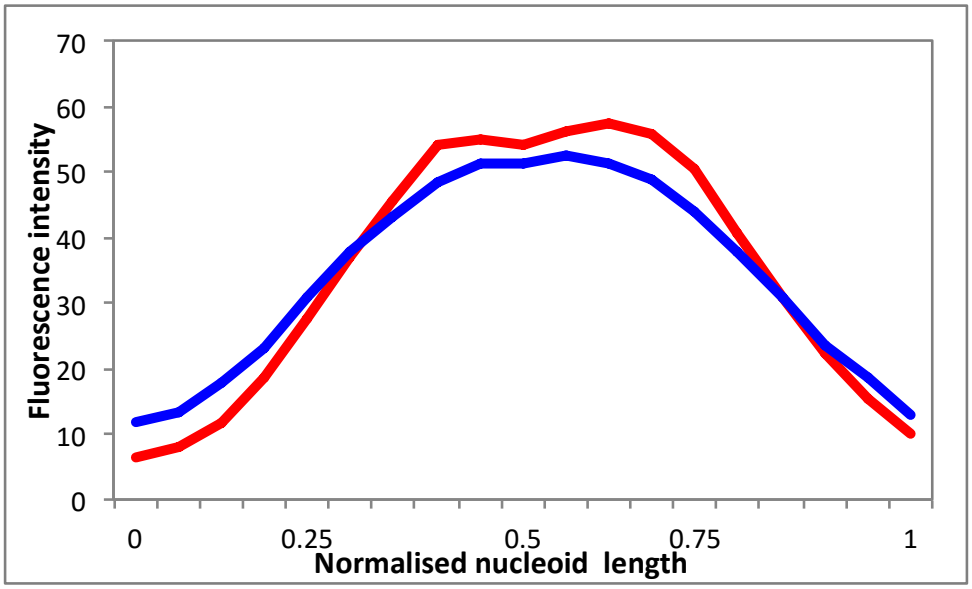

Figure 5.38 - Statistical analysis of ParG position when ParF-K160E-R163E is present. Quantitative analysis of ParG-mCherry localisation from *E. coli* cells harbouring a plasmid carrying the partition cassette *parF-K160E-R163E-parG-mCherry-parH* (pBM20-ParF-K160E-R163E) and a plasmid expressing *parF- K160E-R163E-emerald* from the P_{BAD} promoter (pBM40-ParF-K160E-R163E). The graph shows the average position of ParG-mCherry signal (n = 100 cells). ParG-mCherry signal is shown in red and DAPI-stained nucleoid in blue.

Z-stacks revealed, that like the wild type protein, ParF-K160E-R163E protrudes into the nucleoid volume (Figure 5.39). Although *in vitro* ParF-K160E-R163E displayed disrupted nsDNA binding, it is evident that the mutant protein is still able to associate with the nucleoid in the cell. Therefore these amino acid changes are not sufficient to disrupt nsDNA binding *in vivo* and ParF-K160E-R163E is able to retain some residual nsDNA binding. It is possible that other basic residues are able to compensate and allow DNA binding.

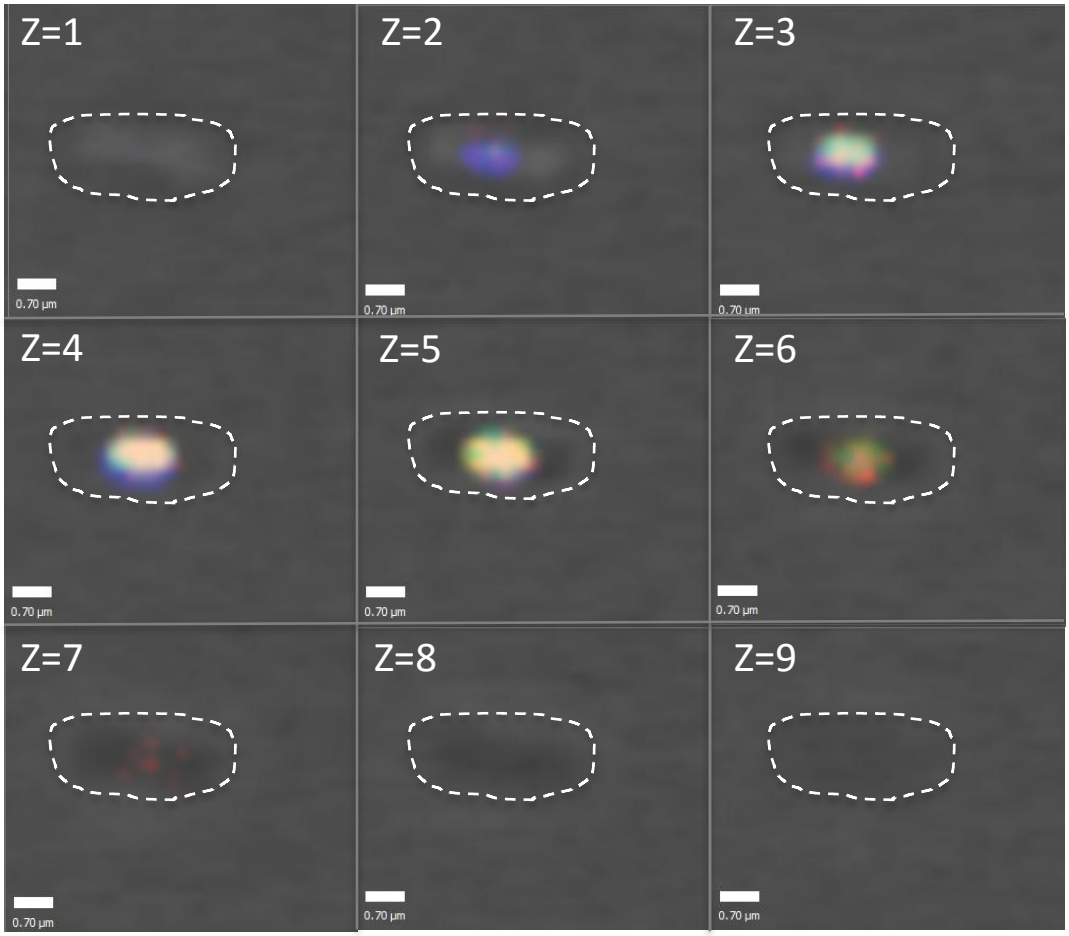

Figure 5.39 – Z stack images of ParF-K160E-R163E and ParG. Images of *E. coli* cells acquired with the confocal microscope. Nine Z-stacks were taken at intervals of 190 nm. Merged image of a cell harbouring the plasmid carrying the *parF-K160E-R163E-parG-mCherry-parH* cassette and a plasmid expressing *parF-K160E-R163E-emerald* from the P_{BAD} promoter. The nucleoid was stained with DAPI. Scale bar = 0.70 µm.

5.5 ParF-R139A, ParF-R169A and ParF-K160E-R163E conclusions

The aim of this part of the project was to identify an interface of ParF that was involved in nsDNA binding. The structure of ParF led to the identification of eight surface exposed basic residues that were potentially involved in nsDNA binding. These eight residues were individually converted to alanine and characterised in terms of the effect the residue change had on plasmid partition. R139A and R169A were shown to have significant effect on plasmid retention and selected for further analysis. However it was proposed that a single amino acid change may not completely abolish DNA binding and therefore a double mutant was also constructed. The two residues selected were initially identified surface exposed basic residues but when individually mutated to alanine had little effect on plasmid segregation. The two residues, K160 and R163 were mutated to glutamic acid with the aim of maintaining the hydrophilic surface of the ParF but to disrupt DNA binding by changing the positively charged residues to a negative charge. ParF-K160E-R163E was shown to have significant effect on plasmid retention and therefore further analysis was carried out.

R139 and R169 had also been identified by Schumacher *et al* (2012) to play an important role in ATP binding of ParF. The side chain of R139 was seen to insert into the ATP binding pocket of ParF and stack over the adenine, which allows R139 to contact the ribose O4 and forms the only hydrogen bond from ParF to the ribose group. Residues 166 -177 were identified as being important in providing contacts that specify the adenine nucleobase. R169 forms the top of the ATP binding site and contacts the adenine N1 group, the side chain of R169 is therefore important in shaping the ATP binding site (Schumacher *et al*., 2012, Dobruk-Serkowska *et al*., 2012). Therefore it was reasonable to suggest that changing these residues to alanine might disrupt ATP binding of ParF with possible consequences on the ability of the protein to interact with nsDNA. It became evident throughout this work that this was the case and ParF-R139A and ParF-R169A displayed very similar phenotypes (Table 5.1).

ParF-R169A was characterised by Dobruk-Serkowska *et al*(2012) and shown to be a hyperactive ATPase likely due to the fact that the change enabled easier access to the ATP binding pocket. ParF-R169A was also shown to have a stronger self-interaction and a higher tendency to self-associate into higher order structures in the absence of nucleotide. ParF-R169A was also shown to have a stronger interaction with ParG

compared to ParF-ParG and it was postulated that the flexible N-terminal tail of ParG might be more rigidly tethered in the ParF-R169A-ParG interaction. In this study ParF-R139A was shown to possess many of the same features. ParF-R139A showed hyperactive ATPase and reduced binding to ATP, which is likely to be due to the fact that the change of arginine to alanine no longer allows the side chain of R139 to contact the ribose group of ATP. ParF-R139A also demonstrated a higher tendency to self-associate into higher order structures in the absence of nucleotide and was unable to undergo ATP-dependent assembly. As suggested by Dobruk-Serkowska *et al*(2012) and as discussed in Chapter 4 of this work, changes in residues close to or involved in the ATP binding pocket may cause a conformational change that favours the self-association of ParF. Therefore it is reasonable to suggest that this may be case for both ParF-R139A and ParF-R169A. Finally, ParF-R139A also displayed a stronger interaction with ParG, as did ParF-R169A. As discussed in Chapter 4, changes at the monomer-monomer interface of ParF not only disrupt the self-interaction but also the interaction with ParG. This is due to the fact that the N-terminal tail of ParG is believed to insert into the ATP binding pocket of ParF at the monomer-monomer interface. Specific residues have been identified that are important in this interaction and changes to these residues result in a weaker interaction with ParG. On the other hand, changes to R139 and R169 result in a stronger binding either due to allowing easier access of the N-terminal tail of ParG or the N-terminal tail being more rigidly tethered.

ParF has been shown to bind nsDNA in an ATP-dependent manner (McLeod et al., 2016) and this work). ParF-R139A and ParF-R169A were unable to bind nsDNA *in vitro*. However *in vivo*, both mutants localised over the nucleoid suggesting that the mutants retain the ability to bind nsDNA. The disruption of nsDNA binding *in vitro* may be caused by the mutants' hyperactive ATPase activity. Firstly, it has been shown for other ParA proteins that binding ATP is crucial for nsDNA binding and secondly, some ParA proteins undergo a conformational change upon ATP binding that enables nsDNA binding. ParF-R139A and ParF-R169A have been shown to (1) display weaker binding to ATP that result in disruption of nsDNA and (2) are hyperactive ATPase proteins so ATP is being hydrolysed to ADP at a quicker rate causing the mutant proteins to 'fall off' the DNA, as they are no longer bound to ATP. The interaction of ParF with DNA appears to be a very transient process and *in vitro* disruption of ATP binding and ATP hydrolysis has a large impact on the ability of ParF to bind DNA. *In vivo*, the concentration of DNA is much greater and this may allow other surface-

exposed basic residues to compensate for R139A or R169A allowing the mutants to retain some residual nsDNA binding.

ParF-R139A and ParF-R169A display complex phenotypes that are linked to the ability of ParF to bind and hydrolyse ATP as well as change in self-interaction and interaction with ParG. In contrast to ParF-R139A and ParF-R169A, ParF-K160E-R163E initially demonstrated almost identical properties to the wild type protein, as was observed to bind and hydrolyse ATP in a similar way to ParF as well as displaying similar self-interactions and a similar interaction with ParG. However the ability of the mutant to self-associate and undergo ATP-dependent assembly into higher order structures was disrupted. ParF K160E-R163E was unable to self-associate into higher order structures in the absence of nucleotide but was able to undergo ATP-dependent assembly into higher order structures. The response of ParF- K160E-R163E to ATP was slower and more gradual compared to wild type ParF but a clear increase in light scattering was observed.

As with ParF-R139A and ParF-R169A, ParF-K160E-R163E was shown to be unable to bind nsDNA *in vitro* potentially suggesting these residues are important in the interaction of ParF with DNA. However *in vivo*, ParF-K160E-R163E localised over the nucleoid suggesting that the mutant had retained the ability to bind nsDNA. As previously discussed, the *in vivo* association with the nucleoid of these mutants might be due to the fact that other exposed basic residues are able to compensate and allow some residual DNA binding.

ParF-K160E-R163E is similar to the wild type protein in some respects however the mutant protein does display reduced activities in nsDNA binding as well as demonstrating a significant reduction in plasmid retention. Despite the fact that ParF-K160E-R163E is able to undergo ATP-dependent assembly into higher order structures, *in vivo* the mutant is homogenously distributed and unable to oscillate, suggesting that the disruption of nsDNA binding is playing a key role in plasmid partition, although the mutant is still capable of association with the nucleoid. This suggests a link between nsDNA binding and the cycling of assembly and disassembly of higher order structures.

Table 5.1 – Summary of *in vitro* and *in vivo* characteristics of ParF-R139A, ParF-R169A and ParF-K160E-R163E in comparison to wild type ParF. If highlighted in red there is a significant difference observed between the ParF mutant and the wild type protein.

	ParF	ParF-R139A	ParF-R169A	ParF-K160E-R163E
Plasmid Retention	~70 %	~ 3%	~ 5%	~ 11%
Binds ATP	Yes. K_d = 0.44 µM	Yes. K_d = 2.11µM	Yes. K_d = > 1µM	Yes. K_d = 0.7 µM
Forms a dimer	Yes. MU = 1300	Yes. MU ~ 100 more than ParF	Yes. MU ~ 300 more than ParF	Yes. Same as ParF
Interacts with ParG	Yes. MU= 839	Yes. MU ~ 300 more than ParF	Yes. MU ~ 300 more than ParF	Yes. Same as ParF
Intrinsic ATPase activity	Weak	Hyperactive	Hyperactive	Weak
ATPase activity stimulated by ParG	Yes	No	No	Yes
Self –associates in the absence of nucleotide	Yes	Yes – higher tendency	Yes- higher tendency	No
ATP dependent assembly into higher order structures	Yes	No – addition of nucleotide solubilises the protein	No– addition of nucleotide solubilises the protein	Yes. Slower response to ATP than ParF
ParG promote assembly into higher order structures	Yes	Yes	Yes	Yes
ParF/ParF mutant cell localisation pattern	Asymmetrically distributed	Homogenously distributed	Homogenously distributed	Homogenously distributed
ParG cell localisation pattern	Distinct ParG foci can be identified within a dispersed signal	Compact focus randomly positioned	Compact focus mostly at midcell	Distinct ParG foci can be identified within a dispersed signal.
Number of ParG foci	1-4	1	1	1-4
Protrudes through the nucleoid	Yes	Yes	Yes	Yes
Oscillates	Yes	No	No	No

5.6 The link between ParF nsDNA binding and assembly into higher order structures

Evidence from this chapter and also previous chapters has suggested that the ns-DNA binding properties of ParF and the ability to assemble into higher order structures may be correlated and it is possible that there is a link between these two important properties of ParF. In order to analyse this potential correlation, a number of *in vitro* experiments, which have previously been used to characterise ParF mutant proteins, were carried out with the addition of DNA and the effects were observed. These included DLS, sedimentation assays, ATPase assays and electron microscopy experiments. However, the results were not entirely conclusive although DLS, sedimentation assays and electron microscopy experiments did appear to demonstrate that the addition of DNA did have an effect on the assembly of ParF into higher order structures. Due to the fact the results were not entirely conclusive and only preliminary experiments were carried out it would be necessary to undertake further work on this in the future to confirm the possible link between ns-DNA binding and assembly into higher order structures of ParF.

5.7 Conclusion of the nsDNA binding properties of ParF

Many ParA proteins have been shown to display non-specific DNA binding properties *in vitro* and have been visualised to localise on the nucleoid *in vivo*. ParF has also been shown to localise on the nucleoid *in vivo* (Ringgaard et al., 2009, McLeod et al., 2016) and has been observed to bind nsDNA in an ATP-dependent manner *in vitro* (McLeod et al., 2016). It has emerged that the non-specific DNA binding properties of ParA proteins are important in the plasmid segregation mechanism and all recently proposed models for plasmid segregation involve ParA proteins associating with the nucleoid. The structure of ParF revealed surface exposed residues, which could be involved in the nsDNA binding of ParF and form a potential DNA binding interface.

In the first part of this study biochemical ensemble and single molecule techniques were employed to confirm that ParF was able to bind nsDNA *in vitro* and to try and gain further understanding of the binding properties. It was evident from the results that ParF was able to bind nsDNA *in vitro* in an ATP-dependent manner. Fluorescence anisotropy

results demonstrated the K_d of this binding was ~ 300 nM, which is not a particularly strong binding affinity. However this is possibly due to the transient nature of DNA binding displayed by ParF. The results from the TPM experiments firstly confirmed that ParF binds nsDNA in an ATP-dependent manner and also provided a better understanding into how ParF potentially binds DNA. The analysis of the TPM results suggested that ParF doesn't form a one-dimensional filament structure on the DNA but in fact multiple ParF-ATP dimers may bind the DNA and then interact with other ParF dimers to form larger higher order structures that result in the bending/looping and ultimately compaction of the DNA.

The roles of individual surface exposed basic residues, identified from the structure of ParF, were then investigated in terms of the effect they have on nsDNA binding and also plasmid segregation. ParF-R139A, ParF-R169A and ParF-K160E-R163E were characterised *in vitro*, all of which demonstrated reduced nsDNA binding. However, ParF-R139A and ParF-R169A were found to be hyperactive ATPase proteins and also displayed disrupted interaction with ParG, which made the direct role of R139 and R169 on nsDNA binding challenging to determine. On the other hand ParF-K160E-R163E demonstrated *in vitro* properties almost identical to those of wild-type ParF, but was unable to bind nsDNA. On further analysis it was evident that the ability of ParF-K160E-R163E to assemble into higher order structures was also disrupted. ParF-K160E-R163E did not demonstrate the ability to self-associate in the absence of nucleotide but did undergo ATP-dependent assembly into higher order structures, although this assembly was slower than that demonstrated by wild type ParF. *In vivo*, ParF-R139A and ParF-R169A displayed similar patterns to previously observed mutant proteins such as ParF-S108A. The ParF mutants were homogenously distributed over the nucleoid and ParG formed compact foci mostly positioned at midcell or the extreme pole of the nucleoid. On the other hand, ParF-K160E-R163E displayed similar patterning to that of ParF other than the fact the mutant was unable to oscillate from one pole of the nucleoid to the other. This was interesting as ParF-K160E-R163E is able to undergo ATP-dependent assembly into higher order structures *in vitro.* This suggested that the disruption of nsDNA binding is playing a role even though the mutant is associated with the nucleoid. This implies a link between nsDNA binding and the assembly and disassembly of ParF higher order structures.

These results, along with previous work in other chapters, suggest that DNA binding and assembly into higher order structures are not independent events and in fact may be

coupled. In the final part of this work DLS, sedimentation assays and electron microscopy results provided some initial support for a link between the two properties of ParF (data not shown). However these results were preliminary and not entirely conclusive. These initial findings would need to be support by further *in vitro* experiments in order to draw a definitive conclusion. A range of experiments would need to be carried out with DNA present and also could be carried out with ParF mutants discussed in this chapter, as well as previous chapters, to test the hypothesis that DNA binding and assembly into higher order structures are linked.

The work described in this chapter has introduced an exciting concept and hypothesis that DNA binding and assembly into higher order structures are not independent events but in fact linked. The work has led to a new mechanism of ParF assembly into higher order structures to be proposed, which is described in Chapter 6. This work also helps to support a newly proposed model for plasmid segregation, which is also discussed in detail in Chapter 6.

Chapter 6: Discussion and Future Work

6.1 Discussion

All cells must be able to carry out accurate DNA segregation to ensure stable genome transmission. In the last couple of decades our understanding of prokaryotic DNA segregation has vastly improved and it is now known that prokaryotes employ active DNA segregation mechanisms. Both bacterial plasmids and chromosomes have been shown to utilise partition (*par*) systems in order to faithfully segregate the genome in the cell (Moller-Jensen *et al*., 2000, Schumacher, 2012). Low copy number plasmids have been important model systems, which have allowed further understanding of partition systems in prokaryotes. Plasmid TP228 is a low copy number, multidrug resistant plasmid originally isolated in *Salmonella newport* that has been shown to utilise a type Ib partition system consisting of two *trans*-acting proteins, ParF and ParG, and a *cis*-acting centromere site *parH* upstream of *parFG*. ParF is a Walker-type ATPase and ParG is a centromere binding protein that has been shown to bind specifically to the partition site *parH* to form a partition complex that is then able to recruit ParF (Barillà and Hayes, 2003, Hayes, 2000, Wu *et al*., 2011a). ParF, the Walker-Type ATPase, is the motor protein of the partition system and is responsible for driving the segregation of the plasmid, the exact mechanism of which is still not fully understood. However ParF has been shown to form higher order structures and this is thought to be important in the plasmid segregation mechanism (Barilla *et al*., 2005). This work has focused on gaining a further understanding of the mechanism involved in the assembly and disassembly of ParF higher order structures. In addition to this, the role of ParF non-specific DNA binding properties was also studied in order to try and dissect the role the nucleoid plays in the plasmid segregation mechanism. The overall objective was to try and gain a better understanding of the molecular mechanism and dynamics employed by this plasmid to ensure accurate plasmid partitioning.

6.1.1 Disruption of the dimer-dimer interface prevents ParF from forming higher order structures

Several ParA proteins have been observed to undergo ATP-dependent polymerisation into higher order structures (Batt et al., 2009, Barilla et al., 2007, Bouet et al., 2006, Ringgaard et al., 2009). This has led to models for plasmid segregation being developed in which polymerisation – depolymerisation cycles were crucial for the segregation process. More recently the ability of many ParA proteins to form higher order structures has been disputed and new models of plasmid segregation have been proposed that do

not involve ParA polymerisation. However, previous work (Barilla *et al*., 2005) clearly demonstrates that ParF is able to undergo ATP-dependent assembly into higher order structures and work here supports this. Vast experimental data, alongside structural data, supports the ability of ParF to form higher order structures and the importance this plays in the segregation process.

The structure of ParF has been solved revealing that ParF is monomeric when bound to ADP and dimeric when bound to ATP (Schumacher *et al*., 2012). It has been previously observed that ParF, when bound to ATP, is able to form higher order filament structures but the exact details of how ParF assembles into these structures is not fully understood. The structural data has allowed further understanding of this process as it was revealed that ParF-ATP dimers interact with each other to form dimer-of-dimer units. It was then proposed that these dimer-of-dimer units formed the building blocks of the ParF polymers and that by disrupting two interfaces on the surface of these ParF dimers ParF polymer formation would be abolished. At these two interfaces (interface 1 and 2), residues that make key interactions were identified and changed to a particular amino acid dependent upon the interaction that needed to be disrupted. A triple mutant harbouring changes at interface 1 was previously constructed (Schumacher *et al*., 2012) and found to disrupt plasmid segregation as the mutant was unable to form higher order structures upon the addition of ATP.

ParF-K64A-V89Y-M96A, a mutant that is shown to be defective in plasmid partitioning, is unable to form higher order structures upon the addition of ATP, even though this mutant is able to bind and hydrolyse ATP. When observed using EM, no higher order structures could be visualised either in the absence or presence of ATP. In the presence of ATP ParF-K64A-V89Y-M96A appeared as small globular structures, almost identical to ParF in the absence of ATP, confirming this mutant was unable to form higher order structures. ParF-K64A-V89Y-M96A was still able to form a dimer, which with all the experimental data gathered supported the theory that disruption of this interface prevents ParF from forming higher order structures.

In vivo, ParF-K64A-V89Y-M96A patterning differs to that of the wild type ParF. ParF-K64A-V89Y-M96A does not form an asymmetric pattern over the nucleoid but in fact is homogenously spread over the nucleoid and furthermore was unable to oscillate from one pole of the nucleoid to the other. The cycling between assembly and disassembly of higher order structures is what drives this oscillation; therefore the fact that ParF-K64A-

V89Y-M96A is unable to do so explains why no oscillation is observed. The *in vivo* studies further support the importance of ParF formation into higher order structures and that disrupting interfaces at the ParF dimer can abolish this. The lack of formation of higher order structures and oscillation of ParF-K64A-V89Y-M96A causes the partition deficient phenotype and indicates assembly of higher order structures plays a critical role in TP228 plasmid partitioning.

6.1.2 The ParF monomer-monomer interface is crucial for both the ParF-ParF interaction and the ParF-ParG interaction

As previously discussed, the structure of ParF revealed that ParF-ATP dimers interacted with each other to form dimer-of-dimer units that formed the building blocks of ParF filaments. Therefore it was reasonable to propose that disrupting the monomer-monomer interface of ParF so that a dimer could not be formed would lead to disruption of this process. In the dimer structure the nucleotide appears to be sandwiched in between the monomers and residues were identified that were involved in the interactions between ParF and the nucleotide. In addition, other residues were identified that were important in forming cross contacts at the monomer-monomer interface of ParF. Schumacher *et al* (2012*)* identified a proline-rich motif in ParF. This motif is seen to insert into the adjacent ParF monomer close to the ATP binding pocket and allows cross contacts to form between subunits within the dimer. In addition to the proline rich motif, additional key residues were identified that make cross contacts within the monomer-monomer interface and with the proline rich motif. Computational alanine scanning was also carried out in order to identify residues that might be important at the ParF monomer-monomer interface.

Mutational studies led to the identification of key residues that played crucial roles at the monomer-monomer interface. However the results were not as predicted and the amino acid substitution of residues in the proline-rich motif did not prevent dimer formation but in fact promoted both stronger dimer formation and the assembly of higher order structures of ParF. In addition, residues at the monomer-monomer interface of ParF were found to be important in the interaction between ParF and ParG. ParF-S108A and ParF-P109R were characterised extensively *in vitro* (and ParF-P107A to some extent) and it was clearly demonstrated that all the mutants were still able to form dimers. The interaction of ParF-S108A-ParF-S108A and ParF-P109R-ParF-P109R was shown to be stronger than that of the wild-type protein indicating that these changes do

have an effect at the monomer-monomer interface. DLS experiments, sedimentation assays and EM revealed that both ParF-S108A and ParF-P109R had a higher tendency to self-associate into higher order structures in the absence of nucleotide compared to wild type ParF, especially ParF-P109R. The addition of any nucleotide inhibited ParF-S108A assembly into higher order structures whereas nucleotides had little effect on ParF-P109R and the protein continued to self-associate into higher order structures, therefore demonstrating both ParF-S108A and ParF-P109R were unable to undergo ATP-dependent assembly into higher order structures. Clearly the monomer-monomer interface was disrupted when these residues were changed: it is likely that the close proximity of the proline rich motif to the ATP binding pocket may alter the conformation of the binding pocket and cause a conformational change that locks ParF in a configuration that favours its self-association. When visualised *in vivo* using confocal microscopy it was evident that the disruption at the monomer-monomer interface prevented the mutants from oscillating from one pole of the nucleoid to the other. ParF-S108A and ParF-P109R displayed slightly different patterning over the nucleoid however both were not asymmetrically distributed like the wild type ParF. The fact that the mutants are unable to undergo ATP-dependent assembly and disassembly of higher order structures leads to the inability to oscillate and thus prevents accurate plasmid segregation.

Another interesting property of ParF-S108A and ParF-P109R was that they displayed significantly weaker interactions with ParG. Both the N-terminal and C-terminal regions of ParG have been shown to interact with ParF (Barillà and Hayes, 2003, Barilla *et al*., 2007). Specifically it has been proposed that the unstructured N-terminal tail of ParG might be inserted close to the ATP binding pocket of ParF to allow an arginine finger motif to stimulate ParF ATPase activity. The co-structure of ParF-ParG is yet to be solved, however some recent work has made progress towards achieving this objective and this has led to a potential ParF-ParG interface being identified (Schumacher, M. – unpublished data). The residues in ParF that were highlighted as being important in the ParF-ParG interaction were S108, P109, L110, F112 and V149. Bacterial-two hybrid assays clearly demonstrated that S108, P109 and L110 were crucial in the interaction with ParG and F112 and V149A to a lesser extent. In the structure of ParF, the triad of residues S108, P109 and L110 appear to protrude more obviously into the monomer-monomer interface. It is likely that the unstructured, flexible N-terminal tail of ParG might be able to insert close to the ATP binding pocket of ParF and therefore it is

reasonable to conclude that these protruding residues are more likely to make key interactions with the ParG N-terminal tail.

These results demonstrated that monomer-monomer interface of ParF is important in both the ParF-ParF interaction and also the ParF-ParG interaction. Disrupting this interface has a knock on effect on the ATP dependent assembly of ParF into higher order structures, due to a conformational change within the ParF dimer. It is predicted that multiple residues would need to be changed to disrupt the monomer-monomer interface in such a way that the ParF dimer would be unable to form.

6.1.3 ParF is able to bind nsDNA and associates with the nucleoid *in vivo*

As like other ParA proteins, ParF has been shown to bind nsDNA in an ATP-dependent manner *in vitro* and localise with the nucleoid *in vivo* (McLeod et al., 2016). This was confirmed in this study using biochemical, single molecule and microscopy techniques. ParF displays moderately strong ATP-dependent DNA binding that is likely to be a highly transient process due to the cycling between ATP binding and hydrolysis. TPM experiments indicated that ParF does not form a 1-dimensional filament structure on the DNA, but in fact that multiple ParF-ATP dimers may bind the DNA and the interaction of different ParF dimers to form larger higher order structures causing bending and compaction of the DNA. These results were interesting as they supported *in vivo* observations in which higher resolution images revealed that ParF appears to protrude into the nucleoid forming a lattice of ParF filaments. Confocal and super resolution microscopy studies confirmed that ParF localises with the nucleoid and time lapse studies demonstrated the ability of ParF to oscillate from one pole of the nucleoid to the other. As previously mentioned higher resolution images revealed that ParF appears to protrude into the nucleoid, this was also confirmed by acquiring Z-stack images of ParF. These observations clearly demonstrated the importance of the nucleoid in TP228 plasmid segregation.

The structure of ParF revealed surface exposed basic residues that could be involved in nsDNA binding and that could be a potential DNA binding interface. It was proposed that if these residues were changed, the DNA binding could be disrupted and thus this would lead to a greater understanding of DNA binding in the segregation process. Initially alanine scanning mutagenesis studies of the surface exposed basic residues revealed three informative mutants that were then characterised *in vitro*. Although all

three mutants were unable to bind DNA *in vitro,* observations *in vivo* revealed that the mutants could still associate with the nucleoid. Two of these mutants, ParF-R139A and ParF-R169A, were in fact found to be crucial in ATP binding and both were hyperactive ATPase proteins that displayed weaker binding to ATP. Therefore this made it hard to determine the direct role these residues played in nsDNA binding. The disruption of nsDNA binding *in vitro* is likely to be due to the fact that both proteins display hyperactive ATPase activity and thus ATP is being hydrolysed to ADP at a quicker rate causing the mutant proteins to 'fall off' the DNA. The interaction of ParF with DNA is clearly a very transient process and *in vitro* disruption of ATP binding and hydrolysis has a large impact on the ability of ParF to bind DNA. *In vivo*, the concentration of DNA is much greater and this may allow other surface exposed basic residues to compensate for R139A or R169A allowing the mutants to retain some residual nsDNA binding.

On the other hand, ParF- K160E-R163E displayed an almost identical phenotype to ParF, but as mentioned was unable to bind nsDNA *in vitro* however did still associate with the nucleoid in *vivo*. Interestingly ParF-K160E-R163E also demonstrated disrupted assembly and disassembly of higher order structures and therefore *in vivo* displayed different patterning to the wild type protein. ParF-K160E-R163E was homogenously distributed over the nucleoid and was unable to oscillate from one pole of the nucleoid to the other. This then led to theory that ParF assembly into higher order structures and DNA binding could be linked and not independent events. It was proposed that to fully disrupt DNA binding multiple residues would need to be changed in order to prevent other surface exposed basic residues from compensating, However the data shown here has led to the conclusion that, in this case, both single and double mutations are not sufficient to abolish DNA binding completely and possibly other multiple residue changes would need to be studied.

To investigate whether ParF assembly into higher order structures and DNA binding is linked, DLS experiments, sedimentation assays and EM were used. The results were not entirely conclusive and therefore further work would need to be carried out in order to determine if ParF assembly and DNA binding are independent events.

6.2 Summary of all ParF mutant proteins

Throughout this work it has become evident that many of the important properties displayed by ParF are in fact all linked. ParF is (1) a weak ATPase protein that is able to

bind and hydrolyse ATP. The binding of ATP leads to two things; (2) the assembly into higher order structures and (3) DNA binding. When all three constituents are functioning correctly ParF is able to successfully drive the segregation of plasmid TP228. When one or more of these properties are disrupted, the segregation of plasmid TP228 becomes significantly less efficient. Interestingly many of the mutant proteins used in this work display disruption in not only one of these properties but often two or all three. This suggests that ParF displays a complex set of properties that are closely interlinked. Table 6.1 and 6.2 summarises the mutant proteins that have been studied in this work and helps to demonstrate this complex behaviour of ParF as well as allowing comparisons and differences to be highlighted. It can be noted that although many of the mutant proteins were constructed with the aim of disrupting different properties of ParF many similarities can be seen among all of them.

Table 6.1 - Summary of ParF mutant proteins *in vitro* phenotypes. If highlighted in red it indicates differences to that of ParF. Grey boxes indicate work not primarily done in this study.

	Plasmid retention	**Binds ATP**	**Forms a dimer**	**Interacts with ParG**	**Intrinsic ATPase activity**	**ATPase activity stimulated by ParG**	**Self-associates in the absence of nucleotide**	**ATP-dependent assembly into higher order structures**	**Binds nsDNA in an ATP-dependent manner *in vitro***
ParF	~70 %	Yes – Kd =0.44 µM	Yes	Yes	Weak	Yes	Yes	Yes	Yes
Chapter 3 – Dimer-dimer interface									
ParF-K64A-V89Y-M96A	~ 40 %	Yes	Yes	Yes	Weak	Yes	Yes, slightly lower tendency	No	No
Chapter 4 – Monomer-monomer interface									
ParF-P104A	~20 %	Yes	Yes	Yes	Hyper active	No	Yes, higher tendency	No	-
ParF-P107A	~60 %	Yes	Yes	Yes	-	-	Yes, higher tendency	No	-
ParF-S108A	~8 %	Yes	Yes	Significantly weaker	Weak	No	Yes, higher tendency	No	-
ParF-P109R	~7 %	Yes	Yes	Significantly weaker	Weak	No	Yes, significantly higher tendency	No	-
ParF-L110A	~10 %	-	-	Significantly weaker	-	-	-	-	-

	Plasmid retention	Binds ATP	Forms a dimer	Interacts with ParG	Intrinsic ATPase activity	ATPase activity stimulated by ParG	Self-associates in the absence of nucleotide	ATP-dependent assembly into higher order structures	Binds nsDNA in an ATP-dependent manner *in vitro*
ParF-F112A	~10 %	-	-	Yes	-	-	-	-	-
ParF-V149F	~26 %	-	-	Yes	-	-	-	-	-
Chapter 5 – ParF nsDNA binding									
ParF-R139A	~3 %	Yes	Yes	Yes slightly stronger	Hyper active	No	Yes, higher tendency	No	No
ParF-R169A	~5 %	Yes	Yes	Yes slightly stronger	Hyper active	No	Yes, higher tendency	No	No
ParF-K160E-R163E	~11 %	Yes	Yes	Yes	Weak	Yes	No	Yes gradually	No

Table 6.2 – Summary of ParF mutant proteins *in vivo* phenotype. If highlighted in red it indicates differences to that of ParF. Grey boxes indicate work not primarily done in this study.

	ParF pattern	**ParG pattern**	**ParG foci number**	**Spread throughout the nucleoid**	**Oscillates from one pole of the nucleoid to the other**
ParF	Asymmetrically distributed on the nucleoid	Dispersed throughout the nucleoid, but often, distinct ParG foci can also be identified within the dispersed signal. Pattern follows ParF	1 -4	Yes	Yes
Chapter 3 – Dimer-dimer interface					
ParF-K64A-V89Y-M96A	Homogenously spread	Homogenously spread	No obvious foci	Yes	No
Chapter 4 – Monomer-monomer interface					
ParF-S108A	Homogenously spread	Compact focus mostly at midcell	Majority of cells have 1 focus	Yes	No
ParF-P109R	Many different patterns	Many different patterns	0-4	Yes	No
Chapter 5 – ParF nsDNA binding					
ParF-R139A	Homogenously spread with foci	Compact focus randomly positioned	Majority of cells have 1 focus	Yes	No
ParF-R169A	Homogenously	Compact focus mostly at midcell	Majority of cells	Yes	No

	spread with foci		have 1 focus		
ParF-K160E-R163E	Homogenously spread	Dispersed throughout the nucleoid, but often, distinct ParG foci can also be identified within the dispersed signal.	1-4	Yes	No

Table 6.3 - Summary of ParF mutant proteins and the effects on the three main properties of ParF.

	1. Disruption in ATPase activity	**2. Disruption in ATP-dependent assembly into higher order structures**	**3. Disruption in DNA binding *in vitro***
ParF-K64A-V89Y-M96A	NO	YES	YES
ParF-P104A	YES	YES	-
ParF-P107A	NO	YES	-
ParF-S108A	NO	YES	YES
ParF-P109R	NO	YES	-
ParF-R139A	YES	YES	YES
ParF-R169A	YES	YES	YES
ParF-K160E-R163E	NO	NO	YES

The ParF mutant proteins investigated here fall into two main groups, those in which the residue that is changed is positioned at, or close to, the monomer-monomer interface of ParF and the other group in which the residues are positioned closer to the surface of the ParF dimer. Those that fall into the first group are: ParF-P104A, ParF-P107A, ParF-S108A, ParF-P109R, ParF-R139A and ParF-R169A. The remaining two, ParF-K64A-V89Y-M96A and ParF-K160E-R163E fall into the latter group. All of the ParF mutant proteins in the first group show disruption in ATP dependent assembly into higher order structures and also display a higher tendency to self-associate into the higher order structures in the absence of nucleotide. This clearly demonstrates the importance of maintaining the integrity of this interface in ensuring the correct assembly of ParF higher order structures. On the other hand, ParF-K64A-V89Y-M96A and ParF-K160E-R163E do display disruption in ATP-dependent assembly into higher order structures but do not self-associate into higher order structures in the absence of nucleotide like the wild type ParF protein. This supports the importance of the dimer-dimer interface in the ability of ParF to form the building blocks of ParF polymers. Although ParF-K160E-R163E was not originally constructed to disrupt the dimer-dimer interface, the positions of these residues is in fact close to that of the second interface identified by Schumacher *et al* (2012). However it should be noted that ParF-K160E-R163E does undergo ATP-dependent assembly into higher order structures but at a much slower rate compared to the wild type protein.

As previously discussed, the residues that are positioned at the interface of ParF not only disrupt the assembly of ParF into higher order structures but also in some cases disrupt the ATP binding and hydrolysis and in others the interaction with ParG. This produces an even more complex phenotype. When visualised *in vivo*, ParF-S108A, ParF-P109R, ParF-R139A and ParF-R169A (ParF-P104A and ParF-P107A currently have not been visualised *in vivo*) display very similar patterning, with ParF-P109R being the only protein that differs slightly. All are homogenously distributed throughout the nucleoid and ParG forms compact foci often positioned at midcell or the extreme pole. If the mutant protein retains its interaction with ParG (in the case of ParF-R139A and ParF-R169A) then some overlap of ParF mutant and ParG foci can be observed. None of the ParF mutants are able to oscillate from one pole of the nucleoid to the other, which is likely due to the disruption of the assembly and disassembly of higher order structures. In addition to the fact that the conversions of these residues appears to lock ParF into a conformation that favours the self-association, the disruption is also

linked to either defects in the ATP binding and hydrolysis (ParF-P104A, ParF-R139A and ParF-R169A) or the alteration in the interaction with ParG (ParF-S108A and ParF-P109R).

Other than the disruption in the ATP-dependent assembly into higher order structures and the reduced tendency to self-associate, ParF-K64A-V89Y-M96A and ParF-K160E-R163E display similar phenotypes to that of the wild-type protein ParF. However both have been shown to be unable bind DNA *in vitro*, although both are still able to associate with the nucleoid *in vivo*. The slower ATP-dependent assembly of ParF-K160E-R163E with the disruption in DNA binding and alongside the fact that ParF-K64A-V89Y-M96A is unable to assemble into higher order structures or bind DNA suggests that one may be necessary for the other to occur. Although work carried out to determine if this was the case was inconclusive and requires further investigation, it is still reasonable to suggest a link between DNA binding and assembly into higher order structures and therefore a model for ParF DNA binding is proposed here (Figure 6.1). In this model ParF either binds to DNA as a dimer or a small polymer. Upon this the ParF dimer or small polymer can either continue to grow along the length of the DNA using the DNA as a scaffold. Alternatively ParF dimers positioned apart on the DNA may interact thus causing looping and compaction of the DNA. The combination of these events enables a network of ParF polymers and dimers to form on the DNA causing an extensive filament network of ParF within the DNA.

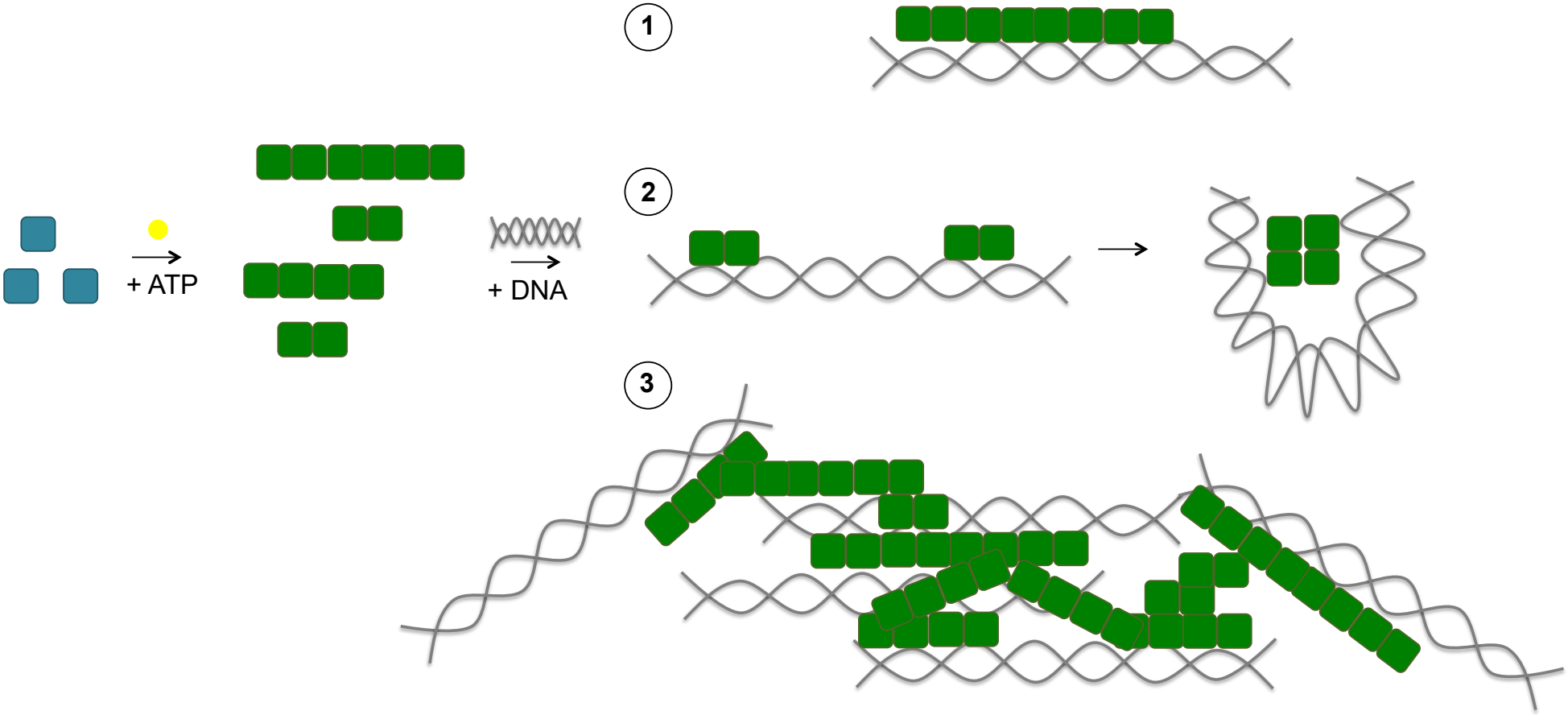

Figure 6.1 - ParF DNA binding model. Upon binding ATP (yellow circle) ParF is able to form a dimer and then can binding DNA and also assemble into higher order structures. This then results in three outcomes. (1) ParF is able to utilise the nucleoid as a scaffold and is able to bind as a dimer or small polymer and then continue to grow. (2) ParF binds the DNA as a dimer and interacts with other ParF dimers to loop and bridge the DNA. (3) ParF forms an extensive network of filaments within the nucleoid. Monomeric ParF is shown in blue and dimeric and polymers are shown in green. DNA is shown in grey.

The ParF mutant proteins analysed in this work have provided a greater understanding of how ParF drives TP228 plasmid segregation. It is essential that ParF is able to bind and hydrolyse ATP correctly to enable the assembly into higher order structures and to enable the protein to bind DNA in a non-specific manner. In addition, the ATPase activity of ParF must be stimulated correctly by ParG to enable the dynamic behaviour of ParF to occur correctly. If ParG is unable to stimulate ParF ATPase activity, either due to the ParF mutant protein being a hyperactive ATPase or because the interaction with ParG is abrogated, the dynamic behaviour of ParF is disrupted. Subsequently plasmid segregation is disrupted due to the inability of ParF to oscillate over the nucleoid therefore leading to incorrect positioning of the plasmids. When some ParF mutants that are defective in plasmid partitioning are visualised *in vivo*, the ParG focus bound to the plasmid is often observed stuck at midcell or at the extreme pole of the nucleoid. The fact that the ParG focus is mostly present at midcell or at the pole suggests that the plasmid-ParG complex is excluded from the nucleoid. This is likely because the interaction between the ParF mutant protein and ParG is disrupted and thus does not correctly recruit the plasmid to the nucleoid region. The focus at midcell is likely to be between separated nucleoids. This would explain the disruption in plasmid segregation. When functioning correctly, ParF binds ATP and assembles into higher order structures and due to the ability of the protein to bind DNA uses the nucleoid as a scaffold to aid this assembly. ParF is continually growing into these higher order structures and the cycling of binding ATP followed by hydrolysis, stimulated by ParG, enables the dynamic relocation of ParF. The interaction between ParF and ParG enables the plasmid to be recruited to the nucleoid and thus allows ParF to relocate the plasmids throughout the nucleoid. If the ability of ParF to bind and hydrolyse ATP, assemble into higher order structures, bind DNA or interact with ParG is disrupted ParF is unable to efficiently drive TP228 plasmid segregation. Figure 6.2 depicts the events that occur when ParF is functioning correctly (Figure 6.2A) and when crucial residues are disrupted. The ParF mutant proteins, with disruptions at the monomer-monomer interface and that display a higher tendency to self-associate in the absence of nucleotide but appear to become solubilised in the presence of nucleotide, do not undergo ATP dependent assembly into higher order structures. This results in the proteins being homogenously spread over the nucleoid and unable to oscillate (Figure 6.2B). ParF-K64A-V89Y-M96A and ParF-K160E-R163E display a similar homogenous pattern over the nucleoid, but the inability of these ParF mutant proteins to

assemble into higher order structures and oscillate is due to disruptions at the dimer-dimer interface and to the disruption of the nsDNA binding properties of ParF (Figure 6.2 C and D, respectively). A new model for TP228 plasmid segregation is discussed in the next section. This has been developed based on results obtained with various ParF mutant proteins discussed in this work alongside further biochemical *in vitro* characterisation of ParF and higher resolution images acquired using super resolution microscopy.

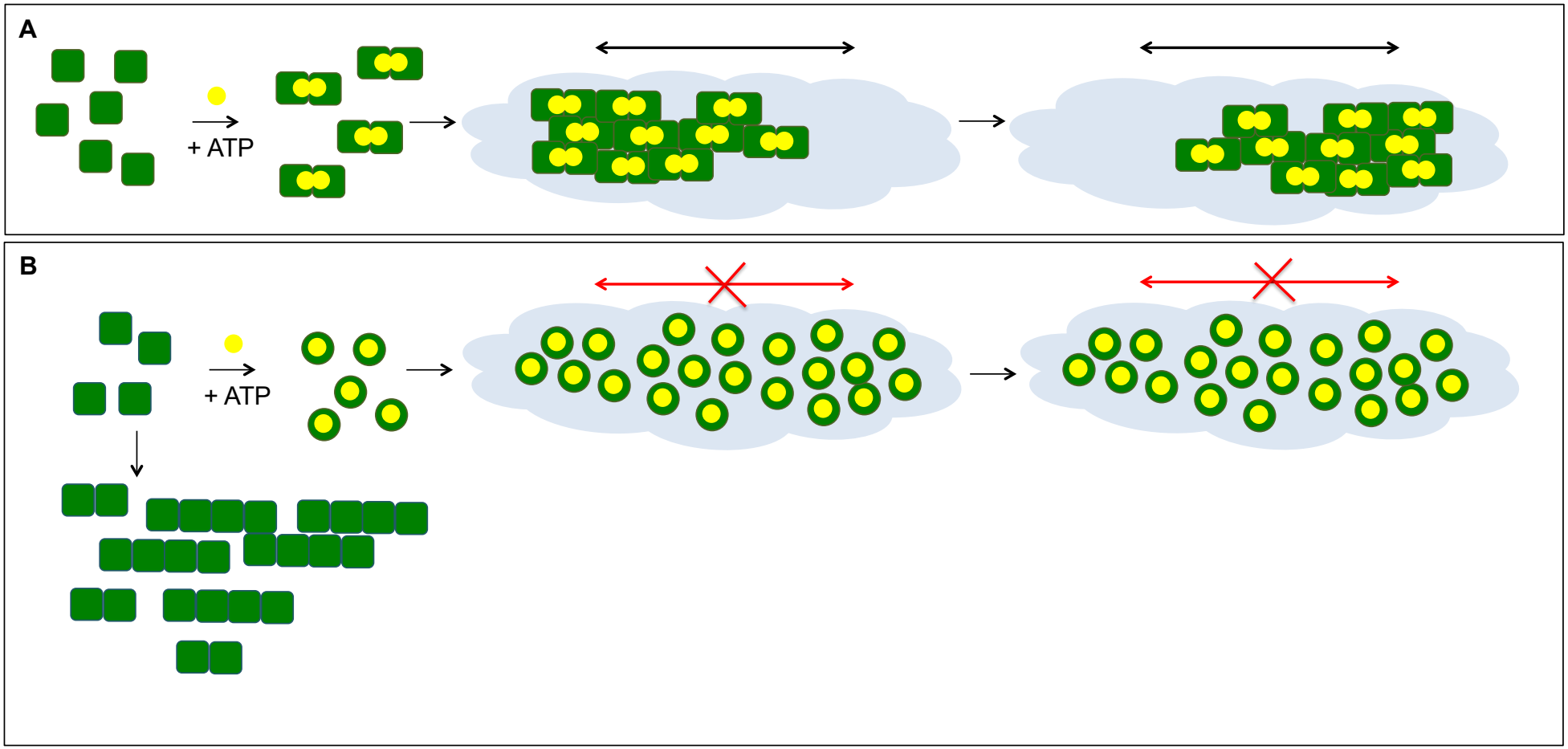
A
+ ATP
B
+ ATP

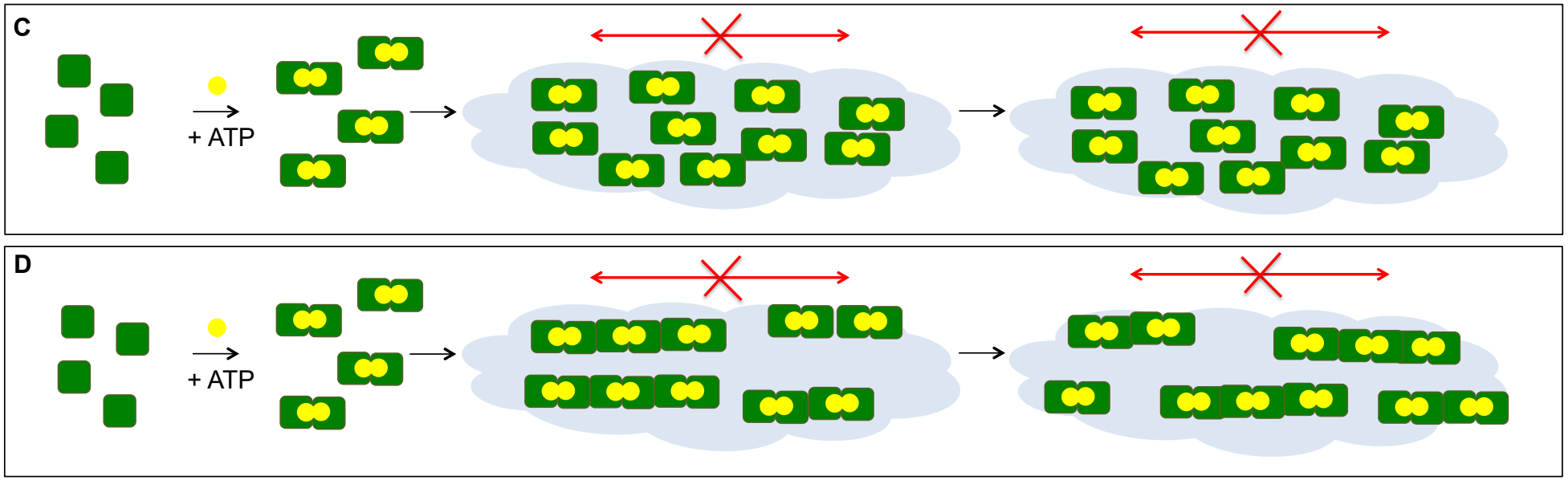

Figure 6.2 - A schematic representation of the behaviour displayed by ParF and ParF mutant proteins. A) Wild type ParF. Monomeric ParF (green square) binds ATP (yellow circle) and forms a dimer. ParF dimers then assemble into higher order structures and oscillate from one pole of the nucleoid as depicted by a black arrow. B) ParF-S108A, ParF-P109R, ParF-R139A and ParF-R169A. These ParF mutant proteins are locked into a configuration that favours the self-association in the absence of nucleotide. The addition of ATP causes the proteins to become solubilised and the proteins are unable to undergo ATP dependent assembly into higher order structures (green circles). The proteins are therefore homogenously distributed throughout the nucleoid and don't display any oscillatory behaviour depicted by a red arrow. C) ParF-K64A-V89Y-M96A. ParF-K64A-V89Y-M96A is able to bind ATP and form a dimer. The protein is unable to form higher order structures due to the disruption at the dimer-dimer interface and therefore is associated with the nucleoid as a dimer in a homogenous and static pattern without displaying any oscillatory behaviours. D) ParF-K160E-R163E. ParF-K160E-R163E is able to bind ATP and form a dimer. However the disruption in the nsDNA binding properties appears to slow down the ATP-assembly into higher order structures and again leads to the homogenous distribution of the protein through the nucleoid without oscillation.

6.3 A model for TP228 plasmid segregation

The molecular mechanism employed by type I partition systems has been under much deliberation in recent years. There are currently two main models of segregation that have been proposed that involve two very different mechanisms of segregation. These models are constantly being reviewed and recently new models have also been proposed. The first of these, the filament model, involves ParA proteins polymerising into a string-like structures. A polymerisation – depolymerisation cycle occurs due to stimulation of the ParA ATPase activity by the partner protein. The ParA polymers, bound to the plasmid via the partner protein, were proposed to either pull the plasmid upon this polymerisation and depolymerisation cycle and therefore moving the plasmids to either poles of the cell. More recently this model was then modified to incorporate the nucleoid acting as a scaffold for the polymerisation of ParA into filaments (Ringgaard *et al*., 2009). The second model, the diffusion-ratchet model, involves ParA-ATP associating with the nucleoid as dimers or small oligomers. The stimulation of ATP hydrolysis by the partner protein enables the dynamic relocation of ParA and this allows ParB, bound to *parS,* to follow a ParA gradient on the nucleoid surface (Vecchiarelli, 2014). A variation on this model has also been proposed, the DNA-relay model, in which chromosome dynamics also play a role in the model (Lim *et al*., 2014). Most recently a 'hitch-hiking' model has been proposed (Le Gall *et al*., 2016). In this model the ParA proteins associate at high-density regions within the nucleoid and the stimulation of the ATPase activity, by the partner protein ParB, enables ParA oligomers to hitch-hike along the high density regions in the nucleoid and the partition complex is moved due to Brownian diffusion and directional bias. Although all the current models differ in the exact mechanism that results in the segregation of the plasmid, many similarities can be noted across all the models. Firstly the nucleoid acting as a scaffold is a common feature in all of the models. The second feature is that all the ParA proteins utilise the energy of nucleotide binding and hydrolysis to drive the plasmid segregation. Finally the ATPase activity of the ParA proteins is stimulated via an interaction with the partner protein, which in most cases is bound to the plasmid.

A new model for TP228 plasmid segregation is proposed here that takes into account findings in this study, together with previous work carried out on the TP228 partition cassette and work on other type I partition systems. In this proposed model, current models are combined, where self-assembly into higher order structures and ParF

forming a gradient on the nucleoid are both important. Higher resolution images showed that ParF localises to the nucleoid but also that it appears to protrude into the nucleoid forming a lattice. It should be noted that in some cases ParF also appears to project out of the nucleoid surface. ParF has been observed *in vitro* to form higher order filament structures and this further supports the formation of the three-dimensional lattice. The nsDNA binding properties demonstrated by ParF enables the protein to use the nucleoid as a scaffold thus aiding the self-assembly into the higher order structures and leading to the formation of the three-dimensional lattice. Often ParG bound to the plasmid looks to be captured in this ParF lattice and this allows the transport of the plasmid from pole to pole of the nucleoid. Therefore the new model of TP228 plasmid segregation involves the nucleoid forming a scaffold for the assembly of a three-dimensional ParF lattice. A pair of ParG-bound plasmids is engulfed by the ParF lattice at midcell, and the ParF-ParG interaction allows the plasmids to be captured. The plasmids are then transported from one pole of the nucleoid to the other. The ParF lattice consists of a leading and lagging edge, which directs the movement. The leading edge consists of compact polymers whereas the lagging edge consists of less densely packed polymers. One plasmid bound to ParG then becomes detached due to ParG stimulation of ParF ATP hydrolysis causing disassembly of the surrounding ParF polymers. The remaining plasmid is then transported to the other pole of the nucleoid where it also becomes detached. The model is shown in Figure 6.3

The ParF mutants that have been investigated in this study support this proposed model. Firstly, this work has shown that if either the monomer-monomer or dimer-dimer interface of ParF is disrupted the protein is unable to undergo ATP dependent assembly into higher order structures. *In vivo*, this results in ParF being homogenously spread over the nucleoid and unable to oscillate. Therefore it is likely that the ParF lattice is unable to be correctly formed or positioned throughout the nucleoid. In addition to this disruption in nsDNA properties of ParF may also contribute to a different structure of the ParF lattice on the nucleoid and as a consequence of both these disruptions, no splitting or positioning of the plasmids occurs.

Secondly, this work has demonstrated that when the interaction between ParF and ParG is disrupted again no splitting or positioning of the plasmids occurs, indicating that ParG is essential for accurate plasmid positioning and partitioning. *In vivo*, ParF mutants that showed a weaker interaction with ParG clearly demonstrated the inability to capture and engulf the ParG bound plasmid. This resulted in the ParG focus bound to

the plasmid often being stuck at midcell or at the extreme pole of the nucleoid. The fact that the ParG focus is mostly present at midcell or at the pole suggests that the plasmid-ParG complex is excluded from the nucleoid due to the fact that ParF is unable to recruit the plasmid to the nucleoid region. This therefore leads to the failure of ParF to position the plasmids correctly. It has been proposed in other partition systems that initially plasmid pairing occurs at midcell before partitioning (Edgar *et al*., 2001) and the observations *in vivo* suggest in some cases the plasmids remain stuck at midcell after pairing if the ParF-ParG interaction is disrupted. It can be observed *in vivo* that ParF mutants that are still able to interact with ParG demonstrate the ability to recruit the ParG-plasmid complex to the nucleoid. In these cases however, as the ParF lattice is disrupted and ParF is homogenously distributed, the ParG bound plasmid is not positioned correctly and effectively is just randomly spread through the nucleoid. As these ParF mutants are unable to oscillate the randomly bound ParG-plasmid complex is not repositioned and thus leads to partitioning defects.

The results gathered from this study help to validate the model discussed in Figure 6.3. Clearly the dynamic ParF lattice distributes a cargo to correctly position the plasmid in a given area, which in this case in the nucleoid. ParG is critical to the model by both enabling the relocation of this cargo as well as ensuring the plasmid is recruited to the ParF lattice via the ParF-ParG interaction.

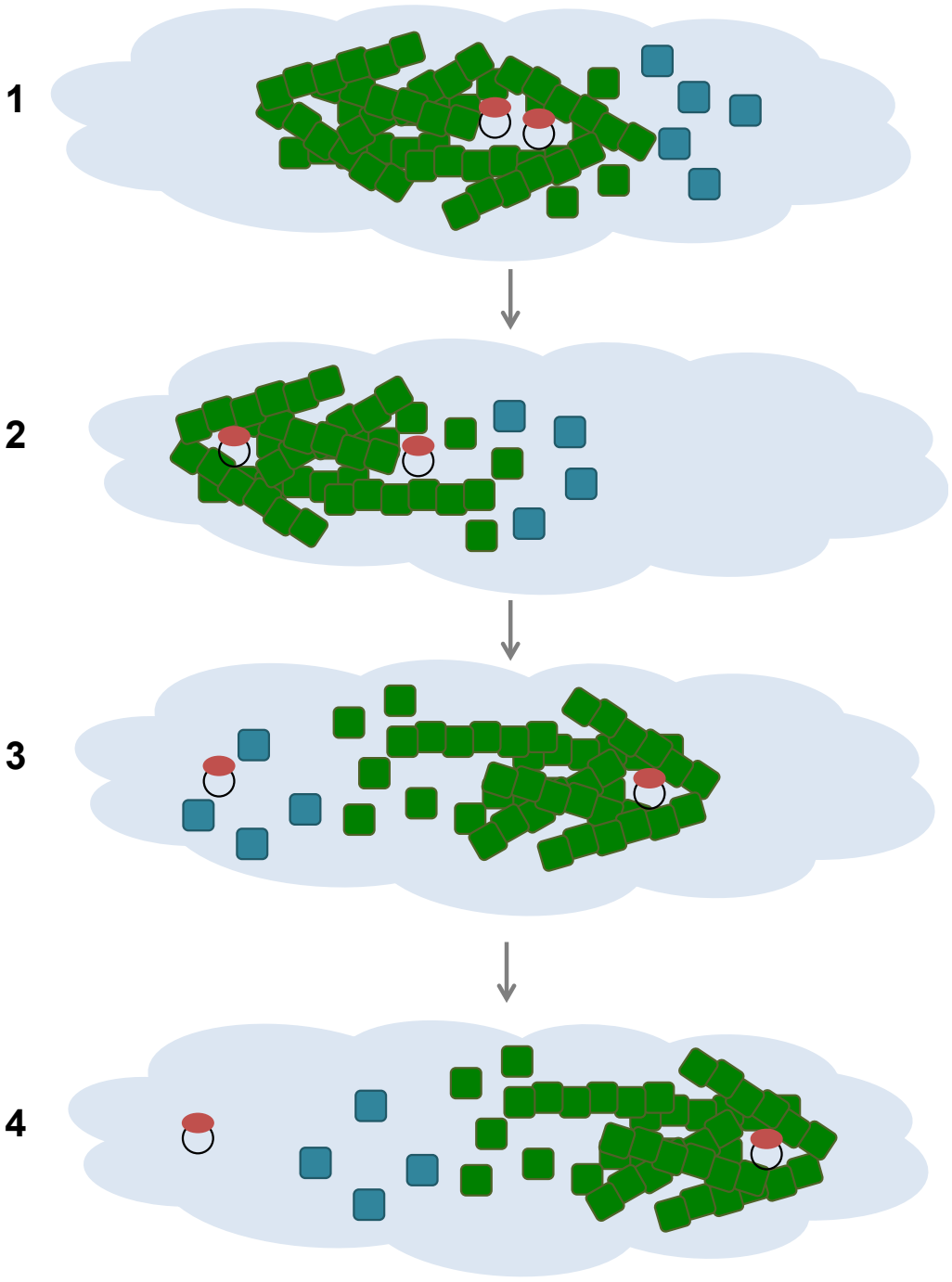

Figure 6.3 - A model for TP228 plasmid segregation. A model of the three-dimensional ParF lattice mediated plasmid segregation. (1) The sister plasmids are captured in the ParF lattice. (2) The plasmids are transported to a pole of the nucleoid directed by the leading edge of the ParF polymer. (3) The plasmids are then transported to the opposite pole of the nucleoid where one of the plasmids is dropped. (4) The other plasmid is then transported to the opposite pole of the nucleoid where it eventually also becomes detached. The nucleoid is shown in grey, plasmid is a black circle with ParG (red) bound. Monomeric ParF is shown as a blue square and dimeric and polymeric ParF is shown by green squares.

6.4 Future work

ParF displays a complex set of phenotypes that are crucial in the protein's ability to correctly and efficiently drive plasmid segregation. In order to gain further understanding of ParF and further develop the TP228 plasmid segregation model a number of other areas need to be investigated further.

Schumacher *et al* (2012) observed that ParF-ATP dimers interact with each other to form dimer-of-dimer units, which then form the building blocks of the ParF polymers. It was suggested that by disrupting two interfaces on the surface of these ParF dimers that ParF polymer formation would be abolished. In this work a triple mutant harbouring changes at one of these interfaces was investigated (interface 1). It would be beneficial if a mutant could be constructed harbouring changes at the other dimer-dimer interface (interface 2) and investigated to further support this model of how ParF assembles into higher order structures. Any additional work on the dimer-dimer interface would give a valuable insight into the assembly of ParF into higher order structures.

Conversion of residues at the monomer-monomer interface of ParF appeared to disrupt many crucial properties of ParF. Firstly, residues that were changed in order to prevent ParF dimer formation in fact showed the opposite effect and locked the protein into a configuration that favoured self-association. Further understanding of this conformational change could be analysed by detecting changes in intrinsic tryptophan fluorescence as previously carried out for ParF-P104A (Dobruk-Serkowska *et al*., 2012). Biophysical techniques that determine a conformational change within a protein, such as hydrogen exchange or second harmonic generation (SHC), alongside computational modelling may also allow a greater understanding of the effect of converting these residues on ParF conformation. The initial aim of this part of the study was to try and disrupt the monomer-monomer interface of ParF to prevent dimer formation. Therefore constructing a ParF mutant that is unable to form a dimer is still a high priority. It would give an invaluable insight into the assembly process of ParF into higher order structures as well as the ability of the protein to bind DNA. If a ParF mutant was constructed that was unable to form a dimer it would be interesting to observe this mutant *in vivo* to see if the protein was associated with the nucleoid or whether, as predicted, dispersed throughout the cell and not confined to the nucleoid. To achieve this, as mentioned in Chapter 4, a double or a triple mutant may need to be constructed by converting residues previously identified to be important in the

monomer-monomer cross contacts (Schumacher *et al*., 2012). Once additional mutants have been constructed chemical crosslinking experiments alongside bacterial two-hybrid assays could again be employed to determine if the mutant could form a dimer.

As well as the monomer-monomer interface of ParF being important in the ability of the ParF to form higher order structures, this work revealed a potential interface for ParG binding and crucial residues that are involved in this binding. The ParF-ParG and ParF mutants - ParG interactions were only tested in a semi-quantitative manner and it would be beneficial to carry out further work on this to further quantify the interactions. Surface plasmon resonance (SPR), isothermal titration calorimetry (ITC) and microscale thermophoresis (MST) would be good techniques to use for this. Also solving the co-structure of ParF-ParG would be a great step towards gaining a better understanding of this interaction.

Achieving further understanding of how ParF binds nsDNA and the role of the nucleoid in the plasmid segregation mechanism would be advantageous in helping to develop the TP228 plasmid segregation model further. This work failed to confirm a DNA binding interface of ParF as all the mutants constructed, although showed disruption of nsDNA *in vitro*, still associated with the nucleoid *in vivo*. As discussed in Chapter 5, other ParF mutants would need to be constructed and analysed. Alternative double mutants could be constructed as well as triple or quadruple mutants. The aim would be to construct a mutant that is unable to associate with the nucleoid. Additional techniques could be used to gain further understanding of the nsDNA binding properties of ParF. Single molecule techniques such as FRET, magnetic tweezers and optical tweezers have been shown to be powerful tools to analyse Protein-DNA interactions. Techniques such as these would help build upon results gathered in this study. The link between DNA binding and ParF assemble into higher order structures also needs further investigation. The DLS, sedimentation assay and EM techniques could be optimised and developed further to analyse the effect DNA has on ParF assembly into higher order structures alongside new techniques. Alternative approaches to DLS such as Nanoparticle Tracking Analysis (NTA) or Resonant mass measurement (RMM) could be employed as these techniques overcome some of the issues raised in DLS. In addition to analysing the wild type ParF protein, analysing ParF mutant proteins that display a disruption in nsDNA binding as well as proteins that demonstrate disruption in the ability to form higher order structures would enable an even greater understanding. Specifically, an experiment that compares the assembly of ParF and ParF-K160E-R163E into higher

order structures could demonstrate whether DNA is able promote this assembly as ParF-K160E-R163E was shown to be unable to bind nsDNA *in vitro*.

Finally, additional microscopy techniques would be beneficial in many ways. Firstly, super resolution microscopy of ParF and ParF mutant proteins would be advantageous as the higher resolution images acquired from this technique have been instrumental in the development of the new TP228 plasmid segregation model. Observing patterns formed by ParF mutant proteins studied in this work as well as new mutants would give a greater insight into the exact mechanism behind TP228 plasmid segregation. In addition to this, as previously mentioned when some ParF mutant proteins are present ParG forms a single compact focus often positioned at midcell. It has been observed that ParG foci co-localise with the plasmid carrying the *parFGH* cassette (McLeod et al., 2016) and therefore clarifying this is the case with the different ParF mutants (ParF-S108A, ParF-R139A and ParF-R169A) and that the plasmid is associated with ParG would further support the model proposed. Previously this has been determined by inserting an array of lac operator sites, $lacO_{120}$ into the plasmid carrying the *parFG-mCherry-parH* cassette. This plasmid, alongside a second plasmid expressing *lacI-ebfp2* encoding the Lac repressor fused to an enhanced version of Blue Fluorescent Protein 2 are then transformed into cells. LacI-EBFP2 binds the *lacO* sites, forming compact blue foci that indicate the position of plasmids. In addition this Fluorescence *in situ* hybridization (FISH) could also be employed to determine the position of the plasmid. These techniques would be also useful if carried out with ParF-K64A-V89Y-M99A and ParF-K160E-R163E as again it could confirm if the plasmids are associated with ParG, which appears to be randomly recruited throughout the nucleoid with the ParF mutants.

Abbreviations

AMPPCP - phosphomethylphosphonic acid adenylate ester

ATP - adenosine 5-triphosphate

3D - three dimentional

3D-SIM - 3 dimensional structured illumination microscopy

°C - Degrees Celsius

µg - Microgram

µl - Microlitres

µm - Micromolar

A - Absorbance

Amp - Ampicillin

AP - Alkaline phosphatase

APS - Ammonium persulphate

ATP - Adenosine triphosphate

ATPase - Adenosine triphosphate hydrolase

Bp - Base pair

BSA - Bovine serum albumin

Cat - Chloramphenicol

CBP - centromere binding protein

DAPI - 4', 6-diamidino-2-phenylindole

dH2O - deionised water

DLS - dynamic light scattering

DMP - dimethyl pimelimidate

DNA - Dexoyribonuclic acid

dNTP - Dexoyribonucleoside-5'-triphosphate

dsDNA - Double stranded dexoyribonuclic acid

E. coli **-** *Escherichia coli*

EM - electron microscopy

EMSA - electrophoretic mobility shift assay

GTP - Guanosine triphosphate

GTPase - Guanosine triphosphate hydrolase

His - Histidine

HTH - helix-turn-helix motif

IHF - integration host factor

IPTG - Isopropyl beta-D-1-thiogalactopyranoside

IR - inverted repeat

ITC - isothermal titration calorimetry

Kan - Kanamycin

kbp - kilobase pairs

K_d - Dissociation constant

kDa - Kilodaltons

L - Litre

LB - Luria-Bertani medium

M - Molar

mg - Milligrams

Min - Minutes

ml - Millilitres

mM - Millimolar

mol - Moles

MST - microscale thermophoresis

MW - Molecular weight

ng - Nanograms

nm - Nanometres

OD_{600} - Optical density at 600 nm

O_F - operator site

ONPG - O-nitrophenyl-β-d-galactopyranoside

PAGE - Polyacrylamide gel electrophoresis

PBS - Phosphate buffered saline

PCR - Polymerase chain reaction

pmol - Picomoles

RHH - ribbon-helix-helix

RT - Room temperature

s - Seconds

SDS - Sodium dodecyl sulphate

Spec - Spectinomycin

SPR - Surface Plasmon Resonance

TA - toxin-antitoxin

TEMED - N,N,N’N’-tetramethyl-ethylenediamine

Tris - Tris (hydroxymethyl) aminomethane

U - Enzyme unit

UV - Ultraviolet

w/v - Weight for volume

θ - theta

References

ADACHI, S., HORI, K. & HIRAGA, S. 2006. Subcellular positioning of F plasmid mediated by dynamic localization of SopA and SopB. *J Mol Biol,* 356**,** 850-63.

AH-SENG, Y., RECH, J., LANE, D. & BOUET, J. Y. 2013. Defining the role of ATP hydrolysis in mitotic segregation of bacterial plasmids. *PLoS Genet,* 9**,** e1003956.

AI, H.-W., SHANER, N. C., CHENG, Z., TSIEN, R. Y. & CAMPBELL, R. E. 2007. Exploration of New Chromophore Structures Leads to the Identification of

Improved Blue Fluorescent Proteins. *Biochemistry,* 46**,** 5904-5910.

AYLETT, C. H. S. & LOWE, J. 2012. Superstructure of the centromeric complex of TubZRC plasmid partitioning systems. *PNAS,* 109**,** 16522-16527.

AYLETT, C. H. S., WANG, Q., MICHIE, K. A., AMOS, L. A. & LOEWE, J. 2010. Filament structure of bacterial tubulin homologue TubZ. *Proceedings of the National Academy of Sciences of the United States of America,* 107**,** 19766-19771.

BARILLA, D., CARMELO, E. & HAYES, F. 2007. The tail of the ParG DNA segregation protein remodels ParF polymers and enhances ATP hydrolysis via an arginine finger-like motif. *Proceedings of the National Academy of Sciences,* 104**,** 1811-1816.

BARILLÀ, D. & HAYES, F. 2003. Architecture of the ParF•ParG protein complex involved in prokaryotic DNA segregation. *Molecular Microbiology,* 49**,** 487-499.

BARILLA, D., ROSENBERG, M. F., NOBBMANN, U. & HAYES, F. 2005. Bacterial DNA segregation dynamics mediated by the polymerizing protein ParF. *Embo Journal,* 24**,** 1453-1464.

BATT, S. M., BINGLE, L. E., DAFFORN, T. R. & THOMAS, C. M. 2009. Bacterial genome partitioning: N-terminal domain of IncC protein encoded by broad-host-range plasmid RK2 modulates oligomerisation and DNA binding. *J Mol Biol,* 385**,** 1361-74.

BAXTER, J. C. & FUNNELL, B. E. 2014. Plasmid Partition Mechanisms. *Microbiology Spectrum,* 2.

BHARAT, T. A., MURSHUDOV, G. N., SACHSE, C. & LOWE, J. 2015. Structures of actin-like ParM filaments show architecture of plasmid-segregating spindles. *Nature,* 523**,** 106-10.

BIGNELL, C. & THOMAS, C. M. 2001. The bacterial ParA-ParB partitioning proteins. *Journal of Biotechnology,* 91**,** 1-34.

BOUET, J.-Y., AH-SENG, Y., BENMERADI, N. & LANE, D. 2006. Polymerization of SopA partition ATPase: regulation by DNA binding and SopB. *Molecular Microbiology,* 63**,** 468-481.

BOUET, J. Y. & FUNNELL, B. E. 1999. P1 ParA interacts with the P1 partition complex at parS and an ATP–ADP switch controls ParA activities. *EMBO J,* 18**,** 1415-1424.

BOUET, J. Y., SURTEES, J. A. & FUNNELL, B. E. 2000. Stoichiometry of P1 Plasmid Partition Complexes. *The Journal of Biological Chemistry,* 275**,** 8213-8219.

CARMELO, E., BARILLA, D., GOLOVANOV, A. P., LIAN, L.-Y., DEROME, A. & HAYES, F. 2005. The Unstructured N-terminal Tail of ParG Modulates Assembly of a Quaternary Nucleoprotein Complex in Transcription Repression. *Journal of Biological Chemistry,* 280**,** 28683-28691.

CASTAING, J. P., BOUET, J. Y. & LANE, D. 2008. F plasmid partition depends on interaction of SopA with non-specific DNA. *Mol Microbiol,* 70**,** 1000-11.

CHEN, B. W., LIN, M. H., CHU, C. H., HSU, C. E. & SUN, Y. J. 2015. Insights into ParB spreading from the complex structure of Spo0J and parS. *Proc Natl Acad Sci U S A,* 112**,** 6613-8.

CHEN, Y. & ERICKSON, H. P. 2008. In vitro assembly studies of FtsZ/tubulin-like proteins (TubZ) from Bacillus plasmids: evidence for a capping mechanism. *J Biol Chem,* 283**,** 8102-9.

CORDELL, S. C. & LOWE, J. 2001. Crystal structure of the bacterial cell division regulator MinD. *FEBS Letters,* 492**,** 160-165.

DAM, M. & GERDES, K. 1994. Ten Direct Repeats Flanking the parA Promoter Constitute a Centromere-like Partition Site parC, that Expresses Incompatibility. *J Mol Biol,* 236**,** 1289-1298.

DAVEY, M. J. & FUNNELL, B. E. 1994. The P1 Plasmid Partition Protein ParA. *J Biol Chem,* 269**,** 29908-29913.

DAVEY, M. J. & FUNNELL, B. E. 1997. Modulation of the P1 Plasmid Partition Protein ParA by ATP, ADP, and P1 ParB. *J Biol Chem,* 272**,** 15286-15292.

DAVIS, M. A., RADNEDGE, L., MARRTIN, K. A., HAYES, F., YOUNGREN, B. & AUSTIN, S. 1996. The P1 ParA protein and its ATPase activity play a direct role in the segregation of plasmid copies to daughter cells. *Mol Microbiol,* 21**,** 1029-1036.

DE BOER, P. A. J., CROSSLEY, R. E. & ROTHFIELD, L. 1992. Roles of MinC and MinD in the Site-Specific Septation Block Mediated by the MinCDE System of Escherichia coli. *J Bacteriol,* 174**,** 63-70.

DEBER, C. M., BRODSKY, B., JOHNSON, R. W. & RATH, A. 2010. Proline residues in Proteins. *eLS*.

DEL SOLAR, G., GIRALDO, R., RUIZ-ECHEVARRIA, J. M., ESPINOSA, M. & DIAZ-OREJAS, R. 1998. Replication and Control of Circular Bacterial Plasmids. *Microbiology and Molecular Biology Reviews,* 62**,** 434-464.

DERMAN, A. I., BECKER, E. C., TRUONG, B. D., FUJIOKA, A., TUCEY, T. M., ERB, M. L., PATTERSON, P. C. & POGLIANO, J. 2009. Phylogenetic analysis identifies many uncharacterized actin-like proteins (Alps) in bacteria: regulated polymerization, dynamic instability and treadmilling in Alp7A. *Mol Microbiol,* 73**,** 534-52.

DERMAN, A. I., NONEJUIE, P., MICHEL, B. C., TRUONG, B. D., FUJIOKA, A., ERB, M. L. & POGLIANO, J. 2012. Alp7R regulates expression of the actin-like protein Alp7A in Bacillus subtilis. *J Bacteriol,* 194**,** 2715-24.

DOBRUK-SERKOWSKA, A., CACCAMO, M., RODRIGUEZ-CASTANEDA, F., WU, M., BRYCE, K., NG, I., SCHUMACHER, M. A., BARILLA, D. & HAYES, F. 2012. Uncoupling of Nucleotide Hydrolysis and Polymerization in the ParA Superfamily Disrupts DNA Segregation Dynamics. *Journal of Biological Chemistry*.

DUNHAM, T. D., XU, W., FUNNELL, B. E. & SCHUMACHER, M. A. 2009. Structural basis for ADP-mediated transcriptional regulation by P1 and P7 ParA. *EMBO J,* 28**,** 1792-802.

EBERSBACH, G. & GERDES, K. 2001. The double par locus of virulence factor pB171: DNA segregation is correlated with oscillation of ParA. *Proceedings of the National Academy of Sciences,* 98**,** 15078-15083.

EBERSBACH, G. & GERDES, K. 2004. Bacterial mitosis: partitioning protein ParA oscillates in spiral-shaped structures and positions plasmids at mid-cell. *Mol Microbiol,* 52**,** 385-98.

EBERSBACH, G. & GERDES, K. 2005. Plasmid segregation mechanisms. *Annual Review of Genetics.*

EBERSBACH, G., RINGGAARD, S., MOLLER-JENSEN, J., WANG, Q., SHERRATT, D. J. & GERDES, K. 2006. Regular cellular distribution of plasmids by oscillating and filament-forming ParA ATPase of plasmid pB171. *Molecular Microbiology,* 61**,** 1428-1442.

EDGAR, R., CHATTORAJ, D. K. & YARMOLINSKY, M. 2001. Pairing of P1 plasmid partition sites by ParB. *Mol Microbiol,* 42**,** 1363-1370.

FIGGE, R. M., EASTER, J. & GOBER, J. W. 2003. Productive interaction between the chromosome partitioning proteins, ParA and ParB, is required for the progression of the cell cycle in Caulobacter crescentus. *Mol Microbiol,* 47**,** 1225-1237.

FINK, G. & LOWE, J. 2015. Reconstitution of a prokaryotic minus end-tracking system using TubRC centromeric complexes and tubulin-like protein TubZ filaments. *Proc Natl Acad Sci U S A,* 112**,** E1845-50.

FOGEL, M. A. & WALDOR, M. K. 2006. A dynamic, mitotic-like mechanism for bacterial chromosome segregation. *Genes & Development,* 20**,** 3269-3282.

FOTHERGILL, T. J. G., BARILLA, D. & HAYES, F. 2005. Protein Diversity Confers Specificity in Plasmid Segregation. *Journal of Bacteriology,* 187**,** 2651-2661.

FUNNELL, B. E. 1991. The P1 Plasmid Partition Complex at parS.The influence of Escherichia coli integration host factor and of substrate topology. *The Journal of Biological Chemistry,* 266**,** 14328-14337.

FUNNELL, B. E. & GAGNIER, L. 1993. The P1 Plasmid Partition Complex at parS. *The Journal of Biological Chemistry,* 268**,** 3616-3624.

GARNER, E. C., CAMPBELL, C. S., WEIBEL, D. B. & MULLINS, R. D. 2007. Reconstitution of DNA Segregation Driven by Assembly of a Prokaryotic Actin Homolog. *Science,* 315**,** 1270-1274.

GERDES, K., HOWARD, M. & SZARDENINGS, F. 2010. Pushing and Pulling in Prokaryotic DNA Segregation. *Cell,* 141**,** 927-942.

GERDES, K., MOLLER-JENSEN, J. & JENSEN, R. B. 2000. Plasmid and chromosome partitioning: surprises from phylogeny. *Molecular Microbiology,* 37**,** 455-466.

GHASRIANI, H., DUCAT, T., HART, C. T., HAFIZI, F., CHANG, N., AL-BALDAWI, A., AYED, S. H., LUNDSTROM, P., DILLON, J. A. & GOTO, N. K. 2010. Appropriation of the MinD protein-interaction motif by the dimeric interface of the bacterial cell division regulator MinE. *Proc Natl Acad Sci U S A,* 107**,** 18416-21.

GHOSAL, D., TRAMBAIOLO, D., AMOS, L. A. & LOWE, J. 2014. MinCD cell division proteins form alternating copolymeric cytomotive filaments. *Nat Commun,* 5**,** 5341.

GOLOVANOV, A. P., BARILLÀ, D., GOLOVANOVA, M., HAYES, F. & LIAN, L.-Y. 2003. ParG, a protein required for active partition of bacterial plasmids, has a dimeric ribbon–helix–helix structure. *Molecular Microbiology,* 50**,** 1141-1153.

GORDON, G. S., SITNIKOV, D., WEBB, C. D., TELEMAN, A., STRAIGHT, A., LOSICK, R., MURRAY, A. W. & WRIGHT, A. 1997. Chromosome and Low Copy Plasmid Segregation in E. coli: Visual Evidence for Distinct Mechanisms. *Cell,* 90**,** 1113-1121.

GRAHAM, T. G. W., WANG, X., SONG, D., ETSON, C. M., VAN OIJEN, A. M., RUDNER, D. Z. & LOPARO, J. J. 2014. ParB spreading requires DNA bridging. *Genes & Development*.

GRUBER, S. & ERRINGTON, J. 2009. Recruitment of condensin to replication origin regions by ParB/SpoOJ promotes chromosome segregation in B. subtilis. *Cell,* 137**,** 685-96.

GUYNET, C. & DE LA CRUZ, F. 2011. Plasmid segregation without partition. *Mobile Genetic Elements,* 1**,** 236-241.

HATANO, T. & NIKI, H. 2010. Partitioning of P1 plasmids by gradual distribution of the ATPase ParA. *Molecular Microbiology,* 78**,** 1182-1198.

HATANO, T., YAMAICHI, Y. & NIKI, H. 2007. Oscillating focus of SopA associated with filamentous structure guides partitioning of F plasmid. *Mol Microbiol,* 64**,** 1198-213.

HAYASHI, I., OYAMA, T. & MORIKAWA, K. 2001. Structural and functional studies of MinD ATPase: implications for the molecular recognition of the bacterial cell division apparatus. *EMBO J,* 20**,** 1819-1828.

HAYES, F. 2000. The partition system of multidrug resistance plasmid TP228 includes a novel protein that epitomizes an evolutionarily distinct subgroup of the ParA superfamily. *Mol Microbiol,* 37**,** 528-541.

HAYES, F. 2003. Toxins-Antitoxins: Plasmid Maintenance, Programmed Cell Death, and Cell Cycle Arrest. *Science,* 301**,** 1496-1499.

HAYES, F. & AUSTIN, S. 1994. Topological Scanning of the P1 Plasmid Partition Site. *J Mol Biol,* 243**,** 190-198.

HAYES, F. & BARILLA, D. 2006. Assembling the bacterial segrosome. *Trends in Biochemical Sciences,* 31**,** 247-250.

HAYES, F. & BARILLÀ, D. 2006. The bacterial segrosome: a dynamic nucleoprotein machine for DNA trafficking and segregation. *Nature Reviews Microbiology,* 4**,** 133-143.

HESTER, C. M. & LUTKENHAUS, J. 2007. Soj (ParA) DNA binding is mediated by conserved arginines and is essential for plasmid segregation. *Proceedings of the National Academy of Sciences,* 104**,** 20326-20331.

HU, L., VECCHIARELLI, A. G., MIZUUCHI, K., NEUMAN, K. C. & LIU, J. 2015. Directed and persistent movement arises from mechanochemistry of the ParA/ParB system. *Proc Natl Acad Sci U S A,* 112**,** E7055-64.

HU, Z., GOGOL, E. P. & LUTKENHAUS, J. 2002. Dynamic assembly of MinD on phospholipid vesicles regulated by ATP and MinE. *Proc Natl Acad Sci U S A,* 99**,** 6761-6.

HU, Z. & LUTKENHAUS, J. 1999. Topological regulation of cell division in Escherichia coli involves rapid pole to pole oscillation of the division inhibitor MinC under the control of MinD and MinE. *Mol Microbiol,* 34**,** 82-90.

HU, Z. & LUTKENHAUS, J. 2000. Analysis of MinC Reveals Two Independent Domains Involved in Interaction with MinD and FtsZ. *J Bacteriol,* 182**,** 3965-3971.

HU, Z. & LUTKENHAUS, J. 2001. Topological Regulation of Cell Division in E. coli: Spatiotemporal Oscillation of MinD Requires Stimulation of Its ATPase by MinE and Phospholipid. *Molecular Cell,* 7**,** 1337-1343.

HWANG, L. C., VECCHIARELLI, A. G., HAN, Y. W., MIZUUCHI, M., HARADA, Y., FUNNELL, B. E. & MIZUUCHI, K. 2013. ParA-mediated plasmid partition driven by protein pattern self-organization. *EMBO J,* 32**,** 1238-49.

IETSWAART, R., SZARDENINGS, F., GERDES, K. & HOWARD, M. 2014. Competing ParA Structures Space Bacterial Plasmids Equally over the Nucleoid. *PLoS Comput Biol,* 10**,** e1004009.

IRETON, K., GUNTHER, N. W. & GROSSMAN, A. D. 1994. spoOJ Is Required for Normal Chromosome Segregation as well astheInitiationofSporulationinBacillussubtilis. *J Bacteriol,* 176**,** 5320-5329.

IVANOV, V. & MIZUUCHI, K. 2010. Multiple modes of interconverting dynamic pattern formation by bacterial cell division proteins. *Proc Natl Acad Sci U S A,* 107**,** 8071-8.

JACOB, F., BRENNER, S. & CUZIN, F. 1963. On the regulation of DNA replication in bacteria. *Cold Spring Harbor Symp Quant Biol,* 28**,** 329-348.

JENSEN, R. B., LURZ, R. & GERDES, K. 1998. Mechanism of DNA segregation in prokaryotes: Replicon pairing by parC of plasmid R1. *Proc Natl Acad Sci U S A,* 95**,** 8550-8555.

JOHNSON, T. J. & NOLAN, L. K. 2009. Pathogenomics of the virulence plasmids of Escherichia coli. *Microbiol Mol Biol Rev,* 73**,** 750-74.

JONES, C. S., OSBORNE, D. J. & STANLEY, J. 1993. Molecular comparison of the IncX plasmids allows division into IncXl and IncX2 subgroups. *Journal of General Microbiology,* 139**,** 735-741.

KARIMOVA, G., PIDOUX, J., ULLMANN, A. & LADANT, D. 1998. A bacterial two-hybrid system based on a reconstituted signal transduction pathway. *Proc Natl Acad Sci U S A,* 95**,** 5752-5756.

KHAN, S. A. 1997. Rolling-Circle Replication of Bacterial Plasmids. *Microbiol Mol Biol Rev,* 61**,** 442-455.

KNIGHT, K. L. & SAUER, R. T. 1989. DNA bindingspecificityoftheArcandMntrepressorsis determined by a short region of N-terminal residues. *PNAS,* 86**,** 797-801.

KORTEMME, T. & BAKER, D. 2002. A simple physical model for binding energy hot spots in protein-protein complexes. *Proc Natl Acad Sci U S A,* 99**,** 14116-21.

LARSEN, R. A., CUSUMANO, C., FUJIOKA, A., LIM-FONG, G., PATTERSON, P. & POGLIANO, J. 2007. Treadmilling of a prokaryotic tubulin-like protein, TubZ, required for plasmid stability in Bacillus thuringiensis. *Genes & Development,* 21**,** 1340-1352.

LAU, I. F., FILIPE, S. R., SØBALLE, B., ØKSTAD, O.-A., BARRE, F.-X. & SHERRATT, D. J. 2004. Spatial and temporal organization of replicating Escherichia coli chromosomes. *Molecular Microbiology,* 49**,** 731-743.

LE GALL, A., CATTONI, D. I., GUILHAS, B., MATHIEU-DEMAZIERE, C., OUDJEDI, L., FICHE, J. B., RECH, J., ABRAHAMSSON, S., MURRAY, H., BOUET, J. Y. & NOLLMANN, M. 2016. Bacterial partition complexes segregate within the volume of the nucleoid. *Nat Commun,* 7**,** 12107.

LEDERBERG, J. 1952. Cell Genetics and Hereditary Symbiosis. *Physiol Rev,* 32**,** 403-430.

LEE, P. S. & GROSSMAN, A. D. 2006. The chromosome partitioning proteins Soj (ParA) and Spo0J (ParB) contribute to accurate chromosome partitioning, separation of replicated sister origins, and regulation of replication initiation in Bacillus subtilis. *Molecular Microbiology,* 60**,** 853-869.

LEIPE, D. D., WOLF, Y. I., KOONIN, E. V. & ARAVIND, L. 2002. Classification and evolution of P-loop GTPases and related ATPases. *J Mol Biol,* 317**,** 41-72.

LEONARD, T. A., BUTLER, P. J. & LOWE, J. 2004. Structural analysis of the chromosome segregation protein Spo0J from Thermus thermophilus. *Mol Microbiol,* 53**,** 419-32.

LEONARD, T. A., BUTLER, P. J. & LOWE, J. 2005. Bacterial chromosome segregation: structure and DNA binding of the Soj dimer - a conserved biological switch. *Embo Journal,* 24**,** 270-282.

LILLY, J. & CAMPS, M. 2015. Mechanisms of Theta Plasmid Replication. *Microbiol Spectr,* 3**,** 1-18.

LIM, H. C., SUROVTSEV, I. V., BELTRAN, B. G., HUANG, F., BEWERSDORF, J. & JACOBS-WAGNER, C. 2014. Evidence for a DNA-relay mechanism in ParABS-mediated chromosome segregation. *Elife,* 3**,** e02758.

LIN, D. C. & GROSSMAN, A. D. 1998. Identification and Characterization of a Bacterial Chromosome Partitioning Site. *Cell,* 92**,** 675-685.

LIVNY, J., YAMAICHI, Y. & WALDOR, M. K. 2007. Distribution of centromere-like parS sites in bacteria: insights from comparative genomics. *J Bacteriol,* 189**,** 8693-703.

LOOSE, M., FISCHER-FRIEDRICH, E., RIES, J., KRUSE, K. & SCHWILLW, P. 2008. Spatial Regulators for Bacterial Cell Division Self-Organize into Surface Waves in Vitro. *Science,* 320**,** 789-792.

LUTKENHAUS, J. 2007. Assembly Dynamics of the Bacterial MinCDE System and Spatial Regulation of the Z Ring. *Annual Review of Biochemistry,* 76**,** 539-562.

LUTKENHAUS, J. 2012. The ParA/MinD family puts things in their place. *Trends in Microbiology,* 20**,** 411-418.

LUTKENHAUS, J. & SUNDARAMOORTHY, M. 2003. MinD and role of the deviant Walker A motif, dimerization and membrane binding in oscillation. *Molecular Microbiology,* 48**,** 295-303.

MACARTNEY, D. P., WILLIAMS, D. R., STAFFORD, T. & THOMAS, C. M. 1997. Divergence and conservation of the partitioning and global regulation functions in the central control region of the IncP plasmids RK2 and R751. *MBio,* 143**,** 2167-2177.

MACHÓN, C., FOTHERGILL, T. J. G., BARILLÀ, D. & HAYES, F. 2007. Promiscuous Stimulation of ParF Protein Polymerization by Heterogeneous Centromere Binding Factors. *Journal of Molecular Biology,* 374**,** 1-8.

MARSTON, A. L. & ERRINGTON, J. 1999. Dynamic Movement of the ParA-like Soj Protein of B. subtilis and Its Dual Role in Nucleoid Organization and Developmental Regulation. *Molecular Cell,* 4**,** 673-682.

MCLEOD, B. N., ALLISON-GAMBLE, G. E., BARGE, M. T., TONTHAT, N. K., SCHUMACHER, M. A., HAYES, F. & BARILLA, D. 2016. A three-dimensional ParF meshwork assembles through the nucleoid to mediate plasmid segregation. *Nucleic Acids Res*.

MILLION-WEAVER, S. & CAMPS, M. 2014. Mechanisms of plasmid segregation: have multicopy plasmids been overlooked? *Plasmid,* 75**,** 27-36.

MOHL, D. A. & GOBER, J. W. 1997. Cell Cycle–Dependent Polar Localization of Chromosome Partitioning Proteins in Caulobacter crescentus. *Cell,* 88**,** 675-684.

MOLLER-JENSEN, J., BORCH, J., DAM, M., JENSEN, R. B., ROEPSTORFF, P. & GERDES, K. 2003. Bacterial Mitosis: ParM of Plasmid R1 Moves Plasmid DNA by an Actin-like Insertional Polymerization Mechanism. *Molecular Cell,* 12**,** 1477-1457.

MOLLER-JENSEN, J., JENSEN, R. B. & GERDES, H. 2000. Plasmid and chromosome segregation in prokaryotes. *Trends in Microbiology,* 8**,** 313-320.

MOLLER-JENSEN, J., JENSEN, R. B., LOWE, J. & GERDES, K. 2002. Prokaryotic DNA segregation by an actin-like filament. *Embo Journal,* 21**,** 3119-3127.

MOLLER-JENSEN, J., RINGGAARD, S., MERCOGLIANO, C. P., GERDES, K. & LOWE, J. 2007. Structural analysis of the ParR/parC plasmid partition complex. *EMBO J,* 26**,** 4413-4422.

MOTALLEBI-VESHAREH, M., ROUCH, D. A. & THOMAS, C. M. 1990. A FAMILY OF ATPASES INVOLVED IN ACTIVE PARTITIONING OF DIVERSE BACTERIAL PLASMIDS. *Molecular Microbiology,* 4**,** 1455-1463.

MURAYAMA, K., ORTH, P., DE LA HOZ, A. B., ALONSO, J. C. & SAENGER, W. 2001. Crystal structure of omega transcriptional repressor encoded by

Streptococcus pyogenes plasmid pSM19035 at 1.5 A resolution. *J Mol Biol,* 314**,** 789-96.

MURRAY, H. & ERRINGTON, J. 2008. Dynamic control of the DNA replication initiation protein DnaA by Soj/ParA. *Cell,* 135**,** 74-84.

MURRAY, H., FERREIRA, H. & ERRINGTON, J. 2006. The bacterial chromosome segregation protein Spo0J spreads along DNA from parS nucleation sites. *Mol Microbiol,* 61**,** 1352-61.

NI, L., XU, W., KUMARASWAMI, M. & SCHUMACHER, M. A. 2010. Plasmid protein TubR uses a distinct mode of HTH-DNA binding and recruits the prokaryotic tubulin homolog TubZ to effect DNA partition. *Proceedings of the National Academy of Sciences,* 107**,** 11763-11768.

NORMAN, A., HANSEN, L. H. & SORENSEN, S. J. 2009. Conjugative plasmids: vessels of the communal gene pool. *Philos Trans R Soc Lond B Biol Sci,* 364**,** 2275-89.

OSAWA, M. & ERICKSON, H. P. 2013. Liposome division by a simple bacterial division machinery. *PNAS,* 110**,** 11000-11004.

PILLET, F., SANCHEZ, A., LANE, D., ANTON LEBERRE, V. & BOUET, J. Y. 2011. Centromere binding specificity in assembly of the F plasmid partition complex. *Nucleic Acids Res,* 39**,** 7477-86.

PRATTO, F., CICEK, A., WEIHOFEN, W. A., LURZ, R., SAENGER, W. & ALONSO, J. C. 2008. Streptococcus pyogenes pSM19035 requires dynamic assembly of ATP-bound ParA and ParB on parS DNA during plasmid segregation. *Nucleic Acids Research,* 36**,** 3676-3689.

PTACIN, J. L., LEE, S. F., GARNER, E. C., TORO, E., ECKART, M., COMOLLI, L. R., MOERNER, W. E. & SHAPIRO, L. 2010. A spindle-like apparatus guides bacterial chromosome segregation. *Nature Cell Biology,* 12**,** 791-798.

QUISEL, J. D., CHI-HONG LIN, D. & GROSSMAN, A. D. 1999. Control of Development by Altered Localization of a Transcription Factor in B. subtilis. *Molecular Cell,* 4**,** 665-672.

REYES-LAMOTHE, R., NICOLAS, E. & SHERRATT, D. J. 2011. Chromosome Replication and Segregation in Bacteria. *Annual Review of Genetics,* 46**,** 120830114430006.

REYES-LAMOTHE, R., TRAN, T., MEAS, D., LEE, L., LI, A. M., SHERRATT, D. J. & TOLMASKY, M. E. 2014. High-copy bacterial plasmids diffuse in the nucleoid-free space, replicate stochastically and are randomly partitioned at cell division. *Nucleic Acids Res,* 42**,** 1042-51.

RINGGAARD, S., LOWE, J. & GERDES, K. 2007. Centromere Pairing by a Plasmid-encoded Type I ParB Protein. *Journal of Biological Chemistry,* 282**,** 28216-28225.

RINGGAARD, S., VAN ZON, J., HOWARD, M. & GERDES, K. 2009. Movement and equipositioning of plasmids by ParA filament disassembly. *Proceedings of the National Academy of Sciences,* 106**,** 19369-19374.

RODIONOV, O., LOBOCKA, M. & YARMOLINSKY, M. 1999. Silencing of genes flanking the P1 plasmid centromere. *Science,* 283**,** 546-549.

SAKAI, N., YAO, M., ITOU, H., WANANABE, N., YUMOTO, F., TANOKURA, M. & TANAKA, I. 2001. The Three-Dimensional Structure of Septum Site-Determining Protein MinD from Pyrococcus horikoshii OT3 in Complex with Mg-ADP. *Structure,* 9**,** 817-826.

SALJE, J., GAYATHRI, P. & LOWE, J. 2010. The ParMRC system: molecular mechanisms of plasmid segregation by actin-like filaments. *Nat Rev Microbiol,* 8**,** 683-92.

SALJE, J. & LOWE, J. 2008. Bacterial actin: architecture of the ParMRC plasmid DNA partitioning complex. *Embo Journal,* 27**,** 2230-2238.

SANCHEZ, A., CATTONI, DIEGO I., WALTER, J.-C., RECH, J., PARMEGGIANI, A., NOLLMANN, M. & BOUET, J.-Y. 2015. Stochastic Self-Assembly of ParB Proteins Builds the Bacterial DNA Segregation Apparatus. *Cell Systems,* 1**,** 163-173.

SCHOLEFIELD, G., WHITING, R., ERRINGTON, J. & MURRAY, H. 2011. Spo0J regulates the oligomeric state of Soj to trigger its switch from an activator to an inhibitor of DNA replication initiation. *Mol Microbiol,* 79**,** 1089-100.

SCHREITER, E. R. & DRENNAN, C. L. 2007. Ribbon-helix-helix transcription factors: variations on a theme. *Nat Rev Microbiol,* 5**,** 710-20.

SCHUMACHER, M. A. 2007. Structural biology of plasmid segregation proteins. *Current Opinion in Structural Biology,* 17**,** 103-109.

SCHUMACHER, MARIA A. 2008. Structural biology of plasmid partition: uncovering the molecular mechanisms of DNA segregation. *Biochemical Journal,* 412**,** 1.

SCHUMACHER, M. A. 2012. Bacterial plasmid partition machinery: a minimalist approach to survival. *Current Opinion in Structural Biology,* 22**,** 72-79.

SCHUMACHER, M. A., GLOVER, T. C., BRZOSKA, A. J., JENSEN, S. O., DUNHAM, T. D., SKURRAY, R. A. & FIRTH, N. 2007. Segrosome structure revealed by a complex of ParR with centromere DNA. *Nature,* 450**,** 1268-1271.

SCHUMACHER, M. A., PIRO, K. M. & XU, W. 2010. Insight into F plasmid DNA segregation revealed by structures of SopB and SopB-DNA complexes. *Nucleic Acids Res,* 38**,** 4514-26.

SCHUMACHER, M. A., YE, Q., BARGE, M. T., ZAMPINI, M., BARILLA, D. & HAYES, F. 2012. Structural Mechanism of ATP-induced Polymerization of the Partition Factor ParF: IMPLICATIONS FOR DNA SEGREGATION. *Journal of Biological Chemistry,* 287**,** 26146-26154.

SHAEVITZ, J. W. & GITAI, Z. 2010. The structure and function of bacterial actin homologs. *Cold Spring Harb Perspect Biol,* 2**,** a000364.

SHELBELUT, C. W., GUBERMAN, J. M., TEEFFELEN, S. V., YAKHNINA, A. A. & GITAI, Z. 2010. Caulobacter chromosome segregation is an ordered multistep process. *PNAS,* 107**,** 14194-14198.

SHIH, Y. L. 2003. Division site selection in Escherichia coli involves dynamic redistribution of Min proteins within coiled structures that extend between the two cell poles. *Proceedings of the National Academy of Sciences,* 100**,** 7865-7870.

SIMPSON, A. E., SKURRAY, R. A. & FIRTH, N. 2003. A Single Gene on the Staphylococcal Multiresistance Plasmid pSK1 Encodes a Novel Partitioning System. *Journal of Bacteriology,* 185**,** 2143-2152.

SOBERON, N. E., LIOY, V. S., PRATTO, F., VOLANTE, A. & ALONSO, J. C. 2011. Molecular anatomy of the Streptococcus pyogenes pSM19035 partition and segrosome complexes. *Nucleic Acids Res,* 39**,** 2624-37.

STIEBER, D., GABANT, P. & SZPIRER, C. Y. 2008. Toxins-Antitoxins: Plasmid Maintenance, Programmed Cell Death, and Cell Cycle Arrest. *Biotechniques,* 45**,** 344-346.

SUEFUJI, K., VALLUZZI, R. & RAYCHAUDHURI, D. 2002. Dynamic assembly of MinD into filament bundles modulated by ATP, phospholipids, and MinE. *Proc Natl Acad Sci U S A,* 99**,** 16776-81.

SULLIVAN, N. L., MARQUIS, K. A. & RUDNER, D. Z. 2009. Recruitment of SMC by ParB-parS organizes the origin region and promotes efficient chromosome segregation. *Cell,* 137**,** 697-707.

TINSLEY, E. & KHAN, S. A. 2006. A novel FtsZ-like protein is involved in replication of the anthrax toxin-encoding pXO1 plasmid in Bacillus anthracis. *J Bacteriol,* 188**,** 2829-35.

TORO, E., HONG, S. H., MCADAMS, H. H. & SHAPIRO, L. 2008. Caulobacter requires a dedicated mechanism to initiate chromosome segregation. *Proc Natl Acad Sci U S A,* 105**,** 15435-40.

TORO, E. & SHAPIRO, L. 2010. Bacterial chromosome organization and segregation. *Cold Spring Harb Perspect Biol,* 2**,** a000349.

VECCHIARELLI, A. G., HAN, Y.-W., TAN, X., MIZUUCHI, M., GHIRLANDO, R., BIERTÜMPFEL, C., FUNNELL, B. E. & MIZUUCHI, K. 2010. ATP control of dynamic P1 ParA-DNA interactions: a key role for the nucleoid in plasmid partition. *Molecular Microbiology***,** 78-91.

VECCHIARELLI, A. G., HWANG, L. C. & MIZUUCHI, K. 2013. Cell-free study of F plasmid partition provides evidence for cargo transport by a diffusion-ratchet mechanism. *Proc Natl Acad Sci U S A,* 110**,** E1390-7.

VECCHIARELLI, A. G., LI, M., MIZUUCHI, M., HWANG, L. C., SEOL, Y., NEUMAN, K. C. & MIZUUCHI, K. 2016. Membrane-bound MinDE complex acts as a toggle switch that drives Min oscillation coupled to cytoplasmic depletion of MinD. *Proc Natl Acad Sci U S A,* 113**,** E1479-88.

VECCHIARELLI, A. G., MIZUUCHI, K. & FUNNELL, B. E. 2012. Surfing biological surfaces: exploiting the nucleoid for partition and transport in bacteria. *Molecular Microbiology,* 86**,** 513-523.

VECCHIARELLI, A. G. N., K. C.; MIZUUCHI, K. 2014. A propagating ATPase gradient drives transport of surface-confined cellular cargo. *PNAS,* 111**,** 4880-4885.

VIOLLIER, P. H., THANBICHLER, M., MCGRATH, P. T., WEST, L., MEEWAN, M., MCADAMS, H. H. & SHAPIRO, L. 2004. Rapid and sequential movement of individual chromosomal loci to specific subcellular locations during bacterial DNA replication. *Proc Natl Acad Sci U S A,* 101**,** 9257-62.

VOLANTE, A. & ALONSO, J. C. 2015. Molecular Anatomy of ParA-ParA and ParA-ParB Interactions during Plasmid Partitioning. *J Biol Chem,* 290**,** 18782-95.

WALKER, J. E., SARASTE, M., RUNSWICK, M. J. & GAY, N. J. 1982. Distantlyrelatedsequences inthea- and f-subunitsofATP synthase, myosin,kinasesandotherATP-requiringenzymesandacommon nucleotidebindingfold. *EMBO J,* 1**,** 945-951.

WANG, X., LLOPIS, P. M. & RUDNER, D. Z. 2013. Organization and segregation of bacterial chromosomes. *Nature Reviews Genetics,* 14**,** 191-203.

WANG, X., MONTERO LLOPIS, P. & RUDNER, D. Z. 2014a. Bacillus subtilis chromosome organization oscillates between two distinct patterns. *Proc Natl Acad Sci U S A,* 111**,** 12877-82.

WANG, X., TANG, O. W., RILEY, E. P. & RUDNER, D. Z. 2014b. The SMC condensin complex is required for origin segregation in Bacillus subtilis. *Curr Biol,* 24**,** 287-92.

WU, M., ZAMPINI, M., BUSSIEK, M., HOISCHEN, C., DIEKMANN, S. & HAYES, F. 2011a. Segrosome assembly at the pliable parH centromere. *Nucleic Acids Research,* 39**,** 5082-5097.

WU, W., PARK, K. T., HOLYOAK, T. & LUTKENHAUS, J. 2011b. Determination of the structure of the MinD-ATP complex reveals the orientation of MinD on the membrane and the relative location of the binding sites for MinE and MinC. *Mol Microbiol,* 79**,** 1515-28.

ZAMPINI, M., DEROME, A., BAILEY, S. E. S., BARILLA, D. & HAYES, F. 2009. Recruitment of the ParG Segregation Protein to Different Affinity DNA Sites. *Journal of Bacteriology,* 191**,** 3832-3841.

ZHOU, H. & LUTKENHAUS, J. 2005. MinC mutants deficient in MinD- and DicB-mediated cell division inhibition due to loss of interaction with MinD, DicB, or a septal component. *J Bacteriol,* 187**,** 2846-57.